



UNIVERSITY OF  
LIVERPOOL

**microRNA:target interactions  
in tendinopathy**

Thesis submitted in accordance with the requirements of the  
University of Liverpool for the degree of Doctor of Philosophy

by

David Alan Bardell

April 2021

orthopaedic  
researchUK



## Contents

Acknowledgements.....	10
Abstract.....	12
Abbreviations.....	13
List of Tables.....	24
List of Figures.....	28
<b>Chapter 1 – Introduction.....</b>	<b>32</b>
<i>1.1 Tendon structure and function.....</i>	<i>32</i>
1.1.1 Extracellular matrix composition.....	34
1.1.2 Cellular content of tendons.....	36
1.1.3 Matrix metabolism.....	37
1.1.4 Mechanical properties of tendon.....	38
1.1.5 Mechanical properties differ between positional and energy storing tendons.....	41
1.1.6 Tendon response to exercise.....	41
1.1.7 Age-related changes.....	42
1.2 Pathophysiology of tendinopathies.....	44
1.2.1 Matrix changes associated with tendinopathies.....	45
1.2.2 Mechanical influences on tendinopathies.....	46
1.2.3 Inflammation in tendinopathy.....	47
1.2.4 Neural influences in tendinopathy.....	48
1.2.5 Vascular influences on tendinopathy.....	48
1.2.6 Endocrine influences on tendinopathy.....	49
1.2.7 Other factors implicated in tendinopathies.....	50
1.2.8 Mechanisms of tendon repair.....	50
1.3 microRNAs and tendinopathy.....	51
1.3.1 microRNA synthesis and function.....	52
1.3.2 Role of microRNAs in tendinopathies/musculoskeletal disease.....	56
1.3.3 Diagnostic, prognostic and therapeutic potential of microRNAs.....	63

1.4 Aims and objectives of project.....	64
<b>Chapter 2 – Materials and methods.....</b>	<b>65</b>
2.1 Tissue sample acquisition.....	65
2.1.1 Human tissue.....	65
2.1.2 Equine tissue.....	67
2.2 Primary tenocyte isolation.....	69
2.2.1 Cell culture media.....	69
2.2.2 Equine primary tenocytes.....	69
2.2.3 Human primary tenocytes.....	71
2.3 Monolayer cell culture techniques.....	72
2.3.1 Monolayer culture.....	72
2.3.2 Laminin coating cover slips.....	73
2.4 Three-dimensional equine tendon construct techniques.....	74
2.4.1 Culture media and reagent preparation.....	74
2.4.2 Preparing Sylgard™ 184 silicone elastomer plates.....	77
2.4.3 Tendon construct methodology.....	78
2.5 Cholesterol conjugated microRNA/oligonucleotide transfection.....	81
2.5.1 Treatment of monolayer cultures.....	82
2.5.2 Transfection of three-dimensional tendon constructs.....	83
2.6 CCCP assay for induced autophagy/mitophagy.....	84
2.6.1 CCCP treatment of miR-181-treated tenocytes.....	85
2.7 Immunocytochemistry.....	86
2.8 RNA extraction.....	88
2.8.1 RNA extraction from equine and human tendons.....	88
2.8.2 RNA extraction from equine tenocyte constructs.....	89
2.8.3 RNA extraction from monolayer cell culture.....	90
2.8.4 MirVana™ RNA extraction protocol.....	91
2.9 RNA quantification and quality assessment.....	93
2.9.1 Agarose gel electrophoresis.....	93

2.9.2 Nanodrop 2000 spectrophotometry.....	94
2.9.3 TapeStation electrophoresis.....	96
2.10 RNA-sequencing.....	97
2.11 cDNA synthesis.....	100
2.11.1 Reverse transcription for miRNAs.....	100
2.11.2 Reverse transcription for mRNAs.....	101
2.12 Quantitative real time PCR (RT-qPCR).....	103
2.12.1 Primer design and optimisation.....	103
2.12.2 RT-qPCR protocol for miRNAs.....	112
2.12.3 RT-qPCR protocol for mRNAs.....	113
2.13 Protein extraction.....	115
2.13.1 Cell monolayer culture (6 well plates).....	115
2.13.2 Protein extraction from equine tenocyte constructs.....	116
2.13.3 Protein concentration assay (Pierce assay).....	117
2.14 SDS-PAGE.....	118
2.14.1 Solutions and reagents for SDS-PAGE.....	118
2.14.2 Casting gels.....	119
2.14.3 Loading and running gels.....	120
2.15 Western blotting.....	121
2.15.1 Solutions required for Western blotting.....	122
2.15.2 Western blotting protocol.....	122
2.16 Histological processing.....	124
2.16.1 Routine histology.....	124
2.16.2 Electron microscopy.....	129
2.17 Statistical analysis.....	130
<b>Chapter 3 – microRNA profiling of human and equine tendon.....</b>	<b>132</b>
3.1 Introduction.....	132
3.2 Methods.....	135
3.2.1 Small RNA-sequencing.....	135

3.2.2 Reverse transcription quantitative real-time polymerase chain reaction validation of small RNA-sequencing data.....	136
3.2.3 Reverse transcription quantitative real-time polymerase chain reaction validation of equine tendinopathy as a model for miRNA dysregulation in human tendon disease.....	137
3.2.4 Statistical analysis.....	139
3.3 Results.....	139
3.3.1 RNA-seq profiling of small non-coding RNA in human tendon.....	139
3.3.2 RT-qPCR validation of microRNAs differentially expressed in human tendon disease.....	143
3.3.3 Validation of equine superficial digital flexor tendinopathy as a model to study miRNA dysregulation in human tendon disease.....	147
3.4 Discussion.....	151
<b>Chapter 4 – Prediction of altered miRNA:target gene interaction in tendinopathy.....</b>	<b>157</b>
4.1 Introduction.....	157
4.2 Methods.....	159
4.2.1 Target prediction and pathway analysis for miRNAs differentially expressed in human tendinopathy.....	159
4.2.2 Target prediction and pathway analysis for differentially expressed miRNAs common to both human and equine tendinopathy.....	159
4.2.3 Statistical analysis.....	160
4.3 Results.....	163
4.3.1 Target prediction and pathway analysis for miRNAs differentially expressed in human tendinopathy.....	163
4.3.2 Target prediction and pathway analysis for differentially expressed miRNAs common to both human and equine tendinopathy.....	174
4.4 Discussion.....	182

<b>Chapter 5 – miR-181 function in equine tenocytes – monolayer cell culture.....</b>	<b>186</b>
5.1 Introduction.....	186
5.2 Methods.....	189
5.2.1 Treatment of tenocyte cultures.....	189
5.2.2 Reverse transcription quantitative real-time polymerase chain reaction.....	189
5.2.3 Induction of mitophagy and immunocytochemistry.....	190
5.2.4 Statistical analysis.....	190
5.3 Results.....	191
5.3.1 Validation of miR-181a-5p overexpression and inhibition in tenocytes.....	191
5.3.2 miR-181a predicted target gene analysis.....	194
5.3.3 The role of miR-181 in regulation of mitochondrial dynamics in equine tenocytes.....	198
5.4 Discussion.....	210
<b>Chapter 6 – Functional analysis of miR-181 in equine tenocytes – 3D tendon constructs.....</b>	<b>217</b>
6.1 Introduction.....	217
6.2 Methods.....	220
6.2.1 Generation of tendon constructs.....	220
6.2.2 Reverse transcription quantitative real-time polymerase chain reaction.....	221
6.2.3 Protein expression.....	221
6.2.4 Histology and transmission electron microscopy.....	222
6.2.5 Statistical analysis.....	222
6.3 Results.....	224
6.3.1 Validation of miR-181a-5p overexpression and inhibition in tendon constructs.....	224
6.3.2 miR-181a predicted target gene analysis.....	226
6.3.3 Protein expression.....	229
6.3.4 Role of miR-181 in regulation of mitochondrial dynamics.....	235
6.3.5 Role of miR-181 in regulation of tendon construct structure.....	238
6.4 Discussion.....	248

<b>Chapter 7 – Validation of miR-181 function in human tenocytes</b> .....	255
7.1 Introduction.....	255
7.2 Methods.....	257
7.2.1 Treatment of tenocyte cultures.....	257
7.2.2 Reverse transcription quantitative real-time polymerase chain reaction.....	257
7.2.3 Protein levels.....	258
7.2.4 Induction of mitophagy and immunocytochemistry.....	258
7.2.5 Statistical analysis.....	258
7.3 Results.....	259
7.3.1 Validation of miR-181a-5p overexpression and inhibition in tenocytes.....	259
7.3.2 miR-181a target gene analysis.....	261
7.3.3 Protein expression (Western blotting).....	263
7.3.4 Role of miR-181 in regulation of mitochondrial dynamics.....	267
7.4 Discussion.....	277
<b>Chapter 8 – General discussion and progression of work</b> .....	283
8.1 Tissue sample collection.....	283
8.2 Comparison of sncRNA transcriptome changes in human and equine tendinopathy.....	285
8.3 Development of a tendon construct model.....	286
8.4 Primer specificity.....	288
8.5 Optimisation of miR-181 transfection protocol.....	288
8.6 Antibody optimisation.....	288
8.7 The role of miR-181 in autophagy and mitochondrial dynamics.....	289
8.8 Concluding remarks.....	291
<b>Appendices</b>	
<b>Appendix 1</b> .....	293
Table A1.1 Reagents, consumables and equipment utilised in this study.....	303

<b>Appendix 2</b> .....	304
<i>Table A2.1 Small nucleolar RNA-61 (SNORD61) demonstrates greater stability of expression than small nucleolar RNA-68 (SNORD68) and small nuclear RNA-U6 (U6) in healthy and diseased equine superficial digital flexor tendon</i> .....	305
<i>Figure A2.1 Boxplots of regularised log counts obtained by RNA-seq for miRNA families subsequently evaluated by RT-qPCR</i> .....	310
<i>Figure A2.2 Differential expression of microRNAs used for RT-qPCR validation of human tendon RNA-seq data, according to tendon type</i> .....	314
<b>Appendix 3</b> .....	315
<i>Table A3.1 Differential expression profiles of non-miRNA small RNA transcripts identified by RNA-seq from six healthy and six diseased human tendon samples</i> .....	337
<i>Table A3.2 Differential expression profiles of miRNA transcripts identified by RNA-seq from six healthy and six diseased human tendon samples</i> .....	349
<b>Appendix 4</b> .....	350
<i>Table A4.1 Predicted mRNA targets of miRNAs significantly differentially expressed in human tendinopathy</i> .....	380
<i>Table A4.2 Predicted mRNA targets of miRNAs identified as significantly differentially expressed in both human and equine tendinopathy</i> .....	382
<b>Appendix 5</b> .....	383
<i>Table A5.1 Small nucleolar RNA-61 (SNORD61) expression in equine primary tenocytes is unaffected by treatment with miR-181a-5p mimic, antagomiR or scrambled control sequence oligonucleotides</i> .....	384
<i>Table A5.2 Glyceraldehyde 3-phosphate dehydrogenase (GAPDH) expression in equine primary tenocytes is unaffected by treatment with miR-181a-5p mimic, antagomiR or scrambled control oligonucleotides</i> .....	385

<i>Figure A5.1 Expression of selected target genes does not differ between scrambled control sequence (SC) treated and untreated (UT) equine tenocytes.....</i>	<i>387</i>
<b>Appendix 6.....</b>	<b>388</b>
<i>Figure A6.1 Comparison between scrambled control (SC) treated and untreated (UT) equine tendon constructs on the expression of selected target genes.....</i>	<i>390</i>
<i>Figure A6.2 Western blot images from mmu-miR-181a-5p mimic (M), antagomiR (AM) and scrambled control (SC) treated equine tendon constructs.....</i>	<i>393</i>
<i>Figure A6.3 Comparison between scrambled control (SC) treated and untreated (UT) equine tendon constructs on histological scoring of H&amp;E and Masson's Trichrome stained sections.....</i>	<i>395</i>
<b>Appendix 7.....</b>	<b>396</b>
<i>Table A7.1 Small nucleolar RNA-61 (SNORD61) expression in human primary tenocytes is unaffected by treatment with miR-181a-5p mimic, antagomiR or scrambled control sequence oligonucleotides.....</i>	<i>397</i>
<i>Table A7.2 Glyceraldehyde 3-phosphate dehydrogenase (GAPDH) expression in human primary tenocytes is unaffected by treatment with miR-181a-5p mimic, antagomiR or scrambled control oligonucleotides.....</i>	<i>397</i>
<i>Figure A7.1 Comparison between scrambled control (SC) treated and untreated (UT) human tenocytes on the expression of selected target genes.....</i>	<i>398</i>
<i>Figure A7.2 Western blot images from mmu-miR-181a-5p mimic (M), antagomiR (AM) and scrambled control (SC) treated human tenocytes for three biological replicates.....</i>	<i>400</i>
<i>Figure A7.3 Comparison between scrambled control (SC) treated and untreated (UT) human tenocytes on the levels of selected target proteins.....</i>	<i>401</i>
<b>References.....</b>	<b>402</b>

## Acknowledgements

There are four individuals without whose support this thesis would not exist.

Firstly, I extend my thanks to my primary supervisor Dr Kasia Whysall whose guidance and expertise in microRNA biology underpinned this project, and who has given me the freedom to make a lot of mistakes and learn a huge amount along the way. Equally, the support, guidance, extensive knowledge and contacts of Professors Pete Clegg and Mandy Peffers have been enormously valuable. Thank you all, sincerely, for giving me the opportunity to step well outside my comfort zone and field of knowledge, and gain an insight into a fascinating and exciting world. Letting an equine veterinary clinician with no laboratory training, loose in a research lab must be akin to letting a bull loose in a china shop. I hope I didn't break too many tea cups.

I could not have done this without the support of my wife Alexa, who is convinced I intend to remain a student for the rest of my life and is, remarkably, still my wife.

Orthopaedic Research UK generously funded the project.

Acquisition of tissue samples relied on the generosity and cooperation of a number of individuals. I am indebted to Drs. Neal Millar and Moeed Akbar from Glasgow University for provision of diseased tendon samples without which this project would have foundered. Moeed was also a font of knowledge on laboratory protocols and I benefitted from this on numerous occasions. In Liverpool, the late Professor Simon Frostick, and Amanda Wood of the Liverpool Biobank were instrumental in ensuring I had access to healthy human tissue samples. Drs. Andy Molloy and Lyndon Mason of the Trauma and Orthopaedic Department, University Hospital Aintree, Liverpool also provided a number of human tendon samples. Dharmesh Patel from Queen Mary University of London cheerfully gave his time to advise me on protocols for isolation of human tenocytes.

Thanks also to the staff at Drury's abattoir, Tockenham, Wiltshire, from where all equine tendon samples were acquired.

Technical staff in what was the Institute of Ageing and Chronic Disease, especially Leif Hunter, Sheila Ryan and Cath Sperinck sorted out technical problems as and when they arose and were gracious enough not to laugh when they were due to my incompetence.

There are many members of various, now restructured, Department of Musculoskeletal Biology I and II lab groups, both fellow PhD students and post-docs, who have advised, helped and supported me along the way. Thank you to Ana, Rachel, Ifigenia, Ben, Katie, Aggie, Mattia, Adam, Shah, Euan, Kiran, Aibek, James, Danae, Yalda, Panos, Phil and Jade.

The individuals below have had a more direct input into this project.

I owe particular thanks to Daniel Green and his understanding of bioinformatics, for his analysis of the RNA-seq data, a skill I could never have hoped to master in the time available.

RNA extracted for a separate project by Roisin Wardle was utilised in part of this study, and I am grateful to her and Mandy Peffers for making this available to me.

Liverpool University Centre for Genomic Research staff, particularly John Kenny, Chris Owen, Pia Koldkjaer, Edith Vamos, Richard Gregory and Sam Haldenby advised on, and performed, the small RNA-sequencing.

Professor Lorenzo Ressel in the Department of Veterinary Anatomy, Physiology and Pathology advised on interpretation of electron micrographs, whilst Marion Pope and Val Tilston performed the electron microscopy and routine histological processing.

Simon Tew allowed me to use his equine primers for some of my PCR work, and along with Liz Canty-Laird, kept an eye on my progress.

Finally, I must thank colleagues in the veterinary teaching hospitals at Leahurst, who, in the face of clinical and teaching demands, cut me as much slack as possible whilst I was writing up, Christine for tea and sympathy, and Beau, Monty and the Owl for their own unique styles of manuscript reviewing.

## **Abstract**

### **microRNA:target interactions in tendinopathy**

**David A Bardell**

Tendon disease is a significant cause of morbidity in both human and equine species, impacting on quality of life, general mobility, capacity to work and ability to participate in recreational sports. Clinically apparent tendinopathy is preceded by asymptomatic degenerative changes, but these are not well understood. Based on their longevity, use and the epidemiological similarities in naturally occurring disease in functionally analogous energy storing tendons, horses present an attractive and relevant model for investigating pathophysiological factors relevant to human tendon.

Non-coding RNAs are important epigenetic modulators of gene expression and one subclass which has attracted significant attention is that of the microRNAs (miRNAs). These 21-25 nucleotide molecules are powerful post-transcriptional regulators of gene expression, typically by inhibiting translation of their mRNA targets into functional gene products. Altered expression of miRNAs, reported in a wide range of diseases, implicates them as important contributors to disease processes.

Using an unbiased approach applied to human energy storing tendon harvested during surgical interventions, this is the first study to thoroughly interrogate changes in the small non-coding RNA (sncRNA) transcriptome occurring with clinical tendinopathy. This thesis presents evidence that the sncRNA transcriptome of tendinopathic tissue differs markedly to that of healthy tendon and may provide novel information on underlying pathogenic mechanism in tendon disease. Following validation of a selected panel of differentially expressed (DE) miRNAs from this data set, the expression of these miRNAs was then investigated in equine superficial digital flexor tendinopathy, identifying three miRNAs (miR-29a, miR-181 and miR-199a) showing similar changes in both species.

Bioinformatics analysis highlighted the observed alteration in miRNA expression was consistent with enhanced cellular proliferation, inhibition of cellular degeneration, and regulation of MAPK and TGF $\beta$  signalling, inflammation, autophagy, mitochondrial homeostasis and oxidative stress response. Focussing on miR-181, gain and loss of function studies in monolayer cultures of primary equine and human tenocytes, and three-dimensional matrix-embedded equine tenocyte constructs, changes in distribution and expression of autophagy related proteins and mitochondrial dynamics were characterised.

Data presented here thus identify that within a sncRNA transcriptome altered significantly in tendinopathy, dysregulation of miRNA expression is preserved/conserved to a degree between human and equine species. Additionally, results suggest miR-181 may have a role in tendinopathy by regulating autophagy and mitochondrial dynamics in equine and human tenocytes via LC3B activity, whilst changes in P62/SQSTM1, NRF2, BNIP3, COXIV and Parkin were observed in equine tenocytes in three-dimensional tissue-engineered constructs.

This thesis supports the use of the horse as a model organism for investigating clinical tendon disease and identifies further avenues for investigating pathophysiological mechanisms active in tendinopathy.

## **Abbreviations**

<b>3'UTR</b>	3' untranslated region
<b>4E-T</b>	eukaryotic translation initiation factor 4E transporter

### **A**

<b>ACAN</b>	aggrecan
<b>ADAM</b>	a disintegrin and metalloproteinase domain-containing protein
<b>ADAMTS</b>	a disintegrin and metalloproteinase with thrombospondin motif
<b>AGO</b>	argonaute
<b>AM</b>	antagomiR
<b>AMP</b>	adenosine monophosphate
<b>AMPK</b>	AMP-activated protein kinase
<b>APS</b>	ammonium persulfate
<b>ARE-BP</b>	AU-rich element binding proteins
<b>ARIH1</b>	Ariadne RBR E3 ubiquitin protein ligase 1
<b>ATG4B</b>	autophagy related 4B cysteine peptidase
<b>ATG3/5/7</b>	autophagy related protein 3/5/7

### **B**

<b>BAK</b>	BCL2 Antagonist/Killer 1
<b>BAX</b>	BCL2 Associated X Apoptosis Regulator
<b>BCL1</b>	cyclin D1
<b>BCL2</b>	B-cell lymphoma 2 apoptosis regulator
<b>BGN</b>	biglycan
<b>BIM</b>	BCL-2 interacting mediator of cell death
<b>BLAST</b>	Basic Local Alignment Search Tool
<b>BMSC</b>	bone marrow derived stem cells
<b>BNIP3</b>	BCL2 interacting protein 3

**bp** base pair  
**BSA** bovine serum albumin

## C

**CCCP** carbonyl cyanide m-chlorophenylhydrazone  
**CCR4-NOT** carbon catabolite repressor 4 - negative on TATA complex  
**CD18** integrin beta chain-2  
**CD90.2** cluster of differentiation 90  
**CDET** common digital extensor tendon  
**cDNA** complimentary DNA  
**CF** carrier free  
**CGRP** calcitonin gene related peptide  
**Chr** chromosome  
**COL1A1** collagen, type I, alpha 1 chain  
**COL1A2** collagen, type I, alpha 2 chain  
**COL2A1** collagen, type II, alpha 1 chain  
**COL3A1** collagen, type III, alpha 1 chain  
**COL5A1** collagen, type V, alpha 1 chain  
**COL6A3** collagen, type VI, alpha 3 chain  
**COL7A1** collagen type VII, alpha 1 chain  
**COL12A1** collagen type XII, alpha 1 chain  
**COL17A1** collagen type XVII, alpha 1 chain  
**COL18A1** collagen type XVIII, alpha 1 chain  
**COL22A1** collagen type XXII, alpha 1 chain  
**COMP** cartilage oligomeric matrix protein  
**COXI** cytochrome c oxidase subunit 1  
**COX2** cyclooxygenase 2  
**COXIV** cytochrome c oxidase subunit 4  
**CRTAP** cartilage associated protein  
**CSA** cross sectional area

**Ct** threshold cycle

## **D**

**DAPI** 4',6-diamidino-2-phenylindole

**DDFT** deep digital flexor tendon

**DDR1** epithelial discoidin domain-containing receptor 1

**DDX6** DEAD-box helicase 6

**DE** differential expression / differentially expressed

**DGCR8** DiGeorge syndrome critical region 8

**DJ-1** protein deglycase DJ-1, also known as Parkinson disease protein 7 (PARK7)

**DMEM** Dulbecco's modified Eagle medium

**DMSO** dimethyl sulfoxide

**DNA** deoxyribonucleic acid

**dNTP** deoxynucleoside triphosphate

**DPBS** Dulbecco's phosphate buffered saline

**DPX** mounting medium

**DRP1** dynamin-related protein 1

**DTT** dithiothreitol

**DUSP2** dual specificity protein phosphatase 2

## **E**

**eca** equine; *Equus caballus*

**ECM** extracellular matrix

**EGR1** early growth response 1

**ERK1/2** extracellular-signal-regulated kinase 1/2

**EVG** elastin van Giesons stain

## F

<b>F</b>	female
<b>FBN1</b>	fibrillin 1
<b>FBS</b>	foetal bovine serum
<b>FDA</b>	Food and Drug Administration
<b>FDR</b>	false discovery rate
<b>FGF2</b>	basic fibroblast growth factor
<b>FITC</b>	fluorescein isothiocyanate
<b>FM</b>	fascicular matrix; freezing medium
<b>FOXO1</b>	forkhead box O1

## G

<b>GAG</b>	glycosaminoglycan
<b>GAPDH</b>	glyceraldehyde 3-phosphate dehydrogenase
<b>GFP</b>	green fluorescent protein
<b>GO</b>	gene ontology
<b>GR</b>	gracilis tendon

## H

<b>H&amp;E</b>	haematoxylin and eosin stain
<b>hFIS1</b>	adaptor fission protein 1
<b>HIF1<math>\alpha</math></b>	hypoxia inducible factor-1 alpha
<b>HOXA11</b>	homeobox protein Hox-A11
<b>HRA</b>	Health Research Authority
<b>HRAS</b>	HRas proto-oncogene, GTPase
<b>Hs</b>	human; <i>Homo sapiens</i>
<b>hsa</b>	human; <i>Homo sapiens</i>
<b>HSC</b>	heat shock protein cognate
<b>HSP</b>	heat shock protein

**HST** hamstring tendon  
**Hz** Hertz, the SI unit of frequency; 1 Hz = 1 cycle per second

## **I**

**ICB** intrafascicular chondroid-like bodies  
**ICTP** carboxyl-terminal telopeptide of type I collagen  
**IFM** interfascicular matrix  
**IGF1** insulin-like growth factor 1  
**IGF1R** insulin-like growth factor I receptor  
**IL** interleukin  
**IL1/6/7/etc.** interleukin 1/6/7/8/10/15/18  
**IL1 $\alpha$**  interleukin 1 alpha  
**IL1 $\beta$**  interleukin 1beta  
**IL1-RAP** interleukin 1 receptor accessory protein  
**INSR** insulin receptor  
**IPA** Ingenuity Pathway Analysis  
**IR** insulin receptor  
**IRAK** interleukin receptor-associated kinase  
**ITGA3** integrin alpha-3

## **J**

**JAK2/STAT** Janus kinase/signal transducer and activator of transcription proteins

## **K**

**kDa** kilo Daltons  
**KEAP1** kelch like ECH associated protein 1

## L

<b>LAMP1</b>	lysosomal-associated membrane protein 1
<b>LC3B</b>	microtubule-associated proteins 1A/1B light chain 3B
<b>LNA</b>	locked nucleic acid
<b>lncRNA</b>	long non-coding RNA
<b>LOXL2</b>	lysyl oxidase like 2
<b>LTBP</b>	latent TGF $\beta$ binding protein

## M

<b>M</b>	male, mimic
<b>MAP1IC3B</b>	microtubule-associated proteins 1A/1B light chain 3B
<b>MAPK</b>	mitogen-activated protein kinase
<b>MCL1</b>	myeloid leukemia cell differentiation protein 1
<b>ME</b>	male entire
<b>MFN1/2</b>	mitofusin 1/2
<b>MHC</b>	myosin heavy chain
<b>MIF</b>	macrophage migration inhibitory factor
<b>miR</b>	microRNA
<b>miRNA</b>	microRNA
<b>MKX</b>	Mohawk
<b>mm</b>	millimetres
<b>mM</b>	millimolar
<b>MMP</b>	matrix metalloprotease
<b>mmu</b>	murine; <i>Mus musculus</i>
<b>MN</b>	male neutered
<b>mRNA</b>	messenger RNA
<b>Ms</b>	mouse
<b>MSC</b>	mesenchymal stem cells
<b>MT-ND1</b>	NADH-ubiquinone oxidoreductase chain 1

**mTOR** mammalian target of rapamycin  
**MUL1** mitochondrial E3 ubiquitin protein ligase 1  
**MYOCD** myocardin

## N

**NCBI** National Center for Biotechnology Information  
**ncRNA** non-coding RNA  
**NFκB** nuclear factor kappa-light-chain-enhancer of activated B cells  
**NID1/NID2** nidogen 1/ nidogen 2  
**NOTCH4** neurogenic locus notch homolog protein 4  
**NR** not recorded  
**NRF2** nuclear factor erythroid 2  
**nt** nucleotide

## O

**OPA1** optic atrophy 1 protein

## P

**P38-MAPK** P38 mitogen-activated protein kinase  
**P62/SQSTM1** ubiquitin-binding protein p62/sequestosome-1  
**PAGE** polyacrylamide gel electrophoresis  
**PAN2-PAN3** poly(A)-nuclease deadenylation complex  
**PARK2/Parkin** E3 ubiquitin-protein ligase Parkin  
**PARK7** Parkinson disease protein 7, also known as protein deglycase DJ-1  
**PARN** poly(A)-specific ribonuclease  
**PCA** principal component analysis  
**PBS** phosphate buffered saline  
**PBS-T** phosphate buffered saline with added Tween20®  
**PCR** polymerase chain reaction

<b>PDGF</b>	platelet derived growth factor
<b>PHP2</b>	prolyl hydroxylase 2
<b>PI3K</b>	phosphatidylinositol 3-kinase
<b>PICP</b>	carboxyl-terminal propeptide of type I collagen
<b>PIN1</b>	peptidyl-prolyl cis-trans isomerase NIMA-interacting 1
<b>PINK1</b>	phosphatase and tensin homologue-induced putative kinase 1
<b>PINP</b>	amino-terminal propeptide of type I collagen
<b>piRNA</b>	piwi-interacting RNA
<b>PLOD2</b>	procollagen-lysine,2-oxoglutarate 5-dioxygenase 2
<b>POL II</b>	RNA polymerase II
<b>PPARGC1A</b>	peroxisome proliferator-activated receptor gamma coactivator 1-alpha
<b>PPE</b>	personal protective equipment
<b>PPM1D</b>	protein phosphatase 1D
<b>PRDX3</b>	peroxiredoxin 3
<b>PRDX6</b>	peroxiredoxin 6
<b>pre-miRNA</b>	precursor microRNA
<b>pri-miRNA</b>	primary microRNA
<b>PTH LH</b>	parathyroid hormone like hormone
<b>PTT</b>	posterior tibial tendon
<b>PVDF</b>	polyvinylidene fluoride

## **R**

<b>RAN-GTP</b>	Ras-related nuclear protein
<b>Rb</b>	rabbit
<b>RCTI</b>	rotator cuff tendon injury
<b>RIPA</b>	radioimmunoprecipitation assay buffer
<b>RISC</b>	RNA-induced silencing complex
<b>RNA</b>	ribonucleic acid
<b>RNA-seq</b>	RNA sequencing
<b>RNAi</b>	RNA interference

<b>ROCK1</b>	rho associated coiled-coil containing protein kinase 1
<b>ROS</b>	reactive oxygen species
<b>rpm</b>	revolutions per minute
<b>rRNA</b>	ribosomal RNA
<b>RT-qPCR</b>	quantitative reverse transcription PCR

## S

<b>SC</b>	scrambled
<b>scaRNA</b>	small Cajal body-specific RNA
<b>SCX</b>	scleraxis
<b>SDFT</b>	superficial digital extensor tendon
<b>sdRNA</b>	snoRNA-derived RNA
<b>SDS</b>	sodium dodecyl sulfate
<b>SFTPA1</b>	pulmonary surfactant-associated protein A1
<b>SIAH1</b>	siah E3 ubiquitin protein ligase 1
<b>siRNA</b>	small interfering RNA
<b>SIRT1</b>	sirtuin 1
<b>SL</b>	suspensory ligament
<b>SLRP</b>	small leucine rich proteoglycan
<b>SMAD2/3/4/7</b>	mothers against decapentaplegic homolog 2/3/4/7
<b>SMN1/2</b>	survival motor neurone 1/2
<b>SMURF1</b>	SMAD specific E3 ubiquitin protein ligase 1
<b>sncRNA</b>	short non-coding RNA
<b>SNORD61</b>	small nucleolar RNA-61
<b>snoRNA</b>	small nucleolar RNA
<b>SNP</b>	single nucleotide polymorphism
<b>snRNA</b>	small nuclear RNA
<b>SOX9</b>	SRY-box transcription factor 9
<b>SSP</b>	supraspinatus tendon
<b>ssRNA</b>	single stranded RNA

**ST** semitendinosus tendon

## **I**

**TCM** tenocyte culture medium

**TCM-NOFBS** tenocyte culture medium-no foetal bovine serum

**TDMD** target-RNA-directed microRNA degradation

**tDR-fragment** tRNA-derived RNA

**TE** transposable element

**TEM** transmission electron microscopy

**TEMED** N,N,N',N'-tetramethylethylenediamine

**TGF $\beta$**  transforming growth factor beta

**TGF $\beta$ 111** transforming growth factor beta-1-induced transcript 1 protein

**TGF $\beta$ R1/2/3** transforming growth factor-beta receptor type 1/2/3

**TGM** tenogenic culture medium

**TGM-C** tenogenic culture medium-complete (addition of TGF $\beta$ 3)

**TIM** translocase of the inner membrane complex

**TIMP** tissue inhibitor of metalloprotease

**tiRNA** 5'tRNA stress-induced fragments

**TLR** toll-like receptor

**TNF $\alpha$**  tumour necrosis factor alpha

**TNMD** tenomodulin

**TNRC6** trinucleotide repeat-containing gene 6A protein

**TOM** translocase of the outer membrane complex

**TOMM20** translocase of outer mitochondrial membrane 20

**TRBP** transactivation response element RNA-binding protein

**TREM-1** triggering receptors expressed on myeloid cells-1

**tRNA** transfer RNA

**TSPC** tendon stem/progenitor cell

## U

**UK** United Kingdom

**UT** untreated

## V

**vt-RNA** vault RNA

## W

**WNT5B** Wnt Family Member 5B

## X

**XRN-2** 5'-3' exoribonuclease 2

## List of Tables

<b>Table 1.1</b> Energy storing and positional tendons commonly reported in association with injury, and/or functional studies in both human and equine species.....	32
<b>Table 1.2</b> Material qualities used to define tendon mechanical properties.....	40
<b>Table 1.3</b> ( <i>includes preceding two pages</i> ) microRNAs identified as significant in tendon ageing and disease.....	62
<b>Table 2.1</b> Details of six human supraspinatus tendon samples harvested from patients with clinically diagnosed rotator cuff disease.....	65
<b>Table 2.2</b> Details of three human posterior tibial tendon samples harvested from patients with clinically diagnosed flat foot deformity.....	66
<b>Table 2.3</b> Details of 17 human hamstring tendon samples harvested from patients undergoing surgical repair of anterior cruciate rupture.....	66
<b>Table 2.4</b> ( <i>includes preceding page</i> ) Details of 53 equine superficial digital flexor tendon (SDFT) samples utilised in various aspects of this study.....	68
<b>Table 2.5</b> Sequences and modifications of Dharmacon™ cholesterol conjugated oligonucleotides utilised in this study.....	81
<b>Table 2.6</b> Details of 12 human tendon samples (six tendinopathic supraspinatus and six healthy control mixed semitendinosus and gracilis tendons) submitted for small RNA-sequencing.....	97
<b>Table 2.7</b> Details of two human supraspinatus tendon samples harvested from patients with clinically diagnosed rotator cuff disease and used in RT-qPCR validation of RNA-seq data.....	99
<b>Table 2.8</b> Details of six human hamstring tendon samples harvested from patients undergoing surgical repair of anterior cruciate rupture and used in RT-qPCR validation of RNA-seq data.....	99
<b>Table 2.9</b> Details of three human posterior tibial tendon (PTT) samples, harvested from patients with clinically diagnosed flat foot deformity, utilised as an independent cohort for RT-qPCR validation of RNA-seq data.....	100
<b>Table 2.10</b> Details of Qiagen miScript primers utilised in this study.....	103
<b>Table 2.11</b> Targets and sequences of equine primers supplied by Primerdesign Ltd (Chandlers Ford, UK) utilised in this study.....	104
<b>Table 2.12</b> Targets and sequences of equine primers supplied by Eurogentec (Camberley, UK) utilised in this study.....	105
<b>Table 2.13</b> Targets and sequences of equine primers supplied by Sigma (Welwyn Garden City, UK) utilised in this study.....	106
<b>Table 2.14</b> Targets and sequences of human primers supplied by Sigma (Welwyn Garden City, UK) utilised in this study.....	106

<b>Table 2.15</b> Relative quantities of reagents for casting gels used for Western blotting.....	119
<b>Table 2.16</b> Grading scheme used to score tendon construct histological appearance.....	128
<b>Table 3.1</b> Donor and tissue details for six diseased and six healthy control human tendon samples processed for RNA extraction for small RNA sequencing.....	135
<b>Table 3.2</b> Donor and tissue details for five diseased and six healthy control human tendon samples used for RT-qPCR validation of small RNA-sequencing data.....	137
<b>Table 3.3</b> Donor and tissue details for 11 horses used for RT-qPCR validation of equine superficial digital flexor tendon (SDFT) disease as a model of human tendinopathy.....	138
<b>Table 3.4</b> Small non-coding RNAs differentially expressed between healthy and diseased tendon samples.....	142
<b>Table 3.5</b> Table 3.5 Up regulated and top 20 down regulated miRNAs, ranked by fold change (FC), identified by RNA-seq as significantly differentially expressed ( $\geq 1.5$ FC; adjusted $P$ -value $< 0.05$ ) between healthy human hamstring tendon (n=6) and tendinopathic supraspinatus tendon (n=6).	142
<b>Table 3.6</b> Summary of RNA-seq validation by RT-qPCR in human tendinopathy and miRNA expression in equine tendinopathy.....	151
<b>Table 4.1</b> Sequences are conserved between human (hsa) and equine (eca) orthologues of miR-29a-3p, miR-199a-5p, miR-181a and miR-181b.....	161
<b>Table 4.2</b> Top biological functions identified by Ingenuity Pathway Analysis of 223 human miRNAs differentially expressed with tendinopathy are associated with cellular development, proliferation, movement and viability.....	165
<b>Table 4.3</b> Ingenuity Pathway Analysis predictions of most significant canonical pathways, diseases and disorders and molecular and cellular functions likely to be implicated as a result of miRNA dysregulation in human tendinopathy.....	170
<b>Table 4.4</b> Top biological functions of 464 predicted target genes regulated by 223 differentially expressed human miRNAs in tendinopathy are associated with cellular development, proliferation, movement and viability.....	171
<b>Table 4.5</b> Biological processes (as described by gene ontology (GO) terms) associated principally with control of cellular proliferation, viability and localisation, signalling and metabolic activity are enriched in the mRNA population targeted by miRNAs DE in human tendinopathy.....	173
<b>Table 4.6</b> Ingenuity Pathway Analysis predictions of most significant canonical pathways, diseases and disorders and molecular and cellular functions implicated as a result of dysregulation of miR-29a-3p, miR-181a-5p and miR-199a-5p common to human and equine tendinopathy.....	176
<b>Table 4.7</b> Biological processes (as described by gene ontology (GO) terms) associated principally with control of cellular recruitment, tissue development and extracellular matrix organisation are enriched in the mRNA population targeted by miR-29a-3p, miR-181a-5p and miR-199a-5p, which show reduced expression in both human and equine tendinopathy.....	181
<b>Table 5.1</b> Identity and genomic location of human and equine miR-181 family members.....	186

<b>Table 5.2</b> Donor and tenocyte passage details for equine superficial digital flexor tendon-derived tenocytes cultured for mmu-miR-181a-5p mimic, antagomiR and scrambled control treatment studies.....	189
<b>Table 5.3</b> miR-181a and b show complete homology between murine (mmu), equine (eca) and human (hsa) species.....	192
<b>Table 6.1</b> Donor and tenocyte passage details for equine superficial digital flexor tendon-derived tenocytes used to generate three-dimensional constructs.....	220
<b>Table 6.2</b> Sequence homology between immunogen epitopes and corresponding equine protein sequences.....	230
<b>Table 6.3</b> Intra-rater repeatability for tendon construct scoring scheme.....	247
<b>Table 6.4</b> Inter-rater repeatability for tendon construct scoring scheme.....	247
<b>Table 7.1</b> Donor and tenocyte passage details for human semitendinosus and gracilis tendon-derived tenocytes cultured for mmu-miR-181a-5p mimic, antagomiR and scrambled control treatment studies.....	257
<b>Table A1.1</b> Reagents, consumables and equipment utilised in this study.....	303
<b>Table A2.1</b> <i>Small nucleolar RNA-61 (SNORD61)</i> demonstrates greater stability of expression than <i>small nucleolar RNA-68 (SNORD68)</i> and <i>small nuclear RNA-U6 (U6)</i> in healthy and diseased equine superficial digital flexor tendon.....	305
<b>Table A3.1</b> Differential expression profiles of non-miRNA small RNA transcripts identified by RNA-seq from six healthy and six diseased human tendon samples.....	337
<b>Table A3.2</b> Differential expression profiles of miRNA transcripts identified by RNA-seq from six healthy and six diseased human tendon samples.....	349
<b>Table A4.1</b> Predicted mRNA targets of miRNAs significantly differentially expressed in human tendinopathy.....	380
<b>Table A4.2</b> Predicted mRNA targets of miRNAs identified as significantly differentially expressed in both human and equine tendinopathy.....	382
<b>Table A5.1</b> <i>Small nucleolar RNA-61 (SNORD61)</i> expression in equine primary tenocytes is unaffected by treatment with miR-181a-5p mimic, antagomiR or scrambled control sequence oligonucleotides.....	384
<b>Table A5.2</b> <i>Glyceraldehyde 3-phosphate dehydrogenase (GAPDH)</i> expression in equine primary tenocytes is unaffected by treatment with miR-181a-5p mimic, antagomiR or scrambled control oligonucleotides.....	385
<b>Table A7.1</b> <i>Small nucleolar RNA-61 (SNORD61)</i> expression in human primary tenocytes is unaffected by treatment with miR-181a-5p mimic, antagomiR or scrambled control sequence oligonucleotides.....	397

**Table A7.2** *Glyceraldehyde 3-phosphate dehydrogenase (GAPDH)* expression in human primary tenocytes is unaffected by treatment with miR-181a-5p mimic, antagomiR or scrambled control oligonucleotides..... 397

## List of Figures

<b>Figure 1.1</b> Schematic representation of tendon structure.....	33
<b>Figure 1.2</b> Age-related changes in force-extension curves for equine superficial digital flexor (SDFT) and common digital extensor (CDET) tendons.....	44
<b>Figure 1.3</b> RNA classification dendrogram illustrating the relationship of non-coding RNAs with other RNA classes and the position of microRNAs within the non-coding subgroup.....	52
<b>Figure 1.4</b> Major miRNA biosynthetic pathways.....	55
<b>Figure 2.1</b> Final appearance of six well plate with polymerised Sylgard™ 184 silicone elastomer coated base and pinned suture construct anchors in place.....	78
<b>Figure 2.2</b> RT-q PCR run cycle protocol for miRNA quantification.....	112
<b>Figure 2.3</b> Standard RT-qPCR cycle run protocol for mRNA quantification.....	113
<b>Figure 2.4</b> Temperature gradient RT-qPCR cycle run protocol for melt curve optimisation.....	114
<b>Figure 3.1</b> RNA-seq identifies differential small RNA profiles between healthy and diseased human tendon tissue.....	141
<b>Figure 3.2</b> ( <i>preceding two pages</i> ) RT-qPCR validation of human tendon RNA-seq data.....	147
<b>Figure 3.3</b> miRNA dysregulation in equine superficial digital flexor tendinopathy demonstrates some similarities with that in human tendinopathy, as identified by RT-qPCR.....	150
<b>Figure 4.1</b> Flowchart illustrating filters applied during target prediction for A. 223 human miRNAs differentially expressed in tendinopathy. B. Four miRNAs differentially expressed in both human and equine tendinopathy.....	162
<b>Figure 4.2</b> Core analysis of 223 human miRNAs differentially expressed with tendinopathy identifies top biological functions most significantly affected are associated with cellular development, proliferation, movement and viability.....	164
<b>Figure 4.3</b> Biological functions A. Apoptosis and B. Necrosis are predicted to be inhibited by the action of multiple miRNAs differentially expressed in human tendinopathy.....	166
<b>Figure 4.4</b> Biological functions A. G1/S phase transition of fibroblast cell lines and B. Maturation of chondrocyte cell lines are predicted to be activated by the action of multiple miRNAs differentially expressed in human tendinopathy.....	167
<b>Figure 4.5</b> Top scoring network identified by Ingenuity Pathway Analysis of 223 differentially expressed human miRNAs identifies potential dysregulation of insulin, SMAD2/3, TGFβ, ERK1/2 and MAP2K1/2 signalling in tendinopathy.....	168

<b>Figure 4.6</b> ( <i>preceding page</i> ) Top scoring networks reflecting dysregulated miRNA:target interactions in human tendinopathy are associated with the terms A. Cell death and survival, gastrointestinal and hepatic system disease (score 49; 31 focus molecules) and B. Cancer, organismal injury and abnormalities reproductive system disease (score 44; 29 focus molecules).....	173
<b>Figure 4.7</b> Top network associated with dysregulation of miR-29a-3p, miR-181a-5p and miR-199a-5p common to both human and equine tendinopathy.....	175
<b>Figure 4.8</b> miR-181a-5p expression regulates cell viability in both human SSP and equine SDFT tendinopathy.....	177
<b>Figure 4.9</b> ( <i>preceding page</i> ) Top scoring networks reflecting dysregulated miRNA:target interactions common to human and equine tendinopathy are associated with the terms: A. Tissue development, connective tissue disorders, organismal injuries and abnormalities (score 34; 15 focus molecules) and B. Tissue development, organismal injury and abnormalities, cancer (score 20; 10 focus molecules).....	179
<b>Figure 4.10</b> Ingenuity Pathway Analysis indicated miRNA dysregulation in both human and equine tendinopathy is associated with chronic inflammation.....	180
<b>Figure 5.1</b> mmu-miR-181a-5p mimic and antagomiR successfully increase and suppress miR-181 expression in equine tenocytes.....	193
<b>Figure 5.2</b> microRNA-181 expression in mmu-miR-181a-5p mimic, antagomiR and scrambled control treated equine primary tenocyte monolayer culture.....	195
<b>Figure 5.3</b> ( <i>includes preceding page</i> ) The effects of miR-181a overexpression and inhibition on expression of selected target genes in equine tenocytes from five biological replicates.....	197
<b>Figure 5.4</b> Mitochondrial network fragmentation in response to incubation with carbonyl cyanide m-chlorophenylhydrazone (CCCP).....	198
<b>Figure 5.5</b> Successful transfection of mmu-miR-181a-5p mimic and antagomiR into primary equine tenocytes.....	199
<b>Figure 5.6</b> Fluorophore-conjugated secondary anti-mouse and anti-rabbit antibodies do not generate a signal following incubation with equine tenocytes in absence of primary antibody.....	200
<b>Figure 5.7</b> Immunofluorescence images of miR-181a-5p mimic, antagomiR and scrambled control treated equine tenocytes subjected to six hours of CCCP/DMSO exposure.....	202
<b>Figure 5.8</b> Immunofluorescence images of miR-181a-5p mimic, antagomiR and scrambled control treated equine tenocytes subjected to six hours of CCCP/DMSO exposure.....	204
<b>Figure 5.9</b> Immunofluorescence images of miR-181a-5p mimic, antagomiR and scrambled control treated equine tenocytes subjected to six hours of CCCP/DMSO exposure.....	207
<b>Figure 5.10</b> Immunofluorescence images of miR-181a-5p mimic, antagomiR and scrambled control treated equine tenocytes subjected to six hours of CCCP/DMSO exposure.....	209
<b>Figure 6.1</b> Modified grading scheme used for construct scoring.....	223
<b>Figure 6.2</b> Equine tenocyte-fibrin gel constructs from biological replicate EqDB12.....	224

<b>Figure 6.3</b> microRNA-181 expression in mmu-miR-181a-5p mimic, antagomiR and scrambled control treated equine tendon constructs.....	225
<b>Figure 6.4</b> ( <i>includes preceding page</i> ) The effects of miR-181a overexpression and inhibition on the expression of selected target genes in three-dimensional equine tenocyte-fibrin gel constructs from five biological replicates.....	228
<b>Figure 6.5</b> Fluorescence associated with Cy5 labelling of mmu-miR-181a-5p mimic treatment is preserved during protein extraction from fibrin gel equine tendon constructs, SDS-PAGE and electrophoretic transfer to polyvinylidene fluoride (PVDF) membrane, and visible on subsequent fluorescent imaging.....	229
<b>Figure 6.6</b> Representative Western blot images from mmu-miR-181a-5p mimic (M), antagomiR (AM) and scrambled control (SC) treated equine tendon constructs.....	233
<b>Figure 6.7</b> ( <i>preceding page</i> ) Target protein levels in mmu-miR-181a-5p mimic (M), antagomiR (AM) and scrambled control (SC) treated equine tendon constructs from five biological replicates.....	235
<b>Figure 6.8</b> Representative transmission electron micrographs of equine tendon construct ultrastructure.....	236
<b>Figure 6.9</b> Representative transmission electron micrographs of mitochondrial morphology of equine tendon constructs.....	237
<b>Figure 6.10</b> Transmission electron micrograph of mmu-miR-181a-5p mimic treated sample.....	238
<b>Figure 6.11</b> Longitudinal and transverse sections of mmu-miR-181a-5p mimic, antagomiR and scrambled control treated equine tendon constructs.....	239
<b>Figure 6.12</b> Differentiation of construct architecture using a novel grading scheme.....	240
<b>Figure 6.13</b> ( <i>includes preceding page</i> ) Tendon construct histological scoring for H&E and Masson's Trichrome stained sections of mmu-miR-181a-5p mimic (M), antagomiR (AM) and scrambled control (SC) treated tendon constructs from seven biological replicates.....	242
<b>Figure 6.14</b> ( <i>includes preceding page</i> ) Tendon construct histological scoring for H&E and Masson's Trichrome stained sections of mmu-miR-181a-5p mimic (M), antagomiR (AM) and scrambled control (SC) treated tendon constructs from seven biological replicates.....	244
<b>Figure 6.15</b> ( <i>includes preceding page</i> ) Tendon construct histological scoring for H&E and Masson's Trichrome stained sections of mmu-miR-181a-5p mimic (M), antagomiR (AM) and scrambled control (SC) treated tendon constructs from seven biological replicates.....	246
<b>Figure 7.1</b> microRNA-181 expression in mmu-miR-181a-5p mimic (M), antagomiR (AM) and scrambled control (SC) treated human primary tenocyte monolayer culture in three biological replicates.....	260
<b>Figure 7.2</b> The effects of miR-181a overexpression and inhibition on expression of selected target genes in human tenocytes from three biological replicates.....	262

<b>Figure 7.3</b> ( <i>includes preceding page</i> ) Representative Western blot images and target protein levels in mmu-miR-181a-5p mimic (M), antagomiR (AM) and scrambled control (SC) treated human tenocytes from three biological replicates.....	266
<b>Figure 7.4</b> Successful transfection of mmu-miR-181a-5p mimic and antagomiR into primary human tenocytes.....	267
<b>Figure 7.5</b> Fluorophore-conjugated secondary anti-mouse and anti-rabbit antibodies do not generate a signal following incubation with human tenocytes in absence of primary antibody.....	268
<b>Figure 7.6</b> Immunofluorescence images of miR-181a-5p mimic, antagomiR and scrambled control treated human tenocytes subjected to six hours of CCCP/DMSO exposure.....	270
<b>Figure 7.7</b> Immunofluorescence images of miR-181a-5p mimic, antagomiR and scrambled control treated human tenocytes subjected to six hours of CCCP/DMSO exposure.....	272
<b>Figure 7.8</b> Immunofluorescence images of miR-181a-5p mimic, antagomiR and scrambled control treated human tenocytes subjected to six hours of CCCP/DMSO exposure.....	274
<b>Figure 7.9</b> Immunofluorescence images of miR-181a-5p mimic, antagomiR and scrambled control treated human tenocytes subjected to six hours of CCCP/DMSO exposure.....	276
<b>Figure A2.1</b> ( <i>includes preceding 4 pages</i> ) Boxplots of regularised log counts obtained by RNA-seq for miRNA families subsequently evaluated by RT-qPCR.....	310
<b>Figure A2.2</b> ( <i>includes preceding 3 pages</i> ) Differential expression of microRNAs used for RT-qPCR validation of human tendon RNA-seq data, according to tendon type.....	314
<b>Figure A5.1</b> ( <i>includes preceding page</i> ) Expression of selected target genes does not differ between scrambled control sequence (SC) treated and untreated (UT) equine tenocytes.....	387
<b>Figure A6.1</b> ( <i>includes preceding page</i> ) Comparison between scrambled control (SC) treated and untreated (UT) equine tendon constructs on the expression of selected target genes.....	390
<b>Figure A6.2</b> ( <i>includes preceding 2 pages</i> ) Western blot images from mmu-miR-181a-5p mimic (M), antagomiR (AM) and scrambled control (SC) treated equine tendon constructs.....	393
<b>Figure A6.3</b> ( <i>includes preceding page</i> ) Comparison between scrambled control (SC) treated and untreated (UT) equine tendon constructs on histological scoring of H&E and Masson's Trichrome stained sections.....	395
<b>Figure A7.1</b> Comparison between scrambled control (SC) treated and untreated (UT) human tenocytes on the expression of selected target genes.....	398
<b>Figure A7.2</b> ( <i>includes preceding page</i> ) Western blot images from mmu-miR-181a-5p mimic (M), antagomiR (AM) and scrambled control (SC) treated human tenocytes for three biological replicates.....	400
<b>Figure A7.3</b> Comparison between scrambled control (SC) treated and untreated (UT) human tenocytes on the levels of selected target proteins.....	401

## Chapter 1 – Introduction

### 1.1 Tendon structure and function

The musculotendinous unit is an anatomical construct with the principle function of generating and transmitting force. This allows for locomotor and as well as postural and positional movements. Although functionally this operates as a continuous unit, the two main component tissues muscle and tendon are very different metabolically, structurally, and biochemically. Within each tissue type further subdivisions occur related to more specialised functional ability. Skeletal muscle is classified into three subtypes biochemically (Type I, Type IIA and Type IIB), with evidence of some ability of fibre types to interconvert (Essen et al 1975). Tendons are designed principally for effective transmission and absorption of uniaxial tensile forces, are poorly vascularised and relatively sparsely populated with cells. However, tendon is a complex tissue. Composition varies not only with development, ageing and functional requirements, but also in response to altered mechanical stimuli. Tendons are broadly classified into those with a principally positional function and those which store and return energy during locomotion. Tendinopathies constitute a common morbidity in both human and veterinary medicine, with over 30 million human tendon-related procedures estimated to take place annually worldwide (Loiacono et al 2019). Despite being a digitigrade quadruped, the horse is frequently cited as a relevant model for investigating mechanical, biochemical and pathophysiological aspects relevant to human tendon (Innes and Clegg 2010, Lui et al 2011, Patterson-Kane and Rich 2014, Thorpe et al 2016a). This is based on equine longevity, use and epidemiological similarities in injury to functionally analogous tendons, with energy storing tendons being overrepresented in both species. Examples of tendons commonly associated with injury, and/or functional studies in human and equine species are listed in Table 1.1.

<u>Equine</u>	<u>Human</u>
<u>Energy storing tendons</u>	
Superficial digital flexor tendon	Achilles tendon
Deep digital flexor tendon	Posterior tibial tendon
Suspensory ligament	Patellar tendon
	Supraspinatus tendon
<u>Positional tendons</u>	
Common digital extensor tendon	Anterior tibial tendon

**Table 1.1 Energy storing and positional tendons commonly reported in association with injury, and/or functional studies in both human and equine species.**

Historically, the collagenous matrix has been extensively studied in order to understand the mechanical properties of tendon and gain insight into tendon deterioration. In recent years however, it has become apparent that differences in mechanical properties between tendon types are determined largely by the composition of the non-collagenous matrix. The hierarchical structure of tendon has been well described (Kastelic et al 1978) and a schematic representation of this is given in Figure 1.1.

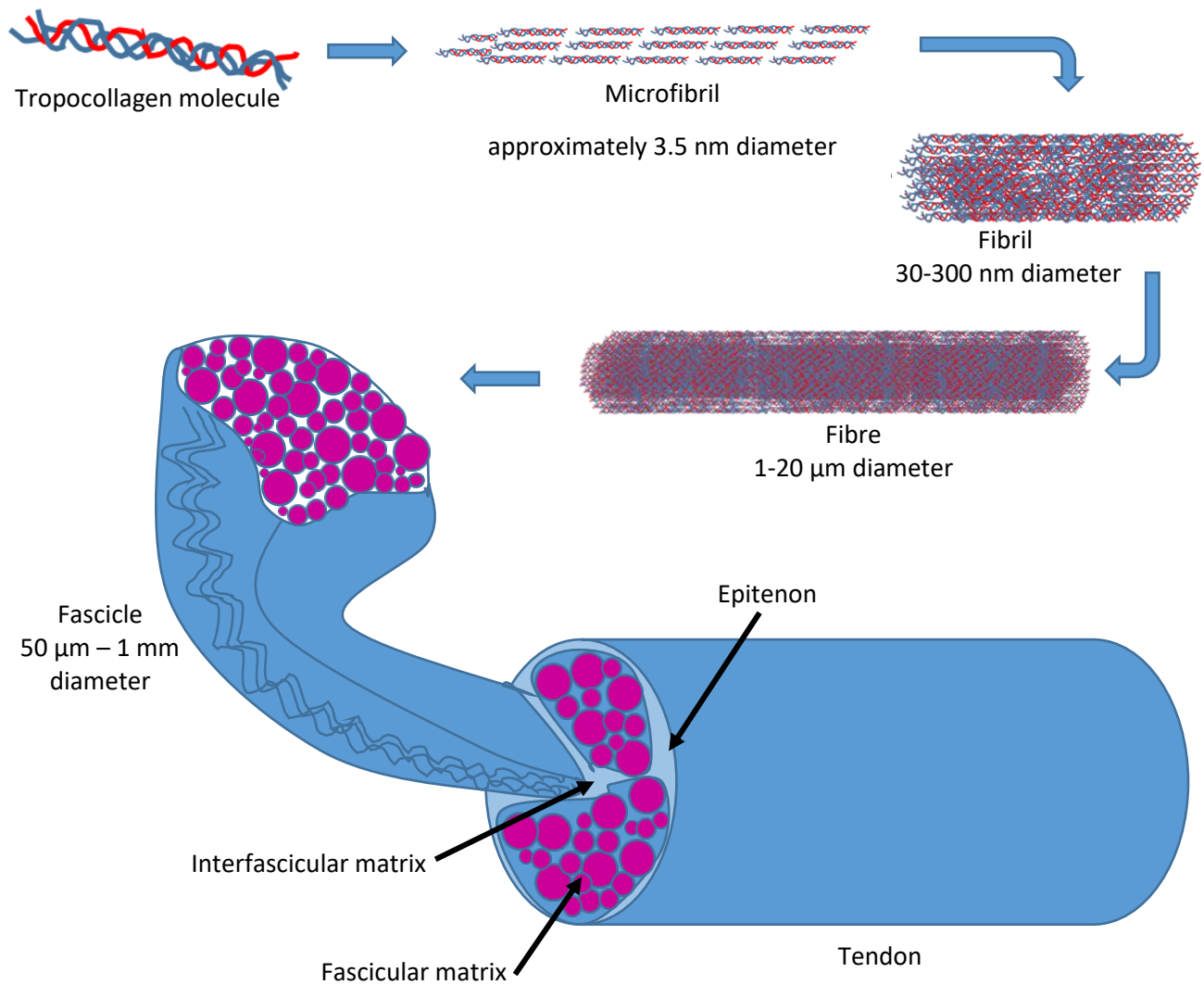


**Figure 1.1 Schematic representation of tendon structure.** Tropocollagen molecules comprising heterotrimeric left handed helical arrangement of collagen molecules aggregate into roughly cylindrical microfibrils. Microfibrils coalesce to form fibrils, and subsequently fibres, of varying diameter. Fibres are grouped into fascicles, each defined in transverse section by surrounding proteoglycan-rich matrix.

### 1.1.1 Extracellular matrix composition

In terms of structure, tendon can be described as a viscoelastic fibre-reinforced composite material. Consisting of 55-70% water, the most abundant protein is collagen (60-85% of dry weight), 60-90% of which is type I (Kjær 2004), with types III, V, XI, XII and XIV present in lesser amounts (Screen et al 2015). The basic type I collagen molecule is a left handed triple helix consisting of two  $\alpha 1$  and one  $\alpha 2$  chains secreted by the fibroblast into the extracellular space, where N- and C- terminal propeptides are cleaved, to produce a mature tropocollagen molecule approximately 280 nm long (Cheng and Screen 2007, Mouw et al 2014). Tropocollagen molecules associate axially and longitudinally, in a quarter-staggered arrangement, stabilised by intra- and inter-molecular covalent crosslinks, to form functionally continuous higher order structures. A variable number of hierarchical levels have been described, but typically consist of microfibrils, fibrils and fascicles (Kastelic et al 1978, Sharma and Maffulli 2005, Cheng and Screen 2007). Collagen fibrils exhibit a crimp waveform which is propagated through the higher level structures due to adjacent fibrils aligning in register (Patterson-Kane and Rich 2014). Fascicles are arranged with varying degrees of helical pitch (Kalson et al 2012, Thorpe et al 2013a). Despite changes in tendon cross sectional area, collagen content as a percentage of dry weight does not alter along the length of SDFT, and total collagen only increases significantly in the region approaching the metacarpophalangeal joint (Birch et al 2002).

A bimodal distribution of collagen fibril diameter develops in the equine superficial digital flexor tendon (SDFT) over the period from neonate to skeletal maturity. This also occurs in the suspensory ligament (SL) and human Achilles tendon, but not common digital extensor tendon (CDET) or deep digital flexor tendon (DDFT), where fibre diameter distribution remains unimodal and significantly larger (Parry et al 1978a, Parry et al 1978b, Birch et al 1999, Magnusson et al 2002). Median fibril diameter is significantly smaller in SDFT (47.8 nm) than DDFT (122.8 nm), with 90% of SDFT and 55% of DDFT fibres less than 150 nm (Birch et al 1999). Mass average SDFT and SL fibril diameter ( $169 \pm 19$  nm and  $122 \pm 14$  nm respectively) are significantly lower than that of the CDET ( $229 \pm 36$  nm), suggesting larger fibril diameters are associated with conferring a stiffer matrix (Birch 2007). Profiles of enzymatically-derived collagen crosslinks also differ between tendon types.

Hydroxylslypyridinoline cross-links predominate in energy storing tendon (SDFT, DDFT and SL), whilst histidinohydroxymesodesmosine is the major type found in CDET.

Histidinohydroxylysinonorleucine and dehydro-hydroxylysinonorleucine are also present in CDET, but largely absent from energy storing tendon types (Birch 2007, Birch et al 2008b). The consequence of these differences is not known, but increasing inter-molecular crosslinking alters the charge profile, affecting intra-fibre and cell-collagen interactions, which can produce major changes in physical properties and cell-matrix interactions (Avery and Bailey 2006).

Fibrils and fascicles are embedded within a complex proteoglycan-rich matrix, which is continuous with the encompassing epitenon. Proteoglycans consist of a core protein covalently linked to glycosaminoglycans (GAGs) – long, linear, charged polysaccharides composed of disaccharide repeats. Differences in structure and steric arrangement of these GAG sidechains confer differing biochemical and hydrodynamic properties, thus contributing to developmental, organisational and mechanical characteristics of tendon infrastructure (Mouw et al 2014). Principal proteoglycans include the small leucine rich proteoglycans (SLRPs) decorin, biglycan, fibromodulin and lumican, tenomodulin and larger proteoglycans aggrecan, versican, cartilage oligomeric matrix protein (COMP), lubricin and tenascin-c. Variably, COMP (Smith et al 1997, Thorpe et al 2013b) and decorin

(Corps et al 2006) are described as the most abundant tendon proteoglycans. COMP is expressed exclusively in load-resisting soft tissues (tendon, ligament, cartilage, meniscus and intervertebral disc) although expression levels vary within and between individual tissues (Smith et al 2002a).

In SDFT, COMP levels show the greatest dynamic change with age and mechanical loading compared to other appendicular tendons and ligaments (Smith et al 1997). Synthesis is critically dependent on appropriate mechanical loading (Smith et al 1999), increasing during musculoskeletal maturation and peaking at approximately 2 years of age. Greatest expression occurs in the mid metacarpal region of SDFT, where tensional forces predominate. Thereafter levels decline exponentially in the metacarpal region of SDFT, whilst remaining constant in other SDFT regions and tendinous structures (Smith et al 1997). COMP is also present in the proliferative zone of articular cartilage, but absent in resting and hypertrophic zones, suggesting a role in cellular proliferation (Smith et al 1997).

Interfascicular boundaries are wider and more clearly delineated in SDFT compared with CDET (Ali et al 2018, Thorpe et al 2012) with more distinct and abundant interfascicular matrix (IFM) which stains more intensely for proteoglycan and glycoprotein (Thorpe et al 2016b). Sulphated GAG composition varies, being significantly lower in CDET ( $2.5 \mu\text{g mg}^{-1}$  dry weight) than either SDFT ( $9.1 \mu\text{g mg}^{-1}$ ), DDFT ( $10.6 \mu\text{g mg}^{-1}$ ) or SL ( $13.2 \mu\text{g mg}^{-1}$ ) (Birch 2007). GAG content is significantly lower in the mid metacarpal region of SDFT relative to the other regions (Birch et al 2002).

Decorin appears to be ubiquitously expressed both between tendon types and matrix sub-compartments, consistent with its importance in collagen fibrillogenesis (Thorpe et al 2016b). However, Thorpe and co-workers (2016c) describe greater expression in SDFT fascicular matrix (FM) than IFM in older horses. Biglycan, which competes for the same collagen binding sites, is suggested to show greater abundance in SDFT IFM than FM (Thorpe et al 2016b).

Lumican and fibromodulin, which share binding sites on collagen type I and modulate collagen fibril organisation, circumferential growth and cross-linking, appear to be preferentially located in CDET, with lumican more abundant in IFM and fibromodulin predominating in FM (Thorpe et al 2016b). However, Thorpe and colleagues (2016c) describe greater fibromodulin expression in SDFT FM than IFM, expression of which decreases with age.

Lubricin (also known as proteoglycan 4 or superficial zone proteoglycan) is localised to IFM of both SDFT and CDET, with elastin significantly located in SDFT IFM and largely absent in CDET (Thorpe et al 2016b).

Further quantitative and qualitative differences in protein expression between SDFT IFM and FM have also been reported (Thorpe et al 2016c). Of the ten types of collagen identified in IFM and FM COL17A1 and COL18A1 were only present in FM, whilst COL7A1 and COL22A1 only in IFM. Proteins expressed in greater abundance in FM were mainly extracellular matrix (ECM) proteins including COL1A1, COL1A2, COL12A1, thrombospondins 1 and 4, fibromodulin, COMP and decorin. In old horses, no difference in COMP between FM and IFM has also been reported (Thorpe et al 2016c). Glycoproteins were more abundant in IFM, with heparin sulphate exclusively identified in IFM, not in FM (Thorpe et al 2016b). Of proteins common to both IFM and FM approximately 80% were more highly expressed in IFM, the majority of which were cellular proteins.

Matrix composition varies not only between positional and energy storing tendons, and fascicular and intrafascicular compartments, but also in response to discrete regional mechanical requirements. The insertion of tendon onto bone is a highly specialised area, with four distinct zones described in this transitional region; tendon proper, fibrocartilage, mineralised fibrocartilage and bone (Thomopoulos et al 2003). Tendons are principally designed to withstand tensile forces, but where they change direction around articulations or bony prominences, tendon may take on a more fibrocartilaginous appearance similar to that seen at the insertion region (Corps et al 2006). Human supraspinatus (SSP) tendon demonstrates this force-dependent regional variation in matrix proteins. Decorin is present throughout the tendon, whilst aggrecan and biglycan expression is highest near the insertion site where compression and shear forces are more likely, and where clinical injury often initiates (Matuszewski et al 2012). Thomopoulos and co-workers (2003) reported similar changes in rat SSP tendon, with increased expression of collagen types II, IX and X and aggrecan at the insertion site, and decorin and biglycan more highly expressed in tensile regions (Thomopoulos et al 2003). These authors also reported a change in tenocyte shape from spindle shaped to rounded, a finding also reported in regions of equine SDFT subjected to compressive forces and demonstrating a more fibrocartilaginous appearance (Webbon 1978).

### 1.1.2 Cellular content of tendons

Tenocytes are specialised fibroblasts, account for 95% of the cellular content of tendon and secrete both collagenous and non-collagenous matrix proteins. A specialised population of tendon stem/progenitor cells (TSPC) has been identified (Bi et al 2007), which reside in ECM rich niches and express tendon-related factors such as scleraxis (SCX), tenomodulin (TNMD), COMP and tenascin-c (TNC). They are closely related to, but distinct from, bone marrow stem cells (BMSC), possessing fibroblast marker CD90.2, but not BMSC marker CD18 (Bi et al 2007). Proliferation and differentiation of TSPCs into functionally competent tenocytes appears to be linked to biglycan and fibromodulin expression (Bi et al 2007). Single cell gene expression analysis has identified three distinct subpopulations, clusters I and II with high expression levels of nestin, which show particularly strong tenogenic and regenerative capacity, with cluster I additionally showing elevated levels of *CD31* and *CD34* expression, and a nestin negative population with elevated expression of *SCX*, *COL1*, *TNC*, thrombospondin 4, Mohawk (*MKX*) and *COMP* (Yin et al 2016).

Embryologically, development of limb tendons occurs progressively in a proximal to distal direction, with loose aggregations of tendon progenitors aligning between differentiating cartilage and muscle tissue prior to condensing to form tendon structures (Huang 2017). Expressed in the early stages of embryological limb development, TGF $\beta$  is a potent and critical inducer of *SCX* expression in early tendon development (Gaut and Duprez 2016). Scleraxis is a transcriptional activator, important in driving commitment and maintenance of progenitor cells to tenogenic differentiation (Pryce et al 2009, Tan et al 2020). In conjunction with *MKX*, *SCX* positively regulates *COL1A1* transcription, additionally activating expression of *TNMD*, another critical regulator of tenocyte differentiation and maturation (Shukunami et al 2018).

Mature tenocytes typically have elongated nuclei and long cytoplasmic extensions. Complex three-dimensional inter-communicating networks of nanotubules up to several hundred micrometers long permit communication between adjacent cells via gap junctions (Egerbacher et al 2020). In regions

where tendons are exposed to compressive forces, and towards the osteo-tendinous junction, they assume a more rounded, chondrocyte-like appearance. Tenocytes are distributed heterogeneously, in linear arrays, throughout tendon substance, cellularity being significantly greater in the IFM than the FM (Thorpe et al 2016b). The IFM cell population is also morphologically distinct, cells being typically rounder in shape with a more stem cell-like appearance than tenocytes resident in the FM, with a shorter population doubling time and tendency to form colonies in culture (Zhang et al 2021). Additionally, cells isolated from IFM of porcine Achilles tendon displayed specific, discriminatory markers differentiating them from tenocytes isolated from FM (Zhang et al 2021). These authors demonstrated CD105, CD31, CD73, CD146,  $\alpha$ -smooth muscle actin, elastin, osteocalcin, tubulin polymerisation promoting protein, substance-P and collagen IV were all highly expressed by IFM tenocytes, but absent, or only weakly expressed by FM tenocytes (Zhang et al 2021). Endothelial cells, neurones and chondrocytes are also present in small amounts.

Histologically, foetal SDFT is indistinguishable from the adjacent energy storing DDFT (Webbon 1978) however, DDFT cellularity decreases with age, unlike in SDFT, where cellularity is maintained (Birch et al 1999, Birch et al 2008a, Birch et al 2008b). Batson and co-workers (2003) also report CDET cellularity is preserved with ageing, although is much lower than that of SDFT. Interestingly, these authors did find a significant reduction in SDFT cellularity with age, although it remained consistently higher than that in age-matched CDET. Frequent regions of acellularity are also reported in core mid-metacarpal SDFT regions compared to peripheral zones (Webbon 1978). These differences in cellularity suggest contrasting metabolic activity in mature tendon both between tendon types and region of matrix and may represent a possible mechanism for repair of accumulated damage (Birch et al 1999, Birch 2007, Thorpe et al 2016c).

### **1.1.3 Matrix metabolism**

Despite differences in cellularity, levels of mRNA for collagens I and III, fibromodulin and lubricin were significantly lower in SDFT than corresponding CDET, whilst COMP and decorin levels were not different between tendon types (Birch et al 2008a).

In a heterogenous equine population, Ribitsch and colleagues (2019) detected COMP, versican and decorin expression in SDFT across the age range examined (1 day to 23 years). However, these authors report expression of collagens I, III and V almost exclusively restricted to individuals less than 4 years of age, with tenascin-c, tenomodulin and scleraxis showing similar expression profiles, suggesting limited turnover of these molecules once skeletal maturity has been reached. Evidence from environmental <sup>14</sup>C levels in human Achilles tendon indicates tendon collagenous matrix deposition occurs during the first 17 years of life, roughly equivalent in terms of musculoskeletal maturation, with little turnover subsequently (Heinemeier et al 2013).

Matrix metabolism can be assessed by markers of synthesis including mRNA expression, and (for type I collagen) levels of carboxyl- and amino-terminal propeptides (PICP and PINP) cleaved during the production of tropocollagen. Degradation markers include the carboxyl-terminal telopeptide of type I collagen (ICTP) and matrix metalloprotease (MMP) expression. MMP1, MMP8 and MMP13 mediate the initial stages of collagen degradation, whilst MMP2 and MMP9 (gelatinases) target denatured collagen. MMP3 (stromelysin) degrades matrix glycoproteins and activates MMP1 and MMP9. Expression of MMP2 and MMP9 (both pro- and active forms) have been shown to be similar

in SDFT and CDET. Significantly higher levels of pro-MMP3 have been detected in CDET, but without mRNA evidence of increased transcription, suggesting CDET is 'constitutively primed' for greater degradative activity (Birch et al 2008a). Significantly higher levels of MMP-generated collagen type I degradation fragments ICTP are detectable in CDET than SDFT (Thorpe et al 2010), consistent with higher MMP1 and MMP13, and lower TIMP3 activity reported by Birch and co-workers (2008a). There is, additionally evidence of disproportionate accumulation of degradation products in SDFT (Thorpe et al 2010).

Collagen cross-linking produced by non-enzymatic glycosylation increases progressively with ageing. These crosslinks exhibit natural fluorescence and tissue fluorescence has been used as an indicator of collagen residence time. Tissue fluorescence significantly increases with age in both SDFT and CDET, Batson and co-workers (2003) describing a good correlation with age of horse, but is consistently and significantly lower in CDET than SDFT (Birch 2007, Thorpe et al 2010). Corroborating this, measurement of spontaneous L-to-D racemic conversion of aspartate (a natural ageing-related phenomenon) shows a linear increase in D:L ratio with age in both tendons, with far greater D-aspartate accumulation in SDFT (Thorpe et al 2010). These authors calculated collagen half-life to be approximately 198 years for SDFT compared with 34 years for CDET. Non-collagenous matrix, by comparison is more labile and, conversely turned over more rapidly in SDFT than CDET, half-lives being calculated as 2.2 years and 3.5 years respectively (Thorpe et al 2010).

Taken together, these data support the theory of more active matrix degradation in CDET than SDFT.

#### **1.1.4 Mechanical properties of tendon**

Mechanical behaviour of tendon is described in terms of stress, strain, stiffness, hysteresis and elastic modulus (Heinemeier and Kjær 2011). These qualities are defined in Table 1.2.

Deformation of tendon under load occurs at many different levels within the structure; straightening of the crimp pattern, elongation of the triple helical tropocollagen molecules, sliding between adjacent tropocollagen molecules, fibrils, and fascicles, and straightening of the fascicular helix (Sharma and Maffulli 2005, Thorpe et al 2013a). Positional tendons are required to be relatively inextensible under physiological loads whilst energy-storing tendons need to be able to stretch and recoil to increase efficiency of locomotion. The helical arrangement of fascicles reported in both human and equine flexor tendons (Kalson et al 2012, Thorpe et al 2013a) is not evident, or greatly reduced, in positional tendons (Thorpe et al 2013a, Thorpe et al 2015a). In response to applied strain, fibre sliding occurs in CDET to a significantly greater extent than in SDFT and at normal physiological loading may be the major mechanism responsible for extension, with little or no fascicle sliding required (Thorpe et al 2013a). In contrast, fascicle sliding may be the major mechanism with SDFT, in conjunction with helical 'unwinding', contributing to greater extension and better recoil characteristics. Fascicle rotation was significantly greater in SDFT than CDET (Thorpe et al 2013a). SDFT fascicles show less hysteresis than CDET, with better recovery characteristics following applied strain.

Strain in energy storing tendons has been measured at approximately 10% and 16% in human Achilles and equine SDFT respectively during intense exercise (Lichtwark and Wilson 2005, Stephens et al 1989). This contrasts with approximately 3% for the positional human anterior tibialis

(Maganaris and Paul 2000) and 2.5% for CDET estimated by Birch and co-workers (2008a). *In vitro* failure strains of 9.9% for Achilles tendon (Wren et al 2001), 12.5-17.3% for SDFT (Dowling and Dart 2005) and 9.7% for CDET (Batson et al 2003), indicate that energy storing tendons operate with little or no safety margin. These data suggest propensity for damage, and importance of matrix homeostasis is therefore greater in elastic tendons, conflicting with the observed indices of metabolic activity described above.

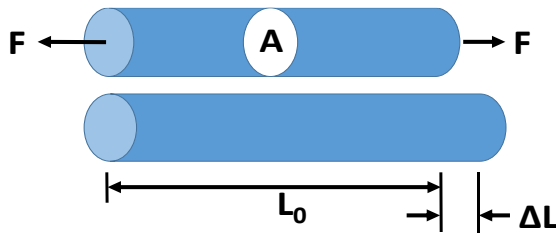
Use of explants for investigating material properties of tendon has produced much useful and detailed data. These methods, however, possess inherent limitations, and material properties of tendon components may not truly reflect *in vivo* behaviour of tendon as a biological entity. Application of load results in stress relaxation, or 'conditioning', a process resulting in a 40-60% reduction in applied stress due to linear stretch (Dudhia et al 2007). Stress relaxation of the IFM occurs to a significantly greater degree in CDET than SDFT. Moreover, this is an age-dependent phenomenon, occurring typically within the first few hours in aged equine explants, but up to 12 hours in tissue derived from younger animals (Dudhia et al 2007). Isolation of fascicles allows independent interrogation of fascicular and interfascicular matrix mechanical properties, but at the expense of incurring artefactual changes. Fascicle isolation results in swelling and non-uniform elongation, producing significantly lower elastic modulus than whole tendon, whilst failing at lower stress and strain (Thorpe et al 2012).

Sample handling protocols also impact on tissue mechanical properties. Dudhia and co-workers (2007) found application of cyclical strain induced a significant age-related reduction in ultimate tensile stress of fresh SDFT explants, which did not occur in explants rendered (and confirmed) non-viable by one 2 hour freeze-thaw cycle to -20°C. Conversely, Huang and colleagues (2011) reported no statistically significant alterations in mechanical properties of human digital flexor tendons subjected to three or less freeze-thaw cycles.

**Viscoelastic:** possessing both viscous and elastic properties in response to an applied force. Viscosity describes resistance of a fluid to flow; elasticity describes the ability of a solid to retain its original form under the influence of an applied force.

**Stress:** force relative to cross sectional area =  $\frac{\text{Force (F)}}{\text{Area (A)}}$

**Strain:** extension under load as a percent of resting length =  $\frac{\text{Change in length } (\Delta L)}{\text{Original length } (L_0)}$



**Ultimate tensile stress:** applied tensile force at which a tendon will fracture.

**Failure strain:** the degree of extension at which a tendon will fail.

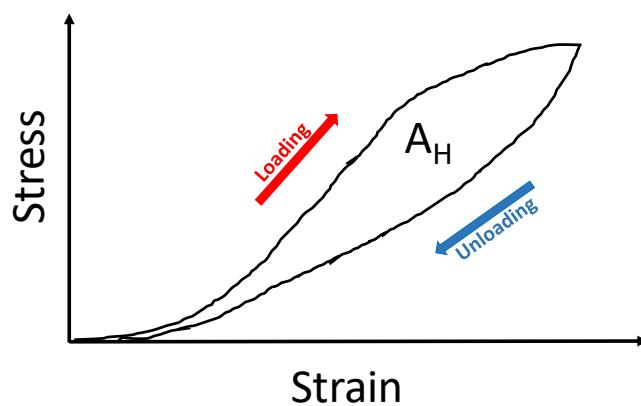
**Stress relaxation:** time dependent reduction in stress when a constant strain is applied.

**Creep:** time dependent increase in strain when a constant stress is applied.

**Stiffness:** change in tendon length in relation to the applied force – proportional to cross sectional area.

**Fatigue loading:** repetitive loading/unloading cycles continued to the point at which structural damage occurs.

**Hysteresis:** energy dissipated (as heat) due to material viscosity. Defined on a stress/strain graph by the area ( $A_H$ ) between the curves generated during one loading/unloading cycle.



**Elastic modulus:** describes the relationship of strain to applied uniaxial stress. Represented by the gradient of a stress/strain plot. Independent of cross sectional area, the higher the modulus, the stiffer the material.

**Table 1.2 Material qualities used to define tendon mechanical properties.**

### 1.1.5 Mechanical properties differ between positional and energy storing tendons

In whole tendon, elastic modulus and ultimate tensile stress are significantly lower in SDFT than CDET. Isolated fascicles demonstrate no difference in these properties between tendon types, but surprisingly, fascicle failure strain was significantly higher in CDET than SDFT (Thorpe et al 2015c). The difference in failure strain between isolated fascicles and parent tendon was 4 times higher in SDFT than in CDET, indicating the importance of the IFM in contributing to tendon mechanical properties (Thorpe et al 2012).

CDET fascicles and IFM demonstrate greater hysteresis than SDFT (Thorpe et al 2012, Thorpe et al 2015c, Thorpe et al 2017). A significant positive correlation between COMP levels and ultimate tensile stress, elastic modulus and stiffness was found in 2 year old horses (Smith et al 2002a). This correlation was absent in older animals, suggesting high levels are important during development (Smith et al 2002b). Water content shows a significant negative correlation with elastic modulus, and is lower in CDET than SDFT, DDFT and SL (Birch 2007). SDFT water content also reduces significantly from the mid metacarpal level distally (Birch et al 2002), indicating regional heterogeneity in elastic modulus.

Both fascicles and IFM of SDFT demonstrate greater fatigue resistance than CDET. Fascicles resist approximately 20 times more cycles before failure, with significantly less hysteresis, and greater resistance to developing creep, indicating greater elasticity of SDFT (Thorpe et al 2016a, Thorpe et al 2017). IFM exhibits similar, but less pronounced differences between tendon types (Thorpe et al 2016a).

### 1.1.6 Tendon response to exercise

Tendon has the capacity to adapt acutely and chronically to increases in mechanical loading. As little as 30 minutes exercise resulted in significant upregulation of COL1A1, scleraxis and tenomodulin in rat Achilles tendon (Mendias et al 2012). *In vitro* evidence suggests TGFβ1 is an important mediator of mechanically induced collagen synthesis in fibroblasts (Heinemeier et al 2007). Electrical stimulation of the sciatic nerve in rats over 4 days resulted in significant upregulation of TGFβ1, COL1A1, COL3A1, MMP2, TIMP1, TIMP2 and lysyl oxidase (Heinemeier et al 2007). COL1A1 expression appears to be associated with acute exercise, rather than chronic. Response to mechanical loading *in vivo* is mediated by induction of growth factors TGFβ1 and IGF1. In a rat exercise model, both degree and distribution of IGF1 expression in Achilles tendon fibroblasts has been shown to vary in a dynamic manner with changes in mechanical loading of the tendon (Hansson et al 1988).

Increased collagen synthesis in response to acute exercise has been demonstrated in human patellar tendon using <sup>13</sup>C labelled amino acids (Miller et al 2005) and Achilles tendon, using peritendinous microdialysis to measure precursor peptides and degradation products (Langberg et al 1999).

Chronic exercise results in approximately 30% increased cross sectional area (CSA) of human Achilles tendon, a change that may also be evident unilaterally in long term physical activity which favours one limb. Short term exercise may result in small, regional changes in CSA (Heinemeier and Kjær 2011). Tendon hypertrophy in response to exercise has not been found consistently in female

athletes (Heinemeier and Kjær 2011). The difference in patellar tendon CSA between trained and untrained men was not detectable in women (Magnusson et al (2007).

Rooney and co-workers (2017) showed distinctly different temporal responses in rat supraspinatus tendon over an eight week exercise period. An initial increase in tendon CSA 24 hrs after onset of exercise was accompanied by reduction in elastic modulus, maximum stress and load. After two weeks, CSA had returned to control values, but tendon stiffness, modulus, maximum load and maximum stress had increased, whilst hysteresis reduced. These changes were maintained until study termination at 8 weeks (Rooney et al 2017). These authors also describe a reduction in MMP activity both in the acute and chronic stages, favouring a more anabolic environment, although MMP identities and degree of reduction are not given. Tenocyte morphology changed within 48 hrs of initiation of exercise, with cells becoming rounder for up to two weeks, returning to normal at eight weeks. Cell density and collagen organisation remained unchanged (Rooney et al 2017). Although critical comparisons are often lacking, these authors indicate that there is a beneficial temporal progression of adaptive changes to non-injurious levels of exercise.

In horses, however, ultimate force, ultimate stress, stiffness index and elastic modulus of SDFT did not differ following an 18 month athletic training regime between exercise and control groups (Birch et al 2008b). Although GAG content decreased in SDFT, DDFT, SL and CDET in response to exercise, gross and histological appearance, cellularity, CSA, collagen content, type, and degree of crosslinking were unchanged (Birch et al 2007, Birch et al 2008b). Following a similar regime, Smith and co-workers (1999) demonstrated lower COMP levels in SDFT than in unexercised controls, whilst Patterson-Kane and colleagues (1997a) identified an alteration in distribution of collagen fibril diameters. A decrease in mean average fibril diameter (from 132 nm to 105 nm) in core SDFT regions, changing fibre diameter distribution from that reported during normal ageing, where no regional variation exists (Birch et al 1999). Greater tensile strength is attributed to large diameter fibrils due to the potential for a higher density of intrafibrillar covalent cross-linking between collagen molecules. Small diameter fibrils are assumed to be more important in terms of promoting elasticity due to increased fibril-ground substance interaction by virtue of their greater surface area (Patterson-Kane et al 1997a).

### **1.1.7 Age-related changes**

In human patellar tendon, no significant differences in mechanical properties or dimensions between old and young men are described. A significant reduction in collagen concentration is reported in old men compared to young, but enzymatic (pyridinoline) and particularly non-enzymatic (pentosidine) crosslinking significantly increases (Couppé et al 2009). The authors postulate this is a mechanism to maintain mechanical properties of ageing tendon in the face of collagen loss. Expression of decorin, aggrecan, biglycan and versican are shown to decrease with age in Achilles tendon (Corps et al 2006). Transcriptomic analysis of Achilles tendon identified over 300 genes differentially expressed between old and young donors (Peffer et al 2015). Both protein coding and non-coding transcripts were represented, but changes in ECM-related genes were not significant. Interestingly, differences in splice variants of ECM relevant proteins COL1A1, COL3A1 and disintegrin and metalloproteinase domain-containing protein 12 (ADAM12) were recognised

between old and young groups. Network analysis of differentially expressed genes implicated cell function, growth and proliferation as most affected, suggesting ageing may impact on tenocyte ability to sense and respond appropriately to environmental stimuli (Peffer et al 2015). Supporting this, an increase in tenocyte senescent phenotype is reported in rat Achilles tendon with ageing, with reduced tenocyte proliferative capacity, and a concurrent increase in expression of MMP2 and MMP9 and down regulation of TIMP1 and TIMP2 (Tsai et al 2011, Yu et al 2013). Additionally, Kohler and co-workers (2013) describe reduced TSPC number and capacity for self-renewal and differentiation in ageing human Achilles tendon (Kohler et al 2013).

Proteomic analysis also identified age related changes in cell phenotype in equine SDFT. A significant reduction in the anti-apoptotic and anti-inflammatory heat shock protein 27 is reported, coupled with increased cytoskeletal and gap junction proteins. No changes in the major structural ECM proteins were evident, with only reductions in SLRPs fibromodulin, mimecan and asporin being identified (Peffer et al 2014). Recently, intrafascicular chondroid-like bodies (ICBs) have been described in SDFT samples from aged horses (Ali et al 2021). These ICBs are discrete spherical to ovoid accumulations of cartilaginous ECM dispersed between tendon fascicles, containing abnormal tenocytes with rounded, rather than fusiform nuclei. Additionally, calcium deposits were present within some. Although the significance of these was unclear, the authors suggested they may represent a response to microtrauma and could potentially impact on the viscoelastic properties of the tendon (Ali et al 2021).

Tenocytes are believed to undergo principally oxidative metabolism (Birch et al 1997), but as the tendon matures, there is a shift towards anaerobic glycolysis, compatible with the reported age-related reduction in blood flow (Astrom 2000, Sharma and Maffulli 2005).

In SDFT, ageing is associated with significant reductions in both number of load cycles to failure and ultimate tensile strength, with increased failure strain (Dudhia et al 2007). Ageing does not affect fascicle or IFM hysteresis, but isolated fascicles and IFM demonstrate an approximately 66-77% decrease in number of cycles to failure in old compared to young horses (Thorpe et al 2017). This is associated with more severe fibre kinking, discontinuity and widening of inter-fibre spaces in older fascicles (Thorpe et al 2014). Collagen fibril crimp angle and length undergo a non-uniform reduction with age in equine SDFT. The greatest change occurs in core relative to peripheral regions, where values decline to 65-75% of those in young animals (Wilmink et al 1992, Patterson-Kane et al 1997b). Crimp straightening then occurs at lower strains in central fibres, leading to non-uniform distribution of force within the tendon. Cross-linking from collagen glycosylation increases with ageing in both CDET and SDFT, but at a greater rate in SDFT.

Thorpe and colleagues (2016c) report little effect of ageing on IFM or FM protein composition of SDFT. Fibromodulin decreases with age in both FM and IFM, with COL6A3 and the SLRP mimecan also decreasing in FM. Percentage of CSA occupied by IFM significantly reduces with age in SDFT, from approximately 15% to 9%, a change not seen in CDET (Thorpe et al 2013b) and reported to be more pronounced in the distal SDFT (Ali et al 2018).

Concurrently, although IFM failure strain does not change (Thorpe et al 2015c), IFM stiffness increases, decreasing capacity for fascicle sliding and rotation, mechanisms of far greater importance to SDFT function than CDET (Thorpe et al 2013b, Thorpe et al 2017). Consequently, a compensatory increase in fibre sliding in response to load occurs, which, coupled with an age related increase in

IFM stress relaxation, reduces recoil and increases hysteresis (Thorpe et al 2013a, Thorpe et al 2014, Thorpe et al 2015a). Fascicle stress relaxation does not increase with age in SDFT, but elastic modulus and failure stress do (Thorpe et al 2015c).

Elastic modulus decreases with age in CDET (Thorpe et al 2015c). No age-related alteration in fibre or fascicle response to applied strain, recovery or hysteresis is reported, although fascicle and IFM stress relaxation increases with age, producing a significant increase in failure extension (Thorpe et al 2015c). Ageing does not affect fascicle or IFM hysteresis or fatigue resistance in CDET (Thorpe et al 2013a, Thorpe et al 2014, Thorpe et al 2017). Figure 1.2 illustrates IFM force-extension curves for SDFT and CDET, demonstrating the far more profound effect of ageing on the former.

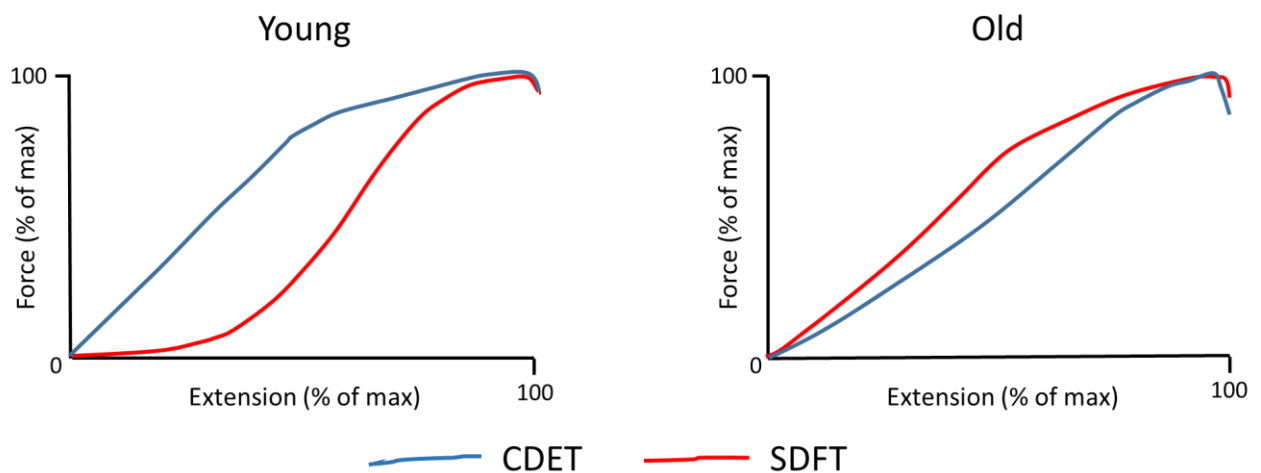


**Figure 1.2 Age-related changes in force-extension curves for equine superficial digital flexor (SDFT) and common digital extensor (CDET) tendon interfascicular matrix.** Significantly greater extension occurs at lower forces in young SDFT than old, demonstrating increased interfascicular matrix stiffening with age. Changes in CDET tend to be opposite, but are minor in comparison and not statistically significant. (Redrawn from Thorpe et al 2013b).

## **1.2 Pathophysiology of tendinopathies**

Musculoskeletal injuries account for 11-24% of all presentations to primary care facilities in the UK (Clarke-Cornwell et al 2006, Jordan et al 2007). Incidence of tendinopathies varies between 0.3-5.5% (Littlewood et al 2013, Albers et al 2014) in the general population, up to 11% for athletic individuals, with a prevalence in some disciplines of 18.5 – 44.6% (Lian et al 2005, Lopes et al 2012). Tendinopathies thus have a major impact both in terms of quality of life and financial consequences from loss of productivity and earnings, compensation and treatment costs (Hopkins et al 2016).

Tendinopathies are also a cause of significant morbidity and wastage in the equine population (Lam et al 2007). Most research into incidence and aetiology has focussed on the Thoroughbred due to the financial importance of the racing industry, although a high incidence of ligament and tendon injuries has also been reported in eventing (Singer et al 2008), show-jumping and dressage disciplines (Murray et al 2006). Musculoskeletal injuries account for up to 82% of all injuries

sustained during flat and National Hunt racing in the UK. Of these 46% involve ligaments or tendons (Williams et al 2001), with the superficial digital tendon (SDFT) of the forelimb particularly susceptible to injury.

The parallels between human and equine tendinopathy are interesting. In both species there is a high prevalence in predominantly energy storing tendons, that is positively associated with ageing and occupational/exercise status and a tendency for recurrent injury (Paavola et al 2002, Ely et al 2009, Thorpe et al 2010, Gajhede-Knudsen et al 2013, Reardon et al 2013). This suggests deterioration in the ability to maintain matrix composition, or maladaptation to mechanical loading during ageing.

### **1.2.1 Matrix changes associated with tendinopathies**

Typically diseased tendon shows gross discolouration, increased cellularity, greater GAG content, greater water content, neovascularisation and greater proportion and altered distribution of type III collagen (Birch et al 1998, Birch et al 2002, Jelinsky et al 2011).

Chondroid metaplasia is a frequent finding in mid metacarpal SDFT of mature horses (Webbon 1978), and conversion to a more fibrocartilagenous phenotype has been identified in rat supraspinatus tendon as a result of overuse, increasing expression of *COL2A1*, aggrecan and *SOX9* (Archambault et al 2007).

In chronic tendinopathies, up-regulation of collagens I and III and down regulation of MMP3 are relatively consistent findings (Ireland et al 2001, Jones et al 2006, Jelinsky et al 2011). Various studies have also reported upregulation of MMP11, ADAM12 (Jones et al 2006), MMP2 (Alfredson et al 2003), MMP9, MMP13, MMP14, MMP19 and TIMP1 (Jelinsky et al 2011) in chronic Achilles tendinopathy.

Proteoglycan expression is also inconsistent. Jelinsky and co-workers (2011) report no change in aggrecan, versican, decorin, biglycan, fibromodulin, or lumican with Achilles tendinopathy. Ireland and colleagues (2001) report increases in tenascin-C, osteonectin, heparin sulphate proteoglycan and biglycan, with reduced aggrecan. Corps and co-workers (2006) showed upregulation of aggrecan and biglycan in painful, intact tendon, but within 48 hours of tendon rupture, report reduction in decorin, with aggrecan, biglycan and versican expression to levels equivalent to control tissue. Chronically painful and ruptured Achilles also express distinctly different metalloproteinase and TIMP profiles, indicating unique proteolytic environments between the two disease states (Jones et al 2006).

In addition to variations due to differences in chronicity and severity of disease, inconsistencies may be due to differences in analysis techniques, specific tendon studied, age and gender of patient. Control tissue may be taken from an unaffected region of the same tendon, one closely anatomically located, or a distant and functionally unrelated one. Robust peripheral clock properties are exhibited by both positional and elastic tendon *in vivo* and primary tenocytes *in vitro* (Yeung et al 2014), potentially adding another confounder.

### 1.2.2 Mechanical influences on tendinopathies

In the horse, weight distribution is unequal between thoracic and pelvic limbs with approximately 60% of body weight borne by the forelimbs at rest. During locomotion, the SDFT is loaded early in the stance phase, undergoing significant extension and recoil during the stride cycle. The adjacent DDFT is loaded later in the stance phase of locomotion and subjected to lower peak forces (Platt et al 1994). During galloping or jumping effort, the forces that these tendons are subjected to are amplified significantly. Muscles of both tendons are similar in architecture, being multipennate with short fibre lengths but muscle fibre types differ. Both muscles are classified as digital flexors but due to fibre length and orientation show limited capacity to shorten, their functionality being more attuned to maximising the efficiency of energy return from passive loading of the musculotendinous unit and damping high frequency vibrations associated with locomotion (Wilson et al 2001). The tendinous component promotes postural stability and potential energy absorption during locomotion (Zarucco et al 2004). The DDF consists of a greater proportion of fast MHC-2A and MHC-2X fibres MHC isoforms, with slow MHC1 oxidative types predominating in the SDF (Butcher et al 2007). This has been one reason proposed as contributing to the predisposition of SDFT lesions, in that the faster DDF fibres fatigue more easily, placing greater reliance for metacarpo-phalangeal joint support on the SDFT which ordinarily operates close to its failure limit during exercise (Butcher et al 2007). The Achilles tendon performs an analogous function in man. It is the largest and strongest tendon in the human body and a compound tendon of the gastrocnemius and soleus muscles, each contributing approximately equally (Cummins et al 1946). Additionally, forces are not distributed uniformly over the cross-sectional area, due to different contributions from the gastrocnemius and soleus muscles, generating significant shear forces within the tendon (Arndt et al 1998). Slow oxidative (Type I) muscle fibres predominate in soleus (80-90%), whilst gastrocnemius has a more even split between Type I and II fibres (Johnson et al 1973), producing differences in fatigue resistance and force generating capacities in the muscular components of the unit. In addition, anatomical malalignment (typically hyperpronation of the foot) is stated as contributing to 60% of disorders due to oblique loading.

Of the four musculotendinous units comprising the rotator cuff complex of the shoulder, the SSP is the most commonly injured component (Matuszewski et al 2012). Due to its anatomical location, it is subject to compression, shear and torsion in addition to tensile loading. Whilst tensional forces are largely resisted by the fibrillar collagens, the non-collagenous matrix is principally responsible for modulating shearing and compressive forces (Screen et al 2015).

Strains of 16.6% have been recorded *in vivo* in SDFT in galloping horses (Stephens et al 1989) and 8.3% in human Achilles tendon (Lichtwark and Wilson 2005). These are similar to the *in vitro* failure strains of 12.5-17.3% reported for SDFT (Dowling and Dart 2005) and 9.9% for Achilles tendon (Wren et al 2001), indicating that these tendons operate with little or no safety margin.

Whilst an acute traumatic event may account for a proportion of tendon injuries, the majority of clinical tendinopathy is understood to be the culmination of preceding, asymptomatic matrix degeneration. Several mechanisms have been proposed as contributors to tendon disease, with histological changes having been classified as hypoxic degeneration, hyaline degeneration, lipid degeneration, mucoid degeneration, fibrinoid degeneration, calcification and fibrocartilaginous or osseous metaplasia (Paavola et al 2002). These can occur independently or concurrently, often with evidence of neovascularisation, but can also be found in up to 30% of Achilles tendons from a

healthy asymptomatic population (Paavola et al 2002). Overuse activity has been implicated in a number of tendinopathies, typically from monotonous, asymmetric and excessive duration and intensity of exercise (Paavola et al 2002). Although the mechanism is not clear it is likely as a result of microtrauma to the matrix. Animal models of repetitive exercise have supported this, with increased tendon vascularity, cellularity and disruption of collagen fibre integrity described (Backman et al 1990, Barbe et al 2003, Soslowky et al 2000). Exercise *per se* does not negatively influence tendon integrity and has been shown to result in no (Huang et al 2004, Birch et al 2008b), or beneficial (Heinemeier et al 2012) effect on tendon properties.

A 24 hour period of physiologically relevant cyclical loading (5% strain at 1 Hz) reduced ultimate tensile strength of fresh equine SDFT explants by approximately 40% compared to unloaded controls (Dudhia et al 2007). These changes were attributed to concurrent upregulation of MMP2 and MMP9, although increase in expression was not shown to be different between age groups (Dudhia et al 2007). The regional transition to a greater proportion of smaller diameter fibrils seen with mechanical loading in equine SDFT is consistent with reducing tensile strength, thus lowering failure strain (Patterson-Kane et al 1997a). This is supported by data comparing fibril size between ruptured Achilles tendons and age and sex matched controls, where site-specific loss of larger diameter fibrils at the rupture site was identified (Magnusson et al 2002). Interestingly, these patients reported rupture was not associated with excessive force generation and absence of pre-existing symptoms. This suggests significant structural changes can occur without clinical symptoms of tendinopathy (Magnusson et al 2002).

### **1.2.3 Inflammation in tendinopathy**

There is ongoing debate and conflicting evidence about the role of inflammation in tendinopathies (Riley 2008, Millar et al 2010, Chisari et al 2019). In a heterogeneous population in terms of age, sex, affected tendon and duration of disease, Jelinsky and co-workers (2011) detected statistically significant upregulation of several cytokines and cytokine-related molecules. However, magnitude of change rarely exceeded the 1.5 fold change predetermined by the authors as necessary to be considered differentially expressed, concluding no evidence for direct regulation of pro-inflammatory cytokines. Inflammatory cytokines are frequently not detected in chronic Achilles disease (Alfredson et al 2003).

Millar and colleagues (2009) identified significant upregulation of 14 inflammation associated genes in a rat model of overuse supraspinatus tendinopathy. Five of these up regulated genes (IL18, IL15, IL6, MIF and TNF $\alpha$ ) were also found to be overexpressed in torn human supraspinatus tendon (Millar et al 2009). In grossly normal subscapularis tendon with histological evidence of moderate to advanced tendinopathy, macrophage, mast cell and T-cell infiltration was significantly higher than in torn supraspinatus tendon harvested from the same joint (Millar et al 2010).

Cyclic loading of fresh SDFT fascicles, designed to initiate overuse damage, increased COX2, MMP13 and IL6 expression, demonstrating an immediate inflammatory response (Thorpe et al 2015b). Cell morphology also altered significantly in loaded samples, with cells becoming rounder, particularly in areas where fibre damage was evident. Similar results are reported in bovine DDFT (Spiesz et al 2015). In naturally occurring equine SDFT tendinopathy, Dakin and co-workers (2012) identified a significant increase in macrophages in the sub-acute phase of injury (3-6 weeks post-injury), with

pro-inflammatory macrophage populations predominating. This changed to predominantly anti-inflammatory phenotype in chronic disease (>3 month post-injury) (Dakin et al 2012).

These data support a role for inflammation in early tendinopathy, which resolves as disease progresses.

#### **1.2.4 Neural influences in tendinopathy**

Tendon is sparsely innervated, but sensory, nociceptive and autonomic nerve fibres have been identified, often in association with blood vessels. Acetylcholine, alpha-adrenergic and muscarinic receptors are also present in tendon-associated vasculature (Scott and Bahr 2009). Sparse sensory innervation may explain why tendinopathic changes identified ultrasonographically or with MRI are clinically asymptomatic. Microvasculature proliferation and sprouting of free nerve endings have been reported in tendinopathy, often in close approximation. Neuroma formation has been reported in both patellar and Achilles tendinopathy. In-growing nerve endings principally express CGRP and substance P, both of which are potent vasodilators, mediate nociceptive signalling (Scott and Bahr 2009) and stimulate production of pro-inflammatory cytokines IL1 $\beta$ , IL6 and TNF $\alpha$  (Hernanz et al 2003). Substance P also stimulates cell growth, proliferation and angiogenesis. This cascade of events is termed 'neurogenic inflammation'. Upregulation of glutamate signalling also occurs in degenerate rat supraspinatus tendon. Glutamate is a potent nociceptive neurotransmitter and vasodilator and can initiate apoptosis (Molloy et al 2006). Neuropeptides may therefore modulate important aspects of tendinopathy including pain, vascular hypertrophy and tissue remodelling (Scott and Bahr 2009).

#### **1.2.5 Vascular influences on tendinopathy**

Tendon is a relatively poorly vascularised tissue and oxygen uptake by human Achilles tendon is approximately one sixth that of the gastrocnemius muscle at rest (Kubo et al 2008). There are three routes of vascularisation, the myotendinous and osteotendinous junctions and through paratenon or synovial structures, the importance of each system varying between tendons. During exercise, both tendon oxygen consumption and blood flow increase significantly, maintaining tissue oxygen saturation (Kubo et al 2008). On cessation of exercise, oxygen uptake returns rapidly resting values whilst blood flow remains higher for longer, generating a relative hyperaemia and producing higher saturation values in recovery. However, blood flow decreases with age and, focally, under mechanical loading. This is particularly compromised at sites of torsion, friction and compression (Sharma and Maffulli 2005). Eighty percent of Achilles ruptures occur in the region 3-6 cm proximal to the calcaneal insertion, the point at which the gastrocnemius and soleus tendons have merged, the tendon is narrowest, and is least vascular (Hess 2010). Correspondingly, the most frequently injured mid metacarpal region of the SDFT is also the least vascular region (Kraus-Hansen et al 1992) with the smallest CSA (Smith et al 1994). The region of the posterior tibial tendon (PTT) most affected by degenerate changes and rupture coincides with a zone of hypovascularity just distal to the medial malleolus (Frey et al 1990). These similarities between regional hypovascularity and common injury sites suggest hypoxia may contribute to tendon degeneration. Apoptosis increases in primary human tenocytes exposed to a hypoxic environment, with significantly increased expression

of BCL1, HIF1 $\alpha$ , clusterin, caspases 3 and 7 and HSP70. Hypoxic culture also elevated IL6 and IL8 levels, indicating the potential for initiating leucocyte recruitment, and dysregulated collagen production, upregulating collagen IIIA and reducing collagen IA (Millar et al 2012). The capacity for hypoxia to initiate and regulate tendinopathy by influencing inflammation, apoptosis and collagen synthesis is supported by clinical evidence. In early stage subscapularis tendinopathy, upregulation of HIF1 $\alpha$ , BCL2 and clusterin is accompanied by elevated inflammatory cell infiltration, with increased collagen III expression in torn supraspinatus tendon in the same joints (Millar et al 2012). Progressive increases in HIF1 $\alpha$  expression are shown to correlate with extent of apoptosis and severity of rotator cuff injury (Benson et al 2010).

Relative paucity of blood flow also reduces efficiency of heat dissipation. A mean core SDFT temperature of 43.3°C was recorded during 5 minutes of galloping exercise, the highest registered temperature being 45.4°C (Wilson and Goodship 1994). These authors suggest this is unlikely to be sufficient to damage the ECM, but exceeds the threshold of 42.5°C for fibroblast viability. Mathematical modelling suggests similar core temperatures are possible in Achilles tendon during running (Wilson and Goodship 1994). Upregulation of heat shock proteins (HSP27 and HSP70) are reported by Millar and co-workers (2009) in a rat model of supraspinatus overuse.

### **1.2.6 Endocrine influences on tendinopathy**

Tendinopathies are known to occur more frequently in diabetic patients (Oliva et al 2016). Blood glucose is normally tightly regulated between 4-7 mM, but in diabetics can rise much higher. The ability of primary human tenocytes to withstand conditions of oxidative stress *in vitro* is significantly compromised under conditions mimicking hyperglycaemia (Poulsen et al 2014). These authors also show that oxidative stress under normoglycaemic conditions results in significant upregulation of COL1A1 and COL1A2 mRNA. This suggests that oxidative stress, lethal to cells exposed to elevated glucose concentrations, is anabolic under conditions mimicking normoglycaemia. Expression of HIF1 $\alpha$  is significantly reduced at glucose concentrations above 6 mM, whilst expression of FOXO1 dramatically increases at higher glucose concentrations. The switch from HIF1 $\alpha$  dominance (prodifferentiation via upregulation of SOX9 and scleraxis) to FOXO1 dominance (proapoptosis) corresponds to the upper level of normoglycaemia (Poulsen et al 2014). Chronically high glucose also increases expression of MMP9 and MMP13 and impairs angiogenesis (Oliva et al 2016).

There is some evidence of a sex predisposition with certain tendinopathies. Posterior tibial tendon dysfunction is three times more common in women than men. Average age at presentation is approximately 40 years and incidence increases with age. Other risk factors, however, include obesity, hypertension, treatment with corticosteroids (either local injection or oral intake) and diabetes mellitus (Holmes and Mann 1992). Tendon collagen synthesis in women varies with menstrual cycle, is affected by oral contraceptives, and increases in post-menopausal women (Magnusson et al 2007). Incidence of Achilles tendon injury is up to 12 times higher in men than women, commonly affecting men in the fourth to fifth decade of life (Hess 2010). This however has been linked to participation in recreational and competitive sport, rather than directly with male gender.

Triiodothyronine and thyroxine are known to affect collagen synthesis and crosslinking (Oliva et al 2016). Clinically, hypothyroidism is associated with tendon calcification, the mechanism postulated

to be increased hypoxaemia-induced apoptosis secondary to perturbed vascularisation (Oliva et al 2016).

### **1.2.7 Other factors implicated in tendinopathies**

A genetic predisposition for developing rotator cuff tears (Harvie et al 2004), Achilles tendinopathy (Abrahams et al 2013) and SDFT injury (Tully et al 2014) has been proposed. The latter two conditions have been associated with sequence variants in both the 3'UTR of the *COL5A1* gene and polymorphisms in the tenascin C gene (Mokone et al 2005, Tully et al 2014). Although type V collagen is a minor component of tendon, it interacts with types I and III and plays an important role in fibril assembly and lateral growth (Birk 2001). The 3'UTR of *COL5A1* contains binding sites for miR-608 and a polymorphic form of this miRNA is also reported, which may also impact on collagen expression (Abrahams et al 2013).

Fluoroquinolone antimicrobials have also been implicated in architectural modification of tendon, by decreasing transcription of decorin, weakening the biomechanical properties (Bernard-Beaubois et al 1998).

Corticosteroid administration is a recognised, although controversial, therapeutic option in tendinopathy. Whilst beneficial in the short term, intermediate to long term outcomes show a reduction in mechanical properties and predisposition to re-injury, with atrophy of Achilles and patellar tendons reported (Hart 2011). Systemic corticosteroid administration, or treatment of adjacent synovial structures, has also been implicated as a risk factor in developing tendinopathies (Pomeroy et al 1999).

### **1.2.8 Mechanisms of tendon repair**

Tenocytes are capable of maintaining and orchestrating beneficial adaptive changes to tendon matrix, despite the apparently lower metabolic activity in those tendons more at risk of injury. However, following matrix damage, reparative mechanisms are inadequate, with increased proteolytic activity, altered tenocyte differentiation pattern to a more fibrochondrogenic phenotype, with altered collagen type deposition. Consequently, there is a high risk of re-injury following an episode of tendinopathy. Approximately 43% re-injury rate is reported for SDFT tendinopathy (Dyson 2004, Reardon et al 2012, Reardon et al 2013) and up to 30% for Achilles tendon (Gajhede-Knudsen et al 2013).

Tendon healing has been classified as occurring in three overlapping phases (Sharma and Maffulli 2005).

- Inflammatory phase – inflammatory cell infiltration occurs with phagocytosis of necrotic material. Angiogenesis is triggered, and epitenon and endotenon tenocyte proliferation is stimulated. Tenocytes migrate to area of tissue damage and type III collagen synthesis begins.
- Proliferative phase – synthesis of type III collagen and glycosaminoglycans peaks, increasing water content of damaged tissue. Neural ingrowth occurs.

- Remodelling phase –
  - 6-10 weeks post injury, tenocyte metabolism remains high but cellularity starts to decrease. Type I collagen synthesis increases, glycosaminoglycan synthesis decreases. Tenocytes and collagen fibres become aligned in direction of stress.
  - 10 weeks to 1 year, maturation of fibrous tissue occurs. Tenocyte metabolism and vascularity decline.

Healing due to intrinsic tenocytes produces improved biomechanics and more collagen and glycosaminoglycans than fibroblasts migrating in from external tissue, resulting in a better quality repair (Sharma and Maffulli 2005). A greater understanding of tenocyte behaviour in response to mechanical and chemical environmental stimuli, and an ability to manipulate this to produce a more effective reparative response is key to developing effective treatment strategies.

### **1.3 microRNAs and tendinopathy**

The term 'epigenetics', first introduced by Waddington (1968) is defined as the 'interactions between genes and their products which bring phenotype into being'. This term, therefore, refers to alterations in gene expression by mechanisms separate to, and independent of, changes in the underlying DNA sequence. Epigenetics was originally considered to encompass two main mechanisms; methylation of cytosine bases within DNA, the pattern and extent of which can enhance or inhibit transcription factor binding, and modification of the histone packing proteins by methylation, acetylation and phosphorylation (Riasat et al 2020). However, this field has now expanded to encompass another system of regulation, since the discovery of microRNAs in the late 1990s and subsequent elucidation of RNA interference mechanisms. Furthermore, it is becoming increasingly recognised that the non-protein coding fraction of the genome has a critical function in normal physiological development and function, as well as the course of many disease processes (Esteller 2011).

The non-coding RNA (ncRNA) family is diverse and subdivided into long (>200 nucleotides) and short (<200 nucleotides) non-coding subgroups (Figure 1.3). microRNAs (miRNAs), a subclass of the small non-coding RNA (sncRNA) group are the most extensively studied. As key players in the RNA interference (RNAi) pathway, miRNAs act as regulators of gene expression, many being highly conserved across species, indicating involvement in critical cellular processes (Bartel 2018). Widespread alterations in miRNA expression have been identified in many different human disorders, generating interest in harnessing them as therapeutic or disease modifying agents (Esteller 2011).

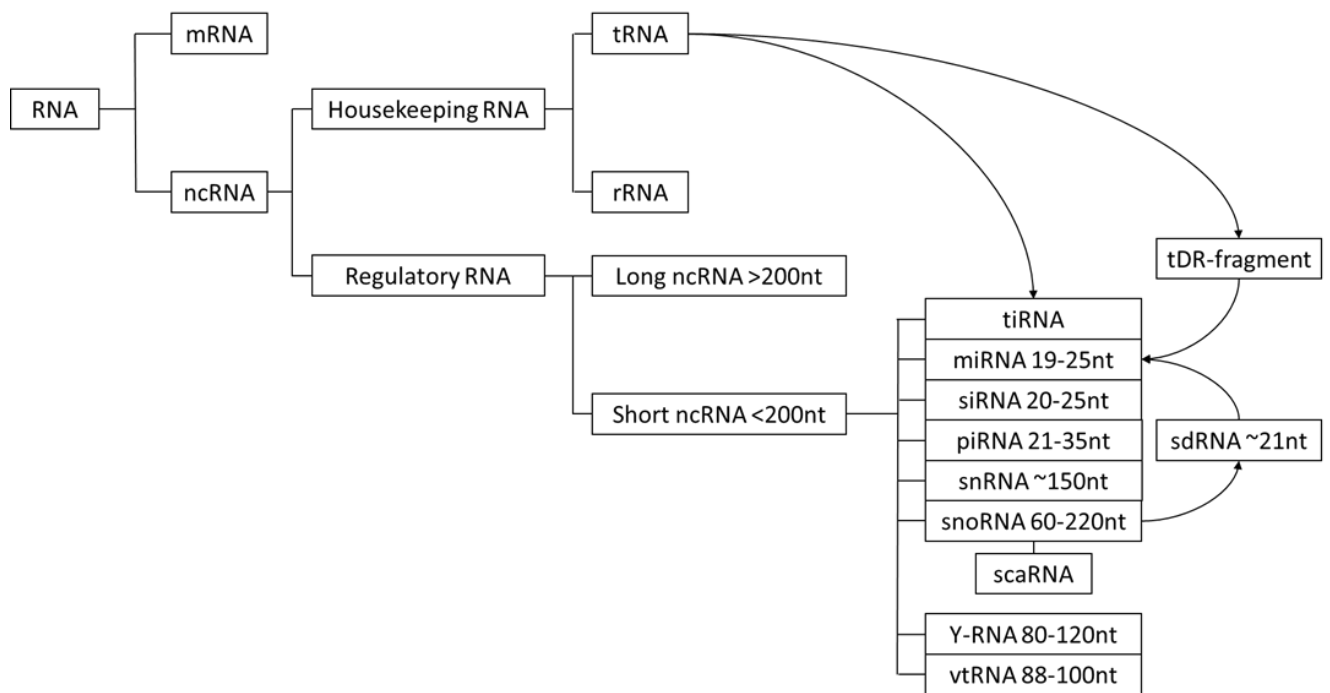


**Figure 1.3 RNA classification dendrogram illustrating the relationship of non-coding RNAs with other RNA classes and the position of microRNAs within the non-coding subgroup.** mRNA = messenger RNA, ncRNA = non-coding RNA, tRNA = transfer RNA, rRNA = ribosomal RNA, tDR = tRNA-derived RNA, tiRNA = 5'-tRNA stress-induced fragments, miRNA = microRNA, siRNA = small interfering RNA, piRNA = PIWI-interacting RNA, snRNA = small nuclear RNA, snoRNA = small nucleolar RNA, sdRNA = snoRNA-derived miRNA, scaRNA = small Cajal body-specific RNA, vtRNA = vault RNA, nt = nucleotide.

### 1.3.1 microRNA synthesis and function

Originally identified in 1993 in *C. elegans* where lin-4 and let-7 RNAs were identified as essential for correct temporal development through four different larval stages. miRNAs are characterised by their size (21-25 nucleotides) and derivation from hairpin precursors.

There are several pathways by which mature miRNAs can be generated (Figure 1.4), but most of the more highly conserved and abundantly expressed are believed to derive from dedicated miRNA gene loci, with expression under direct RNA Polymerase II (POL II) transcriptional control. Approximately 25-30% are processed from introns of protein coding genes, with expression therefore under the same regulatory control as the co-expressed gene (Chiang et al 2010, Bartel 2018). Both dedicated non-coding transcripts and introns of protein coding ones may contain single or multiple primary miRNA (pri-miRNA) sequences. The pri-miRNA, transcribed by POL II is processed in the nucleus by the trimeric microprocessor complex containing the RNase III enzyme Droscha in combination with two molecules of the RNA binding protein DGCR8. This produces a stem-loop structured precursor (pre-miRNA) of approximately 70 nucleotides (35 base pairs), with a two base pair offset, which is exported to the cytoplasm by Exportin-5/RAN-GTP (Bartel 2018). Here a second RNase III enzyme, Dicer I, in combination with binding protein TRBP cleaves the hairpin loop to produce the double stranded miRNA:miRNA\* duplex.

The miRNA:miRNA\* duplex then combines with an Argonaute (AGO) protein (in mammals typically either AGO-1, -3, or -4), facilitated by chaperone proteins HSC70/HSP90. Once combined with AGO, unwinding of the duplex occurs and either the miRNA or miRNA\* strand is selected for retention into the functional multi-protein RNA-induced silencing complex (RISC). The alternate strand is expelled and subsequently degraded. Strand retention is dictated by the configuration of the 5' (5p) terminus of each strand. The Argonaute binding pocket shows preferential affinity for a terminal uracil or adenosine and least stable 5' terminal pairing (Bartel 2018).

The biosynthesis of miRNAs is now known to be far more complex than the canonical pathway originally described, with both Drosha and Dicer independent pathways identified. Some intronic sequences, when processed by the spliceosome, resemble pre-miRNAs, with no, or very short, 5' or 3' flanking sequences which can be removed by alternative nucleases. These structures, called 'mirtrons' then enter the conventional processing pathway downstream of Drosha/DGCR8 having bypassed the need for this step. Additionally, some snoRNA and tRNA transcripts can contain hairpin structures which are processed to yield pre-miRNA substrates for Dicer activity (Stavast and Erkeland 2019). This process is now known to be widespread and conserved (Scott and Ono 2011).

There is also a Dicer/TRBP independent pathway, which so far has only been identified as responsible for production of one annotated miRNA (miR-451) (Cheloufi et al 2010). This requires Drosha/DGCR8 processing of the pri-miR-451 transcript, with final maturation of the pre-miR-451 occurring in combination with Argonaute-2 (which has intrinsic endonuclease activity) and the exoribonuclease PARN (Krol et al 2010).

miRNAs mediate their effects through binding principally to sites within the 3' untranslated region (3'UTR) of their target, with variable, but imperfect complementarity (Filipowicz et al 2008). Target sites are also recognised within coding regions and the 5'UTR of mRNAs, although reportedly of minor importance in both frequency and response effect (Bartel 2009, Filipowicz et al 2008). The result is either repression of mRNA transcription or translation, or enhanced enzymatic mRNA degradation (Selbach et al 2008, Bartel 2009). The latter mechanism is of major importance in plant miRNAs, where miRNA-target binding shows a far higher degree of complementarity. However, in mammals, only 20 gene transcripts susceptible to this mechanism have been identified to date (Bartel 2018). The major method in mammals is translational repression, mediated by two main routes, the relative importance of each being determined by the developmental stage of the organism (Bartel 2018). Recruitment of the adapter protein TNRC6 by Argonaute promotes interaction with the mRNA poly(A) tail and its associated poly(A)-binding protein, additionally recruiting the deadenylase complexes PAN2-PAN3 and CCR4-NOT. The subsequent shortening of the poly(A) tail, destabilising the mRNA. The CCR4-NOT complex additionally recruits DDX6 and 4E-T, which inhibit initiation of translation. This second mechanism occurs rapidly and predominates during embryological development, but is of minor importance in post-embryonic regulation (Bartel 2018).

Binding specificity and activity are both dictated by the sequence at the 5' terminus of the miRNA, centred on nucleotides 2-7. This 'seed' sequence forms Watson-Crick pairing with the target site (typically) within the mRNA 3'UTR. Additional pairing between miRNA nucleotides 1 and 8 are also described, with 7 or 8 base pair matching necessary for effective canonical function. Activity with only six base pair matching frequently results in weak or undetectable efficacy (Bartel 2018). Additional base pairing may occur further downstream from the seed sequence. These are termed

supplementary sites if seed pairing is 7-8 base pairs, or compensatory if seed pairing is imperfect with only six matches (Bartel 2018). A single miRNA may have several binding sites within the 3'UTR of each mRNA (seven have been identified for lin-4 within the 3'UTR of the lin-14 gene (Wightman et al 1993)). The degree of repression is influenced by the number and proximity of seed sequences. A linear correlation is described between number of seed sequences and log<sub>2</sub> fold change of down regulated genes, with a synergistic effect apparent if seed sequences are less than 40 nucleotides apart (Selbach et al 2008). Each miRNA may target multiple mRNAs, with an average target number of 400 proposed (Bartel 2009). A single mRNA may be influenced by multiple miRNAs, with expression of over 60% of human genes predicted to be regulated by miRNAs (Noren Hooten et al 2013).

Once incorporated into the RISC complex, miRNA half-life may extend to several days, and stability is often further enhanced if the RISC is associated with its target mRNA, indicating stability is target-dependent (Krol et al 2010).

Relatively non-specific control of miRNA production is exerted through controlling expression and activity of the microprocessor and Dicer/TRBP complexes. Positive feedback loops have been identified for let-7 miRNAs, with the mature miRNA targetting the pri-miRNA, to enhance processing. Let-7 also targets Dicer mRNA, triggering a more general negative feedback loop (Krol et al 2010). Long non-coding RNA transcripts have been identified which act as miRNA 'sponges', combining with high affinity, preventing their inhibitory effect, such as the interaction described by Lu and co-workers (2017) between lncH19 and miR-29b-3p. A 5' to 3' exonuclease XRN-2 has been identified which catalyses degradation of mature miRNAs, but requires the miRNA to dissociate from the other RISC components (Chatterjee and Grosshans 2009).

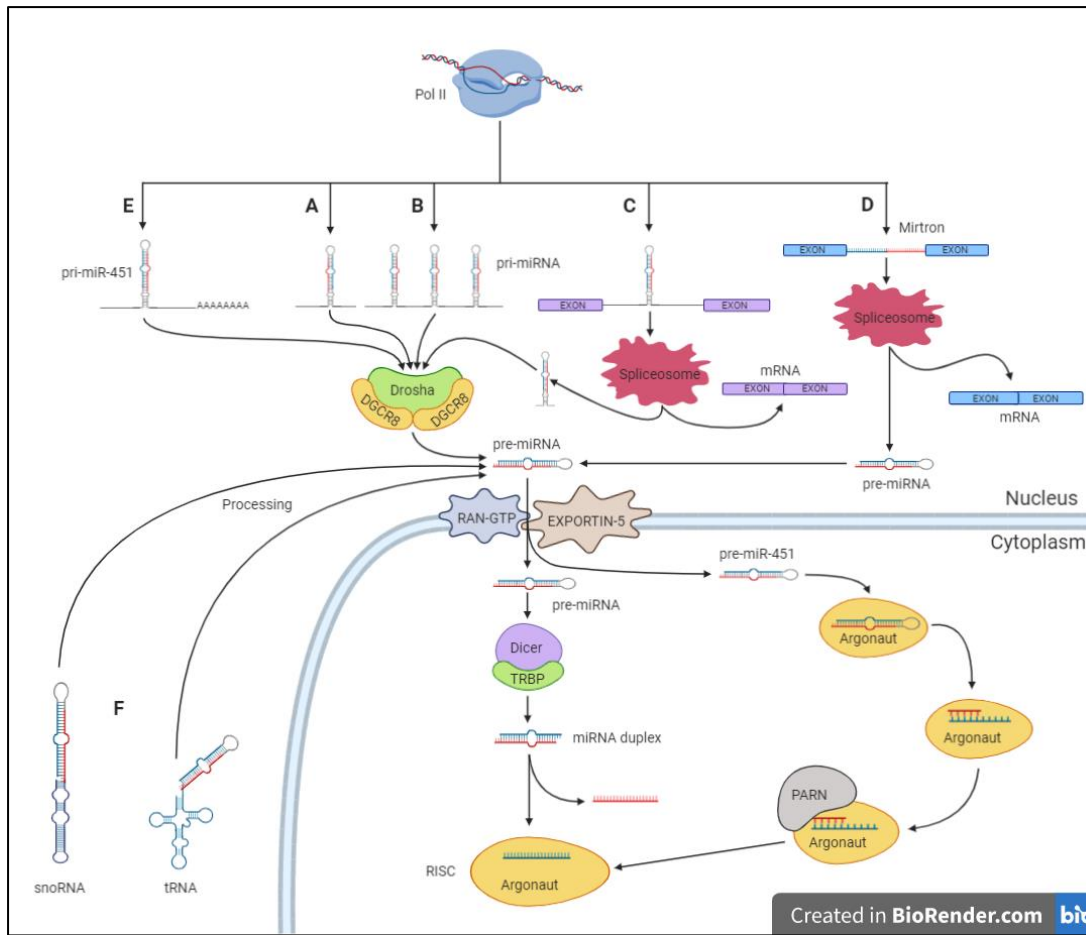


**Figure 1.4 Major miRNA biosynthetic pathways.**

**A-C.** Canonical pathway. Single (A), or clustered (B) primary microRNAs (pri-miRNA) transcribed from dedicated gene loci. Pri-miRNAs co-transcribed in introns of protein coding genes (C) under control of the same promoter as the encoded gene, and spiced out of the encoded gene during production of mature mRNA. The stem of the pri-miRNA hairpin is then further processed by the endoribonuclease Drosha combined with the double-stranded RNA binding protein DGCR8 (DiGeorge Syndrome Critical Region 8). The product, a shorter (~70 base pair) hairpin precursor miRNA (pre-miRNA) is exported to the cytoplasm by the RAN-GTP-Exportin-5 complex. A second endoribonuclease (Dicer) – binding protein (TRBP -transactivation response element RNA-binding protein) complex cuts the loop of the hairpin, producing the miRNA duplex. This is loaded into the Argonaute protein where strand selection occurs. The guide strand (red) is expelled, the active strand (blue) is retained, forming the RNA induced silencing complex (RISC).

**D.** Short intergenic sequences may encode the pre-miRNA with little or no additional bases. Spliceosome processing generates the pre-miRNA, bypassing the requirement for Drosha/DGCR8 activity. Downstream processing then follow the pathway outlined above.

**E.** miR-451 follows a Dicer-independent pathway. Transcribed from a dedicated gene locus, pri-miRNA-451 undergoes Drosha/DGCR8 trimming, but following export to the cytoplasm, pre-miRNA-451 combines directly with Argonaut-2, which itself performs partial cleavage. The functional RISC is completed by the action of RNA exonuclease poly(A)-specific ribonuclease (PARN).

*(legend continues overleaf)*

F. snoRNAs and tRNAs can contain integral pre-miRNA sequences which are liberated during processing, bypassing the requirement for Drosha/DGCR8 activity.

Other regulatory mechanisms include adenosine-to-inosine editing of pri-mRNAs preventing further processing and polyuridylation of 3' end of pre-miRNAs, blocking Dicer interaction and inducing degradation (Bartel 2018). There is evidence that mature miRNAs are generally more stable than mRNA transcripts, this stability being enhanced by 3' adenylation or methylation indicating sequence configuration at the 3' end is important in degradation of miRNAs (Krol et al 2010). This is supported by the phenomenon of target-RNA-directed miRNA degradation (TDMD), where highly complementary miRNA-target binding induces miRNA degradation initiated from the 3' end. This appears to be of particular importance for rapid decay of neuronal miRNAs (de la Mata et al 2015).

As well as acting in an intracrine fashion, miRNAs can exert a more widespread effect, being secreted into the circulation as part of a miRNA binding protein or high-density lipoprotein complex, or as part of the microvesicle/exosome cargo (Jung and Suh 2014).

### **1.3.2 Role of microRNAs in tendinopathies/musculoskeletal disease**

The recognition of the widespread influence of miRNAs in physiological and pathological processes has resulted in an extensive body of research in this area, despite their relatively recent discovery. Tendinopathies are relatively under researched compared to arthroses and myopathies, and their pathogenesis is incompletely understood. Many of the factors believed to be implicated in tendon pathology have been shown to be influenced by miRNAs, but there are limited studies specifically investigating their role. Table 1.3 lists those studies identified which specifically link miRNA expression to tendon.

Multiple metabolic alterations occur during the normal physiological ageing process, including stem cell exhaustion, cellular senescence, mitochondrial dysfunction, deregulated nutrient sensing, pro-inflammatory state and loss of proteostasis (López-Otín et al 2013). miRNAs have been implicated in regulation of all these via their reported interactions with insulin signalling, AMPK/Sirtuin pathway, mTOR signalling, TLR-NFκB-MAPK pathway and HIF1α signalling (Victoria et al 2017). A subset of miRNAs (miR-1/206 and miR-133 families) have been shown to be critical in myoblast proliferation and myocyte differentiation (Goljanek-Whysall et al 2012) and differential expression of miRNAs has been identified in muscle ageing (Soriano-Arroquia et al 2016), sarcopaenia (Brown and Goljanek-Whysall 2015) and disease (Goljanek-Whysall et al 2012). Embryonic development of functional myotendinous junction is known to be dependent on a critical dystroglycan expression gradient controlled by miR-9a in *Drosophila* (Yatsenko et al 2014).

Tendon stem/progenitor cell (TSPC) senescence has been reported to be associated with miR-140-5p upregulation inhibiting Pin1 (Chen et al 2015a). Down regulation of miR-135a with ageing promotes senescence in TSPCs by derepressing ROCK1 expression (Chen et al 2015b). The capacity of TSPCs to differentiate into functional tenocytes decreases with age due to upregulation of miR-217 inhibiting EGR1 expression (Han et al 2017). A similar inhibitory effect on TDSCs via EGR1 has also been identified for miR-124-3p with a subsequent suppression of collagen type 1, fibromodulin and tenascin C expression (Wang et al 2016).

In human Achilles tendon, downregulation of miR-1245a (a driver of cellular proliferation) with age is reported by Peffer and co-workers (2015), whilst Pease and colleagues (2017) identified differential expression of an additional 26 microRNAs with ageing, although direction of change was not stated. Four of these (miR-1287, miR-1304, miR-1909, miR-3614) were common to both male and female-derived tissue and are linked with cellular proliferation.

Noren Hooten and co-workers (2013) identified significant reduction in miR-151a-3p, miR-181a-5p and miR-1248 in the serum of older people. These microRNAs have been shown to target pro-inflammatory cytokines IL6, IL8 (miR-1248, miR-181a-5p), IL1 $\alpha$ , IL1 $\beta$ , TNF $\alpha$  and FGF2 (miR-181a-5p) and anti-inflammatory IL10 and TGF $\beta$  (miR-181a-5p). Olivieri and colleagues (2012) identified overexpression of miR-21 in an aged population. This microRNA targets TGF $\beta$ R1 and TGF $\beta$ R2 subunits, downregulating this anti-inflammatory signalling pathway. Direct secretion of IL6 and TNF $\alpha$  via the NF $\kappa$ B pathway can also be triggered by miR-21 acting as a ligand at TLRs (Fabbri 2012). Downregulation of IRAK expression has also been reported, exerting an anti-inflammatory action (Olivieri et al 2013). The recognition of miR-155, miR-21 and miR-146 as critical regulators of inflammation has led to them being termed 'inflamma-miRs'. The consequence is that ageing predisposes to a more inflammatory phenotype. This may suggest that age-related changes in tendon may be an integral part of body-wide ageing processes (Xu and Tahara 2013).

Although computational analysis has identified miRNA target sites in some cytokines (IL1 $\alpha$ , IL6, IL10, IL11, IL12B, IL13, IL16, IL23, IL25), an additional, indirect regulatory mechanism has been proposed (Asirvatham et al 2009). AU-rich elements within the 3'UTR of cytokine transcripts regulate transcript stability by association with AU-rich element binding proteins (ARE-BP) which either promote or retard transcript stability. ARE-BPs involved in the decay pathway are a richer source of predicted miRNA targets, although few have been functionally confirmed (Asirvatham et al 2009). Chronic inflammation can lead to fibrosis, and both pro- (miR-21, miR-199a-5p, miR-199b) and anti- (miR-29a, b, c) fibrotic miRNAs have been identified, affecting multiple tissue types (O'Reilly 2016). miR-29 has been described as a master regulator of fibrosis, with decreased expression associated with fibrosis in multiple organs (O'Reilly 2016). miR-29a has been shown to regulate collagen expression both directly (Millar et al 2015, Lu et al 2017, Watts et al 2017) and indirectly by influencing the TGF $\beta$  signalling pathway (Chen et al 2014, Ciechomska et al 2014, Lu et al 2017), increasing MMP1 activity by inhibiting TIMP1.

Using microarray analysis, extensive changes in microRNA expression patterns associated with Collagens type I and III, MMP9, MMP2, JAK2/STAT3 signalling pathway, inflammation and energy homeostasis have been identified in both intact and torn tendon in the inflammatory environment of an arthritic joint (Thankam et al 2016, 2018, 2019). Type V collagen is a minor component of tendon, but an important stabiliser of fibril structure. miR-608 targets COL5A1 and a SNP at rs4919510 within the *MIR608* gene is significantly associated with Achilles tendinopathy (Abrahams et al 2013).

Acute exercise alters miRNA expression in rat Achilles tendon (Mendias et al 2012). A single 30 minute exercise session resulted in upregulation of six (miR-378, miR-1, miR-133a, miR-133a\*, miR-133b, miR-206) and down regulation of seven (miR-100, miR-140, miR-let-7a, miR-let-7e, miR-338, miR-381, miR-743a) miRNAs. These miRNAs are associated with cell proliferation and ECM synthesis (miR-378 miR-100), skeletal muscle adaptation (miR-1, miR-133a, miR-133a\*, miR-133b, miR-206), chondrogenesis and neovascularisation (miR-140). miR-338 and miR-381 were predicted to target

scleraxis, and decreased expression of these corresponded with increased scleraxis expression (Mendias et al 2012).

Inhibition of miR-100 and increased miR-378 are associated with increased cell proliferation and angiogenesis. Decreases in miR-let-7a and 7e are consistent with previous reports of an inverse relationship between let-7 expression and cell proliferation. Up regulation of miR-1, miR-133a, (miR-133a\*), miR-133b and miR-206 is consistent with expression profiles seen in striated muscle in response to mechanical loading and ischaemia (Mendias et al 2012).

Hypoxic insult has been implicated in the pathogenesis of tendinopathies (Benson et al 2010, Millar et al 2012) and upregulation of multiple miRNAs following exposure to a hypoxic culture environment has been demonstrated in a variety of cell types (Kulshreshtha et al 2007). Rapid reduction in miR-199a levels, in response to hypoxia derepresses its direct target HIF1 $\alpha$ . A major regulator of altered gene expression in hypoxia, HIF1 $\alpha$  directly upregulates miR-181 and miR-210 expression and promotes p53-mediated cell cycle arrest or apoptosis (Kulshreshtha et al 2007, Rane et al 2009). Downregulation of anti-fibrotic miR-29b has also been reported under hypoxia (Ivan et al 2008).

Hypoxia, mechanical loading, inflammation, and genetic predisposition can all potentially enhance apoptotic tenocyte death (Scott et al 2005, Nell et al 2012, Millar et al 2009, Benson et al 2010). Apoptosis has been identified as important both as a cause (Yuan et al 2002) of tendinopathy and as part of the tissue repair process (Lui et al 2007) and is closely linked with the autophagy and necrosis pathways (Xu et al 2012).

Both intrinsic and extrinsic apoptotic pathways have been shown to be regulated by microRNAs, and apoptotic and autophagic pathways are influenced by common miRNAs. Increased apoptotic activity in tendinopathy may therefore impact on autophagic and necroptosis pathways. Autophagy is a highly conserved eukaryotic cellular recycling process critical to cell survival and maintenance. Three types of autophagy are described in mammalian cells, macro-, micro- and chaperone-mediated autophagy. Chaperone-mediated autophagy is highly specific, restricted to proteins containing a particular pentapeptide motif, common to approximately 30% of cytosolic proteins (Parzych and Klionsky 2014). This motif is recognised by several chaperone proteins which unfold the targeted protein and translocate it directly across the lysosomal membrane for degradation. In contrast, micro- and macroautophagy can be either selective or non-selective. Microautophagy involves direct uptake of cytoplasmic contents into the lysosome by invaginations of the lysosomal membrane, whilst macroautophagy involves *de novo* formation of a double-membrane phagophore which progressively engulfs the cargo to form an autophagosome, which subsequently fuses with a lysosome, forming an autolysosome, leading to degradation of the sequestered cargo by acidic hydrolases. Macroautophagy occurs constitutively at low levels, but is up regulated under conditions of cellular stress (Parzych and Klionsky 2014). Bulk (non-selective) autophagy is used for bulk turnover of cytoplasm under conditions starvation, whilst selective autophagy specifically targets damaged or superfluous organelles and invasive microbes. Reactive oxygen species (ROS) produced as by-product of oxidative phosphorylation induce oxidative damage to mitochondria resulting in increased ROS production and ultimately release of cytochrome c and cellular injury (Song et al 2018). Mitochondrial quality is controlled by several mechanisms, proteolytic degradation of damaged proteins, cycles of mitochondrial fission and fusion and elimination of dysfunctional mitochondria by a selective form of macro-autophagy termed mitophagy (Narendra et al 2010).

Mitophagy can occur through several mechanisms; Type 1, 2 and 3 are described (Lemasters 2014), and pathways are classified as ubiquitin-dependent or -independent (Palikaras et al 2018). Several miRNAs (miR-155, miR-101, miR-204 and miR-224) are known to regulate autophagy (Szekerczés et al 2020), and down regulation of miR-181a with ageing in skeletal muscle disrupts mitophagy, resulting in accumulation of autophagy-related proteins and abnormal mitochondria (Goljanek-Whysall et al 2020).

Author	Gene identity	Organism	Tendon type	Age-related findings
Peffer et al 2015	miR-1245a	Human	Achilles tendon	Reduced expression with ageing.
Peffer et al 2016	miR-500a-5p, miR-548j-5p, miR-618, miR-10	Human	MSCs differentiated into tenogenic tissue	miR-500, miR-548 and miR-618 showed increased expression with ageing. miR-10 methylation significantly increased with ageing.
Pease et al 2017	26 miRs	Human	Achilles tendon	26 DE miRs identified in old v young female-derived tissue, 4 of which (miR-1287, miR-1304, miR-1909, miR-3614) also DE in old versus young male-derived tissue. Direction of change not stated.
Han et al 2017	miR-217	Human	Achilles tendon	Tenogenic differentiation capacity of TSPCs decreases with age due to p16 induced upregulation of miR-217 resulting in reduced EGR1 expression.
Chen et al 2015a	miR-140-5p	Human	Achilles tendon	miR-140-5p associated with TSPC senescence via direct inhibition of Pin1 expression.
Chen et al 2015b	miR-135a	Rat	Achilles tendon	Down regulation of miR-135a with ageing promotes senescence in TSPCs via interaction with ROCK1.
Bardell et al 2018	miR-29a, miR-34a, miR-34b, miR-181b, miR-199a, miR-199b	Equine	SDFT	miR-34b miR-181b up regulated with age miR-29a, miR-34a, miR-199a, miR-199b down regulated with age.
Author	Gene identity	Organism	Tendon type	Mechanical loading related findings
Mendias et al 2012	35 microRNAs associated with cell proliferation and ECM synthesis, skeletal muscle adaptation, chondrogenesis and neovascularisation, the let-7 cluster and microRNAs predicted to bind the 3'-UTR of scleraxis or tenomodulin	Rat	Achilles tendon (exercise),  Primary tendon fibroblasts (TGFβ challenge)	miR-378, miR-1, miR-133a, miR-133a*, miR-133b, miR-206 up regulated in response to 30 minutes exercise.  miR-100, miR-140, miR-let-7a, miR-let-7e, miR-338, miR-381, miR-743a down regulated with exercise.  miR-21, miR-221, miR-222, miR-1, miR-133a, miR-133a*, miR-133b, miR-29a, miR-29b, miR-29c, miR-140 up regulated after TGFβ challenge.  miR-205, miR-338, miR-381, miR-let-7a, miR-let-7b, miR-let-7e down regulated after TGFβ challenge.

Table 1.3 continues overleaf

Author	Gene identity	Organism	Tendon type	Pathology related findings
Yatsenko et al 2014	miR-9a	Drosophila	Myotendinous junction	miR-9a controls dystroglycan expression to establish critical gradient required to establish functional myotendinous junction.
Millar et al 2015	miR-29a	Human Mouse	Primary tenocytes ( <i>in vitro</i> ) Patellar tendon ( <i>in vivo</i> )	IL-33 upregulation in early tendinopathy suppresses miR-29a, promoting COL3A1 expression. Application of exogenous miR-29a directly targets and inhibits COL3A1, but not type I collagens due to alternative polyadenylation sites in type I transcripts.
Watts et al 2017	miR-29a	Equine	SDFT	Application of exogenous miR-29a to collagenase-induced SDFT lesions significantly reduced COL3A1 expression 2 weeks post-treatment, without affecting that of COL1A1, reduced lesion size at 6, 12 and 16 weeks post-injury and improved histological score at 2 and 16 weeks.
Chen et al 2014	miR-29b	Rat	Digital flexor tendon	Chitosan promotes miR-29b and P21 expression and inhibits fibroblast growth, TGFβ-1 and Smad3.
Lu et al 2017	miR-29b-3p	Human Mouse	TDSC ( <i>in vitro</i> ) Patellar tendon ( <i>in vivo</i> )	miR-29b-3p directly targets lncRNA H19, TGFβ-1 and COL1A1, suppressing tenogenic differentiation and tendon repair.
Usman et al 2015	miR-210	Rat	Achilles tendon	Application of exogenous miR-210 following surgical transection accelerated improvements in ultimate tensile strength and capillary density. Increased expression of Col1a1 with larger fibre diameter and improved histological appearance of repair.
Wang et al 2016	miR-124-3p	Human	Hamstring tendon	miR-124-3p directly targets EGR1 reducing tenogenic differentiation of TDSCs and suppressing collagen 1, fibromodulin and tenascin C expression.
Laguet et al 2011	miR-608	Human	DNA derived from blood samples	Functional binding site for miR-608 identified in 3'-UTR of COL5A1 gene.
Abrahams et al 2013	miR-608	Human	DNA derived from blood samples	SNP in miR-608 associated with development of chronic Achilles tendinopathy.

Table 1.3 continues overleaf

Author	Gene identity	Organism	Tendon type	Pathology related findings (cont.)
Bardell et al 2018	miR-29a, miR-34a, miR-34b, miR-181b, miR-199a, miR-199b	Equine	SDFT	miR-29a, miR-181b, miR-199a, miR-199b down regulated with disease.  mir-34a, miR-34b up regulated with disease.
Thankam et al 2016	miR-145-5p, miR-151a-3p, miR-382-5p, miR-199a-5p, miR-21-5p, miR-125a-5p, miR-498	Human	Biceps tendon	miRs associated with COL1A2, COL3A1, MMP9, MMP2 highly significantly altered in intact tendon in an inflammatory environment (glenohumeral arthritis).  miR-498 up regulated, all others down regulated.
Thankam et al 2018	230 miRs significantly DE with tendinopathy	Human	Rotator cuff	196 miRs down regulated ( $\geq -3FC$ ) 34 miRs up regulated ( $\geq +2FC$ ) in RCTI, with extensive associations with JAK2/STAT3 pathway and inflammation.
Thankam et al 2019	13 miRNAs described as highly significantly altered in connection with AMPK and TREM-1 pathways	Human	Rotator cuff	miR-145-5p, miR-991-5p, miR-100-5p, miR-150-5p, miR-193b-3p, miR-103a-3p, miR-31-5p, miR-195-5p, miR-497-5p, miR-15a-5p, miR-16-5p, miR-let-7b-5p down regulated in RCTI.  miR-297 up regulated in RCTI.

**Table 1.3** (includes preceding two pages) **microRNAs identified as significant in tendon ageing and disease.** MSC = mesenchymal stem cells; TSPC = tendon stem progenitor cells; DE = differentially expressed; EGR1 = early growth response 1; PIN1 = Peptidyl-prolyl cis-trans isomerase NIMA-interacting 1; ROCK1 = rho associated coiled-coil containing protein kinase 1; ECM = extracellular matrix; SDFT= superficial digital flexor tendon; UTR = untranslated region; lncRNA = long non-coding RNA; TDSC = tendon derived stem cells; SNP = single nucleotide polymorphism; AMPK = AMP-activated protein kinase; TREM-1 = triggering receptors expressed on myeloid cells-1; RCTI = rotator cuff tendon injury.

### 1.3.3 Diagnostic, prognostic and therapeutic potential of microRNAs

The recognition of microRNAs as key regulators of gene expression, their involvement in critical cellular processes and identification of detectable changes with a range of disease processes renders them potentially useful for diagnostic, prognostic and therapeutic purposes.

The clinicaltrials.gov database lists 398 clinical studies (searched 28/03/2020), including phase 4 trials, investigating microRNAs as biomarkers for the diagnosis and prognosis of multiple diseases and monitoring response to treatment. Currently only phase 1 and 2 clinical trials investigating therapeutic potential are registered. These are exploring miR-16 and miR-29 mimics and miR-21, miR-92, miR-122 and miR-155 antagonists as treatments for a variety of indications including hepatitis C virus, wound healing, T-cell lymphoma and mesothelioma (Hanna et al 2019). Given the pleiotropic capability of microRNAs, significant potential for off-target effects may limit their potential as therapeutic agents. Indeed, phase 1 and phase 2 trials of miR-34 mimic for treatment of solid tumours were terminated due to severe adverse immune responses (Rupaimoole and Slack 2017). RNA therapeutics have however reached the stage of clinical approval. Patisiran (Onpattro®) is a small-interfering RNA targeting transthyretin production by the liver. This received FDA approval in 2018 and has a marketing authorisation in the UK for treating hereditary transthyretin amyloidosis. Nusinersen (Spinraza®) was approved by the European Medicines Agency in May 2017 for treatment of the genetic disease spinal muscular atrophy. This synthetic antisense oligonucleotide compensates for the loss of function mutation in the survival motor neuron (SMN) 1 gene by modulating alternative splicing of the SMN 2 gene product, producing a transcript identical to that of a functional SMN1 gene.

RNA-based therapies have been explored to a small degree in tendon healing. Synthetic oligonucleotides targeting the TGFβ1 gene reduced adhesion formation after digital flexor tenotomy in chickens, but also reduced ultimate tensile strength (Wu et al 2016). Following surgical transection of Achilles tendon in rats, exogenous miR-210 accelerated neovascularisation and improved tensile strength during early healing. Although these differences were only detectable two weeks post-injury, improved histological appearance and increased collagen fibre diameter were evident at 6 weeks (Usman et al 2015). Intra-articular injection of miR-210 also improved meniscal healing in rats following surgically induced injury (Kawanishi et al 2014). Intralesional injection of miR-29a one week after collagenase induced SDF tendinopathy in horses resulted in significant reduction in COL3A1 two weeks post-treatment without affecting type 1 collagen, reduced lesion size and improved histological scores (Watts et al 2017). Although these results should be interpreted with caution as the models do not mimic naturally occurring tendinopathy in their pathogenesis, they demonstrate the potential for this technology to have a positive impact on a recalcitrant clinical problem.

## **1.4 Aims and objectives of project**

The aims of this project were:

- 1)** To characterise expression profiles of sncRNAs in human elastic energy storing tendon, using an unbiased technique (RNA-sequencing) in samples obtained from patients with naturally occurring tendinopathy and healthy control tendon, with the objective of identifying how, and to what extent, sncRNAs are differentially expressed between healthy and diseased states (Chapter 3).
- 2)** To perform a targeted validation of RNA-seq results using RT-qPCR, focussing on a selected panel of 11 miRNAs known, or predicted, to be implicated in processes pertinent to tendinopathy (fibrosis, matrix degradation, inflammation, oxidative stress, cellular differentiation and apoptosis; Chapter 3).
- 3)** To investigate concordance of RT-qPCR results obtained in human tissue with changes in expression of the same miRNAs in healthy and diseased equine SDFT tissue, with the objective of determining if similar dysregulation occurs between species, and identify candidate miRNAs for further investigation of biological networks and cellular pathways common to both species (Chapters 3 and 4).
- 4)** To select the most promising candidate miRNA for further investigation of its role in equine tenocyte function using gain- and loss-of-function studies in both monolayer culture and three-dimensional tissue-engineered constructs, and an induced autophagy/mitophagy model in monolayer culture. Analysis of candidate miRNA-target interactions at biochemical, ultrastructural and histological levels informed the objective of establishing whether manipulation of expression of this miRNA alters tenocyte and/or extracellular matrix interaction and function in a way that may yield potential therapeutic benefit (Chapters 5 and 6).
- 5)** To identify if human tenocytes demonstrate analogous changes to those seen in equine tenocytes when subjected to the same experimental methodologies in monolayer culture, with the objective of determining if equine tenocytes are a valid experimental model for investigation of human tendon disease (Chapter 7).

## **Chapter 2 - Materials and methods**

A full list of reagents, consumables and equipment used is given in Appendix 1.

### **2.1 Tissue sample acquisition**

#### **2.1.1 Human tissue**

Supraspinatus tendon (SSP) was harvested from patients with clinically diagnosed rotator cuff disease, undergoing surgical repair procedures. Collection was performed under Health Research Authority (HRA) ethical approval (16/WS/0207), and with informed patient consent. Sample handling and RNA extraction were performed at University of Glasgow's Institute of Infection, Immunity and Inflammation, courtesy of Dr Neal Millar, Academic Consultant Orthopaedic Surgeon at the University of Glasgow, Scotland. Details of the six samples provided are given in Table 2.1.

Sample number	Sample name	Organism	Sex	Age	Status	Source
SSP1	18139-7 / 0946/18 SSP	Human	F	39	Diseased SSP	Glasgow
SSP2	18139-8 / 0947/18 SSP	Human	F	39	Diseased SSP	Glasgow
SSP3	18139-9 / 0866/18 SSP	Human	M	51	Diseased SSP	Glasgow
SSP4	18139-10 / 0944/18 SSP	Human	M	50	Diseased SSP	Glasgow
SSP5	18139-11 / 0864/18 SSP	Human	M	59	Diseased SSP	Glasgow
SSP6	18139-12 / 0887/18 SSP	Human	F	45	Diseased SSP	Glasgow

**Table 2.1 Details of six human supraspinatus tendon samples harvested from patients with clinically diagnosed rotator cuff disease. M = male; F = female; Age given in years; SSP = supraspinatus tendon.**

Following informed patient consent under HRA ethical approval (17/WM/0099), posterior tibial tendon was harvested from patients with clinically diagnosed acquired flat foot deformity undergoing surgical reconstruction procedures at Aintree University Hospital, Liverpool. Tissue was collected by Andrew Molloy or Professor Lyndon Mason, both Consultant Trauma and Orthopaedic Surgeons at Aintree University Hospital, into RNA $\text{later}^{\text{®}}$  stabilisation solution (Invitrogen) and stored at 4°C until collected by the author. Following equilibration in RNA $\text{later}^{\text{®}}$  stabilisation solution (Invitrogen), at 4°C overnight, samples were removed, blotted dry, weighed and placed in 1.5 mL reaction tubes for storage at -80°C.

Details of the three samples provided are given in Table 2.2.

Sample number	Sample name	Organism	Sex	Age	Status	Source
P1	P1M60081217	Human	M	60	Diseased PTT	Liverpool
P2	P2M71191217	Human	M	71	Diseased PTT	Liverpool
P3	P3M65130318	Human	M	65	Diseased PTT	Liverpool

**Table 2.2** Details of three human posterior tibial tendon samples harvested from patients with clinically diagnosed flat foot deformity. M = male; Age given in years; PTT = posterior tibial tendon.

Hamstring tendon (mixed gracilis and semitendinosus) was obtained from patients undergoing reconstructive surgery following anterior cruciate ligament rupture. Tissue was collected at Broadgreen Hospital, Liverpool, UK under Liverpool Musculoskeletal Biobank HRA ethical approval (15/NW/0661) and following informed patient consent. Samples were collected into RNA<sup>later</sup><sup>®</sup> or tenocyte culture media without foetal calf serum (TCM-NOFBS – see section 2.2). Sample information is given in Table 2.3.

Sample number	Sample name	Organism	Ethnicity	Sex	Age	Status	Source
C1	LMB-KM-249	Human	White British	M	31	Healthy ST/GR	Liverpool
C2	LMB-MBL-252	Human	Malaysian	M	35	Healthy ST/GR	Liverpool
C3	LMB-GA-253	Human	White British	F	17	Healthy ST/GR	Liverpool
C4	LMB-HB-254	Human	Indian	F	23	Healthy ST/GR	Liverpool
C5	LMB-AS-255	Human	White British	F	23	Healthy ST/GR	Liverpool
C6	LMB-MK-257	Human	White British	F	29	Healthy ST/GR	Liverpool
C7	LMB-MH-258	Human	White British	M	24	Healthy ST/GR	Liverpool
C8	LMB-MW-260	Human	White British	M	23	Healthy ST/GR	Liverpool
C9	LMB-RM-261	Human	White British	M	26	Healthy ST/GR	Liverpool
C10	LMB-MM-265	Human	White British	M	48	Healthy ST/GR	Liverpool
C11	LMB-SM-270	Human	White British	M	30	Healthy ST/GR	Liverpool
C12	LMB-AP-278	Human	White British	M	41	Healthy ST/GR	Liverpool
C13	LMB-JL-280	Human	Chinese	M	18	Healthy ST/GR	Liverpool
C14	LMB-SF-282	Human	White British	F	26	Healthy ST/GR	Liverpool
C15	LMB-RL-286	Human	White British	M	24	Healthy ST/GR	Liverpool
C16	LMB-SG-289	Human	White British	M	32	Healthy ST/GR	Liverpool
C17	LMB-MT-291	Human	White British	M	25	Healthy ST/GR	Liverpool

**Table 2.3** Details of 17 human hamstring tendon samples harvested from patients undergoing surgical repair of anterior cruciate rupture. M = male; F = female; Age given in years; ST = semitendinosus tendon; GR = gracilis tendon.

### 2.1.2 Equine tissue

Superficial digital flexor tendon (SDFT) was acquired fresh from horses consigned for slaughter to F. Drury & Sons Ltd, The Abattoir, Tockenham, Wiltshire, UK. Samples were collected as a by-product of the agricultural industry. Specifically, the Animal (Scientific Procedures) Act 1986, Schedule 2, does not define collection from these sources as scientific procedures. Collection of this material therefore did not require ethical approval. Slaughtering was achieved using a firearm to effect brainstem destruction from a free bullet. Once death was confirmed, the distal forelimbs were recovered by disarticulation at the radio-carpal joint.

To determine optimal handling for subsequent RNA extraction, one distal forelimb was left intact, whilst the skin and superficial fascial layers of tissue were removed from the contralateral limb to expose the SDFT. Transverse sections approximately 0.5 cm thick were harvested from the mid-metacarpal region and placed in either RNA<sup>later</sup>® stabilisation solution, ice cold Dulbecco's phosphate buffered saline (DPBS; Sigma-Aldrich) or frozen in dry ice for transport. Following transport to the lab, mid-metacarpal sections of SDFT were dissected from the intact limb and placed in RNA<sup>later</sup>® for RNA extraction, or tenocyte culture media without foetal bovine serum (FBS, TCM-NOFBS – see section 2.2) for tenocyte isolation. Details of equine tendon samples utilised in this study are given in Table 2.4.

Use	Sample name	Organism	Sex	Age	Status	Source
RNA	H1	Equine	NR	3	Normal SDFT	Peppers/Wardle
RNA	H2	Equine	NR	25	Normal SDFT	Peppers/Wardle
RNA	H3	Equine	NR	4	Normal SDFT	Peppers/Wardle
RNA	H16	Equine	NR	3	Normal SDFT	Peppers/Wardle
RNA	H18	Equine	NR	19	Normal SDFT	Peppers/Wardle
RNA	H23N	Equine	NR	6	Normal SDFT	Peppers/Wardle
RNA	H23D	Equine	NR	6	Diseased SDFT	Peppers/Wardle
RNA	H24N	Equine	NR	9	Normal SDFT	Peppers/Wardle
RNA	H24D	Equine	NR	9	Diseased SDFT	Peppers/Wardle
RNA	H27	Equine	NR	18	Normal SDFT	Peppers/Wardle
RNA	H47	Equine	NR	7	Diseased SDFT	Peppers/Wardle
RNA	H52	Equine	NR	6	Diseased SDFT	Peppers/Wardle
RNA	H62	Equine	NR	7	Diseased SDFT	Peppers/Wardle
3D	EqDB1	Equine	F	9	Normal SDFT	Drury & Sons Ltd
3D	EqDB3	Equine	MN	9	Normal SDFT	Drury & Sons Ltd
RNA	EqDB5	Equine	MN	5	Normal SDFT	Drury & Sons Ltd
RNA	EqDB6	Equine	F	11	Normal SDFT	Drury & Sons Ltd
2D, 3D, ICC, RNA	EqDB7	Equine	MN	5	Normal SDFT	Drury & Sons Ltd
RNA	EqDB8	Equine	MN	4	Normal SDFT	Drury & Sons Ltd
2D, 3D, RNA	EqDB9	Equine	F	12	Normal SDFT	Drury & Sons Ltd
2D, 3D, RNA	EqDB10	Equine	F	18	Normal SDFT	Drury & Sons Ltd
2D, RNA	EqDB11	Equine	F	3	Normal SDFT	Drury & Sons Ltd

Table 2.4 continues overleaf

Use	Sample name	Organism	Sex	Age	Status	Source
2D, 3D, RNA	EqDB12	Equine	F	8	Normal SDFT	Drury & Sons Ltd
RNA	EqDB13N	Equine	MN	Aged	Normal SDFT	Drury & Sons Ltd
RNA	EqDB13D	Equine	MN	Aged	Diseased SDFT	Drury & Sons Ltd
RNA	EqDB14	Equine	MN	4	Normal SDFT	Drury & Sons Ltd
RNA	EqDB15	Equine	F	6	Normal SDFT	Drury & Sons Ltd
RNA	EqDB16	Equine	F	16	Normal SDFT	Drury & Sons Ltd
RNA	EqDB17	Equine	MN	17	Normal SDFT	Drury & Sons Ltd
2D, RNA	EqDB18	Equine	MN	9	Normal SDFT	Drury & Sons Ltd
RNA	EqDB19	Equine	MN	15	Normal SDFT	Drury & Sons Ltd
RNA	EqDB20	Equine	F	20	Normal SDFT	Drury & Sons Ltd
RNA	EqDB21	Equine	MN	9	Normal SDFT	Drury & Sons Ltd
RNA	EqDB22	Equine	MN	9	Normal SDFT	Drury & Sons Ltd
RNA	EqDB23	Equine	MN	5	Normal SDFT	Drury & Sons Ltd
3D, RNA	EqDB24	Equine	F	9	Normal SDFT	Drury & Sons Ltd
RNA	EqDB25	Equine	MN	4	Normal SDFT	Drury & Sons Ltd
RNA	EqDB26	Equine	MN	16	Normal SDFT	Drury & Sons Ltd
RNA	EqDB27	Equine	F	15	Normal SDFT	Drury & Sons Ltd
RNA	EqDB28	Equine	MN	13	Normal SDFT	Drury & Sons Ltd
RNA	EqDB29	Equine	F	14	Normal SDFT	Drury & Sons Ltd
RNA	EqDB30	Equine	MN	3	Normal SDFT	Drury & Sons Ltd
RNA	EqDB31	Equine	F	5	Normal SDFT	Drury & Sons Ltd
RNA	EqDB32	Equine	MN	25	Normal SDFT	Drury & Sons Ltd
RNA	EgDB33	Equine	ME	5	Normal SDFT	Drury & Sons Ltd
RNA	EqDB34	Equine	F	9	Normal SDFT	Drury & Sons Ltd
RNA	EqDB35	Equine	MN	19	Normal SDFT	Drury & Sons Ltd
RNA	EqDB36	Equine	F	22	Normal SDFT	Drury & Sons Ltd
RNA	EqDB37	Equine	MN	21	Normal SDFT	Drury & Sons Ltd
RNA	EqDB37	Equine	MN	21	Diseased SDFT	Drury & Sons Ltd
RNA	EqDB38	Equine	F	15	Normal SDFT	Drury & Sons Ltd
RNA	EqDB39	Equine	F	5	Normal SDFT	Drury & Sons Ltd
RNA	EqDB40	Equine	MN	9	Normal SDFT	Drury & Sons Ltd

**Table 2.4** (includes preceding page) **Details of 53 equine superficial digital flexor tendon (SDFT) samples utilised in various aspects of this study.** All horses were euthanised for reasons unrelated to this study and tissue acquired from fresh abattoir material. SDFT = superficial digital flexor tendon; NR = not recorded; ME = male entire; MN = male neutered; F = female; Age given in years; RNA = RNA extraction; ICC = immunocytochemistry; 2D = monolayer cell culture; 3D = tissue-engineered tendon construct.

Samples EqDB1 - EqDB40 (listed in Table 2.4) were collected and processed by the author. Samples H1, H2, H3, H16, H18, H23, H24, H27, H47, H52 and H62 (listed in Table 2.4) were provided by Professor Mandy Peffers, from the University of Liverpool Veterinary School Musculoskeletal

Biobank. RNA extraction was performed by Miss Roisin Wardle and RNA made available for use in this study.

## **2.2 Primary tenocyte isolation**

### **2.2.1 Cell culture media**

#### **Tenocyte culture medium (TCM; TCM-NOFBS without foetal bovine serum)**

To 500 mL DMEM low glucose (1 g L<sup>-1</sup>) phenol red free media (Life Technologies 11880-036), was added:

- 1 mL Amphotericin B 250 µg mL<sup>-1</sup> (ThermoFisher 15290026)
- 5 mL Penicillin-Streptomycin (contains 10,000 U penicillin + 10 mg streptomycin mL<sup>-1</sup>; Sigma P4333-20ML)
- 5 mL L-glutamine solution 200 mM (Sigma G7513-20ML)
- 50 mL Foetal Bovine Serum (Life Technologies 10270106)

Final medium composition: 100 U mL<sup>-1</sup> penicillin, 0.1 mg mL<sup>-1</sup> streptomycin, 0.5µg mL<sup>-1</sup> amphotericin B and 2 mM L-glutamine +/- 10% Foetal Bovine Serum.

NOTE – using phenol red free media will permit fluorescence microscopy.

#### **Freezing medium (FM)**

Foetal bovine serum to which was added 10% by volume DMSO (Sigma-Aldrich D8418)

### **2.2.2 Equine primary tenocyte isolation protocol**

Materials required:

- Sterile 60 mm Petri dishes
- Scalpel blades
- Rat tooth forceps
- Collagenase type II (ThermoFisher 17101015)
- Powdered trypsin (Sigma T4799-5G – lyophilised trypsin from porcine pancreas)
- TCM
- TCM-NOFBS
- DPBS (Sigma-Aldrich D8537)
- 50 mL Falcon centrifuge tubes
- 70 µm cell strainers
- Rotating/shaker incubator set at 37°C
- Haemocytometer
- Trypan Blue solution 0.4% (Sigma-Aldrich T8154)
- FM and cryogenic vials or culture flasks/plates

Work in Class II biological safety cabinet.

Cut up tendon tissue as finely as possible (approximately 2 mm x 2 mm x 2mm cubes) using a scalpel blade.

Place in 50 mL Falcon tube.

Incubate with 20-30 mL TCM-NOFBS containing 0.1% (1 mg mL<sup>-1</sup>) collagenase type II in rotating incubator at 37°C for 20-24 hours.

Centrifuge (260 g for 15 minutes) and remove supernatant.

Re-suspend in 20-30 mL TCM-NOFBS containing 0.4% (4 mg mL<sup>-1</sup>) collagenase type II.

Incubate at 37°C for 4 hrs (rotating incubator).

Centrifuge (260 g for 15 minutes) and remove supernatant.

Re-suspend in 20-30 mL DPBS to wash.

Centrifuge (260 g for 15 minutes) and remove supernatant.

Re-suspend in 20-30 mL TCM-NOFBS containing 0.25% (2.5 mg mL<sup>-1</sup>) trypsin.

Place in rotating incubator at 37°C for 1 hour.

Centrifuge (260 g for 15 minutes) and remove supernatant.

Re-suspend in 20-30 mL DPBS to wash.

Centrifuge (260 g for 15 minutes) and remove supernatant.

Re-suspend in 5-10 mL TCM.

Pass through 70 µm cell strainer to remove undigested tissue debris and produce single cell suspension – may need to flush through strainer with extra TCM.

Count cells and assess viability (Trypan Blue exclusion), freeze, or seed onto T75 or T175 uncoated culture flask, as appropriate.

### **2.2.3. Human primary tenocyte isolation protocol**

Attempts at tenocyte isolation by digestion (as employed with equine tenocytes) failed to yield any viable cells. Tenocyte isolation was performed using an explant method.

Materials required:

- Sterile 60 mm Petri dishes for cutting samples in
- Sterile culture flasks or 6 well plates
- Scalpel blades
- Rat tooth forceps
- DPBS (Sigma-Aldrich D8537)
- TCM
- Serological pipettes and filling gun
- TrypLE Select Enzyme (1x) (Life Technologies 12563029)
- Haemocytometer
- Trypan Blue solution 0.4% (Sigma-Aldrich T8154)
- FM and cryogenic vials or culture flasks/plates

Remove adherent muscle and peritendinous tissue from sample.

Wash in DPBS and weigh sample.

Cut up tendon tissue as finely as possible (approximately 2 mm x 2 mm x 2 mm cubes) and seed into culture flask or 6 well plate containing TCM.

Change media every 2-3 days.

Once tenocytes are visible adjacent to tissue pieces and adherent to vessel surface, remove tissue from culture vessel (aspirate with media using serological pipette).

Continue media changes every 2-3 days until cells reach 75-80% confluence.

Dissociate cells, count and assess viability (Trypan Blue exclusion test) prior to re-seeding or freezing as appropriate (see 2.3.1).

## **2.3 Monolayer cell culture techniques**

### **2.3.1 Monolayer culture**

For cell amplification purposes, tenocytes were seeded at approximately 4000 cells  $\text{cm}^{-2}$  into T75 or T175 culture flasks. For all experimental monolayer culture work, tenocyte seeding density was approximately 10,000  $\text{cm}^{-2}$  in 6 well plates (100,000 cells  $\text{well}^{-1}$ ) and 8,500  $\text{cm}^{-2}$  in 12 well plates (30,000 cells  $\text{well}^{-1}$ ).

Culture surface areas:

- 6 well plate = 9.6  $\text{cm}^2$   $\text{well}^{-1}$
- 12 well plate = 3.5  $\text{cm}^2$   $\text{well}^{-1}$

Cells cultured for immunocytology were seeded into 6 or 12 well plates containing laminin coated cover slips (see 2.3.2).

Equine and human tenocytes were cultured in phenol red free TCM in a 5%  $\text{O}_2$ , 5%  $\text{CO}_2$  atmosphere at 37°C. Medium was changed every 2-3 days, with dissociation of cells for re-seeding or freezing performed when cell growth had resulted in approximately 80% confluence. Dissociation was achieved using TrypLE Select (Life Technologies), a recombinant microbial produced trypsin replacement enzyme, according to the following protocol.

Remove media from culture vessel.

Add warmed DPBS (12 mL for T75, 25 mL for T175, 2 mL  $\text{well}^{-1}$  for 6 well plate), swirl and remove.

Add second aliquot DPBS, swirl and remove.

Add TrypLE Select solution:

- 5 mL T75 flask
- 8 mL T175 flask
- 1 mL  $\text{well}^{-1}$  6 well plate

Incubate at 37°C for 5-7 minutes.

Tap culture vessel sharply several times and view under microscope to confirm cell dissociation.

Add TCM to culture vessel to inactivate enzyme:

- 10 mL T75 flask
- 12 mL T175 flask
- 1 mL  $\text{well}^{-1}$  6 well plate

Aspirate vessel contents and transfer to 15 mL or 50 mL centrifuge tube (combine cell suspensions where appropriate).

Centrifuge at 180 *g* for 5 minutes.

Discard supernatant and resuspend cell pellet in known volume of TCM (typically 5-10 mL).

Take 10  $\mu\text{L}$  of cell suspension and mix with 10  $\mu\text{L}$  Trypan Blue in 1.5 mL reaction tube.

Pipette 10  $\mu\text{L}$  of mix under cover slip of haemocytometer.

Count cells and determine percentage viability.

Then:

- Seed cells into new culture vessel for amplification or experiment
- Freeze
  - Re-centrifuge (180  $g$  for 5 minutes)
  - Remove supernatant
  - Resuspend cells in appropriate volume of FM and aliquot into 1.8 mL cryogenic vials (typically as aliquots of 500,000 or 1 million cells)

### 2.3.2 Laminin coating cover slips

Materials required:

- Laminin (Invitrogen 23017-015 natural mouse laminin 1.10  $\text{mg mL}^{-1}$  – stored at  $-80^\circ\text{C}$  – defrost laminin stock in fridge to prevent solidifying) - working solution 10  $\mu\text{g mL}^{-1}$  in DPBS (keep in fridge)
- Fine point forceps
- DPBS (Sigma-Aldrich D8537)
- (Sterile) 10 mm diameter cover slips (VWR 631-1576 microscope cover glasses)
- 6 or 12 well plates
- 1000  $\mu\text{L}$  and 100  $\mu\text{L}$  pipettes and tips

Work in Class II biological safety cabinet

Transfer coverslips into plate wells (ideally coverslips sterile, but incubate under UV in culture hood for 30 minutes per side otherwise).

Pipette laminin onto cover slip.

- 100  $\mu\text{L well}^{-1}$  for 12 well plate – place first drop onto coverslip and use this to drag coverslip to centre of well, then add remaining volume. Laminin bleb should form a convex meniscus on top of cover slip. If too great a volume used or meniscus breaks, coverslip will float on top of laminin.
- 500 – 1000  $\mu\text{L well}^{-1}$  for 6 well plate if using larger diameter coverslips or 2-3 x 10 mm cover slips well $^{-1}$ .

Incubate at  $37^\circ\text{C}$  for minimum 30 – 60 minutes.

If coverslip floating, turn over.

Aspirate laminin (can be stored at  $4^\circ\text{C}$  and re-used up to five times).

## **2.4 Three-dimensional equine tendon construct techniques**

### **2.4.1 Culture media and reagent preparation**

#### **Tenogenic culture medium (TGM; TGM-C once TGFβ3 has been added)**

To 500 mL tenocyte culture media (TCM – see 2.2.1) was added:

- 10 mg Aprotinin (Sigma A1153-10MG – from bovine lung) – add to 5 mL media then sterile (0.2 μm) filter before adding to rest of media.
- 29 mg Ascorbate-2-phosphate (Sigma A4544-25G – L-ascorbic acid) – add to 5 mL media then sterile (0.2 μm) filter before adding to rest of media.
- 5 mL Non-essential amino acids (100x) (Sigma M7145-100ML).
- 1 μL mL<sup>-1</sup> of 1 ng μL<sup>-1</sup> working solution TGFβ3 (R&D Systems 243-B3-002) - DO NOT ADD YET.

Calculate volume of medium required for batch of constructs being created and aliquot this volume to separate tube. To this add 1 μL mL<sup>-1</sup> of 1 ng μL<sup>-1</sup> working solution TGFβ3 (see below) just before use to achieve final concentration of 1 ng mL<sup>-1</sup> TGFβ3. This forms Tenogenic Complete Medium (TGM-C).

#### **TGFβ3 (R&D Systems 243-B3-002) reconstitution**

To a vial containing 2 μg TGFβ3 powder, add 100 μL 4 mM HCl containing 1 mg mL<sup>-1</sup> bovine serum albumin (BSA) to give stock solution\* of 20 μg mL<sup>-1</sup>.

Take 5 μL of 20 μg mL<sup>-1</sup> stock solution and add to 95 μL 4 mM HCl with 1 mg mL<sup>-1</sup> BSA to give a 1 ng μL<sup>-1</sup> working solution.

Aliquot in 1.5 mL reaction tubes and freeze at -20°C.

Add to TGM at 1 μL mL<sup>-1</sup> media to give 1 ng mL<sup>-1</sup> Tenogenic Complete Medium (TGM-C).

\*product supplied as lyophilised powder as CF (carrier free) or in combination with BSA as a stabiliser. Only need to add BSA if reconstituting CF formulation.

#### **Fibrinogen stock solution (20 mg mL<sup>-1</sup>) preparation protocol**

Materials required:

- DMEM low glucose (1 g L<sup>-1</sup>) medium (Life Technologies 11880-036) with no other additives. NOTE – using TGM may result in solution clotting during freeze/thaw cycle and failure to form adequate clot with construct. Can use DPBS (Sigma-Aldrich D8537), which will result in slightly less thrombin requirements (approx. 10 μL well<sup>-1</sup>, when optimising fibrinogen: thrombin ratios for constructs).
- 500 mg Fibrinogen (Sigma F8630-1G – from bovine plasma)
- 2 x 50 mL sterile Falcon tubes
- 0.2 μm Sartorius Minisart filters (Appleton Woods FC121 – cellulose acetate membrane). Do not use filters with PTFE membrane eg. VWR International – fibrinogen will clog membrane.
- 1.5 mL reaction tubes
- Needles and syringes

- Balance
- Cell culture hood
- Rotating plate (end-over-end) incubator or rotating plate in warm room.

Switch on rotating plate incubator and set temperature to 37°C.

Check balance is level and adjust if necessary. Press CAL, wait for balance to calibrate. Add empty 50mL falcon tube and tare.

Weigh out amount of fibrinogen required to make a 20 mg mL<sup>-1</sup> stock (e.g. 500 mg for 25 mL final volume) carefully into empty sterile 50 mL falcon tube – powder will stick to everything.

Record weight of fibrinogen.

In sterile cell culture hood transfer the volume of medium required to 50 mL Falcon tube containing the fibrinogen. *The fibrinogen will clump and sit on top of the medium and stick to the sides of the tube.*

Swirl gently (most of the fibrinogen will stay on top of the medium) and incubate at 37°C. Do not vortex the solution at any stage.

Place Falcon tube in rotating (end over end) incubator at 37°C (or use rotating plate in warm room). Check every 30 minutes until the fibrinogen is dissolved – may need to tap tube occasionally. After 4 hours the fibrinogen should be dissolved.

In the cell culture hood, sterile filter the fibrinogen stock solution using a syringe and 0.2 µm sterile disposable 'button' filter. Aliquot filtrate into 1.5 mL reaction tubes and store at -20°C.

*Each batch should be tested for the optimal amount of thrombin required when making constructs. (Similarly each batch of thrombin requires testing separately (see 'optimising fibrinogen/thrombin ratios for tendon constructs' below).*

### **Thrombin stock solution (200 U mL<sup>-1</sup>) preparation protocol**

Materials required:

- Thrombin (Sigma T4648-1KU – from bovine plasma)
- DMEM low glucose (1 g L<sup>-1</sup>) media (Life Technologies 11880-036) – with no other additives
- 0.2 µm Sartorius Minisart filters (Appleton Woods FC121) (or Sigma 16534K Minisart filters)
- 5 mL syringe and needle
- 1.5 mL reaction tubes and rack

Add 5 mL media to 1 KU vial of thrombin powder and ensure thoroughly mixed.

Sterilise by passing through 0.2  $\mu\text{m}$  filter and aliquot into 1.5 mL sterile reaction tubes and freeze at -20°C.

### Optimising fibrinogen/thrombin ratios for tendon constructs

Materials required:

- Cell culture hood
- 200  $\mu\text{L}$  and 1000  $\mu\text{L}$  pipettes and tips
- 6 well plate
- 7 mL Bijou tubes
- Fibrinogen 20  $\text{mg mL}^{-1}$  stock solution
- Thrombin 200 U  $\text{mL}^{-1}$  stock solution
- TGM-C (see 2.4.1)
- Ice tray

Work in Class II biological safety cabinet and keep tubes of stock solutions on ice.

In Bijou tube mix 400  $\mu\text{L}$  TGM-C with 100  $\mu\text{L}$  Fibrinogen 20  $\text{mg mL}^{-1}$  stock solution for each well (2400  $\mu\text{L}$  media : 600  $\mu\text{L}$  Fibrinogen solution for 6 well plate).

Pipette 500  $\mu\text{L}$  of this mix into each well.

Working one well at a time, optimal thrombin dose is established as follows:

- Mix 20  $\mu\text{L}$ \* Thrombin stock solution with 500  $\mu\text{L}$  TGM-C in a clean Bijou and pipette entire volume into first well, ensuring thorough mixing by pipetting with Fibrinogen/TGM-C solution already there.
- Rock plate backwards and forwards gently to ensure even covering of well floor and watch for setting. Needs to set fairly quickly but giving enough time to ensure even distribution within well. Looking for even, firm clot with no watery component and adherent to circumference without contracting.
- Repeat steps above, using increasing (or decreasing) volumes of Thrombin stock solution each time –\*suggest 20  $\mu\text{L}$ , 25  $\mu\text{L}$ , 30  $\mu\text{L}$ , 35  $\mu\text{L}$ , 40  $\mu\text{L}$  and 45  $\mu\text{L}$ .

## 2.4.2 Preparation of Sylgard™ 184 silicone elastomer plates

Materials required:

- Sylgard™ 184 silicone elastomer base (World Precision Instruments SYLG184)
- 5 mL serological pipettes and filling gun
- 50 mL Falcon tube
- 6 x 6 well plates
- Minutien insect pins (Fine Science Tools 26002-20)
- Size 0 (3.5 Metric) braided silk suture (Ethicon Mersilk)
- Forceps
- Ruler
- Permanent marker
- Rotor mixer
- Incubator (set to 60°C)
- Cell culture hood

Set incubator to 60°C.

Transfer 45 mL Sylgard™ base (highly viscous, easier to pour than pipette) to a 50 mL Falcon tube.

Add 5 mL of curing reagent and invert on a rotor mixer at room temperature for 10 minutes to ensure complete mixing.

Distribute Sylgard™ between six plates by pouring - equivalent to a depth of approximately 2 mm and a volume of 1.5 mL in each of 36 wells.

Replace lids on plates and cure at 55-60°C overnight.

### **Pinning construct anchors into Sylgard™ plates:**

On the underside of the plate mark two dots 1.25 cm apart in the middle of each well using a ruler and permanent marker pen.

Cut 0.8 cm pieces of suture (two for each well).

Place minutien insect pin through one end of the suture (braided suture easily unravels) and pin into the Sylgard™ over one of the dots.

Place a second pin through the other end of the suture in line with the dots but pointing towards the outside edge of the well.

Repeat for the other dot to produce two diametrically pinned lengths of suture material with a 1.2 cm gap between them (Figure 2.1).

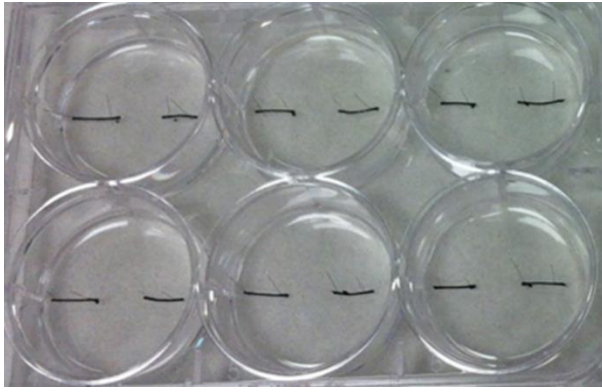


**Figure 2.1 Final appearance of six well plate with polymerised Sylgard™ 184 silicone elastomer coated base and pinned suture construct anchors in place.**

Store pinned plates at room temperature.

To sterilise plates, soak in 100% ethanol for 0.5-1.5 hours under UV light in cell culture hood.

Drain off excess ethanol in the hood.

Before use, rinse plates once in 5 mL DPBS for 5 minutes.

### 2.4.3 Tendon construct methodology

Materials required:

- TGM (3.5 mL construct<sup>-1</sup>)
- DPBS (Sigma-Aldrich D8537)
- TrypLE Solution
- Thrombin (200 U mL<sup>-1</sup> stock solution) – 35 µL construct<sup>-1</sup> \*
- Fibrinogen (20 mg mL<sup>-1</sup> stock solution) – 100 µL construct<sup>-1</sup>
- TGFβ3 (1 ng µL<sup>-1</sup> stock solution) – 3.5 µL construct<sup>-1</sup>
- Tenocyte suspension (600,000 cells construct<sup>-1</sup>, suspended in TCM)
- 10 µL, 100 µL and 1000 µL pipettes and tips
- 7 mL Bijou tubes (1 per construct)
- 15 mL centrifuge tubes
- 50 mL Falcon tubes
- Haemocytometer
- 1.5 mL reaction tubes and rack
- Trypan Blue solution 0.4%
- Cell culture hood
- Sylgard™ 6 well plates (pre-prepared - see 2.4.2)
- 5 mL and 10 mL serological pipettes and filling gun

Warmed to 37°C

Stock solutions (stored at -20°C) and defrosted on ice for use

\* volume of thrombin will vary depending on previous optimisation of thrombin:fibrinogen ratio (see 2.4.1).

Rinse Sylgard™ plates before use – 5 mL DPBS per well for 5 minutes.

To TGM, add 1  $\mu\text{L mL}^{-1}$  TGF $\beta$ 3 stock solution to make Tenogenic Complete Medium (TGM-C).

Aliquot a volume of TGM-C equivalent to 500  $\mu\text{L construct}^{-1}$  to a separate tube and add a volume of Thrombin stock solution equivalent to 35  $\mu\text{L}^*$   $\text{construct}^{-1}$ .

\* volume of thrombin will vary depending on previous optimisation of thrombin:fibrinogen ratio (see 2.4.1).

Drain DPBS from plate wells.

Add 535  $\mu\text{L}$  TGM-C/Thrombin mix to each well (volume will vary depending on volume of thrombin added after optimisation).

Spin down cells (180 *g* for 5 minutes) and resuspend in a volume of TGM-C equivalent to 400  $\mu\text{L construct}^{-1}$ , to make a suspension of  $1.5 \times 10^6$  cells  $\text{mL}^{-1}$ .

Make fibrinogen/cell suspension mix – do this individually for each construct as gel sets very quickly:

- Aliquot 400  $\mu\text{L}$  of cell suspension (equivalent to 600,000 cells) to clean Bijou tube
- Reset pipette to 500  $\mu\text{L}$ .
- Add 100  $\mu\text{L}$  Fibrinogen stock solution to cell suspension.
- Mix well and immediately pipette entire volume into well containing TGM-C/Thrombin solution.
- Mix well by pipetting up and down 2-3 times (Total volume =  $\sim 1$  mL fibrin gel/cell suspension per well).
- Move plate backwards and forwards rapidly to ensure mixture forms a flat layer covering the entire well floor and is in contact with the pins before the fibrin gel forms.

Incubate at 37°C for 5 minutes to set.

Repeat for each well required.

Add 2.5 mL TGM-C to each well.

Place in 37°C incubator (5% CO<sub>2</sub>, 5% O<sub>2</sub>).

Change media the following day and score carefully around the edge of each well with pipette tip to breakdown adhesions.

Change media every 2-3 days, scoring with pipette tip towards the middle of the well at every media change to break down adhesions to the well, until the gel has formed a linear construct – usually by 5-7 days.

Harvest constructs at 28 days and process as follows:

- Histology – make two cuts in the Sylgard™ base of each well parallel to the pinned construct using a scalpel blade. Remove constructs, still pinned to a strip of Sylgard™, from well, rinse briefly in DPBS and place in 7 mL Bijou tubes containing fixative:
  - 4% paraformaldehyde (Sigma 441244-1KG) for routine histology.
  - 2.5% glutaraldehyde (Taab Laboratories Equipment G002) in 0.1 M sodium cacodylate (Taab Laboratories Equipment S011) buffer for electron microscopy.
- RNA extraction – make two cuts in the Sylgard™ base of each well parallel to the pinned construct using a scalpel blade. Remove constructs, still pinned to a strip of Sylgard™, from well, rinse briefly in DPBS and place in 7 mL Bijou tubes containing RNA<sup>later</sup>® (Life Technologies AM7021). Following equilibration at 4°C overnight, remove anchor pins and suture material, blot constructs dry, weigh and place in 1.5 mL reaction tubes for storage at -80°C.
- Protein extraction – remove anchor pins, rinse constructs in DPBS, place in 1.5 mL reaction tubes and snap freeze in liquid nitrogen prior to storage at -80°C.

## 2.5 Cholesterol conjugated microRNA/oligonucleotide transfection

Dharmacon™ cholesterol conjugated oligonucleotides were obtained from GE Healthcare Ltd, Little Chalfont UK. Sequence details and modifications are given in Table 2.5.

Product Description	Modifications	Sequence
<u>miR-181 Mimic</u> Modified catalogue product C-310435-05 miRIDIAN microRNA mimic mmu-miR-181a-5p (MIMAT0000210)	miRIDIAN mimic 5'Cholesterol on passenger strand; 3'Cy5 on guide strand	5'- AACAUUCAACGCUGUCGGUGAGU -3'
<u>miR-181 antagomiR</u> ssRNA-23 mer	5' Fluorescein 23 x Methoxys 6 x Phosphorothioates 3' Cholesterol	5'- Fl - mA*mC*mUmCmAmCmCmGmAmCmAm GmCmGmUmUmGmAmA*mU*mG*mU* mU-Cholesterol-3'
<u>Scrambled control sequence</u> ssRNA-21 mer	21 x Methoxys 6 x Phosphorothioates 3' Cholesterol	5' - mC(*)mA(*)mGmUmAmCmUmUmUmUm GmUmGmUmAmGmUmA(*)mC(*)mA(*) mA-Cholesterol-3'

**Table 2.5 Sequences and modifications of Dharmacon™ cholesterol conjugated oligonucleotides utilised in this study.** \* = phosphorothionate modified nucleotide; m = 2'-O-methylation modified nucleotide

Manufacturer supplied, concentrated oligonucleotides were diluted with RNase free water according to manufacturer's siRNA resuspension protocol to produce a stock solution of 100 µM. Final concentration was verified spectrophotometrically by measuring absorbance at 260 nm (A260) (Nanodrop 2000; ThermoScientific), then calculating concentration using Beer's Law, according to:

$A_{260} = \epsilon CL$  where  $\epsilon$  is the extinction coefficient (from the Product Transfer Form), C is the siRNA concentration, and L is the path length.

Therefore  $C = A_{260}/\epsilon L$

Stock solutions were stored in aliquots in 0.2 mL PCR tubes at -20°C and defrosted on ice immediately prior to use. Working solutions were produced by further dilution in either TCM (monolayer cultures) or TGM-C (3D constructs) according to:

- Mimic and scrambled control - 100 nM - equivalent to 1 µL stock solution mL<sup>-1</sup> medium
- AntagomiR - 200 nM - equivalent to 2 µL stock solution mL<sup>-1</sup> medium

### 2.5.1 Treatment protocol for monolayer cultures

Each treatment was duplicated for each biological replicate.

Materials required:

- Dissociated tenocytes suspended in TCM at known concentration
- TCM
- 6 or 12 well cell culture plates
- 10 $\mu$ L, 200  $\mu$ L and 1000  $\mu$ L pipettes and tips
- 100  $\mu$ M stock solutions of mmu-miR-181a-5p mimic, antagomiR and scrambled control oligonucleotides defrosted on ice
- Cell culture hood
- 30 mL or 60 mL tubes

#### Day 1

Seed cells into plate wells:

- 6 well plate - 100,000 cells per well
- 12 well plate – 30,000 cells per well

Add additional TCM if needed.

Incubate plates overnight at 37°C in a 5% O<sub>2</sub>, 5% CO<sub>2</sub> atmosphere.

#### Day 2

Prepare 3 aliquots of TCM of appropriate volume for transfection (6 well plate = 2 mL well<sup>-1</sup>; 12 well plate = 1 mL well<sup>-1</sup>).

To one aliquot add 1  $\mu$ L mL<sup>-1</sup> 100  $\mu$ M mimic stock solution = 100 nM.

To one aliquot add 2  $\mu$ L mL<sup>-1</sup> 100  $\mu$ M antagomiR stock solution = 200 nM.

To one aliquot add 1  $\mu$ L mL<sup>-1</sup> 100  $\mu$ M scrambled control stock solution = 100 nM.

Aspirate TCM from wells and replace with appropriate treated TCM.

Return plates to incubator.

#### Day 3

Can check uptake of mimic and antagomiR treatments under fluorescence microscope (uptake in 50% of cells is good enough).

#### Day 4

Proceed to RNA extraction (see 2.8.3), protein extraction (see 2.13.1) or immunocytochemistry (see 2.7).

### **2.5.2 Treatment protocol for three-dimensional tendon constructs**

Tenocytes were seeded into a fibrin gel matrix (see 2.4.3). Twenty four hours after seeding, at the first media change, TGM-C was replaced with TGM-C spiked with either mmu-miR-181a-5p mimic, antagomiR or scrambled control oligonucleotide at the concentrations specified above. Treatment was repeated at every subsequent media change until constructs were harvested at 28 days.

## **2.6 CCCP assay for induced autophagy/mitophagy**

Carbonyl cyanide m-chlorophenylhydrazone (CCCP) is a protonophore ( $H^+$  ionophore), causing uncoupling of the proton gradient that is established during the normal activity of electron carriers in the mitochondrial electron transport chain, reducing the ability of ATP synthase to function optimally. It also has a number of effects on cellular calcium.

Materials required:

- Cell cultures (12 well plates)
- CCCP 20 mM stock solution thawed on ice (C2759 Sigma-Aldrich; Molecular weight 204.62, powder for reconstitution in DMSO)
- TCM
- DMSO (D8418 Sigma-Aldrich Dimethyl sulfoxide for molecular biology)
- 10  $\mu$ L, 200  $\mu$ L and 1000  $\mu$ L pipettes and tips
- 7 mL Bijou tubes

### **Optimising time and concentration variables for tenocyte exposure to CCCP**

Three experiments were run to optimise CCCP concentration and time of exposure consistent with highest concentration compatible with cell survival and assessed by immunocytochemistry against two target proteins TOMM20 and P62/SQSM1:

- 1) 10 or 20  $\mu$ M CCCP solution for 4 or 6 hours
- 2) 20  $\mu$ M CCCP solution for 8 hours
- 3) 20  $\mu$ M CCCP solution for 1, 2, 3, 4, 5 and 6 hours

Calculate volumes of CCCP/DMSO dilutions needed (1 mL well<sup>-1</sup> for 12 well plate).

Make up required CCCP dilutions and DMSO equivalents in Bijous:

- For 10  $\mu$ M CCCP solution, add 0.5  $\mu$ L 20 mM stock mL<sup>-1</sup> media.
- For 20  $\mu$ M CCCP solution, add 1  $\mu$ L 20 mM stock mL<sup>-1</sup> media.
- For DMSO controls, add equivalent volume DMSO mL<sup>-1</sup> media.

Aspirate media from wells and add 1 mL appropriate CCCP dilutions to each designated well.

Three sets of control wells were prepared:

- Equivalent DMSO concentration for subsequent incubation with primary antibody.
- DMSO control wells of equivalent concentration for subsequent incubation without primary antibody.
- Untreated controls (TCM only).

Return plates to incubator for designated time prior to immunocytochemical analysis (see 2.7).

## **2.6.1 CCCP treatment protocol for miR-181-treated tenocytes**

### **Day 1**

Seed cells into plate wells:

- Protein extraction
  - 6 well plate – 100,000 cells per well = 1.2 million cells per donor (2 plates per donor).
  - Add 2 mL culture media.
- RNA extraction or immunocytochemistry
  - 12 well plate – 30,000 cells per well = 360,000 cells per donor (1 plate per donor).
  - Add 1.5 mL culture media.

### **Day 2**

Change media – replace with mmu-miR-181a-5p mimic, antagomiR and scrambled control oligonucleotide treated TCM (see 2.5.1):

- 6 well plate - 2 mL well<sup>-1</sup>
- 12 well plate - 1 mL well<sup>-1</sup>

### **Day 3 (24hrs after transfection)**

Treat with CCCP to achieve 20  $\mu$ M concentration:

- 6 well plate - add 2  $\mu$ L 20mM CCCP stock solution or DMSO.
- 12 well plate – add 1  $\mu$ L 20mM CCCP stock solution or DMSO.

NOTE: Add CCCP/DMSO stock solutions directly to mmu-miR-181a-5p mimic, antagomiR and scrambled control oligonucleotide treated TCM already in wells.

Return plates to incubator for 6 hours.

Proceed to RNA extraction (see 2.8.3), protein extraction (see 2.13.1) or immunocytochemistry (see 2.7).

## 2.7 Immunocytochemistry

Materials required:

- Cell cultures
- Methanol -pre-chilled in -40°C freezer (Fisher Scientific M/4000/15)
- Relevant primary antibodies (defrosted on ice)
- Relevant secondary antibodies (in fridge at 4°C)
- DAPI diluted in DPBS 1:10,000 (Sigma-Aldrich D9542-1MG; DAPI powder, reconstituted in DPBS (Sigma-Aldrich D8537) to 1 mg mL<sup>-1</sup> stock solution. Add 1 µL to 10 mL DPBS to achieve working solution.
- Hydromount® (National Diagnostics HS-106)
- 10 µL, 200 µL, and 1000 µL pipettes and tips
- Serological pipettes and filling gun
- Glass microscope slides
- DPBS (Sigma-Aldrich D8537)
- Bovine Serum Albumin (Sigma-Aldrich A2153; lyophilised powder ≥96% (agarose gel electrophoresis).
- Horse serum (ThermoFisher Scientific (Gibco™) 16050122; horse serum New Zealand origin)
- Glycine (Sigma-Aldrich G8898; glycine powder for electrophoresis ≥99%).
- Tween® 20 (Sigma-Aldrich P1379; non-ionic detergent).

Make up blocking solution:

1% (10 mg mL<sup>-1</sup>) BSA

10% horse serum

0.3 M glycine (75.07g mol<sup>-1</sup> ≡ 22.52mg mL<sup>-1</sup>)

0.1% DPBS-Tween

DPBS

To 100 mL DPBS add:
1 g BSA
10 mL horse serum
2.2521 g glycine
100 µL Tween 20®

Remove media from wells.

Wash with DPBS and remove.

Fix in ice cold methanol for 5 minutes – put on rocker at room temperature.

Remove methanol and wash with DPBS.

Remove DPBS and add 500 µL blocking solution per well (12 well plate).

Incubate in blocking solution for 1 hour on rocker at room temperature.

Dilute primary antibodies in blocking solution:

- anti-TOMM20 (ab186734 rabbit) use at 1:75 dilution
- anti-TOMM20 (ab56783 mouse) use at 1:75 dilution
- anti-LC3B (ab192890 rabbit) use at 1:100 dilution
- anti-p62/SQSTM1 (ab109012 rabbit) use at 1:100 dilution
- anti-Parkin 1:100 (ab15954 rabbit) – discontinued
- anti-Parkin (ab77924 mouse) use at 1:100 dilution
- anti-Peroxiredoxin 6 (ab133348 rabbit) use at 1:100 dilution

Remove blocking solution from wells.

Add primary antibody diluted in blocking solution (100  $\mu\text{L}$  well<sup>-1</sup> for 12 well plate).

Incubate overnight on rocker in cold room (4°C).

Remove primary antibody (can be reused up to 5 times).

Perform 3 x 5 minute DPBS washes.

Dilute secondary antibody in blocking solution –150  $\mu\text{L}$  per well for 12 well plate - keep protected from light:

- Red (532) Goat anti-mouse IgG (Invitrogen A11002) use at 1:1000 dilution.
- Red (532) Goat anti-rabbit IgG (Invitrogen A11009) use at 1:1000 dilution.
- Green (488) Goat anti-rabbit IgG (Invitrogen A11008) use at 1:1000 dilution.

Incubate at room temperature for 1 hour - keep protected from light.

Remove secondary antibody – discard.

Perform 3 x 5 minute DPBS washes - keep protected from light.

Add 300  $\mu\text{L}$  DAPI: 1:10000 in DPBS, incubate for 10 minutes at room temperature - keep protected from light.

Remove DAPI – discard.

Wash in DPBS for 10 minutes at room temperature - keep protected from light.

Mount in Hydromount:

- Spot Hydromount onto glass slide.
- Take cover slip out of well, turn over and mount face down on glass slide.

Cure overnight at room temperature - keep protected from light.

Store at 4°C - keep protected from light.

(Dilutions: 1:100 = 10  $\mu\text{L}$  mL<sup>-1</sup>; 1:1000 = 1  $\mu\text{L}$  mL<sup>-1</sup>; 1:10000 = 1  $\mu\text{L}$  10mL<sup>-1</sup>)

For antibodies to be used on samples of unproven reactivity, check antigenic conservation with species of interest. Specific antibody data sheet should give amino acid sequence of the antigen (immunogen) which the antibody was raised against (may be a short sequence, or whole peptide as antigen used to raise antibody).

Data sheet may have a direct link to NCBI BLAST for relevant sequence – if so click on this. Page listing ‘Sequences producing significant alignments’ will open. Scroll down to find species of interest and click on it to access sequence comparison and identity.

If the UniProt protein identifier is given, click on this to open Uniprot page and scroll down to find ‘Sequence’ section. This will give the amino acid sequence of the protein. To the left of the sequence box is a link to BLAST; click on GO button. Alignments with various species will come up; scroll down to find species of interest and click on ‘View alignment’ link. Detailed report of sequence and identity will open.

## **2.8 RNA extraction**

### **2.8.1 RNA extraction protocol for equine and human tendons**

Materials required:

- Tendon samples in liquid nitrogen or on dry ice
- BBraun MIKRO-DISMEMBRATOR U
- Sample capsules and ball bearings for above
- Clean Dewar of liquid nitrogen
- Long handled haemostats with locking ratchet for liquid nitrogen immersion
- 60 mm diameter Petri dishes
- Scalpel blades
- Fine point forceps
- 1000 µL pipette and tips
- 1.5 mL reaction tubes and rack
- 7 mL Bijou tubes
- 70% ethanol and 1% Distel to clean surfaces and instruments
- Tissue lysis buffer (from MirVana™ kit)

Ensure appropriate PPE available for liquid nitrogen work.

Switch on dismembrator and set to 2000 rpm and 1 minute 30 seconds.

Weigh sample – aim for approximately 100 mg tissue.

Place in Petri dish and chop finely (approximately 2 mm x 2 mm x 2 mm cubes).

Transfer to dry 7 mL Bijou tube and drop into liquid nitrogen.

Grasp dismembranator capsule body and lid with long handled haemostats (ensure ball bearing is in body of capsule) and lower into liquid nitrogen.

When boiling stops, remove capsule and drain excess liquid nitrogen, taking care ball bearing does not get lost.

Place on work surface – work quickly during this stage to minimise warming of capsule and sample.

Remove Bijou containing sample from liquid nitrogen and tap sharply on work surface 3-4 times to loosen sample. Transfer sample to body of dismembranator capsule.

Push lid firmly on to capsule body and place in dismembranator clamp.

Switch on dismembranator – hold machine whilst running to reduce noise and vibration.

Remove capsule from dismembranator and tap sharply on work surface 3-4 times to move sample to base of capsule.

Open capsule and add lysis buffer:

- Equine – 1500  $\mu$ L for 100 mg tendon tissue results in fairly good solution, will fit easily into capsule and resulting solution will just fit into a 1.5 mL reaction tube.
- Human – 1 mL lysis buffer per 100 mg powdered tissue.

Lysis buffer will freeze. Replace lid on capsule and leave to thaw.

Process next sample/s.

When all samples have been processed to the stage they are in lysis buffer, pipette solutions vigorously to ensure completely solubilised and transfer to 1.5 mL reaction tubes.

Store at  $-80^{\circ}\text{C}$  or proceed to next stage of extraction (see 2.8.4 MirVana™ RNA extraction protocol).

## **2.8.2 RNA extraction protocol for equine tenocyte constructs**

Materials required:

- Construct samples (previously weighed)
- Mortar and pestle
- 2 clean Dewar flasks of liquid nitrogen
- Long handled haemostats with locking ratchet for liquid nitrogen immersion
- Dipping beaker for liquid nitrogen
- Narrow blade spatula
- Fine point forceps
- 60 mm diameter Petri dish to use as sterile instrument tray
- 1000  $\mu$ L pipette and tips
- 1.5 mL reaction tubes and rack
- 70% ethanol and 1% Distel to clean surfaces and instruments
- Tissue lysis buffer (from MirVana™ kit)

Ensure appropriate PPE available for liquid nitrogen work.

Transfer samples to dry reaction tube and drop into liquid nitrogen in one Dewar.

Using long handled haemostats and dipping beaker, pour liquid nitrogen from second Dewar into mortar to cool mortar and pestle – the colder these are, the easier processing will be; work quickly during this stage to minimise warming of mortar, pestle and sample.

Remove reaction tube containing sample from liquid nitrogen, pinch hinge between thumb and forefinger for a few seconds to prevent hinge snapping when tube opened and tap sharply on work surface to loosen sample.

Transfer sample to mortar whilst still some liquid nitrogen left.

Grind sample using pestle – may add more liquid nitrogen to mortar to keep cold.

CARE – sample is very brittle and can easily be lost from mortar unless broken up gently.

Add 500 µL lysis buffer (kit instructions recommend 10x volumes of lysis buffer per tissue mass).

Lysis buffer will freeze – continue to grind to reduce to powder.

Immerse one end of spatula in liquid nitrogen. When boiling stops, remove spatula and use to scrape frozen powder from mortar and pestle and transfer into 1.5 mL reaction tube.

As mortar warms, powder will turn to sludge, then liquid. Use pipette to suck up residual sample and pipette vigorously to mix thoroughly in reaction tube.

Clean mortar and pestle and any instruments used with 1% Distel then 70% ethanol prior to processing next sample.

Transfer reaction tube to liquid nitrogen / -80°C freezer or proceed to next stage of extraction (see 2.8.4 MirVana™ RNA extraction protocol).

### **2.8.3 RNA extraction protocol for monolayer cell cultures**

Materials required:

- Cell cultures (6 or 12 well plates)
- 1000 µL pipettes and tips
- DPBS - cold from fridge (Sigma-Aldrich D8537)
- Lysis buffer (from MirVana™ kit)
- Cell scrapers (Sarstedt 83.1830)
- Ice tray
- 1.5 mL reaction tubes and rack

Aspirate and discard culture medium.

Wash with DPBS and place culture plate on ice.

Remove DPBS and add 600µL lysis buffer (from MirVana™ kit) per well (12 well plate).

Collect lysate with cell scraper and transfer to labelled 1.5 mL reaction tube.

Pipette vigorously to ensure complete lysis.

Transfer reaction tube to liquid nitrogen / -80°C freezer or proceed to next stage of extraction (see 2.8.4 MirVana™ RNA extraction protocol).

### **2.8.4 MirVana™ RNA extraction protocol**

The MirVana™ RNA extraction kit is designed to prevent loss of small RNAs during processing. The protocol for total RNA retrieval without small RNA enrichment was followed.

Materials required:

- MirVana™ miRNA Isolation Kit (Invitrogen AM1560) contains:
  - Sample tubes and filters at room temperature
  - Acid-Phenol:Chloroform at 4°C
  - Homogenate Additive at 4°C
  - Wash Solution 1 and 2/3 at room temperature
  - Elution Solution (or use RNase free water) at 95°C
- Heating block set to 95°C
- Molecular grade ethanol (100%) at room temperature (Sigma-Aldrich 51976-500ML-F)
- 100 µL pipette and tips
- 1000 µL pipette and tips
- 1.5 mL reaction tubes and rack

Transfer sample/lysis buffer solution to clean 1.5 mL reaction tube:

- 600 µL for tendon tissue - aliquot any surplus solution into separate reaction tubes and freeze at -80°C.
- 500 µL for tendon constructs – entire volume.
- 600 µL Cell culture (12 well plate)

Add Homogenate Additive:

- 60 µL per sample (tendon tissue)
- 50 µL per sample (tendon construct) (10% of sample volume)
- 60 µL Cell culture (from 12 well plate)

Vortex briefly to mix.

Incubate on ice for 10 minutes.

In fume hood add Acid-Phenol:Chloroform:

- 600  $\mu\text{L}$  (tendon tissue) = same volume as original sample.
- 500  $\mu\text{L}$  (tendon construct) = same volume as original sample.
- 600  $\mu\text{L}$  cCell monolayer culture (12 well plate).

Vortex tubes for 60 seconds.

Centrifuge at room temperature at 10,000  $g$  for 10 minutes to separate phases.

Transfer top aqueous phase to clean 1.5 mL reaction tube and note volume removed (approximately 350 – 400  $\mu\text{L}$  yield from 500  $\mu\text{L}$  original sample volume).

Add 1.25 x harvested volume of 100% ethanol at room temperature (438  $\mu\text{L}$  ethanol for 350  $\mu\text{L}$  sample volume; 500  $\mu\text{L}$  ethanol for 400  $\mu\text{L}$  sample volume).

Place filter cartridge into new sample tube (from kit) for each sample.

Pipette sample/ethanol mix into filter cartridge, this can hold maximum 700  $\mu\text{L}$  at a time (from 400  $\mu\text{L}$  sample + 1.25 x  $\mu\text{L}$  ethanol = ~900  $\mu\text{L}$  – will need to add in 2 stages).

Centrifuge tubes at room temperature at 10,000  $g$  for 30 seconds.

Discard flow through, repeat with any residual sample volume and discard second flow through.

Using the same collection tube, replace filter cartridge and add 700  $\mu\text{L}$  Wash Solution 1 into filter cartridge.

Centrifuge at room temperature at 10,000  $g$  for 30 seconds.

Discard flow through, replace filter cartridge in same tube and add 500  $\mu\text{L}$  Wash Solution 2/3.

Centrifuge at room temperature at 10,000  $g$  for 30 seconds.

Discard flow through, replace filter cartridge and add second 500  $\mu\text{L}$  volume of Wash Solution 2/3

Centrifuge at room temperature at 10,000  $g$  for 30 seconds.

Discard flow through, replace filter cartridge and re-centrifuge for 1 minute at room temperature at 10,000  $g$  to remove all residual fluid from cartridge.

Transfer filter cartridge to clean sample tube (from kit).

Add 100  $\mu\text{L}$  RNase free water (or use Elution Solution provided in kit) at 95°C.

Centrifuge at room temperature at 10,000  $g$  for 30 seconds.

Remove filter cartridge and dispose.

Eluate contains RNA which can then be stored at -80°C.

## **2.9 RNA quantification and quality assessment**

### **2.9.1 Agarose gel electrophoresis**

Materials required:

- RNA samples defrosted on ice (can also use PCR products to check primer integrity).
- Agarose powder (Sigma-Aldrich A9639-100G)
- Midori green DNA stain (Geneflow S6-0016)
- 6x Blue loading dye
- 1L 1x TAE (Tris/Acetic acid/EDTA) buffer - autoclaved to ensure RNase free (diluted from 50x TAE Buffer, Bio-Rad 1610743)
- 250 mL conical flask
- 1 L beaker
- 0.2 mL PCR tubes
- 10  $\mu$ L pipette and tips
- Microwave oven
- Gel unit (horizontal) (Geneflow G9-0036)

Place autoclave tape across 2 sides of tank tray to contain gel.

Weigh out 1.0 g agarose powder (to make 100 mL 1% w/v gel).

Mix agarose with 100 mL TAE buffer in conical flask.

Microwave to dissolve agarose – swirl flask regularly to ensure mixing (solution may well boil).

Allow to cool slightly, add 10  $\mu$ L Midori green DNA stain and mix well.

Pour into gel tray and place comb to create wells.

Mix samples with loading dye in PCR tubes:

1 $\mu$ L RNA sample
1 $\mu$ L loading dye
4 $\mu$ L RNase free water
(Load all into well)

5 $\mu$ L PCR products
1 $\mu$ L loading dye

Mix same volumes and ratios of ladder:dye as sample:dye.

Mix well.

Centrifuge to collect all liquid in bottom of tubes.

Remove autoclave tape from gel tray once gel set.

Place gel tray in tank and pour over the rest of the TAE buffer to cover the gel (will take all the remaining buffer).

Remove comb from gel.

Load sample/dye mix into wells in gel – do this gently to avoid damaging wells and ensure mix stays within the well.

Put lid on tank.

Attach leads (red-red; black-black).

Switch on power supply.

Ensure set to Volts not mA.

Set voltage using up/down arrows (70 – 90V).

Press run.

## 2.9.2 Nanodrop 2000 spectrophotometry

Materials required:

- RNA samples defrosted on ice
- RNase free water (and buffer used to elute RNA into, if different)
- 10 µL pipette and tips
- Lint-free tissue
- NanoDrop 2000 spectrophotometer (ThermoFisher Scientific)

Open Nanodrop software.

Click on 'Nucleic Acid' application (top left of options).

(Automatic dialogue box may open requesting wave length verification – if so ensure sample pedestal and sampling arm contact are clean, close arm and click 'OK').

Open drop down menu in 'Type' box (top right of screen) and select 'RNA' (the number 40 should appear in the box immediately to the right).

Ensure that 'Add to report' box is ticked (top of right hand panel, under 'Measure' icon).

Clean NanoDrop pedestal and sampling arm contact with RNase free water and lint-free tissue.

Pipette 1 µL RNase free water (or elution buffer) onto pedestal and close arm.

Click on 'Blank' (top left of screen) – Blank must be measured before sample.

Wipe pedestal/sampling arm contact clean.

Pipette 1 µL sample onto pedestal and close arm.

Type sample ID into 'Sample ID' box top right of screen.

Click on 'Measure' (top left of screen).

When measurement completed, graph displays absorbance spectrum between 220 and 350 nm. RNA concentration ( $\text{ng } \mu\text{L}^{-1}$ ), absorbance at 260 nm ( $A_{260}$ ), 280 nm ( $A_{280}$ ), ratio of absorbance at 260 and 280 nm ( $260/280$ ) and 260 and 230 nm ( $260/230$ ) are reported.

Absorbance (A) is calculated as  $A = -\log(\text{Intensity}_{\text{sample}} / \text{Intensity}_{\text{blank}})$ .

Note: device measures absorbance using a 1 mm path length, but reports absorbance characteristics normalised to a 10 mm path length.

Concentration is calculated using a modification of the Beer-Lambert equation  $c = A\epsilon/L$ , where  $c$  = concentration,  $A$  = absorbance,  $\epsilon$  = extinction coefficient (taken as  $40 \text{ ng-cm } \mu\text{L}^{-1}$ ),  $L$  = path length (in cm). RNA extinction coefficient automatically selected when inputting sample type before starting analyses.

Record results.

Wipe pedestal/sampling arm contact clean.

Repeat for each sample.

If measuring a lot of samples it is worth repeating the blank (manufacturer recommends doing this after 30 minutes) – can also measure blanking solution as a sample to check; reported absorbance characteristics should not vary by more than 0.04 A from original spectra. Also performing consecutive measurements on same sample periodically will check operational integrity (sample homogeneity and reproducibility of results).

### 2.9.3 TapeStation electrophoresis

Materials required:

- RNA samples – thawed on ice
  - RNA Screen Tapes and reagents, either:
    - RNA Screen Tape (Agilent Technologies 5067-5576) -
    - RNA Screen Tape Sample Buffer (Agilent Technologies 5067-5577)
    - RNA Screen Tape Ladder (Agilent Technologies 5067-5578)
- or:
- High Sensitivity RNA Screen Tape (Agilent Technologies 5067-5579)
  - High Sensitivity RNA Screen Tape Sample Buffer (Agilent Technologies 5067-5580)
  - High Sensitivity RNA Screen Tape Ladder ‡ (Agilent Technologies 5067-5581)
- Quantitative and RIN<sup>e</sup> \* functional range 25-500 ng  $\mu\text{L}^{-1}$
- Quantitative range 500-10,000 pg  $\mu\text{L}^{-1}$ , RIN<sup>e</sup> \* functional range 1000-25,000 pg  $\mu\text{L}^{-1}$

‡ requires dilution; add 10  $\mu\text{L}$  RNase free water to vial and vortex to mix

- Loading tips (Agilent Technologies 5067-5153)
- Optical tube strips (8x Strip) (Agilent Technologies 401428)
- Optical tube strip caps (8x Strip) (Agilent Technologies 401425)
- Vortex mixer with adapter for holding tubes (IKA Laboratory Equipment MS3 5067-5700/4674100)
- Heating block set to 72°C (Grant Instruments BTA)
- 10  $\mu\text{L}$  pipette and tips
- Ice tray
- Agilent 2200 Tape Station Instrument (Agilent Technologies)

\* RIN – RNA Integrity Number – an automatically calculated value to describe RNA integrity. Utilises an algorithm which incorporates the ratio of the areas under the 18S and 28S rRNA peaks on an electrophoretogram to the total area under the graph, the height of the 28S peak and the fast area (region between the 18S and 5S peaks) ratio (Schroeder et al 2006). RIN<sup>e</sup> – RNA Integrity Number equivalent; value derived using the relative ratio of the fast zone signal to the 18S peak signal (Agilent Technologies).

Equilibrate all reagents to room temperature and set heating block to 72°C.

Briefly vortex and centrifuge buffer and ladder tubes prior to use.

Add 5  $\mu\text{L}$  Sample Buffer (1  $\mu\text{L}$  if using High Sensitivity Buffer) to required number of tubes (no. of samples + 1).

Add 1  $\mu\text{L}$  RNA Ladder (2  $\mu\text{L}$  if using diluted High Sensitivity Ladder) to one tube.

Add 1  $\mu\text{L}$  RNA sample (2  $\mu\text{L}$  sample if using High Sensitivity reagents) to the remainder of tubes and cap tubes.

Briefly centrifuge tubes to collect contents at bottom.

Vortex tubes for 1 minute at 2000 rpm.

Briefly re-centrifuge samples.

Heat ladder and samples at 72°C for 3 minutes.

Place on ice for 2 minutes.

Re-centrifuge to ensure all sample at base of tubes.

Load samples, Screen Tape and loading tips into Tape Station 2200 instrument for analysis (can take 16 optical tubes per analysis run).

## **2.10 RNA-sequencing**

RNA was extracted from human tendon tissue derived from six patients with rotator cuff (supraspinatus tendon) tendinopathy and six patients undergoing anterior cruciate ligament reconstruction surgery (mixed semitendinosus and gracilis tendon). Details of these samples are given in Table 2.6.

Sample number	Sample name	Organism	Sex	Age	Status	Source
18139_7	0946/18 SSP	Human	F	39	Diseased	Glasgow
18139_8	0947/18 SSP	Human	F	39	Diseased	Glasgow
18139_9	0866/18 SSP	Human	M	51	Diseased	Glasgow
18139_10	0944/18 SSP	Human	M	50	Diseased	Glasgow
18139_11	0864/18 SSP	Human	M	59	Diseased	Glasgow
18139_12	0887/18 SSP	Human	F	45	Diseased	Glasgow
18139_13	LMB-KM-249	Human	M	31	Healthy	Liverpool
18139_14	LMB-GA-253	Human	F	17	Healthy	Liverpool
18139_15	LMB-HB-254	Human	F	23	Healthy	Liverpool
18139_16	LMB-AS-255	Human	F	23	Healthy	Liverpool
18139_17	LMB-MW-260	Human	M	23	Healthy	Liverpool
18139_18	LMB-RM-261	Human	M	26	Healthy	Liverpool

**Table 2.6 Details of 12 human tendon samples (six tendinopathic supraspinatus and six healthy control mixed semitendinosus and gracilis tendons) submitted for small RNA-sequencing. M = male; F = female; Age is given in years.**

Following elution into RNase free water and quantification (Nanodrop), samples were submitted to the Centre for Genomic Research, University of Liverpool, for library preparation and small RNA-sequencing. Total RNA concentration and integrity was confirmed using Qubit (ThermoFisher), but for 3 samples, concentration was too low and a Bioanalyser (Agilent) was used.

Fifty five nanograms of total RNA per sample were used to prepare twelve libraries using a commercially available small RNA library preparation kit (NEBNext small RNA library prep kit) which retains strand selective information. This kit is developed to capture any small RNAs possessing a 5' monophosphorylated and a 3' hydroxylated end. No specific ribosomal RNA depletion step was included, therefore library preparation used total RNA. PCR amplification used 15 cycles.

Library for sequencing was size selected at 120-300 base pairs (bp) (library preparation adds approximately 126 bp to length of original sequences as adapter/primers).

Paired-end, 150 bp sequencing was performed in a single lane on an Illumina HiSeq 4000 machine, generating data from >280 M clusters (sequencing depth was approximately 23 M reads per sample).

Data were processed using CASAVA (version 1.8.2) to generate output in FASTQ format. Raw FASTQ files were trimmed for the presence of adapter sequences using Cutadapt (version 1.2.1) with the option `-O3`, ensuring any reads which matched the adapter sequence for three bp or more were removed. Reads were further trimmed for quality using Sickle (version 1.200) using a minimum Phred (Q) score of 20. Reads shorter than 12 bp after trimming were discarded. If only one read of a pair passed this process, it was included in the R0 file.

Trimmed R1-R2 read pairs were aligned using a Gencode fasta (.fa) file to reference genome (Gencode GRCh38.p12) using Bowtie2 (version 2.3.5). Reads from aligned BAM files were subsequently counted using featureCounts (version 1.6.4) against the Gencode reference annotation file (Gencode (GRCh38.p12) gtf file) for non-miRNAs, and miRBase (hsa.gff3 file, release 22.1) for miRNAs, using Bowtie2 (version 2.3.5). Any counts to miRNAs from the Gencode file were removed to avoid duplication in downstream analysis.

BAM files of small RNAs were counted separately against respective annotation files. Information on 3p/5p identity of miRNAs is included in miRBase, but absent in the Gencode annotation file. The Gencode annotation file was used to maximise identification and quantification of other (non-miRNA) small RNA families as this information is unavailable in miRBase.

Raw read counts (as .csv files) were then imported into the Bioconductor package DESeq2 (version 1.22.2) for differential gene expression analysis. This pipeline normalises raw data based on the assumption that most genes are not differentially expressed (DE), using the median of read count/mean read count ratio for each gene to generate a scaling factor. DESeq2 models data as a negative binomial distribution to account for biological and technical variation using local regression to estimate the relationship between mean and variance of each gene (Dillies et al 2012). Normalised counts are log<sub>2</sub> transformed prior to application of a modified Fisher exact test to return exact *P*-values. The Benjamini-Hochberg procedure for multiple hypothesis correction is then

applied. Results are reported as log<sub>2</sub> fold change of normalised data and genes considered DE if log<sub>2</sub> fold change  $\geq 1.5$  with a Benjamini-Hochberg adjusted *P*-value  $< 0.05$ .

Principal component analysis (PCA) was used to visualise sources of variance in the data. All PCA calculations were performed in R (version 4.0.1, R Core Team (2020)), using the *prcomp* function within the package on regularised log transcript abundances, to extract principal components. Once extracted, principal components one and two were plotted using the *ggplot2* plotting package, and samples were coloured according to the disease state of the tissue (red = diseased, blue = healthy). The variance each principal component explained was calculated manually as the square of the standard deviation.

### PCR validation

RNA-Seq library preparation consumed all available RNA from four of the six SSP tendinopathy samples. Only two samples from the original cohort, both from 39 year old female patients, were therefore available for PCR validation purposes (Table 2.7).

Sample number	Sample name	Organism	Sex	Age	Status	Source
18139_7	0946/18 SSP	Human	F	39	Diseased SSP	Glasgow
18139_8	0947/18 SSP	Human	F	39	Diseased SSP	Glasgow

**Table 2.7** Details of two human supraspinatus tendon samples harvested from patients with clinically diagnosed rotator cuff disease and used in RT-qPCR validation of RNA-seq data. F = female; SSP = supraspinatus tendon; Age is given in years.

RNA was available from all six original control samples (Table 2.8).

Sample number	Sample name	Organism	Sex	Age	Status	Source
18139_13	LMB-KM-249	Human	M	31	Healthy ST/GR	Liverpool
18139_14	LMB-GA-253	Human	F	17	Healthy ST/GR	Liverpool
18139_15	LMB-HB-254	Human	F	23	Healthy ST/GR	Liverpool
18139_16	LMB-AS-255	Human	F	23	Healthy ST/GR	Liverpool
18139_17	LMB-MW-260	Human	M	23	Healthy ST/GR	Liverpool
18139_18	LMB-RM-261	Human	M	26	Healthy ST/GR	Liverpool

**Table 2.8** Details of six human hamstring tendon samples harvested from patients undergoing surgical repair of anterior cruciate rupture and used in RT-qPCR validation of RNA-seq data. M = male; F = female; ST = semitendinosus tendon; GR = gracilis tendon; Age is given in years.

RNA was extracted from three independent samples of diseased posterior tibial tendon to increase sample number available for RT-qPCR validation (Table 2.9).

Sample number	Sample name	Organism	Sex	Age	Status	Source
P1	P1M60081217	Human	M	60	Diseased PTT	Liverpool
P2	P2M71191217	Human	M	71	Diseased PTT	Liverpool
P3	P3M65130318	Human	M	65	Diseased PTT	Liverpool

**Table 2.9** Details of three human posterior tibial tendon (PTT) samples, harvested from patients with clinically diagnosed flat foot deformity, utilised as an independent cohort for RT-qPCR validation of RNA-seq data. M = male; Age is given in years.

30 ng total RNA was reverse transcribed into cDNA for RT-qPCR.

## **2.11 cDNA synthesis**

### **2.11.1 Reverse transcription protocol for miRNAs**

Selective conversion of mature miRNAs in the RNA template was performed by polyadenylation of mature miRNAs using poly(A) polymerase prior to conversion into cDNA by reverse transcriptase, using oligo-dT priming.

Materials required:

- RNA samples defrosted on ice
- RNase free water (Sigma 3098)
- miScript II RT Kit (Qiagen 218161) defrosted on ice – contains:
  - miScript HiSpec Buffer (5x)
  - miScript Nucleics Mix (10x)
  - miScript Reverse Transcriptase mix (Qiagen)
- 1.5 mL reaction tubes and rack
- 10 µL, 200 µL and 1000 µL pipettes and tips
- 0.2 mL PCR tubes
- 96 well freezer block
- Ice tray
- Thermal cycler (T100 BioRad)

Keep reagents in ice and PCR tubes in freezer block.

Calculate volume of each RNA sample required to provide 30 ng, 50 ng or 100 ng of template, using RNA concentration obtained from spectrophotometric analysis (NanoDrop 2000).

Calculate volume of RNase free water required to add to RNA template to make volume up to 12  $\mu\text{L}$ .

Prepare reaction mix as follows:

- 5  $\mu\text{L}$  miScript HiSpec Buffer (5x)
  - 2  $\mu\text{L}$  miScript Nucleics Mix (10x)
  - 1  $\mu\text{L}$  miScript Reverse Transcriptase mix
- } per reaction

Pipette 8  $\mu\text{L}$  of reaction mix into each PCR tube required.

Add calculated volumes of RNase free water and RNA template to bring total volume per tube to 20  $\mu\text{L}$ .

Briefly centrifuge PCR tubes to collect contents at base and transfer to thermal cycler.

Perform a single step reaction:

- Incubate at 37°C for 60 minutes
- Reaction inactivation at 95°C for 5 minutes
- Cool to 4°C

Dilute samples with 180  $\mu\text{L}$  RNase free water prior to storing at -20°C.

### 2.11.2 Reverse transcription protocol for mRNAs

Materials required:

- RNA samples defrosted on ice
- RNase free water (Sigma 3098)
- Random hexamers (50  $\mu\text{M}$ ) (Invitrogen N8080127)
- First Strand Buffer (5x) (Invitrogen Y02321)
- DTT (0.1 M) (Invitrogen Y00147)
- dNTPs (from 10 mM stock) (Sigma D4788-1MMO, T9656-1MMO, D5038-1MMO, D4913-1MMO)
- Superscript II Reverse Transcriptase (Invitrogen 18064014)
- Ribolock (40 U  $\text{mL}^{-1}$ ) (ThermoFisher EO0381)
- 1.5 mL reaction tubes and rack
- 10  $\mu\text{L}$ , 200  $\mu\text{L}$  and 1000  $\mu\text{L}$  pipettes and tips
- 0.2 mL PCR tubes
- 96 well freezer block
- Thermal cycler (T100 BioRad)

Keep reagents in ice and PCR tubes in freezer block.

Calculate volume of each RNA sample required to provide 500 ng, 200 ng, 100 ng or 50 ng of template (depending on application), using RNA concentration obtained from spectrophotometric analysis (NanoDrop 2000).

Calculated volume of RNase free water required to add to RNA template to bring total volume per sample to 10.5  $\mu\text{L}$  (11  $\mu\text{L}$  if using 500 ng template).

Prepare reaction mix as follows:

- 4  $\mu\text{L}$  First Strand Buffer (5x)
  - 2  $\mu\text{L}$  DTT (0.1 M)
  - 1  $\mu\text{L}$  dNTP (from 10 mM stock)
  - Superscript II RT
    - 1  $\mu\text{L}$  for 500 ng template
    - 0.5  $\mu\text{L}$  for  $\leq 200$  ng template
  - 1  $\mu\text{L}$  Ribolock (40 U  $\mu\text{L}^{-1}$ )
- } per reaction

Perform a two step reaction:

Prepare reaction tubes by mixing RNase free water, template and random hexamers as follows:

- X  $\mu\text{L}$  RNA template
  - Y  $\mu\text{L}$  RNase free water
  - 1  $\mu\text{L}$  Random hexamers (50  $\mu\text{M}$ )
- } where X + Y = 10.5  $\mu\text{L}$   
(X + Y = 11  $\mu\text{L}$  if using 500 ng template)

- Run at 65°C for 10 minutes to denature and prime template.

Place on ice immediately after to avoid RNA renaturing.

Add 8.5  $\mu\text{L}$  reaction mix per tube (9  $\mu\text{L}$  if using 500 ng template)

- Run at 42°C for 60 minutes
- Cool to 4°C

Dilute samples with 180  $\mu\text{L}$  RNase free water prior to storing at -20°C.

## 2.12 Quantitative real time PCR (RT-qPCR)

### 2.12.1 Primer design and optimisation

#### microRNAs

miRNA-specific forward primers were purchased from Qiagen miScript Primer Assay range (Table 2.10) as lyophilised powder and reconstituted with 550  $\mu$ L RNase free water according to manufacturer's instructions.

Primer Identity	Catalogue Number	Mature miRNA Sequence	
Hs_SNORD61_11	218300/MS00033705	N/A	
Hs_RNU6-2_11	18300/MS00033740	N/A	
Hs_let-7f_1	MIMAT0000067	218300/MS00006489	5'UGAGGUAGUAGAUUGUAGUAGUU
Hs_miR-29a_1	MIMAT0000086	218300/MS00003262	5'UAGCACCAUCUGAAAUCGGUUA
Hs_miR-34a_1	MIMAT0000255	218300/MS00003318	5'UGGCAGUGUCUUAGCUGGUUGU
Mm_miR-34b-5p_1	MIMAT0000382	218300/MS00007910	5'AGGCAGUGUAAUUAGCUGAUUGU
Hs_miR-34b*_2	MIMAT0000685	218300/MS00031780	5'UAGGCAGUGUCAUUAGCUGAUUG
Hs_miR-34c_1	MIMAT0000686	218300/MS00003332	5'AGGCAGUGUAGUUAGCUGAUUGC
Hs_miR-181a*_1	MIMAT0000270	218300/MS00006692	5'ACCAUCGACCGUUGAUUGUACC
Hs_miR-181a_2	MIMAT0000256	218300/MS00008827	5'AACAUUCAACGCUGUCGGUGAGU
Hs_miR-181b_1	MIMAT0000257	218300/MS00006699	5'AACAUUCAUUGCUGUCGGUGGGU
Hs_miR-181c_2	MIMAT0000258	218300/MS00008841	5'AACAUUCAACCUGUCGGUGAGU
Hs_miR-181d_2	MIMAT0002821	218300/MS00031500	5'AACAUUCAUUGUUGUCGGUGGGU
Hs_miR-199a_1	MIMAT0000231	218300/MS00006741	5'CCCAGUGUUCAGACUACCGUUC
Hs_miR-199b_1	MIMAT0000263	218300/MS00003731	5'CCCAGUGUUUAGACUAUCUGUUC

**Table 2.10 Details of Qiagen miScript primers utilised in this study.** Hs = *Homo sapiens*; Mm = *Mus musculus*.

Reverse priming was achieved using Universal Primer Assay (Qiagen).

#### Messenger RNAs

Gene specific primers for were purchased from Primerdesign Ltd, Chandlers Ford, UK (Table 2.11 ), Eurogentec, Camberley, UK (Table 2.12), or Sigma, Welwyn Garden City, UK (Tables 2.13. and 2.14).

Primers supplied by Primerdesign (Table 2.11) utilised the design and optimisation service offered by the company and were provided as a lyophilised powder of pre-mixed forward and reverse primers and were resuspended in 660  $\mu$ L RNase-free water, to produce a 6  $\mu$ M stock solution.

Target	Species	Primer sequence
IL-1RAP F	Equine	ATGAGATTTGGTGGACCATTGATG
IL-1RAP R	Equine	CTCCATTCATCTTCTGTTAGAGTCTG
IL-7 F	Equine	GACCAGGGTCCTGGGAGT
IL-7R	Equine	GGGGAGGAATTCCAAAGATATACC
Insulin-like Growth Factor 1 F	Equine	TCAGTTCGTGTGTGGAGACAG
Insulin-like Growth Factor 1 R	Equine	TCCAGCCTCCTCAGATCACAG
ILGF1 receptor F	Equine	GGGAATGGAGTGCTGTATGCA
ILGF1 receptor R	Equine	GCTCTCGGCTCATGGTGATC
Insulin receptor F	Equine	CTGGATCAACCCGACAATTGTC
Insulin receptor R	Equine	TCGACAATCTCCAGGAAGGTC
NFκB2 F	Equine	GTGATCGTCGAACAGCCTAAG
NFκB2 R	Equine	GAGGCACCTGGCAGTCC
p38-MAPK (MAPK14) F	Equine	TGAATGAAGACTGCGAGCTGA
p38-MAPK (MAPK14) R	Equine	CTGGTTGTAATGCATCCAGTTCA
P62 (SQSTM1) F	Equine	TGTGAATTCCTCAAGAACGTAGG
P62 (SQSTM1) R	Equine	CCTGGAGAGACGGAGGTCA
PARK7 F	Equine	GAAGGAACAAGAAAAGAGGAAAGGC
PARK7 R	Equine	TAGCCTGTGGGTGTGTTGTAAC
PRDX3 F	Equine	TGCTTGACAAATGTATTGTGGTC
PRDX3 R	Equine	GTGCTGGGTGACGGCAG
PRDX6 F	Equine	GCTCTCTCAATAGACAGTGTGAAG
PRDX6 R	Equine	AGGTCTCGATTCTTATCATCAATGATG
SIRT1 F	Equine	TGCTGAAGCAGTAAGAAAGTGC
SIRT1 R	Equine	CATGGAAAATGTAACGATTTGGTGG
SMAD7 F	Equine	TCCAGATGCTGTGCCTTCC
SMAD7 R	Equine	TCTCCTCCCAGTATGCCACC
TGFβ-R1 F	Equine	GTGCCGACATCTATGCAATGG
TGFβ-R1 R	Equine	TCATAATAAGGCAGCTGGTAATCTTC
TGFβ-R2 F	Equine	CCTGTGTCGAAAGCATGAAGG
TGFβ-R2 R	Equine	GGTCAGAGTCTCACACACCATC
TNF F	Equine	TACCGAATGCCTTCCAGTCAATC
TNF R	Equine	GGGTTTGCTACAACATGGGCTA

**Table 2.11 Targets and sequences of equine primers supplied by Primerdesign Ltd (Chandlers Ford, UK) utilised in this study. F = forward; R = reverse.**

Primers supplied by Eurogentec (Table 2.12) were previously designed by Dr Simon Tew and made available for use in this project. Eurogentec primers were reconstituted in RNase-free water according to the manufacturers' Technical Data Sheet to produce 100  $\mu\text{M}$  stock solutions. These were further diluted with RNase-free water to 20  $\mu\text{M}$  for use.

Target	Species	Primer sequence
TNF F	Equine	CCTTCCAGTCAATCAACCCTCT
TNF R	Equine	CACGCCCACTCAGCCACT
IL1 F	Equine	GCCTAAGAATACTACATCCAGAGA
IL1 R	Equine	GGCATTGATTAGACAACAGTGAA
GAPDH F	Equine	GCATCGTGGAGGGACTCA
GAPDH R	Equine	GCCACATCTTCCCAGAGG

**Table 2.12 Targets and sequences of equine primers supplied by Eurogentec (Camberley, UK) utilised in this study.** F = forward; R= reverse.

Primers supplied by Sigma (Tables 2.13 and 2.14) were designed by the author (with the exception of the mouse TOMM20-directed primer), according to the protocol given below, and ordered as the following formulation:

- Synthesis scale – 0.025  $\mu\text{mole}$
- Purification – Desalt
- Format – Dry

Sigma primers were reconstituted in RNase-free water according to the manufacturers' Technical Data Sheet to produce 100  $\mu\text{M}$  stock solutions. These were further diluted with RNase-free water to 20  $\mu\text{M}$  for use.

Stock solutions were stored at  $-20^{\circ}\text{C}$  and final concentration in PCR reactions was 0.3  $\mu\text{M}$  for all primers.

Target	Species	Primer sequence
IL1a F	Equine	GGCAAAGAAATCAAGATGGCGA
IL1a R	Equine	TTCAGAGTCTTCCCCTTGCC
PARK2 F	Equine	AGTGAGCATGATCGTGTTTGT
PARK2 R	Equine	TTAGCAACCGCCTCCTTGAG
TGFβ1 F	Equine	CAGCATGTGGAGCTGTACCA
TGFβ1 R	Equine	GGAAGTGAACCCGTTGATGC
TGFβ2 F	Equine	GAAGCAAGATTCGCAGACTTGA
TGFβ2 R	Equine	TCGATCTGGGTGTTTTGCC
TGFβ3 F	Equine	ACCAATTACTGCTCCGCAAC
TGFβ3 R	Equine	GTCAATGTAGAGAGGGCGCA

**Table 2.13 Targets and sequences of equine primers supplied by Sigma (Welwyn Garden City, UK) utilised in this study.** F = forward; R = reverse.

Target	Species	Primer sequence
GAPDH F	Human	CAAGGTCATCCATGACAACCTTTG
GAPDH R	Human	GGCCATCCACAGTCTTCTGG
COX IV F	Human	TGGGAGTGTTGTGAAGAGTGA
COX IV R	Human	GCAGTGAAGCCGATGAAGAAC
TOMM20 F	Mouse	AGTCGAGCGAAGATGGTGG
TOMM20 R	Mouse	GCCTTTTGC GGTCGAAGTAG
PARK2 F	Human	CCCAGTGACCATGATAGTGTTTG
PARK2 R	Human	TGCTGGTGTGAGAATCGACC
P62/SQSTM1 F	Human	CCGTGAAGGCCTACCTTCTG
P62/SQSTM1 R	Human	CGTCCTCATCGCGGTAGTG
P62/SQSTM1 F	Human	GTGAAGGCCTACCTTCTGGG
P62/SQSTM1 R	Human	GTCCTCATCGCGGTAGTGC
MAP1LC3B F	Human	CCGCACCTTCGAACAAAGAG
MAP1LC3B R	Human	AGATTGGTGTGGAGACGCTG
COXI F	Human	CTGCTATAGTGGAGGCCGGA
COXI R	Human	GGGTGGAGTAGTCCCTGC
INSR F	Human	GCCCTGTGACGCATGAAATC
INSR R	Human	GGACGTCTAAATAGTCTGTACGTA

**Table 2.14 Targets and sequences of human primers supplied by Sigma (Welwyn Garden City, UK) utilised in this study.** F = forward; R = reverse.

## Protocol for primer design

Open the following applications:

- NCBI Primer-BLAST <https://www.ncbi.nlm.nih.gov/tools/primer-blast/>
- NCBI Gene <https://www.ncbi.nlm.nih.gov/gene>

In NCBI Gene, type the name of the gene of interest in the search box.

Click on the result relevant to the species of interest eg TOMM20 *Homo sapiens*:

How To

Gene  Search

Create RSS Save search Advanced

Tabular 20 per page Sort by Relevance Send to

GENE Was this helpful?

**TOMM20** – translocase of outer mitochondrial membrane 20

*Homo sapiens* (human)

Also known as: MAS20, MOM19, TOM20

GeneID: 9804

RefSeq transcripts (1) RefSeq proteins (1) PubMed (65)

Orthologs Genome Browser BLAST Download

RefSeq Sequences +

Search results

Items: 1 to 20 of 180

See also 1 discontinued or replaced items

Name/Gene ID	Description	Location	Aliases	MIM
<input type="checkbox"/> TOMM20 ID: 9804	translocase of outer mitochondrial membrane 20 [ <i>Homo sapiens</i> (human)]	Chromosome 1, NC_000001.11 (235109341..235128837, complement)	MAS20, MOM19, TOM20	601848
<input type="checkbox"/> KRAS ID: 2548	KRAS proto-oncogene, GTPase [ <i>Homo sapiens</i> (human)]	Chromosome 12, NC_000012.12 (75702748..75702758, complement)	C-K-RAS, C-K-RAS, CFC2, K-RAS2A, K-RAS2B, K-RAS4A, K-RAS4B, K-RAS4C, K-RAS4D, K-RAS4E, K-RAS4F, K-RAS4G, K-RAS4H, K-RAS4I, K-RAS4J, K-RAS4K, K-RAS4L, K-RAS4M, K-RAS4N, K-RAS4O, K-RAS4P, K-RAS4Q, K-RAS4R, K-RAS4S, K-RAS4T, K-RAS4U, K-RAS4V, K-RAS4W, K-RAS4X, K-RAS4Y, K-RAS4Z, K-RAS4AA, K-RAS4AB, K-RAS4AC, K-RAS4AD, K-RAS4AE, K-RAS4AF, K-RAS4AG, K-RAS4AH, K-RAS4AI, K-RAS4AJ, K-RAS4AK, K-RAS4AL, K-RAS4AM, K-RAS4AN, K-RAS4AO, K-RAS4AP, K-RAS4AQ, K-RAS4AR, K-RAS4AS, K-RAS4AT, K-RAS4AU, K-RAS4AV, K-RAS4AW, K-RAS4AX, K-RAS4AY, K-RAS4AZ, K-RAS4BA, K-RAS4BB, K-RAS4BC, K-RAS4BD, K-RAS4BE, K-RAS4BF, K-RAS4BG, K-RAS4BH, K-RAS4BI, K-RAS4BJ, K-RAS4BK, K-RAS4BL, K-RAS4BM, K-RAS4BN, K-RAS4BO, K-RAS4BP, K-RAS4BQ, K-RAS4BR, K-RAS4BS, K-RAS4BT, K-RAS4BU, K-RAS4BV, K-RAS4BW, K-RAS4BX, K-RAS4BY, K-RAS4BZ, K-RAS4CA, K-RAS4CB, K-RAS4CC, K-RAS4CD, K-RAS4CE, K-RAS4CF, K-RAS4CG, K-RAS4CH, K-RAS4CI, K-RAS4CJ, K-RAS4CK, K-RAS4CL, K-RAS4CM, K-RAS4CN, K-RAS4CO, K-RAS4CP, K-RAS4CQ, K-RAS4CR, K-RAS4CS, K-RAS4CT, K-RAS4CU, K-RAS4CV, K-RAS4CW, K-RAS4CX, K-RAS4CY, K-RAS4CZ, K-RAS4DA, K-RAS4DB, K-RAS4DC, K-RAS4DD, K-RAS4DE, K-RAS4DF, K-RAS4DG, K-RAS4DH, K-RAS4DI, K-RAS4DJ, K-RAS4DK, K-RAS4DL, K-RAS4DM, K-RAS4DN, K-RAS4DO, K-RAS4DP, K-RAS4DQ, K-RAS4DR, K-RAS4DS, K-RAS4DT, K-RAS4DU, K-RAS4DV, K-RAS4DW, K-RAS4DX, K-RAS4DY, K-RAS4DZ, K-RAS4EA, K-RAS4EB, K-RAS4EC, K-RAS4ED, K-RAS4EE, K-RAS4EF, K-RAS4EG, K-RAS4EH, K-RAS4EI, K-RAS4EJ, K-RAS4EK, K-RAS4EL, K-RAS4EM, K-RAS4EN, K-RAS4EO, K-RAS4EP, K-RAS4EQ, K-RAS4ER, K-RAS4ES, K-RAS4ET, K-RAS4EU, K-RAS4EV, K-RAS4EW, K-RAS4EX, K-RAS4EY, K-RAS4EZ, K-RAS4FA, K-RAS4FB, K-RAS4FC, K-RAS4FD, K-RAS4FE, K-RAS4FF, K-RAS4FG, K-RAS4FH, K-RAS4FI, K-RAS4FJ, K-RAS4FK, K-RAS4FL, K-RAS4FM, K-RAS4FN, K-RAS4FO, K-RAS4FP, K-RAS4FQ, K-RAS4FR, K-RAS4FS, K-RAS4FT, K-RAS4FU, K-RAS4FV, K-RAS4FW, K-RAS4FX, K-RAS4FY, K-RAS4FZ, K-RAS4GA, K-RAS4GB, K-RAS4GC, K-RAS4GD, K-RAS4GE, K-RAS4GF, K-RAS4GG, K-RAS4GH, K-RAS4GI, K-RAS4GJ, K-RAS4GK, K-RAS4GL, K-RAS4GM, K-RAS4GN, K-RAS4GO, K-RAS4GP, K-RAS4GQ, K-RAS4GR, K-RAS4GS, K-RAS4GT, K-RAS4GU, K-RAS4GV, K-RAS4GW, K-RAS4GX, K-RAS4GY, K-RAS4GZ, K-RAS4HA, K-RAS4HB, K-RAS4HC, K-RAS4HD, K-RAS4HE, K-RAS4HF, K-RAS4HG, K-RAS4HH, K-RAS4HI, K-RAS4HJ, K-RAS4HK, K-RAS4HL, K-RAS4HM, K-RAS4HN, K-RAS4HO, K-RAS4HP, K-RAS4HQ, K-RAS4HR, K-RAS4HS, K-RAS4HT, K-RAS4HU, K-RAS4HV, K-RAS4HW, K-RAS4HX, K-RAS4HY, K-RAS4HZ, K-RAS4IA, K-RAS4IB, K-RAS4IC, K-RAS4ID, K-RAS4IE, K-RAS4IF, K-RAS4IG, K-RAS4IH, K-RAS4IJ, K-RAS4IK, K-RAS4IL, K-RAS4IM, K-RAS4IN, K-RAS4IO, K-RAS4IP, K-RAS4IQ, K-RAS4IR, K-RAS4IS, K-RAS4IT, K-RAS4IU, K-RAS4IV, K-RAS4IW, K-RAS4IX, K-RAS4IY, K-RAS4IZ, K-RAS4JA, K-RAS4JB, K-RAS4JC, K-RAS4JD, K-RAS4JE, K-RAS4JF, K-RAS4JG, K-RAS4JH, K-RAS4JI, K-RAS4JJ, K-RAS4JK, K-RAS4JL, K-RAS4JM, K-RAS4JN, K-RAS4JO, K-RAS4JP, K-RAS4JQ, K-RAS4JR, K-RAS4JS, K-RAS4JT, K-RAS4JU, K-RAS4JV, K-RAS4JW, K-RAS4JX, K-RAS4JY, K-RAS4JZ, K-RAS4KA, K-RAS4KB, K-RAS4KC, K-RAS4KD, K-RAS4KE, K-RAS4KF, K-RAS4KG, K-RAS4KH, K-RAS4KI, K-RAS4KJ, K-RAS4KK, K-RAS4KL, K-RAS4KM, K-RAS4KN, K-RAS4KO, K-RAS4KP, K-RAS4KQ, K-RAS4KR, K-RAS4KS, K-RAS4KT, K-RAS4KU, K-RAS4KV, K-RAS4KW, K-RAS4KX, K-RAS4KY, K-RAS4KZ, K-RAS4LA, K-RAS4LB, K-RAS4LC, K-RAS4LD, K-RAS4LE, K-RAS4LF, K-RAS4LG, K-RAS4LH, K-RAS4LI, K-RAS4LJ, K-RAS4LK, K-RAS4LL, K-RAS4LM, K-RAS4LN, K-RAS4LO, K-RAS4LP, K-RAS4LQ, K-RAS4LR, K-RAS4LS, K-RAS4LT, K-RAS4LU, K-RAS4LV, K-RAS4LW, K-RAS4LX, K-RAS4LY, K-RAS4LZ, K-RAS4MA, K-RAS4MB, K-RAS4MC, K-RAS4MD, K-RAS4ME, K-RAS4MF, K-RAS4MG, K-RAS4MH, K-RAS4MI, K-RAS4MJ, K-RAS4MK, K-RAS4ML, K-RAS4MM, K-RAS4MN, K-RAS4MO, K-RAS4MP, K-RAS4MQ, K-RAS4MR, K-RAS4MS, K-RAS4MT, K-RAS4MU, K-RAS4MV, K-RAS4MW, K-RAS4MX, K-RAS4MY, K-RAS4MZ, K-RAS4NA, K-RAS4NB, K-RAS4NC, K-RAS4ND, K-RAS4NE, K-RAS4NF, K-RAS4NG, K-RAS4NH, K-RAS4NI, K-RAS4NJ, K-RAS4NK, K-RAS4NL, K-RAS4NM, K-RAS4NN, K-RAS4NO, K-RAS4NP, K-RAS4NQ, K-RAS4NR, K-RAS4NS, K-RAS4NT, K-RAS4NU, K-RAS4NV, K-RAS4NW, K-RAS4NX, K-RAS4NY, K-RAS4NZ, K-RAS4OA, K-RAS4OB, K-RAS4OC, K-RAS4OD, K-RAS4OE, K-RAS4OF, K-RAS4OG, K-RAS4OH, K-RAS4OI, K-RAS4OJ, K-RAS4OK, K-RAS4OL, K-RAS4OM, K-RAS4ON, K-RAS4OO, K-RAS4OP, K-RAS4OQ, K-RAS4OR, K-RAS4OS, K-RAS4OT, K-RAS4OU, K-RAS4OV, K-RAS4OW, K-RAS4OX, K-RAS4OY, K-RAS4OZ, K-RAS4PA, K-RAS4PB, K-RAS4PC, K-RAS4PD, K-RAS4PE, K-RAS4PF, K-RAS4PG, K-RAS4PH, K-RAS4PI, K-RAS4PJ, K-RAS4PK, K-RAS4PL, K-RAS4PM, K-RAS4PN, K-RAS4PO, K-RAS4PP, K-RAS4PQ, K-RAS4PR, K-RAS4PS, K-RAS4PT, K-RAS4PU, K-RAS4PV, K-RAS4PW, K-RAS4PX, K-RAS4PY, K-RAS4PZ, K-RAS4QA, K-RAS4QB, K-RAS4QC, K-RAS4QD, K-RAS4QE, K-RAS4QF, K-RAS4QG, K-RAS4QH, K-RAS4QI, K-RAS4QJ, K-RAS4QK, K-RAS4QL, K-RAS4QM, K-RAS4QN, K-RAS4QO, K-RAS4QP, K-RAS4QQ, K-RAS4QR, K-RAS4QS, K-RAS4QT, K-RAS4QU, K-RAS4QV, K-RAS4QW, K-RAS4QX, K-RAS4QY, K-RAS4QZ, K-RAS4RA, K-RAS4RB, K-RAS4RC, K-RAS4RD, K-RAS4RE, K-RAS4RF, K-RAS4RG, K-RAS4RH, K-RAS4RI, K-RAS4RJ, K-RAS4RK, K-RAS4RL, K-RAS4RM, K-RAS4RN, K-RAS4RO, K-RAS4RP, K-RAS4RQ, K-RAS4RR, K-RAS4RS, K-RAS4RT, K-RAS4RU, K-RAS4RV, K-RAS4RW, K-RAS4RX, K-RAS4RY, K-RAS4RZ, K-RAS4SA, K-RAS4SB, K-RAS4SC, K-RAS4SD, K-RAS4SE, K-RAS4SF, K-RAS4SG, K-RAS4SH, K-RAS4SI, K-RAS4SJ, K-RAS4SK, K-RAS4SL, K-RAS4SM, K-RAS4SN, K-RAS4SO, K-RAS4SP, K-RAS4SQ, K-RAS4SR, K-RAS4SS, K-RAS4ST, K-RAS4SU, K-RAS4SV, K-RAS4SW, K-RAS4SX, K-RAS4SY, K-RAS4SZ, K-RAS4TA, K-RAS4TB, K-RAS4TC, K-RAS4TD, K-RAS4TE, K-RAS4TF, K-RAS4TG, K-RAS4TH, K-RAS4TI, K-RAS4TJ, K-RAS4TK, K-RAS4TL, K-RAS4TM, K-RAS4TN, K-RAS4TO, K-RAS4TP, K-RAS4TQ, K-RAS4TR, K-RAS4TS, K-RAS4TT, K-RAS4TU, K-RAS4TV, K-RAS4TW, K-RAS4TX, K-RAS4TY, K-RAS4TZ, K-RAS4UA, K-RAS4UB, K-RAS4UC, K-RAS4UD, K-RAS4UE, K-RAS4UF, K-RAS4UG, K-RAS4UH, K-RAS4UI, K-RAS4UJ, K-RAS4UK, K-RAS4UL, K-RAS4UM, K-RAS4UN, K-RAS4UO, K-RAS4UP, K-RAS4UQ, K-RAS4UR, K-RAS4US, K-RAS4UT, K-RAS4UU, K-RAS4UV, K-RAS4UW, K-RAS4UX, K-RAS4UY, K-RAS4UZ, K-RAS4VA, K-RAS4VB, K-RAS4VC, K-RAS4VD, K-RAS4VE, K-RAS4VF, K-RAS4VG, K-RAS4VH, K-RAS4VI, K-RAS4VJ, K-RAS4VK, K-RAS4VL, K-RAS4VM, K-RAS4VN, K-RAS4VO, K-RAS4VP, K-RAS4VQ, K-RAS4VR, K-RAS4VS, K-RAS4VT, K-RAS4VU, K-RAS4VV, K-RAS4VW, K-RAS4VX, K-RAS4VY, K-RAS4VZ, K-RAS4WA, K-RAS4WB, K-RAS4WC, K-RAS4WD, K-RAS4WE, K-RAS4WF, K-RAS4WG, K-RAS4WH, K-RAS4WI, K-RAS4WJ, K-RAS4WK, K-RAS4WL, K-RAS4WM, K-RAS4WN, K-RAS4WO, K-RAS4WP, K-RAS4WQ, K-RAS4WR, K-RAS4WS, K-RAS4WT, K-RAS4WU, K-RAS4WV, K-RAS4WW, K-RAS4WX, K-RAS4WY, K-RAS4WZ, K-RAS4XA, K-RAS4XB, K-RAS4XC, K-RAS4XD, K-RAS4XE, K-RAS4XF, K-RAS4XG, K-RAS4XH, K-RAS4XI, K-RAS4XJ, K-RAS4XK, K-RAS4XL, K-RAS4XM, K-RAS4XN, K-RAS4XO, K-RAS4XP, K-RAS4XQ, K-RAS4XR, K-RAS4XS, K-RAS4XT, K-RAS4XU, K-RAS4XV, K-RAS4XW, K-RAS4XX, K-RAS4XY, K-RAS4XZ, K-RAS4YA, K-RAS4YB, K-RAS4YC, K-RAS4YD, K-RAS4YE, K-RAS4YF, K-RAS4YG, K-RAS4YH, K-RAS4YI, K-RAS4YJ, K-RAS4YK, K-RAS4YL, K-RAS4YM, K-RAS4YN, K-RAS4YO, K-RAS4YP, K-RAS4YQ, K-RAS4YR, K-RAS4YS, K-RAS4YT, K-RAS4YU, K-RAS4YV, K-RAS4YW, K-RAS4YX, K-RAS4YY, K-RAS4YZ, K-RAS4ZA, K-RAS4ZB, K-RAS4ZC, K-RAS4ZD, K-RAS4ZE, K-RAS4ZF, K-RAS4ZG, K-RAS4ZH, K-RAS4ZI, K-RAS4ZJ, K-RAS4ZK, K-RAS4ZL, K-RAS4ZM, K-RAS4ZN, K-RAS4ZO, K-RAS4ZP, K-RAS4ZQ, K-RAS4ZR, K-RAS4ZS, K-RAS4ZT, K-RAS4ZU, K-RAS4ZV, K-RAS4ZW, K-RAS4ZX, K-RAS4ZY, K-RAS4ZZ	190070

The following screen comes up with all the information on the selected gene:

NCBI Resources How To Sign In to NCBI

Gene  Search

Advanced Help

Full Report - Send to - Hide sidebar >>

**TOMM20** translocase of outer mitochondrial membrane 20 [*Homo sapiens* (human)]

Gene ID: 9804, updated on 9-Feb-2020

**Summary**

Official Symbol TOMM20 provided by HGNC

Official Full Name translocase of outer mitochondrial membrane 20 provided by HGNC

Primary source HGNC:HGNC:20947

See related Ensembl:ENSG00000173726 MIM:601848

Gene type protein coding

RefSeq status VALIDATED

Organism *Homo sapiens*

Lineage Eukaryota; Metazoa; Chordata; Craniata; Vertebrata; Euteleostomi; Mammalia; Eutheria; Euarchontoglires; Primates; Haplorhini; Catarrhini; Hominidae; Homo

Also known as MAS20, MOM19, TOM20

Expression Ubiquitous expression in thyroid (RPKM 101.1), brain (RPKM 96.3) and 25 other tissues [See more](#)

Orthologs [mouse](#) [all](#)

**Genomic context**

Location: 1q42.3 See TOMM20 in [Genome Data Viewer](#)

Exon count: 5

Annotation release	Status	Assembly	Chr	Location
109.20191205	current	GRCh38.p13 (GCF_000001465.39)	1	NC_000001.11 (235109341..235128837, complement)
105	previous assembly	GRCh37.p13 (GCF_000001465.25)	1	NC_000001.10 (235272656..235292256, complement)

Chromosome 1 - NC\_000001.11

Genomic Sequence: [NC\\_000001.11 Chromosome 1 Reference GRCh38.p13 Primary Assembly](#)

Go to [reference sequence details](#)

Go to [nucleotide](#): [Graphics](#) [FASTA](#) [GenBank](#) [3D structures](#)

**Table of contents**

- Summary
- Genomic context
- Genomic regions, transcripts, and products
- Expression
- Bibliography
- Phenotypes
- Variation
- HIV-1 interactions
- Pathways from PubChem
- Interactions
- General gene information
  - Markers, Related pseudogenes(s), Clone Names, Homology, Gene Ontology
- General protein information
- NCBI Reference Sequences (RefSeq)
- Related sequences
- Additional links
- Genome Browsers
- Genome Data Viewer
- Variation Viewer (GRCh37.p13)
- Variation Viewer (GRCh38)
- 1000 Genomes Browser (GRCh37.p13)
- Ensembl
- UCSC
- Related information
  - Order cDNA clone

Scroll down to 'mRNA and Protein(s)' under the heading 'NCBI Reference Sequences (RefSeq)':

**General protein information**

Preferred Names  
mitochondrial import receptor subunit TOM20 homolog

Names  
mitochondrial 20 kDa outer membrane protein  
outer mitochondrial membrane receptor Tom20  
translocase of outer mitochondrial membrane 20 homolog type 1

**NCBI Reference Sequences (RefSeq)**

RefSeqs maintained independently of Annotated Genomes

These reference sequences exist independently of genome builds. [Explain](#)

**mRNA and Protein(s)**

1. [NM\\_014765.3](#) → [NP\\_055580.1](#) mitochondrial import receptor subunit TOM20 homolog  
[See identical proteins and their annotated locations for NP\\_055580.1](#)

Status: **VALIDATED**

Source sequence(s)	<a href="#">AK289810</a> , <a href="#">BC009886</a> , <a href="#">BC100286</a> , <a href="#">D13641</a>
Consensus CDS	<a href="#">CCDS1603.1</a>
UniProtKB/Swiss-Prot	<a href="#">Q15388</a>
UniProtKB/TrEMBL	<a href="#">A0A024R3W2</a>
Related	<a href="#">ENSP00000355566.4</a> , <a href="#">ENST00000366607.5</a>

Conserved Domains (1) [summary](#)

<a href="#">pfam02064</a>	MAS20, MAS20 protein import receptor
Location:	13 → 124

Click on the hyperlinked code of the transcript of interest. There may be multiple transcript options representing different lengths, isoforms or variants. Select the one(s) of interest:

**NCBI Reference Sequences (RefSeq)**

RefSeqs maintained independently of Annotated Genomes

These reference sequences exist independently of genome builds. [Explain](#)

**mRNA and Protein(s)**

1. **NM\_014765.3** → [NP\\_055580.1](#) mitochondrial import receptor subunit TOM20 homolog  
[See identical proteins and their annotated locations for NP\\_055580.1](#)

Status: **VALIDATED**

Source sequence(s)	<a href="#">AK289810</a> , <a href="#">BC009886</a> , <a href="#">BC100286</a> , <a href="#">D13641</a>
Consensus CDS	<a href="#">CCDS1603.1</a>
UniProtKB/Swiss-Prot	<a href="#">Q15388</a>
UniProtKB/TrEMBL	<a href="#">A0A024R3W2</a>
Related	<a href="#">ENSP00000355566.4</a> , <a href="#">ENST00000366607.5</a>

Conserved Domains (1) [summary](#)

<a href="#">pfam02064</a>	MAS20, MAS20 protein import receptor
Location:	13 → 124

('NM' - manually curated protein-coding transcripts; 'XM' - predicted protein-coding models).

The following screen will open:

The screenshot shows the NCBI GenBank entry for the Homo sapiens translocase of outer mitochondrial membrane 20 (TOMM20), mRNA. The accession number NM\_014765.3 is highlighted in red. The page includes fields for Nucleotide search, GenBank links, and various analysis tools like Run BLAST, Pick Primers, and Highlight Sequence Features. The main content area displays the following information:

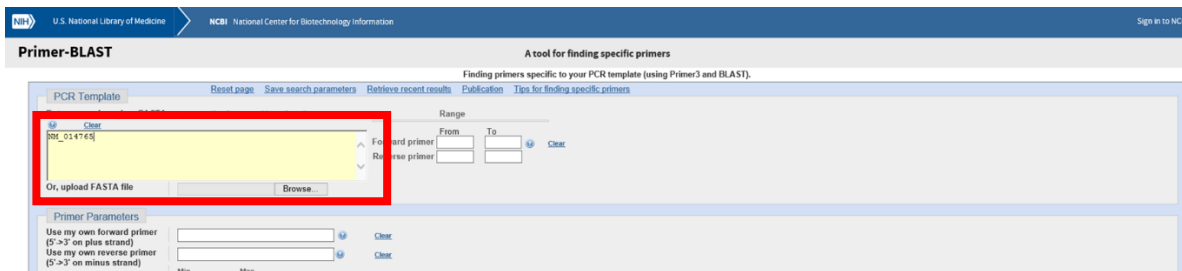
**LOCUS** NM\_014765 3283 bp mRNA linear FRI 10-JUL-2019  
**DEFINITION** Homo sapiens translocase of outer mitochondrial membrane 20 (TOMM20), mRNA.  
**ACCESSION** NM\_014765  
**VERSION** NM\_014765.3  
**KEYWORDS** RefSeq; MANE Select.  
**SOURCE** Homo sapiens (human)  
**ORGANISM** [Homo sapiens](#)  
Eukaryota; Metazoa; Chordata; Craniata; Vertebrata; Euteleostomi; Mammalia; Eutheria; Euarchontoglires; Primates; Haplorrhini; Catarrhini; Hominidae; Homo.  
**REFERENCE** 1 (bases 1 to 3283)  
**AUTHORS** Filadi R, Leal NS, Schreiner B, Rossi A, Dentoni G, Pinho CM, Wiehager B, Cieri D, Cali T, Pizzo P and Ankaracrona M.  
**TITLE** TOM70 Sustains Cell Bioenergetics by Promoting IP3R3-Mediated ER to Mitochondria Ca(2+) Transfer  
**JOURNAL** Curr. Biol. 28 (3), 369-382 (2018)  
**PUBMED** 29395920  
**REMARK** GeneRIF: TOM70, but not TOM20, clusters in distinct OMM foci, frequently overlapping with sites in which the endoplasmic reticulum (ER) contacts mitochondria. Functionally, TOM70 depletion specifically impairs inositol triphosphates (IP3)-linked ER to mitochondria Ca(2+) transfer. This phenomenon is dependent on the capacity of TOM70 to interact with IP3-receptors and favor their functional recruitment close to mitochondria.  
**REFERENCE** 2 (bases 1 to 3283)  
**AUTHORS** Mikkilineni L, Whitaker-Menezes D, Domingo-Vidal M, Sprandio J, Arana P, Cotzia P, Dulau-Florea A, Gong J, Uppal G, Zhan T, Leiby B, Lin Z, Pro B, Soccia F, Lisanti MF and Martinez-Guachoorn U.  
**TITLE** Hodgkin lymphoma: A complex metabolic ecosystem with glycolytic reprogramming of the tumor microenvironment  
**JOURNAL** Semin. Oncol. 44 (3), 218-225 (2017)  
**PUBMED** 29248133  
**REMARK** GeneRIF: TOMM20, MCT1, and MCT4 expression was significantly different in Hodgkin and Reed Sternberg (HRS) cells. HRS have high expression of TOMM20, while tumor associated macrophages have absent TOMM20 expression. Tumor-infiltrating lymphocytes have low TOMM20 expression. Reactive lymph nodes in contrast to cHL tumors had low TOMM20, MCT1, and MCT4 expression in lymphocytes and

Copy the 'ACCESSION' number ...

The screenshot shows the NCBI GenBank entry for the Homo sapiens translocase of outer mitochondrial membrane 20 (TOMM20), mRNA. The accession number NM\_014765 is highlighted in red. The page includes fields for Nucleotide search, GenBank links, and various analysis tools like Run BLAST, Pick Primers, and Highlight Sequence Features. The main content area displays the following information:

**LOCUS** NM\_014765 3283 bp mRNA linear FRI 10-JUL-2019  
**DEFINITION** Homo sapiens translocase of outer mitochondrial membrane 20 (TOMM20), mRNA.  
**ACCESSION** NM\_014765  
**KEYWORDS** RefSeq; MANE Select.  
**SOURCE** Homo sapiens (human)  
**ORGANISM** [Homo sapiens](#)  
Eukaryota; Metazoa; Chordata; Craniata; Vertebrata; Euteleostomi; Mammalia; Eutheria; Euarchontoglires; Primates; Haplorrhini; Catarrhini; Hominidae; Homo.  
**REFERENCE** 1 (bases 1 to 3283)  
**AUTHORS** Filadi R, Leal NS, Schreiner B, Rossi A, Dentoni G, Pinho CM, Wiehager B, Cieri D, Cali T, Pizzo P and Ankaracrona M.  
**TITLE** TOM70 Sustains Cell Bioenergetics by Promoting IP3R3-Mediated ER to Mitochondria Ca(2+) Transfer

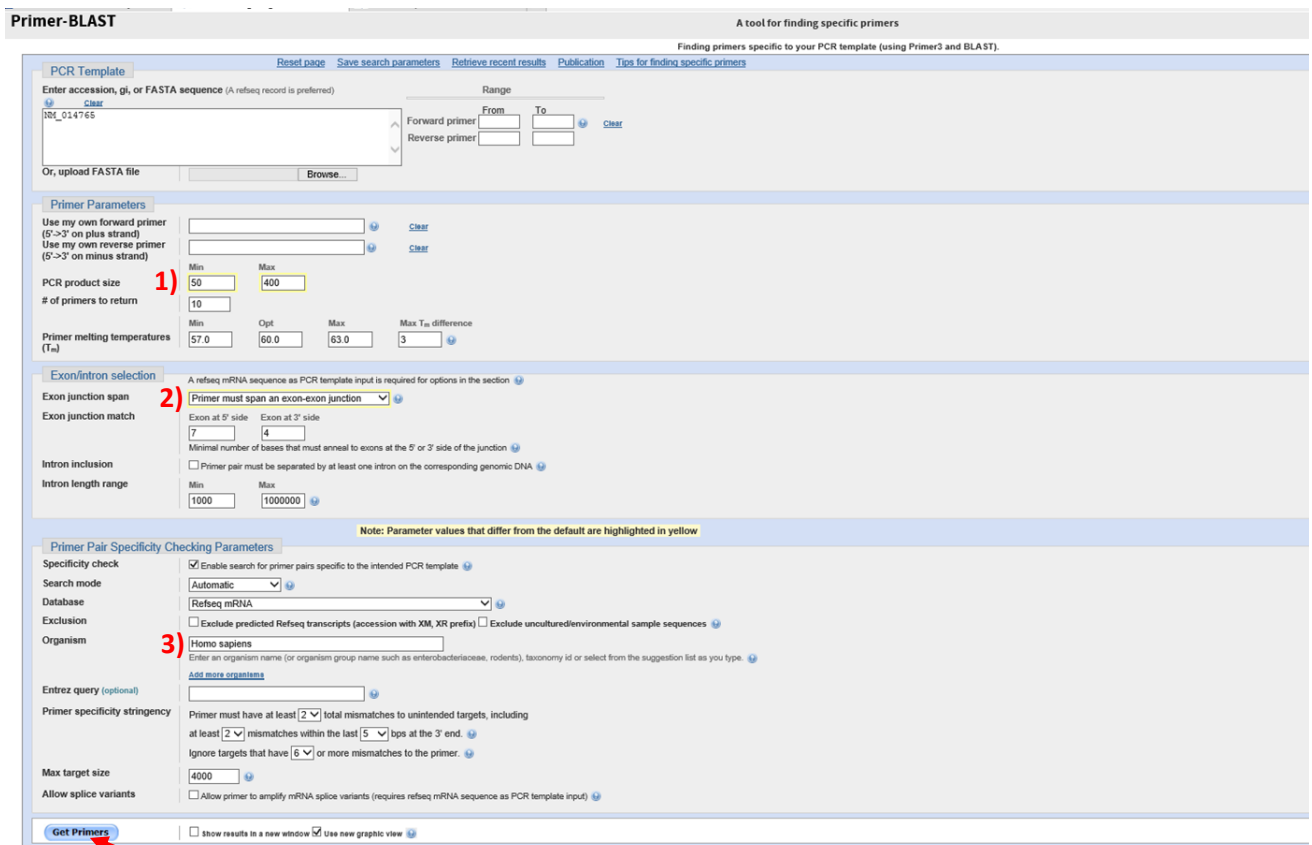
... and paste it to the "Primer-BLAST" window, on the box underneath "PCR Template":



Enter details:

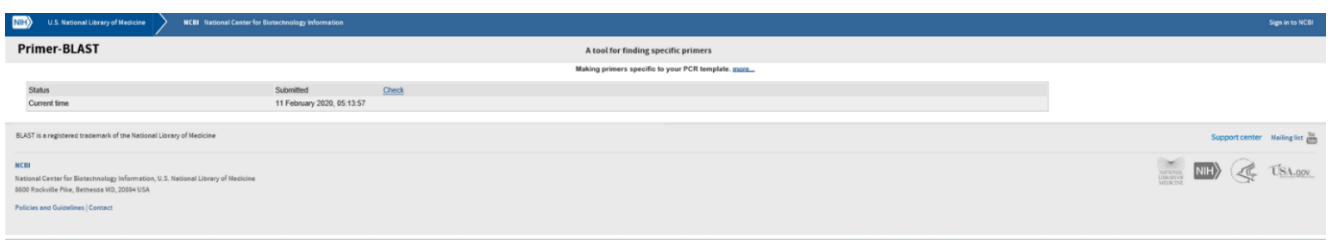
- 1) PCR product size – Min 50, Max 400 bp.
- 2) Exon junction span - select 'Primer must span an exon-exon junction' from drop down list.
- 3) Organism – enter species of interest (default is Homo sapiens).

*Note: Can change the 'Primer melting temperatures (Tm)' or the '#of primers to return' if required.*



Click on 'Get Primers'.

The following screen will come up while the database is processing information:



Once primers have been designed, the following screen will open listing (usually) 10 primer pairs and their characteristics including length, T<sub>m</sub>, self-complementarity etc.

The screenshot displays the Primer-BLAST results page. At the top, it shows the input PCR template: **NM\_014785.3 Homo sapiens translocase of outer mitochondrial membrane 20 (TOM20), mRNA**. Below this, there are sections for 'Graphical view of primer pairs' and 'Detailed primer reports'.

**Graphical view of primer pairs:** This section shows a genomic map with several primer pairs indicated by arrows. The x-axis represents the genomic position in base pairs, ranging from approximately 100 to 3,000.

**Detailed primer reports:** This section provides specific data for two primer pairs.

Primer pair 1	Sequence (5'-3')	Template strand	Length	Start	Stop	T <sub>m</sub>	GC%	Self complementarity	Self 3' complementarity
Forward primer	GGGCTTTCGAAGTACCTGAC	Plus	21	279	299	58.84	52.38	5.06	2.00
Reverse primer	TGTGAGATGGTCTAGGCCCT	Minus	20	404	385	60.32	55.80	3.00	2.00
Product length	126								
Exon junction	290/281 (forward primer) on template <a href="#">NM_014785.3</a>								

Products on intended targets:  
 >[NM\\_014785.3](#) Homo sapiens translocase of outer mitochondrial membrane 20 (TOM20), mRNA  
 product length = 126  
 Forward primer 1 GGGCTTTCGAAGTACCTGAC 21  
 Template 279 ..... 299  
 Reverse primer 1 TGTGAGATGGTCTAGGCCCT 20  
 Template 404 ..... 385

**Primer pair 2**

Aim for primer pairs with:

- No additional products
- GC content ~50% (40-55% OK)
- 1-2°C difference max for T<sub>m</sub>
- Lowest complementarity
- Short (100-200bp) products (not >500bp)

Other things to consider:

The following points should be considered when designing PCR primers and are common to all types of PCR:

- T<sub>m</sub> calculation: 2°C x (A+T) + 4°C x (G+C)
- Avoid complementarity in the 2–3 bases at the 3' end of the primer pairs
- Avoid mismatches between the 3' end of the primer and the template
- Avoid runs of 3 or more Cs or Gs at the 3' end of the primer
- Avoid complementarity within primers and between the primer pair
- Avoid a T as ultimate base at the 3' end
- Ensure primer sequence is unique for the template sequence
- Use a concentration of 0.1–1.0 μM of each primer. For many applications, a primer concentration of 0.2 μM will be sufficient

Lyophilized primers should be dissolved in a small volume of distilled water or TE to make a concentrated stock solution. Prepare small aliquots of working solutions containing 10 pmol/μl to avoid repeated thawing and freezing. Store all primer solutions at –20°C. Primer quality can be checked on a denaturing polyacrylamide gel; a single band should be seen.

(Source: <https://www.qiagen.com/gb/resources/molecular-biology-methods/pcr/>)

## 2.12.2 RT-qPCR protocol for miRNAs

Fluorescence based RT-qPCR reaction mix was prepared as follows:

Per reaction:

- 5  $\mu$ L SYBR Green Supermix (PrecisionPLUS, Primerdesign)
- 0.7  $\mu$ L miR-specific forward primer (miScript 10x Primer Assay, Qiagen)
- 0.7  $\mu$ L reverse primer (miScript 10x Universal Primer Assay, Qiagen)
- 0.6  $\mu$ L RNase free water (Sigma)

To this was added:

- 5  $\mu$ L pre-diluted cDNA sample

To give a total reaction volume of 12  $\mu$ L.

### RT-qPCR run cycle (Bio-Rad CFX)

A two stage amplification cycle protocol was employed. The initial denaturation step (95°C) being followed by a combined annealing and extension phase. Forty amplification cycles were run, followed by melt curve generation (55-95°C in 0.5°C increments) Annealing temperature was set to 58°C for miR-181 primers, 55°C for all other miR-specific primers (Figure 2.2).

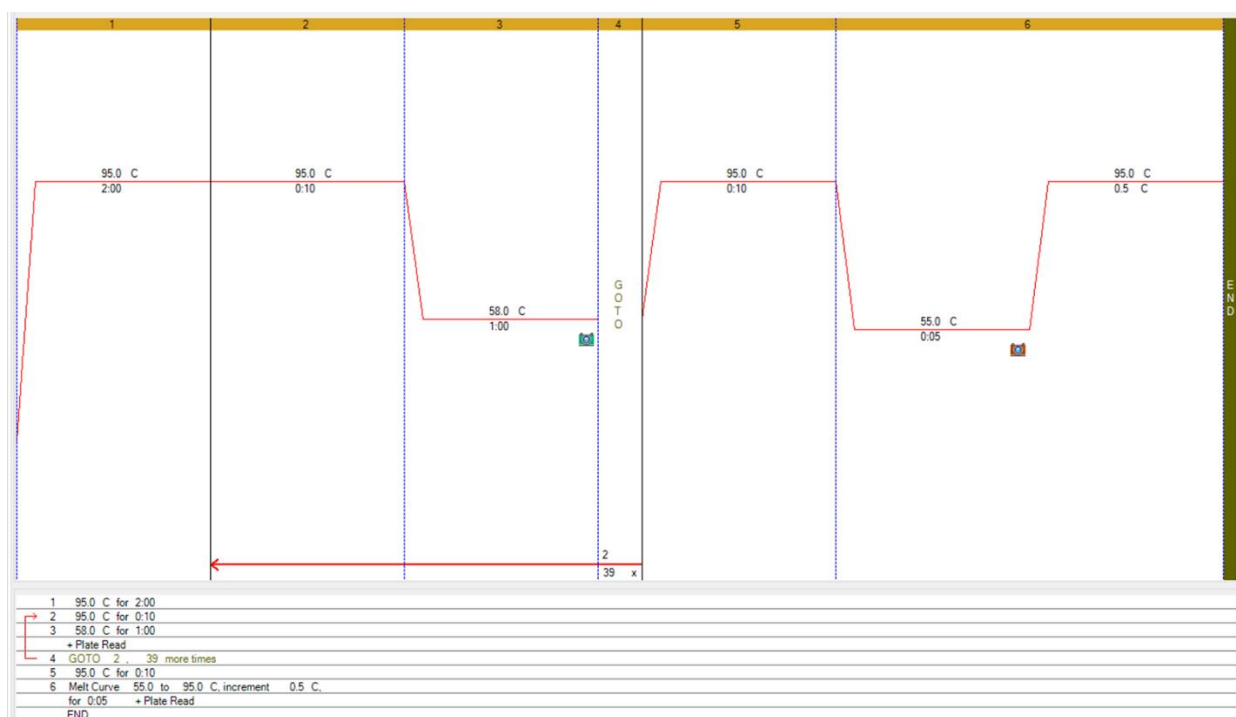


**Figure 2.2 RT-q PCR run cycle protocol for miRNA quantification.**

Technical replicates were run in triplicate. Expression relative to *SNORD61* was calculated using the delta Ct method. Calculation of *P*-values was by either Kruskal Wallis, Mann Whitney U, or Student's *t*-test with significance defined as  $P < 0.05$  (GraphPad Prism version 5.01 for Windows, GraphPad Software, San Diego California USA, [www.graphpad.com](http://www.graphpad.com)).

### 2.12.3 RT-qPCR protocol for mRNAs

Fluorescence based RT-qPCR reaction mix was prepared as follows (volumes are per reaction):

Primerdesign primers:

- 5 µL SYBR Green Mastermix (PrecisionPLUS, Primerdesign)
- 0.6 µL Forward/Reverse primer mix
- 1.4 µL RNase free water

Eurogentec or Sigma primers:

- 5 µL SYBR Green Mastermix (PrecisionPLUS, Primerdesign)
- 0.18 µL 20 µM Forward primer solution
- 0.18 µL 20 µM R primer solution
- 1.64 µL RNase free water (Sigma)

To this was added:

- 5 µL pre-diluted cDNA sample

To give a total reaction volume of 12 µL.

#### RT-qPCR run cycle (Bio-Rad CFX)

A two stage amplification cycle protocol was employed. The initial denaturation step (95°C) being followed by a combined annealing and extension phase, run at a default temperature of 60°C. Forty amplification cycles were run, followed by melt curve generation (65-95°C in 0.5°C increments) (Figure 2.3). If aberrant melt curves were generated, a temperature gradient plate was run (Figure 2.4) to optimise the annealing temperature and samples re-run.

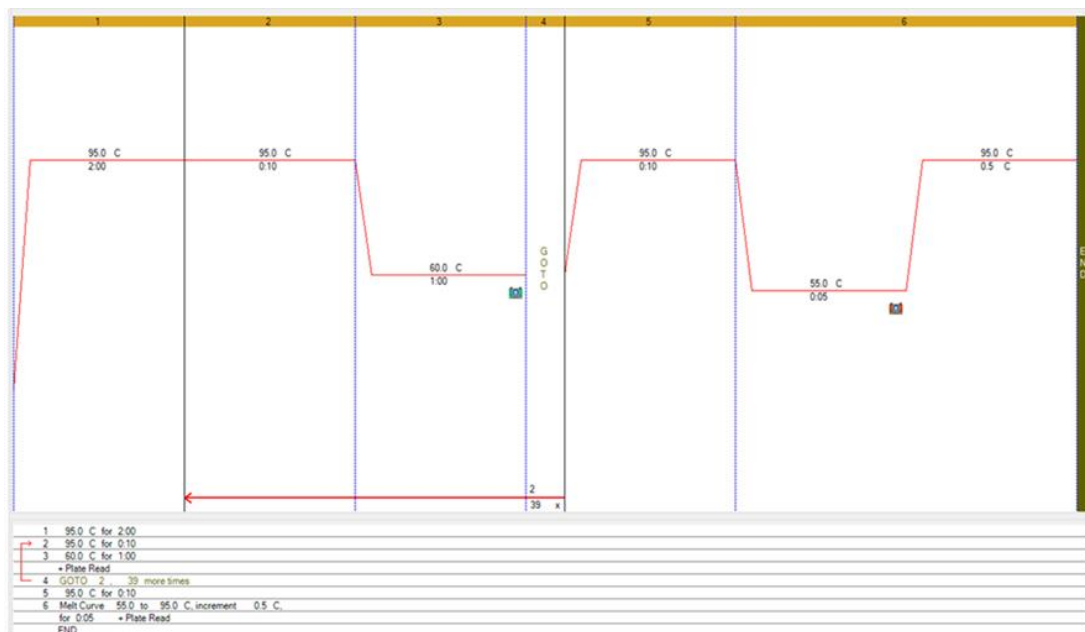


Figure 2.3 Standard RT-qPCR cycle run protocol for mRNA quantification.



## **2.13 Protein extraction**

### **2.13.1 Protein extraction protocol for cell monolayer culture (6 well plates)**

Materials required:

- Cell cultures
- 1000  $\mu$ L pipette and tips
- DPBS - cold from fridge (Sigma-Aldrich D8537)
- RIPA buffer (Sigma R0278-50ML)
- Protease inhibitor (Roche cOMplete ULTRA Tablets, Mini, EDTA-free protease inhibitor cocktail, Sigma 05892791001)
- Ice tray
- Cell scrapers
- 1.5 mL reaction tubes and rack
- Centrifuge
- Shaker incubator at 4°C

Dissolve 1 protease inhibitor tablet in 10 mL RIPA buffer - 150  $\mu$ L needed per construct.

Aspirate and discard TCM/treated TCM from wells.

Wash with DPBS x 2 and place culture plate on ice.

Remove DPBS and add 1 mL RIPA buffer with added protease inhibitor per well (6 well plates).

Incubate for 5 minutes on ice.

Collect lysate with cell scraper and transfer to labelled 1.5 mL reaction tube in ice.

Pipette vigorously to ensure complete lysis and place on shaker incubator in cold room (4°C) for 30 minutes.

Centrifuge tubes at 14,000 *g* for 10 minutes at 4°C.

Collect and measure supernatant into clean reaction tube and discard pellet.

Freeze at -80°C or perform Pierce Assay for protein concentration determination (see 2.13.3).

### 2.13.2 Protein extraction protocol for equine tenocyte constructs

Materials required:

- Samples - on dry ice or in liquid nitrogen
- Metal dismembrator capsules (from BBraun MIKRO-DISMEMBRATOR U)
- Pestle (narrow plastic ended pestle from Sartorius Potter S motorised pestle)
- 2 clean Dewars of liquid nitrogen
- Long handled haemostats with locking ratchet for liquid nitrogen immersion
- Dipping beaker and haemostats for liquid nitrogen
- Fine point forceps
- 60 mm diameter Petri dish to use as sterile instrument tray
- 100  $\mu$ L pipette and tips
- 1.5 mL reaction tubes and rack in ice
- 70% ethanol and 1% Distel to clean surfaces and instruments
- RIPA buffer (Sigma R0278-50ML)
- Protease inhibitor (Roche cOMplete ULTRA Tablets, Mini, EDTA-free protease inhibitor cocktail, Sigma 05892791001)

Dissolve 1 protease inhibitor tablet in 10 mL RIPA buffer - 150  $\mu$ L needed per construct.

Ensure appropriate PPE available for liquid nitrogen work.

Remove any residual suture material from constructs and weigh samples.

Using long handled haemostats immerse one half of a dismembrator capsule and pestle into liquid nitrogen – this will act as the mortar when grinding sample.

When boiling stops, remove capsule and pestle. Place pestle on sterile Petri dish, drain liquid N<sub>2</sub> from capsule and place on work surface.

Remove reaction tube containing sample from liquid nitrogen/dry ice, pinch hinge between thumb and forefinger for a few seconds to prevent hinge snapping when tube opened and tap sharply on work surface to loosen sample.

Transfer sample to mortar and add liquid N<sub>2</sub> from second Dewar.

Work quickly during this stage to minimise warming of capsule and sample. Wrap mortar in thick band of paper towel to hold.

Grind sample using pestle (add more liquid nitrogen to mortar if boils dry before powder formed).

CARE – sample is very brittle and can easily be lost from mortar unless broken up gently. Grinding the sample with liquid N<sub>2</sub> in the mortar reduces the risk of sample being lost from the mortar when it fragments.

Add 100  $\mu$ L RIPA buffer/protease inhibitor mix once sample reduced to powder. DO NOT add buffer until sample is powdered, as buffer will freeze and sample will not grind properly.

Place to one side and start processing next sample.

As mortar warms, buffer will melt and dissolve powdered sample. When liquid, use pipette to suck up buffer/sample solution to mix and transfer to 1.5 mL reaction tube.

Rinse mortar with 50  $\mu$ L RIPA buffer/protease mix and add this to reaction tube with sample.

Place reaction tube on ice whilst processing remaining samples.

Clean pestle (and mortar if need to reuse it) and any instruments used with 1% Distel then 70% ethanol prior to processing next sample.

Transfer all reaction tubes in a rack onto the orbital shaker in the cold room (4°C) and run shaker at 200 rpm overnight.

Centrifuge at 14000 *g* for 10 minutes at 4°C.

Collect (and measure) supernatant (discrete coherent pellet will form so easy to pipette off liquid).

Freeze at -80°C or perform Pierce Assay for protein concentration determination (see 2.13.3).

### **2.13.3 Protein concentration assay (Pierce assay)**

Materials required:

- Samples of protein extracts thawed on ice
- Bovine serum albumin standards (ThermoFisher 23208 - Pre-diluted Protein Assay Standards. Bovine Serum Albumin (BSA) set: 2000, 1500, 1000, 750, 500, 250 and 125  $\mu$ g mL<sup>-1</sup>) (or make your own).
- 96 well cell culture plate
- Pierce Assay Reagent (ThermoFisher 226600 – Pierce 660 nm Protein Assay Reagent.
- 10  $\mu$ L, 100  $\mu$ L and 1000  $\mu$ L pipettes and tips
- SPECTROstar Nano spectrometer-based absorbance microplate reader (BMG Labtech).

In 96 well plate add 10  $\mu$ L of standards/sample in duplicates or triplicates + 150  $\mu$ L Pierce Assay Reagent.

Put on plate shaker for 1 minute or just tap gently to mix – CARE solution does not splash onto plate lid and ensure all bubbles are removed (use 1000  $\mu$ L pipette to gently ‘blow’ on wells to remove bubbles).

Incubate at room temperature for 5 minutes.

Read absorbance at 660 nm wavelength on microplate reader.

Calculate standard curve and sample protein concentrations using Excel spreadsheet (anchor line of best fit through zero to obtain gradient for calculations).

## **2.14 SDS-PAGE**

Materials required:

- ProtoGel 30% w/v Acrylamide (National Diagnostics EC-890).
- ProtoGel Resolving Buffer (4x) (National Diagnostics EC-892).
- ProtoGel Stacking Buffer (National Diagnostics EC-893).
- 10% Ammonium persulfate (APS) stock solution (pre-prepared from ammonium persulfate; Sigma-Aldrich A3678).
- N,N,N',N'-Tetramethylethylenediamine (TEMED) (Sigma T9281-100ML).
- Tris-Glycine-SDS PAGE Buffer (10x) (National Diagnostics EC-870) or:
  - Tris base (Trizma® base – Sigma T6066-1KG)
  - Glycine powder for electrophoresis (Sigma-Aldrich G8898)
  - Sodium dodecyl sulfate (SDS) (Sigma L3771-100G)
  
- Protein Loading Buffer (x5) (National Diagnostics EC-887).
- Isopropanol (Sigma-Aldrich I9516-500ML).
- Distilled water
- Water - Molecular Biology Reagent (Sigma W4502-1L) – for protein dilution.
- Chameleon Duo Pre-stained Protein Ladder (LI-COR 928-60000).
- 5 mL and 10 mL serological pipettes and gun.
- 10 and 200 µL pipettes and tips.
- Pasteur pipettes.
- 30 mL Universals or 15 mL Falcon tubes.
- Heating block set to 95°C.
- PowerPac Basic Power Supply (Bio-Rad 1645050).
- Electrophoresis tank (Bio-Rad Mini-PROTEAN Tetra System 165-8006) – includes 1.5 mm gel casting glasses and apparatus.

### **2.14.1 Solutions and reagents for SDS-PAGE**

**1x Running Buffer** – need 1 L.

Dilute 10x Tris-Glycine-SDS PAGE buffer in distilled water, or make up:

- 3.03 g Tris base (0.025 M)
- 14.4 g Glycine (0.192 M)
- 1 g SDS (0.1%)
- 1000 mL distilled water

pH 8.5 (do not adjust pH).

Prepared in advance and store at 4°C.

### 10% ammonium persulfate (APS) stock solution

Dissolve 500 mg ammonium persulfate powder (Sigma-Aldrich A3678) in 5 mL of distilled water. Freeze at -20°C in 250 µL aliquots (enough to make 2 x gels).

### 2.14.2 Protocol for casting gels

Set up gel casting stand. Make sure base of casting glasses are level and held tightly together to prevent leaking (use plates for 1.5 mm gel).

Prepare two tubes for the resolving and stacking gel solutions as indicated in Table 2.15 (do not add APS or TEMED yet, as the solution will polymerise – add these just before pouring the solution into the casting glasses).

Reagent	Resolving gel (12%)		Stacking gel (4%)
	1 gel	2 gels	2 gels
ProtoGel 30% Acrylamide	4 mL	8 mL	1.3 mL
ProtoGel Resolving Buffer (4x)	2.5 mL	5 mL	N/A
ProtoGel Stacking Buffer	N/A	N/A	2.5 mL
Distilled water	3.3 mL	6.6 mL	6.1 mL
APS (10% stock solution)	100 µL	200 µL	50 µL
TEMED	20 µL	40 µL	25 µL

**Table 2.15** Relative quantities of reagents for casting gels used for Western blotting.

Add APS and TEMED to the resolving gel solution, mix by inverting. Using 10 mL serological pipette, add ~8 mL of the resolving gel solution into the gap between the two glasses, leaving 2 cm below the bottom of the comb level – avoid creating bubbles.

Quickly add a ~1 mL of isopropanol on top of the resolving gel to obtain a flat interface and remove surface bubbles. Leave to polymerise for 30 minutes at room temperature.

Once polymerised, pour off isopropanol and carefully rinse with distilled water several times. Remove any excess of liquid with a filter paper – do not touch gel.

Add APS and TEMED to the stacking gel solution, mix by inverting and pour onto top of resolving gel (~3 mL per gel to form positive meniscus at top of short plate). Carefully place the appropriate comb avoiding bubbles. Leave to polymerise at room temperature for at least 30 minutes.

Once polymerised, gently remove comb for use, or store with comb in place, wrapped in tissue paper soaked with distilled water and sealed in a plastic bag (up to 2 days at 4°C).

### 2.14.3 Protocol for loading and running gels

Calculate the volume of protein sample needed to obtain required mass of protein for all samples and volumes of molecular grade water and 5x loading buffer needed to make up required total loading volume. Use 5-30 µg protein.

Mix samples and water first, then add 1:5 (loading buffer:undiluted sample) of 5x protein loading buffer – do this in fume hood. Protein with loading buffer can be prepared in advance and stored at -20°C until use.

Maximum loading volumes (Sample + buffer + water) for 1.5 mm thick gels:

- 30 µL if using 15 well comb
- 60 µL if using 10 well comb

Heat the samples at 95°C for 5 minutes in heating block. Briefly centrifuge to collect sample at base of tube (this must be done just before loading the samples).

Place the gel in the electrophoresis tank, with the wells facing the interior of the tank. If running only one gel, place a plastic buffer dam on the opposite side of the gel box.

Pour cold running buffer into the electrophoresis tank between the gels, making sure that the reservoir between the gels is completely filled and that the buffer level comes to the mark on the side of the tank. Note: running buffer must be cold - put the electrophoresis tank over ice box.

Load molecular marker (Chameleon Duo, LI-COR) in the first well; 5 µL for 10 well gel; 3 µL for 15 well gel. Then load samples in their respective wells. Do this in fume hood. Tilting gel holder in tank makes it easier to see wells.

Top up running buffer if necessary – CARE – use serological pipette to avoid disturbing samples.

Close electrophoresis tank making sure that the red (positive) and black (negative) electrode wires are correctly connected to the power supply.

Use constant voltage setting on power supply. Apply a voltage of 120 V for 1<sup>1</sup>/<sub>2</sub> hours. Check current is running by looking for bubbles forming on the electrodes. Run until the loading buffer reaches the bottom of the gel – may need to run for another 10 minutes or so, but monitor progress of loading dye.

## **2.15 Western blotting**

Materials required:

- Tris base (Trizma® base – Sigma T6066-1KG)
- Methanol (Sigma-Aldrich 322415-1L)
- 6-amino-n-hexanoic acid (Sigma-Aldrich 07260-500G)
- 3MM Chr Chromatography Paper 10 cm x 100 m (GE Healthcare Whatman 3030-672)
- Ponceau S Solution (Sigma-Aldrich P7170-1L)
- TWEEN 20 (Sigma-Aldrich P1379-500ML)
- Distilled water
- Phosphate Buffered Saline Tablets (Sigma-Aldrich P4417-50TAB)
- PVDF Western Blotting Membrane (Roche 03010040001)
- Marvel Original Dried Skimmed Milk Powder (Premier Foods)
- Odyssey Blocking Buffer (now discontinued)
  - TBS (LI-COR 927-50000)
  - PBS (LI-COR 927-40000)
- Intercept Blocking Buffer
  - PBS (LI-COR 927-7000)
- Primary antibodies:
  - Rb anti-LC3B (ab192890) - use at 1:1000 dilution
  - Ms anti-MFN1 (ab57602) - use at 1:1000 dilution
  - Ms anti-MFN2 (ab56889) - use at 1:1000 dilution
  - Rb anti-NRF2 C-20 (sc-722) - use at 1:400 dilution
  - Ms anti-P62 (ab56416) - use at 1:1000 dilution
  - Ms anti-PARKIN (ab77924) - use at 1:200 dilution
  - Rb anti-TOMM20 (ab186734) - use at 1:1000 dilution
  - Rb anti-BNIP3 (ab109362) - use at 1:1000 dilution
  - Rb anti-COXIV (ab16056) - use at 1:1000 dilution
  - Rb anti-LAMP1 (ab62562) - use at 1:500 dilution
  - Ms anti-Vinculin (ab130007) - use at 1:1000 dilution
- Secondary antibodies:
  - IRDye 800CW Goat anti-Rabbit IgG (LI-COR 926-32211) – use at 1:10,000 dilution
  - IRDye 800CW Goat anti-Mouse IgG (LI-COR 925-32210) – use at 1:10,000 dilution
  - IRDye 680RD Goat anti-Mouse IgG (LI-COR 926-68070) – use at 1:10,000 dilution
- Trans-Blot SD Semi-Dry Transfer Cell (Bio-Rad 170-3940)
- Chemi Doc XRS+ Imaging System (Bio-Rad 1708265)
- Odyssey CLx Imaging System (LI-COR 9140-PRE)

### 2.15.1 Solutions required for Western blotting

**PBS-T:** (0.05% Tween20® in PBS)

- 5 Phosphate buffered saline tablets (Sigma P4417-50TAB)
- 1000 mL distilled water
- 50 µL Tween20® (Sigma P7949-500ML)

(Note: if looking at phosphorylated proteins use **TBS-T** – also need **TBS** blocking buffer).

**Anode I Buffer:** 0.3 M Tris in 20% methanol solution, pH 10.4.

- 36.34 g Tris base
- 800 mL distilled water
- 200 mL methanol

**Anode II Buffer:** 25 mM Tris in 20% methanol solution, pH 10.4.

- 3.02 g Tris base
- 800 mL distilled water
- 200 mL methanol

**Cathode Buffer:** 40 mM 6-amino-n-hexanoic acid in 20% methanol solution, pH 7.6.

- 5.24 g 6-amino n hexanoic acid
- 800 mL distilled water
- 200 mL methanol

### 2.15.2 Western blotting protocol

Remove gel from glass plates. Trim wells from top of gel and place in Anode II buffer to equilibrate for ≥10 minutes.

Cut approximately 6 cm x 8.5cm square of PVDF membrane. Do not touch membrane - handle using tissue forceps. Activate membrane by incubating in methanol on rocker for ≥10 minutes and then rinse in Anode II solution.

For each gel cut 18 pieces of chromatography paper slightly larger than gel (8 cm x 10 cm). Soak in transfer buffers as follows:

- 6 papers in Anode I buffer
- 3 papers in Anode II buffer
- 9 papers in Cathode buffer

Load the transfer cell in the following order:

- Cathode (-) (top)
- 9 papers soaked in Cathode solution
- Gel
- Membrane
- 3 papers soaked in Anode II solution
- 6 papers soaked in Anode I solution
- Anode (+) (bottom)

Remove air bubbles by rolling.

Soak up any excess transfer buffers next to the blot with paper towel and close cell.

Run transfer unit at 200 mA for 1 hour (The transfer time may vary depending on the properties of the proteins, and should be determined empirically).

Remove membrane carefully, rinse with distilled water and stain with Ponceau S.

Return Ponceau S stain to bottle and wash membrane 3-4 times with distilled water until background staining removed and the bands are clearly visible. Do not wash with PBS-T before imaging or all bands will become weaker and image quality will be poor.

Image Ponceau staining using BIO-RAD Chemi Doc.

Wash the membrane 3 x 5 minutes with PBS-T until Ponceau staining completely removed.

Block membrane with 10 mL 3% milk in PBS-T or LI-COR Odyssey or Intercept Blocking Buffer for 60 minutes at room temperature on rocker (keep blocking solution to dilute secondary antibody in later).

Incubate overnight at 4°C on rocker with primary antibody diluted in 3% milk/PBS-T or LI-COR Blocking Buffer.

Wash 3 times for 5 minutes with PBS-T.

Incubate for 1 hour at room temperature with secondary antibody diluted in 10 mL 3% milk/PBS-T or LI-COR Blocking Buffer.

Wash 3 times for 5 minutes with PBS-T.

Image membrane with LI-COR Odyssey CLx Imaging System.

## **2.16 Histological processing**

Tendon constructs for histological evaluation were submitted pinned to a backing of silicone elastomer (Sylgard™, Dow Corning Corporation) in appropriate fixative (see 2.4.3). All processing was performed by Miss Valerie Tilston of the University of Liverpool Veterinary Laboratory Services Group, Leahurst Campus.

### **2.16.1 Routine histology**

Processing for light microscopy was performed by Mrs Valerie Tilston and consisted of paraffin embedding, sectioning, mounting and staining with haematoxylin and eosin, Masson's trichrome and elastin von Gieson's stains.

Materials required:

- Potassium permanganate (Sigma-Aldrich 223468-500G)
- Oxalic acid 1% (TCS Biosciences HK015)
- Ethanol (Sigma-Aldrich 51976-500ML-F)
- Millers Stain (HD Supplies HS235-500)
- Van Giesons Stain (TCS Biosciences HS780-500)
- Xylene (Fisher Scientific X/0250/17)
- Haematoxylin 95% monohydrate (Atom Scientific RRBD61-X or TCS Biosciences HD1475)
- Sodium iodate (Acros Organics 201761000)
- Aluminium Potassium Sulphate (Acros Organics 217485000,)
- Glacial Acetic Acid (Fisher Scientific A/0360/PB17)
- Eosin Y Stain (TCS Biosciences Ltd HS250-1L)
- Celestine Blue (Sigma-Aldrich 206342)
- Ferric Ammonium Sulphate (BDH Chemicals 271644)
- Glycerol (VWR International 24388.295)
- Ponceau de Xylidine (HD Supplies HD1800)
- Acid Fuchsin (Biostain Ready Reagents RRBD93/X)
- Phosphomolybdic acid (Acros Organics 206381000)
- Light Green (HD Supplies HD1535)
- DPX (Thermo Scientific LAMB/DPX)
- Distilled water
- Microscope slides (Solmedia MSS61012S, MSS4511YW)
- Cover slips (FisherScientific FB58670)
- Tissue processing/embedding cassettes (Fisher Scientific 10746851)
- Tissue processor (Sakura Fintek Tissue-Tek Vacuum Infiltration Processor)
- Paraffin wax (Solmedia Ultraplast premium embedding medium WAX060)
- Microtome (Leica RM 2125 RT microtome Leica Microsystems (UK) Ltd, Milton Keynes, UK)

Dehydration and infiltration of formalin fixed tissue was performed in a Tissue-Tek vacuum infiltration automatic tissue processor overnight, using the following protocol:

- 10% formalin for 1 hour 45 minutes
- 70% ethanol for 30 minutes
- 70% ethanol for 30 minutes
- 86% ethanol for 30 minutes
- 96% ethanol for 1 hour 30 minutes
- Absolute ethanol for 1 hour 30 minutes
- Absolute ethanol for 1 hour 30 minutes
- Xylene for 1 hour
- Xylene for 2 hours
- Wax 1 for 1 hour
- Wax 2 for 1 hour
- Wax 3 for 1 hour
- Wax 4 for 1 hour
- End

Samples were embedded in paraffin, 4 µm paraffin sections cut on a Leica RM2125 RT microtome, floated on a waterbath and placed on slides. Dewaxing, rehydration, staining and dehydration of sections was performed as detailed below. Mounting was completed by application of DPX and cover slip.

#### **Millers Elastin Stain (EVG) staining method**

Dewax sections in xylene for 5 minutes.

Transfer sections to fresh xylene and rehydrate by taking through descending concentrations of ethanol; 100% → 96% → 85% → 70% → distilled water.

Treat sections with 1% potassium permanganate for 5 minutes.

Rinse in distilled water.

Decolourise in 1% oxalic acid for 1 minute.

Wash briefly in running water.

Rinse in 95% ethanol.

Stain in Millers stain (HD Supplies, HS235-500) for 3 hours.

Rinse in 95% ethanol to remove excess stain.

Wash in running water.

Counterstain with Van Giesons stain (TCS Biosciences, HS780-500) for 4 minutes.

Blot, air dry and dehydrate in absolute ethanol.

Clear in xylene and mount in DPX.

*Elastin tissue stains deep blue; collagen stains red; other tissues stain yellow.*

### **Mayers Haematoxylin formulation**

- 1 g Haematoxylin 95% monohydrate (RRBD61-X, Atom Scientific, Manchester, UK or TCS Biosciences Ltd HD1475).
- 0.2 g Sodium iodate (Acros Organics 201761000).
- 50 g Aluminium Potassium Sulphate (Acros Organics 217485000).
- 1 L distilled water.
- 20 mL glacial acetic acid (Fisher Scientific A/0360/PB17).

Dissolve haematoxylin in distilled water using gentle heat.

Add aluminium potassium sulphate and dissolve using gentle heat.

Cool, add sodium iodate and mix.

Filter the solution and add 20 mL glacial acetic acid.

### **Eosin stain formulation**

- 50 mL 1% Eosin Y Stain (TCS Biosciences Ltd HS250-1L).
- 390 mL 95% ethanol.
- 2 mL glacial acetic acid (Fisher Scientific A/0360/PB17).

### **Haematoxylin and eosin (H&E) staining method**

Dewax sections in xylene for 5 minutes.

Transfer sections to fresh xylene and rehydrate by taking through descending concentrations of ethanol; 100% → 96% → 85% → 70% → distilled water.

Stain sections in Haematoxylin for 5 minutes.

'Blue' sections under running tap water for 6 minutes.

Stain sections in Eosin for 2 minutes.

3 x 1 minute washes in 96% alcohol (dip sections up and down to remove excess Eosin).

3 x washes in 100% alcohol.

2 x washes in xylene.

Mount sections in DPX and coverslip.

*Haematoxylin – basic dye staining basophilic structures (ribosomes, nucleus, RNA-rich regions) blue-purple.*

*Eosin – alcohol based acidic dye colours eosinophilic structures (protein rich) pink.*

*Structures do not have to be acidic or basic, the terms basophilic and eosinophilic reflects the affinity to the dyes.*

### **Masson Trichrome stain formulation**

- **Celestine Blue Solution**
  - 2.5 g Celestine Blue (Sigma-Aldrich 206342).
  - 25 g Ferric Ammonium Sulphate (BDH Chemicals 271644).
  - 70 mL Glycerol (VWR International 24388.295).
  - 500 mL distilled water.
- **Cytoplasmic Stain**
  - 2 parts 1% Ponceau de Xylidine (HD Supplies HD1800).
  - 1 part 1% Acid Fuchsin (Biostain Ready Reagents RRBD93/X) in 1% acetic acid.
- **1% Phosphomolybdic acid** (Acros Organics 206381000).
- **2% Light Green** (HD Supplies HD1535).

### **Masson's Trichrome staining method:**

Dewax sections in xylene for 5 minutes.

Transfer sections to fresh xylene and rehydrate by taking through descending concentrations of ethanol; 100% → 96% → 85% → 70% → distilled water.

Stain in Celestine Blue for 5 minutes.

Rinse with tap water and stain with Mayers Haematoxylin for 5 minutes.

'Blue' in tap water for 6 minutes.

Stain with Cytoplasmic Stain for 7 minutes.

Rinse in tap water.

Differentiate in 1% phosphomolybdic acid for 5 minutes.

Rinse in tap water.

Counterstain in 2% Light Green (dilute 1:10 in 1% acetic acid) for 5 minutes.

Differentiate in 1% acetic acid for 1-2 minutes to remove excess green.

Blot with fibre free blotting paper.

Dehydrate through increasing grades of alcohol (70%, 85%, 96%, 100%) clear in xylene and mount with DPX ((LAMB/DPX).

*Nuclei stain black; muscle, red blood cells, fibrin and cytoplasmic granules stain red; collagen, reticulin, amyloid and mucin stain green.*

### Grading histological appearance of tendon constructs

Constructs were graded according to the modified scheme given in Table 2.16.

Characteristic	Score
<b>Extracellular Matrix organisation</b> <ul style="list-style-type: none"> <li>- Compact</li> <li>- In part compact, in part loose</li> <li>- Loosely composed, not orderly</li> </ul>	 2 1 0
<b>Cell Shape</b> <ul style="list-style-type: none"> <li>- Spindle-shaped (normal)</li> <li>- Mixture of spindle and round cells</li> <li>- Oval to rounded shape</li> </ul>	 2 1 0
<b>Cell Distribution</b> <ul style="list-style-type: none"> <li>- Homogenous Distribution of cells</li> <li>- Focal areas of altered cell density</li> </ul>	 1 0
<b>Cellular Alignment</b> <ul style="list-style-type: none"> <li>- Uniaxial</li> <li>- More than 50% of cell with no uniaxial alignment</li> </ul>	 1 0
<b>Cellularity</b> <ul style="list-style-type: none"> <li>- Low Cellularity</li> <li>- Intermediate Cellularity</li> <li>- High Cellularity</li> </ul>	 2 1 0
<b>Collagen arrangement</b> <ul style="list-style-type: none"> <li>- Parallel arrangement, tight cohesive bundles, homogenous polarisation pattern, normal crimping</li> <li>- Separation of individual fibre bundles, maintenance of overall bundle architecture</li> <li>- Bundle changes; loss of demarcation of bundles, loss of normal polarisation pattern</li> <li>- Marked separation of bundles, complete loss of architecture</li> </ul>	 3 2 1 0

**Table 2.16 Grading scheme used to score tendon construct histological appearance.** The scheme is modified from elements contained in the Bonar (Cook et al 2004) and Movin (Movin et al 1997) scores for classification of the histopathological appearance of diseased tendon.

Histological scores were compared across treatment groups using the Kruskal Wallis test with Dunn's multiple comparison test. Inter- and intra-rater reliability of scoring investigated using weighted Cohen's kappa coefficient (GraphPad Prism version 5.01 for Windows, GraphPad Software, San Diego California USA, [www.graphpad.com](http://www.graphpad.com)).

### 2.16.2 Electron microscopy

Processing for transmission electron microscopy (TEM) was performed by Mrs Marion Pope and consisted of resin embedding, sectioning, mounting and staining with Toluidine blue (for light microscopy evaluation) and uranyl acetate and lead citrate staining (TEM evaluation).

Materials required:

- Glutaraldehyde 25% E.M. Grade (Taab Laboratories Equipment G002).
- Sodium cacodylate (Taab Laboratories Equipment S011).
- Osmium tetroxide (Taab Laboratories Equipment O001).
- Uranyl acetate (Taab Laboratories Equipment U007).
- Maleic acid (Taab Laboratories Equipment M003).
- Ethanol, absolute (Taab Laboratories Equipment E047).
- Acetone E.M. grade (Taab Laboratories Equipment A018).
- Taab epoxy resin components (Taab Laboratories Equipment T001, D025, M011, D032).
- Embedding moulds (Taab Laboratories Equipment E095).
- Toluidine blue (Taab Laboratories Equipment SD211).
- Borax (Taab Laboratories Equipment B021).
- Methanol (Taab Laboratories Equipment M023).
- Reynold's lead citrate stain 3% (Taab Laboratories Equipment L037).
- Curing oven at 60°C (Genlab Ltd MINO/4/CLAD).
- Richert-Jung Ultracut ultramicrotome (Leica Microsystems (UK) Ltd).
- Diatome ultra diamond knife (Agar Scientific AGG3397).
- 200 mesh TEM thin bar copper grids (Agar Scientific AGG2700C).
- Phillips EM208S Transmission Electron Microscope (Thermo Fisher Scientific).

#### Fixation:

Primary: 2.5% glutaraldehyde in 0.1 M sodium cacodylate buffer pH 7.4 for 4 hours.

Wash 0.1 M sodium cacodylate buffer pH 7.4 for 30 minutes.

Secondary fixation and contrast stain: osmium tetroxide 1% aqueous for 1 hour.

Wash 0.1 M sodium cacodylate buffer pH 7.4 for 30 minutes.

'en bloc' staining 2% uranyl acetate in 0.69% maleic acid pH 4.5 for 1 hour.

Dehydrate in ascending concentrations of ethanol 50% → 70% → 90% for 2 x 5 minutes each.

100% ethanol 3 x 10 minutes each.

100% acetone 3 x 5 minutes each.

Infiltrate with epoxy resin in ascending resin: acetone mixes:

- resin 1 : 3 acetone for 1 hour.
- resin 2 : 2 acetone for 1 hour.
- resin 3 : 1 acetone for 1 hour.
- 100% resin 2 x 1 hour.

Embed in 100% epoxy resin in flat embedding mould.

Polymerise at 60°C overnight.

### **Sectioning :**

For light microscopy evaluation:

- Semi-thin sections (0.5  $\mu\text{m}$ ) cut on Reichert-Jung Ultracut ultramicrotome.
- Stained with 1% Toluidine blue in 1 % borax.

### **For TEM:**

- Ultrathin Sections (60-90 nm) cut with Diatome diamond knife on Reichert-Jung Ultracut ultramicrotome.
- Mount on 200 mesh copper grids.
- Contrast stain with saturated solution of uranyl acetate in 50% methanol for 5 minutes.
- Incubate with *Reynold's Lead citrate stain* for 5 minutes.

Viewed and imaged in Phillips EM208S Transmission Electron Microscope at 80 kV.

## **2.17 Statistical analysis**

Small RNA-sequencing data were analysed for differential gene expression using the Bioconductor package DESeq2 (version 1.22.2). Genes were considered DE if log<sub>2</sub> fold change  $\geq 1.5$  with a Benjamini-Hochberg adjusted *P*-value  $< 0.05$ . All principal component analysis calculations were performed in R (version 4.0.1, R Core Team (2020)), using the *prcomp* function, with principal components one and two plotted using the *ggplot2* plotting package. See Chapter 3 for further details.

miRNA:target interactions, associated network and pathway analysis was performed using\_QIAGEN Ingenuity Pathway Analysis (QIAGEN Inc., Redwood City, CA, USA, <https://www.qiagenbioinformatics.com/products/ingenuity-pathway-analysis>, Krämer et al 2014). See Chapter 4 for further details.

Analysis of inter- and intra-rater repeatability of the modified grading system applied to tissue-engineered three-dimensional equine tendon constructs (Chapter 6) was investigated using Cohen's kappa coefficient ( $\kappa$ ), calculated in Excel (Microsoft Corporation, 2018. Microsoft Excel, available at: <https://office.microsoft.com/excel>). Tables were constructed for total score and each component of the grading scheme for both repeated, blinded grading by the same operator and blinded grading by two independent operators. Agreement due to chance was calculated and subtracted from both the sum of number of agreements and total number of comparisons possible, with the ratio of the residuals defining Cohen's kappa for each component, which varied between 0 (agreement equivalent to chance alone) and 1 (perfect agreement).

All other statistical analyses were performed using GraphPad Prism version 5.01 for Windows (GraphPad Software, San Diego California USA, [www.graphpad.com](http://www.graphpad.com)).

RT-qPCR data were analysed non-parametrically. In Chapter 3, comparison of relative miRNA expression between tendinopathic tissue and controls for both human and equine data, human tendinopathy validation work and comparisons between control and posterior tibial tendon (PTT) tissue utilised the Mann-Whitney test as conditions for its application were satisfied. Comparisons between control and supraspinatus (SSP) tissue, and between SSP and PTT samples (Chapter 3), utilised the Student t test, as less than three data points were present in the SSP comparator group, which precluded the use of non-parametric analysis. These results are presented in Appendix 2, Figure A2.2. Comparison of ages between donors of tendinopathic and control tissue utilised the Student t-test.

Analysis of gene expression (Chapters 5, 6 and 7) and tissue-engineered three-dimensional tendon construct grading data (Chapter 6), between miR-181a mimic, antagomiR and scrambled control sequence treated groups were analysed using the Kruskal Wallis test with Dunn's test for pairwise comparisons. Comparison of target gene expression (Chapter 5, 6 and 7) and histological grading scores (Chapter 6) between scrambled control sequence treated and untreated groups, where performed, utilised the Mann-Whitney test when conditions for its application were satisfied. Results are presented in Appendix 5, Figure A5.1, Appendix 6, Figures A6.1 and A6.3, and Appendix 7, Figure A7.1 respectively. Where less than three data points were present in one comparator group, the Student t test was used. Histological scoring between scrambled control and untreated constructs contained some categories where all data points in the untreated group had the same numerical value, it was therefore not possible to generate *P*-values for these categories.

Protein levels between miR-181a mimic, antagomiR and scrambled control sequence treated groups derived from Western blot images (Chapters 6 and 7) were analysed using one way ANOVA with Tukey's multiple comparison test for pair-wise comparisons. Comparisons between scrambled control sequence treated and untreated groups (Chapter 7) utilised the Student-t test and are presented in Appendix 7, Figure A7.3.

Further details are given in the relevant chapters. In all cases, significance was determined at  $P < 0.05$ .

## **Chapter 3 - microRNA profiling of human and equine tendon**

### **3.1 Introduction**

Non-coding RNAs (ncRNA) are broadly classified into long (>200 nucleotides) and short (<200 nucleotides) subgroups (see Chapter 1, Figure 1.3). Within the short non-coding RNA (sncRNA) subgroup, several distinct families are recognised, including ones derived from fragmentation of transfer RNA (tRNA) which possess a regulatory function (tRNA-derived RNA (tDR) and 5'-tRNA stress-induced fragments (tiRNA)), microRNAs (miRNA), small interfering RNAs (siRNA), PIWI-interacting RNAs (piRNA), small nuclear RNAs (snRNA), small nucleolar RNAs (snoRNA; within which, small Cajal body-specific RNA (scaRNA) and sno-derived RNA (sdRNA) are distinctly identifiable components), Y-RNAs, and vault RNAs (vtRNA).

Highly abundant in the nucleus, snRNAs are important in intron splicing, stabilisation and maturation of mRNA. Regulation of histone gene transcription, and translational repression of several mRNAs by binding to their 3'UTR, thereby preventing polyadenylation and facilitating degradation, is also reported (Valadkhan and Gunawardane 2013).

There are two major classes of snoRNAs; box C/D and box H/ACA snoRNAs, which guide 2'-O-ribose-methylation, and pseudouridylation of target mRNAs respectively. Within the H/ACA class, location of a specific subset is restricted to within Cajal bodies (a nuclear organelle), with these subsequently referred to as scaRNA. snoRNAs act to modify ribosomal RNA during ribosomal biogenesis, but also target snRNAs and mRNAs (Mattick and Makunin 2006).

miRNAs and siRNAs are both approximately 20-25 nucleotides in length and function in a similar manner, directing mRNA cleavage or translational repression. Distinguished by differences in their biogenesis, miRNAs are processed from transcripts which form hairpin structures, with each hairpin precursor yielding a single miRNA:miRNA\* duplex. Conversely, siRNAs are derived from linear double stranded RNA duplexes each of which can generate multiple siRNA duplexes. Target specificity also differs, with miRNAs able to repress translation of genes from multiple different loci, whereas siRNAs tend to act on genes from adjacent genomic locations (Bartel 2004). Other RNA species possessing hairpin elements, such as tRNA and snoRNA can, additionally, be processed into miRNAs (see Chapter 1, Figures 1.3 and 1.4).

PIWI-interacting RNAs are 21-35 nucleotide RNAs processed from long, single stranded precursor transcripts derived principally, but not exclusively, from transposable element (TE) sequences and show great diversity between species. Mature piRNAs bind to a specific clade of Argonaute proteins and exert their effect in a similar manner to miRNA and siRNAs, interacting with target mRNAs through base pairing, which are then cleaved by the endonuclease activity of the Argonaute protein (Rojas-Ríos and Simonelig 2018). Due to their derivation from, and targeting of, TE mRNA, they provide a flexible mechanism for gene silencing, as they are not constrained by the conserved nature of miRNAs and siRNAs (Ozata et al 2018).

Y-RNAs are essential for initiation of chromosomal DNA replication and, in association with the Ro60 protein are associated with RNA stability and cellular stress responses (Kowalski and Krude 2015).

In humans, four vtRNA paralogues have been identified, vtRNA1-1, vtRNA1-2, vtRNA1-3 and vtRNA2-1. These are integral components of the vault complex which is involved in nucleo-cytoplasmic transport, intracellular detoxification processes, signalling, resistance to apoptosis and nuclear pore complex formation (Amort et al 2015).

Although the function of many of these sncRNA species is not fully understood, their importance as epigenetic modifiers of phenotype is being increasingly recognised. Of the sncRNAs, miRNAs have been the most extensively studied, and were the family which we were principally interested to explore in relation to tendon disease.

The number of identified microRNAs (miRNAs) recorded in publically available data bases, such as miRMaster (Fehlmann et al 2017), miRCarta (Backes et al 2018), miRGeneDB (Fromm et al 2020) and miRBase (Kozomara et al 2019) has increased dramatically in recent years, with 2,656 mature human miRNAs listed in the most recent release (v22) of miRBase (Kozomara et al 2019, Alles et al 2019). The number of miRNAs listed, however, differs between databases, which vary in their remit and stringency of inclusion criteria. The total number of true miRNAs is unknown, as not only are there potentially as yet undiscovered miRNAs, but only 26% of human miRNAs listed in miRBase release 22 are annotated with a high level of confidence, the majority lacking robust experimental validation (Alles et al 2019; Friedländer et al 2008). Traditional experimental approaches to identification of miRNAs including cloning and Sanger sequencing have been complemented more recently by computational predictions analysing genomic DNA for sequences resembling known miRNA precursors, adjacent to known miRNA genes, or conserved sequences lying outwith known protein coding regions, which have the potential to form stem-loop structures (Bartel 2004, Friedländer et al 2008). It is therefore possible that databases contain a high number of false-positives from computational predictions. Against this background, the increasing interest in the role of miRNA dysregulation in several disease states, has stimulated research into determining differential expression (DE) profiles of these regulatory RNAs using a number of technologies. Of these, reverse transcription quantitative PCR (RT-qPCR) offers the narrowest approach, relying on *a priori* selection of a small number of miRNAs identified from computational prediction, or previous research, as relevant to the disease process of interest. Microarrays are a dye-based detection system utilising sequence specific probe hybridisation and offer a relatively cost effective technology for dramatically increasing the number of targets investigated in transcriptome analysis. However, their use requires that arrays are available for the species and targets of interest. Hybridisation artefacts can, however, produce a non-uniform effect on expression measurement, result in loss of sensitivity in differentiating targets with high sequence similarity, and sequence content may influence detected probe intensities (Oshlack et al 2010). Background signal and cross-hybridisation also confound identification of low abundance transcripts and small changes in transcript expression, both of which may carry biological significance ('t Hoen et al 2008). The development of high-throughput sequencing technologies and their application to measuring RNA expression levels (RNA-seq) offers a powerful tool to gain an insight into profiling gene expression levels without any prior knowledge of the organism or disease process being investigated (Rapaport et al 2013). Expression of each transcript is measured by the number of 'reads' which map to the same sequence code, which in turn is determined by the sequencing depth – the total number of reads obtained from

each sample during a sequencing run. Whilst offering a far wider dynamic range, lower technical variability and higher sensitivity than RT-qPCR or microarray techniques, RNA-seq is expensive and generates large, complex datasets requiring a sophisticated analytical pipeline (Oshlack et al 2010). High throughput sequencing has also been shown to be biased towards certain small RNAs (those with high CG content), independent of sequencing platform, but strongly linked to the method of library preparation (Linsen et al 2009). Indeed, using an equimolar mixture of 473 synthetic human miRNAs, Linsen and co-workers (2009) reported profiling results indicating up to four orders of magnitude difference between least and most frequently detected miRNAs. However, whilst this precludes determination of absolute transcript abundance, these biases are systematic, reproducible and affect miRNAs over the entire read frequency distribution, allowing determination of differences in relative expression between samples (Linsen et al 2009). Differential expression profiling determined using RNA-seq has also been shown to positively correlate to qPCR results, as this latter technique also demonstrates similar quantification biases (Linsen et al 2009, Pradervand et al 2010).

Despite the limitations stated above, small RNA profiling by RNA-seq is considered the method of choice for studying small RNA expression (Linsen et al 2009), as it is not susceptible to hybridisation artefacts inherent in using microarrays, can accurately discriminate miRNA family members differing by only a single nucleotide, can detect 5' and 3' variants, and requires no pre-existing knowledge or assumptions of which miRNAs are relevant to the studied condition (Linsen et al 2009). Additionally, this technology is applicable to all species, including those for which limited genomic data is available (Rapaport et al 2013). Although we were principally interested in how miRNA expression changed with disease in tendinopathy, we broadened our RNA-seq analysis to capture other sncRNAs by expanding our library size selection to include sequences of 120 to 300 base pairs. Although this would give us a greater breadth of coverage within our samples, this does come at the potential cost of reducing sequencing depth for the miRNA component.

Our aim was to establish sncRNA profiles for both healthy and diseased human elastic energy storing tendon using RNA-seq and ascertain which sncRNAs showed significant DE between cohorts. Having demonstrated sncRNA transcriptomes differ significantly between healthy and diseased tissue, we then undertook to validate a selection of miRNAs (miRs -let-7f, -29a, -34a, -34b, -34c, -181a, -181b, -181c, -181d, -199a and -199b) using RT-qPCR. These miRNAs were chosen based on their predicted or validated targeting of pathological processes believed to be important in tendinopathy (fibrosis, matrix degradation, inflammation, oxidative stress, cellular differentiation and apoptosis).

Further, as equine tendon has frequently been proposed as a model for investigation of human tendon biomechanics and disease (Dudhia et al 2007, Innes and Clegg 2010, Lui et al 2011, Thorpe et al 2014), we were interested if analogous miRNA expression changes occurred in equine as in human tendinopathy. To this end, using RT-qPCR, we investigated expression of these same miRNAs in equine superficial digital flexor tendon (SDFT), comparing clinically normal and diseased tissue.

RT-qPCR validation of RNA-seq data was achieved for nine of the 11 miRNAs investigated, with four of these miRNAs also showing some level of agreement in equine SDFT, suggesting similarity in disruption of cellular processes between species.

## 3.2 Methods

### 3.2.1 Small RNA-sequencing

RNA was extracted from human supraspinatus (SSP) tendon tissue collected from six patients with rotator cuff tendinopathy undergoing surgical repair, and from mixed semitendinosis and gracilis (hamstring) tendon from six patients undergoing anterior cruciate ligament reconstruction surgery (Table 3.1).

Sample number	Sample name	Organism	Sex	Age (years)	Tissue	Source
18139_7	0946/18 SSP	Human	F	39	Diseased SSP	Glasgow
18139_8	0947/18 SSP	Human	F	39	Diseased SSP	Glasgow
18139_9	0866/18 SSP	Human	M	51	Diseased SSP	Glasgow
18139_10	0944/18 SSP	Human	M	50	Diseased SSP	Glasgow
18139_11	0864/18 SSP	Human	M	59	Diseased SSP	Glasgow
18139_12	0887/18 SSP	Human	F	45	Diseased SSP	Glasgow
18139_13	LMB-KM-249	Human	M	31	Healthy HST	Liverpool
18139_14	LMB-GA-253	Human	F	17	Healthy HST	Liverpool
18139_15	LMB-HB-254	Human	F	23	Healthy HST	Liverpool
18139_16	LMB-AS-255	Human	F	23	Healthy HST	Liverpool
18139_17	LMB-MW-260	Human	M	23	Healthy HST	Liverpool
18139_18	LMB-RM-261	Human	M	26	Healthy HST	Liverpool

**Table 3.1 Donor and tissue details for six diseased and six healthy control human tendon samples processed for RNA extraction for small RNA sequencing.** F = female, M = male, SSP = supraspinatus tendon, HST = hamstring (mixed semitendinosis and gracilis) tendon.

Following elution into RNase free water, RNA concentration and quality were assessed, and samples submitted to the Centre for Genomic Research, University of Liverpool, for library preparation and small RNA-sequencing. Fifty five nanograms of total RNA per sample were used for library preparation using a commercially available small RNA library preparation kit (NEBNext small RNA library prep kit). Library preparation adds approximately 126 bp to the original sequence length, and library for sequencing was size selected at 120-300 base pairs (bp). Paired-end, 150 bp sequencing was performed in a single lane on an Illumina HiSeq 4000 machine, generating data from >280 M clusters (sequencing depth approximately 23 M reads per sample).

Data were processed using CASAVA (version 1.8.2) to generate output in FASTQ format.

Raw FASTQ files were trimmed for the presence of adapter sequences using Cutadapt (version 1.2.1) with the option `-O3`, ensuring any reads which matched the adapter sequence for three bp or more

were removed. Reads were further trimmed for quality using Sickle (version 1.200) using a minimum Phred (Q) score of 20. Reads shorter than 12 bp after trimming were discarded.

Trimmed read pairs were aligned to reference genome (Gencode GRCh38.p12) using Bowtie2 (version 2.3.5) and subsequently counted using featureCounts (version 1.6.4) against the Gencode reference annotation file (Gencode (GRCh38.p12) gtf file) for non-miRNAs, and miRBase (hsa.gff3 file, release 22.1) for miRNAs, using Bowtie2 (version 2.3.5). Any counts to miRNAs from the Gencode file were removed to avoid duplication in downstream analysis.

Principal component analysis (PCA) was used to visualise sources of variance in the data. All PCA calculations were performed in R (version 4.0.1, R Core Team (2020)), using the *prcomp* function within the package on regularised log transcript abundances, to extract principal components. Once extracted, principal components one and two were plotted using the *ggplot2* plotting package, and samples were coloured according to the disease state of the tissue (red = diseased, blue = healthy). The variance each principal component explained was calculated manually as the square of the standard deviation.

### **3.2.2 Reverse transcription quantitative real-time polymerase chain reaction validation of small RNA-sequencing data**

Library preparation for RNA-sequencing consumed all available RNA from four of the six SSP tendinopathy samples, only two samples, both from 39 year old female patients were therefore available for RT-qPCR validation purposes. Total RNA was extracted from three independent samples of diseased posterior tibial tendon (PTT), according to the protocol detailed in Chapter 2, sections 2.8.1 and 2.8.4. RNA was available from all six original control samples. RT-qPCR validation of RNA-seq results was, therefore, performed on both dependent (six healthy control and two tendinopathic SSP samples) and independent (three tendinopathic PTT samples) cohorts.

Details of donor and tissue samples used in validation experiments are given in Table 3.2.

Sample number	Sample name	Organism	Sex	Age (years)	Tissue	Source
18139_7	0946/18 SSP	Human	F	39	Diseased SSP	Glasgow
18139_8	0947/18 SSP	Human	F	39	Diseased SSP	Glasgow
P1	P1M60081217	Human	M	60	Diseased PTT	Liverpool
P2	P2M71191217	Human	M	71	Diseased PTT	Liverpool
P3	P3M65130318	Human	M	65	Diseased PTT	Liverpool
18139_13	LMB-KM-249	Human	M	31	Healthy	Liverpool
18139_14	LMB-GA-253	Human	F	17	Healthy	Liverpool
18139_15	LMB-HB-254	Human	F	23	Healthy	Liverpool
18139_16	LMB-AS-255	Human	F	23	Healthy	Liverpool
18139_17	LMB-MW-260	Human	M	23	Healthy	Liverpool
18139_18	LMB-RM-261	Human	M	26	Healthy	Liverpool

**Table 3.2 Donor and tissue details for five diseased and six healthy control human tendon samples used for RT-qPCR validation of small RNA-sequencing data.** F = female, M = male, SSP = supraspinatus tendon, PTT = posterior tibial tendon.

Reverse transcription to cDNA used 30 ng total RNA template for miRNA expression analysis. Protocol details are given in Chapter 2, section 2.11.1. Levels of miRNAs -29a-3p, -34a-5p, -34b-5p, -34c-5p, -181a-3p, -181b-5p, -181c-5p, -181d-5p, -199a-5p, -199b-5p and -let-7f-5p were determined using commercially available primers (Qiagen, Manchester, UK) and normalised to *SNORD61* as internal control (validated for this purpose as a stable small non-coding RNA in human tenocytes (Appendix 7, Table A7.1)). Primer sequences and RT-qPCR details are listed in Chapter 2, sections 2.12.1 (Table 2.10) and 2.12.2 (Figure 2.2) respectively. For all RT-qPCR data, technical replicates were run in triplicate and expression relative to *SNORD61* calculated using the delta Ct method (Livak and Schmittgen 2001).

### 3.2.3 Reverse transcription quantitative real-time polymerase chain reaction validation of equine tendinopathy as a model for miRNA dysregulation in human tendon disease

Total RNA extracted from equine superficial digital flexor tendons (SDFT) for use in a separate study was made available for validation purposes (courtesy of Professor Mandy Peffers and Miss Roisin Wardle). This cohort consisted of six horses with normal SDFT, three horses with diseased SDFT and two horses from which both normal and diseased SDFT tissue had been collected (Table 3.3).

Sample name	Organism	Age (years)	Tissue
H1	Equine	3	Normal SDFT
H2	Equine	25	Normal SDFT
H3	Equine	4	Normal SDFT
H16	Equine	3	Normal SDFT
H18	Equine	19	Normal SDFT
H23N	Equine	6	Normal SDFT
H23D	Equine	6	Diseased SDFT
H24N	Equine	9	Normal SDFT
H24D	Equine	9	Diseased SDFT
H27	Equine	18	Normal SDFT
H47	Equine	7	Diseased SDFT
H52	Equine	6	Diseased SDFT
H62	Equine	7	Diseased SDFT

**Table 3.3 Donor and tissue details for 11 horses used for RT-qPCR validation of equine superficial digital flexor tendon (SDFT) disease as a model of human tendinopathy.** NB. Information on sex of animals was not available.

Reverse transcription to cDNA used 100 ng RNA template for miRNA expression analysis. Protocol details are given in Chapter 2, section 2.11.1.

Three candidate small non-coding RNA reference genes were investigated for use as internal controls. Based on previous reports (Sperveslage et al 2014, Bignotti et al 2016), expression of *small nuclear RNA-U6*, *small nucleolar RNA-61 (SNORD61)*, and *small nucleolar RNA-68* was assessed. Of these, *SNORD61* demonstrated least variation in expression. Across all biological replicates, and between those with normal or diseased SDFT, *SNORD61* threshold cycle (Ct) values varied by less than, or equal to, three cycles. Where normal and diseased tissue from the same individuals was available, *SNORD61* Ct values varied by  $\leq 0.75$  cycles (Appendix 2, Table A2.1). Levels of miRNAs - 29a, -34a, -34b, -34c, -181a, -181b, -181c, -181d, -199a, -199b and -let-7f were determined using commercially available primers (Qiagen, Manchester, UK) and normalised to *SNORD61* as internal control. Mature sequences of equine (eca) miRNAs -let-7f, -29a, -34a, -34c, -181a, -181b, -199a and -199b are identical to those reported for *Homo sapiens* (hsa), justifying our use of the same primers. Sequences for eca-miR-181c and eca-miR-181d are not reported, but we were interested to determine if expression of these miRNAs could be detected in equine tissue. The sequence for eca-miR-34b differs substantially from that of hsa-miR-34b, therefore we utilised a primer designed to target the murine orthologue of this miRNA, as this has an identical sequence to the equine version. Primer sequences and RT-qPCR details are listed in Chapter 2, sections 2.12.1 (Table 2.10) and 2.12.2 (Figure 2.2) respectively. For all RT-qPCR data, technical replicates were run in triplicate and expression relative to *SNORD61* calculated using the delta Ct method (Livak and Schmittgen 2001).

### 3.2.4 Statistical analysis

For small RNA-sequencing data, raw read counts (as .csv files) were imported into the Bioconductor package DESeq2 (version 1.22.2) for differential gene expression analysis. Normalised counts were log<sub>2</sub> transformed prior to application of a modified Fisher exact test to return exact *P*-values. The Benjamini-Hochberg procedure for multiple hypothesis correction was then applied. Results are reported as log<sub>2</sub> fold change of normalised data and genes considered differentially expressed if log<sub>2</sub> fold change ≥1.5 with a Benjamini-Hochberg adjusted *P*-value <0.05.

Statistical analysis of RT-qPCR data was performed using GraphPad Prism version 5.01 for Windows (GraphPad Software, San Diego California USA, www.graphpad.com). Comparison of relative microRNA expression between tendinopathic tissue and controls for both human and equine data were analysed non-parametrically using the Mann Whitney test. For human tendinopathy validation work, comparisons between control and PTT tissue utilised the Mann-Whitney test as conditions for its application were satisfied. Comparisons between control and SSP tissue, and between SSP and PTT samples, utilised the Student *t* test, where less than three data points were present in the SSP comparator group, which precluded the use of non-parametric analysis. These results are presented in Appendix 2, Figure A2.2. Comparison of ages between donors of tendinopathic and control tissue utilised the Student *t*-test. Significance was assumed if *P*<0.05.

## 3.3 Results

### 3.3.1 RNA-seq profiling of small non-coding RNA in human tendon

Donors of tendinopathic SSP tissue were significantly older than donors of healthy control tissue (47.2±7.8 yrs and 23.8±4.6 yrs respectively; *P*<0.0001).

Concentrations of RNA submitted for sequencing varied between 4.8 and 51.2 ng μL<sup>-1</sup>. Quality, as indicated by RNA integrity number was moderate, varying between 3.4 and 6.9, but was not different between groups (*P*=0.98).

We identified a total of 1311 small RNA transcripts using small RNA-seq. Read mapping to the Gencode GRCh38.p12 GTF file gave 98.4% alignment. Identification of transcripts mapped to miRNAs was performed separately using miRBase hsa.gff3 file (release 22.1) to identify 3p and 5p variants. 716 transcripts were from non-miRNA RNA (three protein coding, four vault RNA, nine small Cajal body-specific RNA, 39 small nuclear RNA, 244 small nucleolar RNAs (80 H/ACA, 64 C/D box), 208 Y-RNAs and 209 pseudogenes (see Appendix 3, Table A3.1 for full list of transcript identities, expression changes and *P*-values). There were 565 annotated miRNA transcripts identified, representing 347 miRNA families, with between one and 16 member miRNAs expressed per family. Additionally, two previously annotated miRNAs subsequently removed from the most recent update of the miRBase database (release 22), due to lack of experimental validation (miR-4461 and miR-6723) and one novel predicted miRNA were identified. Of the annotated miRNAs, duplicate counts

were returned for 35, triplicate counts for three, quadruplicate for two and quintuplicate for one, representing transcripts for the same mature miRNA derived from different gene loci. Deduplication of miRNAs was performed prior to statistical analysis, giving 148 up regulated, 415 down regulated in diseased supraspinatus (SSP) tendon compared to control samples, and two which were unchanged (see Appendix 3, Table A3.2 for full list of annotated miRNAs, expression changes and *P*-values). Magnitude and direction of fold change of all identified transcripts is illustrated in Figure 3.1 (A). Principal component analysis (PCA) of datasets identified separation of diseased and healthy control samples, healthy controls clustering more tightly than diseased, with >80% of the variation between cohorts explained by the first two principal components (Figure 3.1 (B)).

A total of 385 small RNAs were significantly DE ( $\log_2$  fold change  $\geq 1.5$  with Benjaminin-Hochberg adjusted *P*-value  $< 0.05$ ) between tendinopathic samples and healthy controls (Figure 3.1 (C)). Of these, 162 were non-miRNA transcripts, identified as pseudogenes ( $n=31$ ), Y-RNAs ( $n=46$ ), C/D box class snoRNAs ( $n= 48$ , representing 20 specific SNORDs), H/ACA class snoRNAs ( $n=22$ , representing 18 specific SNORAs), snRNAs ( $n=9$ , representing 6 snRNAs), scaRNAs ( $n=2$ ), vault RNA ( $n=1$ ) and protein coding RNAs ( $n=3$ ) (Table 3.4).

A total of 223 miRNAs were significantly DE ( $\log_2$  fold change  $\geq 1.5$  with Benjaminin-Hochberg adjusted *P*-value  $< 0.05$ ) between tendinopathic samples and healthy controls. The majority were down regulated ( $n=207$ ), with 16 up regulated (Table 3.4). All up regulated miRNAs and the top 20 (by fold change) down regulated miRNAs are listed in Table 3.5.

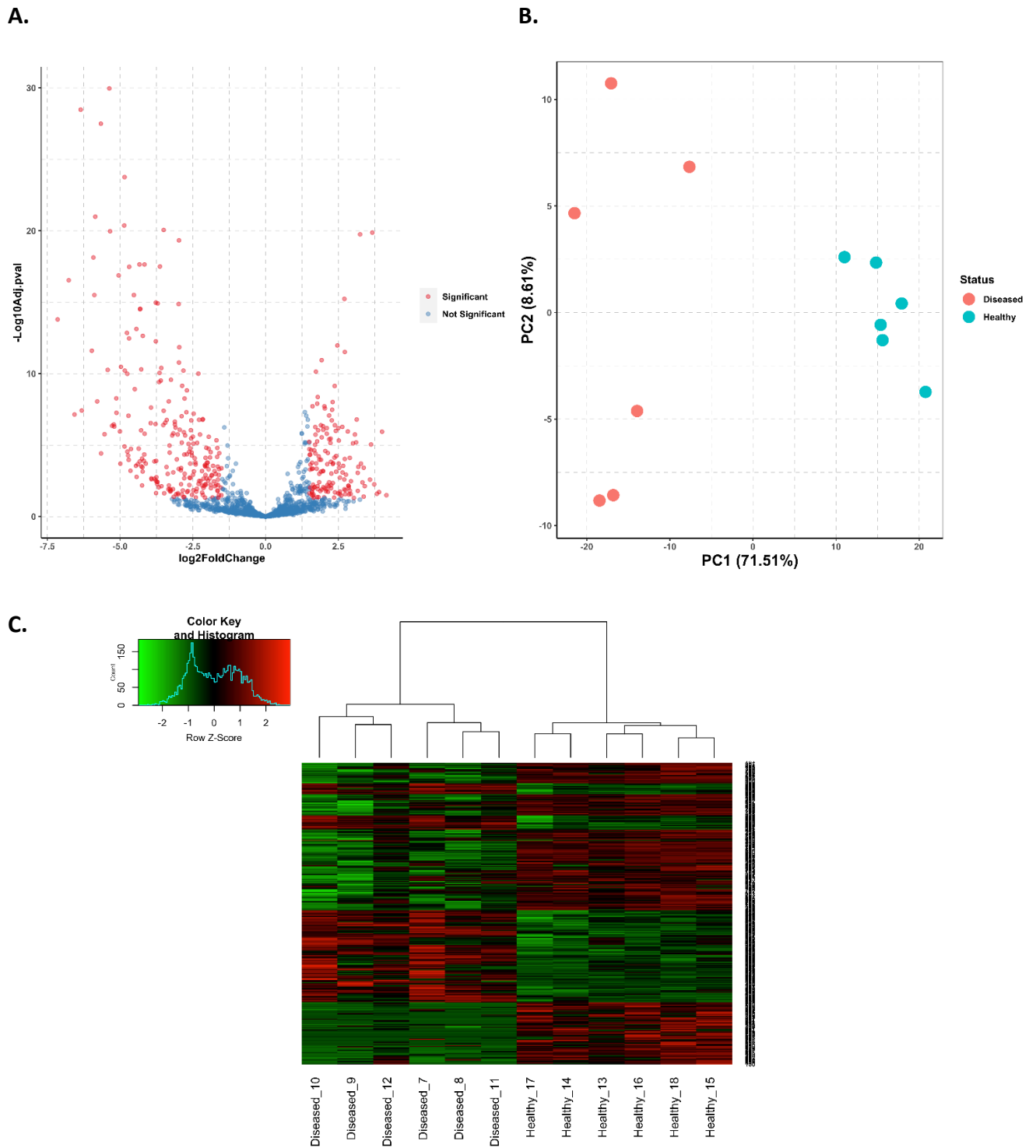


**Figure 3.1 RNA-seq identifies differential small RNA profiles between healthy and diseased human tendon tissue. A.** Volcano plot illustrating direction, magnitude and significance of all annotated non-miRNA and miRNA transcripts. **B.** Principal Component Analysis plot demonstrating separation and clustering of diseased and healthy cohorts. **C.** Heat map and consensus dendrogram of all 385 significantly DE small non-coding RNAs. Samples were from healthy hamstring tendon (n=6) and tendinopathic supraspinatus tendon (n=6). Significance was defined as  $\geq 1.5$  log<sub>2</sub> fold change with adjusted *P*-value  $< 0.05$ .

RNA Species	Number		
	Differentially Expressed	Up regulated	Down regulated
Vault RNA	1	1	0
Small Cajal body-specific RNA	2	2	0
Small nuclear RNA	6	2	4
Pseudogenes	31	14	17
Small nucleolar RNA	38	34	4
Y-RNA	46	46	0
microRNA	223	16	207

**Table 3.4 Small non-coding RNAs differentially expressed between healthy and diseased tendon samples.** Samples were from healthy hamstring tendon (n=6) and tendinopathic supraspinatus tendon (n=6). Significance was defined as  $\geq 1.5$  log<sub>2</sub> fold change with adjusted *P*-value <0.05.

Up regulated miRNAs			Down regulated miRNAs		
Identity	Log <sub>2</sub> FC	Adjusted <i>P</i> -value	Identity	Log <sub>2</sub> FC	Adjusted <i>P</i> -value
hsa-miR-6724-5p	4.00	1.16E-06	hsa-miR-451a	-7.15	1.63E-14
hsa-miR-4667-3p	3.90	0.019236	hsa-miR-374a-3p	-6.76	2.92E-17
hsa-miR-4485-3p	3.73	0.005572	hsa-miR-19b-3p	-6.57	7.27E-08
hsa-miR-3652	2.93	0.003391	hsa-miR-101-3p	-6.35	3.38E-29
hsa-miR-612	2.86	0.028223	hsa-miR-144-5p	-6.32	3.82E-08
hsa-miR-3917	2.64	0.000822	hsa-miR-32-5p	-5.97	2.50E-12
hsa-miR-632	2.50	6.48E-07	hsa-miR-3613-5p	-5.92	7.49E-19
hsa-miR-3654	2.38	0.020232	hsa-miR-335-5p	-5.88	3.17E-16
hsa-miR-193b-5p	2.18	0.007485	hsa-miR-660-5p	-5.85	1.04E-21
hsa-miR-12136	2.14	0.018255	hsa-miR-130a-3p	-5.79	8.79E-09
hsa-miR-10392-5p	2.12	0.000215	hsa-miR-340-5p	-5.66	3.21E-28
hsa-miR-2110	2.05	2.59E-05	hsa-miR-383-5p	-5.65	3.81E-05
hsa-miR-1291	1.90	4.08E-07	hsa-miR-598-3p	-5.53	1.74E-06
hsa-miR-3655	1.78	0.007444	hsa-miR-142-3p	-5.42	5.47E-11
hsa-miR-10394-3p	1.77	0.044227	hsa-miR-140-5p	-5.37	1.10E-30
hsa-miR-6125	1.67	0.008724	hsa-miR-374a-5p	-5.34	1.09E-20
			hsa-miR-30d-3p	-5.27	4.42E-07
			hsa-miR-653-5p	-5.22	3.62E-07
			hsa-miR-374b-3p	-5.20	5.04E-07
			hsa-miR-382-3p	-5.13	5.39E-09
			<i>hsa-miR-199a-5p</i>	-2.98	1.68E-11
			<i>hsa-miR-181d-5p</i>	-2.82	6.14E-11
			<i>hsa-miR-181c-5p</i>	-2.59	0.000197
			<i>hsa-miR-29a-3p</i>	-1.91	7.22E-05

**Table 3.5 Up regulated and top 20 down regulated miRNAs, ranked by fold change (FC), identified by RNA-seq as significantly differentially expressed ( $\geq 1.5$  FC; adjusted *P*-value <0.05) between healthy human hamstring tendon (n=6) and tendinopathic supraspinatus tendon (n=6). miRNAs in italics (ranked 117, 128, 141 and 185 by FC) are also shown, as down regulation of related miRNAs was subsequently observed in equine superficial digital flexor tendinopathy. hsa = *Homo sapiens*.**

### 3.3.2. RT-qPCR validation of microRNAs differentially expressed in human tendon disease

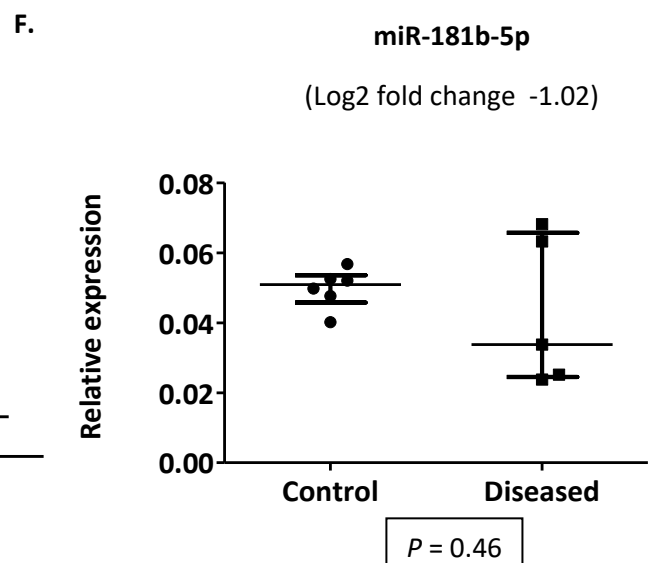
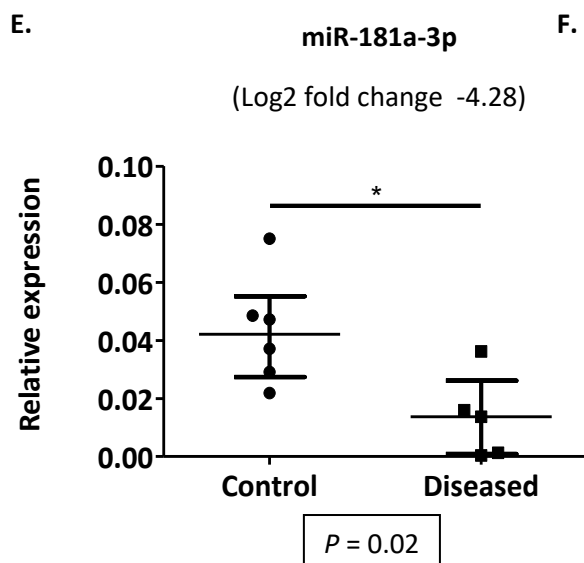
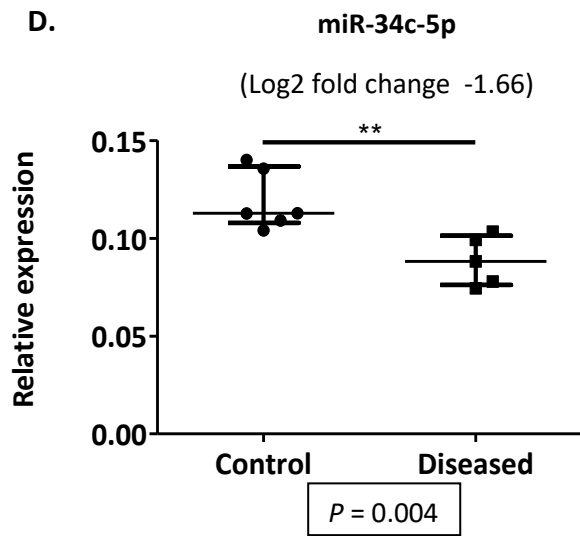
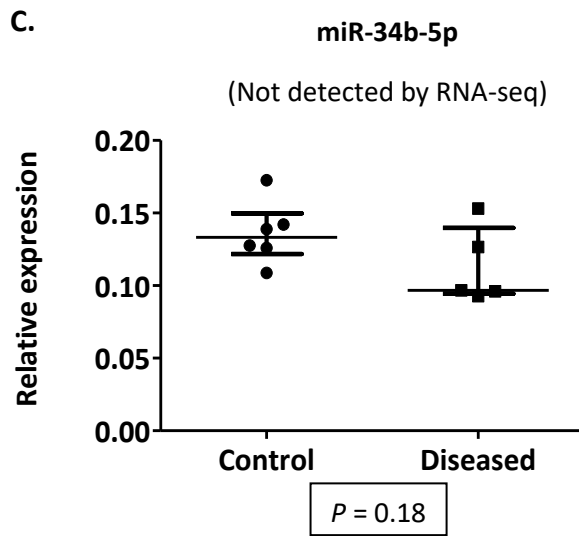
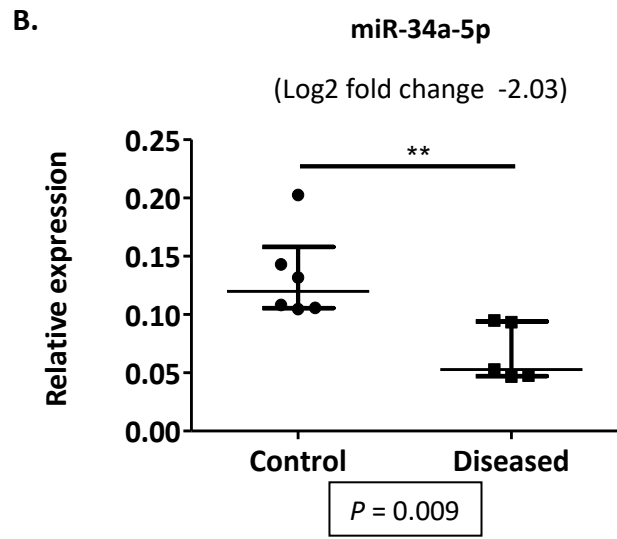
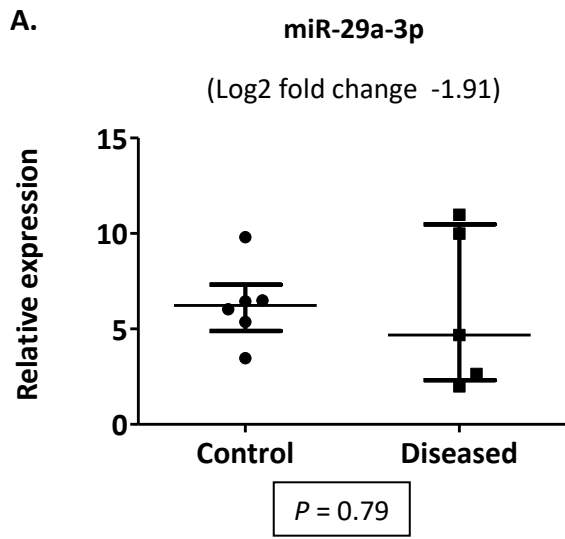
Next, using RT-qPCR, we undertook to validate a selected panel of miRNAs identified by RNA-seq. Library preparation for RNA-seq had depleted all available RNA from four of the six SSP tendinopathic samples, therefore three additional tendon samples were utilised for validation. These consisted of tendinopathic posterior tibial tendon (PTT). Although from different anatomical locations, both SSP and PTT are classified as elastic, energy storing tendons. RT-qPCR validation of RNA-seq results in the tendinopathic cohort therefore consisted of two SSP samples for which RNA-seq data was available (dependent validation) and three PTT samples (independent validation). Samples from the control cohort had all previously been submitted for RNA-seq analysis.

Donors of tendinopathic (SSP and PTT) tissue were significantly older than donors of healthy control tissue ( $54.8 \pm 14.9$  yrs and  $23.8 \pm 4.6$  yrs respectively;  $P < 0.0009$ ).

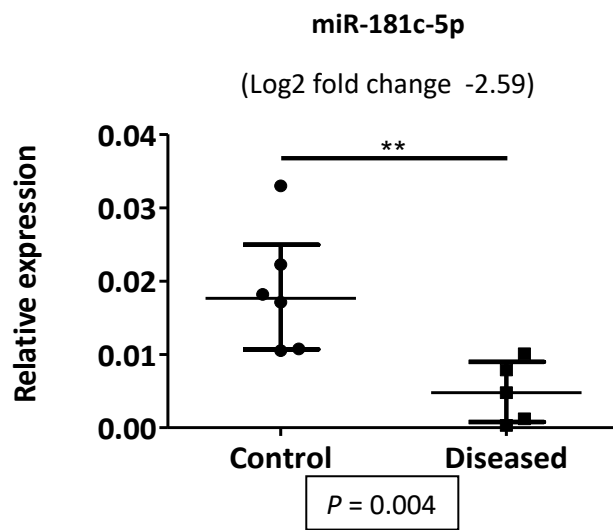
For RT-qPCR validation, 30 ng total RNA was reverse transcribed into cDNA and RT-qPCR performed for miRNAs -29a-3p, -34a-5p, -34b-5p, -34c-5p, -181a-3p, -181b-5p, -181c-5p, -181d-5p, -199a-5p, -199b-5p and -let-7f-5p. These miRNAs were chosen based on their (or their family's) involvement in the following processes relevant to tendon homeostasis and disease. Known to directly target *COL1A1* and *COL3A1* (Maurer et al 2010) and *MMP2* (Jones et al 2011), miR-29a expression is reduced in tendinopathy (Millar et al 2015). This impacts on the transition from type I to type III collagen deposition in early stage disease and facilitate matrix degradation. miR-34 is an important regulator of cell proliferation, differentiation and apoptosis, inducing cellular senescence and apoptosis in human and murine fibroblasts respectively (He et al 2007). miR-34a also regulates fibrosis in an age- and context-dependent manner (Cui et al 2017), whilst down regulation of miRs -34b and -34c caused accumulation of abnormal, dysfunctional mitochondria and impaired clearance from degenerate neuronal cells (Miñones-Moyano et al 2011). Processes regulated by the miR-181 family pertinent to tendinopathy are inflammation (Xie et al 2013, Lu et al 2015), fibrosis (Chen et al 2018), apoptosis and autophagy (Liu et al 2017, Pop-Bica et al 2018, Rezaei et al 2019). Upregulation of miR-181 is important in skeletal muscle differentiation and regeneration (Naguibneva et al 2006), with reduced miR-181a expression implicated in age-related degenerative changes such as disrupted MAPK and TGF $\beta$  signalling and mitochondrial function (Soriano-Arroquia et al 2016, Goljanek-Whysall et al 2020). Expression of several miR-181 family members is also sensitive to hypoxia (Kulshreshtha et al 2007, Nallamshetty et al 2013), as is expression of miR-199a (Rane et al 2009). Additionally, miRs -199a and -199b both regulate fibrosis, upregulation being associated with a number of fibrotic diseases (da Costa Martins et al 2010, Lino Cardenas et al 2013). The highly conserved let-7 family of miRNAs have important functions in developmental progression, one of which is cellular differentiation. We investigated expression of miR-let-7f as a potential marker of tendon stem/progenitor cell proliferation and differentiation capacity, as age-related reduction in expression is associated with reduced capacity for these processes in bone marrow derived mesenchymal stem cells (Yu et al 2011).

Our chosen panel of miRNAs represent, in the majority, ones identified by RNA-seq as showing significantly reduced expression in our tendinopathic cohort. However, miR-34b-5p was not detected by RNA-seq and miR-181b-5p was detected, but not DE. We included these in our validation to confirm these negative findings.

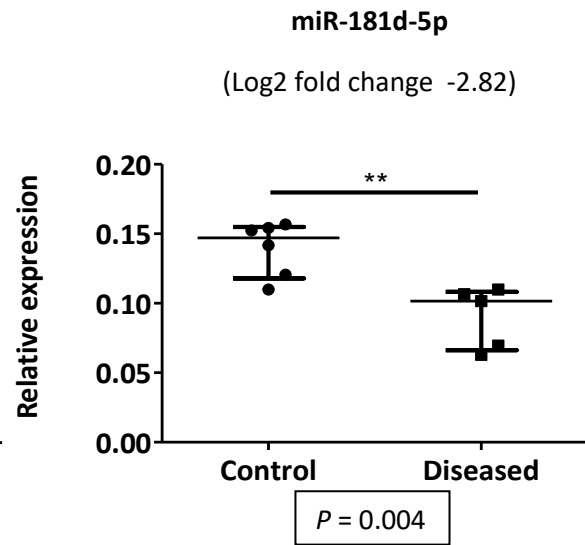
Considering all tendinopathic samples as a single cohort, RT-qPCR validation of RNA-seq results was achieved for nine of the 11 chosen miRNAs, with only miR-29a and miR-let-7f failing. Graphical results are presented in Figure 3.2, with boxplots of regularised log counts obtained by RNA-seq for these miRNA families given in Appendix 2, Figure A2.1). Further evaluation of these results identified that for miR-29a, changes in expression differed with tendon type, expression increasing significantly relative to controls for SSP tendon, contradicting RNA-seq findings, whilst expression in PTT tendon significantly reduced, corroborating RNA-seq data (Appendix 2, Figure A2.2 (A)). Indeed, there did appear to be some effect of tendon type on expression change, with miRNAs -34b, -181a, -199a and -199b showing some difference, although the small numbers involved in this sub-analysis demand these results are interpreted with caution. No significant difference in miR-let-7f expression was found with any tendon grouping (see Appendix 2, Figure A2.2 for full details of miRNA expression according to tendon type). Table 3.6 illustrates comparison between RNA-seq results and those of RT-qPCR validation.



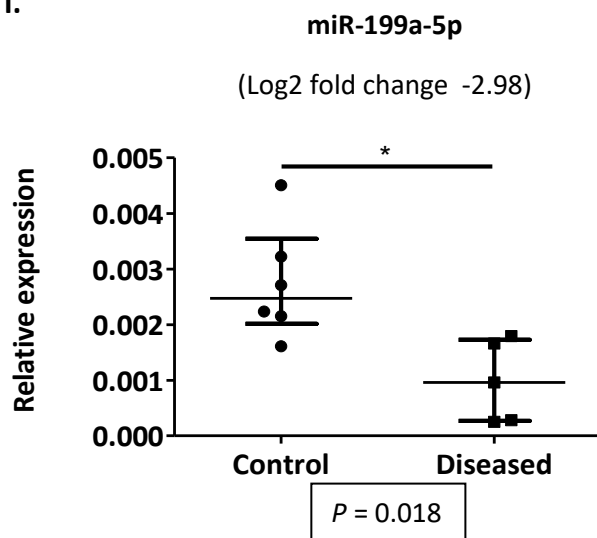
G.



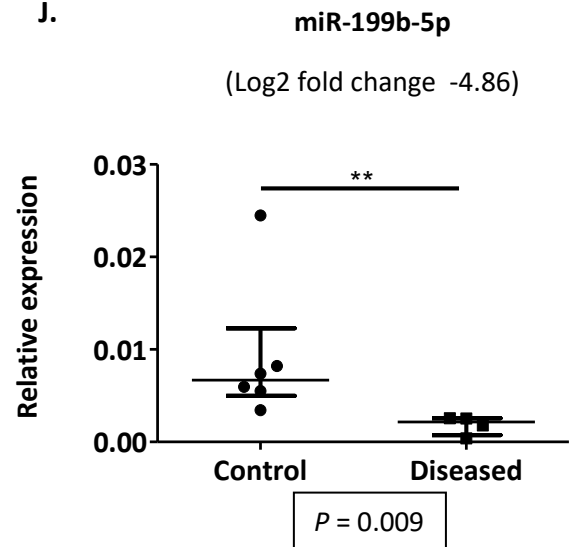
H.



I.



J.



K.

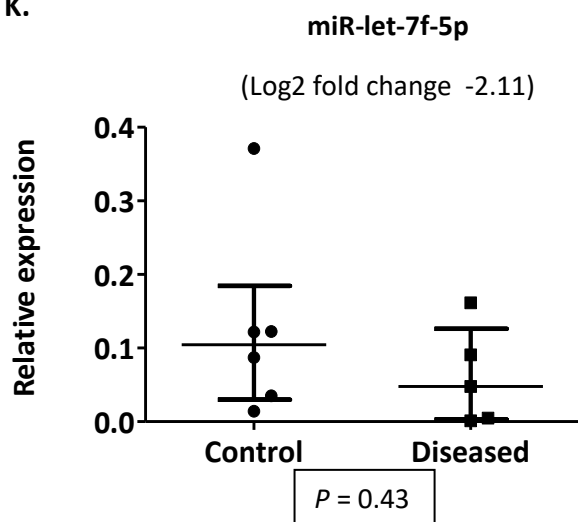
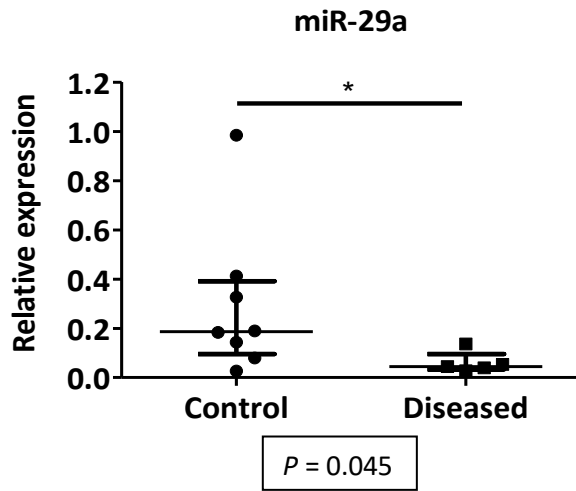


**Figure 3.2** (preceding two pages) **RT-qPCR validation of human tendon RNA-seq data.** Relative expression of **A.** miR-29a-3p, **B.** miR-34a-5p, **C.** miR-34b-5p, **D.** miR-34c-5p, **E.** miR-181a-3p, **F.** miR-181b-5p, **G.** miR-181c-5p, **H.** miR-181d-5p, **I.** miR-199a-5p, **J.** miR-199b-5p, **K.** miR-let-7f-5p between Control (healthy hamstring tendon) and Diseased (tendinopathic supraspinatus and posterior tibial tendon). Data were normalised to *SNORD61* expression. Graphs show median and inter-quartile range. Mann Whitney U test; \* =  $P < 0.05$ ; \*\* =  $P < 0.01$ . Log<sub>2</sub> fold change values for each miRNA, as determined by RNA-seq are given in parentheses with each graph for comparison.

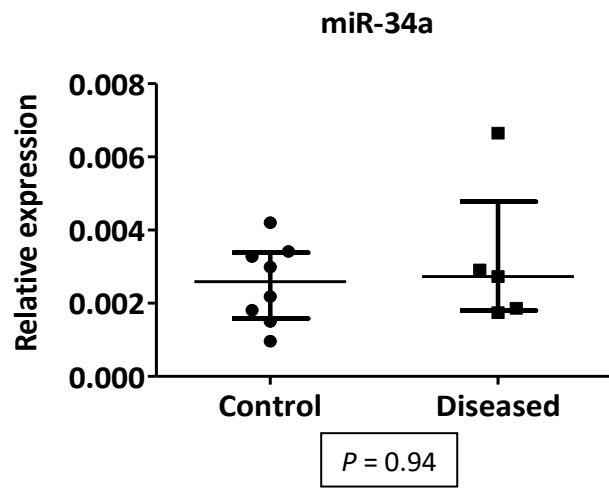
### **3.3.3 Validation of equine superficial digital flexor tendinopathy as a model to study miRNA dysregulation in human tendon disease**

Following successful validation of RNA-seq data from human tissue, we next employed RT-qPCR to determine expression of the same miRNAs in the energy storing equine SDFT, to explore any commonality between species. Three miRNAs, miR-29a, -181b and -199a showed significantly reduced expression in equine tendinopathic SDFT compared to healthy controls (Figure 3.3). Two miRNAs showed complete agreement across RNA-seq and RT-qPCR results in both human and equine tissues, miR-34b, which showed no change in expression with disease, and miR-199a, which showed reduced expression in tendinopathic tissue in both species (Table 3.6). Interestingly, miRNAs -181a, -181c and 181d, all of which showed reduced expression with human tendinopathy (RNA-seq data being supported by RT-qPCR), showed no change in equine tissue with disease. However, miRNA 181-b, which was validated as unchanged in human disease, was significantly reduced in the equine samples (Figure 3.3 (F)). A summary comparison of results across human and equine tissue by both RNA-seq and RT-qPCR is presented in Table 3.6. Coincidentally, we have separately identified miR-181b to be significantly up regulated in equine SDFT with ageing (Figure 3.3 (L)). This suggests that miR-181b may be the dominant family member in this species, and, interestingly, that ageing and disease may promote different expression changes. Reduction in expression of miR-29a and miR-199a has previously been reported in association with tendon disease (Millar et al 2015, Thankam et al 2016), however, alteration in miR-181 expression has not.

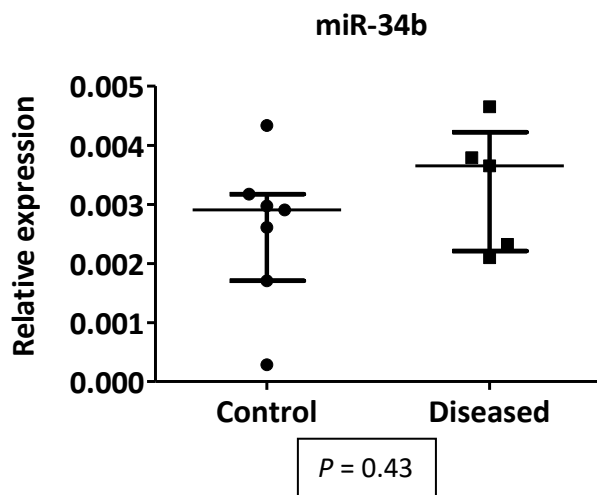
A.



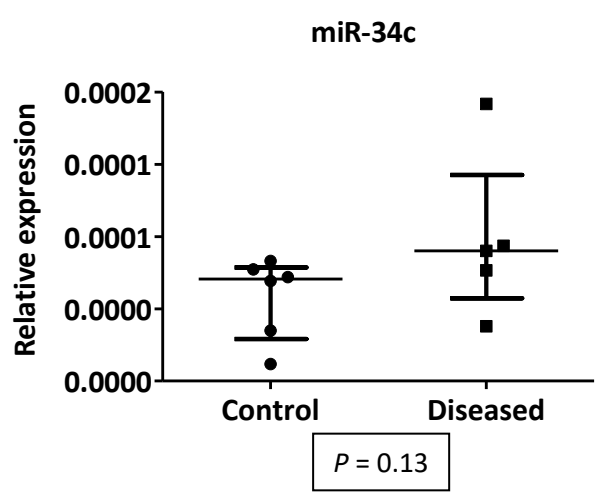
B.



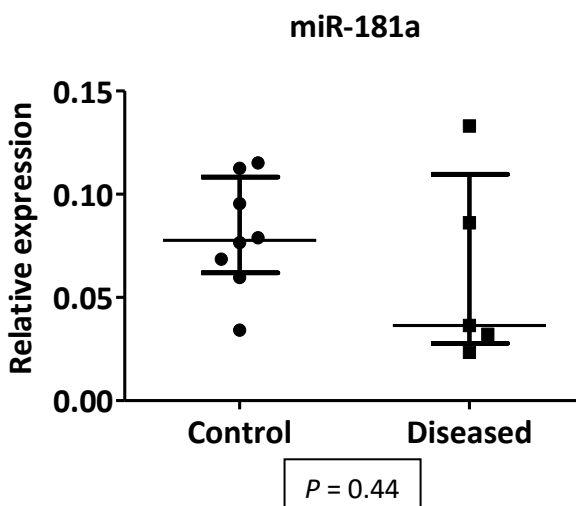
C.



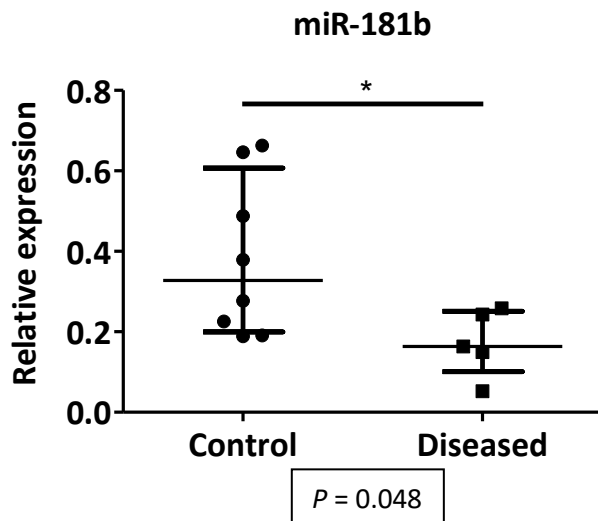
D.



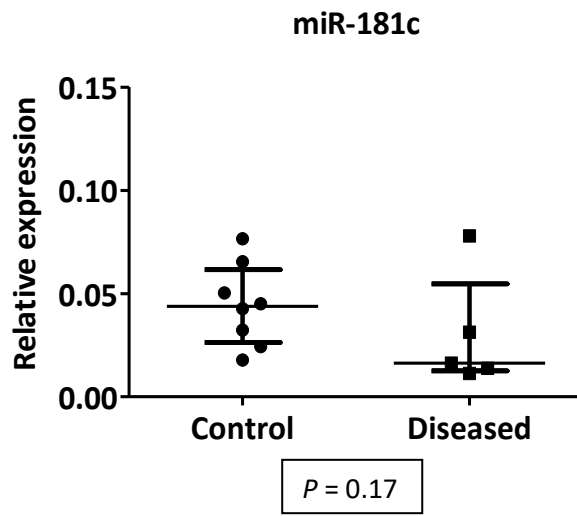
E.



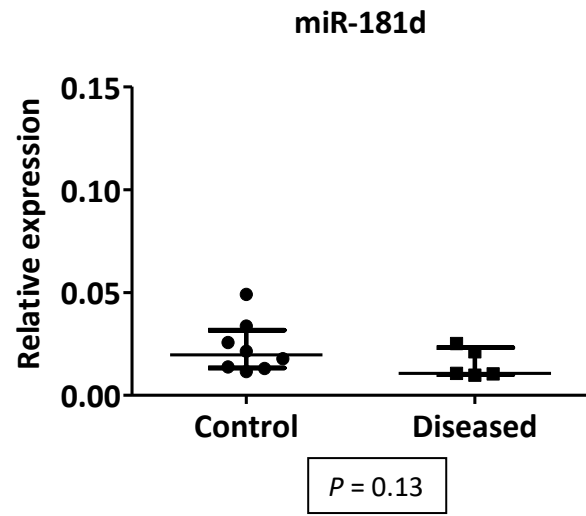
F.



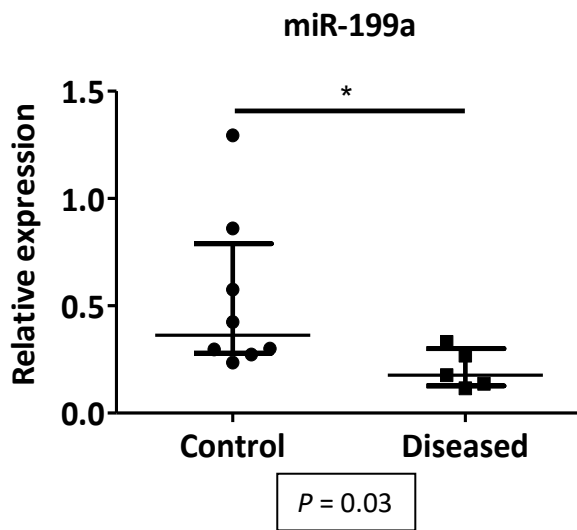
G.



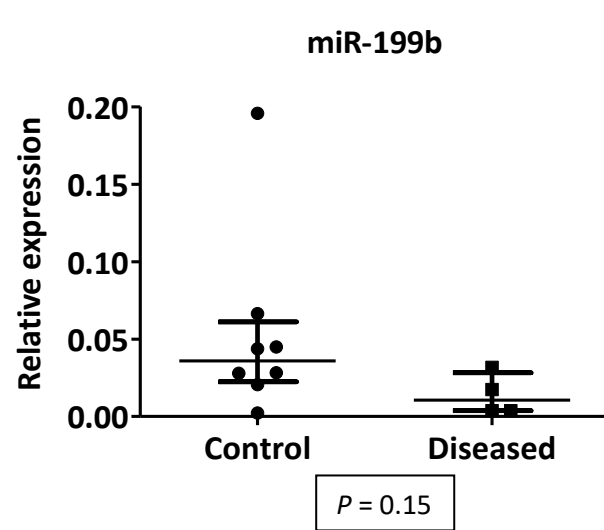
H.



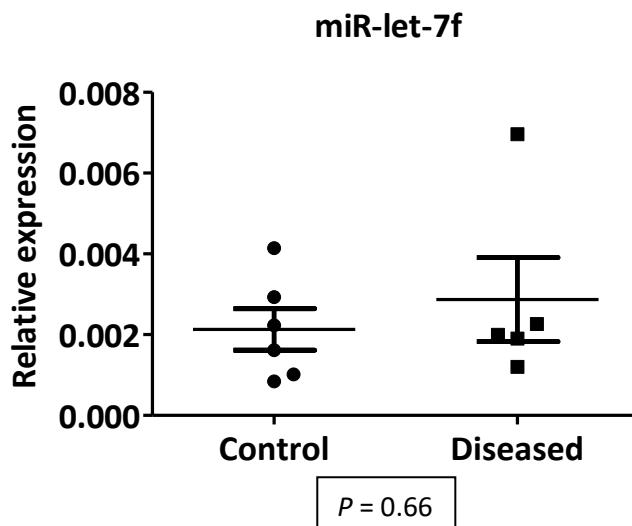
I.



J.



K.



L.

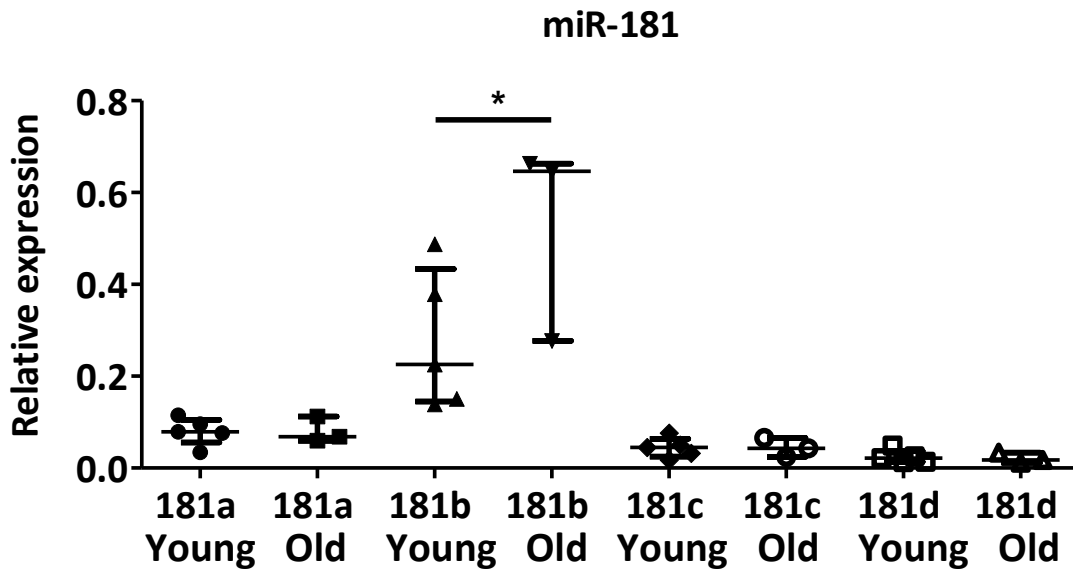


**Figure 3.3 miRNA dysregulation in equine superficial digital flexor tendinopathy demonstrates some similarities with that in human tendinopathy, as identified by RT-qPCR.** Relative expression of **A.** miR-29a, **B.** miR-34a, **C.** miR-34b, **D.** miR-34c, **E.** miR-181a, **F.** miR-181b, **G.** miR-181c, **H.** miR-181d, **I.** miR-199a, **J.**miR-199b, **K.** miR-let-7f, between healthy (Control; n= 8) and Diseased (n = 5) equine SDFT. **L.** miR-181 expression in young (n =5) versus old (n = 3) clinically normal equine SDFT tissue for comparison. Data were normalised to *SNORD61* expression. Graphs show median and inter-quartile range. \* =  $P < 0.05$  (Mann Whitney U test).

Identity	Human		Equine	
	RNA-seq		RT- qPCR	RT-qPCR
	Detected	Significant change		
miR-29a	3p,	↓ (3p)	- (3p)	↓ (3p)
miR-34a	5p,	↓ (5p)	↓ (5p)	- (5p)
miR-34b	3p	-	- (5p)	- (5p)
miR-34c	3p, 5p,	↓ (5p)	↓ (5p)	- (5p)
miR-181a	3p, 5p	↓ (3p)	↓ (3p)	- (3p + 5p)
miR-181b	3p, 5p	-	- (5p)	↓ (5p)
miR-181c	3p, 5p	↓ (3p + 5p)	↓ (5p)	- (5p)
miR-181d	5p	↓ (5p)	↓ (5p)	- (5p)
miR-199a	3p, 5p	↓ (3p + 5p)	↓ (5p)	↓ (5p)
miR-199b	3p, 5p	↓ (3p + 5p)	↓ (5p)	- (5p)
miR-let-7f	3p, 5p	↓ (5p)	- (5p)	- (5p)

**Table 3.6 Summary of RNA-seq validation by RT-qPCR in human tendinopathy and miRNA expression in equine tendinopathy.** 3p, 5p = miRNA variants detected; (3p), (5p) in RT-qPCR columns indicates variant against which primer directed. ↓ = significant down regulation of expression with disease, - = no significant change detected between healthy and diseased tissue.

### **3.4 Discussion**

In this chapter we established sncRNA expression profiles in human energy storing tendon and demonstrated that these transcriptomes differ substantially between healthy and diseased cohorts. Furthermore, we utilised RT-qPCR to validate these findings in a small number of miRNAs. Additionally, we have identified similar changes for some of these miRNAs occurring in tendinopathy of the equine energy storing superficial digital flexor tendon.

RNA-seq has been described as the technology of choice to investigate small RNA expression patterns as it requires no pre-existing knowledge or assumptions about the samples, can discriminate between transcripts differing by only a single nucleotide and is subject to less technical variation and artefactual errors than alternative methods (Linsen et al 2009). Library preparation is reported to be the step in sample preparation that is most likely to result in bias, due to the requirement for reverse transcription to cDNA. During this step, any post-translational modifications, tendency to form secondary structures, variability in transcript lengths, CG content and specific enzymes used can all affect efficiency of reverse transcription and therefore the representation in the sequencing data (Gebetsberger et al 2015). These inherent quantification biases prevent accurate determination of absolute transcript numbers, but still permit analysis of differential expression between samples. Similar biases have been shown to occur with RT-qPCR quantification, with results showing good correlation between technologies, making RT-qPCR a valid method of validation (Linsen et al 2009).

With RNA-seq reads, we achieved very good alignment (98.4%) to the reference genome (Gencode GRCh38.p12). As miRNA expression was the primary focus of this study, transcripts identified as miRNAs were separately mapped using miRBase hsa.gff3 file (release 22.1), as this database contains more detailed miRNA-specific information (such as differentiating 3p and 5p variants). Identification of 41 miRNAs was replicated between two and five times, reflecting presence of immature transcripts derived from different gene loci. Where this occurred, read counts for each miRNA were combined prior to further analysis, as we were interested in DE of each miRNA, rather than from which locus each transcript was derived.

The panel of miRNAs used for RT-qPCR validation (miRNAs -29a, -34a, -34b, -34c, -181a, -181b, -181c, -181d, -199a, -199b and -let-7f) were chosen based on their predicted or validated targeting of pathological processes believed to be important in tendinopathy (as outlined in section 3.3.2).

RNA-seq data identified eight let-7 miRNAs, with three members (let-7a, let-7c and let-7f) significantly down regulated with disease. The seminal let-7 family of miRNAs were originally identified due to their essential role in the transition of the larval L4 stage of *Caenorhabditis elegans* to the adult nematode. Let-7 family miRNAs are highly conserved across multiple animal species, both in terms of sequence, and the developmental stage at which they are expressed. There are ten mature human let-7 sequences, with let-7f formed from precursors from two distinct genomic locations (Roush and Slack 2008). Whilst a direct role for let-7 in vertebrate development has not been conclusively shown, one of the major functions attributed to this miRNA family is promotion of cellular differentiation (Roush and Slack 2008). Down regulation of miR-let-7f has been reported in bone marrow derived mesenchymal stem cells with ageing, concurrent with reduced potential for proliferation, differentiation and production of heat shock proteins by these cells (Yu et al 2011). We therefore chose to explore expression of this miRNA, as a potential marker of tendon stem/progenitor cell proliferative and differentiation capacity in tendinopathy, in our RT-qPCR validation panel. However, RNA-seq findings were not supported by RT-qPCR data in either human or equine tissue (Figure 3.2 (K), Figure 3.3 (K) and Table 3.6). Whilst this could represent a real finding, it may relate to the differences in analytical technique. RT-qPCR relies on stability of reference gene expression for normalisation of data, and primer specificity to the target of interest. Sequences of the 5p variants of all hsa-let-7 family members only differ from each other by one or two bases. High levels of sequence similarity may result in primer hybridisation artefacts and high levels of background signal, reducing sensitivity (Wang et al 2009, Oshlack et al 2010). Divested of these limitations, and by quantifying individual sequence reads against the reference genome, RNA-seq offers greater sensitivity and accuracy than RT-qPCR, able to detect subtle changes in expression, down to 10%.

Our findings with miR-29a were interesting. RNA-seq data demonstrated a significant reduction with disease in human SSP tendon (Appendix 3, Table A3.1), as did RT-qPCR data for equine SDFT (Figure 3.3 (A)), supporting previous work (Millar et al 2015). However, RT-qPCR validation of RNA-seq was contradictory, indicating no significant change overall with disease (Figure 3.2 (A)). Examined in more detail, the expression of miR-29a varied with tendon type, being up regulated in diseased SSP, contradicting the findings of Millar and co-workers (2015), whilst down regulated in diseased PTT (Appendix 2, Figure A2.2 (A)). Both SSP and PTT are classified functionally as elastic energy storing tendons, although they do exhibit significant morphological differences, and our RT-qPCR results

suggest that miR-29a expression with disease may differ depending on specific tendon identity. Of all the miRNAs we investigated in our validation, miR-29a was unique in this respect; all others demonstrated much greater concordance in expression levels between SSP and PTT tendons (Appendix 2, Figure A2.2 (B-K)). This could reflect differences in the stage of disease at the time of tissue harvest, the fact that the two SSP samples were from female donors, whereas the PTT samples were from males, or that SSP donors were younger (39 years) than those from which PTT was obtained (60-71 years). The cohort of SSP tendinopathy patients reported by Miller and co-workers (2015) was older (35-70 years) than ours and biased towards male patients, at a ratio of 2:1. The possibility of tendon-specific responses to disease is an intriguing one, but should be interpreted with caution due to the small numbers involved (n=2 for SSP; n=3 for PTT) and the other confounding factors outlined above.

Probably the most extensively investigated miRNA in respect to tendon disease, miR-29a appears to regulate tendon mechanobiology in a number of ways. Using human clinical samples of SSP tendinopathy, a murine model of patellar tendinopathy, and *in vitro* gain- and loss- of function studies, Millar and co-workers (2015) demonstrated miR-29a to be significantly reduced with tendon disease, and play a critical role in the interaction between inflammatory cytokines and extracellular matrix changes. Known to directly target *COL1A1* and *COL3A1* transcripts (Maurer et al 2010), miR-29a exerts a more profound inhibitory effect on *COL3A1* mRNA than that presaging type I collagen. This is due to *COL1A1* and *COL1A2* transcripts possessing alternative polyadenylation signals, which reduce the length of their 3'UTRs, with subsequent loss of microRNA recognition elements, thus rendering them insensitive to translational repression. This does not appear to occur with *COL3A1* transcripts (Millar et al 2015). Millar and colleagues (2015) also demonstrated miR-29a to be key in the transition from type I to type III collagen deposition in early tendinopathy, by regulating IL33 effect (Millar et al 2015). IL33 is up regulated in early tendinopathy and mediates the transition from collagen type 1 to type 3 synthesis. The cytosolic IL33 receptor is a direct miR-29a target, but IL33 indirectly reduces miR-29a expression via phosphorylation of NFκB, thereby, in early tendinopathy, facilitating increased *COL3A1* expression (Millar et al 2015).

In addition to affecting synthetic function, miR-29a also plays a role in matrix degradation. Validated *in vitro* to target MMP2, reduced miR-29a levels are reported in aneurysmal, relative to normal thoracic aortic tissue (Jones et al 2011). Down regulation of miR-29a corresponded to an increase in both total MMP2 levels and ratio of active:inactive form of the enzyme, resulting in vessel dilation from pathological remodelling of the aortic extracellular matrix (Jones et al 2011). However, in dermal fibroblasts, upregulation of miR-29a reduced TIMP1 secretion by targeting TGFβ activated kinase 1 binding protein 1, an upstream regulator of TIMP1. This produced a functional increase in MMP1 levels, leading to collagen degradation (Ciechomska et al 2014).

The therapeutic use of miR-29a has also been explored in experimentally induced injury models of murine patellar tendon and equine SDFT (Millar et al 2015, Watts et al 2017). Application of exogenous miR-29a at the site of injury significantly reduced type III collagen synthesis in early stage repair, without affecting collagen I synthesis.

Due to limited sample availability, we were unable to use the same cohort of tendinopathic samples exclusively for RT-qPCR validation of RNA-seq data. In addition to the two remaining SSP samples, we also included three samples of tendinopathic PTT from an independent cohort. Ideally, full validation of data requires results are replicated, using an alternative analytical method, in both

dependent and independent samples. Notwithstanding the fact we utilised tendinopathic samples which conform to these descriptions, the low numbers involved need to be considered. Although miR-29a expression was dramatically different between diseased SSP and PTT tendons, this was exceptional, as the other miRNAs investigated demonstrated far greater concordance in this respect (Appendix 2, Figure A2.2 (B-K)). For the purpose of investigating the influence of miRNA dysregulation on basic processes relevant to tendinopathy in general, we therefore elected to group all diseased tendon together as a single cohort for further consideration.

RT-qPCR detected significant reductions in miR-34a and miR-34c expression in human tendinopathic tissue (Figure 3.2 (B) and (D) respectively), confirming RNA-seq data (Table 3.6). Neither of these were observed to change however in diseased equine SDFT (Figure 3.3 (B) and (D) respectively). No change in miR-34b with disease was detected in either species, using either analytical technique, validating stable expression of this miRNA (Table 3.6). Both pro- and anti-fibrotic activity of miR-34a is reported in a murine model of pulmonary fibrosis, with the effect appearing to be age dependent (Cui et al 2017). Young miR-34a<sup>-/-</sup> mice developed more severe fibrosis than young wild type, whereas miR-34a was up regulated in the fibrotic lungs of old mice.

Depletion of miR-34b and miR-34c is reported in degenerate neurological tissue from human Parkinson's Disease patients (Miñones-Moyano et al 2011). Differentiated neuronal cells treated with specific miR-34b and miR-34c inhibitors demonstrated abnormal mitochondrial morphology, with evidence of mitochondrial depolarisation, increased ROS generation and reduced cellular ATP content (Miñones-Moyano et al 2011). These changes were accompanied by a concurrent reduction in protein deglycase DJ-1 and the E3 ubiquitin ligase Parkin, both essential for the clearance of dysfunctional mitochondria.

Additionally, miR-34 plays an important role in cell proliferation, differentiation and apoptosis. Ectopic expression of miR-34 induced cell cycle arrest in both primary and tumour-derived murine and human cell lines, cellular senescence in primary human fibroblasts, and apoptosis in mouse embryonic fibroblasts, reducing proliferative potential (He et al 2007). The transcriptional activator protein p53 accumulates in response to a variety of cellular stressors and DNA damage, resulting ultimately in the endpoints of apoptosis, senescence or cell cycle arrest (He et al 2007). Genes encoding all three miR-34 family isoforms are direct transcriptional targets of p53, providing a mechanism for indirect p53-mediated suppression of gene expression, indeed, overexpression of miR-34a in colorectal cancer cells resulted in a disproportionate downregulation of mRNA and proteins involved in cell cycle regulation (Kaller et al 2011). In addition to being regulated by p53, miR-34a also acts to indirectly increase activity of the p53 signalling pathway by directly targeting silent mating type information regulation 2 homolog 1 (sirtuin 1; SIRT1) (Yamakuchi et al 2008). SIRT1 deacetylates p53, rendering it inactive and promoting its degradation. Therefore, miR-34a suppression of SIRT1 promotes accumulation of active p53, creating a positive feedback loop increasing activity of the p53 signalling pathway (Yamakuchi et al 2008). Our findings suggest a possible role for miR-34a and miR-34c in human tendinopathy, with reduced expression impacting on mitochondrial dynamics and promoting cellular proliferation. Our data however does not support a similar role in equine tendinopathy.

RNA-seq data identified miRs -181a, -181c and -181d as being down regulated in human SSP tendon with disease (Appendix 3, Table A3.2). RT-qPCR validation confirmed these findings (Figure 3.2 (E), (G) and (H) respectively), but interestingly, this was not replicated in equine tissue (Figure 3.3 (E), (G) and (H)). However, miR-181b, the only family member not altered in human tissue, was significantly reduced with equine SDFT disease (Figure 3.3 (F)). Equine variants of miRs -181c and -181d are currently not described (miRBase release 22.1, Kozomara et al 2019). However, seed sequences, critical for miRNA:target interactions, are highly conserved between miR-181 family members, and across species, indicating that in horses, miR-181b may perform an analogous regulatory function to that of -181a, -181c and -181d in humans. Downregulation of miR-181b in human SSP tendinopathy was detected by RNA-seq (Appendix 3, Table A3.2), but did not reach statistical significance, as was confirmed by RT-qPCR (Figure 3.2 (F)). In humans, miR-181a is mapped to two genomic loci, on chromosomes 1 and 9, in both cases clustered with miR-181b. In the equine genome, two locations are also listed for miR-181a, but on chromosomes 25 and 30, only clustering with miR-181b on chromosome 25 (miRBase release 22.1, Kozomara et al 2019). This difference in chromosomal location and cluster frequency may explain the disparity in observed expression of these family members between species. Further detail on miR-181 family members, including species comparison, sequences and genomic location is given in Chapter 4, Table 4.1 and Chapter 5, Tables 5.1 and 5.3. The miR-181 family is implicated in a wide range of processes pertinent to tendinopathy: inflammation (Xie et al 2013), fibrosis (Chen et al 2018), autophagy (Liu et al 2017), and mitochondrial biogenesis and function (Indrieri et al 2019, Goljanek-Whysall et al 2020). Validated miR-181 targets include SIRT1, ubiquitin-binding protein p62, Parkin, protein deglycase DJ-1, cytochrome c oxidase I, interleukin 1 alpha, peroxiredoxin 3 and tumour necrosis factor. Both pro- and anti-apoptotic effects have been described for miR-181a (Pop-Bica et al 2018, Rezaei et al 2019), with miRs -181a, -181b and -181c shown to be induced by hypoxia (Kulshreshtha et al 2007, Nallamshetty et al 2013). Strongly up regulated during differentiation, miR-181 participates in both establishing and regenerating the skeletal muscle phenotype, in part by downregulating the homeobox protein HOXA11 - a repressor of the differentiation process (Naguibneva et al 2006). Our group has shown miR-181a reduction is a consistent finding in human and murine skeletal muscle with ageing and is implicated in age-related degenerative changes. These include defective insulin, MAPK and TGF $\beta$  signalling (Soriano-Arroquia et al 2016) and disrupted mitochondrial dynamics and autophagy (Goljanek-Whysall et al 2020). Thus, as tendon is a functionally integral and anatomically adjacent component of the musculotendinous unit, it was interesting to see that several miR-181 family members demonstrated reduced expression in tendon pathology. However, it is also important to note that donors of tendinopathic SSP and PTT tissue were significantly older than those from whom control tissue was obtained and an age effect cannot be ruled out. Incidence of tendinopathy in both human and equine species increases with age (Paavola et al 2002, Ely et al 2009, Thorpe et al 2010), and intriguingly, we have previously shown miR-181b expression to be up regulated with ageing in clinically normal equine SDFT (Figure 3.3 (L), Bardell et al 2018). This disparity between normal age-related changes in miR-181b expression and that seen with disease, suggests this family of miRNAs may be important in determining differentiation between healthy and pathological phenotypes.

We detected reductions in miR-199a and miR-199b in tendinopathic human SSP samples, and decreased expression of miR-199b in diseased equine SDFT (Table 3.6). Both miR-199a and -199b are pro-fibrotic, with miR-199a-5p up regulated in idiopathic pulmonary fibrosis and following bleomycin

induced lung injury in mice (Lino Cardenas et al 2013). Expression is up regulated following TGF $\beta$  exposure, and enhances its signalling pathways by reducing receptor internalisation, secondary to down regulation of caveolin 1. Upregulation of miR-199a-5p is also reported in renal and hepatic fibrosis, whilst miR-199b over expression is associated with myocardial fibrosis (da Costa Martins et al 2010). In porcine heart, miR-199a expression is abolished by a period of transient ischaemia, promoting increased levels of its targets SIRT1 and HIF1 $\alpha$  (Rane et al 2009). Rapidly induced by hypoxia, HIF1 $\alpha$  is a potent transcription factor, involved in promoting transcription of approximately 90% of genes that are up regulated during hypoxia and protective against hypoxia-induced mitochondrial damage (Rane et al 2009). As discussed above with miR-34a, enhanced accumulation of SIRT1 consequent to miR-199a downregulation, promotes deactivation and degradation of p53, reinforcing this effect. Accumulation of SIRT1 under hypoxic conditions stabilises HIF1 $\alpha$  by downregulating prolyl hydroxylase 2 (PHD2). This enzyme additionally catalyses the formation of hydroxyproline and is therefore important in the stability of collagen. Knockdown of miR-199a results in almost complete reduction in PHD2 expression in cardiac myocytes, an effect reversed by inactivation of SIRT1 (Rane et al 2009). Downregulation of miR-199a and miR-199b observed in diseased human and equine tendon, could therefore reflect a response to a hypoxic insult, with subsequent impaired production and stabilisation of ECM proteins.

Here we have demonstrated that in humans, tendinopathy results in significant changes to the small non-coding RNA transcriptome, and validated these findings in a small, selected cohort of miRNAs known to be involved in relevant pathological processes. Additionally, we have presented evidence that some of these miRNAs show similar changes in equine SDFT tendinopathy. Whilst this is encouraging for the purposes of supporting equine tendon as a valid model for studying human tendinopathy, the extensive differences in miRNA profiles between healthy and diseased tissue warrants investigation of this dataset as a whole. This will be addressed in the following chapter, employing bioinformatics techniques to explore target interactions and pathways.

## **Chapter 4 – Prediction of altered miRNA:target gene interaction in tendinopathy**

### **4.1 Introduction**

In the previous chapter we identified significant alterations in miRNA expression profile with disease in the energy storing human SSP tendon compared with clinically normal control tissue. We further validated differential expression of a number of these miRNAs using RT-qPCR, and demonstrated comparable changes in the functionally similar equine SDFT. miRNAs function to repress translation of their target mRNA, thereby modulating gene expression. Critical to understanding the functional consequences of altered miRNA expression on cell phenotype, is, therefore identifying these target genes and how their interactions and downstream effects contribute to the disease state. With an average of 400 targets per miRNA proposed (Bartel 2009), it is estimated that 60% of human genes are regulated by miRNA targeting (Friedman et al 2009), conferring a profound influence on phenotype.

Plant miRNAs demonstrate extensive complementarity to their mRNA target, facilitating target prediction through identification of complementary base sequences. However, the situation is more difficult in animals, with binding heavily influenced by the six to eight nucleotide seed sequence at the 5' terminal of the miRNA. There are a number of different target prediction tools, but all incorporate this primary functional interaction within their algorithms, focussing on conservation of the miRNA seed sequence and subsequent Watson-Crick pairing to a complementary conserved nucleotide sequence in the 3'UTR of the mRNA target. Target prediction is however, further complicated by the number of contiguous Watson-Crick pairings necessary for effective target binding. This can vary between eight (8mer) and six (6mer), and, additionally by whether binding incorporates the terminal miRNA nucleotide or is offset, with the first one or two nucleotides being functionally redundant. Shorter 6mer sequences are generally reported to have reduced efficacy, are more likely to result in false positive predictions due to the increased probability of complementary sequences arising by chance, and therefore may be disregarded by more stringent prediction algorithms (Bartel 2009, Bartel 2018). Additionally, non-canonical binding can occur, with non-contiguous Watson-Crick pairing, arising from seed sequence mismatches, compensated for by additional binding sites usually centred on nucleotides 13-16 towards the 3' region of the miRNA (Bartel 2009). Other relevant factors which may be incorporated into target prediction algorithms include the accessibility of the mRNA binding region and the calculated thermodynamic stability of binding (Bentwich 2005, Kim et al 2016). As the field of miRNA research has developed, the number of experimentally validated miRNA targets has grown, confirming (or refuting) predictions from computational bioinformatic algorithms. This has led to the creation of manually curated databases such as miRecords (Xiao et al 2009), TarBase (Karagkouni et al 2018) and miRTarBase (Huang et al 2020) which assimilate evidence of validated interactions, providing another resource for investigative research if discovery of novel miRNA:target binding is not the principal focus.

QIAGEN Ingenuity Pathway Analysis (IPA) (QIAGEN Inc., Redwood City, CA, USA, <https://www.qiagenbioinformatics.com/products/ingenuity-pathway-analysis>, Krämer et al 2014) is an analytical tool drawn from an extensive database integrating both computational and manual curation methods for investigating miRNA:target interactions, the networks and pathways which these interactions influence and their ontological consequences. The microRNA Target Filter function within IPA incorporates computationally predicted miRNA-mRNA binding relationships derived from TargetScan (Agarwal et al 2015) and experimentally validated miRNA-mRNA interactions derived from TarBase (Karagkouni et al 2018), miRecords (Xiao et al 2009) and Ingenuity Knowledge Base (QIAGEN Inc., Redwood City, CA, USA). Accordingly, this provides one of the most comprehensive and robust resources for investigation of the functional consequences of altered miRNA expression over life course or associated with pathological conditions.

Age-related changes in miRNA expression in uninjured human Achilles tendon have previously been reported (Peffer et al 2015), as have age- and disease-related changes in equine SDFT (Bardell et al 2018). In this chapter, we utilised IPA to interrogate our dataset of miRNAs DE in human tendinopathy to identify targets and networks likely to be affected as a consequence. With such a large data set (223 miRNAs), the knowledge that each miRNA may target multiple gene transcripts, and transcripts are potentially targeted by more than one miRNA, we additionally employed a functional enrichment programme (ToppFun, Chen et al 2009, <http://toppgene.cchmc.org>) to investigate if certain biological processes were preferentially affected. Using this approach, we identified processes associated with maintaining cell viability, increasing cellularity, inflammation and fibrosis, and insulin, SMAD2/3, TGF $\beta$ , ERK1/2 and MAP2K1/2 signalling as being impacted by miRNA dysregulation.

Having validated DE of a small panel of miRNAs in human tendinopathy, and identified three (miR-29a, miR-181 and miR-199a) that were similarly DE with tendinopathy in equine SDFT, we then repeated this process with these miRNAs to identify mechanistic processes common to both species. Analysis underscored the processes identified above, reinforcing the importance of extracellular matrix (ECM) deposition and organisation (both collagenous and non-collagenous components), inflammation, and cell population dynamics. Thus we have identified processes active in clinical tendinopathy which are common to both human and equine species, and identified three miRNAs similarly dysregulated in both species which influence these processes.

## **4.2 Methods**

### **4.2.1 Target prediction and pathway analysis for miRNAs differentially expressed in human tendinopathy**

The QIAGEN IPA tool was used to assess the biological inference of the 223 miRNAs significantly DE (log<sub>2</sub> fold change ≥1.5 with Benjamin-Hochberg adjusted *P*-value <0.05) between tendinopathic SSP samples and healthy controls (listed in Appendix 3, Table A3.2). Data were uploaded using both miRBase (Kozomara et al 2019) and Ensembl (release 102, Yates et al 2019, <https://www.ensembl.org>) identifiers, with log<sub>2</sub> fold change. This produced 186 analysis ready molecules (170 down regulated, 16 up regulated) following deduplication performed by the software, which clusters mature miRNAs sharing the same seed sequences. Core Analysis was run using default software settings.

To identify potential miRNA targets, we then utilised the microRNA Target Filter function available in IPA. All 223 miRNAs were uploaded into the microRNA Target Filter programme, of which 182 miRNAs had targeting information available, returning 17,547 putative mRNA targets. The data set was then filtered (Figure 4.1 (A)) for confidence of miRNA:target interactions (Experimentally Observed and High (predicted)), which reduced our dataset to 182 miRNAs targeting 11,295 mRNAs. Further filters were then applied for 'Disease' ('Connective Tissue Disorders' and 'Skeletal and Muscular Disorders' - reducing to 182 miRNAs targeting 4534 mRNAs) and 'Tissue/Cell Line' ('Tissues and Primary Cells' and 'Fibroblasts') giving 167 miRNAs targeting 464 mRNAs (Appendix 4, Table A4.1). These 464 molecules were assigned a log<sub>2</sub> fold change value of zero, as DE data was not available. These were uploaded to IPA in combination with the identity and log<sub>2</sub> fold change values of the DE miRNAs. The initial dataset of 687 molecules reduced to 650 analysis ready molecules following deduplication, and Core Analysis of these genes was run. Canonical pathways, diseases and biological functions, and gene networks relevant to these were then further explored.

Functional enrichment of the target genes identified was then investigated using the ToppFun function of the ToppGene Suite software (Chen et al 2009, <http://toppgene.cchmc.org>). The HGNC gene identifier symbols for all 464 target genes were uploaded and functional enrichment analysis run, analysing for the feature 'GO: Biological Process'. Significance was determined by incorporating FDR correction with *P*-value cut off set to 0.05 into the calculation function.

### **4.2.2. Target prediction and pathway analysis for differentially expressed miRNAs common to both human and equine tendinopathy**

In the previous chapter, we identified miR-29a-3p and miR-199a-5p and members of the miR-181 family (hsa-miR-181a-3p, hsa-miR-181c-3p and -5p, hsa-miR-181d-5p, and eca-miR-181b) as showing significant downregulation in both human and equine tendinopathy (Chapter 3, Table 3.6). We therefore next focussed target prediction and network analysis on these miRNAs.

In formatting data for uploading to IPA, the Ensembl and miRBase gene identifiers for the human orthologues of each miRNA were used, as only human, mouse and rat content are fully supported in

IPA. Based on sequence similarity, four miRNAs with corresponding log<sub>2</sub> fold change values were uploaded: hsa-miR-29a-3p and hsa-miR-199a-5p, both of which have identical sequences between human and equine species (Table 4.1), and hsa-miR-181b-5p (for which an arbitrary log<sub>2</sub> fold change value of -1.5 was assigned, thereby defining it as meeting the minimal requirements for significance) and hsa-miR-181d-5p. Equine variants of miR-181c and miR-181d are not described (miRBase release 22.1, Kozomara et al 2019), however hsa-miR-181d only differs from eca-miR-181b by a single base, and hsa-miR-181b-5p and eca-miR-181b have identical sequences (Table 4.1). Additionally, 3p/5p variants of miR-181 family members are not described in the equine species (miRBase release 22.1, Kozomara et al 2019). This resulted in three analysis ready molecules: miR-29b-3p (representing hsa-miR-29a-3p/eca-miR-29a), miR-181a-5p (representing hsa-miR-181d-5p and hsa-miR-181b-5p/eca-miR-181b) and miR-199a-5p (representing hsa-miR-199a-5p/eca-miR-199a-5p), following grouping of mature miRNAs into clusters based on common seed sequences by the IPA software. Core Analysis was run using default software settings.

To identify potential targets for these miRNAs, we then utilised the microRNA Target Filter function as described above (Section 4.2.1), following the same filtering process (Figure 4.1 (B)). Initial analysis predicted 2630 mRNA targets for these three seed sequence configurations. This reduced to 727 after filtering for confidence of miRNA:target interactions (Experimentally Observed and High (predicted)), 326 mRNAs after filtering for 'Disease' (Connective Tissue Disorders and Skeletal and Muscular Disorders), and further to 48 mRNA targets after applying filters for 'Tissue/Cell Line' (Tissues and Primary Cells and Fibroblasts). These targets are listed in Appendix 4, Table A4.2. These 48 molecules were assigned a log<sub>2</sub> fold change value of zero, as DE data was not available and uploaded to IPA, in combination with the identity and log<sub>2</sub> fold change values of the four DE miRNAs. The initial dataset of 53 molecules reduced to 51 analysis ready molecules following deduplication of miRNAs and targets, and Core Analysis was then run. Canonical pathways, diseases and biological functions, and gene networks relevant to these were then further explored.

Functional enrichment of target genes was investigated using the ToppFun function of the ToppGene Suite software (Chen et al 2009, <http://toppgene.cchmc.org>). The HGNC gene identifier symbols for the 48 target genes were uploaded and functional enrichment analysis run, analysing for the feature 'GO: Biological Process'. Significance was determined by incorporating FDR correction with *P*-value cut off set to 0.05 into the calculation function.

### 4.2.3. Statistical analysis

QIAGEN IPA performs two primary statistical tests. The *P*-value of overlap is calculated using a right-tailed Fisher's Exact test for all analyses (canonical pathways, disease and functions, regulator effects and networks), with significance indicated if  $P \leq 0.05$ .

Inclusion of directional expression data permits calculation of z-scores for the functions canonical pathways, upstream regulators and diseases and functions. Z-scores predict downstream effects based on correlation between the expression pattern of molecules in the experimental dataset with that reported in published databases, from which Ingenuity Knowledge Base is populated. A z-score  $\geq 2$  predicts activation, whilst a z-score  $\leq -2$  predicts inhibition.

Additionally, for networks identified as significant ( $P \leq 0.05$ ) using a right-tailed Fisher's Exact test, a network score is reported. This numerical value ranks significant networks according to the degree of relevance of network eligible ('analysis ready') molecules in the experimental dataset to networks contained in the Ingenuity Knowledge Base. The network score is based on the  $P$ -value calculated from the right-tailed Fisher's Exact test, according to the formula: Network Score =  $-\log_{10}(P\text{-value})$ .

miRNA Identity	Sequence																						
hsa-miR-29a-3p	u	a	g	c	a	c	c	a	u	c	u	g	a	a	a	u	c	g	g	u	u	a	
eca-miR-29a	u	a	g	c	a	c	c	a	u	c	u	g	a	a	a	u	c	g	g	u	u	a	
hsa-miR-199a-5p	c	c	c	a	g	u	g	u	u	c	a	g	a	c	u	a	c	c	u	g	u	u	c
eca-miR-199a-5p	c	c	c	a	g	u	g	u	u	c	a	g	a	c	u	a	c	c	u	g	u	u	c
hsa-miR-181a-5p	a	a	c	a	u	u	c	a	a	c	g	c	u	g	u	c	g	g	u	g	a	g	u
eca-miR-181a	a	a	c	a	u	u	c	a	a	c	g	c	u	g	u	c	g	g	u	g	a	g	u
hsa-miR-181b-5p	a	a	c	a	u	u	c	a	u	u	g	c	u	g	u	c	g	g	u	g	g	g	u
eca-miR-181b	a	a	c	a	u	u	c	a	u	u	g	c	u	g	u	c	g	g	u	g	g	g	u
hsa-miR-181c-5p	a	a	c	a	u	u	c	a	a	c	c	u	g	u	c	g	g	u	g	a	g	u	
hsa-miR-181d-5p	a	a	c	a	u	u	c	a	u	u	g	u	u	g	u	c	g	g	u	g	g	g	u
hsa-miR-181a-3p	a	c	c	a	u	c	g	a	c	c	g	u	u	g	a	u	u	g	u	a	c	c	
hsa-miR-181b-3p	c	u	c	a	c	u	g	a	a	c	a	a	u	g	a	a	u	g	c	a	a		
hsa-miR-181c-3p	a	a	c	c	a	u	c	g	a	c	c	g	u	u	g	a	g	u	g	g	a	c	
hsa-miR-181d-3p	c	c	a	c	c	g	g	g	g	g	a	u	g	a	a	u	g	u	c	a	c		

**Table 4.1 Sequences are conserved between human (hsa) and equine (eca) orthologues of miR-29a-3p, miR-199a-5p, miR-181a and miR-181b.** Seed sequences of 5p variants of all four human miR-181 family members are identical, but this feature is not conserved in the corresponding 3p variants. In the equine species, miR-181c and miR-181d are not recognised, nor are 5p/3p variants of miR-181a or miR-181b. Seed sequences are shown in red. Sequences obtained from miRBase (release 22.1, Kozomara et al 2019).

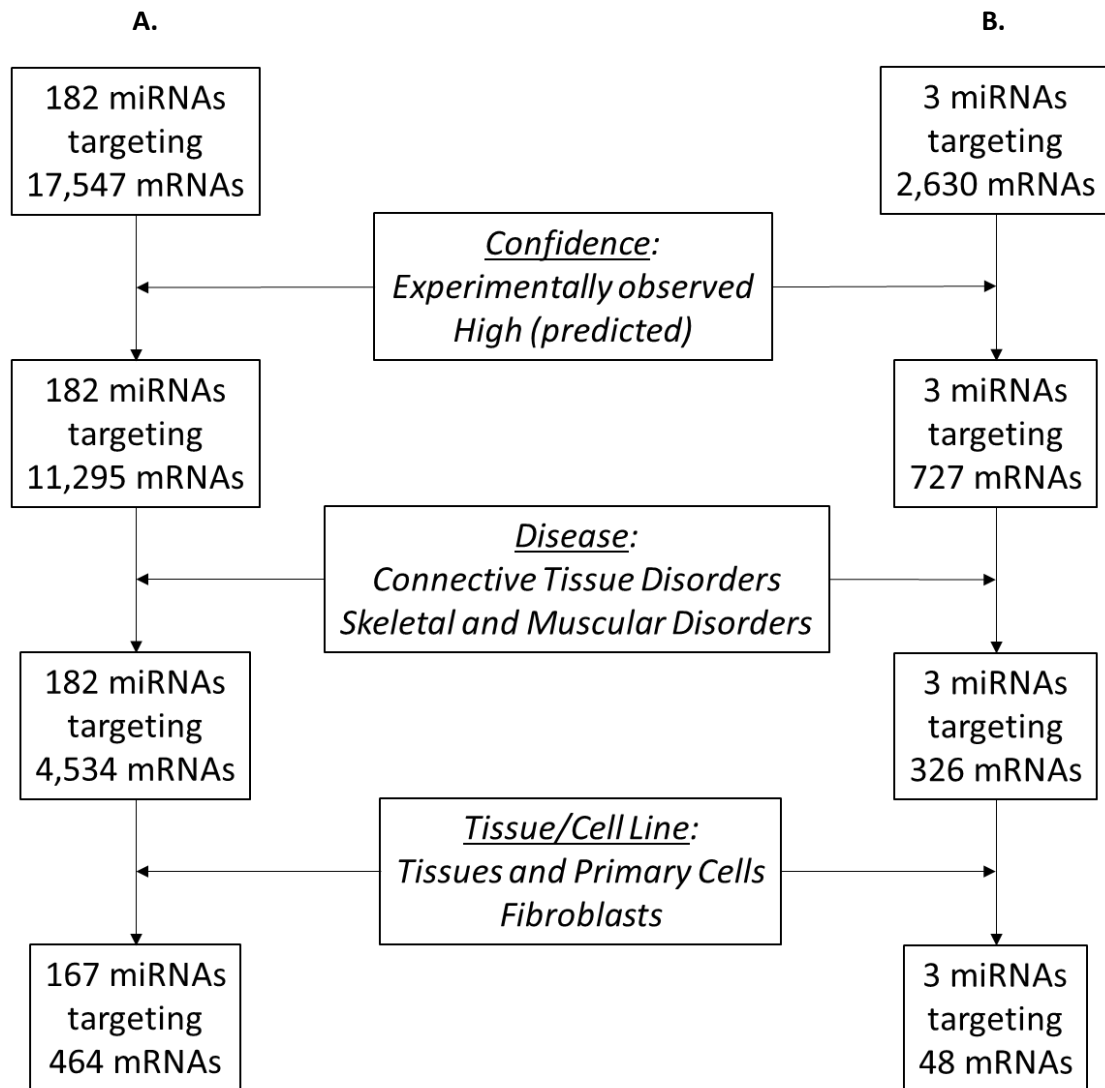


**Figure 4.1** Flowchart illustrating filters applied during target prediction for: **A) 223 human miRNAs differentially expressed in tendinopathy.** **B) Three miRNAs differentially expressed in both human and equine tendinopathy.** Target prediction and filtering performed using Ingenuity Pathway Analysis (IPA; [www.qiagenbioinformatics.com/products/ingenuity-pathway-analysis](http://www.qiagenbioinformatics.com/products/ingenuity-pathway-analysis)) microRNA Target Filter function which clusters miRNAs on the basis of common seed sequences (see text for details). Applied filters are given in *italics*.

## **4.3 Results**

### **4.3.1 Target prediction and pathway analysis for miRNAs differentially expressed in human tendinopathy**

#### **Core Analysis of DE miRNAs**

Initial Core Analysis of all 223 miRNAs previously identified as significantly DE returned top biological functions of cellular development ( $P = 4.70E-02 - 5.29E-15$ ), growth and proliferation ( $P = 4.70E-02 - 5.29E-15$ ) and movement ( $P = 4.70E-02 - 3.34E-11$ ), cell death and survival ( $P = 4.32E-02 - 5.10E-07$ ), and cell cycle ( $P = 4.61E-02 - 8.37E-06$ ). Figure 4.2 illustrates a heat map, sized by number of genes and coloured according to activity (z-score), with all disease and function categories demonstrating significant activation ( $P < 0.05$ , z-score  $\geq 2$ , orange) or deactivation ( $P < 0.05$ , z-score  $\leq -2$ , blue) listed in Table 4.2. Interestingly, activity of inflammatory response or inflammatory disease, or connective tissue disorders, were not predicted to be significantly affected.

Annotated functions 'Apoptosis' and 'Necrosis' and 'G1/S phase transition of fibroblast cell lines' and 'Maturation of chondrocyte cell lines' were further explored for associated miRNAs. Inhibited functions apoptosis and necrosis were associated with 36 miRNAs (Figure 4.3 (A)) and 39 miRNAs (Figure 4.3 (B)) respectively. Activated functions G1/S phase transition of fibroblast cell lines and maturation of chondrocyte cell lines were both associated with four miRNAs (Figures 4.4 (A) and (B) respectively).

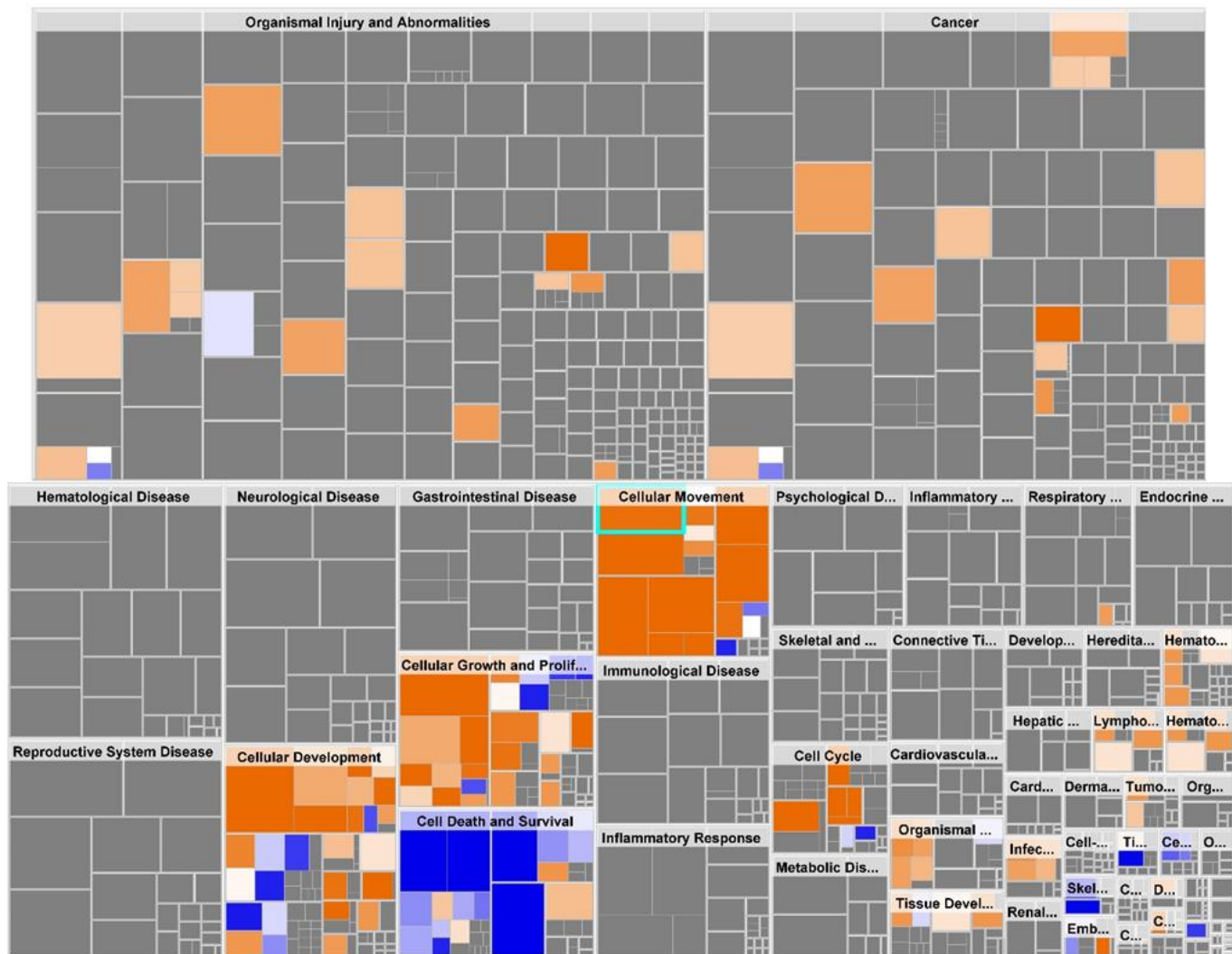


**Figure 4.2 Core analysis of 223 human miRNAs differentially expressed with tendinopathy identifies top biological functions most significantly affected are associated with cellular development, proliferation, movement and viability.** Heatmap squares sized according to number of associated miRNAs and coloured according to activation (z-score;  $\geq 2$  = activation (orange);  $\leq -2$  = inhibition (blue)). Intensity of colour reflects magnitude of z-score ( $< -2$  or  $> 2$ ). Where the software cannot predict activation or inhibition of biological functions from the available database, squares are coloured grey. See Table 4.2 for additional details.

Categories	Diseases or Functions Annotation	P -value	Predicted Activation State	Activation z-score
Cell Death and Survival	Cell death of tumor cell lines	0.0000243	Decreased	-3.503
Cell Death and Survival	Apoptosis of tumor cell lines	0.00000051	Decreased	-3.396
Cell Death and Survival	Apoptosis	0.0194	Decreased	-3.287
Cell Death and Survival	Necrosis	0.00553	Decreased	-3.147
Skeletal and Muscular System Development and Function, Tissue Morphology	Quantity of muscle cell lines	0.0000701	Decreased	-2.449
Cellular Development, Skeletal and Muscular System Development and Function	Differentiation of muscle cell lines	0.000359	Decreased	-2.121
Cellular Development, Cellular Growth and Proliferation	Proliferation of pancreatic cancer cell lines	0.000678	Decreased	-2.012
Cell Cycle, Embryonic Development	G1/S phase transition of embryonic cell line	0.00000837	Increased	2
Cell Cycle, Connective Tissue Development and Function	G1/S phase transition of fibroblast cell lines	0.0000704	Increased	2
Cellular Movement	Cell movement of melanoma cell lines	0.000135	Increased	2
Cellular Development	Maturation of chondrocyte cell lines	0.00000214	Increased	2
Cellular Movement	Cell movement of breast cancer cell lines	0.0145	Increased	2.135
Cancer, Organismal Injury and Abnormalities	Growth of tumor	0.0115	Increased	2.152
Cell Cycle	G1 phase	0.00651	Increased	2.202
Cell Cycle	Interphase	0.0218	Increased	2.202
Cell Cycle	G1/S phase transition	0.0441	Increased	2.202
Cellular Development, Cellular Growth and Proliferation	Development of tumor cell lines	0.013	Increased	2.261
Cellular Movement	Migration of tumor cell lines	1.3E-10	Increased	2.354
Cellular Movement	Cell movement	0.00214	Increased	2.384
Cellular Development, Cellular Growth and Proliferation	Cell proliferation of hepatoma cell lines	0.0000342	Increased	2.471
Cellular Development, Cellular Growth and Proliferation	Cell proliferation of tumor cell lines	5.29E-15	Increased	2.721
Cellular Movement	Cell movement of tumor cell lines	4.83E-10	Increased	2.899
Cellular Movement	Invasion of cells	1.68E-09	Increased	2.915
Cellular Development, Cellular Growth and Proliferation	Cell proliferation of lymphoma cell lines	0.0000104	Increased	2.96
Cellular Movement	Invasion of tumor cell lines	3.34E-11	Increased	3.007

**Table 4.2 Top biological functions identified by Ingenuity Pathway Analysis of 223 human miRNAs differentially expressed with tendinopathy are associated with cellular development, proliferation, movement and viability.** Blue fill indicates predicted inhibition of associated biological function (negative z-score), orange fill indicates predicted activation of associated biological function (positive z-score).

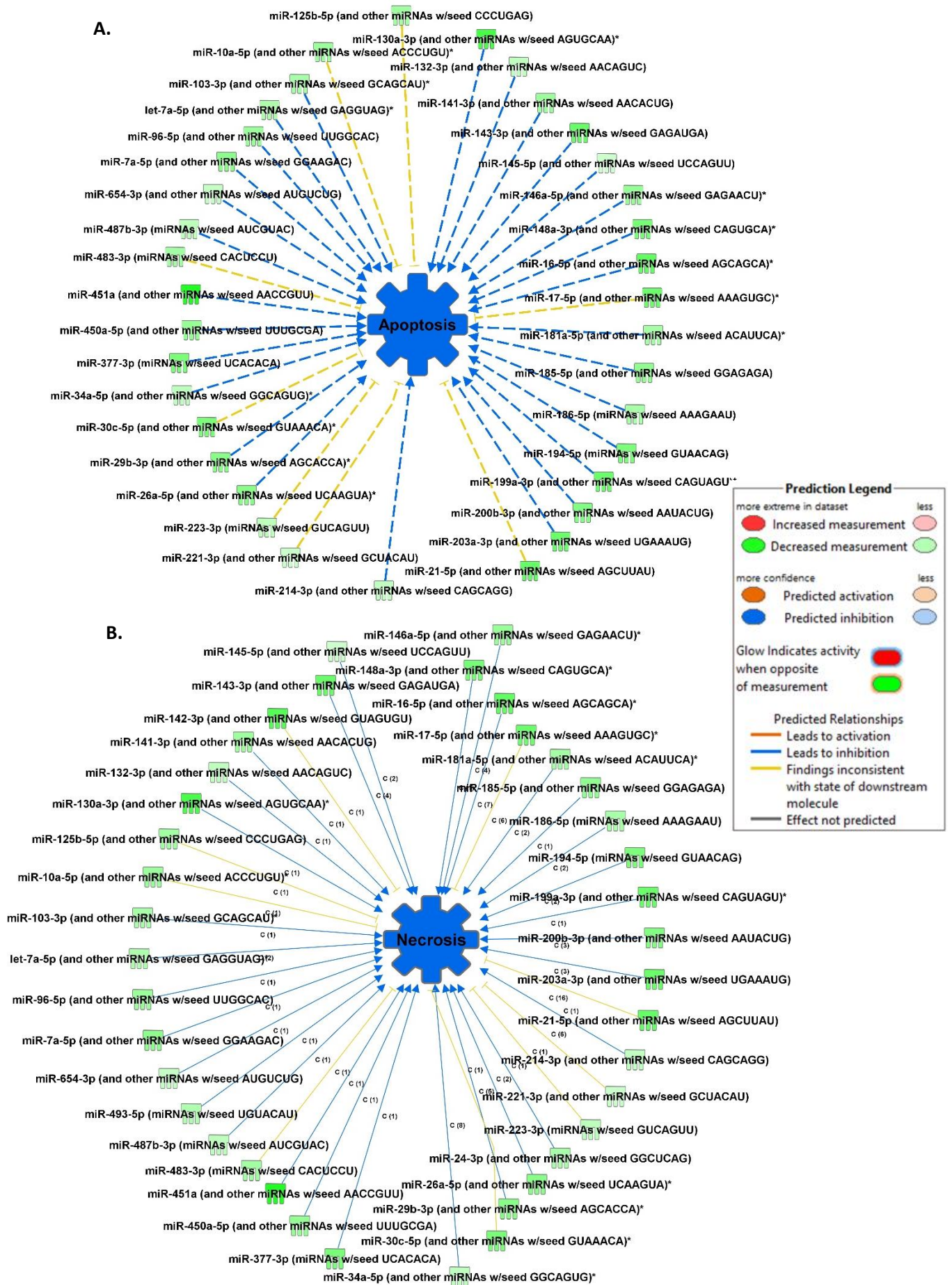
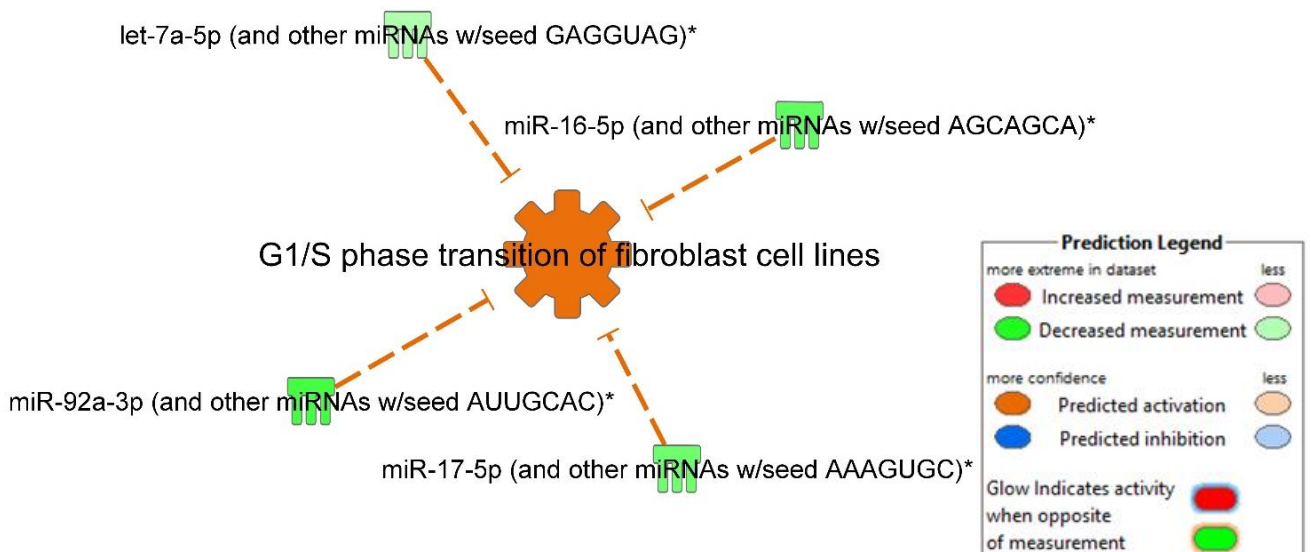


**Figure 4.3 Biological functions A. Apoptosis and B. Necrosis are predicted to be inhibited by the action of multiple miRNAs differentially expressed in human tendinopathy.**

A.



B.

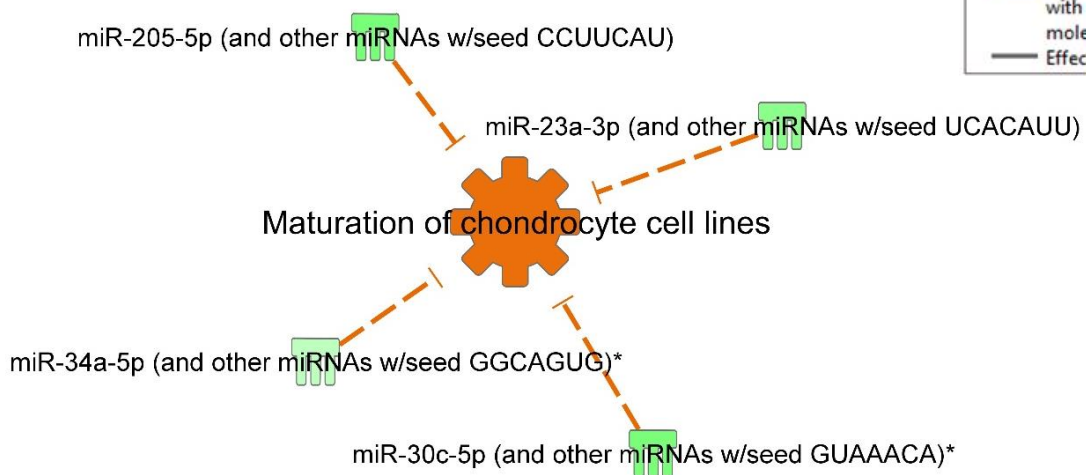


**Figure 4.4 Biological functions A. G1/S phase transition of fibroblast cell lines and B. Maturation of chondrocyte cell lines are predicted to be activated by the action of multiple miRNAs differentially expressed in human tendinopathy.**

Top scoring network, both in terms of score (57) and number of focus molecules (28) was associated with the terms neurological disease, organismal injury and abnormalities, and psychological disorders. Removal of the molecules chorionic gonadotrophin (CG) and follicle stimulating hormone (FSH) from the network reduced this to 23 focus molecules. This network implicated insulin, SMAD 2/3, TGF $\beta$ , ERK1/2 and MAP2K1/2 as important signalling pathways impacted by altered miRNA expression in tendinopathy (Figure 4.5).

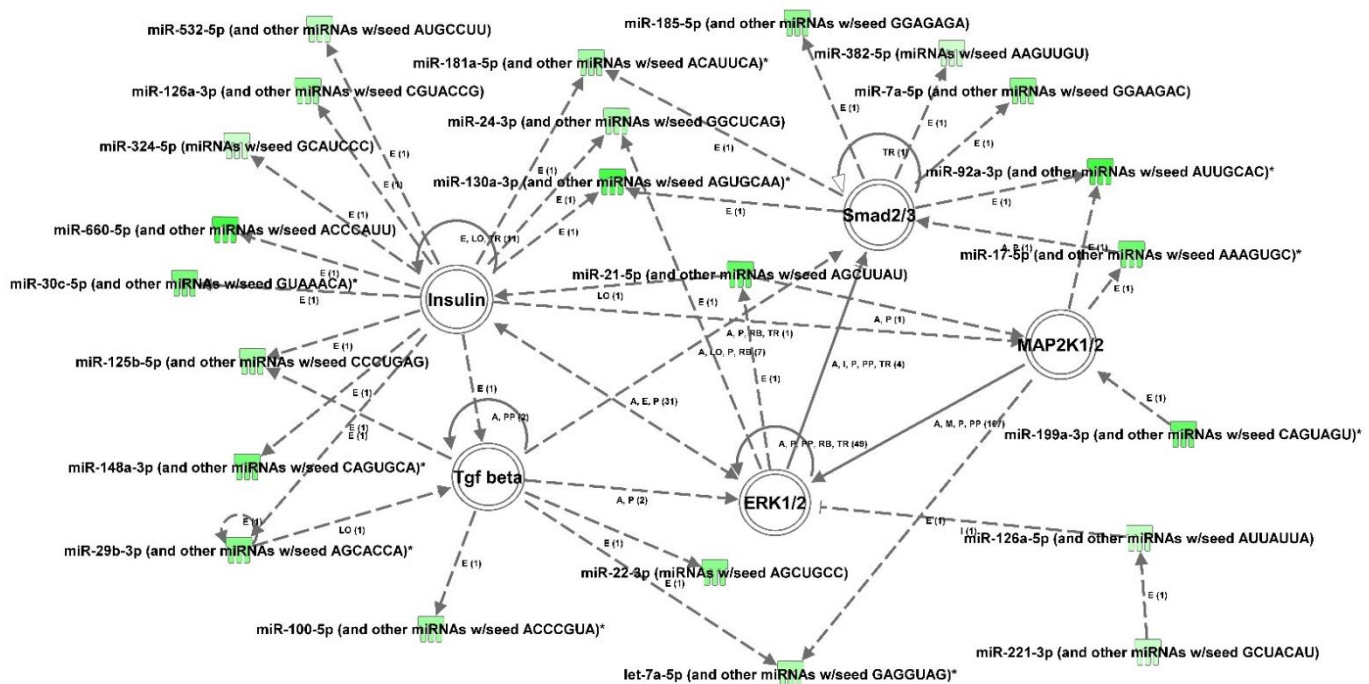


**Figure 4.5** Top scoring network identified by Ingenuity Pathway Analysis of 223 differentially expressed human miRNAs identifies potential dysregulation of insulin, SMAD2/3, TGF $\beta$ , ERK1/2 and MAP2K1/2 signalling in tendinopathy. Network represented following removal of Follicle Stimulating Hormone (FSH) and Chorionic Gonadotrophin (CG). Green indicates miRNA expression reduced in tendinopathy, intensity of colour reflects magnitude of reduction. Grey indicates relationship effect not predicted.

### Core analysis of DE miR target genes

We then investigated target interactions for the 650 analysis ready molecules identified by the IPA microRNA Target Filter function subsequent to our applied filters (section 4.2.1, Figure 4.1 (A)) and deduplication by the software.

Core analysis of the 464 mRNA targets derived following application of these filters identified top diseases and functions associated with the terms cancer, organismal injury and abnormalities, inflammation and connective tissue disorders (Table 4.3). Predicted activation (z-scores) indicated decreased activation of apoptosis and necrosis, with increased activity of functions related to cellular growth, migration and proliferation (Table 4.4). Top molecular and cellular functions identified were associated with cell activity, development and viability (Table 4.3), whilst top canonical pathways implicated were related to tumour microenvironment, fibrosis and inflammation (Table 4.3). The two top scoring networks were associated with the terms cell death and survival, gastrointestinal and hepatic system disease (score 49, 31 focus molecules, Figure 4.6 (A)) and cancer, organismal injury and abnormalities and reproductive system (score 44, 29 focus molecules, Figure 4.6 (B)). Significant upstream regulators were identified as TNF ( $P = 1.44E-144$ ), IL1 $\beta$  ( $P = 3.68E-127$ ) and TGF $\beta$ 1 ( $P = 2.81E-124$ ).

Functional enrichment of identified target genes was then investigated using the ToppFun function of the ToppGene Suite software (Chen et al 2009, <http://toppgene.cchmc.org>). The HGNC gene identifier symbols for all 464 target genes were uploaded and functional enrichment analysis run using the calculation function with FDR correction and  $P$ -value cut off set to 0.05, for the feature 'GO: Biological Process'. Top ten gene ontology (GO) terms ranked in terms of number of molecules in target list and level of statistical significance achieved are listed in Table 4.5.

Canonical Pathway		P-value
Tumour microenvironment		8.35E-53
Hepatic fibrosis signalling		7.27E-47
Hepatic fibrosis/hepatic stellate cell activation		6.28E-46
Role of macrophages, fibroblasts and endothelial cells in rheumatoid arthritis		2.62E-42
Role of osteoblasts, osteoclasts and chondrocytes in rheumatoid arthritis		2.16E-40
Diseases and Disorders	P-value range	Number of molecules
Cancer	1.62E-40 – 4.56E-138	546
Organismal injury and abnormalities	1.10E-39 – 4.56E-138	572
Inflammatory response	5.83E-40 – 2.21E-128	409
Connective tissue disorders	6.77E-40 – 1.94E-107	322
Inflammatory disease	1.04E-40 – 1.94E-107	370
Molecular and Cellular Functions		
Cellular movement	5.41E-40 – 1.50E-137	376
Cellular development	4.28E-40 – 1.81E-129	451
Cellular growth and proliferation	4.28E-40 – 1.81E-129	439
Cell death and survival	7.19E-40 – 4.39E-124	407
Cell-to-cell signalling and interaction	5.83E-40 – 4.77E-103	325

**Table 4.3 Ingenuity Pathway Analysis predictions of most significant canonical pathways, diseases and disorders and molecular and cellular functions likely to be implicated as a result of miRNA dysregulation in human tendinopathy.** Core analysis performed on 464 putative mRNA targets of 167 miRNAs; see text (section 4.2) for details of target filters applied.

Categories	Diseases or Functions Annotation	P -value	Predicted Activation State	Activation z-score
Cell Death and Survival	Cell death of tumor cell lines	1.18E-90	Decreased	-3.503
Cell Death and Survival	Apoptosis of tumor cell lines	1.65E-102	Decreased	-3.396
Cell Death and Survival	Apoptosis	1.13E-123	Decreased	-3.287
Cell Death and Survival	Necrosis	4.39E-124	Decreased	-3.147
Cellular Movement	Migration of breast cancer cell lines	4.26E-49	Increased	2
Cellular Movement	Cell movement of breast cancer cell lines	1.45E-56	Increased	2.135
Cancer, Organismal Injury and Abnormalities	Growth of tumor	2.68E-119	Increased	2.152
Cell Cycle	Interphase	2.71E-56	Increased	2.202
Cell Cycle	G1 phase	5.26E-50	Increased	2.202
Cellular Development, Cellular Growth and Proliferation	Development of tumor cell lines	3.99E-58	Increased	2.261
Cellular Movement	Migration of tumor cell lines	1.98E-104	Increased	2.354
Cellular Movement	Cell movement	3E-131	Increased	2.384
Cellular Development, Cellular Growth and Proliferation	Cell proliferation of tumor cell lines	1.81E-129	Increased	2.721
Cellular Movement	Cell movement of tumor cell lines	4.42E-112	Increased	2.899
Cellular Movement	Invasion of cells	1.4E-117	Increased	2.915
Cellular Movement	Invasion of tumor cell lines	2.65E-102	Increased	3.007

**Table 4.4 Top biological functions of 464 predicted target genes regulated by 223 differentially expressed human miRNAs in tendinopathy are associated with cellular development, proliferation, movement and viability.** Analysis performed using Ingenuity Pathway Analysis. Blue fill indicates predicted inhibition of associated biological function (negative z-score), orange fill indicates predicted activation of associated biological function (positive z-score).



**Figure 4.6 (preceding page) Top scoring networks reflecting dysregulated miRNA:target interactions in human tendinopathy are associated with the terms: A. Cell death and survival, gastrointestinal and hepatic system disease (score 49, 31 focus molecules) and B. Cancer, organismal injury and abnormalities reproductive system disease (score 44, 29 focus molecules).** Green indicates miRNA expression reduced in tendinopathy, red indicates miRNA expression increased in tendinopathy. Intensity of colour reflects magnitude of reduction. Grey indicates relationship effect not predicted.

Gene Ontology		P-value	q-value FDR BH	Hit Count in Query List
ID	Term			
<b>Ranked by number of associated target molecules</b>				
GO:0042127	Regulation of cell population proliferation	3.99E-109	3.36E-105	227
GO:0010941	Regulation of cell death	1.31E-79	1.38E-76	198
GO:0009719	Response to endogenous stimulus	2.22E-83	6.23E-80	196
GO:1901700	Response to oxygen-containing compound	3.63E-83	7.63E-80	196
GO:0009967	Positive regulation of signal transduction	6.08E-83	1.02E-79	195
GO:0019220	Regulation of phosphate metabolic process	2.58E-74	1.32E-71	193
GO:0051174	Regulation of phosphorus metabolic process	2.82E-74	1.32E-71	193
GO:0048870	Cell motility	4.11E-74	1.65E-71	190
GO:0051674	Localization of cell	4.11E-74	1.65E-71	190
GO:0016477	Cell migration	1.93E-79	1.81E-76	188
<b>Ranked by q-value for FDR</b>				
GO:0042127	Regulation of cell population proliferation	3.99E-109	3.36E-105	227
GO:0008284	Positive regulation of cell population proliferation	3.66E-86	1.54E-82	160
GO:0009719	Response to endogenous stimulus	2.22E-83	6.23E-80	196
GO:1901700	Response to oxygen-containing compound	3.63E-83	7.63E-80	196
GO:0009967	Positive regulation of signal transduction	6.08E-83	1.02E-79	195
GO:0035295	Tube development	8.67E-83	1.22E-79	167
GO:0051094	Positive regulation of developmental process	2.66E-81	3.20E-78	184
GO:0010941	Regulation of cell death	1.31E-79	1.38E-76	198
GO:0016477	Cell migration	1.93E-79	1.81E-76	188
GO:0030334	Regulation of cell migration	1.05E-77	8.85E-75	149

**Table 4.5 Biological processes (as described by gene ontology (GO) terms) associated principally with control of cellular proliferation, viability and localisation, signalling and metabolic activity are enriched in the mRNA population targeted by miRNAs DE in human tendinopathy.** Target gene identification and functional enrichment analysis performed using IPA microRNA Target Filter ([www.qiagenbioinformatics.com/products/ingenuity-pathway-analysis](http://www.qiagenbioinformatics.com/products/ingenuity-pathway-analysis)) and Toppgene Suite ([toppgene.cchmc.org](http://toppgene.cchmc.org)) respectively. Highlighted terms are common to rankings by both hit count and q-value. FDR BH = False Discovery Rate derived using Benjamini Hochberg correction.

### 4.3.2. Target prediction and pathway analysis for differentially expressed miRNAs common to both human and equine tendinopathy

To investigate mechanistic processes common to human and equine tendinopathy, a separate analysis was then run focussing on miR-29a-3p, miR-199a-5p and members of the miR-181 family, which had shown significantly reduced expression in tendinopathic tissue from both human and equine species (see Chapter 3, Table 3.6).

#### Core analysis of the four DE miRs common to horse and man

Core Analysis of the human orthologues of these four dysregulated miRNAs (three clusters following grouping of mature miRNAs based on common seed sequences by the IPA software) returned top biological functions of cellular movement ( $P = 2.32E-02 - 1.89E-04$ ), cell-to-cell signalling and interaction ( $P = 6.57E-04 - 3.94E-04$ ), cell death and survival ( $P = 4.98E-02 - 5.26E-04$ ) and cellular development, growth and proliferation ( $P = 4.84E-02 - 5.58E-04$ ).

The only identified network containing all three focus molecules was associated with the terms connective tissue disorders, organismal injury and abnormalities and skeletal and muscular disorders (Figure 4.7). Over represented in the 27 organic molecules identified in this network, were those associated with composition and organisation of the extracellular matrix. Both collagenous (collagens COL1A1, COL4A1, COL4A5, COL5A1, COL5A2, COL5A3, COL14A1) and non-collagenous (biglycan (BGN), fibrillin 1 (FBN1)) matrix proteins were identified, together with those associated with matrix organisation, maturation and homeostasis; cartilage associated protein (CRTAP), lysyl oxidase like 2 (LOXL2), procollagen-lysine,2-oxoglutarate 5-dioxygenase 2 (PLOD2), disintegrin and metalloproteinase with thrombospondin motifs family members 2 and 14 (ADAMTS2, ADAMTS14), integrin alpha-3 (ITGA3) and epithelial discoidin domain-containing receptor 1 (DDR1), which, additionally regulates cell-matrix interactions and cell migration, proliferation, differentiation and survival. Other network proteins also related to these latter processes were dual specificity protein phosphatase 2 (DUSP2), neurogenic locus notch homolog protein 4 (NOTCH4) and protein phosphatase 1D (PPM1D). Reinforcing the maturation of chondrocyte cell lines function identified in the main dataset (Figure 4.4 (B)), this network also included homeobox protein Hox-A11 (HOXA11) and Wnt Family Member 5B (WNT5B).

Other network proteins implicated in cell-matrix interactions in addition to DDR1 were basement membrane proteins nidogen 1 and nidogen 2 (NID1, NID2), important in cell adhesion and critical in establishment of tissue architecture during organ development (Bader et al 2005). Inflammation associated proteins DUSP2 and pulmonary surfactant-associated protein A1 (SFTPA1) were also identified (Figure 4.7).

Regulators and components of the transforming growth factor beta/mothers against decapentaplegic (TGF $\beta$ /SMAD) signalling were also represented, with promoters myocardin (MYOCD) and transforming growth factor beta-1-induced transcript 1 protein (TGFB1I1) being identified, as well as and transforming growth factor beta receptor type 3 (TGFB3).

The presence of hydrogen peroxide in this network also alluded to an association of these miRNAs with oxidative stress (Figure 4.7).

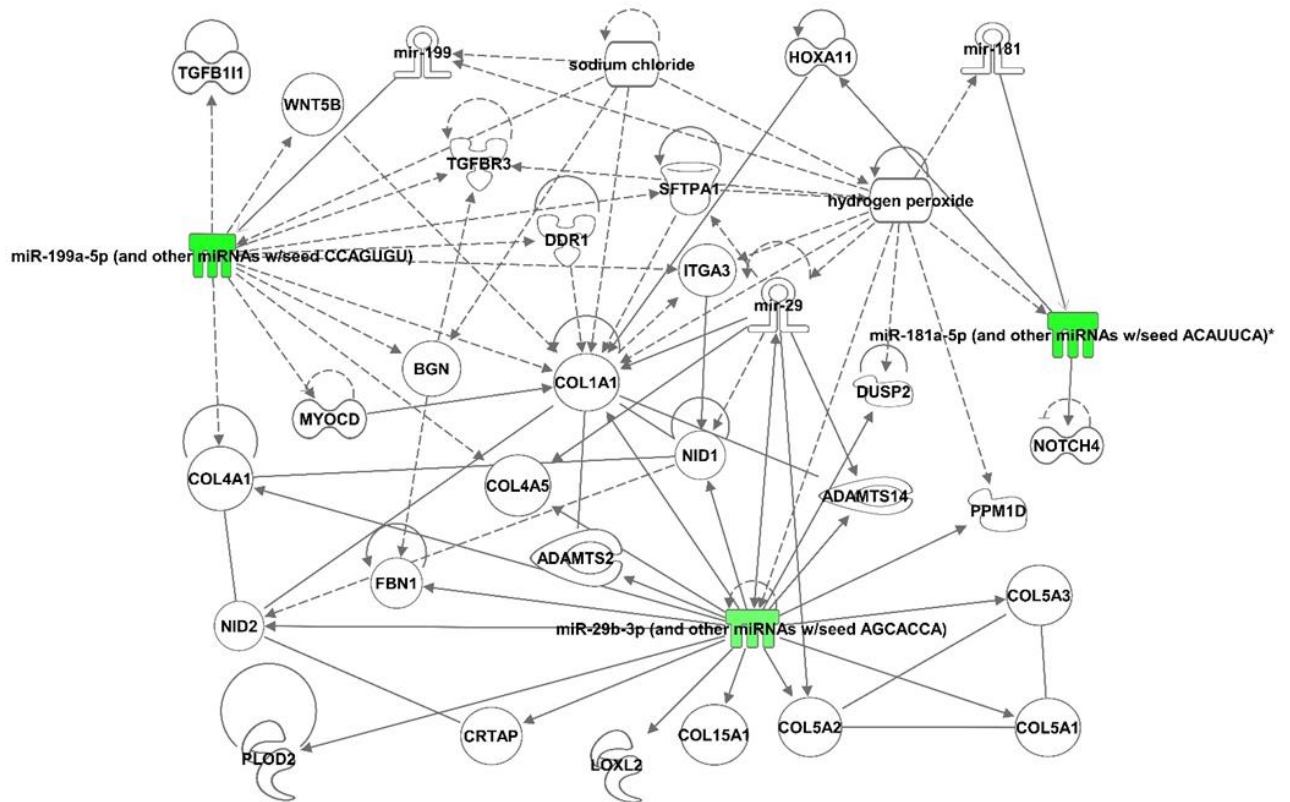


**Figure 4.7** Top network associated with dysregulation of miR-29a-3p, miR-181a-5p and miR-199a-5p common to both human and equine tendinopathy. This was the only network containing all three miRNAs and was associated with the terms connective tissue disorders, organismal injury and abnormalities and skeletal and muscular disorders. Green indicates miRNA expression reduced in tendinopathy, intensity of colour reflects magnitude of reduction. Grey indicates relationship effect not predicted.

### Core analysis of the mRNA targets of four DE miRs

Using the same filtering criteria previously applied within the IPA microRNA Target Filter function (section 4.2.1, Figure 4.1 (B)), we next identified 48 mRNA targets for these three focus molecules (Appendix 4, Table A4.2). Core analysis of these 48 mRNA targets identified top canonical pathways related to fibrosis signalling and activation, tumour microenvironment and signalling associated with epithelial-mesenchymal transition and pancreatic neoplasia (Table 4.6). Top diseases and functions were associated with the terms cancer, organismal injury and abnormalities, and skeletal and muscular disorders (Table 4.6). Activation (z-scores) indicated either no net activity pattern was predicted, or it was not possible to calculate from the data contained within the IPA database. Top molecular and cellular functions identified were associated with cellular movement and signalling, and cell proliferation, development and viability (Table 4.6).

Canonical Pathway		P-value
Hepatic fibrosis signalling		1.00E-19
Hepatic fibrosis/hepatic stellate cell activation		3.46E-18
Tumour microenvironment		8.06E-17
Regulation of epithelial mesenchymal transition by growth factors		8.24E-15
Pancreatic adenocarcinoma signalling		2.38E-12
Diseases and Disorders	P-value range	Number of molecules
Cancer	8.59E-08 – 3.52E-23	51
Organismal injury and abnormalities	8.63E-08 – 3.52E-23	51
Skeletal and muscular disorders	6.48E-08 – 3.07E-19	45
Cardiovascular disease	8.26E-08 – 3.60E-18	36
Reproductive system disease	6.48E-08 – 1.65E-17	46
Molecular and Cellular Functions		
Cellular movement	6.64E-08 – 4.68E-21	39
Cell-to-cell signalling and interaction	6.82E-08 – 1.86E-17	32
Cellular development	7.40E-08 – 1.08E-16	43
Cellular growth and proliferation	7.40E-08 – 1.08E-16	39
Cell death and survival	7.87E-08 – 1.49E-16	38

**Table 4.6 Ingenuity Pathway Analysis predictions of most significant canonical pathways, diseases and disorders and molecular and cellular functions implicated as a result of dysregulation of miR-29a-3p, miR-181a-5p and miR-199a-5p common to human and equine tendinopathy.** Core analysis performed on 48 putative mRNA targets of four miRNAs. IPA analysis utilised human orthologues of relevant miRNAs and clustered miRNAs sharing common seed sequences (see text for details). See text (section 4.2) for details of target filters applied.

Interrogating the database for the term cell viability, implicated miR-181a-5p as the key miRNA for this function (Figure 4.8). The top scoring network (score 34, 15 focus molecules) was associated with the functions tissue development, connective tissue disorders and organismal injury and abnormalities (Figure 4.9 (A)), whilst the second scoring network (score 20, 10 focus molecules) was associated with tissue development, organismal injury and abnormalities and cancer (Figure 4.9 (B)). Upstream regulators identified were SMAD3 ( $P = 8.30E-21$ ) and HRas proto-oncogene, GTPase (HRAS;  $P = 1.01E-19$ ), involved in regulation of cell proliferation and signal transduction.

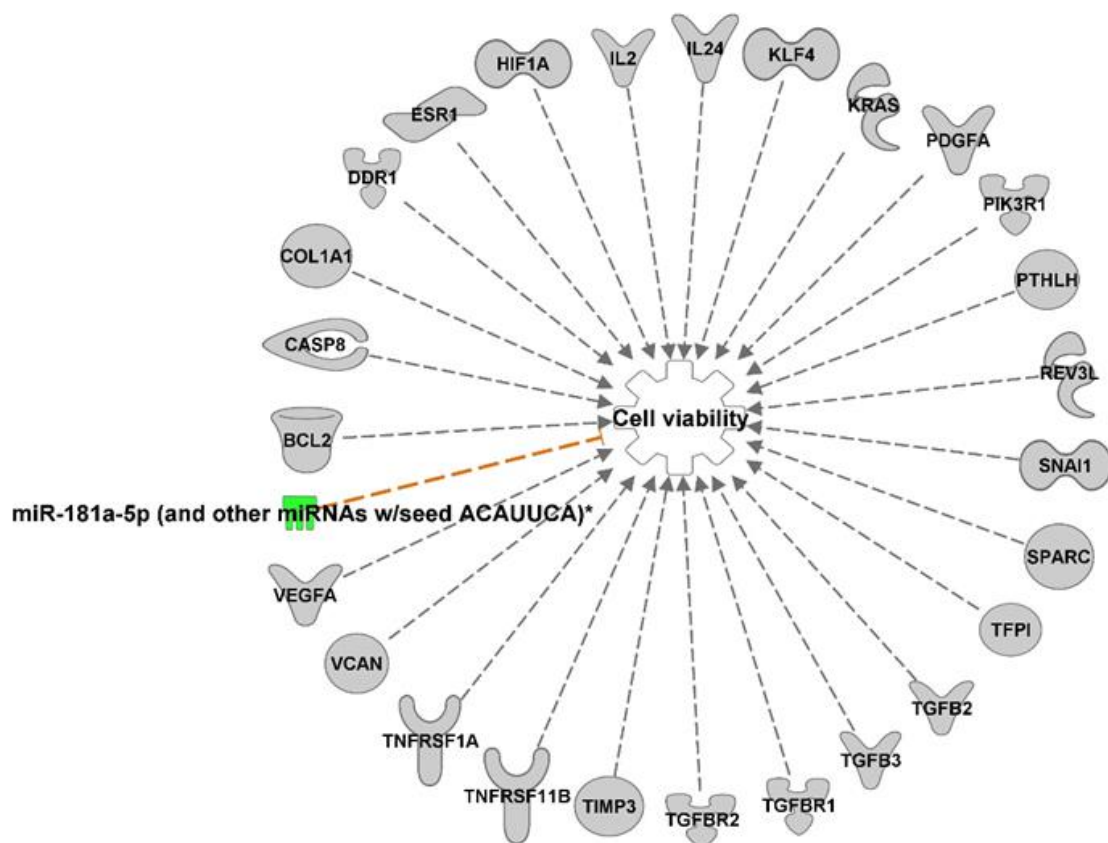
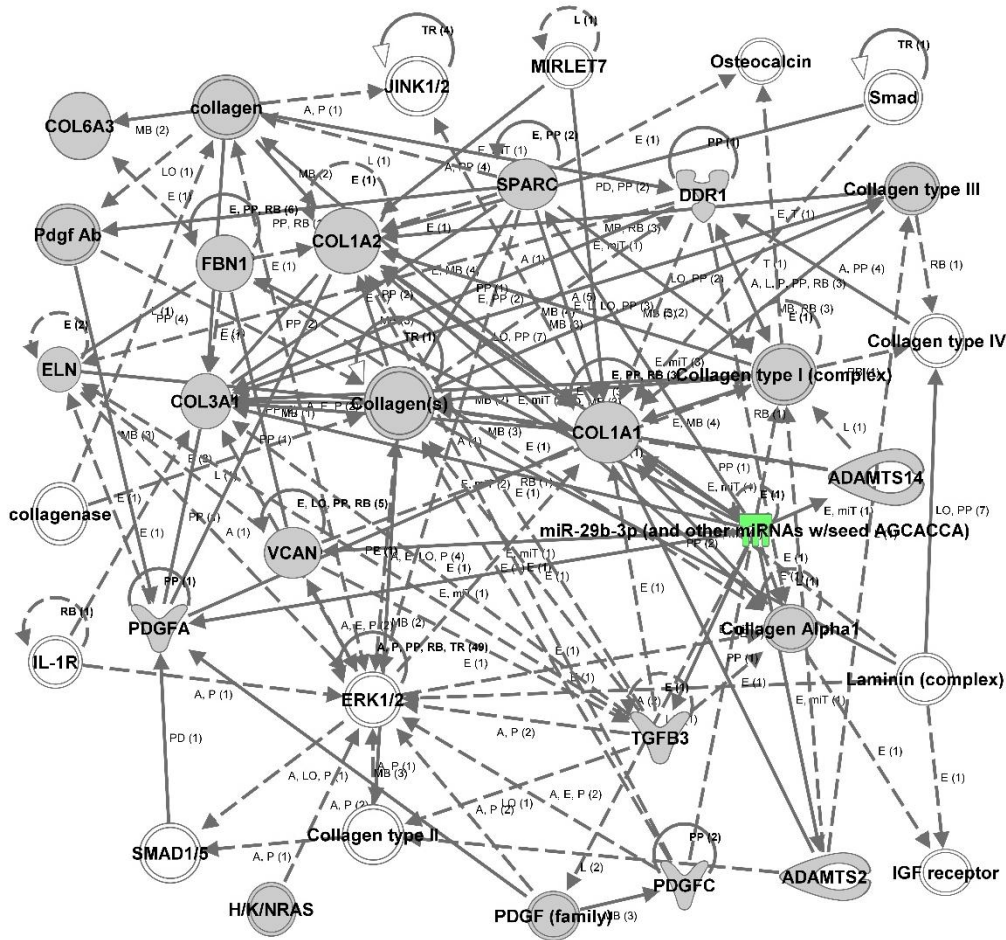


**Figure 4.8 miR-181a-5p expression regulates cell viability in both human SSP and equine SDFT tendinopathy.** Green indicates miRNA expression reduced in tendinopathy, intensity of colour reflects magnitude of reduction. Orange dashed line indicates relationship is predicted activation, grey indicates relationship effect not predicted.

A.



B.

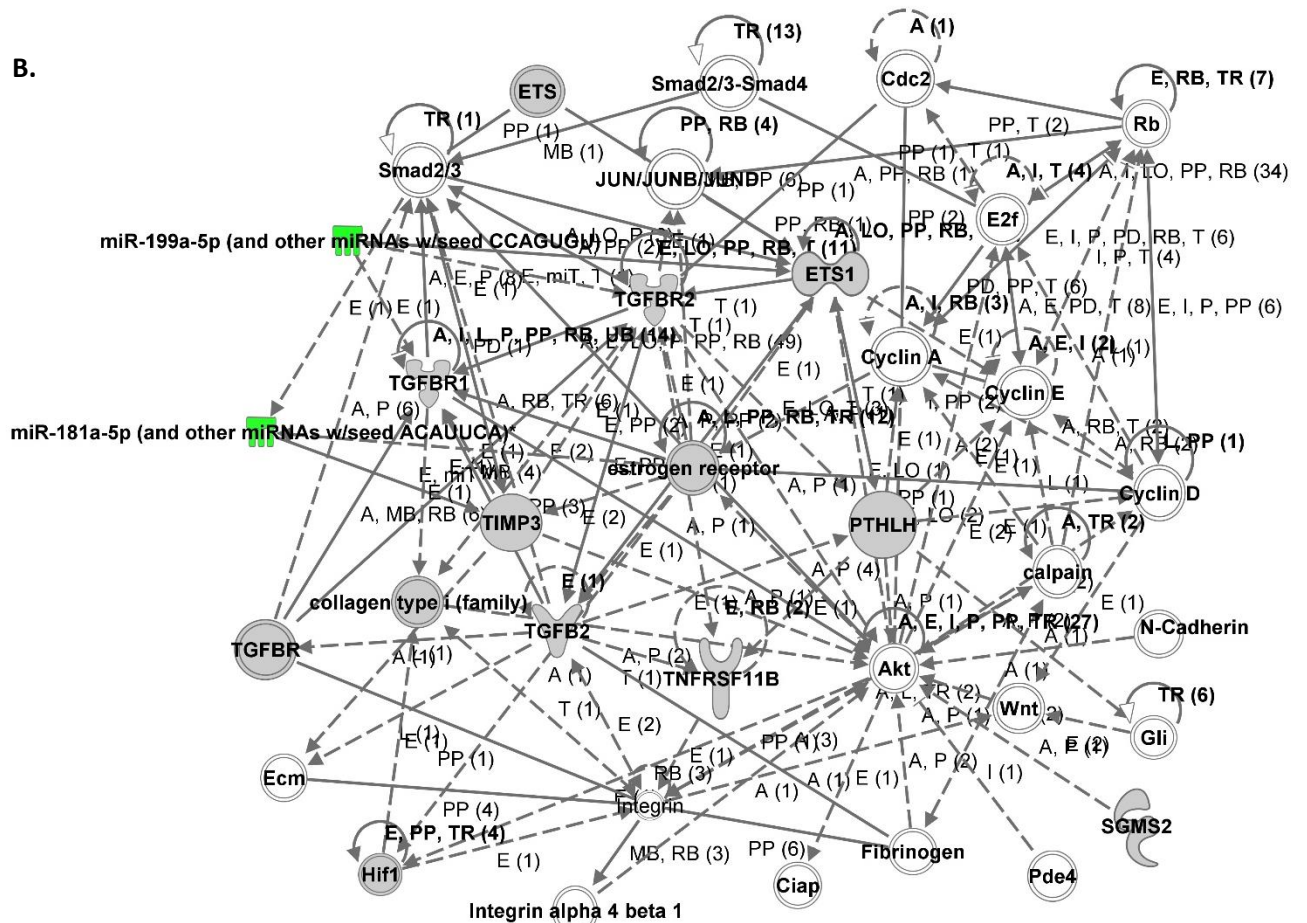


**Figure 4.9** (*preceding page*) **Top scoring networks reflecting dysregulated miRNA:target interactions common to human and equine tendinopathy are associated with the terms: A.** Tissue development, connective tissue disorders, organismal injuries and abnormalities (score 34, 15 focus molecules) and **B.** Tissue development, organismal injury and abnormalities, cancer (score 20, 10 focus molecules). Green indicates miRNA expression reduced in tendinopathy, intensity of colour reflects magnitude of reduction. Grey indicates relationship effect not predicted.

### **Chronic inflammation is regulated by miRNAs in both human and equine tendinopathy**

Inflammatory disease and response was identified as significant by core analysis of predicted target genes regulated by DE miRNAs in our human tendinopathy dataset (Table 4.3). This was not, however, replicated by core analysis of genes targeted by miRs -29a, -181 and -199a common to both human and equine tendinopathy. We therefore revisited the full dataset of human DE miRNAs and interrogated it using the term 'chronic inflammatory disorder'. This resulted in identification of 21 miRNAs associated with this process, which contained the three focus miRNAs common to human and equine tendinopathic samples (Figure 4.10 (A)). Further, we then interrogated our core analysis of predicted targets for these miRNAs using the same term, which confirmed all three miRNAs and 22 of the 48 predicted target genes associated with chronic inflammation (Figure 4.10 (B)).

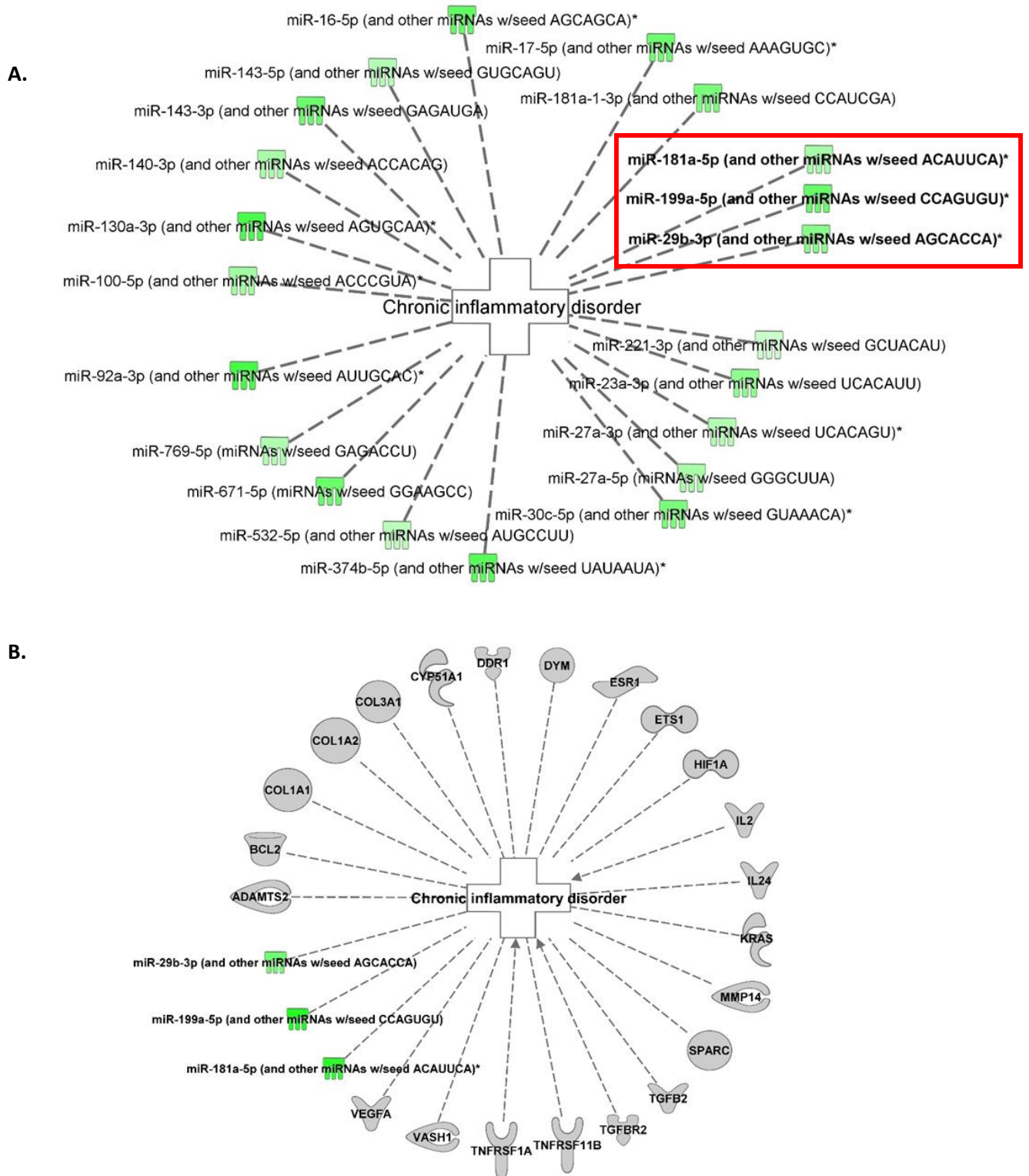


**Figure 4.10 Ingenuity Pathway Analysis indicated miRNA dysregulation in both human and equine tendinopathy is associated with chronic inflammation. A.** miRNAs identified from DE human miRNA dataset in SSP tendinopathy, showing significantly reduced expression associated with chronic inflammation; miRNAs contained within red box were also identified as significantly reduced in diseased equine SDFT. **B.** Predicted targets of miRNAs significantly reduced in both equine SDFT and human SSP tendinopathy associated with chronic inflammation. Green indicates miRNA expression reduced in tendinopathy, intensity of colour reflects magnitude of reduction. Grey indicates relationship effect not predicted.

Functional enrichment of the target genes identified was then investigated using the ToppFun function of the ToppGene Suite software (Chen et al 2009, <http://toppgene.cchmc.org>). The HGNC gene identifier symbols for all 48 target genes were uploaded and functional enrichment analysis run using the calculation function with FDR correction and *P*-value cut off set to 0.05, for the feature 'GO: Biological Process'. Top ten gene ontology (GO) terms ranked in terms of number of molecules in target list and level of statistical significance achieved are listed in Table 4.7.

Gene Ontology		<i>P</i> -value	q-value FDR BH	Hit Count in Query List
ID	Term			
<b>Ranked by number of associated target molecules</b>				
GO:0035295	Tube development	3.86E-19	3.01E-16	26
GO:0051241	Negative regulation of multicellular organismal process	3.97E-15	1.55E-12	24
GO:0009887	Animal organ morphogenesis	8.14E-16	5.08E-13	23
GO:0072359	Circulatory system development	3.24E-15	1.45E-12	23
GO:0016477	Cell migration	1.35E-12	2.64E-10	23
GO:0051674	Localization of cell	9.71E-12	1.26E-09	23
GO:0048870	Cell motility	9.71E-12	1.26E-09	23
GO:0051094	Positive regulation of developmental process	2.95E-12	4.99E-10	22
GO:0030198	Extracellular matrix organization	1.38E-23	4.31E-20	21
GO:0043062	Extracellular structure organization	2.33E-21	3.63E-18	21
<b>Ranked by q-value for FDR</b>				
GO:0030198	Extracellular matrix organization	1.38E-23	4.31E-20	21
GO:0043062	Extracellular structure organization	2.33E-21	3.63E-18	21
GO:0001501	Skeletal system development	3.57E-20	3.71E-17	21
GO:0035295	Tube development	3.86E-19	3.01E-16	26
GO:0009887	Animal organ morphogenesis	8.14E-16	5.08E-13	23
GO:0009611	Response to wounding	2.71E-15	1.41E-12	19
GO:0072359	Circulatory system development	3.24E-15	1.45E-12	23
GO:0051241	Negative regulation of multicellular organismal process	3.97E-15	1.55E-12	24
GO:0035239	Tube morphogenesis	4.95E-15	1.72E-12	21
GO:0001568	Blood vessel development	3.26E-13	1.02E-10	18

**Table 4.7 Biological processes (as described by gene ontology (GO) terms) associated principally with control of cellular recruitment, tissue development and extracellular matrix organisation are enriched in the mRNA population targeted by miR-29a-3p, miR-181a-5p and miR-199a-5p, which show reduced expression in both human and equine tendinopathy.** Target gene identification and functional enrichment analysis performed using IPA microRNA Target Filter ([www.qiagenbioinformatics.com/products/ingenuity-pathway-analysis](http://www.qiagenbioinformatics.com/products/ingenuity-pathway-analysis)) and Toppgene Suite (toppgene.cchmc.org) respectively. Highlighted terms are common to rankings by both hit count and q-value. FDR BH = False Discovery Rate derived using Benjamini Hochberg correction.

## **4.4 Discussion**

Alterations in extracellular matrix composition and organisation are known to be important precursors and consequences of clinical tendinopathy (Archambault et al 2007, Corps et al 2006, Jelinsky et al 2011, Magnusson et al 2002). In this chapter, we have identified enhancement of cellular proliferation and inhibition of cellular degeneration as fundamental processes influenced by altered miRNA expression in human SSP tendinopathy. Additionally, the three miRNAs we validated as showing reduced expression in both human SSP and equine SDFT tendinopathy (miR-29a-3p, miR-181a-5p and miR-199a-5p), recapitulated regulation of cell differentiation, proliferation and fate, as well as inflammation, as important mechanisms common to both species.

The appearance of terms associated with neoplastic disease (tumour microenvironment, cancer and pancreatic adenocarcinoma; Tables 4.3 and 4.6) in IPA output may seem surprising. However, this reflects overrepresentation of experimental data, generated from this research field, incorporated into the Ingenuity Knowledge Base resource. Nevertheless, neoplastic transformation is consistent with modified control of apoptosis and cell cycle regulation, and increased cellular proliferation. In accordance with this, core analyses run on both miRNA data sets returned top biological functions associated with cellular movement, development, growth and proliferation and viability (Figures 4.2 and 4.3, Tables 4.2 and 4.4). Similarly, the term hepatic fibrosis (Tables 4.3 and 4.6) was interpreted as representative of general fibrotic disease processes. Despite filtering all DE miRNAs from the human tendinopathy dataset for the terms connective tissue disorders and fibroblasts, the absence of predicted activation or inhibition of connective tissue disorders reported in Figure 4.2 and Table 4.2, likewise reflects the lack of published, validated evidence, or low confidence of computationally predicted interactions of these miRNAs in regulating connective tissue disorders. Thus interpretation of the IPA output must be undertaken with caution and an understanding of the limitations inherent in the database from which the output is derived.

The dataset of DE human miRNAs derived from RNA-seq implicated processes associated with neurodegenerative disease, whilst analysis of those miRNAs also DE in equine SDFT tendinopathy, implied musculoskeletal and connective tissue associations. Both, however, identified TGF $\beta$ /SMAD and mitogen-activated protein kinase/extracellular-signal-regulated kinase (MAPK/ERK) signalling as being relevant, within the top scoring networks, and as significant upstream regulators (Figures 4.5 and 4.7). Both datasets additionally suggest a transition of fibroblasts to a more cartilaginous phenotype as part of the response to injury. Reduced expression of miRs -23a-3p, -30c-5p, -34a-5p and -205-5p is associated with increased activation of chondrocyte maturation (Figure 4.4 (B)). Additionally, HOXA11 and WNT5B, both identified in the top network containing miRs -29a, -181 and -199a (Figure 4.7), regulate chondrocyte proliferation and differentiation (Gross et al 2012, Yang et al 2003).

TGF $\beta$  signalling is important in immunity, inflammation, fibrosis and neoplastic disease (Massagué 2012), mediating cellular proliferation, differentiation, apoptosis and migration (Hu et al 2018). At the cellular level, TGF $\beta$  family members regulate cell growth, differentiation, adhesion, migration and death, in a strongly developmental, context-dependent and cell type-specific manner. These multifunctional cytokines are able to inhibit cell proliferation whilst promoting cell growth and enhancing stem cell pluripotency, as well as also driving differentiation (Massagué 2012, Morikawa

et al 2016). Canonical TGF $\beta$  signalling occurs via the activation (phosphorylation) of SMAD transcription factors, which act to integrate regulatory inputs, and are pivotal in the context-dependent modulation of TGF $\beta$  signalling (Massagué 2012). Activated SMAD2 and SMAD3 molecules form heterotrimeric oligomers with SMAD4, and are imported into the nucleus where they function to control transcriptional regulation. The ultimate cellular response is therefore influenced by the intensity of the TGF $\beta$  signal, the interaction of SMAD proteins with other, potentially lineage specific, transcription factors (thus forming complexes with diverse regulatory consequences on transcription), and epigenetic influences (such as DNA methylation, chromatin remodelling and expression of non-coding RNA species) (Massagué 2012). SMAD proteins also participate in non-canonical pathways and are phosphorylated by mitogen-activated protein kinases (MAPKs) subsequent to growth factor expression, cellular stress and cyclin-dependent kinase 4 expression during G1 phase progression in the cell cycle (Massagué 2012).

SMAD 2 and 3, identified in the top scoring miRNA network from our human dataset, are the two major regulators promoting TGF $\beta$ 1 mediated fibrosis. SMAD7 acts as a negative feedback regulator of the pathway, blocking SMAD3 expression (Hu et al 2018), and facilitating polyubiquitylation and hence degradation of TGF $\beta$  receptors (Massagué 2012). Myocardin (MYOCD), identified in our network in Figure 4.7, promotes SMAD3-mediated TGF $\beta$  signalling in mouse fibroblast cells (Tong et al 2020).

Activated SMAD proteins are also known to stimulate maturation of a specific set of miRNAs in human vascular smooth muscle cells, including hsa-miR-199a-5p (Davis et al 2010), which we identified as significant in both our human and equine datasets.

As well as intracellular effects, TGF $\beta$  is secreted in an inactive, complexed form (Rifkin 2005). These latent TGF $\beta$  binding protein (LTBP) complexes interact with a number of matrix components including collagen, fibronectin and fibrillin-1. This targets TGF $\beta$  to regions of the ECM, but LTBP-ECM binding also controls activation. Therefore, disruption to ECM protein composition during tendinopathy may disrupted growth factor activation and signalling (Rifkin 2005).

MAPK signalling pathways are highly evolutionarily conserved, key signalling pathways consisting of a cascade of three sequentially activated kinases. Three MAPK families have been characterised, extracellular-signal-regulated kinases (ERKs), Jun amino-terminal kinases (JNKs) and stress-activated protein kinases (p38/SAPKs) (Zhang and Liu 2002). Identified as components of the top scoring network from our human miRNA dataset, MAP2K1/2 and ERK1/2 (Figure 4.5) act as intermediate (MAP2K1/2) and terminal (ERK1/2) elements of the ERK cascade. This 'module' responds primarily to growth factors and mitogens, to induce cell growth, differentiation, adhesion and survival (Morrison 2012). Additionally, the MAPK/ERK cascade promotes apoptosis and regulates lysosomal dynamics (Toy-Miou-Leong et al 2004).

Applying filters for musculoskeletal and connective tissue disorders and fibroblast cell type will fundamentally skew the output for predicted target molecules and therefore the processes and networks identified as being impacted. Consequently, terms associated with fibrotic, connective tissue and musculoskeletal diseases, and networks and pathways incorporating proteins involved in ECM deposition, organisation and turnover are to be expected, and were indeed evident (Tables 4.3 and 4.6, Figures 4.6 and 4.9). However, terms associated with cellular proliferation, recruitment, signalling and viability, as well as inflammation remained prominent (Tables 4.3 and 4.6). It therefore

seems that clinical tendinopathy engenders a state favouring an increase in cell population and protective against cellular degeneration.

In refining our investigation to include only those miRNAs validated by RT-qPCR that showed DE in both human and equine tendinopathy, we focussed on miR-29a-3p, miR-199a-5p and miR-181. Mature sequences for hsa-miR-29a-3p and eca-miR-29a are identical, as are mature sequences for hsa-miR-199a-5p and eca-miR-199a-5p (Table 4.1), facilitating direct comparison. For miR-181, the situation is more complex. Family members miR-181c and miR-181d (both showing significantly reduced expression in human tendinopathy) are not recognised in the equine species. However, miR-181b, whilst not DE in our human samples, was significantly reduced in our equine tendinopathic cohort. Additionally, miR-181b sequences are identical between human and equine species and hsa-miR-181d-5p differs from hsa-miR-181b-5p (and, therefore, also eca-miR-181b) by only a single nucleotide (Table 4.1).

IPA microRNA Target Filter clusters miRNAs according to the seed sequence of the mature miRNA. For instance, hsa-miR-29a-3p, hsa-miR-29b-3p and hsa-miR-29c-3p all share the seed sequence UAGCACCA and are all represented by hsa-miR-29b-3p in the IPA output (Figures 4.3, 4.5, 4.7 and 4.10). hsa-miR-199a-5p and hsa-miR-199b-5p share the seed sequence CCCAGUGU, so although identified as hsa-miR-199a-5p in the output (Figures 4.7 and 4.10), this also represents hsa-miR-199b-5p.

As all four hsa-miR-181-5p variants, and both eca-miR-181 family members, share a common seed sequence (Table 4.1) indicating they share similar targets, and, as the IPA software clusters mature miRNAs sharing the same seed sequences for target prediction purposes, incorporating one miR-181-5p variant into IPA analysis will capture targets predicted for 5p variants of all four human and both equine family members. Seed sequences differ between all four 3p variants of hsa-miR-181, however, precluding extension of this assumption to these variants (Table 4.1). Although miR-181a-3p and miR-181c-3p were significantly DE in human tendinopathy, corresponding equine variants of these sequences are not recognised. Consequently, 3p variants were not included in IPA Core and Target Filter analyses.

miR-29a is known to be reduced in human SSP tendinopathy (Millar et al 2015), to directly target *COL1A1* and *COL3A1* transcripts (Maurer et al 2010) and, by regulating the effect of IL33, play a key role in the transition from type I to type III collagen deposition in early tendinopathy (Millar et al 2015). miR-199a expression is up regulated in fibrotic diseases (Lino Cardenas et al 2013), whilst downregulation, as we observed in both equine and human tendinopathic samples, is observed in hypoxia, secondary to ischaemia, and associated with impaired collagen production and crosslink formation (Rane et al 2009).

Whilst there is little information on the direct relationship between miR-181 and tendon disease, this miRNA has a pervasive influence on biological processes. Reduced expression of miR-181, as we observed with tendinopathic samples, is reported in a wide range of neoplastic diseases, associated with increased cellular proliferation, migration and neoplastic transformation, and inhibited apoptosis (Pop-Bica et al 2018, Rezaei et al 2019). Treatment of mouse embryonic fibroblasts (3T3-L1 pre-adipocytes) with miR-181a-5p mimic promoted adipogenesis, and inhibited proliferation by inducing cell cycle arrest in G1 phase (Ouyang et al 2016). These authors demonstrated that miR-181a-5p directly targets SMAD7. Reduced levels of inhibitory SMAD7

increased phosphorylation of SMAD3, enhanced TGF $\beta$  signalling, resulting in cell cycle arrest. Wang and co-workers (2015) showed miR-181b directly targets TGF $\beta$ R1 and caused cell cycle arrest in G1 phase. Upregulation of miR-181b, however, reduced activation of SMAD3 in non small cell lung cancer cell lines (Wang et al 2015). Although TGF $\beta$ R1 was identified as a target by the IPA microRNA Target Filter software in our analysis, it was predicted to be a target of miR-29a-3p, not miR-181 (Appendix 4, Table A4.2).

The role of inflammation in tendinopathy is controversial, but it has been shown to be important in early human rotator cuff tendinopathy (Millar et al 2010, Mosca et al 2018). Additionally, failure of resolution of an early inflammatory response is an important driver of chronic human Achilles and equine tendinopathy (Dakin et al 2014, Dakin et al 2018). Core Analysis of the human miRNA-target gene dataset identified the pro-inflammatory cytokines IL1 $\beta$  and TNF as significant upstream regulators. Network analysis of the genes targeted by the three miRNAs DE in both human and equine tendinopathy additionally identified inflammation-associated molecules. DUSP2, a mitogen and stress induced phosphatase located in the cell nucleus, interacts with MAPK signalling pathways and regulates T-cell differentiation, activation, and expression of IL6, IL17, TNF and IL1 $\beta$  (Lu et al 2015). SFTPA1 acts through the Toll-like receptor 4 (TLR4) signalling pathway. Inflammatory responses are regulated by miR-181 in osteoarthritis through the NF $\kappa$ B pathway (Zhu and Yang 2019) and in human fibroblasts via Toll-like receptor signalling pathway (Galicja et al 2014).

Regulation of MAPK signalling by miR-181 also impacts on the competency of apoptotic and autophagic processes, with miR-181a implicated in deficiency of these processes, by this mechanism, in the neurodegenerative condition Parkinson's Disease (Liu et al 2017). Of the three miRNAs demonstrating reduced expression in both human and equine tendinopathy, miR-181a-5p was the only one associated with cell viability (Figure 4.8). Age-associated downregulation of miR-181a in murine myocytes is associated with defective mitochondrial biogenesis and function (Goljanek-Whysall et al 2020). The inclusion of hydrogen peroxide in our top network of miRNAs from both human and equine tendinopathy (Figure 4.7) alludes to the relevance of oxidative stress, a consequence of mitochondrial dysfunction, in tendinopathy.

We have shown that tendinopathy engenders a physiological milieu promoting cellular proliferation and differentiation, whilst inhibiting necrotic and apoptotic pathways. These changes appear to be consistent in both human and equine species, and occur concurrently with chronic inflammation.

With miR-181 reported to regulate so many of the biological processes considered to be relevant in the development of tendinopathy, and our data showing that miR-181 expression was reduced in both human and equine tendinopathy, we were interested to further explore the ramifications of altered miR-181 levels in tenocytes. We hypothesised that the role of miR-181 in multiple biological processes such as inflammation, autophagy and mitochondrial dynamics indicate it may have an important influence in tendinopathy, by regulating these processes. In the next chapter, we utilise gain and loss of function of miR-181a-5p to determine how this impacts on expression of genes relevant to inflammation, autophagy, TGF $\beta$  signalling, mitochondrial function and oxidative stress.

## **Chapter 5 - miR-181 function in equine tenocytes - monolayer cell culture**

### **5.1 Introduction**

The reduction in miR-181 expression in both human and equine clinical tendinopathy identified in Chapter 3 suggests this family of miRNAs are important regulators of pertinent biochemical functions in tendon across species.

The miR-181 family consists of four highly conserved members, miR-181a, b, c and d. In humans, miR-181a and b are clustered together at two distinct genomic loci, on chromosomes 1 and 9, with miR-181c and d clustered together on chromosome 19. In the horse, miR-181a and b cluster together on chromosome 25, with miR-181a also mapping to a second locus on chromosome 30 (Table 5.1). Family members miR-181c and miR-181d are not described in this species (miRBase release 22.1, Kozomara et al 2019).

<b>Identity</b>	<b>Accession number</b>	<b>Chromosome</b>	<b>Start</b>	<b>End</b>
<b>Human</b>				
hsa-miR-181a-1	MI0000289	1	198859044	198859153
hsa-miR-181a-2	MI0000269	9	124692442	124692551
hsa-miR-181b-1	MI0000270	1	198858873	198858982
hsa-miR-181b-2	MI0000683	9	124693710	124693798
hsa-miR-181c	MI0000271	19	13874699	13874808
hsa-miR-181d	MI0003139	19	13874875	13875011
<b>Equine</b>				
eca-miR-181a	MI0012920	25	28672622	28672731
eca-miR-181a-2	MI0012936	30	26398918	26399027
eca-miR-181b	MI0012921	25	28673901	28673989

**Table 5.1 Identity and genomic location of human and equine miR-181 family members.** Details from miRBase release 22.1 (Kozomara et al 2019). hsa = *Homo sapiens*, eca= *Equus caballus*.

TargetScan (release 7.2, 2018, Agarwal et al 2015, www.targetscan.org) lists 1371 putative human transcripts as miR-181 targets, conferring the ability of this family to affect multiple pathways

concurrently. It is also one of the most abundant miRNAs carried in human plasma exosomes (Huang et al 2013). Unsurprisingly, considering these factors, miR-181 has been associated with a diverse and often contradictory range of effects. Whilst divergent effects may be expected in different tissues, they have also been reported within the same cell type. Both pro- and anti-oncogenic roles are reported (Yang et al 2017), as well as protective and detrimental effects on myocardial function (Das et al 2017). Yang and co-workers (2017) report a reduction in cell viability with increasing miR-181a expression up to a concentration of 50 nM. Above this, the reverse effect is observed, with promotion of cell growth. In myocardiocytes, differences in subcellular compartmentalisation of different miR-181 family members is attributed to the conflicting phenotypes observed (Das et al 2017). Participation in both feedforward and feedback regulatory loops adds another level of complexity to their function (Tsang et al 2007, Ye et al 2018).

miR-181 is known to be associated with mitochondrial biogenesis and function (Indrieri et al 2019, Goljanek-Whysall et al 2020), autophagy (Liu et al 2017), fibrosis (Chen et al 2018) and inflammation (Xie et al 2013), all processes implicated in the pathogenesis of tendinopathy. An association between miR-181 dysregulation and tendinopathy has not, however, previously been reported.

We performed gain and loss of function studies to assess the impact of miR-181 dysregulation on tenocyte function in equine tenocyte monolayer culture, to assess its potential role in tendinopathy. Intracellular delivery of Cy5-labelled miR-181a mimic and FITC-labelled antagomiR reagents was confirmed visually by fluorescence microscopy and quantitatively by RT-qPCR. Transcript levels of miR-181 validated targets relevant to the pathways above (sirtuin 1 (*SIRT1*), ubiquitin-binding protein p62 (*P62/SQSTM1*), Parkin (*PARK2*), protein deglycase DJ-1 (*PARK7/DJ-1*), cytochrome c oxidase I (*COXI*), interleukin 1 alpha (*IL1 $\alpha$* ), peroxiredoxin 3 (*PRDX3*) and tumour necrosis factor (*TNF*)), were determined by RT-qPCR.

SIRT1 has protective effects against hypoxia, inflammation, cellular senescence and apoptosis (Rahman and Islam 2011). Tendon stem cells constitutively express SIRT1, and up- or down-regulation is associated with altered differentiation into osteogenic or adipogenic lineages (Liu et al 2016). Cellular stress upregulates mitophagy to remove dysfunctional mitochondria and preserve cellular energy metabolism. Disruption of this process results in accumulation of key autophagy related proteins Parkin (product of the *PARK2* gene) and P62/SQSTM1, precipitating cellular degeneration (Goljanek-Whysall et al 2020). Cytochrome c oxidase (COX) is the terminal enzyme in the energy transducing respiratory chain. Complexes I, II and III of this 13 subunit structure are encoded by the mitochondrial genome and are the site of reactive oxygen species production. COXI is involved in formation of the transmembrane proton gradient and is one of the main sites of reactive oxygen species production (Lenaz et al 2006). DJ-1 protein is sensitive to oxidative stress and co-localises with COXI, itself becoming oxidised and stabilising mitochondrial membrane potential (Hayashi et al 2009). Expression of *PRDX3* and peroxiredoxin 5 (*PRDX5*) is restricted to mitochondria. Human tenocytes constitutively express *PRDX5* and expression is up regulated in tendinopathy, supporting the role of oxidative stress in this disease (Wang et al 2001). We investigated expression of *PRDX3* which is crucial for mitochondrial homeostasis in skeletal muscle (Lee et al 2014). Evidence supports an inflammatory component to tendinopathy (Millar et al 2010) and IL1 $\alpha$  and TNF are among the most frequently studied cytokines in this area (Morita et al 2017). Both IL1 $\alpha$  and TNF are suggested to be up regulated in early disease, although clinical and experimental evidence is not consistent (Morita et al 2017).

Additionally, expression of genes interacting with the targets above, or active in the same pathways were investigated. Interestingly, a permissive relationship has been identified between peroxiredoxin 6 (PRDX6) and IL1 and TNF signalling. PRDX6 exhibits dual functions, with both antioxidant and phospholipase A<sub>2</sub> activity (Kim et al 2011). This confers pro-inflammatory and pro-apoptotic effects by upregulating the pro-inflammatory cytokine IL1 $\beta$  and caspase activation. PRDX6 also enhances TNF induced leukotriene production. Therefore, we broadened our targeting of IL1 signalling, including interleukin 1 beta (*IL1 $\beta$* ) and interleukin 1 receptor accessory protein (*IL1RAP*) expression. We also included nuclear factor kappa-light-chain-enhancer of activated B cells (*NF $\kappa$ B*), mothers against decapentaplegic homolog 7 (*SMAD7*) and interleukin 7 (*IL7*). NF $\kappa$ B signalling is linked to inflammation in chronic tendinopathy (Abraham et al 2019) and SMAD7 regulates TGF $\beta$ -driven fibrosis and inflammation (Zhu et al 2011). Fibroblasts subjected to chronic and autoimmune-driven inflammation express IL7 to stimulate proliferation and infiltration of inflammatory cells (Harada et al 1999).

To further explore mitochondrial functionality and dynamics in the context of tendinopathy, cytochrome c oxidase subunit IV (*COXIV*) and translocase of outer mitochondrial membrane 20 (*TOMM20*) expression were investigated. COXIV is encoded by genomic DNA and expression is up regulated in response to HIF1 $\alpha$  released under oxidative stress, protecting mitochondrial function (Hao et al 2018). TOMM20 is an integral part of the import channel for mitochondrial targeted proteins and expression levels can provide an indication of mitochondrial architecture and mass.

We were interested to explore mitochondrial morphology and dynamics in cultured tenocytes and the influence of miR-181 on mitochondrial autophagy. To investigate this, we induced mitochondrial depolarisation using the oxidative phosphorylation uncoupling agent carbonyl cyanide m-chlorophenylhydrazone (CCCP) and determined localisation of TOMM20, microtubule-associated proteins 1A/1B light chain 3B (LC3B), DJ-1, autophagosome adaptor protein P62/SQSTM1 and the E3 ubiquitin ligase Parkin, using immunocytochemistry. TOMM20 staining permits mitochondrial morphology to be visualised, indicating the degree of interconnectivity or fragmentation of these organelles (Tan et al 2019). Mitochondrial fragmentation releases cytochrome c into the cell cytoplasm, recruiting protein DJ-1 to mitigate oxidative damage. Depolarisation of the mitochondrial membrane stabilises phosphatase and tensin homologue-induced putative kinase 1 (PINK1) causing recruitment of Parkin, which mediates polyubiquitination of outer mitochondrial membrane proteins (Palikaras et al 2018). P62/SQSTM1 possesses both ubiquitin and LC3B binding regions, thereby interacting with both the ubiquitinated dysfunctional mitochondria and the autophagosome membrane-associated protein LC3B, initiating autophagosome formation and targeting damaged mitochondria for selective degradation (Sánchez-Martín and Komatsu 2018). P62/SQSTM1 can also interact with the soluble, non-membrane bound form of LC3B, permitting assessment of the autophagosomes compartment functionality in mitochondrial clearance (McCoy and Cookson 2011).

Whilst we found no significant differences in transcript levels between treatment groups of the 16 targets assessed by RT-qPCR, this may indicate that regulation of these genes occurred by altering translation rather than transcript stability. However, intracellular distribution patterns of TOMM20, LC3B, DJ-1, P62/SQSTM1 and Parkin suggested miR-181 has a regulatory effect on mitochondrial dynamics.

## 5.2 Methods

### 5.2.1 Treatment of tenocyte cultures

Primary equine tenocytes from eight donors (Table 5.2) were propagated for 24 hours prior to treatment with cholesterol-conjugated Cy5-tagged mmu-miR-181a-5p mimic, fluorescein-tagged 23 nucleotide (nt) single strand RNA antagomiR, or 21 nt single strand RNA scrambled control sequence. Final treatment concentrations were 100 nM (mimic and scrambled control) and 200 nM (antagomiR). Live cell imaging to confirm uptake of fluorescence was performed using a Nikon Eclipse Ti-E fluorescent microscope.

Sample ID	Sex	Age (years)	Passage number
EqDB5	MN	5	4
EqDB30	MN	3	2
EqDB7	MN	5	2
EqDB9	F	12	4
EqDB10	F	18	3
EqDB11	F	3	2
EqDB12	F	8	3
EqDB18	MN	9	4

**Table 5.2 Donor and tenocyte passage details for equine superficial digital flexor tendon-derived tenocytes cultured for mmu-miR-181a-5p mimic, antagomiR and scrambled control treatment studies.** F = female, MN = male neutered.

### 5.2.2 Reverse transcription quantitative real-time polymerase chain reaction

Forty eight hours after transfection, cells were lysed for RNA extraction and gene expression analysis. Reverse transcription to cDNA used 500 ng RNA template for gene expression and 100 ng RNA template for miRNA expression analyses.

Recapitulating our work in normal and diseased equine superficial digital flexor tendon, and based on previous reports (Sperveslage et al 2014, Bignotti et al 2016), three candidate reference genes, *small nuclear RNA-U6*, *small nucleolar RNA-61 (SNORD61)*, and *small nucleolar RNA-68 (SNORD68)* were investigated for use as internal control. Reinforcing our previous findings (Chapter 3, section 3.2.3 and Appendix 2, Table A2.1), *SNORD61* demonstrated the greatest stability of expression

between treatment groups, with threshold cycle (Ct) values varying by less than four cycles between biological replicates, and less than two across treatment groups (Appendix 5, Table A5.1). Levels of miR-181a, b, c and d were determined using commercially available primers (Qiagen, Manchester, UK) and normalised to *SNORD61* expression. Relative expression values were then summed to give total miR-181 expression for each sample.

Stability of *glyceraldehyde 3-phosphate dehydrogenase (GAPDH)* expression across treatment groups was confirmed, with Ct values varying by less than two cycles between biological replicates, and less than 1.4 across treatment groups (Appendix 5, Table A5.2), justifying its use as internal control for normalisation of target gene expression (Panina et al 2018). Primers were designed for eight validated miR-181 targets (*SIRT1*, *P62/SQSTM1*, *PARK2/Parkin*, *PARK7/DJ-1*, *COXI*, *IL1 $\alpha$* , *PRDX3* and *TNF*) and a further eight genes associated with oxidative stress (*PRDX6*), apoptotic (*COXIV*, *IL7*, *TOMM20*) and inflammatory (*IL1 $\beta$* , *IL1RAP*, *NF $\kappa$ B*, *SMAD7*) pathways. Target gene expression was calculated relative to that of *GAPDH*.

Primer sequences and RT-qPCR details are given in Chapter 2, section 2.12.1, Tables 2.11, 2.12 and 2.13, and section 2.12.3, Figure 2.3 respectively. For all RT-qPCR data, technical replicates were run in triplicate and expression relative to *SNORD61* or *GAPDH* calculated using the delta Ct method (Livak and Schmittgen 2001). For graphical representation, transcript expression was normalised to that of the scrambled control treatment group.

### 5.2.3 Induction of mitophagy and immunocytochemistry

For immunocytochemistry, tenocytes were exposed to the oxidative phosphorylation uncoupling agent carbonyl cyanide m-chlorophenylhydrazone (CCCP) at a concentration of 20  $\mu$ M, dissolved in dimethyl sulfoxide (DMSO), or DMSO alone, for six hours, 24 hours after mimic, antagomiR or scrambled control treatment. Tenocytes were then fixed in ice cold methanol and immunostained for autophagy markers as described in Chapter 2, section 2.7. Mounted preparations were produced in triplicate and preparations examined for overall cellular distribution and quality and consistency of staining. Images were obtained using a Zeiss Axio Imager M2 fluorescent microscope with Zeiss ZEN Imaging software (blue edition 3.1). Images showing consistent patterns of fluorescence, representative of all sections from each treatment group were selected for detailed description of protein localisation in response to treatments.

### 5.2.4 Statistical analysis

Statistical analysis of gene expression was performed using GraphPad Prism version 5.01 for Windows (GraphPad Software, San Diego California USA, [www.graphpad.com](http://www.graphpad.com)). Data were analysed non-parametrically using the Kruskal Wallis test with Dunn's test for pairwise comparisons, to include mimic, antagomiR and scrambled control sequence treated groups. Comparisons between scrambled control sequence treated and untreated groups, where performed, utilised the Mann-Whitney test and are presented in Appendix 5, Figure A5.1. Significance was assumed if  $P < 0.05$ .

Immunocytochemistry results are reported qualitatively.

## **5.3 Results**

### **5.3.1 Validation of miR-181a-5p overexpression and inhibition in tenocytes**

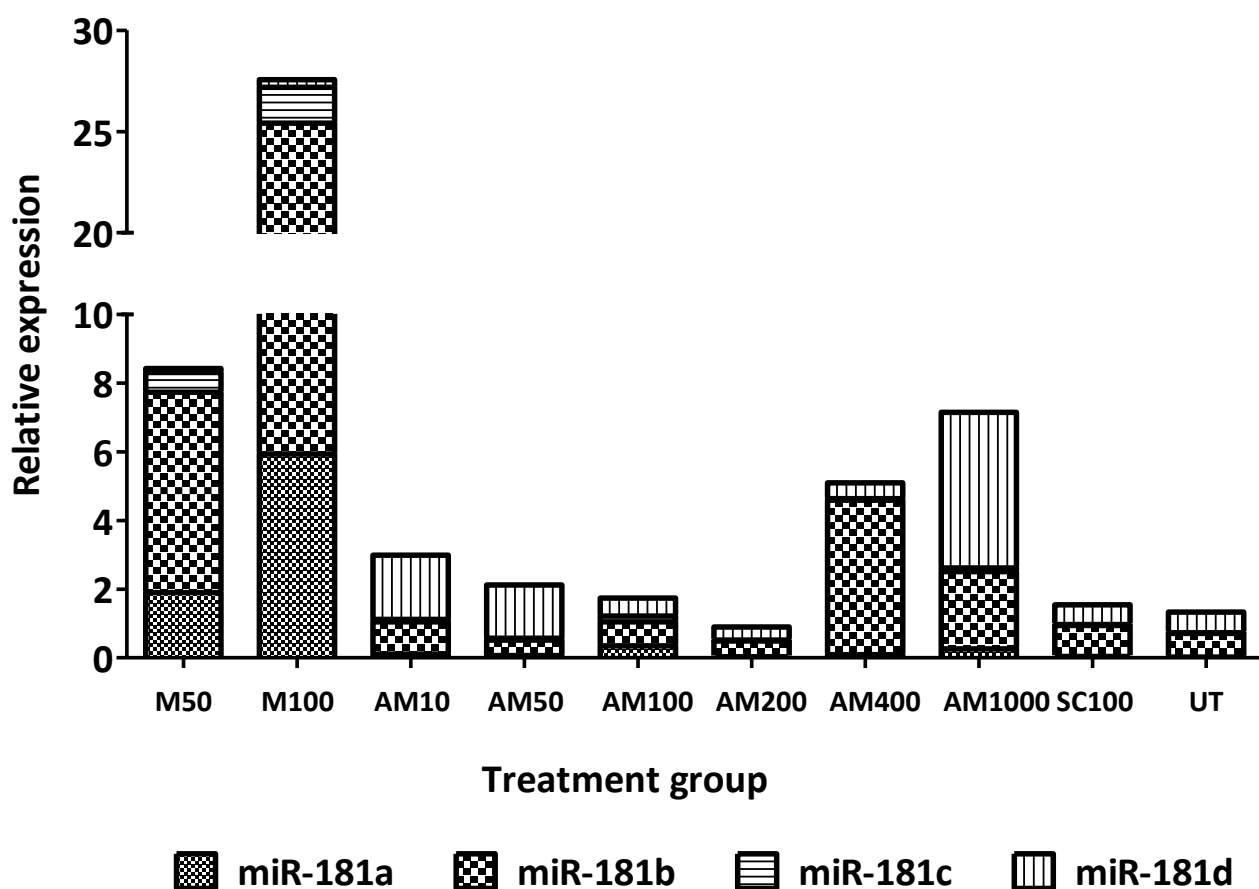
Sequence homology for microRNA-181 family members across murine, equine and human species was confirmed, justifying use of transfection reagents based on murine sequences and human sequence-directed primers (Table 5.3). Sequences for equine variants of miR-181c or miR-181d, however, are not reported (miRBase release 22.1, Kozomara et al 2019).

We first established optimal final working concentrations for our intended treatments. Based on previous work in myoblasts by our group (Soriano-Arroquia et al 2016), tenocyte cultures were incubated for 48 hours with concentrations of 50 and 100 nM mmu-miR-181a-5p mimic, 10, 50, 100, 200, 400 nM and 1  $\mu$ M antagomiR and 100 nM scrambled control oligonucleotide. Total miR-181 expression was then determined using RT-qPCR. Results indicated that concentrations of 100 nM for mimic and scrambled control oligonucleotide, and 200 nM for antagomiR were suitable (Figure 5.1). The apparent increase in total miR-181 expression detected with the 400 nM and 1  $\mu$ M antagomiR treatments was interesting. This could reflect high levels of the antagomiR activating a feedback mechanism, stimulating miR-181 expression, or be artefactual, resulting from the specific formulation of this treatment, or interaction between antagomiR oligonucleotides at high concentrations.

miRNA Identity	Sequence																						
mmu-miR-181a-5p	a	a	c	a	u	u	c	a	a	c	g	c	u	g	u	c	g	g	u	g	a	g	u
eca-miR-181a	a	a	c	a	u	u	c	a	a	c	g	c	u	g	u	c	g	g	u	g	a	g	u
hsa-miR-181a-5p	a	a	c	a	u	u	c	a	a	c	g	c	u	g	u	c	g	g	u	g	a	g	u
mmu-miR-181b-5p	a	a	c	a	u	u	c	a	u	u	g	c	u	g	u	c	g	g	u	g	g	g	u
eca-miR-181b	a	a	c	a	u	u	c	a	u	u	g	c	u	g	u	c	g	g	u	g	g	g	u
hsa-miR-181b-5p	a	a	c	a	u	u	c	a	u	u	g	c	u	g	u	c	g	g	u	g	g	g	u
mmu-miR-181c-5p	a	a	c	a	u	u	c	a	a	c	c	u	g	u	c	g	g	u	g	a	g	u	
hsa-miR-181c-5p	a	a	c	a	u	u	c	a	a	c	c	u	g	u	c	g	g	u	g	a	g	u	
mmu-miR-181d-5p	a	a	c	a	u	u	c	a	u	u	g	u	u	g	u	c	g	g	u	g	g	g	u
hsa-miR-181d-5p	a	a	c	a	u	u	c	a	u	u	g	u	u	g	u	c	g	g	u	g	g	g	u

**Table 5.3 miR-181a and b show complete homology between murine (mmu), equine (eca) and human (hsa) species.** miR-181c and -d are conserved between murine and human species, equine variants of these are not reported. Sequences were obtained from miRBase (release 22.1). Seed sequence shown in red.

## Total miR-181 expression



	Mimic		AntagomiR						Scrambled 100 nM	Untreated
	50 nM	100 nM	10 nM	50 nM	100 nM	200 nM	400 nM	1 $\mu$ M		
<b>181a</b>	1.90	5.94	0.11	0.07	0.35	0.03	0.09	0.26	0.04	0.02
<b>181b</b>	5.84	19.48	0.94	0.45	0.70	0.46	4.50	2.25	0.90	0.69
<b>181c</b>	0.57	1.77	0.07	0.05	0.17	0.03	0.05	0.11	0.03	0.02
<b>181d</b>	0.12	0.37	1.87	1.55	0.52	0.38	0.46	4.53	0.58	0.60
<b>Total</b>	<b>8.43</b>	<b>27.55</b>	<b>2.99</b>	<b>2.13</b>	<b>1.74</b>	<b>0.89</b>	<b>5.09</b>	<b>7.15</b>	<b>1.56</b>	<b>1.33</b>

**Figure 5.1 mmu-miR-181a-5p mimic and antagomiR successfully increase and suppress miR-181 expression in equine tenocytes.** Values represent relative expression, normalised to *SNORD61*, for all four miR-181 family members and total miR-181. In graphical representation, M = miR-181a-5p mimic, AM = antagomiR, SC = scrambled control, UT = untreated control. Number following treatment group identifier indicates concentration (nM) of respective treatment. Relative expression values are given in the table below graph.

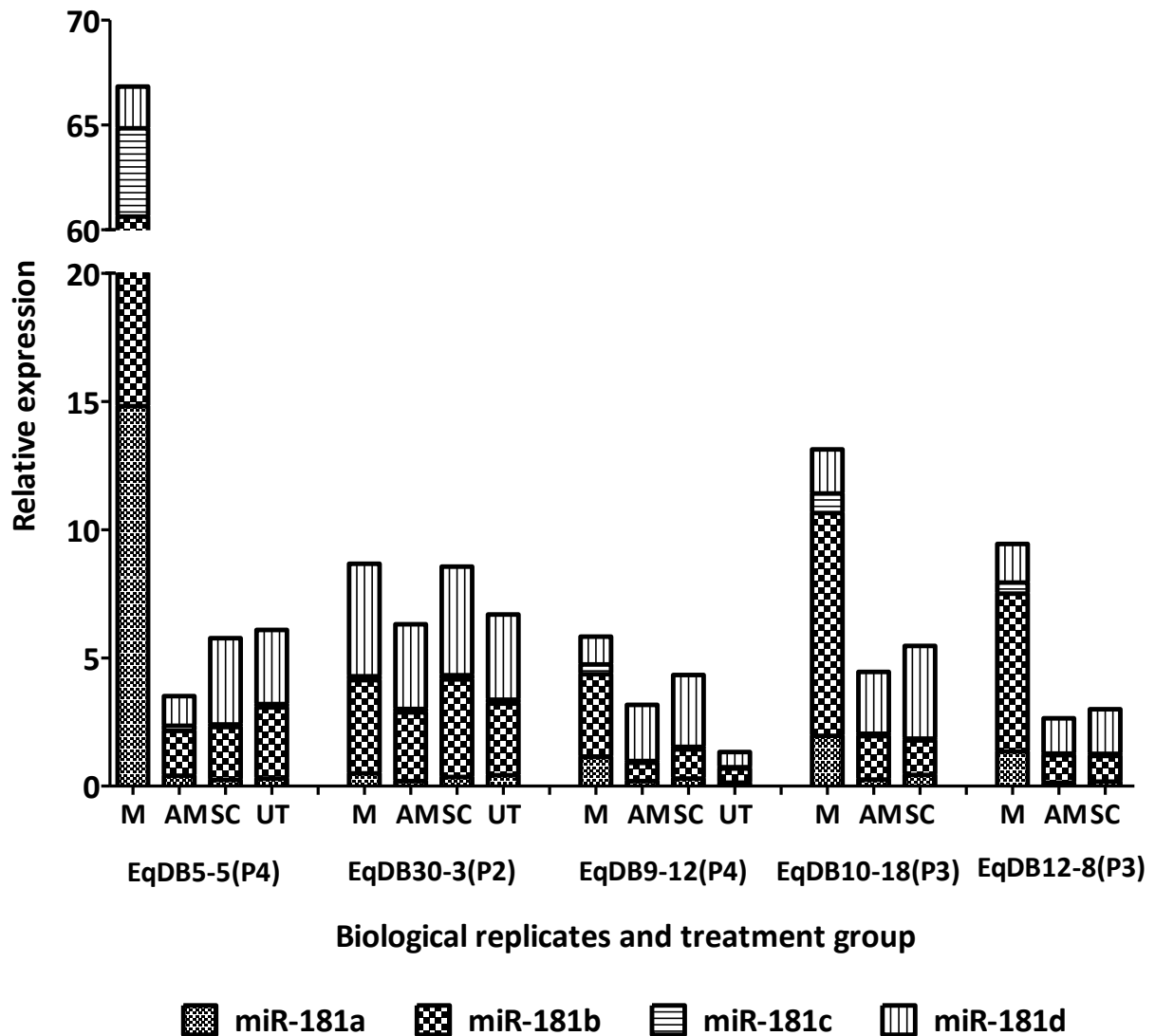
### 5.3.2 miR-181a predicted target gene analysis

We next investigated the expression of miR-181 target genes in response to miR-181a gain or loss of function. Equine primary tenocytes from eight donors (Table 5.2) were treated with mmu-miR-181a-5p mimic, antagomiR or scrambled control sequence oligonucleotides, RNA isolated and RT-qPCR performed.

Based on RT-qPCR evaluation, the success of treatment was variable. All miR-181a mimic treated cultures showed upregulation of total miR-181. Typically, of the four miR-181 family members, miR-181b showed greatest increase, being responsible for 42-69% of the total miR-181 expression in this treatment group. Response to antagomiR treatment was more subtle and varied. In antagomiR treated cultures from five donors, total miR-181 expression were lower than that exhibited by the scrambled control treated group (Figure 5.2).

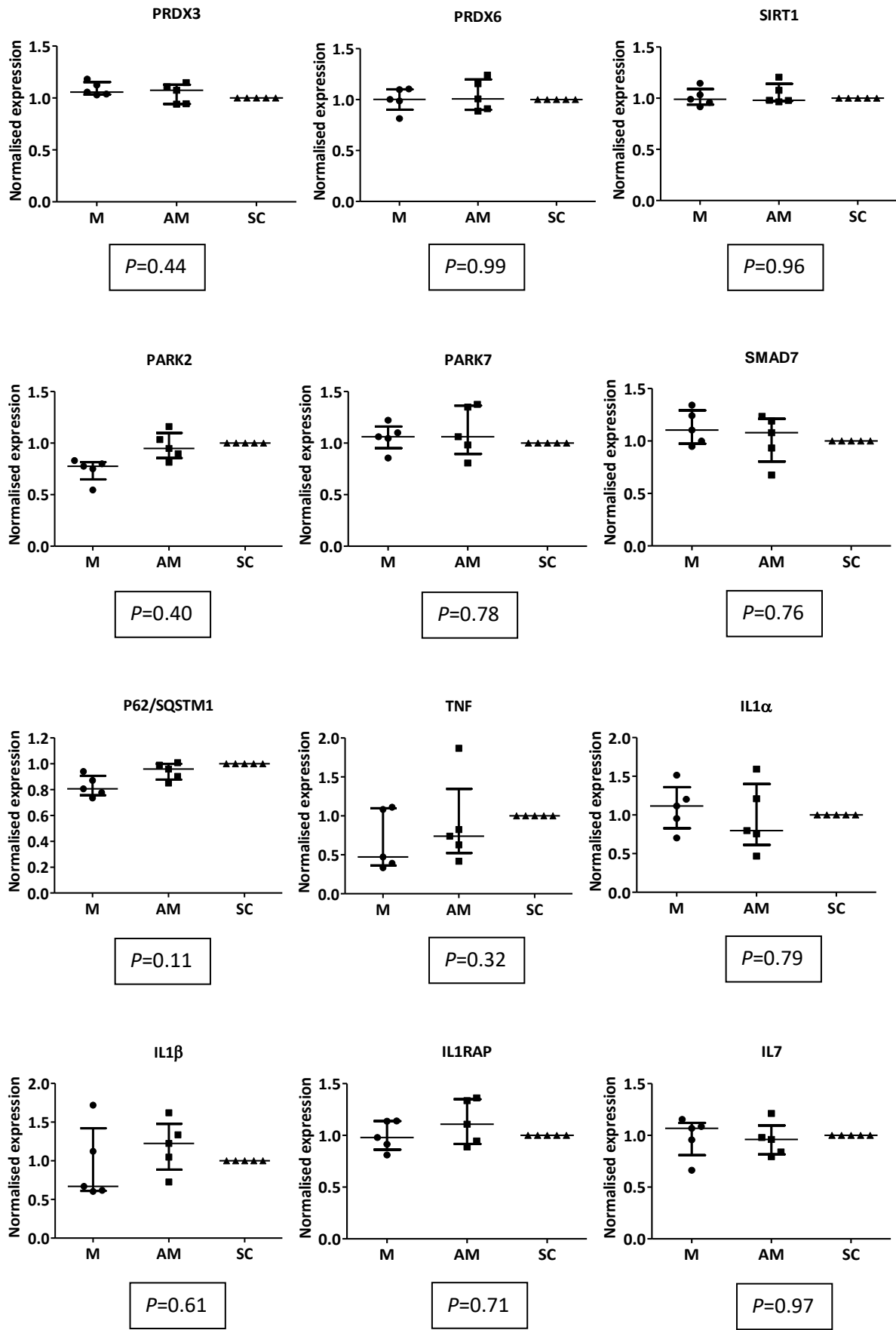
Target gene expression was only investigated in the five biological replicates in which total miR-181 expression was lower in the antagomiR treated group than the scrambled control treated group. Results represent comparisons between mimic, antagomiR and scrambled control sequence treated groups. Comparisons between scrambled control sequence treated and untreated cultures, when performed, are presented in Appendix 5, Figure A5.1. None of the 16 targets examined showed significantly different expression between treatment groups. Normalising transcript expression to that of the scrambled control group showed the greatest variation in response to gain or loss of miR-181 function was demonstrated by *P62/SQSTM1* and *PARK2* (Figure 5.3). In addition to transcript expression, quantification of protein product by Western blot analysis would have strengthened our data. The omission of this aspect represents a limitation of this study.

### Total miR-181 expression



	EqDB5-5(P4)				EqDB30-3(P2)				EqDB9-12(P4)				EqDB10-18(P3)			EqDB12-8(P3)		
	Mimic	AntagomiR	Scrambled	Untreated	Mimic	AntagomiR	Scrambled	Untreated	Mimic	AntagomiR	Scrambled	Untreated	Mimic	AntagomiR	Scrambled	Mimic	AntagomiR	Scrambled
<b>181a</b>	14.81	0.41	0.25	0.30	0.50	0.20	0.36	0.43	1.14	0.20	0.30	0.14	1.96	0.26	0.44	1.35	0.14	0.18
<b>181b</b>	45.82	1.74	2.05	2.77	3.63	2.68	3.80	2.79	3.22	0.71	1.13	0.55	8.69	1.69	1.34	6.16	1.07	1.00
<b>181c</b>	4.22	0.20	0.10	0.13	0.15	0.13	0.16	0.15	0.38	0.07	0.10	0.05	0.76	0.09	0.07	0.43	0.06	0.08
<b>181d</b>	1.99	1.16	3.37	2.89	4.39	3.30	4.24	3.32	1.09	2.19	2.80	0.59	1.72	2.41	3.62	1.50	1.38	1.74
<b>Total</b>	<b>66.83</b>	<b>3.50</b>	<b>5.77</b>	<b>6.09</b>	<b>8.67</b>	<b>6.31</b>	<b>8.56</b>	<b>6.68</b>	<b>5.83</b>	<b>3.16</b>	<b>4.32</b>	<b>1.33</b>	<b>13.13</b>	<b>4.44</b>	<b>5.47</b>	<b>9.45</b>	<b>2.65</b>	<b>3.00</b>

**Figure 5.2 microRNA-181 expression in mmu-miR-181a-5p mimic, antagomiR and scrambled control treated equine primary tenocyte monolayer culture.** Values represent relative expression, normalised to *SNORD61*, for all four miR-181 family members and total miR-181. Five biological replicates were used for gene expression analysis. In graphical representation, M = miR-181a-5p mimic, AM = antagomiR, SC = scrambled control, UT = untreated control. Relative expression values are given in table below graph.



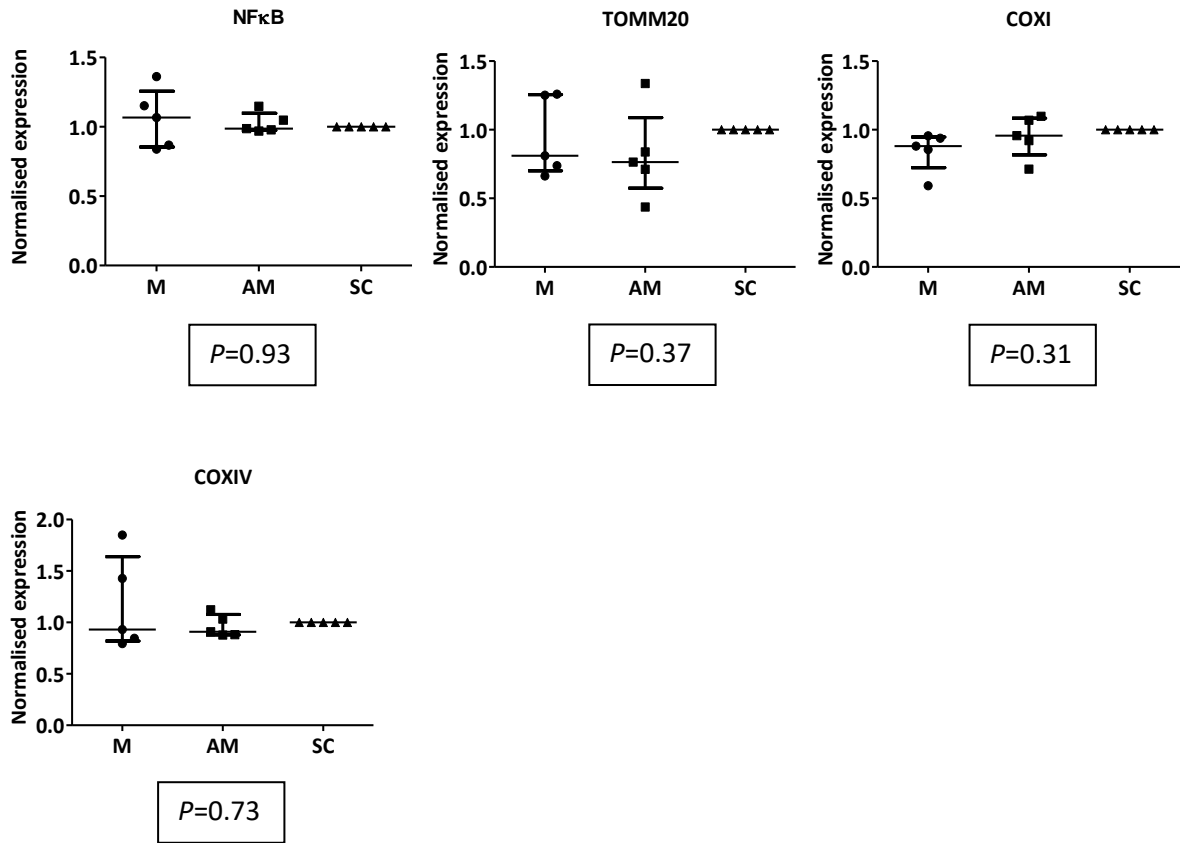


**Figure 5.3 (includes preceding page) The effects of miR-181a overexpression and inhibition on expression of selected target genes in equine tenocytes from five biological replicates.** Y-axis values represent expression relative to *glyceraldehyde 3-phosphate dehydrogenase (GAPDH)*, normalised to scrambled control treatment group. M = miR-181a-5p mimic, AM = antagomiR, SC = scrambled control. P-values calculated from delta Ct values, using Kruskal-Wallis test with Dunn's test for pairwise comparisons. Graphs show median and interquartile range.

### 5.3.3 The role of miR-181 in regulation of mitochondrial dynamics in equine tenocytes

In order to investigate the role of miR-181 in regulation of autophagy and mitochondrial dynamics, mitochondrial depolarisation was induced in primary equine tenocytes using the oxidative phosphorylation uncoupling agent carbonyl cyanide m-chlorophenylhydrazone (CCCP). To confirm treatment effect, tenocytes were incubated with 20  $\mu\text{M}$  CCCP for six hours (Kagan et al 2016, Webb et al 2017), followed by immunofluorescent staining for the outer mitochondrial membrane protein TOMM20. In DMSO treated tenocytes, mitochondria appeared to form extensive interconnected networks. In CCCP treated tenocytes, fragmentation of mitochondrial networks, with a punctate, granular appearance was evident, consistent with that reported by Miyazono and co-workers (2018) (Figure 5.4).

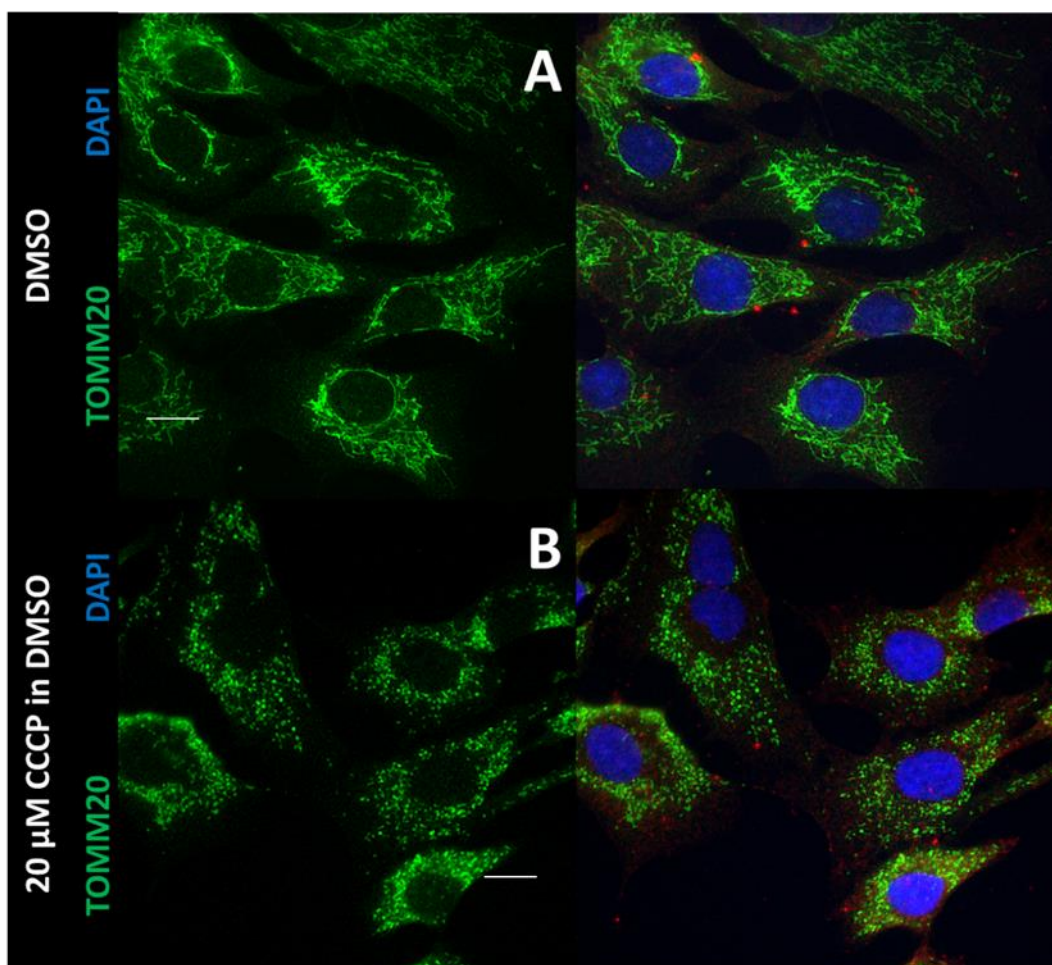


**Figure 5.4 Mitochondrial network fragmentation in response to incubation with carbonyl cyanide m-chlorophenylhydrazone (CCCP).** Equine tenocytes incubated with A) dimethyl sulfoxide (DMSO) for six hours, B) 20  $\mu\text{M}$  CCCP in DMSO for six hours. TOMM20 = translocase of outer mitochondrial membrane 20, DAPI = 4',6-diamidino-2-phenylindole. Bar = 10  $\mu\text{m}$ .

Next, to investigate the effect of miR-181 on autophagy-associated proteins, mitophagy was induced in mmu-miR-181a-5p mimic, antagomiR and scrambled control treated tenocytes by incubation with 20  $\mu$ M CCCP or DMSO control for six hours. Uptake of mimic and antagomiR treatments was confirmed by fluorescence imaging of live cell cultures immediately prior to cells being fixed, permeabilised and processed for immunostaining (Figure 5.5). No-primary-antibody controls were performed and confirmed no detectable residual fluorescence from mimic or antagomiR treatments, absence of background signal and lack of non-specific binding of secondary fluorophore-conjugated antibody (Figure 5.6). Fluorescence associated with Cy5 and FITC labelling of miR-181 mimic and antagomiR treatments was therefore degraded by processing for immunostaining.

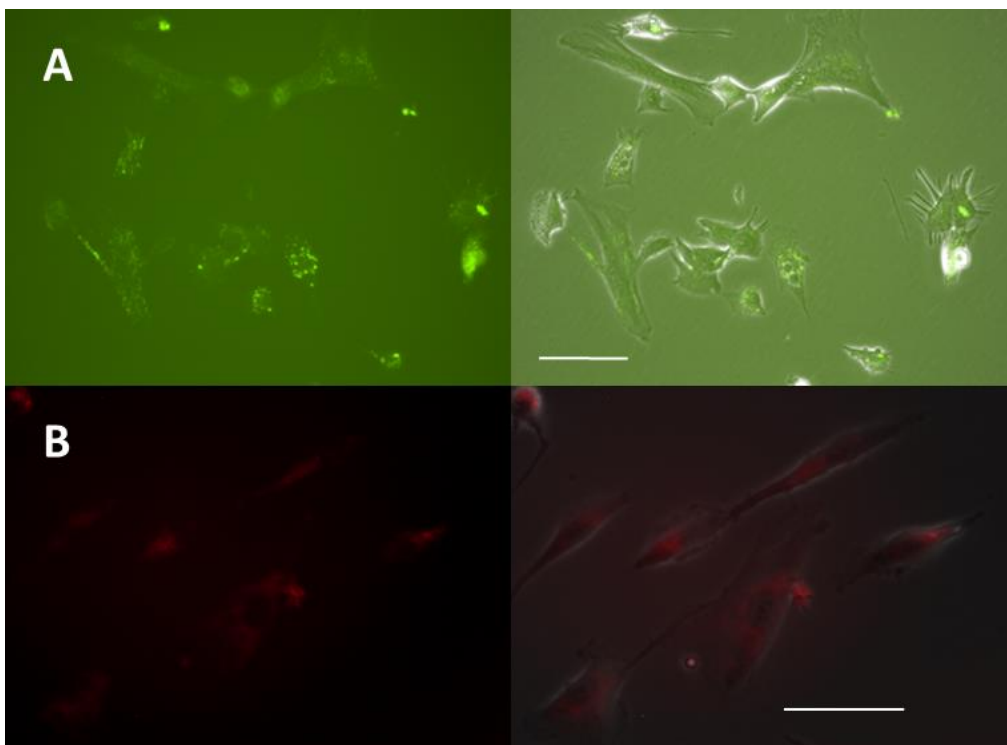


**Figure 5.5 Successful transfection of mmu-miR-181a-5p mimic and antagomiR into primary equine tenocytes.** Live cell images of transfection reagent uptake 48 hours after treatment and immediately prior to processing for immunocytochemistry. A) Fluorescein labelled single strand RNA-23 nucleotide antagomiR treatment, B) Cy5 labelled mmu-miR-181a-5p mimic treatment. Bar = 50  $\mu$ m.

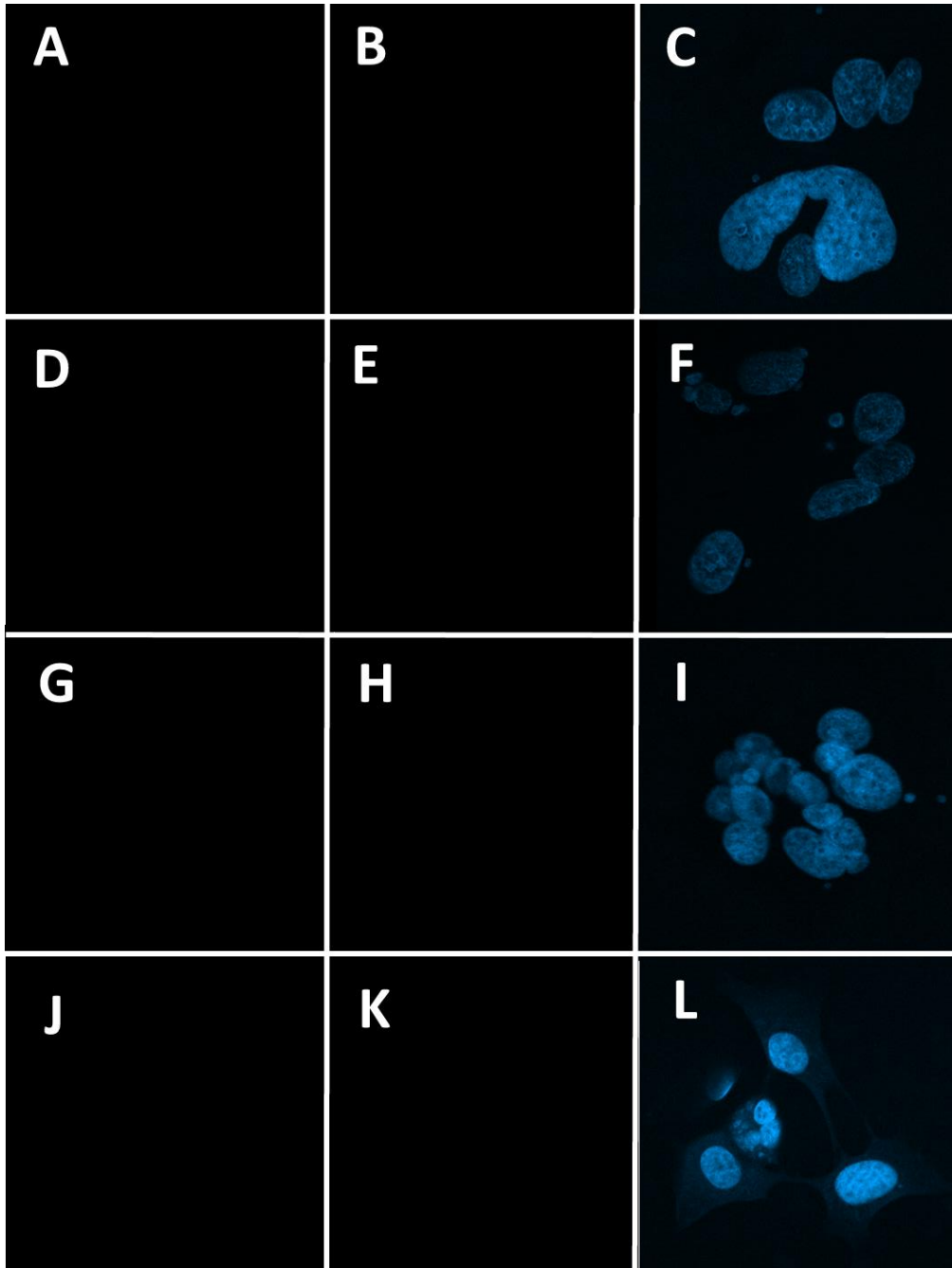


**Figure 5.6 Fluorophore-conjugated secondary anti-mouse and anti-rabbit antibodies do not generate a signal following incubation with equine tenocytes in absence of primary antibody.** Tenocytes incubated for six hours with DMSO prior to fixing, permeabilisation and incubation for one hour with: A-C Alexa Fluor 488-conjugated goat anti-mouse antibody, D-F Alexa Fluor™ 488-conjugated goat anti-rabbit antibody, G-I Alexa Fluor™ 594-conjugated goat anti-rabbit antibody, J-L Alexa Fluor 594-conjugated goat anti-mouse antibody. Images obtained at 593 nm (A, D, G, J), 510 nm (B, E, H, K), 447 nm (C, F, I, L). Nuclear counterstaining with DAPI (4',6-diamidino-2-phenylindole). DMSO = dimethyl sulfoxide.

The regulation of autophagy and mitochondrial turnover was next established by immunostaining for LC3B, DJ-1, P62/SQSTM1, Parkin and TOMM20. Increased mitochondrial biogenesis and clearance exert protective effects in the face of mitochondrial dysfunction (Indrieri et al 2019). Terminally differentiated tenocytes show a slow rate of turnover, with proliferation and apoptotic indices reported as 5-8% and less than 25% respectively in adult tendon (Chuen et al 2004, Russo et al 2015). In such cells, mitochondrial homeostasis plays a pivotal role in maintaining cellular viability and longevity (Okatsu et al 2010).

LC3B positive aggregates (punctae) are considered to be specific markers for autophagosomes, and can be indicative of both autophagy induction and impairment (Runwal et al 2019). Co-staining for the outer mitochondrial membrane protein TOMM20 reveals how mitochondrial morphology is affected by treatment protocols, indicating the degree of connectivity or fragmentation, and permits examination of interactions between mitochondria and autophagosomes (Tan et al 2019). In DMSO treated cells, TOMM20 staining revealed mitochondrial connectivity was preserved, with networks present in all treatment groups. Scattered LC3B punctae were evident in mimic and antagomiR, but rare in scrambled treated groups, indicating that miR-181 levels may be affecting autophagic activity (Figure 5.7). LC3B punctae were negative for TOMM20, indicating either effective degradation of autophagosome-encapsulated mitochondria, or phagophore nucleation had occurred around an alternative substrate. CCCP treatment resulted in formation of LC3B punctae evenly dispersed throughout the cytoplasm of scrambled treated tenocytes, but no apparent increase in punctae formation in mimic or antagomiR treated groups. LC3B punctae again appeared to be negative for TOMM20 staining. Following CCCP exposure, presence of TOMM20 positive punctae, with predominantly perinuclear localisation, in all treatment groups indicated disaggregation of mitochondrial networks. In the miR-181 mimic treated group, these aggregations were particularly prominent and spatially distinct from regions of increased LC3B fluorescence, which were localised towards the periphery of the tenocytes (Figure 5.7). Depolarised, ubiquitinated mitochondria are known to accumulate in the perinuclear region prior to degradation, proposed as a protective cellular response to aid compartmentalisation of abnormal protein aggregates (Okatsu et al 2010). In antagomiR and scrambled treated groups, LC3B distribution was more uniform. Less pronounced perinuclear accumulation of TOMM20 positive punctae was evident in antagomiR treated tenocytes, potentially indicating effective mitophagic clearance, however, overall TOMM20 staining intensity appeared decreased, suggesting a reduction in mitochondrial population, which was maintained in the mimic treated group. Consistent with this, distribution of LC3B positive punctae tended to be more closely associated with regions of increased TOMM20 positive structures (Figure 5.7). These data can be interpreted as either an increase in autophagic flux in miR-181 mimic treated cells, or that increased miR-181 levels prevent recruitment of LC3B to damaged mitochondria. These data present inconclusive evidence for the role of miR-181 in an induced mitophagy model of autophagic flux, therefore we investigated further proteins involved in the earlier stages of autophagy.

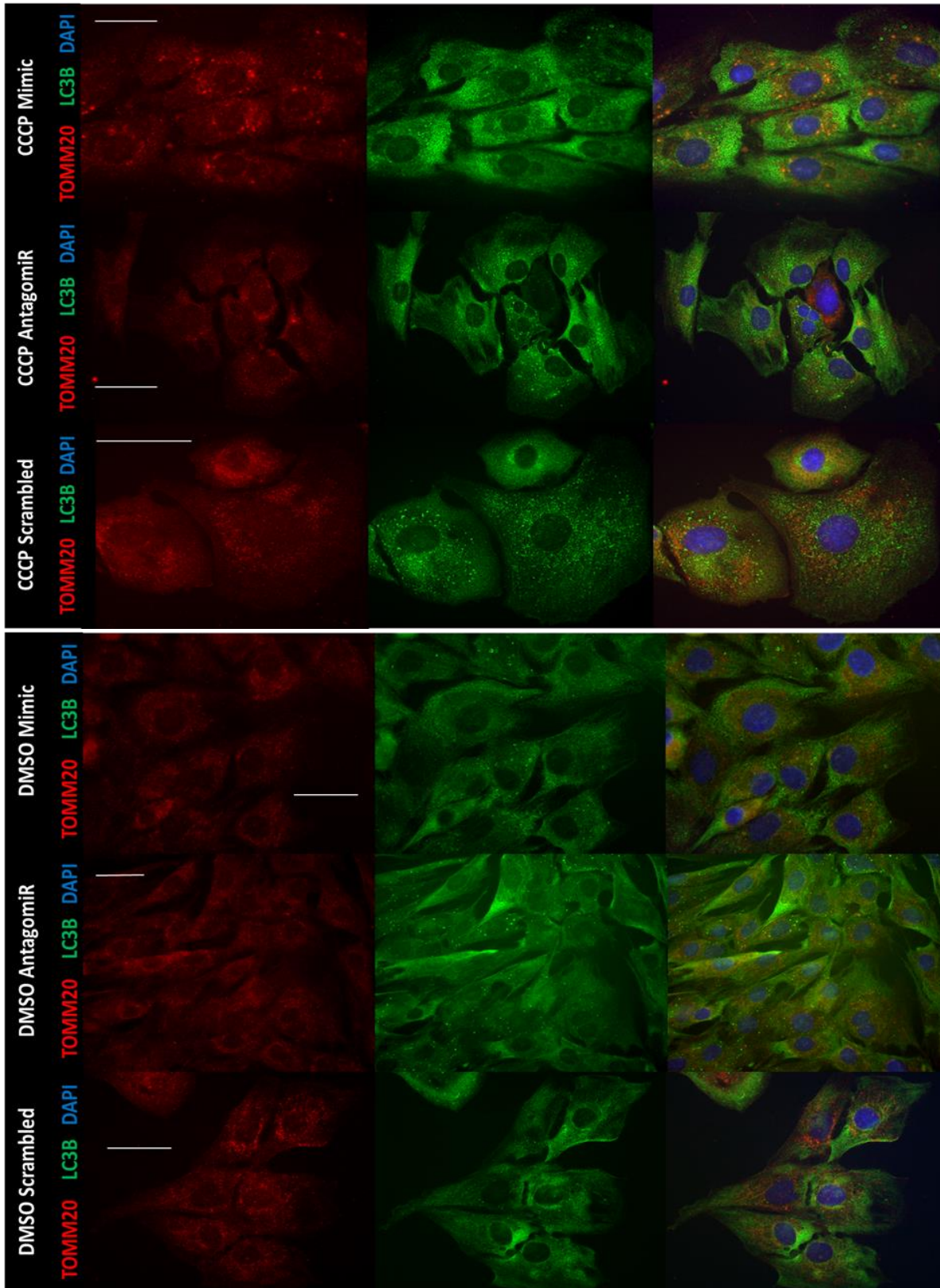


**Figure 5.7** Immunofluorescence images of miR-181a-5p mimic, antagomiR and scrambled control treated equine tenocytes subjected to six hours of CCCP/DMSO exposure. TOMM20 = Translocase of outer mitochondrial membrane 20, LC3B = Microtubule-associated proteins 1A/1B light chain 3B, DAPI = 4',6-diamidino-2-phenylindole, CCCP = carbonyl cyanide m-chlorophenylhydrazone, DMSO = dimethyl sulfoxide. Images 63 x magnification, oil immersion lens, bar = 50  $\mu$ m.

We next looked at the distribution of DJ-1, a protein recruited rapidly to depolarised mitochondria as a protective mechanism against oxidative damage (Taira et al 2004). Uniformly dispersed DJ-1 punctae were present throughout the cytoplasm in all DMSO treated tenocytes, with no distinct pattern of distribution. In tenocytes incubated with DMSO, mitochondrial networks seemed to be preserved in antagomiR and scrambled treated cells, with miR-181 mimic treatment resulting in more mitochondrial remodelling as indicated by the presence of TOMM20-positive punctae rather than mitochondrial networks (Figure 5.8). In CCCP treated tenocytes, mitochondrial punctae rather than networks were detected in miR-181 mimic-, antagomiR- and scrambled treated cells (Figure 5.8) confirming that CCCP induced autophagy. Moreover, in antagomiR treated cells, mitochondrial loss seemed to occur, whereas this was not the case for mimic treated cells, as compared to controls (Figure 5.8). Distribution patterns of TOMM20 positive aggregates differed between treatment groups, being predominantly perinuclear in miR-181 mimic treated cells, peripheral in antagomiR treated cells and intermediate in scrambled control treated cells (Figure 5.8).

CCCP treatment resulted in fewer DJ-1 positive punctae present in tenocytes treated with mimic, antagomiR or scrambled control. These punctae showed a less uniform distribution pattern than DMSO controls, with a tendency for dense perinuclear localisation in miR-181 mimic treated, and more peripheral location in antagomiR treated cells. Scrambled control treated tenocytes showed an intermediate distribution pattern (Figure 5.8). In CCCP treated tenocytes, DJ-1 colocalised with areas more densely populated with mitochondrial punctae in mimic-, antagomiR- and scrambled treated tenocytes. CCCP induces reactive oxygen species (ROS) mediated apoptosis (Park et al 2015) and DJ-1 is known to localise to the mitochondria under conditions of oxidative stress, where it has a protective function (Taira et al 2004).

Our data suggest a role of miR-181 in mitochondrial turnover as shown by TOMM20 positive punctae rather than networks in DMSO treated controls. Following induction of mitophagy, a more appropriate perinuclear condensation of TOMM20 positive staining occurred in miR-181 mimic and scrambled control treated tenocytes, but not in antagomiR treated ones. We were not able to determine definite treatment-dependent changes in co-localisation or levels of DJ-1 with mitochondrial marker TOMM20, suggesting that DJ-1 recruitment to damaged mitochondria occurs in a miR-181 independent manner.

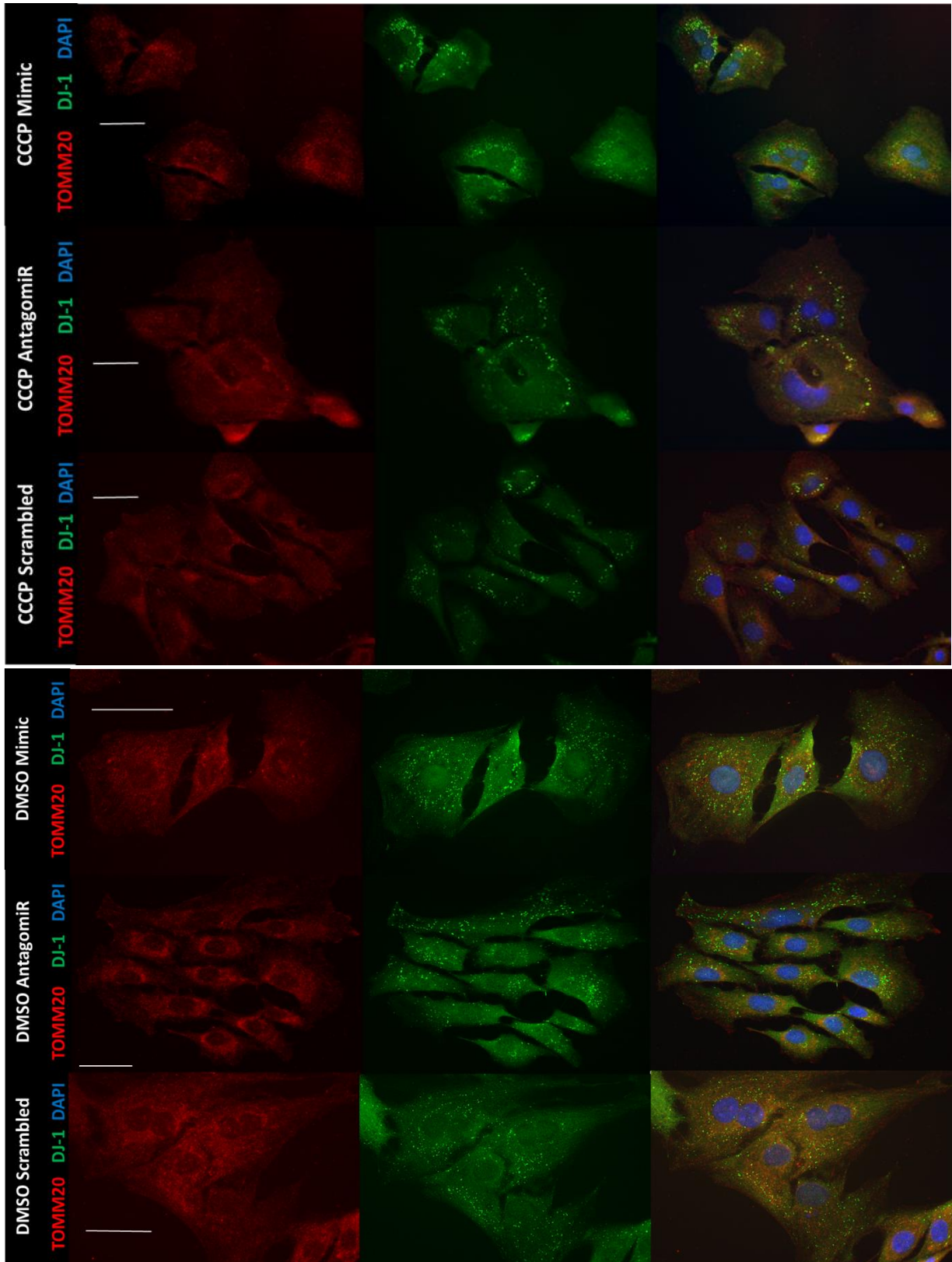


**Figure 5.8 Immunofluorescence images of miR-181a-5p mimic, antagomiR and scrambled control treated equine tenocytes subjected to six hours of CCCP/DMSO exposure.** TOMM20 = Translocase of outer mitochondrial membrane 20, DJ-1 = Protein deglycase DJ-1 (PARK7), DAPI = 4',6-diamidino-2-phenylindole, CCCP = carbonyl cyanide m-chlorophenylhydrazine, DMSO = dimethyl sulfoxide. Images 63 x magnification, oil immersion lens, bar = 50  $\mu$ m.

We then investigated P62/SQSTM1, an autophagy receptor protein up regulated during mitophagy, which interacts with both ubiquitin and LC3B and plays a protective role in ROS-mediated cell death through induction of the NRF2 pathway (Sánchez-Martín and Komatsu 2018).

In DMSO controls, antagomiR treated tenocytes demonstrated a generalised loss of mitochondria as evidenced by a reduction in TOMM20 positive structures overall. In miR-181 mimic treated cells, TOMM20 positive structures were punctiform indicating lack of mitochondrial networks. Similarly, following CCCP exposure, TOMM20 staining revealed a more punctate than networked appearance of mitochondria in mimic treated cells, indicating greater remodelling. Weaker TOMM20 signal potentially indicating mitochondrial loss, was evident in the antagomiR and scrambled treated groups.

In DMSO controls, cells from all treatment groups showed a well demarcated, distinct perinuclear localisation of P62/SQSTM1 similar to that reported by Viiri and co-workers (2010) (Figure 5.9). These authors showed, in proteasome-inhibited human retinal pigment epithelial cells, that P62/SQSTM1 promoted perinuclear accumulation of ubiquitinated proteins in lysosomal vesicles, where P62/SQSTM1 colocalised strongly with the chaperone protein HSP70 (heat shock protein 70) (Viiri et al 2010). There appeared to be subtle differences between treatment groups, with a more 'concentrated' perinuclear appearance in the miR-181 mimic group, slightly less so in the antagomiR treated group, and more diffuse, although still predominantly perinuclear in the scrambled treated group (Figure 5.9).

In CCCP treated tenocytes, P62/SQSTM1 localisation appeared less organised in comparison. Distribution was still predominantly perinuclear, but showed a more disrupted and fragmented pattern. Punctae were more widely dispersed throughout the cytoplasm in mimic, compared to antagomiR or scrambled treated cells, consistent with an up regulation of P62/SQSTM1 labelling of substrates targeted for autophagy, although these did not map to TOMM20 positive punctae (Figure 5.9). In scrambled treated cells, localisation was less concentrated around the nuclei, with diffuse cytoplasmic staining evident, whereas in mimic and antagomiR treated cells, localisation was more clearly defined.

There appeared to be no consistent association between localisation of TOMM20 and P62/SQSTM1 positive regions. Whilst P62/SQSTM1 is reported to be widely distributed at the subcellular level (Sánchez-Martín and Komatsu 2018), perinuclear localisation of P62/SQSTM1 has been reported following CCCP treatment of HeLa cells and mouse embryonic fibroblasts (MEFs), reflecting perinuclear clustering of depolarised mitochondria (Okatsu et al 2010). Moreover, these authors report that although P62/SQSTM1 is not essential for mitochondrial degradation, it is critical for the normal perinuclear clustering of defective mitochondria.

Taken together, these data suggest that miR-181 is associated with increased turnover of mitochondria as evidenced by TOMM20 positive punctate morphology, with preservation of overall mitochondrial population, whilst weaker TOMM20 signal in DMSO- and CCCP-exposed antagomiR treated tenocytes appeared to reduce mitochondrial population. miR-181 appeared to exert some effect on P62/SQSTM1 localisation, but no conclusive interaction could be determined from our data. The preponderance for perinuclear accumulation of P62/SQSTM1 observed consistently, albeit to varying degrees, in all treatment groups may represent a cell type-specific distribution pattern, or reflect a role for this protein unrelated to autophagy. Indeed, P62/SQSTM1 is known to function as a

central signalling molecule in multiple cellular pathways including adipogenesis, antioxidant responses, endosomal trafficking, apoptosis and inflammation (Sánchez-Martín and Komatsu 2018). Autophagic degradation of depolarised mitochondria has been shown to occur in MEFs in the absence of P62/SQSTM1 in a Parkin-dependent manner (Okatsu et al 2010), therefore we next investigated the distribution of the E3 ubiquitin ligase Parkin in our model.

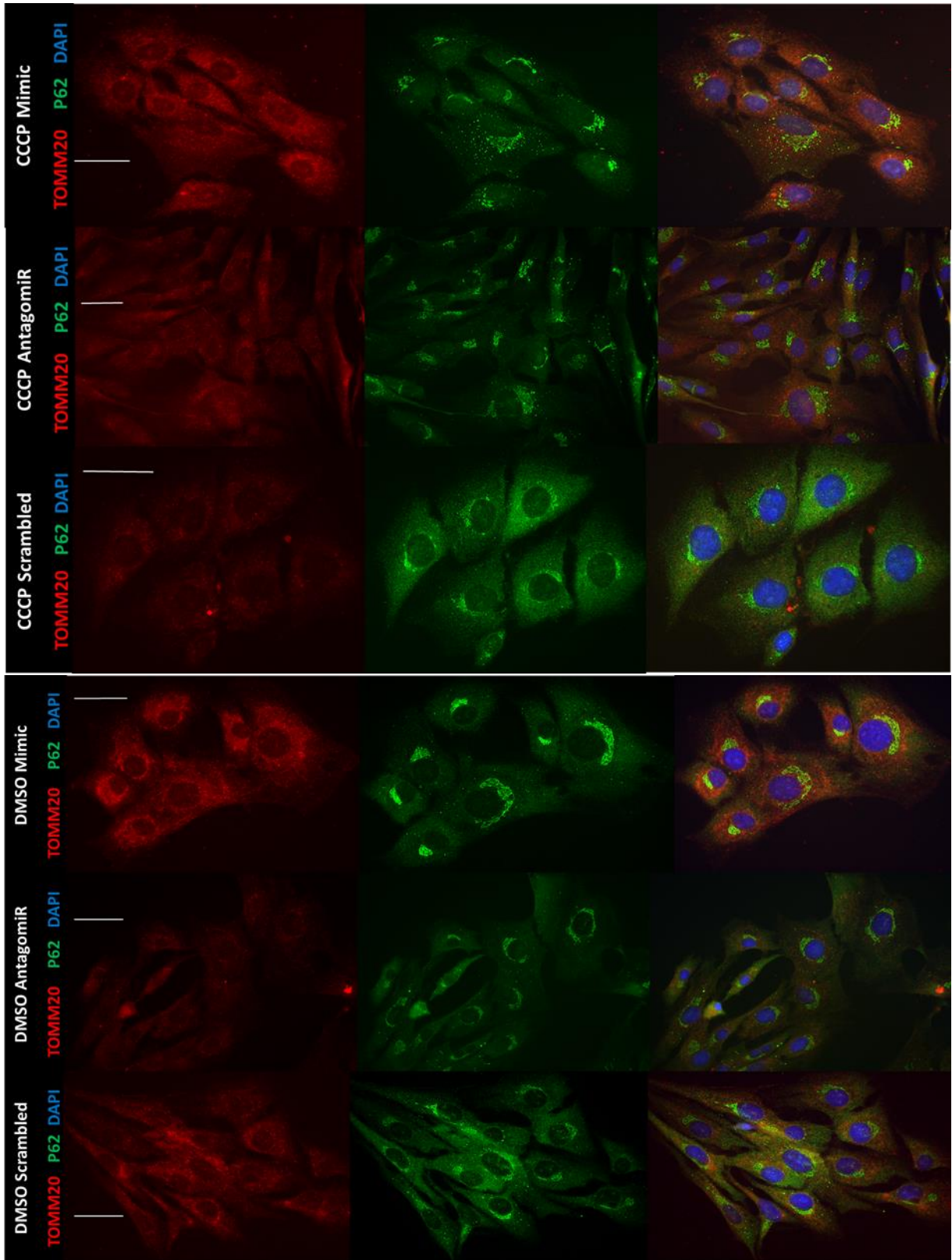


**Figure 5.9** Immunofluorescence images of miR-181a-5p mimic, antagomiR and scrambled control treated equine tenocytes subjected to six hours of CCCP/DMSO exposure. TOMM20 = Translocase of outer mitochondrial membrane 20, P62 = ubiquitin-binding protein p62, DAPI = 4',6-diamidino-2-phenylindole, CCCP = carbonyl cyanide m-chlorophenylhydrazone, DMSO = dimethyl sulfoxide. Images 63 x magnification, oil immersion lens, bar = 50  $\mu$ m.

Parkin is rapidly and robustly recruited to depolarised mitochondria where it ubiquitinates outer mitochondrial membrane proteins, targeting these organelles for autophagic elimination. Parkin also becomes ubiquitinated and degraded during this process (Seirafi et al 2015). In miR-181 mimic, antagomiR and scrambled treated tenocytes exposed to DMSO, uniform cytoplasmic distribution of Parkin was evident, although staining was weak. Networked mitochondria, as indicated by TOMM20 staining, were seen, indicating little mitophagic activity (Figure 5.10). Following incubation with CCCP, Parkin distribution remained uniform and weak, in miR-181 mimic and scrambled treated groups. In antagomiR treated tenocytes however, Parkin accumulation was evident in association with more dense regions of TOMM20 positive mitochondrial staining (Figure 5.10). Mitochondrial connectivity seemed to be preserved to some extent in antagomiR treated cells, although networks appeared contracted and centralised towards the perinuclear region. The presence of TOMM20 positive punctae revealed complete disruption of mitochondrial networks in the mimic and scrambled treated groups (Figure 5.10). Following exposure to CCCP, recruitment of Parkin to depolarised mitochondria and subsequent ubiquitination occurs rapidly (within 1 hour) with subsequent concentration to the perinuclear region in under 4 hours prior to degradation (Okatsu et al 2010). Treatment of cells with CCCP produces rapid depolarisation of the entire mitochondrial network, resulting in levels of damaged mitochondria not seen under physiological conditions (Seirafi et al 2015). It is possible therefore that in miR-181 mimic treated tenocytes incubated with CCCP for six hours, mitophagy had already occurred and TOMM20 positive staining revealed residual mitochondria remaining as a consequence of mitophagic clearance being overwhelmed.

Based on these data, it appears that miR-181 may regulate the levels of Parkin in mitophagy-inducing conditions, such as CCCP treatment. Specifically, inhibition of miR-181 in CCCP treated tenocytes resulted in accumulation of Parkin in these cells. Some co-localisation between Parkin and TOMM20 was observed in the CCCP/antagomiR treated cells, and mitochondrial networks seemed 'shrunk' rather than disaggregated into punctae as in scrambled/CCCP treated cells (Figure 5.10). This suggest that the recruitment of Parkin to mitochondria is not affected by inhibition of miR-181 activity, but autophagy is stalled as indicated by the lack of TOMM20 positive punctae. These data also suggest that miR-181 may promote mitophagy through regulating progression of autophagy rather than recruitment of mitophagic proteins to critically damaged mitochondria.

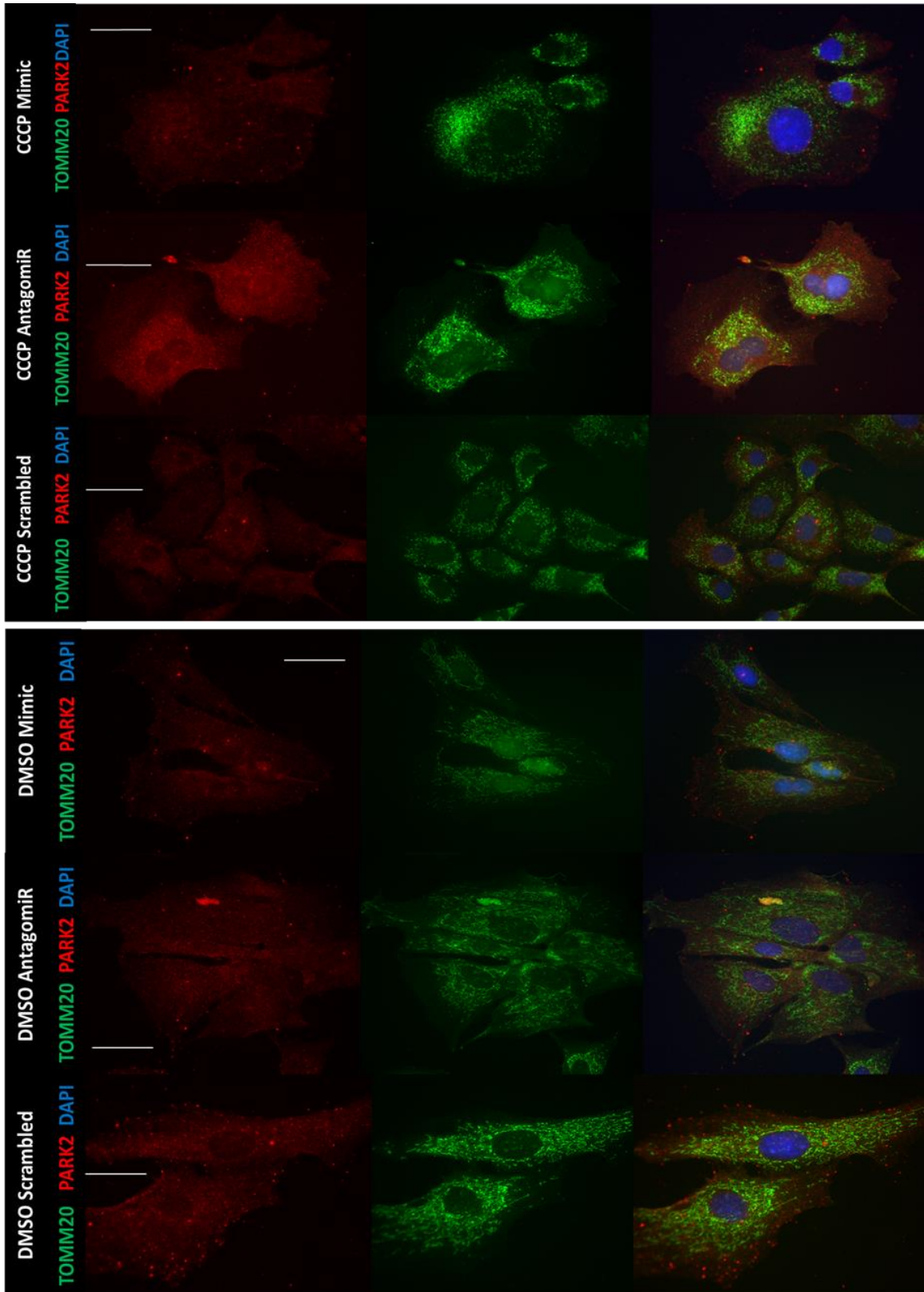


**Figure 5.10** Immunofluorescence images of miR-181a-5p mimic, antagomiR and scrambled control treated equine tenocytes subjected to six hours of CCCP/DMSO exposure. TOMM20 = Translocase of outer mitochondrial membrane 20, PARK2 = Parkin, DAPI = 4',6-diamidino-2-phenylindole, CCCP = carbonyl cyanide m-chlorophenylhydrazine, DMSO = dimethyl sulfoxide. Images 63 x magnification, oil immersion lens, bar = 50  $\mu$ m.

## **5.4 Discussion**

In this chapter, we investigated the effect of miR-181 overexpression and inhibition on selected target gene expression in primary equine tenocytes, following treatment with miR-181a mimic, antagomiR or scrambled control. Additionally we utilised a model of induced mitophagy to determine the effect of miR-181 on mitochondrial dynamics and remodelling. Our results suggest miR-181 regulates mitochondrial turnover.

Due to their involvement in cell differentiation, proliferation and apoptosis, the miR-181 family has been extensively studied in cancer development and progression, with family members miR-181a and -b most frequently reported. Both pro- and anti-apoptotic effects have been described for miR-181a in breast cancer, by targeting both B-cell lymphoma 2 (BCL2) and BCL-2 interacting mediator of cell death (BIM) respectively. Downregulation in a wide range of cancer types resulted in increased cellular proliferation, migration and neoplastic transformation, with inhibition of apoptosis (Pop-Bica et al 2018, Rezaei et al 2019). However, upregulation of miR-181a in breast, gastric, and colorectal cancer and lymphoblastic leukaemia is also associated with increased cellular proliferation and migration. Inhibition of apoptosis and autophagy has also been described, by promoting BCL2 activity and targeting autophagy related gene 5 (Rezaei et al 2019). Over expression of miR-181b, also reported in numerous types of cancer, disrupts the cell cycle, increasing the proportion of quiescent cells and triggering apoptosis. In lung cancer, tumour suppressive actions have been ascribed to targeting transcription factor SOX6, disrupting cell differentiation and proliferation (Zhou et al 2019). Suppressed proliferation and induced apoptosis have also been described in astrocytoma (Zhi et al 2014). Conversely, miR-181b upregulation is associated with cellular proliferation and invasion in ovarian cancer. Many of the oncogenic effects of miR-181a and -b have been associated with promotion of TNF, IL1, MAPK, TGF $\beta$ , and TIMP3 activity (Rezaei et al 2019). miR-181c and miR-181d are less frequently reported, but have been described as tumour suppressive in glioblastomas and ovarian cancer, with downregulation promoting TGF $\beta$  and MAPK activity, favouring cell proliferation, malignant transformation and a pro-inflammatory environment (Rezaei et al 2019). Evidence from studies of neoplastic diseases suggests expression patterns and functional consequences of miR-181 are highly variable and cell-type specific. Contradictory effects both between and within tissue types have been attributed to selective intracellular compartmentalisation and concentration dependent effects (Yang et al 2017). A 'context-dependent' role has also been reported for other miRNAs, where expression may occur predominantly at a particular stage of development, within a particular cell type, or be localised to a specific subcellular compartment. These contextual determinants illustrate that the presence of a functional target site is not, in isolation, sufficient for regulation to occur, as the immediate intracellular environment may under certain circumstances, prevent silencing complex functionality (Carroll et al 2013, Erhard et al 2014).

The greatest increase in miR-181 expression we observed in response to mimic treatment was in miR-181b. The mimic transfection reagent was based on the murine miR-181a-5p sequence and primers used to confirm transfection success were designed to target mature 5p variants of all four human miR-181 family members. Sequence identity is conserved across murine, equine and human species and differences between family members are minor (Table 5.3). Only a single nucleotide

deletion (guanine at position 11) accounts for the difference between miR-181a and miR-181c, whilst miR-181b and miR-181d differ from miR-181a only by three and four nucleotide substitutions respectively. Whilst miR-181b was the most highly expressed of the miR-181 family in equine tendon identified in Chapter 3, (Figure 3.3 (F and L)), changes in expression of miR-181 family members -c and -d, which are not recognised in miRBase, could represent mis-priming events during PCR amplification. Discrimination between targets with very similar sequences can be problematic using PCR technology due to mis-priming events, with primer design, cycle parameters and reagent factors all impacting on quantitative accuracy. Boyle and co-workers (2009) investigated maximising PCR discrimination between targets containing single nucleotide polymorphisms (SNP). Conditions that favour primer-template annealing, including lower cycling temperature relative to primer melting temperature and longer annealing and elongation times maximised accuracy. These authors also found SNP location at the 3' end of the primer influenced quantification more strongly than the same SNP located at the 5' end. Additionally, results varied with different master mixes, using the same primers and cycle settings (Boyle et al 2009). We used commercially available primers, specified as directed against individual miR-181 family members (Qiagen Ltd, Manchester, UK). Short sequence length targets offer limited ability to alter primer sequences, however primer sensitivity and specificity is reportedly enhanced by using locked nucleic acid (LNA) oligonucleotides when detecting and differentiating small or highly similar DNA or RNA targets. These nucleotides contain a methylene bridge connecting the ribose 2'-oxygen and 4'-carbon, increasing conformational stability (Qiagen Ltd., Manchester, UK, technical support, personal communication). It would be interesting to incorporate this in future work. These factors underpin the importance of protocol optimisation and consistency.

Using RT-qPCR, we did not detect statistically significant differences in the expression of the eight validated target genes (*SIRT1*, *P62/SQSTM1*, *PARK2*, *PARK7/DJ-1*, *COX1*, *IL1 $\alpha$* , *PRDX3* and *TNF*) following gain and loss of miR-181 function (Figure 5.3). Similarly, transcript expression of *PRDX6*, *IL16*, *IL1RAP*, *NF $\kappa$ B*, *SMAD7*, *IL7*, *COXIV* and *TOMM20*, genes which interact with them, or are involved in pathways relevant to inflammation, apoptosis, or mitochondrial dynamics were not different (Figure 5.3). This was disappointing, but may be due to miR-181 inhibiting translation, rather than promoting degradation of these transcripts as shown previously (Soriano-Arroquia et al 2016, Bartel 2018).

Oligonucleotides are charged, non-biologically stable molecules, which require modification or formulation to enable cellular delivery. Efficacy is defined by both the ability to be delivered to, and biological availability within the cell (Ly et al 2017). We used cholesterol-conjugated and phosphorothionate and 2'-O-methylation modified oligonucleotides to improve cellular penetrance and stability. Uptake of mimic and antagomiR treatments was confirmed visually and using RT-qPCR, indicating treatments were effectively delivered. Quantification of miR-181 expression by RT-qPCR did show variable efficacy of treatments however (Figure 5.2). This may consequently have increased variation in target gene expression, accounting for lack of significant differential gene expression between treatment groups (Figure 5.3). AntagomiR treatment was only considered successful in five out of eight biological replicates, based on antagomiR treated levels of total miR-181 being below those of the scrambled control treated group (Figure 5.2). We chose to perform gene expression analysis only on these five biological replicates, to increase confidence in results. Cholesterol conjugated 2'-O-Me antagomiRs (such as we used) are reported to promote miRNA degradation (Stenvang et al 2012). If miR-181 is not degraded by interaction with the antagomiR, however, then

it will still be detected by RT-qPCR, even though in the intracellular environment it would still be susceptible to inhibition. This may have resulted in unnecessary exclusion of valid data sets. Conversely, it has been reported that the majority of internalised compounds are trapped unproductively in lysosomes and other 'oligonucleotide sinks', and that the addition of serum to culture media strongly inhibits functional efficacy of cholesterol modified siRNAs (Ly et al 2017). Further work could assess efficacy of alternative transfection protocols such as use of cationic liposome transfection reagents or electroporation, or reduction or absence of serum enrichment to culture media. Additionally, a greater number of technical replicates may allow selection of samples with more consistent transfection results between biological replicates.

In a heterogenous population, variation in baseline gene expression and response to cell treatments between biological replicates is to be expected, and consistent with the context-dependent effect of miRNAs referred to above. Tenocytes used were derived from horses on the basis of availability, and therefore subject to a range of environmental, genetic and epigenetic factors. A more homogenous sample population would have been preferable. Additionally, increasing the number of biological replicates would be useful to counteract inherent variability and that of treatment efficiency. Gene expression was only assessed at the transcript level which may account for the lack of observed effect. miRNAs act principally as post transcriptional regulators of gene expression, so it may be assumed that transcript levels will not be affected, only translation into the functional protein. However, the effect on translational repression, although rapid, is reported to be weak and of limited importance in the post-embryonic state (Eichhorn et al 2014). Destabilisation of mRNA is believed to be the major mechanism by which miRNAs mediate gene expression control, with mRNA levels reputedly providing an almost quantitative reflection of miRNA mediated repression (Bartel 2018). Moreover, the function of the protein products depends of their post-translational modification and their turnover is fast, therefore levels of these proteins may not be indicative of their function (Goljanek-Whysall et al 2020). This would support our assessment of gain and loss of function effects by quantifying only transcript expression. However, gain and loss of miR-181a function significantly affects SIRT1 protein expression in myotubes, without corresponding alterations in mRNA levels (Soriano-Arroquia et al 2016). Robust assessment of gene expression should, therefore include quantification of both transcript and protein product. Protein quantification would have provided an additional, complementary analysis of effect and the absence of this is a major limitation to interpretation of our results.

We therefore investigated autophagy-related protein function by analysing localisation of TOMM20, LC3B, DJ-1, P62/SQSTM1 and Parkin, in control conditions (DMSO) and following mitophagy induction using the decoupling agent CCCP (Figures 5.7, 5.8, 5.9, 5.10). Using immunocytochemistry, we identified treatment-related changes in localisation of, principally, Parkin and to a lesser extent P62/SQSTM1 and LC3B following mitochondrial membrane destabilisation. However we were not able to quantify the co-localisation of mitophagic and autophagic proteins with TOMM20 to determine the exact process by which miR-181 regulated mitochondrial turnover. Distribution and co-localisation of proteins labelled with spectrally distinct fluorescent markers can be assessed by several methods. Simple descriptive techniques, such as reported here, assess colour overlay of green and red fluorescence. Overlapping signals produce predominantly yellow pixels, indicating co-localisation within subcellular compartments (Comeau et al 2006). This, however, requires comparable fluorescence intensities of the two markers and does not permit quantification of degree co-localisation (Moser et al 2017). This is overcome by statistical analysis of pixel-intensity correlation,

commonly using Pearson's correlation coefficient to measure covariance between signals, but becomes inaccurate in samples with unequal numbers of densities detected by each channel. Accuracy is improved by calculation of co-localised coefficients (termed M1 and M2), with defined threshold values for each channel, which correlate pixel intensity detected by the two fluorescence channels relative to the total fluorescence in each channel. These methods are incorporated into plug-ins for commercially available or free software, and could have been utilised to quantify co-localisation using the ImageJ software (Rasband, W.S. U. S. National Institutes of Health, Bethesda, Maryland, USA, <https://imagej.nih.gov/ij/>, 1997-2018), employed in Chapters 6 and 7 for band densitometry analysis of Western blot images. The dynamic range and accuracy of these methods is, however, still debated (Comeau et al 2006). Combination of these techniques with object recognition to calculate an object-corrected Pearson coefficient has been proposed as a more robust measure of co-localisation (Moser et al 2017). Co-localisation does not, however, imply functional interaction between the molecules of interest.

Mitochondria are dynamic organelles, with the capacity to undergo both movement and morphological changes. Brownian motion, short and long range stochastic, directed motion (at speeds reaching  $1 \mu\text{m s}^{-1}$  at  $37^\circ\text{C}$ ), extension and retraction, fission and fusion all contribute to frequent dynamic reorganisation (McCarron et al 2013). Mitochondrial morphology and distribution vary considerably with cell type, between cultured and native cells, and between embryonic and mature tissue. Mitochondrial appearance can also vary regionally within cells (McCarron et al 2013). In fibroblasts, mitochondria are usually filamentous structures 1-10  $\mu\text{m}$  in length and approximately 700 nm in diameter, with the ability to form reticular networks. In mammalian cells, however, network formation appears to be far more prevalent in cultured than native cells (McCarron et al 2013). Formation of continuous networks permits rapid diffusion of solutes within the organelle and mitigation of focal dysfunctionality from mutated mitochondrial DNA or dysfunctional membrane and matrix proteins, thereby maintaining oxidative capacity within the cell (Karbowski and Youle 2003). Fusion and fission occurring as an obligatory physiological function, are more frequently reported in cultured rather than native cells. These events usually occur at equal frequency, to maintain overall mitochondrial number and morphology. Fusion is dependent on the proteins mitofusin 1 and 2 (MFN1, MFN2) and optic atrophy 1 protein (OPA1), whilst fission requires dynamin-related protein 1 (DRP1) and its outer mitochondrial membrane adaptor fission protein 1 (hFIS1). Mutations in these proteins are fatal in mice, whilst in humans, mutations in the fusion proteins cause serious neurological deficits. Morphological and distribution changes may be associated with altered cellular energy requirements (increased connectivity increasing respiratory activity), calcium signalling, or ROS signalling (McCarron et al 2013).

Fission and fusion have also been associated with apoptosis and as a means of controlling mitochondrial quality through autophagy. In early apoptosis, mitochondrial networks disintegrate, producing punctiform fragmented structures. Release of proteins such as cytochrome c from the intermembrane space during this process can activate procaspase-9 and subsequently apoptotic effector proteases caspase-3 and -7 (Karbowski and Youle 2003). Inhibiting fission has been shown to be protective, reducing cardiomyocyte death, myocardial infarct size and renal tubular cell apoptosis in models of ischaemia-reperfusion injury. However, enhanced fission, driven by overexpression of DRP1, maintained viability of HeLa cells by preventing calcium dependent apoptosis (Szabadkai et al 2004), suggesting fission may also be a protective mechanism to separate dysfunctional or damaged mitochondria for targeted degradation.

Of the proteins assessed by immunocytochemistry, pattern of TOMM20 staining indicates whether mitochondrial networks are intact or dispersed, reflecting degree of mitochondrial remodelling. Mitochondrial network disruption occurred in response to induced mitochondrial depolarisation, confirming effect of CCCP treatment. In miR-181 mimic treated tenocytes, mitochondrial content appeared to be preserved, suggesting mitochondrial turnover was enhanced with miR-181 upregulation. In the majority of samples, Alexa Fluor™ 594 (red) conjugated secondary antibody was used to image TOMM20 localisation. The exception was in those cells co-stained for Parkin, in which Alexa Fluor™ 488 (green) was used. This inconsistency was a function of convenience, reflecting availability of relevant compatible primary and secondary antibodies. Image resolution and definition was superior for proteins labelled with the green rather than red fluorophore-conjugated secondary antibody. This may have facilitated observation of more subtle changes in mitochondrial morphology in association with Parkin co-staining, whilst precluding identification of these in the other samples. Indeed, we identified CCCP induced mitochondrial network disintegration in all samples with the exception of miR-181 antagomiR treated cells co-stained for Parkin, where a mitochondrial pattern intermediate between punctiform and networked was evident (Figure 5.10). This could suggest inhibition of miR-181 produced some measure of protection against mitochondrial degradation, or progression of the degradative process had been interrupted. Accumulation of the other proteins investigated can indicate upregulation of autophagy, or disruption to autophagic flux, with impaired clearance from the cell.

Although not statistically significant at the transcript level, localisation of proteins P62/SQSTM1 and Parkin demonstrated the most obvious alterations with miR-181 overexpression or inhibition following mitochondrial depolarisation (Figures 5.9, 5.10). P62/SQSTM1 is an autophagosome adaptor protein, targeting other proteins for selective autophagy by virtue of possessing both LC3B-interacting and ubiquitin binding regions. Parkin is recruited to the outer membrane of damaged mitochondria following phosphatase and tensin homologue-induced putative kinase 1 (PINK1) stabilisation, where it mediates polyubiquitination of outer mitochondrial membrane proteins, targeting them for proteasomal degradation (Palikaras et al 2018).

Autophagy is part of a suite of highly conserved cellular processes, including apoptosis and necroptosis which initiate and regulate programmed cell death (Su et al 2015). These processes operate with a basal level of activity that alters in response to a range of cellular stressors (Sánchez-Martín and Komatsu 2018). Each mechanism consists of well-defined sophisticated pathways which interact through several key intermediates, one of which is P62/SQSTM1 (Su et al 2015). Dysregulation of miR-181 and subsequent expression of *P62/SQSTM1* and co-targets *PARK2* and *DJ-1* is associated with disrupted autophagic pathways and degenerative changes in skeletal muscle (Goljanek-Whysall et al 2020). On this basis, we investigated how miR-181 influenced the distribution of LC3B, P62/SQSTM1, DJ-1, and Parkin following mitochondrial uncoupling. LC3B is an autophagosome membrane-associated protein that targets receptors expressed on the surface of damaged mitochondria and is a marker of enhanced autophagic sequestration or reduced clearance (McCoy and Cookson 2011). In addition to functioning in catabolic pathways, P62/SQSTM1 plays a protective role in ROS-mediated cell death by binding kelch like ECH associated protein 1 (KEAP1), preventing it targeting nuclear factor erythroid 2 (NRF2) for proteasomal degradation. Stabilisation of NRF2 results in its accumulation and nuclear translocation, activating transcription of antioxidant enzymes (Park et al 2015). DJ-1 is recruited to depolarised mitochondria as a protective mechanism against oxidative damage, becoming directly oxidised, and stimulating mitochondrial fusion (Taira et

al 2004, McCoy and Cookson 2011). The outer mitochondrial membrane kinase PINK1 recruits Parkin following mitochondrial depolarisation, initiating ubiquitin-dependent mitophagy and enhancing cell survival by suppressing both mitochondria-dependent and independent apoptosis (Palikaras et al 2018).

Goljanek-Whysall and co-workers (2020) reported that the downregulation of miR-181a with ageing is associated with defective mitochondrial dynamics and a dysfunctional autophagic response in myoblasts, characterised by accumulation of autophagy-associated proteins and abnormal mitochondria. Overexpression of miR-181a/b is also reported to stimulate mitochondrial metabolism and osteogenic induction in human chondrocytes (Zheng et al 2019). Conversely, Ouyang and colleagues (2012) reported inhibition of miR-181a in murine astrocytes is associated with a reduction in oxidative stress and cell death, with preserved mitochondrial function. Although these authors did not measure mitophagic flux, they reported miR-181a inhibition increased levels of the anti-apoptotic proteins myeloid leukaemia cell differentiation protein (MCL1) and BCL2, to which they attributed their findings (Ouyang et al 2012). Investigating mitochondrially-mediated central neurodegeneration both *in vitro* and *in vivo*, Indrieri and co-workers (2019) reported inhibition of miR-181a and -b was protective against cell death following protonophore treatment of neurones in a model of induced autophagy similar to the one we employed. Deletion of miR-181a and -b in mice resulted in increased expression of *NRF2* and *PPARGC1A* (peroxisome proliferator-activated receptor gamma coactivator 1-alpha) transcripts and mitochondrial DNA, indicating increased mitochondrial biogenesis. Concurrently, *PARK2* was up regulated and Parkin and P62/SQSTM1 were enriched in the mitochondrial compared to the cytosolic cell fraction, although overall levels of Parkin and P62/SQSTM1 were reduced (Indrieri et al 2019). These authors concluded that miR-181 inhibition stimulated mitochondrial turnover and increased autophagic flux in CNS tissues, maintaining neuronal viability.

Our results show elements that are consistent with miR-181 upregulation enhancing mitochondrial turnover, thereby maintaining a functional population in the cell, or miR-181 inhibition exerting a protective effect by mitigating mitochondrial damage and preventing degradation. Precipitation of mitochondrial dysfunction resulted in LC3B accumulation in mimic treated cells that did not coincide with regions of punctate TOMM20 staining. This distribution pattern could suggest either failure of LC3B to localise to damaged mitochondria, leading to accumulation within the cell, or that recruitment to damaged mitochondria and degradation of lysosome-associated LC3B had already occurred. Peripheral LC3B positive regions may represent an increase in production of LC3B in the soluble form prior to becoming bound to lysosomal membrane. Whilst DJ-1 and TOMM20 localisation patterns showed a degree of similarity in mimic treated cells, corresponding with the expected response, this appeared more precise in antagomiR treated cells, although overall mitochondrial content seemed reduced (Figure 5.8). The more dense perinuclear clustering of DJ-1 and TOMM20 positive punctae in the CCCP/miR-181 mimic treated cells could reflect an increase in ROS production associated with mitochondrial biogenesis (Yoboue and Devin 2012). The role of P62/SQSTM1 is complex. P62/SQSTM1 condensate dispersal throughout the cytoplasm, seen particularly in mimic treated cells, would be consistent with its role in inducing nucleation of autophagosomal membranes through its interaction with LC3B (Sánchez-Martín and Komatsu 2018). Two forms of LC3B are present in the cell, unconjugated LC3BI and lipid membrane conjugated LC3BII. Classically, LC3B positive aggregates (punctae) are considered to be specific markers for autophagosomes, but LC3BI can form accumulations with P62/SQSTM1 in autophagy-impaired cells

(Runwal et al 2019). Co-staining of P62/SQSTM1 and LC3B in future work could confirm whether this occurs with altered miR-181 expression.

P62/SQSTM1 accumulation may be beneficial in oxidative stress by stabilising NRF2, which then induces expression of multiple antioxidant related genes, autophagy related proteins and further expression of P62/SQSTM1 itself (Sánchez-Martín and Komatsu 2018). However, as P62/SQSTM1 is removed mainly by autophagy, once bound it should be removed rapidly, and accumulation of P62/SQSTM1 inclusions are commonly interpreted as a marker of autophagy impairment (Lippai and Löw 2014). The more widespread distribution of punctate P62/SQSTM1 inclusions in the mimic treated group would be consistent with labelling of substrates for targeted autophagic degradation, although the difference between mimic and antagomiR treatments is less marked than with other proteins investigated. Parkin accumulation was evident in antagomiR treated tenocytes, but mitochondrial clusters were still visible, indicating stalled autophagy in CCCP treated cells. Distribution, however, was more concordant with that of mitochondrial staining, suggesting recruitment to dysfunctional mitochondria. Extensive mitochondrial network disruption into punctae, suggesting active mitophagy following CCCP exposure, was evident in the mimic and scrambled treated groups, but Parkin staining was inconclusive.

In conclusion, we believe our data supports the hypothesis that miR-181 regulates mitochondrial dynamics, with miR-181 upregulation increasing mitochondrial turnover, whilst inhibition of miR-181 function impedes autophagic flux. Although the mechanism remains unclear, the accumulation of Parkin in association with abnormal, 'condensed' mitochondrial networks suggests that recruitment or activation of this enzyme may be an important step. The observed downregulation of miR-181 with clinical tendinopathy in both human and equine species may, therefore, represent a reduced capacity to remove dysfunctional mitochondria and stimulate regeneration. Further investigation of the effects of miR-181 on tenocyte function is warranted, and is investigated further in Chapter 6, in a more physiologically representative model, using three-dimensional tendon constructs to further assess gene expression in concert with structural effects.

## **Chapter 6 - Functional analysis of miR-181 in equine tenocytes - 3D tendon constructs**

### **6.1 Introduction**

The investigation of pathophysiological changes occurring in tendinopathy using clinical samples from human patients often yields inconsistent results (see Chapter 1, section 1.2.1). This may be due to sample acquisition from a highly heterogeneous population with different genetic, epigenetic and lifestyle factors. Compounding this, adherence to ethical and informed consent requirements further impacts on access to samples, limiting sample numbers and uniformity of age, sex and stage and severity of disease. Typically, by the time tissues are acquired, non-surgical interventions have been attempted and disease is usually advanced. Additionally, healthy tissue without comorbidities is difficult to obtain, making tendon one of the more challenging tissues to investigate in man.

Animal models of tendinopathy present an alternative option, offering the capability for limiting environmental, population and disease variables. In addition to ethical considerations, however, there are considerable limitations in translatable integrity to human clinical disease. There is also no single, reliable mechanism for induction of clinically relevant disease in an animal model (Lui et al 2011).

Cell culture techniques allow for ultimate control over environmental conditions, and detailed interrogation of biochemical pathways, but at the expense of cells being in a very artificial milieu. Tenocytes naturally form nanotubular processes 100-500 nm in diameter, extending for several hundred micrometers and forming complex three-dimensional networks within an abundant, complex and well-organised extracellular matrix structure. Gap junctions occur between adjacent tenocytes, demonstrating a capacity for intercellular communication (Egerbacher et al 2020).

The mechanoresponsive nature of tenocytes suggests that behaviour in monolayer culture, with cells adherent to rigid tissue culture plastic, may not fully reflect the *in vivo* situation. Tissue engineering techniques involve cultivation of cells within an artificial three-dimensional extracellular matrix, providing a more physiologically appropriate environment in which to investigate function. The use of both collagen and fibrin gel scaffolds have been described for producing tendon-like tissue (Kapacee et al 2008, Kapacee et al 2010, Kharaz et al 2016). Static tension generated by maturation-contraction of a fibrin gel matrix stimulates embedded tenocytes to produce fibroblasts and linearly aligned collagen fibril bundles absent in transected, tension-free constructs or monolayer culture conditions (Kapacee et al 2008). Histological analysis of tissue-engineered tendon and ligament constructs has however demonstrated significant differences to native tissue. Kharaz and co-workers (2016) reported greater cellularity in artificially synthesised tissues, with canine-derived tenocytes exhibiting a more fibroblastic appearance than in native tendon, and a much looser matrix architecture. Additionally, natural and engineered tissues demonstrate distinctly different proteomes. Although several matrix proteins were common to both tissue types (including collagens type 1, 3, 5 and 6, decorin, biglycan, lumican and tenascin c), they represented a much smaller proportion of the overall proteins in engineered versus natural tissue (Kharaz et al 2016).

Our data from monolayer tenocyte culture suggested miR-181 levels may regulate mitochondrial turnover. Therefore, we undertook gain and loss of miR-181 function studies in fibrin gel constructs generated using equine tendon derived tenocytes. Additionally, network analysis results reported in Chapter 4 (section 4.3.2), implicated miR-181a interaction with insulin and MAPK signalling pathways (Figure 4.5). Consequently, we extended investigation of target gene expression performed in monolayer culture in Chapter 5, to include insulin-like growth factor I (*IGF1*), insulin-like growth factor I receptor (*IGF1R*), insulin receptor (*IR*) and mitogen activated protein kinase 14 (*MAPK*). Interestingly, miR-181a is one of only seven miRNAs shown to be consistently down regulated in murine and human skeletal muscle during ageing (Soriano-Arroquia et al 2016). This may imply disruption to insulin and MAPK signalling is important in age-related deterioration of skeletal muscle as well as pathological changes in tendon.

The polypeptide hormones insulin and IGF1 regulate similar cellular functions, including promoting cellular growth and differentiation, vesicle trafficking, activation of protein kinases and transcriptional activation and repression (Saltiel and Pessin 2002). The insulin and IGF1 receptors share significant sequence homology, with both consisting of disulphide-linked dimers capable of binding and activation by insulin and IGF1 (Ward and Lawrence 2009). Both phosphatidylinositol 3-kinase (PI3K) and MAPK pathways are activated downstream of insulin and IGF1, and are responsible for the majority of the mitogenic and anabolic effects of receptor activation (Rains and Jain 2011, Disser et al 2019). IGF1 is critical in tenocyte proliferation and tendon development and growth in mice, inducing expression of the transcription factors early growth response 1 and 2 and scleraxis (Disser et al 2019). IGF1 injection into the patellar tendon of men increases protein production, irrespective of recipient age (Nielsen et al 2014). In an equine model of tendinopathy, injection of IGF1 into collagenase-induced lesions increased cellularity and hydroxyproline levels (Dahlgren et al 2002). The latter study also reported reduced lesion size and perilesional swelling with IGF1 treatment, although no increase in collagen, glycosaminoglycan production, nor any histological or mechanical benefit were identified.

MAPK activation represents a point of convergence of IR/IGF1 and TGF $\beta$  signalling pathways. TGF $\beta$  is a potent inducer of scleraxis, an important regulator of extracellular matrix deposition, and critical in commitment and maintenance of progenitor cells to tenogenic differentiation (Pryce et al 2009, Tan et al 2020).

To further investigate the disruption to mitochondrial dynamics and autophagy-associated proteins suggested in Chapter 5, levels of the proteins translocase of outer mitochondrial membrane 20 (TOMM20), cytochrome c oxidase subunit 4 (COXIV), microtubule-associated proteins 1A/1B light chain 3B (LC3B), ubiquitin-binding protein p62 (P62/SQSTM1) and Parkin (PARK2), were analysed by Western blotting. Additionally, we included BCL-2 interacting protein 3 (BNIP3), lysosomal-associated membrane protein 1 (LAMP1), mitofusin 1 (MFN1), mitofusin 2 (MFN2) and nuclear factor erythroid 2 (NRF2) in our analysis.

BNIP3 can induce different forms of cell death including apoptosis, necrosis, and autophagy. The predominant mechanism is dependent on cell type and context, being associated with and without cytochrome c oxidase release, and with both caspase dependent and independent pathways. Expression is induced by hypoxia, through interaction of HIF1 $\alpha$  with binding sites in the promoter region and BNIP3 then localises to the mitochondrial membrane, inducing opening of the

mitochondrial permeability transition pore, resulting in mitochondrial depolarisation (Zhang and Ney 2009).

LAMP1 is an abundant membrane spanning glycoprotein component of the lysosomal membrane. In concert with the structurally similar LAMP2, it is estimated these produce a nearly continuous carbohydrate layer on the inner surface of the lysosomal membrane (Andrejewski et al 1999). The presence of LAMP molecules is one of the defining features of the lysosomal compartment, and their abundance and specificity are important in maintaining structural integrity of lysosomal membranes, functional competence in transmembrane trafficking and interaction with other cellular components (Eskelinen 2006). Indeed, LAMPs are critical for lysosome-autophagosome fusion in the final stages of autophagy, with autophagic activity regulating LAMP expression (Morell et al 2016).

Mitochondria are dynamic organelles, with networks undergoing frequent fusion and fission. MFN1 and MFN2 function independently and cooperatively to promote mitochondrial fusion. This process is both facilitatory for mitochondrial function and protective, providing a mechanism to restore and maintain mitochondrial membrane potential (Chen et al 2003). Three distinct molecular complexes are generated, MFN1 and MFN2 homotypic oligomers and MFN1-MFN2 heterotypic oligomers. Although both mitofusin homotypes are capable of driving mitochondrial fusion independently, their relative importance is cell type specific, and disruption to either MFN1 or MFN2 expression can lead to severe mitochondrial fragmentation (Chen et al 2003).

NRF2 is a critical transcription factor involved in the regulation of cellular antioxidant defence mechanisms. Basal levels of NRF2 are low due to KEAP1 facilitated ubiquitination. Exposure to reactive oxygen species, however, renders KEAP1 unable to bind NRF2, promoting its accumulation and subsequent transcription of cytoprotective genes (Komatsu et al 2010). NRF2 is also up regulated in response to P62/SQSTM1 accumulation occurring as a consequence of increased activation or interruption of autophagy (Komatsu et al 2010, Lau et al 2010). Increased cellular NRF2 levels also upregulate both mitochondrial biogenesis and mitophagy (Piantadosi et al 2008, Fang et al 2017).

As tendon structure is highly specialised to support its mechanical function, we additionally investigated the architectural consequences of manipulation of miR-181 levels. Histological and ultrastructural examination of constructs using transmission electron microscopy (TEM) allowed us to gain additional information on mitochondrial morphology, and a more complete picture of the impact of how miR-181 upregulation and inhibition in tenocytes influences extracellular matrix production and organisation. Our data suggests that miR-181a treated tenocytes demonstrate an increased level of autophagy and mitochondrial turnover.

## **6.2 Methods**

### **6.2.1 Generation of tendon constructs**

Tenocytes were isolated from equine SDFT samples acquired from seven donors (Table 6.1).

<b>Sample ID</b>	<b>Sex</b>	<b>Age (years)</b>	<b>Passage number</b>
EqDB1	F	9	3
EqDB3	MN	9	3
EqDB7	MN	5	3
EqDB9	F	12	3
EqDB10	F	18	3
EqDB12	F	8	4
EqDB24	F	9	3

**Table 6.1 Donor and tenocyte passage details for equine superficial digital flexor tendon-derived tenocytes used to generate three-dimensional constructs.** F = female, MN = male neutered.

Eighteen constructs were generated from each biological replicate, to allow duplicate treatments with miR-181a mimic, antagomiR and scrambled sequence control to be processed for histology, RNA and protein extraction. Additionally, untreated controls were produced for three of the biological replicates. Superficial digital flexor tendon-derived tenocytes (600,000 per construct) were seeded into pre-prepared six well plates (Chapter 2, section 2.4.2) in a fibrinogen/thrombin matrix, as described in Chapter 2, section 2.4.3 and incubated at 37°C in a 5% CO<sub>2</sub>, 5% O<sub>2</sub> atmosphere. Twenty four hours later (day 1), complete tenogenic culture medium (see Chapter 2, section 2.4.1) was treated with cholesterol-conjugated Cy5-tagged mmu-miR-181a-5p mimic, FITC-tagged 23 nucleotide (nt) single strand RNA antagomiR, or 21 nt single strand RNA scrambled control sequence oligonucleotides. Final treatment concentrations of 100 nM (miR-181a mimic and scrambled control) and 200 nM (antagomiR) were based on those optimised for use in monolayer culture (Chapter 5, section 5.3.1). Media was changed and treatments repeated every 2-3 days until constructs were harvested on day 28, when they were randomly allocated for downstream processing for either RNA extraction, protein extraction, or histological analysis (Chapter 2, section 2.4.3).

### 6.2.2 Reverse transcription quantitative real-time polymerase chain reaction

Total RNA extraction was performed on constructs from all donors. Reverse transcription to cDNA used 100 ng RNA template for gene expression and 50 ng RNA template for miRNA expression analyses. Expression of miR-181a/b/c/d was determined using commercially available primers (Qiagen, Manchester, UK, see Chapter 2, Table 2.10) and normalised to *SNORD61* as internal control (previously validated for this purpose as a stable small non-coding RNA (Chapter 5, section 5.2.2; Appendix 5, Table A5.1)). Relative expression values were then summed to give total miR-181 expression for each sample.

Primers were designed for insulin-like growth factor I (*IGF1*), insulin-like growth factor I receptor (*IGF1R*), insulin receptor (*IR*) and mitogen activated protein kinase 14 (*MAPK*), in addition to the targets previously investigated in monolayer culture (Chapter 5, section 5.2.2; peroxiredoxin 3 (*PRDX3*), peroxiredoxin 6 (*PRDX6*), sirtuin 1 (*SIRT1*), Parkin (*PARK2*), protein deglycase DJ-1 (*PARK7*), mothers against decapentaplegic homolog 7 (*SMAD7*), ubiquitin-binding protein p62 (*P62/SQSTM1*), tumour necrosis factor (*TNF*), interleukin 1 alpha (*IL1 $\alpha$* ), interleukin 1 beta (*IL1 $\beta$* ), interleukin 1 receptor accessory protein (*IL1RAP*), interleukin 7 (*IL7*), nuclear factor kappa-light-chain-enhancer of activated B cells (*NF $\kappa$ B*), translocase of outer mitochondrial membrane 20 (*TOMM20*), cytochrome c oxidase subunit I (*COXI*), cytochrome c oxidase subunit 4 (*COXIV*)).

Target expression was normalised to that of the housekeeping gene *glyceraldehyde 3-phosphate dehydrogenase* (*GAPDH*; previously demonstrated to exhibit acceptable stability for this purpose (Chapter 5, section 5.2.2; Appendix 5, Table A5.2)). Primer sequences and RT-qPCR details are listed in Chapter 2, section 2.12, Tables 2.11, 2.12 and 2.13 and Figures 2.2 and 2.3 respectively). For all RT-qPCR data, technical replicates were run in triplicate and expression relative to *SNORD61* or *GAPDH* calculated using the delta Ct method (Livak and Schmittgen 2001). For graphical representation, transcript expression was normalised to that of the scrambled control treatment group.

### 6.2.3 Protein expression

Protein extraction was performed on constructs from all donors. Following protein extraction and quantification (Chapter 2, sections 2.13.2 and 2.13.3), sodium dodecyl sulfate-polyacrylamide gel electrophoresis (SDS-PAGE) was performed using five micrograms of protein in 15  $\mu$ L loading volume. Semi-dry transfer to polyvinylidene fluoride (PVDF) membrane was confirmed using Ponceau staining prior to immunofluorescent evaluation of target proteins TOMM20, BNIP3, LAMP1, COXIV, LC3B, P62/SQSTM1, Parkin, MFN1, MFN2 and NRF2. Vinculin was used as loading control for normalisation. Images were acquired using the LI-COR Odyssey CLx Imaging System at emission wavelengths of 700 nm and 800 nm. Details of protocols and antibodies are given in Chapter 2, sections 2.14 and 2.15.

Semi-quantitative analysis of protein expression was performed by band densitometry using ImageJ 1.52 software (Rasband, W.S. U. S. National Institutes of Health, Bethesda, Maryland, USA, <https://imagej.nih.gov/ij/>, 1997-2018). Target protein band densities were measured and normalised to band intensity of corresponding vinculin loading control. Graphical representation of relative expression between groups is given in Figure 6.7.

#### **6.2.4 Histology and transmission electron microscopy**

Histological assessment was performed on constructs from all donors. For light microscopy, mounted sections were stained with haematoxylin and eosin, Masson's trichrome and elastin von Gieson's stains and imaged using a Nikon Eclipse 80i microscope (Chapter 2, section 2.16.1). Histological appearance was assessed using a novel grading scheme based on Bonar (Cook et al 2004) and Movin (Movin et al 1997) scales. Variables assessed were extracellular matrix organisation, cell shape, cell distribution cellular alignment, cellularity and collagen arrangement (Figure 6.1).

Constructs from four donors were processed for TEM. Ultrathin (60-90 nm) resin embedded sections were stained with uranyl acetate and lead citrate and viewed and imaged on a Phillips EM208S Transmission Electron Microscope at 80 kV (Chapter 2, section 2.16.2).

#### **6.2.5 Statistical analysis**

Transcript expression, protein levels and construct scoring data were analysed using GraphPad Prism version 5.01 for Windows (GraphPad Software, San Diego California USA, [www.graphpad.com](http://www.graphpad.com)). Transcript expression and construct scoring data were analysed non-parametrically using the Kruskal Wallis test with Dunn's test for pairwise comparisons. Analysis was performed between miR-181a mimic, antagomiR and scrambled control sequence treated groups. Comparisons between scrambled control sequence treated and untreated groups, where performed, utilised the Mann-Whitney test when conditions for its application were satisfied, or the Student t test where less than three data points were present in one comparator group. These results are presented in Appendix 6, Figures A6.1 and A6.3. Significance was assumed if  $P < 0.05$ . One way ANOVA was also run on histology scores for interest, but did not affect outcomes.

Protein levels derived from Western blot images were analysed using one way ANOVA with Tukey's multiple comparison test for pair-wise comparisons. Analysis was performed between miR-181a mimic, antagomiR and scrambled control sequence treated groups. Significance was assumed if  $P < 0.05$ .

Electron microscopy results are reported descriptively.

Characteristic	Score
<b>Extracellular Matrix organisation</b> <ul style="list-style-type: none"> <li>- Compact</li> <li>- In part compact, in part loose</li> <li>- Loosely composed, not orderly</li> </ul>	 2  1  0
<b>Cell Shape</b> <ul style="list-style-type: none"> <li>- Spindle-shaped (normal)</li> <li>- Mixture of spindle and round cells</li> <li>- Oval to rounded shape</li> </ul>	 2  1  0
<b>Cell Distribution</b> <ul style="list-style-type: none"> <li>- Homogenous Distribution of cells</li> <li>- Focal areas of altered cell density</li> </ul>	 1  0
<b>Cellular Alignment</b> <ul style="list-style-type: none"> <li>- Uniaxial</li> <li>- More than 50% of cell with no uniaxial alignment</li> </ul>	 1  0
<b>Cellularity</b> <ul style="list-style-type: none"> <li>- Low Cellularity</li> <li>- Intermediate Cellularity</li> <li>- High Cellularity</li> </ul>	 2  1  0
<b>Collagen arrangement</b> <ul style="list-style-type: none"> <li>- Parallel arrangement, tight cohesive bundles, homogenous polarisation pattern, normal crimping</li> <li>- Separation of individual fibre bundles, maintenance of overall bundle architecture</li> <li>- Bundle changes; loss of demarcation of bundles, loss of normal polarisation pattern</li> <li>- Marked separation of bundles, complete loss of architecture</li> </ul>	 3  2  1  0

**Figure 6.1 Modified grading scheme used for construct scoring.** Scoring system based on the Bonar (Cook et al 2004) and Movin (Movin et al 1997) scores for classification of histopathological findings of tendinopathy.

## 6.3 Results

All constructs were produced from third passage tenocytes except those from donor EqDB12. This was due to an error in thrombin/fibrinogen ratio used during preparation, resulting in batch failure three days after seeding. A subsequent set of constructs was produced successfully, but from passage four cells (Figure 6.2).

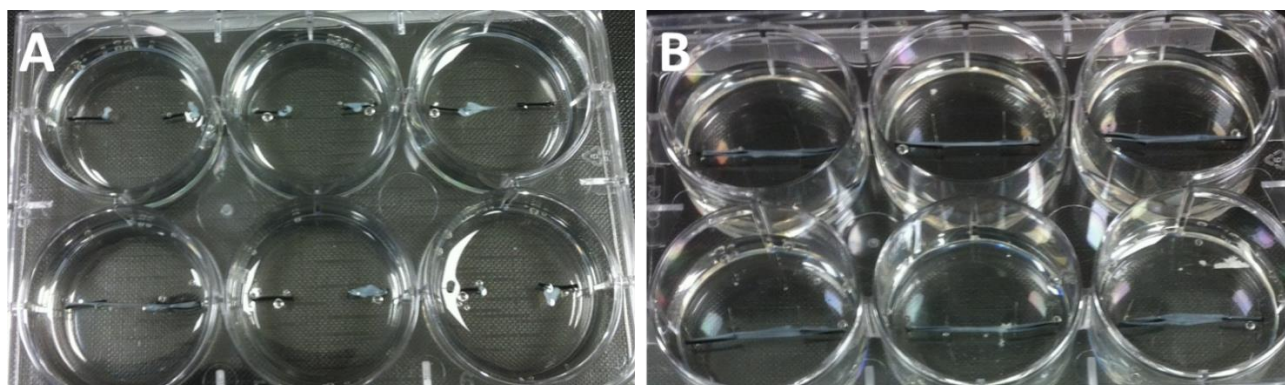


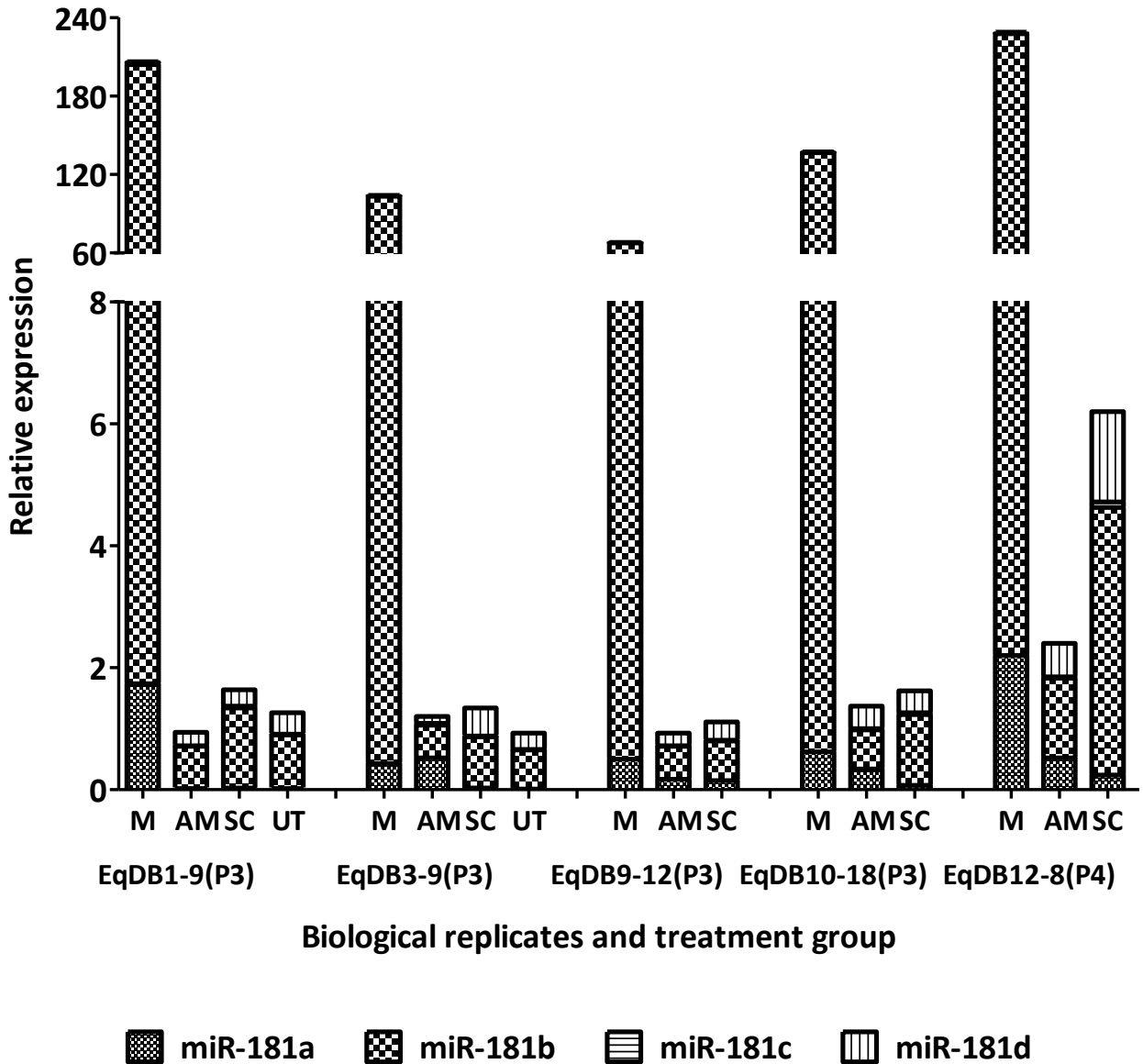
**Figure 6.2 Equine tenocyte-fibrin gel constructs from biological replicate EqDB12. A.** Constructs created from third passage tenocytes failed at 3 days due to incorrect thrombin:fibrin ratio used during preparation. **B.** Replacement constructs created using fourth passage tenocytes and correct thrombin:fibrin ratio.

Mature constructs were non-adherent to the Sylgard™ base in all cases, attached only to the anchor points at each end. Wet weights (mean  $\pm$  SD) for constructs used for RNA extraction were  $6.97 \pm 2.55$  mg and did not differ between treatment groups ( $P = 0.50$ ). Constructs for protein extraction were  $9.02 \pm 2.45$  mg; weights did not differ between treatment groups ( $P = 0.58$ ). Despite random allocation to processing pipeline, constructs used for protein extraction were significantly ( $P < 0.0001$ ) heavier than those used for RNA extraction.

### 6.3.1 Validation of miR-181a-5p overexpression and inhibition in tendon constructs

Constructs were created from seven donors. We first confirmed treatment effect by RT-qPCR evaluation of relative total miR-181 expression, normalised to *SNORD61*. Response to treatment was variable, but in all constructs analysed, miR-181a mimic treatment resulted in substantial upregulation of total miR-181. Of the four miR-181 family members, miR-181b showed greatest increase in expression in response to miR-181a mimic treatment, being responsible for 98-99% of the total miR-181 expression in this treatment group. Response to antagomiR treatment was more subtle and varied. In antagomiR treated constructs from five donors, total miR-181 expression was lower than that exhibited by the scrambled control treated group (Figure 6.3).

## Total miR-181 expression



	EqDB1				EqDB3				EqDB9			EqDB10			EqDB12		
	Mimic	AntagomiR	Scrambled	Untreated	Mimic	AntagomiR	Scrambled	Untreated	Mimic	AntagomiR	Scrambled	Mimic	AntagomiR	Scrambled	Mimic	AntagomiR	Scrambled
<b>181a</b>	1.738	0.022	0.028	0.024	0.428	0.519	0.029	0.012	0.499	0.174	0.146	0.623	0.336	0.070	2.200	0.522	0.240
<b>181b</b>	202.330	0.691	1.307	0.885	102.912	0.537	0.845	0.639	67.125	0.544	0.653	135.953	0.638	1.157	225.348	1.308	4.389
<b>181c</b>	1.449	0.005	0.030	0.006	0.253	0.025	0.012	0.010	0.171	0.008	0.008	0.320	0.020	0.034	0.574	0.022	0.087
<b>181d</b>	0.715	0.218	0.266	0.347	0.370	0.108	0.463	0.272	0.128	0.214	0.301	0.278	0.374	0.361	0.735	0.549	1.484
<b>Total 181</b>	<b>206.232</b>	<b>0.937</b>	<b>1.631</b>	<b>1.262</b>	<b>103.964</b>	<b>1.190</b>	<b>1.349</b>	<b>0.934</b>	<b>67.922</b>	<b>0.940</b>	<b>1.108</b>	<b>137.174</b>	<b>1.368</b>	<b>1.622</b>	<b>228.856</b>	<b>2.401</b>	<b>6.200</b>

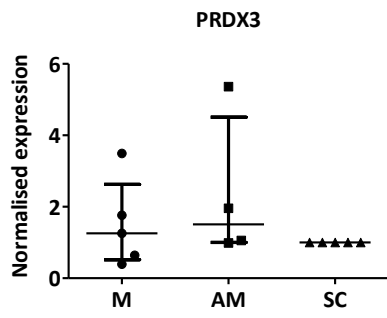
**Figure 6.3** microRNA-181 expression in mmu-miR-181a-5p mimic, antagomiR and scrambled control treated equine tendon constructs. Values represent relative expression, normalised to *SNORD61*, for all four miR-181 family members and total miR-181. Five biological replicates used for gene expression analysis. In graphical representation, M = miR-181a-5p mimic, AM = antagomiR, SC = scrambled control, UT = untreated control. Relative expression values are given in the table below graph.

### 6.3.2 miR-181a predicted target gene analysis

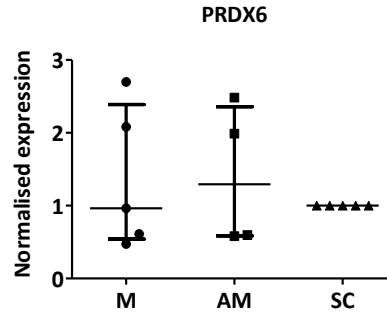
Once treatment effect was determined, target gene expression was analysed in constructs from the five donors demonstrating total miR-181 expression in the antagomiR treated group below that of the scrambled control group. Data showed considerable variability, with data points indicating exaggerated increases in relative expression displayed for *PRDX3*: antagomiR (AM) and scrambled control (SC), *PARK7*: mimic (M), *IL7*: AM, *P62/SQSTM1*: AM, *TNF*: AM, *NFκB*: AM, *PARK2*: AM, *TOMM20*: AM and SC and *COXI*: SC.

On re-examination of RT-qPCR data, the EqDB10 antagomiR treated sample was removed from analysis as the *GAPDH* Ct value was five cycles (more than three times the standard deviation) higher than the mean values for all samples. This is consistent with producing artificially elevated target gene expression values. EqDB9 was responsible for AM and SC group outliers for *PRDX3* and group M for *PARK7*. EqDB3 was responsible for SC group outliers for *TOMM20* and *COXI*. No reason to justify exclusion of these data points could be determined, therefore they were retained in the analysis.

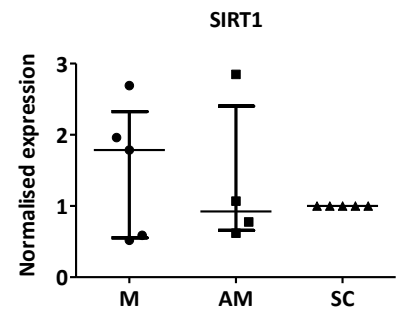
None of the 20 targets examined showed significantly different expression between treatment groups at the transcript level (Figure 6.4).



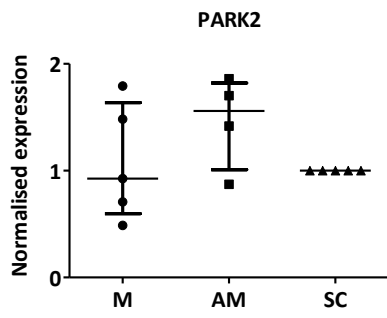
$P=0.44$



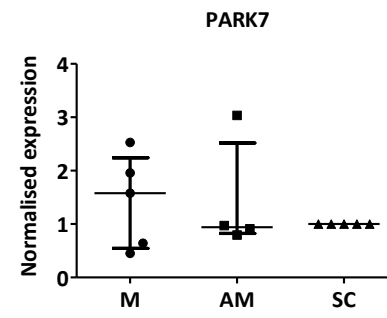
$P=0.77$



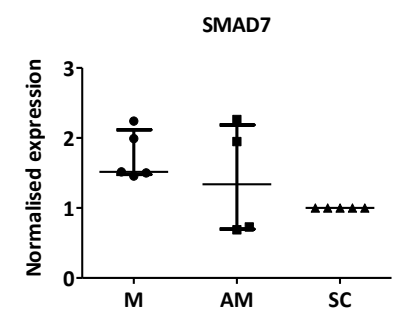
$P=0.79$



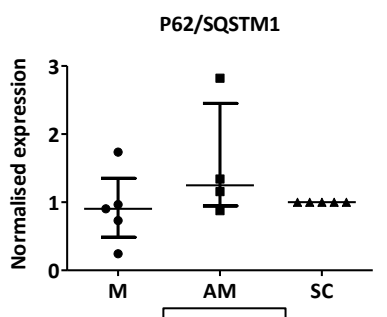
$P=0.78$



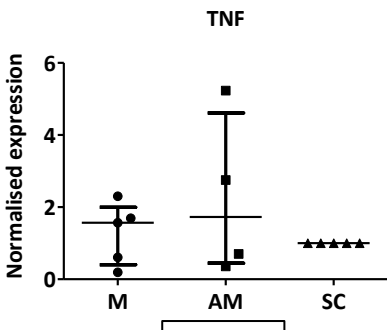
$P=0.77$



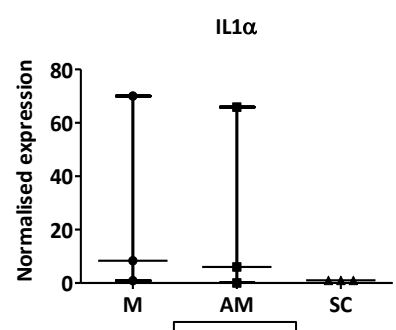
$P=0.53$



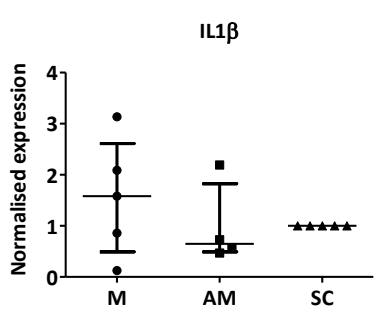
$P=0.26$



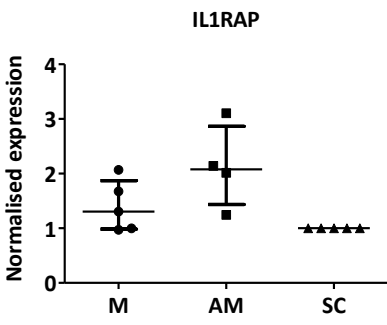
$P=0.91$



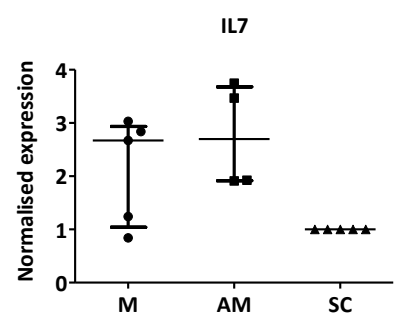
$P=0.27$



$P=0.87$



$P=0.24$



$P=0.33$

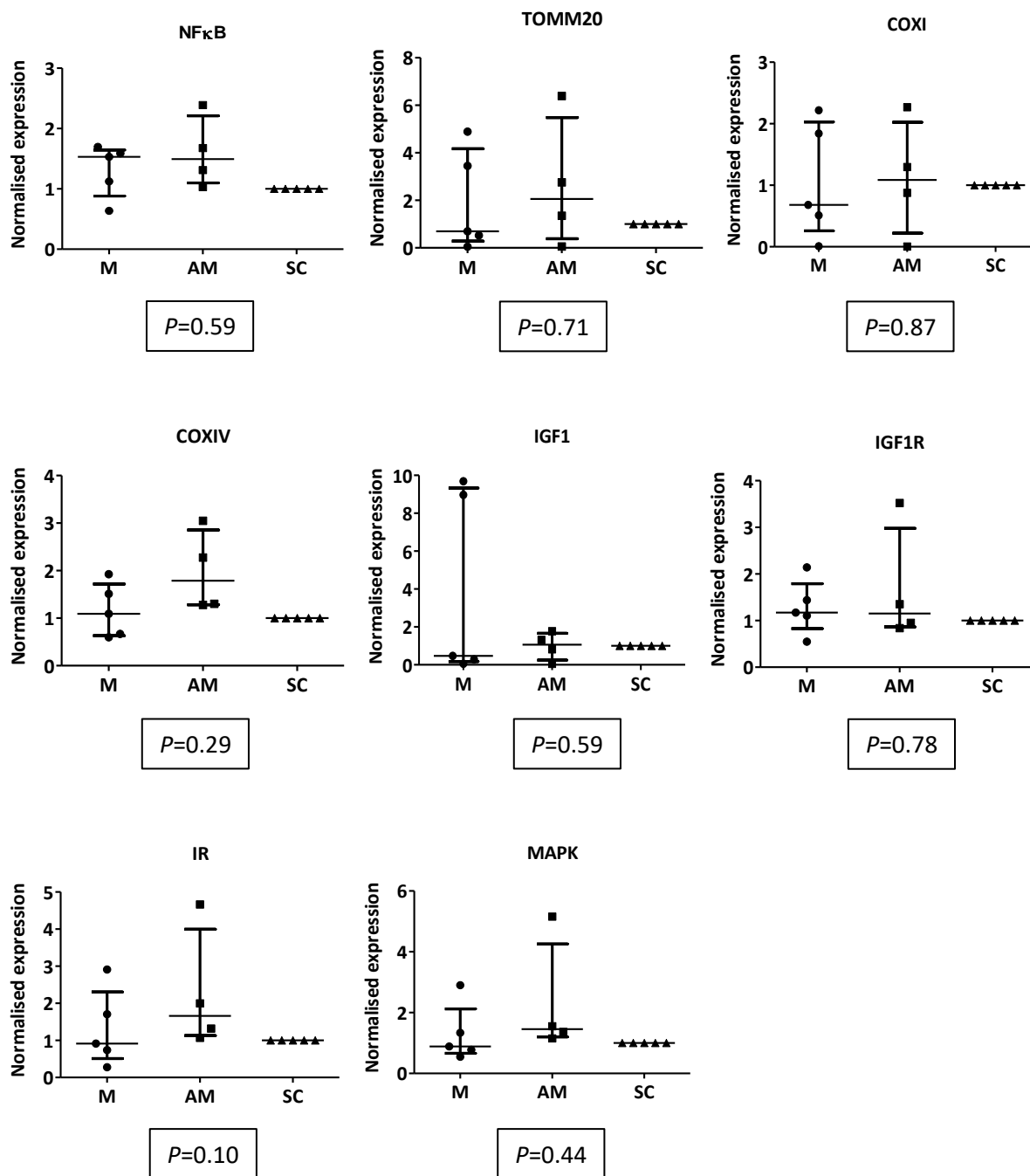


**Figure 6.4 (includes preceding page) The effects of miR-181a overexpression and inhibition on the expression of selected target genes in three-dimensional equine tenocyte-fibrin gel constructs from five biological replicates.** Y-axis values represent expression relative to *glyceraldehyde 3-phosphate dehydrogenase (GAPDH)*, normalised to scrambled control treatment group. M = miR-181a-5p mimic, AM = antagomiR, SC = scrambled control. P-values calculated from delta Ct values, using Kruskal-Wallis test with Dunn's test for pairwise comparisons. Graphs show median and interquartile range.

### 6.3.3 Protein expression

As miRNAs can regulate the expression of their targets via mRNA degradation or inhibition of translation, based on the mitochondrial turnover phenotype identified in Chapter 5, we next investigated the effect of miR-181a mimic and antagomiR treatments on expression of the autophagy- and mitochondria-related proteins TOMM20, COXIV, LC3B, P62/SQSTM1, Parkin, BNIP3, LAMP1, MFN1, MFN2 and NRF2. Size of constructs precluded division for processing for both protein and RNA extraction to confirm miR-181a treatment effect. Results from constructs for all seven donors are therefore presented.

Loading 5 µg protein per lane for SDS-PAGE generated detectable fluorescent signal for TOMM20, BNIP3, LAMP1, COXIV, LC3B and P62/SQSTM1, but not MFN1, MFN2, NRF2 or Parkin. Samples were re-run for these targets using 10 µg protein per lane, and produced useable data for NRF2 and Parkin, but still failed to produce detectable signal for MFN1 and MFN2.

All mmu-miR-181a-5p mimic treated constructs demonstrated a strong, broad signal at approximately six kilo Daltons (kDa), with two to three fainter parallel bands proximally, between the 8 and 15 kDa markers. This phenomenon was evident prior to membrane incubation with Ponceau stain, primary, or secondary antibodies (Figure 6.5), and following incubation with primary and secondary antibodies directed against all targets (see Appendix 6, Figure A6.2). Whilst this may be due to protein degradation, it is most likely artefact related to the fluorescent Cy5 label carried by the miR-181a mimic treatment. Interestingly, we did not see this signal in the immunofluorescence images from monolayer culture work reported in Chapter 5 (Figure 5.5). Emission maximum for Cy5 is 694 nm, consistent with observed signal detection at 700 nm, but absent at 800 nm on the imaging platform used. The signal was also detected directly after electrophoretic transfer of protein to PVDF membranes, prior to incubation with any stains or antibodies. The mass of the double stranded RNA mimic is approximately 13 kDa and that of the denatured fluorescent strand approximately 6.5 kDa, consistent with the position of the bands observed (Horizon Discovery Ltd, Cambridge, UK, technical support, personal communication).



**Figure 6.5 Fluorescence associated with Cy5 labelling of mmu-miR-181a-5p mimic treatment is preserved during protein extraction from fibrin gel equine tendon constructs, SDS-PAGE and electrophoretic transfer to polyvinylidene fluoride (PVDF) membrane, and visible on subsequent fluorescent imaging.** Images are of PVDF membranes from seven biological replicates prior to application of Ponceau stain or incubation with primary or secondary antibodies. SDS-PAGE = sodium dodecyl sulfate-polyacrylamide gel electrophoresis, M = mimic treated, AM = antagomiR treated, SC = scrambled control treated, UT = untreated. Images acquired using LI-COR Odyssey CLx Imaging System at 700 nm wavelength.

We assumed miR-181a treatment success in constructs analysed for protein levels, was analogous to that determined by RT-qPCR in constructs processed for gene expression (Figure 6.3). Additionally, none of the primary antibodies used have documented reactivity with equine proteins. Specific immunogenic sequences against which antibodies were raised were available for anti-BNIP3, -COXIV, -LAMP1, -LC3B, -MFN1, -MFN2 and -NRF2 antibodies. For those directed against P62/SQSTM1, Parkin, TOMM20 and Vinculin, immunisation was specified as being against the full length protein (abcam plc, Cambridge, UK, technical support, personal communication). Sequence alignment was performed to determine homology with the corresponding equine proteins using the Basic Local Alignment Search Tool (BLAST; National Center for Biotechnology Information, Bethesda, USA), with results given in Table 6.2. Greater than 85% homology of immunogen sequences is recommended to support likely cross-reactivity with a novel protein (abcam plc, Cambridge, UK, technical support, personal communication).

Protein	Epitope	Homology (%)
BNIP3	Amino acids 95-200	95
COXIV	Amino acids 128-169	76
LAMP1	Amino acids 76-311	73
LC3B	Amino acids 1-100	100
MFN1	Amino acids 1-741	59
MFN2	Amino acids 661-757	98
NRF2	Amino acids 108-413	86
P62/SQSTM1	Whole protein	93
Parkin	Amino acids 399-465	94
TOMM20	Whole protein	99
Vinculin	Whole protein	89

**Table 6.2 Sequence homology between immunogen epitopes and corresponding equine protein sequences.** BNIP3 = BCL-2 interacting protein 3, COXIV = cytochrome c oxidase subunit 4, LAMP1 = lysosomal-associated membrane protein 1, LC3B = microtubule-associated proteins 1A/1B light chain 3B, MFN1 = mitofusin 1, MFN2 = mitofusin 2, NRF2 = nuclear factor erythroid 2, P62/SQSTM1 = ubiquitin-binding protein p62, PARK2 = Parkin, TOMM20 = translocase of outer mitochondrial membrane 20. Sequence homology determined using Protein BLAST (National Center for Biotechnology Information, Bethesda, USA).

Images of sufficient quality for semi-quantitative analysis of protein expression were obtained with all samples for TOMM20, five samples for LC3B and NRF2, four samples for BNIP3 and three samples for Parkin, P62/SQSTM1, LAMP1 and COXIV. MFN1 and MFN2 were not quantifiable.

The autophagy receptor protein P62/SQSTM1 was significantly up regulated with antagomiR treatment, indicating either an increase in autophagy, or a chronic elevation consistent with autophagy stalling (Figure 6.6 (E) and Figure 6.7). Accumulation of P62/SQSTM1 is protective in ROS-mediated cell death, by exerting a permissive effect on NRF2 mediated upregulation of antioxidant gene transcription (Park et al 2015). However, P62/SQSTM1 is removed mainly by autophagy and, once bound to a ubiquitinated substrate, is rapidly degraded. Accumulation is therefore commonly interpreted as a marker of autophagy impairment (Lippai and Löw 2014). However, poor quality Western blots, with undetectable signal in four of the biological replicates, limited the number of samples available for analysis.

The transcription factor NRF2 was quantifiable in five of the biological replicates, with undetectable signal in the remaining two. Significant upregulation of NRF2 was seen in miR-181a mimic treated constructs (Figure 6.6 (C) and and Figure 6.7). This was interesting, given the elevation of P62/SQSTM1 identified in the antagomiR treated group, and the reported effect of P62/SQSTM1 accumulation on stabilising NRF2 levels (Park et al 2015). However, this is still consistent with a cellular response to oxidative stress and upregulation of both mitochondrial biogenesis and mitophagy in the miR-181a mimic treated group, and suggests that permissive effect of P62/SQSTM1 on NRF2 levels may be weak and obscured by a more robust direct response associated with mitochondrial turnover (Piantadosi et al 2008, Fang et al 2017).

Despite low sequence homology, COXIV signal was detectable in all biological replicates as two bands of approximately 15 and 20 kDa, but was only quantifiable in three of these (Figure 6.6 (H), Appendix 6, Figure A6.2). COXIV is an important regulatory subunit of the cytochrome *c* oxidase complex and, whilst located on the inner mitochondrial membrane, is encoded by nuclear DNA (Hao et al 2018). Two isoforms of COXIV, COXIV-1 and COXIV-2 have been identified (Hüttemann et al 2001), but only differ in molecular weight by approximately 1 kDa. Previous work in our group with other cell types identified the lower molecular weight band as the region of interest and we used this for quantification. Based on this, COXIV demonstrated a significant upregulation in the miR-181a mimic treated group (Figure 6.7), consistent with increased mitochondrial biogenesis and optimising efficiency of the mitochondrial respiratory chain (Hao et al 2018), supporting the finding of increased NRF2 in this group. COXIV undergoes a range of post-translational modifications (acetylation, methylation, succinylation, phosphorylation and ubiquitination are all described (Hornbeck et al 2015)) which may result in detection of unexpected molecular weight products. Alternatively, this may be an off-target interaction.

TOMM20 is a major component of the mitochondrial translocation complex, with a crucial role in mitochondrial biogenesis, capable of direct recognition of cytosolic mitochondrial protein precursors (Hernández et al 1999). TOMM20 was detected and quantifiable in all samples, but its expression did not differ between treatment groups. Encoded by the nuclear genome, the stability of this marker of mitochondrial abundance implies a balance in mitochondrial biogenesis irrespective of applied treatment (Figure 6.6 (A) and Appendix 6, Figure A6.2).

BNIP3 specifically localises to mitochondria. Under conditions of oxidative stress, BNIP3 expression is up regulated by HIF1 and activated by oxidation of an N-terminal cysteine residue (Gustafsson 2011). Activation results in depolarisation of the mitochondrial membrane, mediated by the proapoptotic BCL2 family members BAX and BAK, and/or opening of the mitochondrial permeability transition pore. These mechanisms precipitate apoptosis via cytochrome *c* and reactive oxygen species (ROS) release, with or without caspase activation (Zhang and Ney 2009, Gustafsson 2011). BNIP3 also possesses an LC3B-interacting domain, conferring ability to facilitate mitochondrial turnover by targeting mitochondria for removal by autophagosomes (Gustafsson 2011). BNIP3 quantification was possible in four of the biological replicates, with undetectable signal in the remaining three. Similar to NRF2 and COXIV, BNIP3 was significantly up regulated in miR-181a mimic treated constructs, indicating an increase in mitophagy and mitochondrial-mediated catabolic pathways in this group (Figure 6.6 (D) and Figure 6.7).

LC3B signal was detected in all samples as two bands at approximately 14 and 16 kDa. This is consistent with cleavage of the LC3B precursor molecule by autophagy related 4B cysteine peptidase (ATG4B) to form LC3BI (detected at 16 kDa). LC3BI is activated by autophagy-related protein 7 (ATG7), transferred to autophagy-related protein 3 (ATG3) and conjugated to phospholipid to form LC3BII. LC3BII is the form associated with isolation membranes and autophagosomes, and detected at 14 kDa (Mizushima and Yoshimori 2007). Failure of transfer of the loading control precluded quantification in two of the replicates. Neither LC3BI or II were differentially expressed between treatment groups, but the relative proportions of the two forms, as expressed by the LC3BII/I ratio, appeared to alter. A higher ratio was found in the miR-181a mimic treated group, but this difference did not reach statistical significance (Figure 6.6 (B) and Figure 6.7).

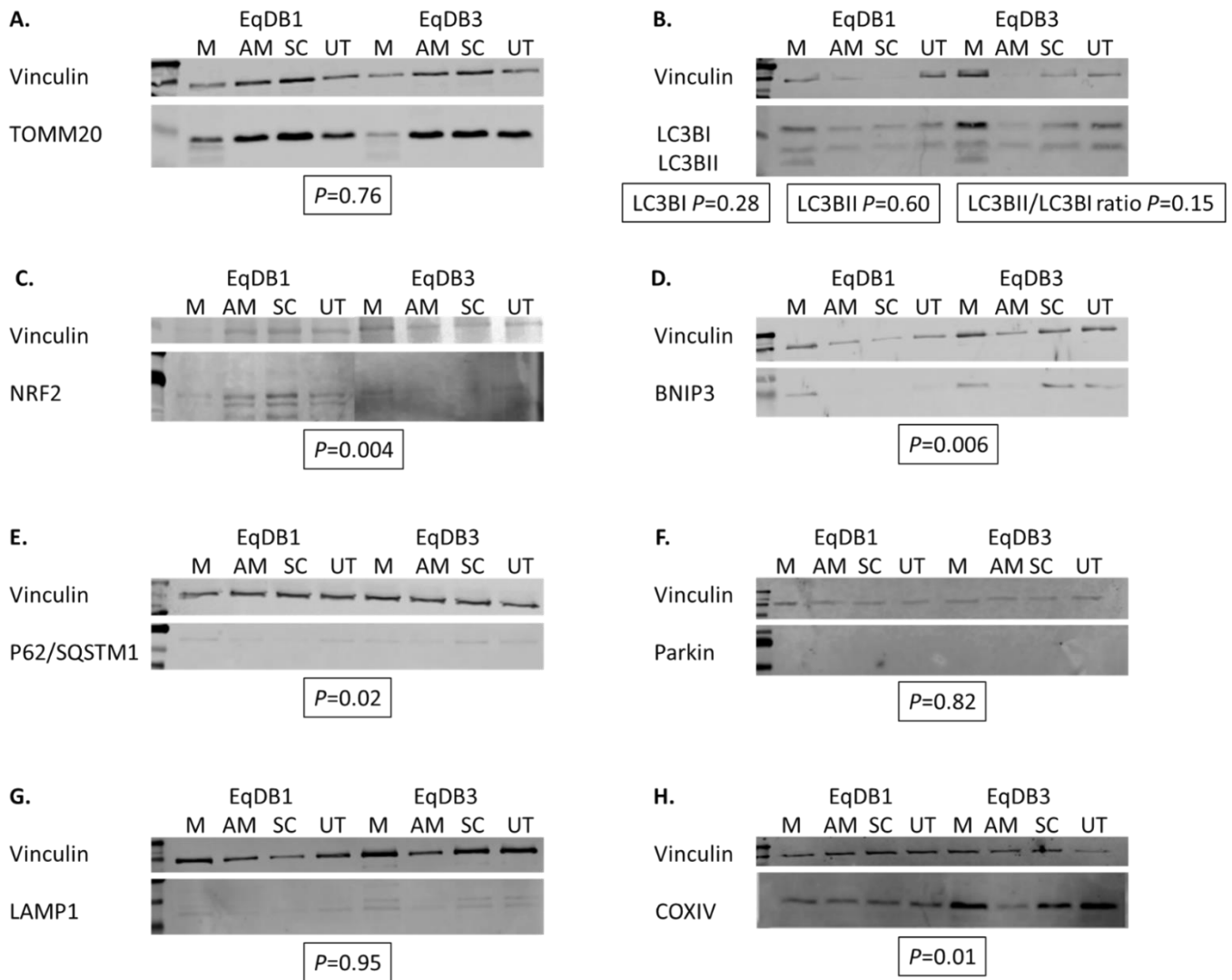


**Figure 6.6 Representative Western blot images from mmu-miR-181a-5p mimic (M), antagomiR (AM) and scrambled control (SC) treated equine tendon constructs. A.** TOMM20 predicted molecular weight 16 kDa. **B.** LC3B predicted molecular weights; LC3BI 16 kDa, LC3BII 14 kDa. **C.** NRF2 predicted molecular weight 61 kDa. **D.** BNIP3 predicted molecular weight 22 kDa. **E.** P62/SQSTM1 predicted molecular weight 61 kDa. **F.** Parkin predicted molecular weight 52 kDa. **G.** LAMP1 predicted molecular weight 45 kDa. **H.** COXIV predicted molecular weight 17 kDa. Vinculin used as loading control, predicted molecular weight 124 kDa. UT = untreated. Images acquired using LI-COR Odyssey CLx Imaging System at emission wavelengths 700 nm (vinculin) and 800 nm (all other targets). *P*-values calculated using one way ANOVA with Tukey's multiple comparison test for pairwise comparisons (see also Figure 6.7). See Appendix 6, Figure A6.2 for all images.

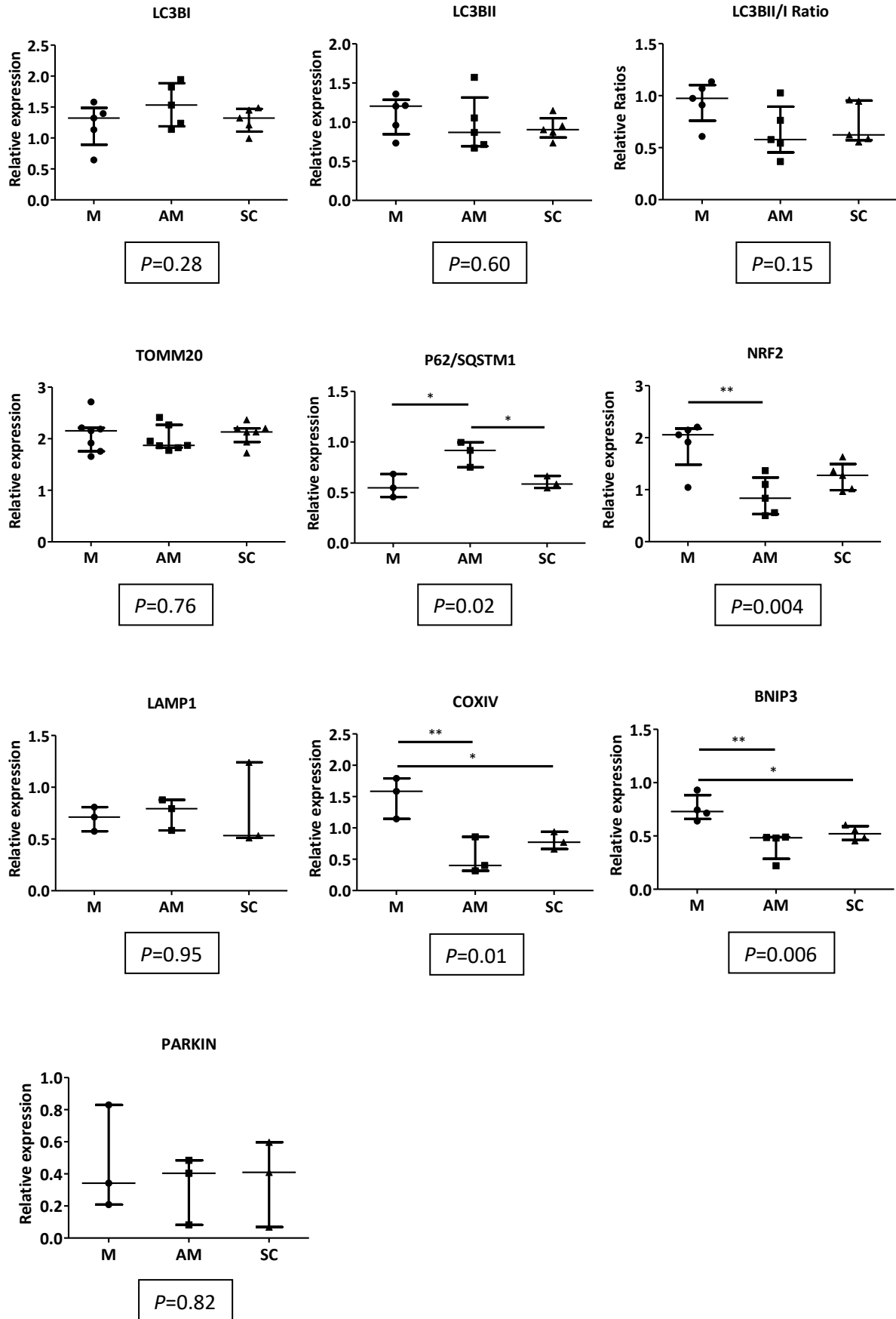


**Figure 6.7 (preceding page) Target protein levels in mmu-miR-181a-5p mimic (M), antagomiR (AM) and scrambled control (SC) treated equine tendon constructs from five biological replicates.**

Fluorescent images acquired using LI-COR Odyssey CLx Imaging System at emission wavelengths 700 nm (vinculin) and 800 nm (all other targets). Expression calculated using densitometric analysis in ImageJ 1.52 software (<https://imagej.nih.gov/ij/>, 1997-2018), normalised to vinculin as loading control. *P*-values calculated using one way ANOVA with Tukey's multiple comparison test for pairwise comparisons. \* = *P* < 0.05, \*\* = *P* < 0.01.

### **6.3.4 Role of miR-181 in regulation of mitochondrial dynamics**

Next, to evaluate mitochondrial morphology and evidence of autophagy, we evaluated construct cellular morphology at the ultrastructural level using TEM. Representative electron micrographs are shown in Figure 6.8. Scattered necrotic and apoptotic cells were evident in all samples, but in general cells appeared alive with a good nuclear morphology. In scrambled control treated samples, some mitochondria were swollen, but most were of normal appearance (Figure 6.9). Swelling of mitochondria, with loss of cristae was seen in some antagomiR treated samples, showing a general degenerative process, which could potentially lead to cell death (Figure 6.9). In miR-181a mimic treated samples there were normal and swollen mitochondria, although number of abnormal mitochondria appeared to be greatest in this group. There was also an increased number of structures consistent with lysosomes. Some structures identified in the miR-181a mimic treated constructs could represent late stage autophagolysosomes containing mitochondria (Figures 6.9 and 6.10). These data suggest that miR-181a up regulated mitophagy, consistent with data in Chapter 5 showing changes in mitochondrial turnover in response to miR-181a mimic treatment or inhibition.

Three types of mitophagy have been described. Types 1 and 2 result in production of mitophagosomes, membrane bound vesicles containing degenerate mitochondria, which subsequently fuse with lysosomes. Type 3 mitophagy, also termed micromitophagy, results in formation of distinctive multivesicular bodies from sequestration of small mitochondrial-derived vesicles (Lemasters 2014). Some rare doughnut shaped or ring mitochondria were evident, which may be consistent with Type 1 or 2 mitophagy (Figure 6.10). There was no evidence of micromitophagy in any of the samples. None of the structures identified were definitive for mitophagy, or micromitophagy, but equally, these cannot be ruled out. These processes can only be definitively proven by visualising the early phase where a mitochondrion is surrounded by a membrane or a multivesicular body is formed (Lemasters 2014). Myelin figures were also present in both miR-181a mimic and antagomiR treated samples, which could be representative for autodigestion of material.

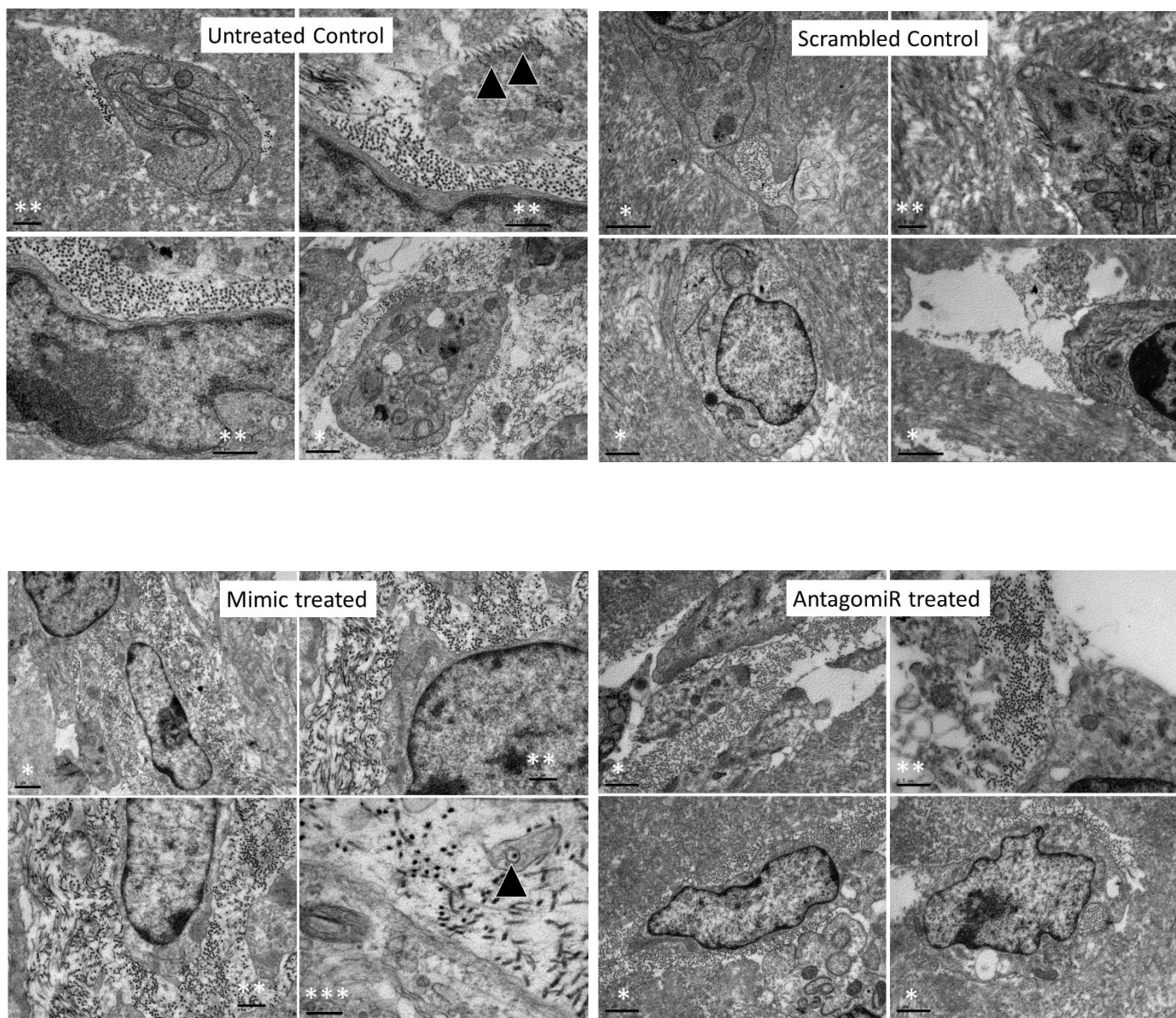


**Figure 6.8 Representative transmission electron micrographs of equine tendon construct ultrastructure.** Black arrowheads indicate fibripositors (untreated control and miR-181a mimic treated sections). Bar: \* = 1  $\mu\text{m}$ , \*\* = 0.5  $\mu\text{m}$ , \*\*\* = 0.2  $\mu\text{m}$ .

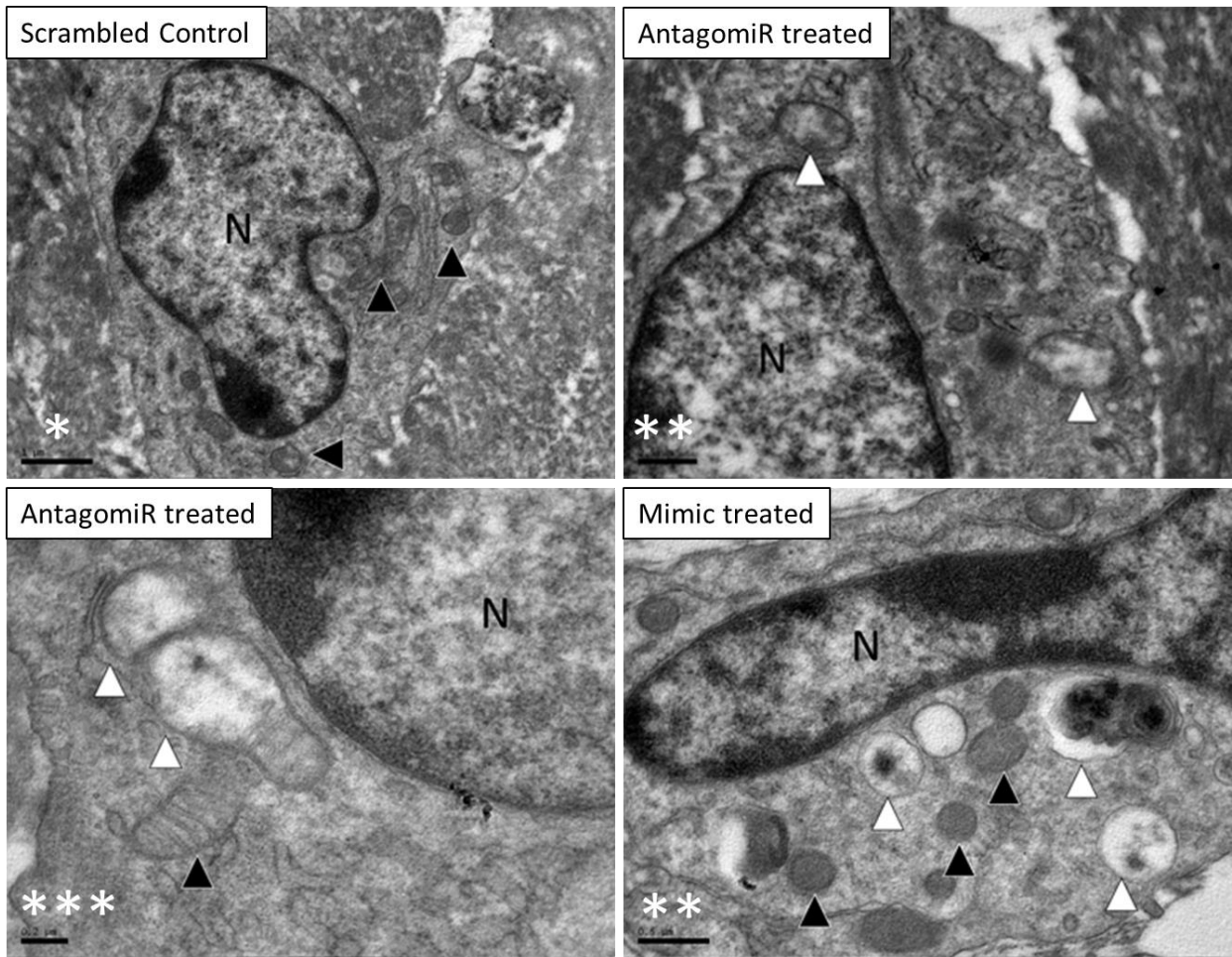


**Figure 6.9 Representative transmission electron micrographs of mitochondrial morphology of equine tendon constructs.** N = nucleus, black arrowheads = normal mitochondria, white arrowheads = pathological mitochondria demonstrating swollen appearance with loss of cristae. Bar: \* = 1 μm, \*\* = 0.5 μm, \*\*\* = 0.2 μm.

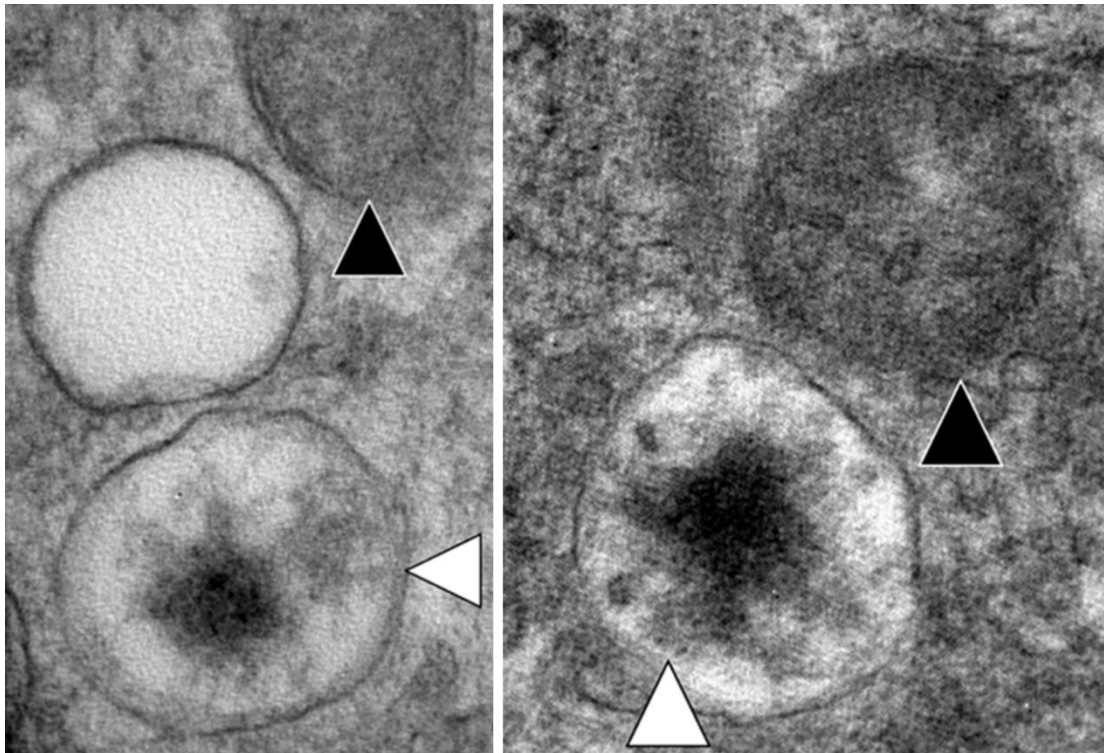


**Figure 6.10 Transmission electron micrograph of mmu-miR-181a-5p mimic treated sample.** Image showing higher magnification of mitochondria. Black arrowheads indicate normal mitochondria, white arrowheads indicate possible late stage pathological mitochondria, characterised by ring or doughnut shape, consistent with the appearance of late stage autophagolysosomes containing mitochondria.

### 6.3.5 Role of miR-181 in regulation of tendon construct structure

Finally, to assess whether manipulation of miR-181 levels resulted in observable structural differences in our constructs, we evaluated TEM images in conjunction with routine histological preparations of constructs from all seven biological replicates.

In TEM images, collagen fibrils were evident in sections from all treatment groups, showing typically parallel arrangement and alignment with the long axis of the constructs. Structures consistent with the appearance of fibrilpositors were occasionally identified in sections from untreated control and miR-181a mimic treated groups, indicating active collagen fibril deposition in the extracellular matrix (Figure 6.8). Despite the lack of observed fibrilpositors in antagomiR and scrambled treated constructs, alignment and arrangement of collagen fibrils indicated that fibril deposition had occurred by a similar mechanism to those in the miR-181a mimic and untreated control groups.

Transverse sections demonstrated constructs were roughly cylindrical in shape, with distinct septae dividing regions of more densely staining tissue, reminiscent of tendon fascicular structure. Subjectively, miR-181a mimic treated constructs presented a more irregular, disorganised structure than other treatment groups (Figure 6.11).

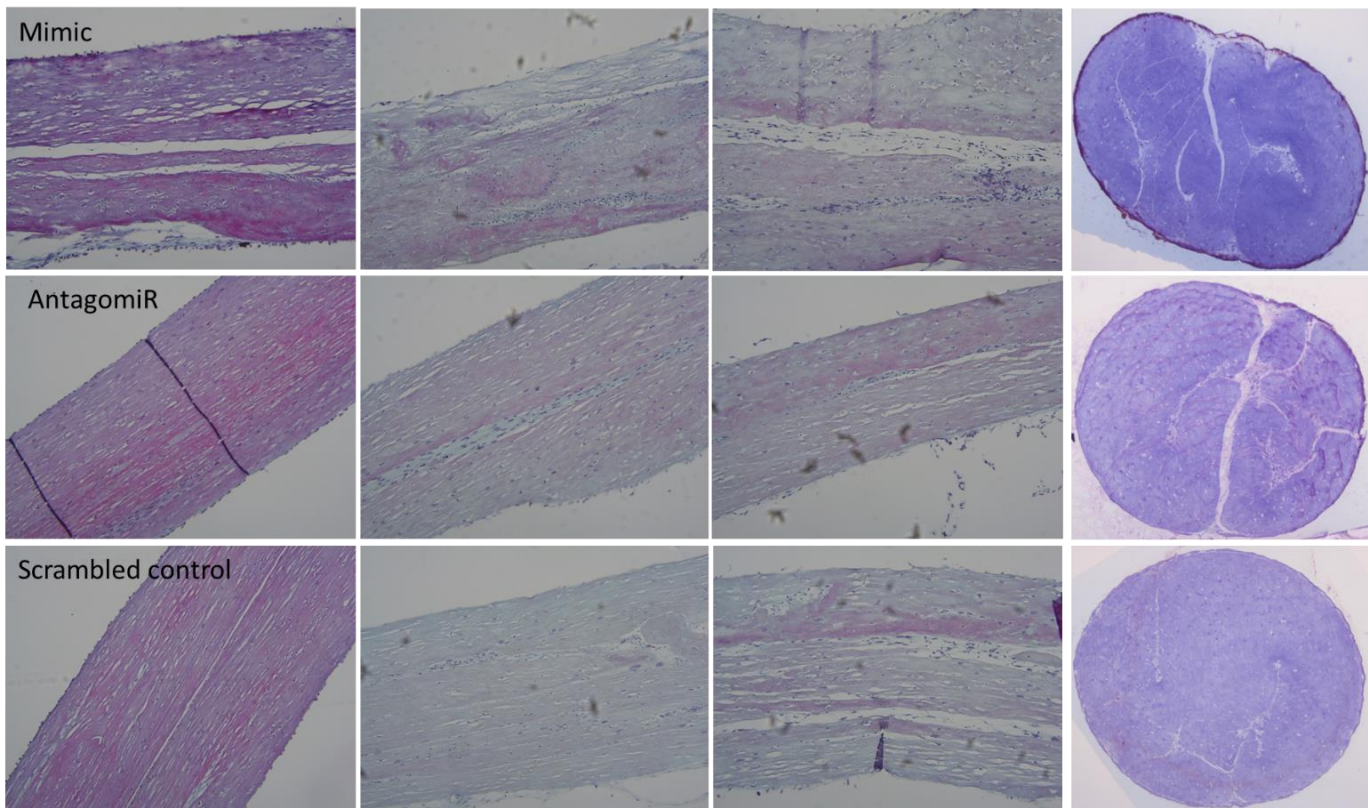


**Figure 6.11** Longitudinal and transverse sections of mmu-miR-181a-5p mimic, antagomiR and scrambled control treated equine tendon constructs. Representative images from one donor illustrate: top row - mimic treated constructs, middle row – antagomiR treated constructs; bottom row scrambled control treated constructs. 10 x magnification, longitudinal sections stained with Masson's Trichrome, transverse sections with Toluidine blue stain.

To objectively assess the effects of miR-181a mimic and antagomiR treatment on the histological appearance, we employed a novel grading scheme. This scheme evaluated six attributes of the constructs, generating a total score between zero and 11. We first confirmed the ability of our devised scheme to differentiate between constructs subjectively evaluated as representative of extremes of histological appearance (Figure 6.12).

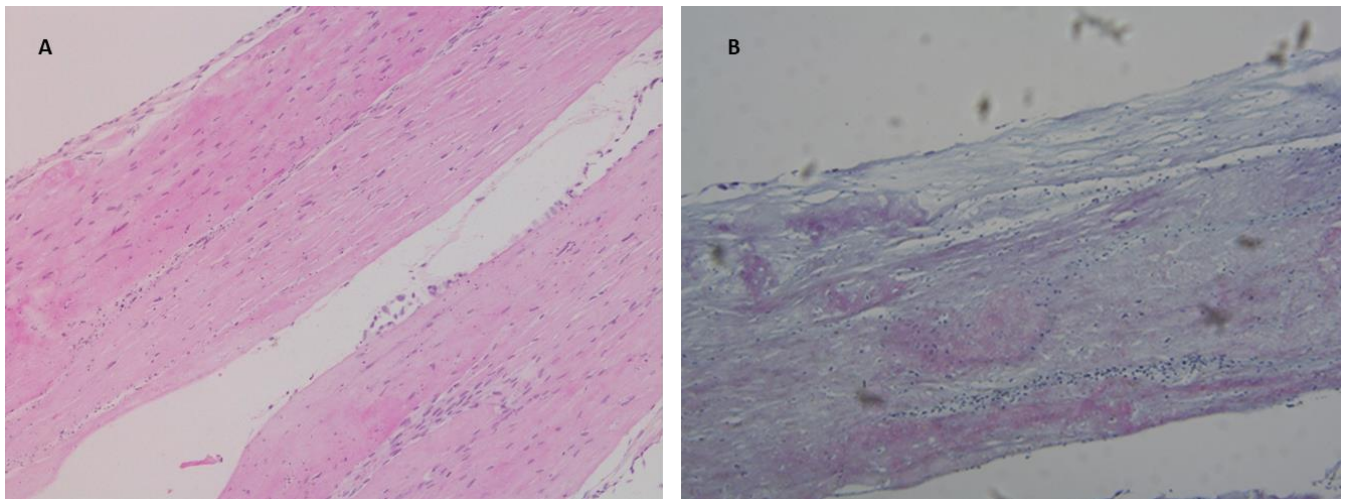
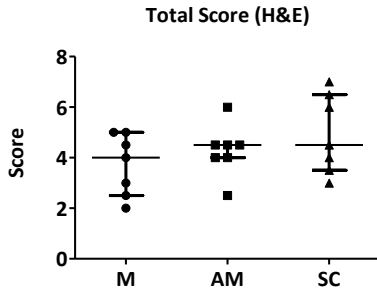


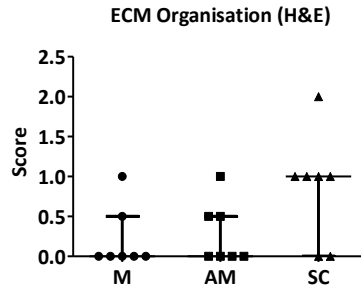
**Figure 6.12 Differentiation of construct architecture using a novel grading scheme. A.** Total score = 0 - 'normal' tendon structure (H&E 10 x magnification). **B.** Total score = 10, - 'abnormal' tendon structure (Masson's Trichrome 10 x magnification).

Elastin von Gieson's staining was poor, resulting in 16/144 (11%) missing values. Consequently, these sections were excluded from further analysis and only haematoxylin and eosin (H&E) and Masson's Trichrome stained sections evaluated. Constructs were graded independently by two operators blinded to treatment group. Results of independent gradings and the average of their combined scores are given in Figures 6.13, 6.14 and 6.15 respectively. There was no significant difference between treatment group scores generated using either total score or assessing each variable independently. This applied to analyses from each independent grader's scoring, or if both grader's scores were averaged. This did not change if results were analysed either by one way ANOVA or Kruskal Wallis tests. Comparison of histology of scrambled control treated and untreated constructs is given in Appendix 6, Figure A6.3.

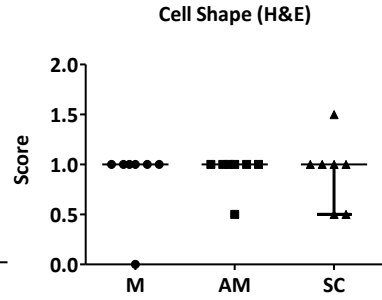
We investigated inter- and intra-rater repeatability of the scoring system using Cohen's kappa coefficient ( $\kappa$ ). Intra-rater repeatability showed substantial agreement for total scores, whilst individual components of the grading scheme varied widely from agreement equivalent to chance to near perfect agreement (Table 6.3). There was a difference between individual components depending on staining method used, with cell distribution performing worst in H&E stained sections and cell shape weakest in Trichrome stained sections.



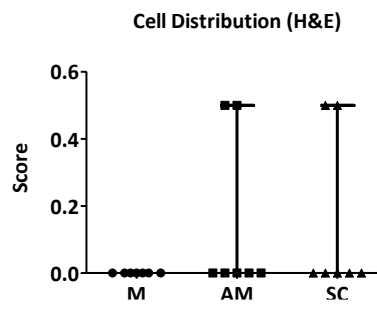
$P = 0.45$



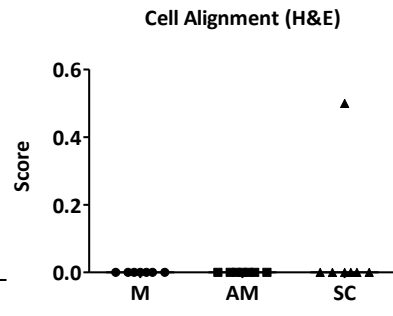
$P = 0.10$



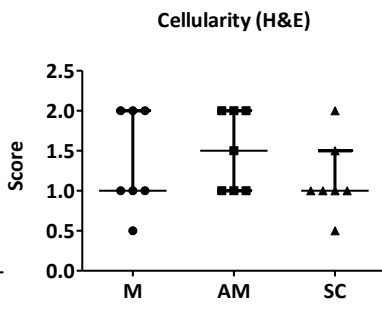
$P = 0.99$



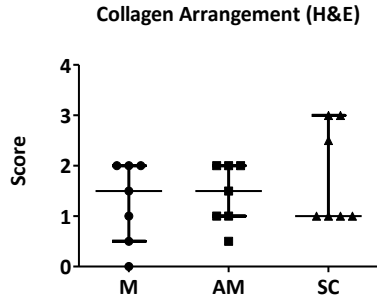
$P = 0.31$



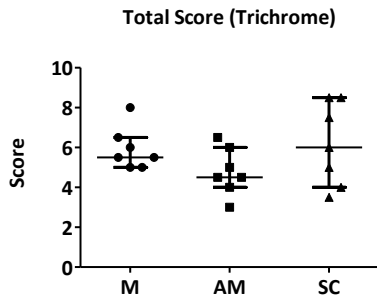
$P = 0.37$



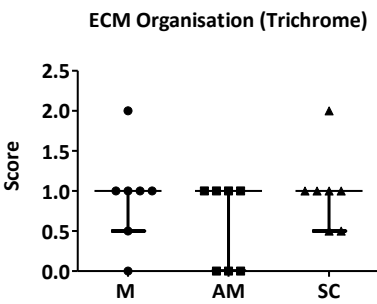
$P = 0.45$



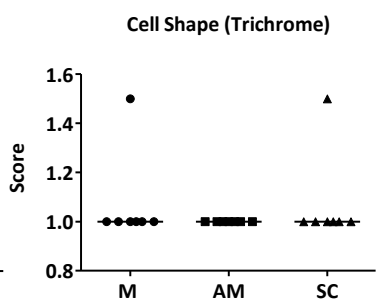
$P = 0.67$



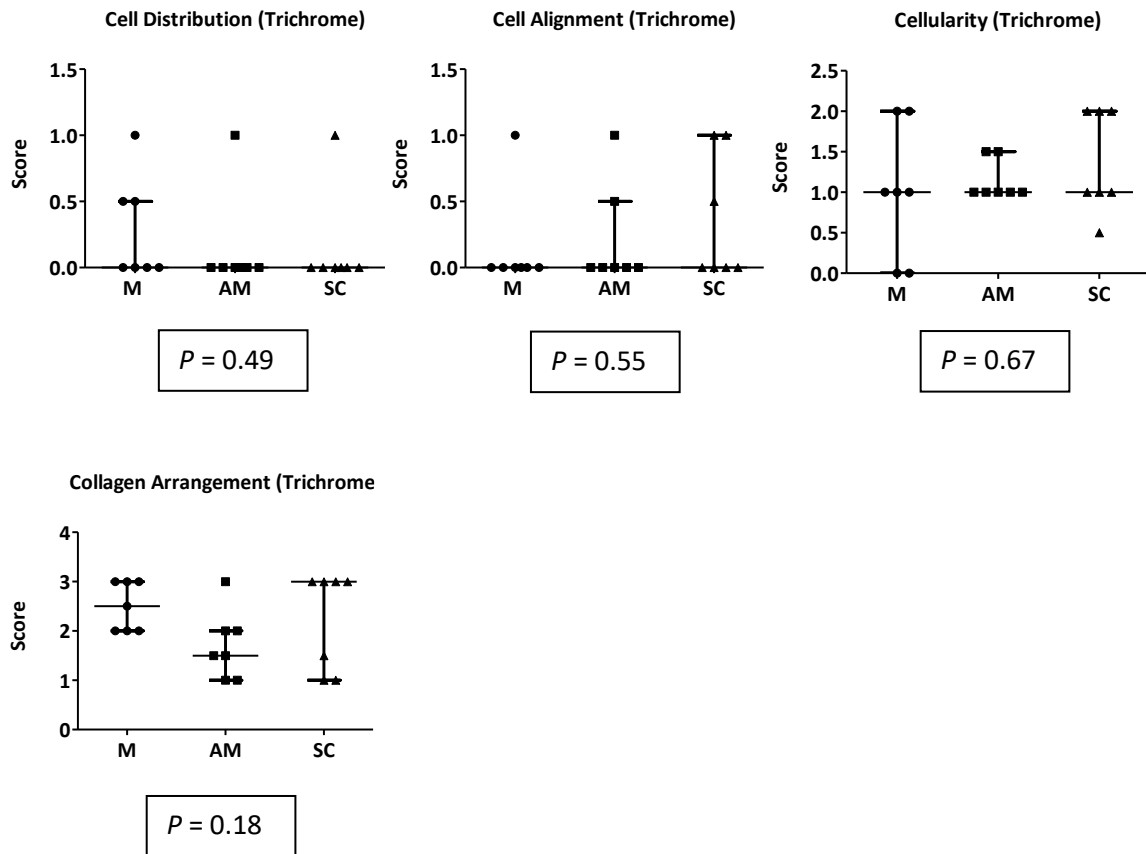
$P = 0.24$



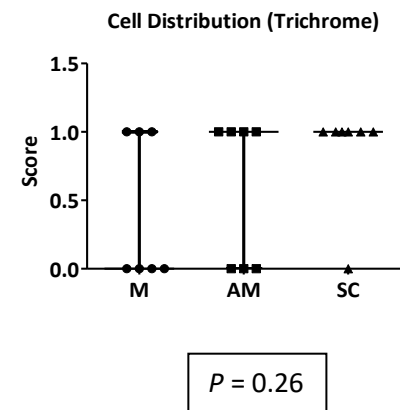
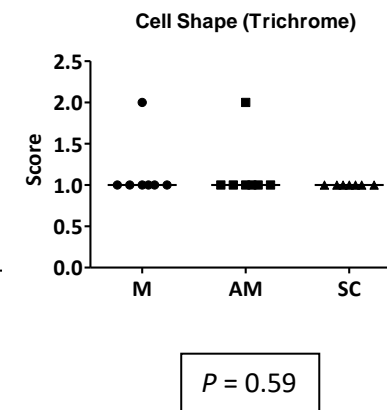
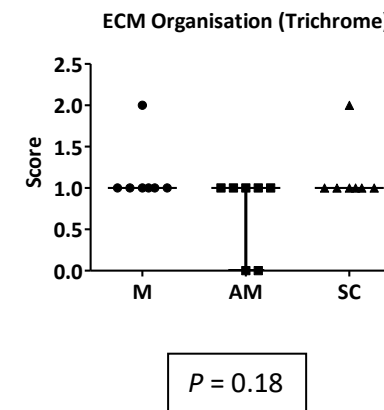
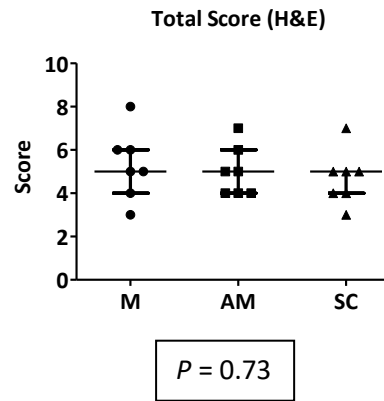
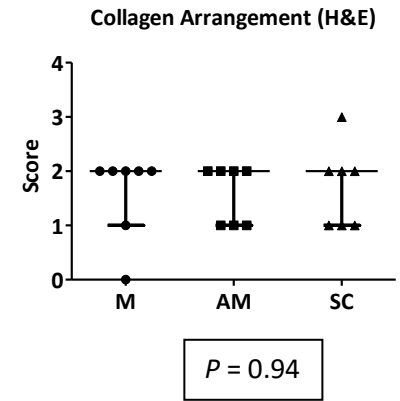
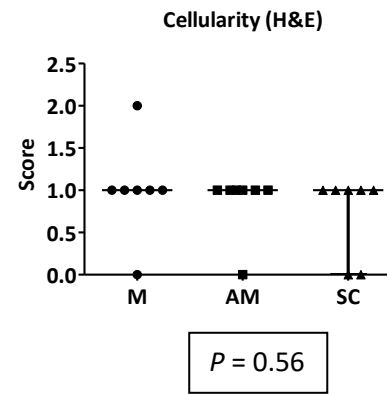
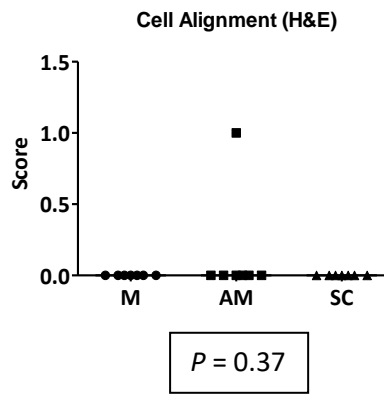
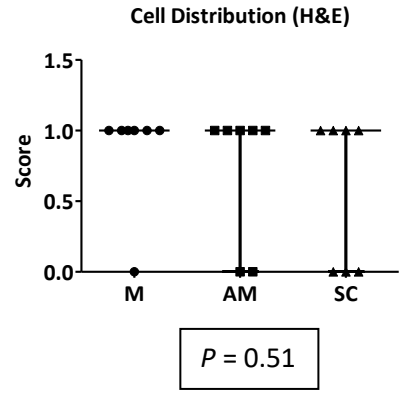
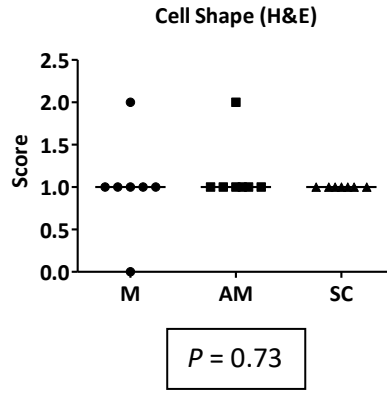
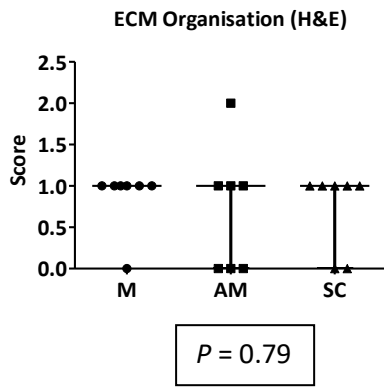
$P = 0.43$



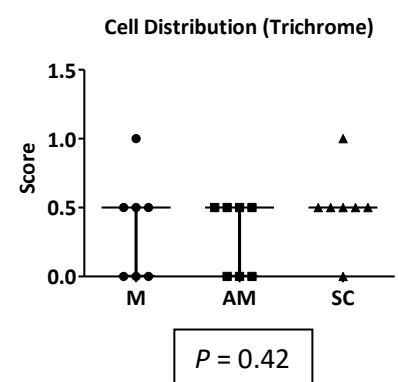
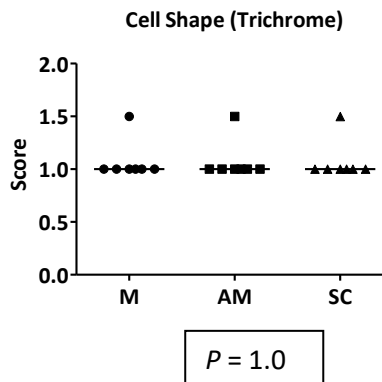
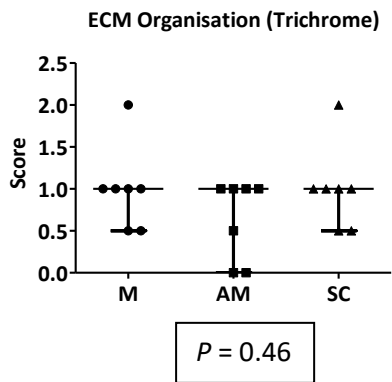
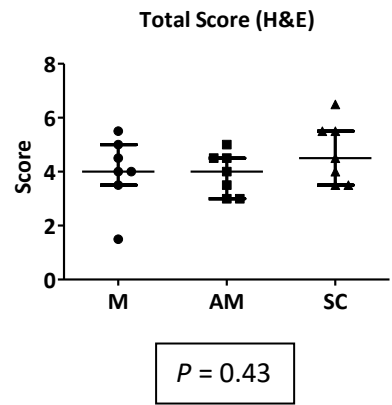
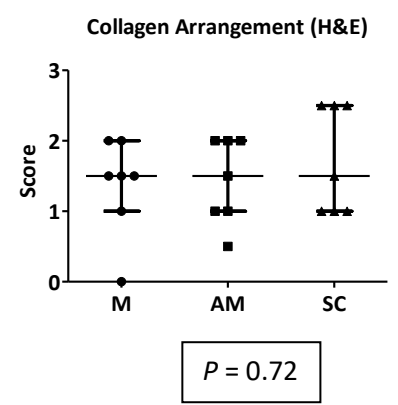
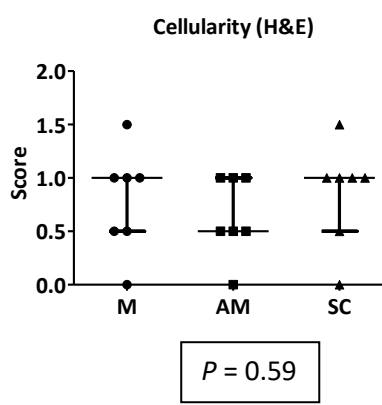
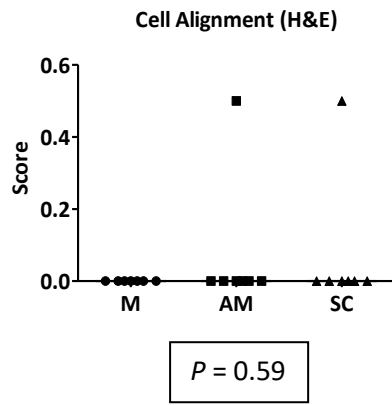
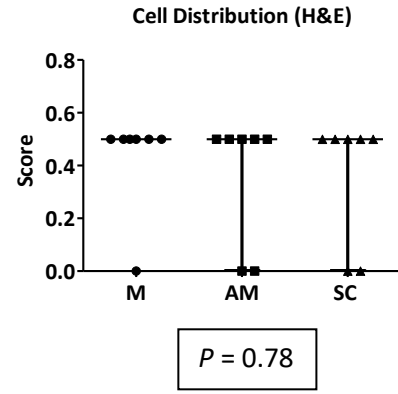
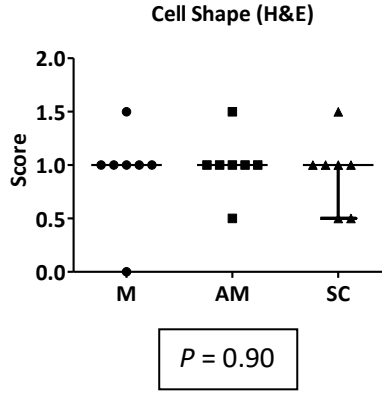
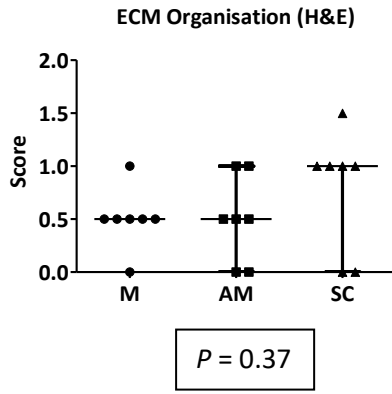
$P = 0.59$



**Figure 6.13** (includes preceding page) **Tendon construct histological scoring for H&E and Masson's Trichrome stained sections of mmu-miR-181a-5p mimic (M), antagomiR (AM) and scrambled control (SC) treated tendon constructs from seven biological replicates.** Results show the average of two consecutive blinded gradings by the same operator (First grader).  $P$ -values obtained using Kruskal-Wallis test with Dunn's test for pairwise comparisons. Graphs show median and interquartile range.







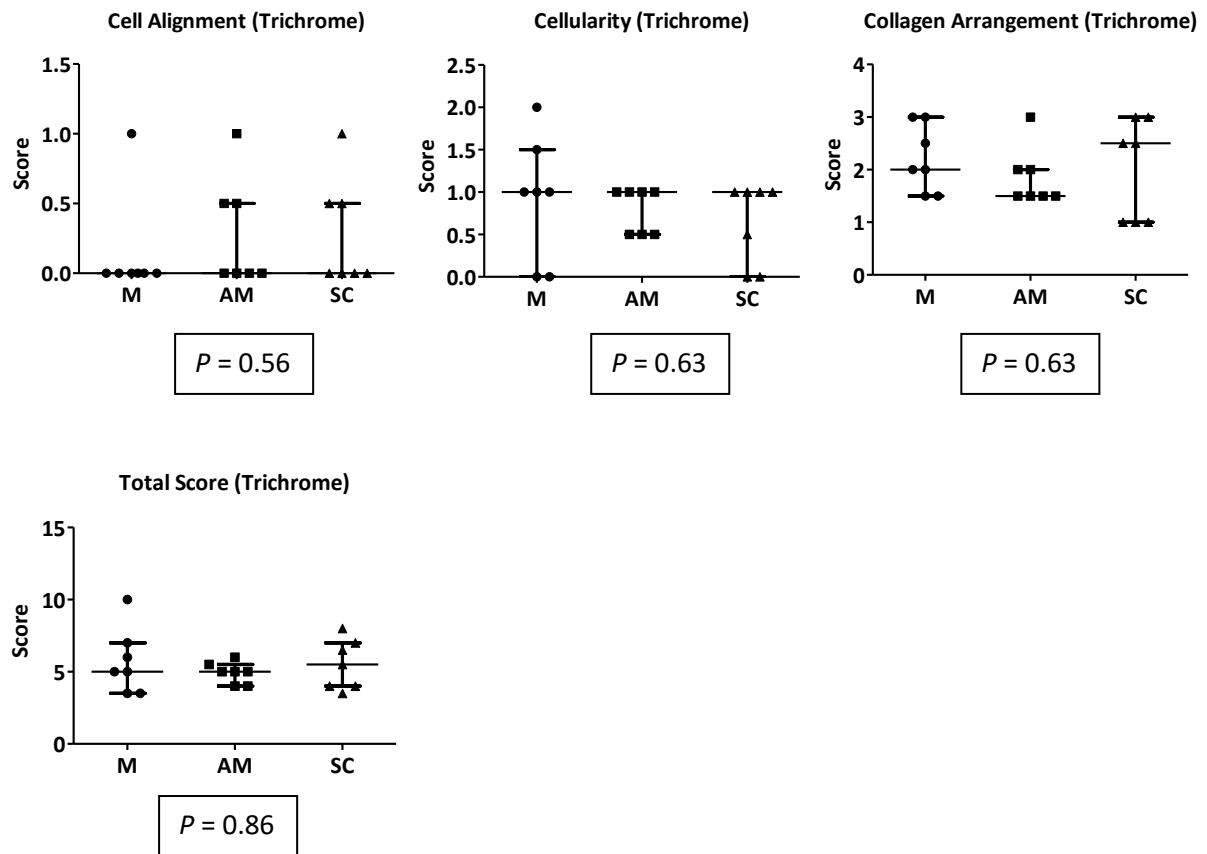


**Figure 6.15** (includes preceding page) Tendon construct histological scoring for H&E and Masson's Trichrome stained sections of mmu-miR-181a-5p mimic (M), antagomiR (AM) and scrambled control (SC) treated tendon constructs from seven biological replicates. Results show the average of two independent, blinded gradings by two operators (First and Second graders). P-values obtained using Kruskal-Wallis test with Dunn's test for pairwise comparisons. Graphs show median and interquartile range.

Variable	H&E κ	Trichrome κ	κ Interpretation
ECM Organisation	0.77	0.78	0 = agreement equivalent to chance
Cell Shape	0.29	-0.04	0.1 - 0.20 = slight agreement
Cell Distribution	-0.07	0.70	0.21 - 0.40 = fair agreement
Cell Alignment	0.47	0.78	0.41 - 0.60 = moderate agreement
Cellularity	0.71	0.82	0.61 - 0.80 = substantial agreement
Collagen Arrangement	0.67	0.73	0.81 - 0.99 = near perfect agreement
Total Score	0.68	0.64	1 = perfect agreement

**Table 6.3 Intra-rater repeatability for tendon construct scoring scheme.** Weighted Cohen's kappa coefficients ( $\kappa$ ) for both haematoxylin and eosin (H&E) and Masson's Trichrome stained sections. ECM = extra cellular matrix. Interpretation values taken from [www.statisticshowto.datasciencecentral.com/cohens-kappa-statistic/](http://www.statisticshowto.datasciencecentral.com/cohens-kappa-statistic/)

Inter-rater repeatability was poor, particularly with H&E stained sections (Table 6.4). Three variables, including total score gave agreement equivalent to that obtained by chance alone. Total score with Trichrome stained sections showed only fair agreement, with no individual component returning better than moderate agreement.

Variable	H&E κ	Trichrome κ
ECM Organisation	0.20	0.51
Cell Shape	0.20	0.06
Cell Distribution	0.09	0.03
Cell Alignment	0.07	0.56
Cellularity	0.29	0.53
Collagen Arrangement	0.29	0.51
Total Score	0.04	0.38

**Table 6.4 Inter-rater repeatability for tendon construct scoring scheme.** Weighted Cohen's kappa coefficients ( $\kappa$ ) for both haematoxylin and eosin (H&E) and Masson's Trichrome stained sections. ECM = extra cellular matrix. See Table 6.3 for interpretation of values.

## **6.4 Discussion**

In this chapter, we have shown that miR-181 influences autophagy and mitochondrial turnover, as supported by the increase in BNIP3, NRF2 and COXIV levels in miR-181a treated constructs, and elevated P62/SQSTM1 in antagomiR treated ones. Additionally, investigation of ultrastructural changes in our constructs identified evidence of increased mitochondrial degradation with miR-181a mimic treatment, although this was not quantified.

Consistent with results obtained in monolayer culture, comparative expression of miR-181 family members indicated miR-181b was most abundant in miR-181a mimic treated constructs. Family members a, and c were also consistently increased, but at levels several orders of magnitude lower than miR-181b. Variable expression was evident for miR-181d. In four of the biological replicates, miR-181d expression in miR-181a mimic treated constructs was below that seen in the scrambled control constructs, and in two of these, miR-181d expression was also lower than that of the antagomiR treated samples (Figure 6.2). Sequence similarity of miR-181 family members, conservation between species and limitations of quantification by RT-qPCR have been previously discussed in Chapter 5.

miR-181a mimic treatment appears to possess very good stability, evidenced by very high levels of miR-181 detected. This presumably results from accumulation of repeated treatments during construct maturation, in comparison with levels detected following a single treatment in monolayer culture (Chapter 5, Figure 5.3). Additionally, Cy5 fluorescence detection during imaging of Western blots was not observed following a single treatment of human tenocytes in monolayer culture (Chapter 7, Figure 7.3; Appendix 7, Figure A7.2).

Similar to the situation in monolayer culture reported in Chapter 5, miR-181a mimic treatment consistently resulted in increased (although variably so) total miR-181 expression, whilst antagomiR treatment produced less consistent results. Accumulation of active molecules resulting in higher than intended cellular concentrations may have resulted in aberrant cellular responses and impacted on our results. Treatment concentrations used were those optimised for a single treatment regime in monolayer tenocyte culture, based on previous evidence of efficacy in myoblast cultures (Soriano-Arroquia et al 2016, Goljanek-Whysall et al 2020). In primary mouse astrocytes, a 50 pM concentration of miR-181a and b mimic have been shown to result in degenerative mitochondrial changes, with 10 pM mimic producing a 16-fold increase in detected miR-181a (Ouyang et al 2012). Experimental evidence of alterations in miRNA expression suggest far smaller fold changes are associated with significant pathological processes.

Effective treatment concentrations will depend on the cell type studied. Neural cells typically show long population doubling times, with between 144 hours and up to 350 hours reported for rat and human astrocytes respectively (Geisert et al 1996, Lundin et al 2018). A relatively static cell population will favour stability of intracellular concentration of treatment reagents. Whilst population doubling times of approximately 350 hours have been reported in murine tenocytes (Lee et al 2018), equine tenocytes proliferate at a much higher rate, with a doubling time of approximately 40 hours (Bavin et al 2017), necessitating higher or more frequent treatment dosing to compensate for this. Considering the context-dependent effect of miRNAs and the variable and

conflicting reports of the consequences of altered miR-181a expression, comparison between cell types must be undertaken with caution.

Further work could assess the efficacy of alternative transfection protocols or the inclusion of a greater number of technical replicates, as discussed in Chapter 5, to allow selection of samples with more consistent treatment results between biological replicates. Indeed, opposing effects on cell viability have been reported in human retinoblastoma, MCF-7 breast cancer and umbilical vein endothelial cells following an increase in concentration of miR-181a to which cells were exposed, from 50 nM to 80 nM (Yang et al 2017). Additionally, it would be interesting to determine if there is a temporal effect of chronic exposure to altered miR-181 expression by harvesting constructs at different time points during maturation, or by exposing mature constructs to a single treatment.

As previous target network analysis identified miR-181 involvement in insulin and MAPK signalling pathways (Chapter 4, section 4.3.2), we included *IR*, *IGF1*, *IGF1R*, and *MAPK* in our gene expression analysis, in addition to those targets investigated in monolayer culture. None of the targets investigated demonstrated evidence of differential expression at the transcript level in our three-dimensional model. Transcript expression level however may not truly reflect functional consequences of miRNA up or down regulation if the miRNA does not act as an upstream regulator of transcript expression, or influence mRNA degradation. Additional factors that may have impacted on the results are the disparity in age and sex of biological donors. Both age and sex influence gene expression in native and tissue engineered tendon (Pease et al 2017). We included constructs derived from two male (neutered) and five female horses between five and 18 years of age. These inconsistencies may have been sufficient to obscure miR-181 induced effects.

The primary antibodies used in protein detection were not validated for use with equine proteins. However, all but COXIV, LAMP1, MFN1 might be expected to work based on sequence conservation. COXIV and LAMP1, however, generated useable data, whilst MFN2 failed to generate a detectable signal despite theoretical compatibility. The quality of Western blots was variable, limiting the number of samples that could be analysed with confidence, and the volume of material available precluded further attempts at improving results for protein expression. Results were however, generated for eight of the targets investigated.

A lack of detectable signal may have been expected with MFN1, LAMP1, COXIV and potentially NRF2, on the basis of differences of sequence identity between intended target and the equine homologues (Table 6.2). However, we achieved some success with LAMP1, COXIV and NRF2, whilst MFN2 failed, despite good sequence conservation between species. The lack of detectable signal may therefore represent shortcomings in the experimental methods.

LAMP1, P62/SQSTM1, COXIV and Parkin signal was either poorly expressed or inconsistent (Figure 6.4 (G), (E), (H) and (F) respectively and Appendix 6, Figure A6.2). For LAMP1 and COXIV, this may reflect weak affinity of the primary antibody for the equine protein due to poor sequence homology (Table 6.2). For P62/SQSTM1 and Parkin, sequence homology was above 90%, indicating the likelihood of cross-reactivity, therefore this may reflect inadequate protein loading or failure of electrophoretic transfer. Neither LAMP1 or Parkin demonstrated altered expression between treatment groups (Figure 6.6 (G) and (F) respectively and Figure 6.7), although Western blots were of poor quality (Appendix 6, Figure A6.2). The lack of significance in *PARK2* expression and Parkin level is interesting, as, of the proteins assessed in Chapter 5, Parkin demonstrated perhaps the most

striking change in accumulation and localisation in response to altered miR-181 activity (Chapter 5, section 5.3.3). Significant upregulation of BNIP3 with miR-181a mimic treatment indicated an upregulation in programmed cell death pathways. BNIP3 localises to mitochondria when overexpressed, where it interacts with the mitochondrial permeability transition pore, causing depolarisation and autophagosome formation. BNIP3 induced autophagy has been shown to have a protective effect against cell death in ischaemia-reperfusion injury models as well as precipitating autophagic cell death either by excessive autophagy, or alternative pathways (Zhang and Ney 2009).

LC3B is the most widely used marker of autophagy (Mizushima and Yoshimori 2007) and we were able to assess expression in five of our biological replicates. Although LC3BII has a higher molecular weight than LC3BI, due to its conjugation with phosphatidylethanolamine it migrates faster during electrophoresis than LC3BI to generate a signal at approximately 14 kDa. Quantity of LC3BII reportedly correlates with number of autophagosomes, but is also degraded by autophagy. LC3BII additionally demonstrates a greater degree of immune reactivity than LC3BI. This frequently results in a stronger LC3BII signal, without necessarily indicating increased amount of LC3BII. This appears to be particularly evident when the antibody is raised against the N-terminus of the peptide. Within-sample analysis of total LC3B or ratio of LC3BI to LC3BII is therefore controversial as an indicator of autophagy. However, between-sample comparison of LC3B signal intensity should be an appropriate method of comparing autophagic activity (Mizushima and Yoshimori 2007). Expression of LC3BI and II was not significantly different between treatment groups, but LC3BI/LC3BII ratios did appear to differ, in a manner consistent with increased autophagy in the miR-181a mimic treated group.

P62/SQSTM1 is an important component of the autophagic process and expression can be used to support LC3B expression data (Mizushima and Yoshimori 2007). P62/SQSTM1 is primarily degraded through selective autophagy and reduced expression is frequently used as a marker of autophagic flux (Sánchez-Martín and Komatsu 2018). However, a protective effect has also been described by P62/SQSTM1 mediated inactivation of KEAP1, promoting NRF2 accumulation. This activates the cellular stress response, counteracting apoptotic cell death (Komatsu et al 2010, Park et al 2015). Interestingly, elevated P62/SQSTM1 associated with increased mitophagy and autophagic flux and has been reported with down regulation of miR-181a and b in murine tissue (Indrieri et al 2019). Accumulation of P62/SQSTM1 with inhibition of miR-181a has also been reported in C2C12 myoblasts, and *in vivo* in murine muscle, associated with impaired autophagy (Goljanek-Whysall et al 2020). In monolayer equine tenocyte culture, P62/SQSTM1 was indicated as being reduced following miR-181 over expression (Chapter 5, Figure 5.3), and a similar, but non-significant change was evident in the constructs. Results should be interpreted with caution due to the low number of Western blots of sufficient quality for analysis, which may account for the failure to achieve significance.

We identified a significant increase in NRF2 expression with miR-181a mimic treatment, which is consistent with a protective cellular response and an increase in mitochondrial turnover, maintaining functional mitochondrial mass (Piantadosi et al 2008, Fang et al 2017). Supporting this, COXIV expression was also increased in this treatment group. COXIV is the terminal enzyme in the respiratory chain located on the inner mitochondrial membrane and encoded by nuclear DNA. In a microwave-induced model of oxidative stress in neurones, upregulation of COXIV protected mitochondrial function and was associated with mitochondrial regeneration (Hao et al 2018). The presence of two COXIV isoforms has been described in yeast, fish, human, rat and mouse,

(Hüttemann et al 2001) and their relative expression alters with cellular metabolic activity. We detected two distinct bands close to the predicted molecular weight of COXIV, although we cannot say that this represents expression of two isoforms in equine cells. The upregulation of COXIV in the miR-181a mimic treated group is consistent with an increase in mitochondrial biogenesis, although expression of TOMM20 was unchanged, which may have been expected to increase in parallel. However, stability of TOMM20 levels demonstrated that mitochondrial mass was maintained in the face of increased autophagy. This suggests an overall increase in mitochondrial turnover, consistent with maintaining an appropriate balance between mitochondrial regeneration and autophagic degradation. The upregulation of COXIV may additionally represent altered relative levels of COXIV isoforms with upregulation of miR-181, to optimise COX activity, O<sub>2</sub> consumption, and ROS generation, with the target of reduced oxidative damage (Hao et al 2018). It would be interesting to investigate expression ratios of these isoforms in future work.

In addition to the variability in quality of Western blots precluding some samples from analysis, we did not perform RT-qPCR to assess miR-181 expression in constructs processed for protein extraction, to confirm success of treatment uptake. We assumed an equivalent effect to that determined in the constructs processed for gene expression analysis. However, this may have been an incorrect assumption and may have resulted in inclusion of constructs in which antagomiR treatment had failed using the criteria we applied for gene expression analysis, where only five of the seven biological replicates were included.

We did not further explore the role of miR-181 in regulating mitophagy by using CCCP or bafilomycin, to induce mitophagy or inhibit autophagic flux, respectively, in our model. This represents a limitation to interpretation of our findings, but could be incorporated in future work. Additionally, transfection of tenocytes with a dual fluorophore, pH sensitive, mitochondrial-targeted reporter construct could be included to more accurately assess lysosomal turnover of mitochondria (Allen et al 2013).

Analysis of TEM images indicated occasional necrotic and apoptotic cells in all treatment groups, but overall there was good cell viability in all constructs from all treatment groups. Narrow diameter fibrils arranged in parallel orientated bundles were evident in all constructs examined, consistent with the appearance of collagen fibrils (Kapacee et al 2008). Structures resembling fibripositors were occasionally seen, but only in untreated control and miR-181a mimic treated sections (Figure 6.10). These axially aligned protrusions of plasma membrane represent the sites of collagen fibril alignment and deposition and are responsible for orchestrating the parallel alignment and organisation of collagen in the extracellular matrix in embryonic tendon (Canty et al 2004). Indeed, fibripositors are crucial to initiate collagen fibril deposition in this manner (Kapacee et al 2008). In post-embryonic tendon, fibripositors are absent, with continued increase in collagen fibril diameter occurring by accretion of extracellular collagen (Canty et al 2004). We only identified occasional fibripositors, and then only in miR-181a mimic and untreated constructs (Figure 6.8). This may be a stochastic function of the sections examined, as parallelism of collagen fibrils in all sections examined would suggest fibripositors had been present in all treatment groups (Kapacee et al 2008). Absence of identifiable fibripositors in antagomiR and scrambled treated constructs could represent accelerated maturation in these treatment groups, although Kapacee and co-workers (2008) reported that they persist for at least 12 weeks post-contraction in fibrin gel tendon constructs.

Alternatively, as tension is required for production and function of fibroblasts (Kapacec et al 2008), static tension may have dissipated to a degree incompatible with their maintenance.

TEM also permitted further investigation of altered miR-181 levels on mitochondrial dynamics. Some swollen mitochondria, with a loss of cristae were seen in scrambled control and antagomiR treated samples, indicating degenerative changes (Figure 6.9). Normal and swollen mitochondria were evident in miR-181a mimic treated samples, but also increased numbers of structures consistent with autophagolysosomes. Autophagy is a highly conserved catabolic process designed to promote cell survival under conditions of stress (Dikic and Elazar 2018). Damaged mitochondria release pro-apoptotic proteins and reactive oxygen species, and three types of selective mitochondrial autophagy are described. Type 1 is classically described in response to nutrient deprivation, and is suppressed following insulin release. Type 2 is typically initiated in response to mitochondrial depolarisation. Type 3 mitophagy is a very selective process for removal of damaged mitochondrial components, rather than the whole organelle. All three types can be triggered in response to oxidative stress (Lemasters 2014). Types 1 and 2 both involve LC3B and isolation of damaged mitochondria into autophagosomes, but by distinct mechanisms. Type 1 progresses by small LC3B-phospholipid conjugates adjacent to the targeted mitochondria coalescing, to progressively surround and envelope it. This process often occurs simultaneously with mitochondrial fission. Once isolation is complete, these mitophagosomes fuse with lysosomes, resulting in mitochondrial digestion. Type 2 differs in that LC3B is recruited directly to the surface of the damaged mitochondria until complete enclosure is achieved, and occurs without evidence of mitochondrial fission. Once mitophagosomes have been formed, Types 1 and 2 are morphologically indistinguishable. Structures consistent with Type 1 or 2 mitophagy were observed in miR-181a mimic treated samples (Figure 6.10). Elevation of BNIP3 levels in miR-181a mimic treated constructs would support this finding, as this mitochondrial membrane protein is known to interact with LC3B, targeting mitochondria for autophagosomal degradation (Gustafsson 2011). In Type 3 mitophagy, vesicles highly enriched for oxidised proteins bud off from the parent mitochondria. These subsequently accumulate into highly characteristic multivesicular bodies prior to lysosomal fusion. We did not identify any of these multivesicular bodies in any sections examined. Type 2 mitophagy is dependent on phosphatase and tensin homologue-induced putative kinase 1 (PINK1) mediated Parkin recruitment. This is also suggested to be essential for Type 3 mitophagy, whereas Type 1 occurs prior to mitochondrial depolarisation in a PINK1-Parkin independent manner (Lemasters 2014). We did not demonstrate any changes in *PARK2* transcript or Parkin protein abundance with miR-181 expression.

Numerous histopathological scoring systems have been used by researchers to evaluate human tendinopathy and animal models of induced disease (Lui et al 2011). Scoring systems have been devised to quantitatively evaluate histological features of tendon rupture, tendinopathies, enthesiopathies and tendon and enthesis repair (Loppini et al 2015). These systems contain elements, such as degree of vascularisation, that are not applicable to artificially produced constructs *in vitro*. Indeed, there are no universally recognised grading systems specifically for tissue engineered tendon constructs *in vitro*. It is recommended that scoring systems investigating *in vitro* tissue engineered tendon should evaluate cellularity, collagen type, collagen architecture, fibroblasts, inflammatory infiltrate and angiogenesis (Loppini et al 2015). Inflammatory infiltrate and angiogenesis however are only applicable to assessing healing response following grafting of *in vitro* engineered tissue into the *in vivo* environment.

For our scoring system we devised a scale, utilising factors described in two well recognised and widely applied tendinopathy scoring systems, the Movin and Bonar grading schemes. These scoring systems show a high level of correlation, producing comparable assessment of similar characteristics in tendon tissue (Maffulli et al 2008). The Bonar score has four categories, and the Movin score is more detailed, with eight. One category in each score is dedicated to cellular morphology, one to vascularity and the remainder to extra cellular matrix (ECM) characteristics. Both utilise a four-point scale within each category with zero representing normal and four markedly abnormal. Our scheme had six categories, two assessing ECM qualities and four tenocyte morphology and distribution. The final grading scheme was biased to cellular characteristics based on the findings of Cook and co-workers (2004) and Doroski and colleagues (2007). The former authors report that morphological changes in tenocytes are more prevalent than ECM changes in asymptomatic tendinopathy. Doroski et al (2007) recommend that success of tendon tissue-engineering techniques should consider viability and proliferation of cells in the construct, in addition to amount and type of ECM production and spatial organisation. We utilised staining protocols commonly employed for assessment of tendon integrity; haematoxylin and eosin (H&E) for cellularity and collagen degeneration, Masson's trichrome and von Gieson's stains for collagen and other matrix proteins (Loppini et al 2015).

Initial application of the scoring scheme indicated it could differentiate between constructs subjectively described as well-organised tendon-like tissue and those with abnormal, irregular architecture (Figure 6.7). Subjectively, miR-181a mimic treated constructs appeared to exhibit a more disorganised structure, but this was not confirmed by our grading scheme where wider application failed to detect a significant difference between constructs from different treatment groups. This may reflect a true finding, that miR-181 treatments did not influence outcome, or reveal a lack of sensitivity at identifying more subtle differences. There was considerable variability between constructs within each treatment group, which may account for lack of significant difference between them. Additionally, whole constructs were processed for histology, therefore, as with the analysis of protein expression, we did not evaluate miR-181 levels in these samples. We assumed miR-181a mimic treatment would be universally successful, as shown with RT-qPCR analysis for those constructs used in gene expression analysis. However, we have previously identified inconsistent results with either success of the antagomiR treatment, or the ability to identify its success, both in monolayer culture (Chapter 5, section 5.3.2) and three-dimensional constructs (section 6.3.1). This represents a limitation to interpretation of data from the antagomiR treated group.

A grading system should be easily applicable, sensitive and repeatable, generating consistent data whether used repeatedly by one individual, or by several individuals (Maffulli et al 2008, McHugh 2012). Staining technique influenced scoring, and assessment of inter-rater repeatability indicates the scheme requires refinement. The schemes on which ours was based were devised for use in native tendon, the Movin score for Achilles tendon, the Bonar for patellar tendon (Maffulli et al 2008). Both schemes use semi quantitative assessment descriptors, which we adapted in our descriptors. This introduces a subjective element to assessment. Inclusion of more precisely defined quantitative elements, such as used in the modified Watkins score for tendon repair (Ide et al 2009), may improve discriminative power. We were unable to demonstrate a difference in tendon construct architecture between treatment groups using our scheme and this requires further development. There remains a need for a scoring system to accurately describe tendon construct structure *in vitro*.

Our data suggest that lysosomal activity and mitochondrial turnover is greater in miR-181a mimic treated tendon constructs. We observed differences in cellularity and organisation and structure of the extracellular matrix of constructs, but the grading scheme we employed did not demonstrate these were significantly different between treatments. The modified scheme we employed requires refinement to increase its sensitivity and reproducibility. Identification of similarities and differences in the response of human tenocytes to miR-181a treatment will form the focus of the next chapter.

## **Chapter 7 - Validation of miR-181 function in human tenocytes**

### **7.1 Introduction**

The reduction in miR-181 expression in both human and equine clinical tendinopathy identified in Chapter 3 suggests this family of microRNAs are important regulators of tenocyte biochemical function in both species. Mitochondrial dynamics and function (Indrieri et al 2019, Goljanek-Whysall et al 2020) and autophagy (Liu et al 2017), key factors in maintaining cell viability and function, are known to be regulated by miR-181. Gain and loss of function studies are thus critical to the assessment of miR-181 dysregulation on tenocyte function and we have demonstrated success in employing these techniques in equine tenocytes in both monolayer culture (Chapter 5) and three-dimensional tissue engineered tendon constructs (Chapter 6).

Human tendon is a difficult tissue to study as healthy tissue is challenging to obtain, whilst pathological tissue is usually only available once disease is well advanced, and often following unsuccessful conservative or medical interventions. Equine tendon has been described as a good model for investigation of biomechanical function and pathological processes in human tendon (Dudhia et al 2007, Innes and Clegg 2010, Lui et al 2011, Thorpe et al 2014). To support this, authors quote the similarities in mechanical function between equine and human energy storing tendons, longevity and athletic function of both species, and their predisposition to naturally occurring age and overuse related disease. For equine tendon to be truly considered a robust model, it is important to elucidate if there are similarities in the biochemical pathways disrupted during disease, as only then can research utilising this more readily available tissue be considered truly translational to the human field. Alteration in intracellular distribution of LC3B, DJ-1, P62/SQSTM1 and Parkin with gain and loss of miR-181 function in equine monolayer culture implicated miR-181 activity as influencing autophagy and mitochondrial dynamics (Chapter 5, section 5.3.3). This effect was reinforced by changes in levels of autophagy and mitochondrial related proteins P62/SQSTM1, NRF2, COXIV and BNIP3 in response to altered miR-181 activity. Additionally, we have shown ultrastructural evidence of up regulated mitophagy with increased miR-181 activity in three-dimensional tissue engineered constructs (Chapter 6, Figures 6.7 and 6.9). We were interested, therefore, in determining whether these changes were reproducible in human tenocytes cultured under similar conditions.

Mitochondria are dynamic organelles both in terms of absolute intracellular mass and morphology. Mitochondrial content reflects the bioenergetic requirements of the cell, whilst morphology is controlled by fission and fusion, processes fundamental to maintaining mitochondrial integrity (Karbowski and Youle 2003, Palikaras et al 2018). In addition to ATP generation, mitochondria are also critical participants in cell cycle control, inflammation, calcium signalling and calcium induced apoptosis and redox signalling (Archer 2013).

Selective autophagic clearance of mitochondria (mitophagy) occurs at a basal rate dictated by specific tissue requirements to maintain mitochondrial quality, and is up regulated under conditions of cellular stress, independent of bulk (non-selective) autophagy (Palikaras et al 2018). Additionally, mitochondrial clearance has been described in several cell types as a natural component of tissue development, reflecting a change from oxidative phosphorylation to glycolysis (Palikaras et al 2018).

Tenocytes switch from predominantly oxidative phosphorylation to anaerobic glycolysis during maturation of tendon, with reversal of this process during injury and repair (Birch et al 1997, Thankam et al 2018). Thus, appropriate control of tenocyte mitochondrial content and function may form a critical aspect of tendon homeostasis, adaptation and response to injury.

Impairment of mitophagy results in progressive accumulation of defective mitochondria, decline in cellular function and tissue damage (Palikaras et al 2018) and is associated with age related deterioration in skeletal muscle mass and function (Goljanek-Whysall et al 2020), neurodegenerative diseases (Chen et al 2019), proliferative, apoptosis resistant diseases (Archer 2013) and cardiomyopathies (Palikaras et al 2018). Increased mass of mitochondria coupled with a reduction in their functional competence is also a feature of the senescent phenotype in fibroblasts (Passos et al 2010). Dysfunctional mitochondria generate higher levels of reactive oxygen species (ROS) which can trigger development of the senescence-associated secretory phenotype (Chapman et al 2019). In chondrocytes, elevated ROS production is associated with increased production of matrix metalloproteinases 1 and 3, indicating a role in enhanced matrix degradation (Reed et al 2014). Superoxide anion ( $O_2^-$ ) radicals, the most prominent ROS produced by electron leak from the electron transport chain, are capable of non-enzymatic degradation of Type I collagen (Monboisse et al 1983).

The emerging role of miR-181 in influencing mitochondrial dynamics was introduced in Chapter 5. Downregulation of miR-181a in skeletal muscle reduced mitophagy and resulted in accumulation of abnormal mitochondria (Goljanek-Whysall et al 2020). Overexpression of miR-181a and b stimulated mitochondrial metabolism in human chondrocytes (Zheng et al 2019). In astrocytes, miR-181a downregulation was protective of mitochondrial membrane potential and reduced production of ROS (Ouyang et al 2012), whilst deletion of miR-181a and b in neuronal cells increased expression of *PPARGC1A* and mitochondrial DNA, indicating a role in mitochondrial biogenesis (Indrieri et al 2019). In murine cardiac myocytes, deletion of miR-181c and d increased COXIV levels (Das et al 2017).

In this chapter, we have extended our investigation of altered miR-181 activity on levels and distribution of mitochondrial and autophagy related proteins seen in equine primary tenocytes, to human primary tenocytes. We have demonstrated successful delivery of miR-181a mimic and antagomiR treatments to human tenocytes, confirmed by visualisation of intracellular fluorescence from tagged mimic and antagomiR reagents and reinforced by RT-qPCR. Focussing on mitochondrial and autophagy related genes *P62/SQSTM1*, *PARK2*, *COXI*, *COXIV*, *LC3B*, *TOMM20* and *IR*, we have additionally demonstrated that, as with equine tenocytes, transcript levels are not affected by miR-181a activity, but miR-181 appears to act through regulation of translation and localisation of autophagy related proteins. Consequently, we believe this work supports the hypothesis that equine tenocytes can serve as an acceptable model for investigation of the effects of pathological processes on human tenocytes.

## **7.2 Methods**

### **7.2.1 Treatment of tenocyte cultures**

Primary human tenocytes from three donors (Table 7.1) were propagated for 24 hours prior to treatment with cholesterol-conjugated Cy5-tagged mmu-miR-181a-5p mimic, FITC-tagged 23 nucleotide (nt) single strand RNA antagomiR, or 21 nt single strand RNA scrambled control sequence. Final treatment concentrations were 100 nM (mimic and scrambled control) and 200 nM (antagomiR). Live cell imaging to confirm uptake of fluorescence was performed using a Nikon Eclipse Ti-E fluorescent microscope. Forty-eight hours after treatment, cells were lysed for either RNA or protein extraction.

Sample ID	Sex	Age (years)	Ethnicity	Passage number
LMB-JL-280	Male	18	Chinese	2
LMB-SF-282	Female	26	White British	3
LMB-RL-286	Male	24	White British	3

**Table 7.1 Donor and tenocyte passage details for human semitendinosus and gracilis tendon-derived tenocytes cultured for mmu-miR-181a-5p mimic, antagomiR and scrambled control treatment studies.**

### **7.2.2 Reverse transcription quantitative real-time polymerase chain reaction**

Total RNA extraction was followed by reverse transcription to cDNA, for which 50 ng RNA template was used for both gene and miRNA expression analyses.

Expression of miR-181a/b/c/d was determined using commercially available primers (Qiagen, Manchester, UK; Chapter 2, section 2.12.1, Table 2.10) and normalised to *SNORD61* as internal control (previously validated for this purpose as a stable small non-coding RNA in equine tenocytes (Chapter 3, section 3.2.3; Appendix 2, Table A2.1 and Chapter 5, section 5.2.2; Appendix 5, Table A5.1) and confirmed in human tenocytes (Appendix 7, Table A7.1)). Relative expression values were then summed to give total miR-181 expression for each sample.

Primers were designed for three validated miR-181 targets (*P62/SQSTM1*, *PARK2/Parkin* and *COX1*) and a further four genes (*LC3B*, *TOMM20*, *IR* and *COXIV*). Target gene expression was normalised to that of the housekeeping gene *glyceraldehyde 3-phosphate dehydrogenase (GAPDH)*; previously demonstrated to exhibit acceptable stability for this purpose in equine tenocytes (Chapter 5, section 5.2.2; Appendix 5, Table A5.2) and confirmed in human tenocytes (Appendix 7, Table A7.2)).

Primer sequences and RT-qPCR details are listed in Chapter 2, sections 2.12.1 (Table 2.14), 2.12.2 (Figure 2.2) and 2.12.3 (Figure 2.3) respectively. For all RT-qPCR data, technical replicates were run in

triplicate and expression relative to *SNORD61* or *GAPDH* calculated using the delta Ct method (Livak and Schmittgen 2001). For graphical representation, transcript expression was normalised to that of the scrambled control treatment group.

### 7.2.3 Protein levels

Protein extraction was performed on cultures from all three biological replicates. Following protein extraction and quantification (Chapter 2, sections 2.13.2 and 2.13.3), sodium dodecyl sulfate-polyacrylamide gel electrophoresis (SDS-PAGE) was performed, initially using 5 µg protein in 15 µL loading volume. If this generated blots of inadequate quality for analytical purposes, protein loading was increased up to a maximum of 20 µg protein in 60 µL loading volume. Semi-dry transfer to polyvinylidene fluoride (PVDF) membrane was confirmed using Ponceau staining prior to immunofluorescent evaluation of target proteins TOMM20, LC3B, P62/SQSTM1, COXIV and Parkin. Vinculin was used as loading control for normalisation. Images were acquired using the LI-COR Odyssey CLx Imaging System at emission wavelengths of 700 nm and 800 nm. Details of protocols and antibodies are given in Chapter 2, sections 2.14 and 2.15.

Semi-quantitative analysis of protein expression was performed by band densitometry using ImageJ 1.52 software (Rasband, W.S. U. S. National Institutes of Health, Bethesda, Maryland, USA, <https://imagej.nih.gov/ij/>, 1997-2018). Target protein band densities were measured and normalised to band intensity of corresponding vinculin loading control. Graphical representation of relative expression between groups is given in Figure 7.3.

### 7.2.4 Induction of mitophagy and immunocytochemistry

For immunocytochemistry, tenocytes were exposed to the oxidative phosphorylation uncoupling agent carbonyl cyanide m-chlorophenylhydrazone (CCCP) for six hours, at a concentration of 20 µM, dissolved in dimethyl sulfoxide (DMSO), or DMSO alone, 24 hours after miR-181a mimic, antagomiR or scrambled control treatment. Tenocytes were then fixed in ice cold methanol and immunostained for mitochondrial and autophagy markers as described in Chapter 2, section 2.7. Images were obtained using a Zeiss Axio Imager M2 fluorescent microscope with Zeiss ZEN Imaging software (blue edition 3.1).

### 7.2.5 Statistical analysis

Statistical analysis was performed using GraphPad Prism version 5.01 for Windows (GraphPad Software, San Diego, California, USA, [www.graphpad.com](http://www.graphpad.com)). Gene expression data were analysed non-parametrically using the Kruskal Wallis test with Dunn's test for pairwise comparisons, to include miR-181a mimic, antagomiR and scrambled control sequence treated groups. Comparisons between scrambled control sequence treated and untreated groups utilised the Mann-Whitney test and are presented in Appendix 7, Figure A7.1. Significance was assumed if  $P < 0.05$ .

Protein levels derived from Western blot images were analysed using one way ANOVA with Tukey's multiple comparison test for pair-wise comparisons. Analysis was performed between miR-181a mimic, antagomiR and scrambled control sequence treated groups. Comparisons between scrambled control sequence treated and untreated groups utilised the Student-t test and are presented in Appendix 7, Figure A7.3. Significance was assumed if  $P < 0.05$ .

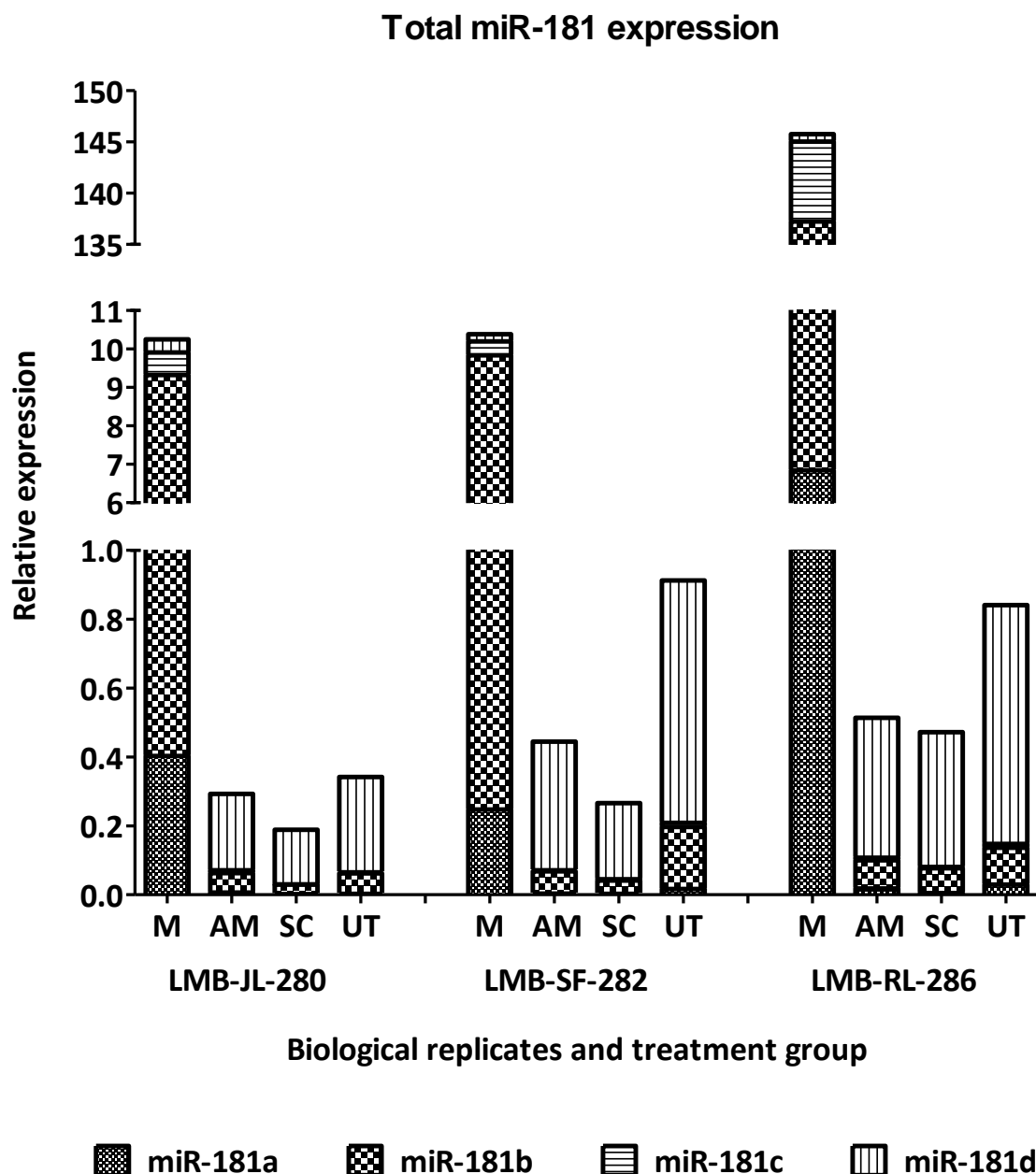
Immunocytochemistry results are reported qualitatively.

## **7.3 Results**

### **7.3.1 Validation of miR-181a-5p overexpression and inhibition in tenocytes**

Human tenocytes from three donors (Table 7.1) were treated with mmu-miR-181a-5p mimic, antagomiR and scrambled control sequence oligonucleotides. Sequence homology between murine and human orthologues/paralogues of miR-181 family members was previously confirmed, and reported in Chapter 5 (Table 5.3), validating our use of treatments based on murine sequence data and human sequence-directed primers. Data were analysed based on relative total miR-181 expression as determined by RT-qPCR, normalised to *SNORD61*.

Based on RT-qPCR evaluation, all miR-181a mimic treated cultures demonstrated substantially increased total miR-181 levels, with levels in one of the replicates approximately fourteen times that of the other two (Figure 7.1). Similar to the situation in equine tenocytes, miR-181b was identified as responsible for the greatest proportion (87-92%) of the increase in total miR-181 levels (Figure 7.1). Total miR-181 levels were much lower in all other treatment groups by comparison, and more equivalent between all three biological replicates (Figure 7.1). The same pattern of expression, with total miR-181 levels in antagomiR treated cultures higher than those detected in the scrambled control treated group, but lower than that in the untreated control groups was also common to all biological replicates (Figure 7.1).



	LMB-JL-280				LMB-SF-282				LMB-RL-286			
	Mimic	AntagomiR	Scrambled	Untreated	Mimic	AntagomiR	Scrambled	Untreated	Mimic	AntagomiR	Scrambled	Untreated
miR-181a	0.403	0.006	0.002	0.002	0.247	0.004	0.003	0.017	6.840	0.018	0.005	0.029
miR-181b	8.920	0.057	0.027	0.060	9.586	0.065	0.039	0.180	130.397	0.081	0.072	0.108
miR-181c	0.587	0.008	0.001	0.003	0.364	0.003	0.004	0.011	7.809	0.008	0.004	0.011
miR-181d	0.342	0.222	0.159	0.277	0.184	0.373	0.221	0.704	0.720	0.406	0.391	0.693
<b>Total miR-181</b>	<b>10.251</b>	<b>0.293</b>	<b>0.189</b>	<b>0.342</b>	<b>10.382</b>	<b>0.444</b>	<b>0.266</b>	<b>0.913</b>	<b>145.767</b>	<b>0.514</b>	<b>0.472</b>	<b>0.841</b>

**Figure 7.1** microRNA-181 expression in mmu-miR-181a-5p mimic (M), antagomiR (AM) and scrambled control (SC) treated human primary tenocyte monolayer culture in three biological replicates. Values represent relative expression, normalised to *SNORD61*, for all four miR-181 family members and total miR-181. UT = untreated control. Relative expression values are given in the table below graph.

### 7.3.2 miR-181a target gene analysis

Following determination of treatment effect, expression of seven selected genes (*COXI*, *COXIV*, *TOMM20*, *PARK2*, *P62/SQSTM1*, *LC3B* and *IR*) was investigated in all three biological replicates. Data were analysed using the non-parametric Kruskal-Wallis test with Dunn's test for pairwise comparisons, significance was assumed if  $P < 0.05$ . Comparisons between mimic, antagomiR and scrambled control sequence treated groups are presented in Figure 7.2. Comparisons between scrambled control sequence treated and untreated cultures are presented in Appendix 7, Figure A7.1. Similar to our results following miR-181 gain and loss of function equine tenocyte, we detected no difference in transcript expression between treatment groups for any of the targets investigated (Figure 7.2).

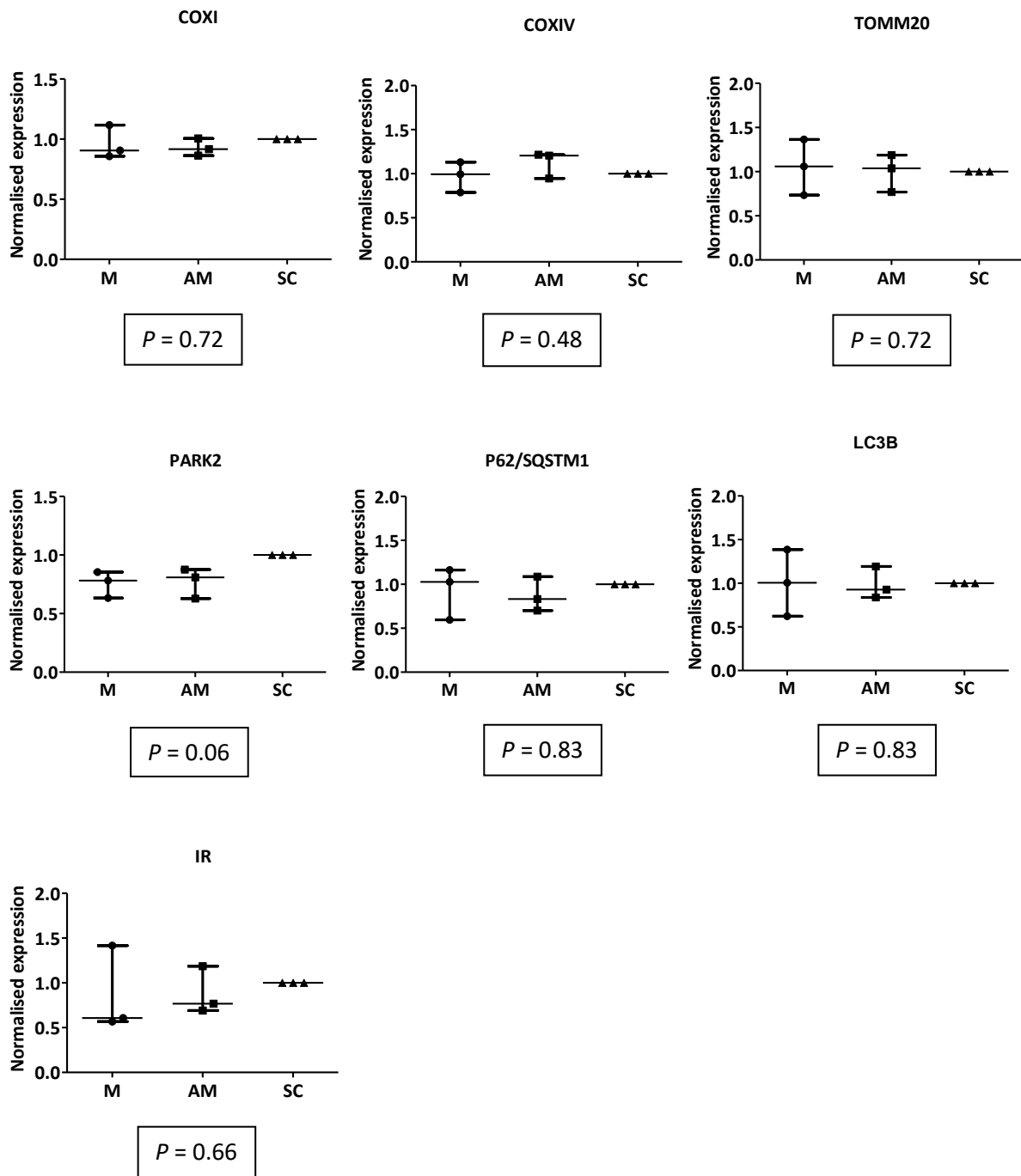


**Figure 7.2** The effects of miR-181a overexpression and inhibition on expression of selected target genes in human tenocytes from three biological replicates. Y-axis values represent expression relative to *glyceraldehyde 3-phosphate dehydrogenase (GAPDH)*, normalised to scrambled control treatment group. M = miR-181a-5p mimic, AM = antagomiR, SC = scrambled control. P-values calculated from delta Ct values, using Kruskal-Wallis test with Dunn's test for pairwise comparisons. Graphs show median and interquartile range.

### 7.3.3 Protein expression (Western blotting)

As miR-181 levels did not appear to influence target gene transcript stability, we next investigated the effect of miR-181 function on protein translation. Levels of the protein product of five of the previously selected genes (*TOMM20*, *P62/SQSTM1*, *LC3B*, *COXIV* and *PARK2*) were investigated by SDS-PAGE and Western blotting. Protein extracts from mmu-miR-181a-5p mimic, antagomiR and scrambled control treated tenocytes were probed using primary antibodies directed against the proteins TOMM20, P62/SQSTM1, LC3B, COXIV and Parkin, with vinculin used as loading control for normalisation.

Images of sufficient quality for semi-quantitative analysis of protein levels were obtained for all samples using 5 µg protein per well for COXIV, 15 µg protein per well for P62/SQSTM1 and 20 µg protein per well for TOMM20 and LC3B. No signal was detected in any of the samples for Parkin using 5, 10 or 20 µg of protein per well. Parkin was therefore unquantifiable. Representative images are shown in Figure 7.3; all images are shown in Appendix 7, Figure A7.2.

LC3B signal was detected in all samples as two bands at approximately 14 and 16 kDa. Signal at the 16 kDa level, consistent with identification of the soluble, unconjugated form LC3BI (Mizushima and Yoshimori 2007), was prominent and did not differ between treatment groups (Figure 7.3 (A)). The signal generated at 14 kDa, consistent with the phospholipid conjugated form LC3BII (Mizushima and Yoshimori 2007), was distinct but much weaker (Figure 7.3 (A)). Significantly ( $P < 0.001$ ) lower levels of LC3BII were detected in miR-181a mimic treated tenocytes than in other treatment groups (Figure 7.3 (A)). No difference in LC3BII levels was evident between antagomiR and scrambled control treatments. Consequently, the LC3BII/LC3BI ratio was significantly ( $P = 0.002$ ) lower in miR-181a mimic treated, versus comparator groups (Figure 7.3 (A)). LC3BII is considered to be a standard marker for autophagosomes, but is itself degraded by the process of autophagy (Runwal et al 2019). Reduced levels are therefore consistent with enhanced autophagic activity or reduced autophagosome formation. The similarity of LC3BI levels between treatment groups would tend to support the latter scenario, as classically, during increased autophagic activity LC3BI levels decrease, with a concomitant increase in LC3BII, with prolonged periods of enhanced autophagy resulting in reduced levels of both forms (Mizushima and Yoshimori 2007).

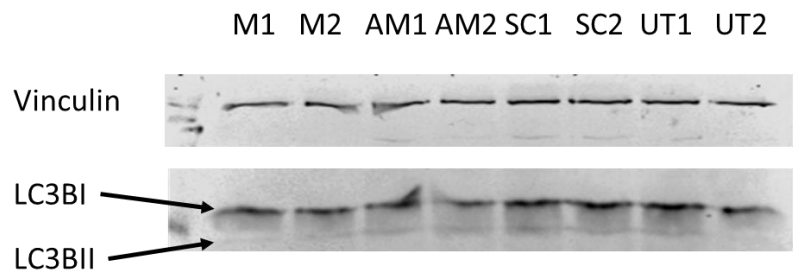
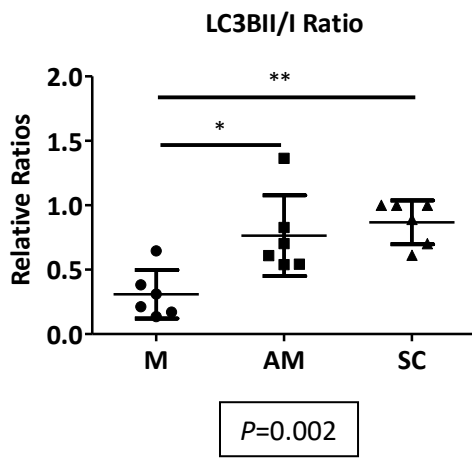
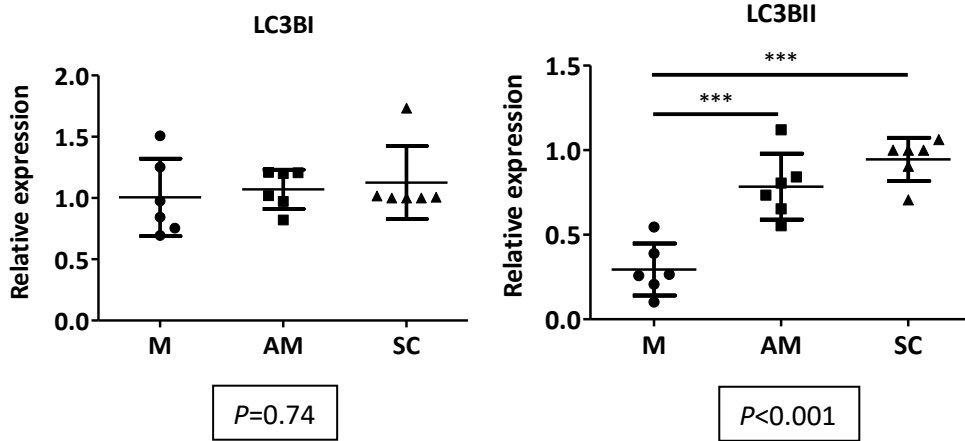
The outer mitochondrial membrane transport complex component TOMM20 showed significantly ( $P = 0.002$ ) lower levels in the miR-181a mimic treated group than the scrambled control, but not antagomiR treated tenocytes (Figure 7.3 (B)). AntagomiR treatment resulted in TOMM20 levels intermediate between those following miR-181a mimic and scrambled control treatments, but was not statistically significantly different from either (Figure 7.3 (B)). This nuclear genome-encoded protein is frequently used as, and considered a reliable marker of, mitochondrial mass (Song et al 2018, Buso et al 2019). Reduced levels in the miR-181a mimic treated group indicated an imbalance between mitophagy and mitochondrial biogenesis. This suggest that, consistent with the reduction in LC3BII levels, TOMM20 is degraded by increased miR-181 activity due to enhanced autophagic clearance of mitochondria.

No significant differences between groups were detected for levels of autophagy receptor protein P62/SQSTM1, or cytochrome c oxidase regulatory subunit COXIV, (Figure 7.3 (C) and 7.3 (D) respectively). Whilst P62/SQSTM1 has been described as essential for Parkin-mediated mitophagy (Youle and Narendra 2010), it also promotes aggregation of ubiquitinated mitochondria targeted for

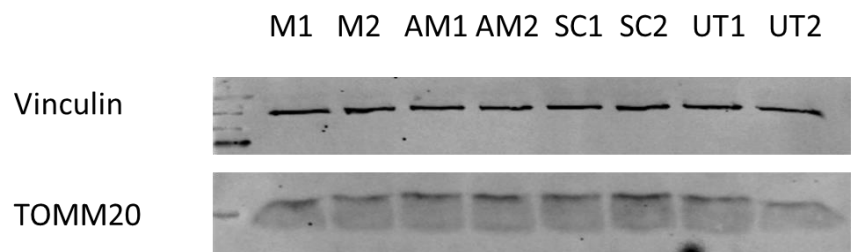
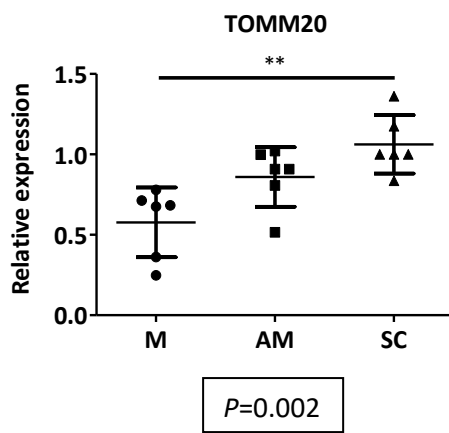
degradation independent of mitophagy (Narendra et al 2010). This may explain the lack of difference in P62/SQSTM1 levels between treatment groups in the face of evidence compatible with increased mitophagy outlined above.

Similar to the situation in equine tenocytes, two distinct bands were consistently detected for COXIV at approximately 15 and 20 kDa (Appendix 7, Figure A7.2D). As stated in Chapter 6 (section 6.3.3), two isoforms of COXIV are described (Hüttemann et al 2001), but these differ in molecular weight only by approximately 1 kDa. We postulated this could be due to an off target interaction in equine tenocytes, but the presence of a similar phenomenon in human cells where these antibodies have validated activity, suggests this most likely represents post-translational modification of this nuclear encoded protein (Hornbeck et al 2015). We determined quantification using the lower (15 kDa) band, consistent with our applied methodology in equine tenocytes (Chapter 6, section 6.3.3). Similar levels detected in all treatment groups suggests occurrence of equivalent mitochondrial biogenesis irrespective of miR-181 activity.

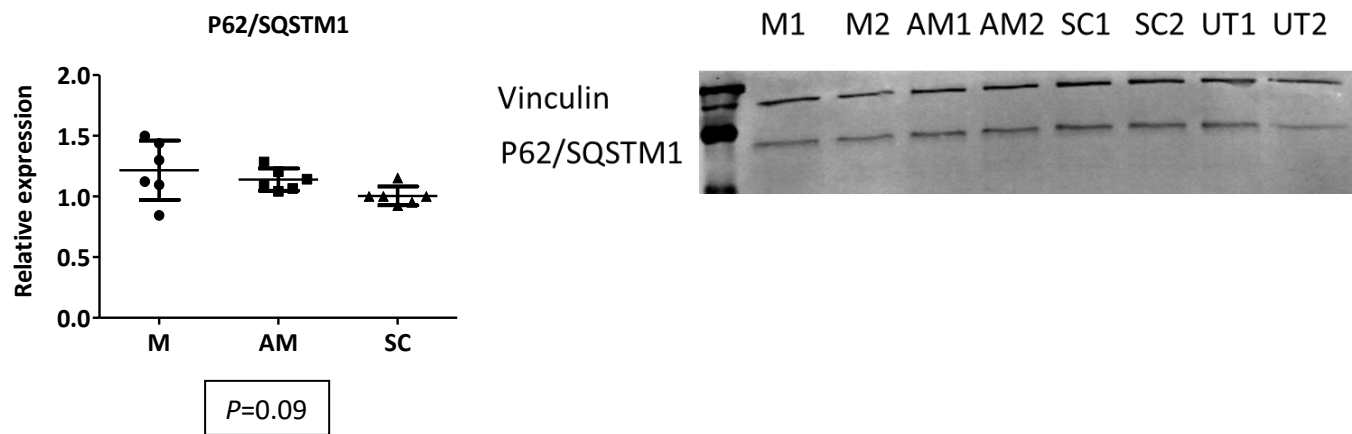
A.



B.



C.



D.

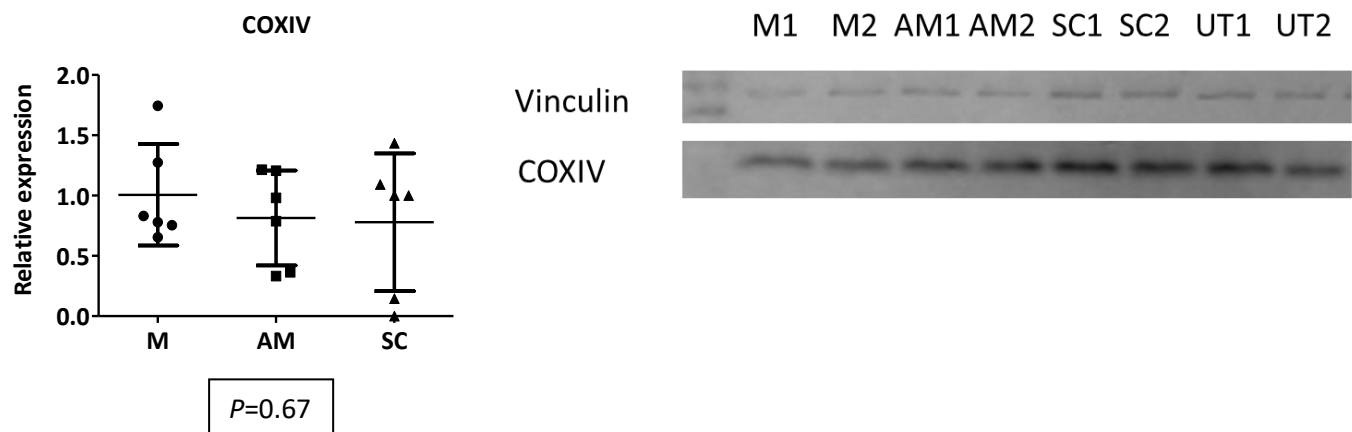


**Figure 7.3 (includes preceding page) Representative Western blot images and target protein levels in mmu-miR-181a-5p mimic (M), antagomiR (AM) and scrambled control (SC) treated human tenocytes from three biological replicates. A.** LC3B predicted molecular weights; LC3BI 16 kDa, LC3BII 14 kDa. **B.** TOMM20 predicted molecular weight 16 kDa. **C.** P62/SQSTM1 predicted molecular weight 61 kDa. **D.** COXIV predicted molecular weight 17 kDa. Vinculin used as loading control, predicted molecular weight 124 kDa. UT = untreated. Images acquired using LI-COR Odyssey CLx Imaging System at emission wavelengths 700 nm (vinculin) and 800 nm (all other targets). See Appendix 7, Figure A7.2 for all images. Protein levels calculated using densitometric analysis in ImageJ 1.52 software (<https://imagej.nih.gov/ij/>, 1997-2018), normalised to vinculin as loading control. *P*-values calculated using one way ANOVA with Tukey's multiple comparison test for pairwise comparisons. \* =  $P < 0.05$ , \*\* =  $P < 0.01$ , \*\*\* =  $P < 0.001$ .

### 7.3.4 Role of miR-181 in regulation of mitochondrial dynamics

To further investigate the effects of miR-181 on mitochondrial dynamics and autophagy-associated proteins, mitophagy was induced in mmu-miR-181a-5p mimic, antagomiR and scrambled control treated tenocytes. As conducted in equine tenocyte culture (Chapter 5, section 5.3.3), treated human tenocytes were incubated for six hours with a 20  $\mu$ M solution of the oxidative phosphorylation uncoupling agent carbonyl cyanide m-chlorophenylhydrazone (CCCP) dissolved in DMSO, or DMSO alone, as control (Kagan et al 2016, Webb et al 2017). We confirmed uptake of mimic and antagomiR treatments by fluorescence imaging of live cell cultures immediately prior to cells being fixed, permeabilised and processed for immunostaining (Figure 7.4). No-primary-antibody controls were performed and confirmed no residual, detectable fluorescence from miR-181a mimic or antagomiR treatments (Figure 7.5). Additionally, neither background signal, nor non-specific binding of secondary fluorophore-conjugated antibody were evident (Figure 7.5). Consistent with the situation in equine tenocytes, fluorescence associated with Cy5 and FITC labelling of miR-181 mimic and antagomiR treatments was degraded by processing for immunostaining.

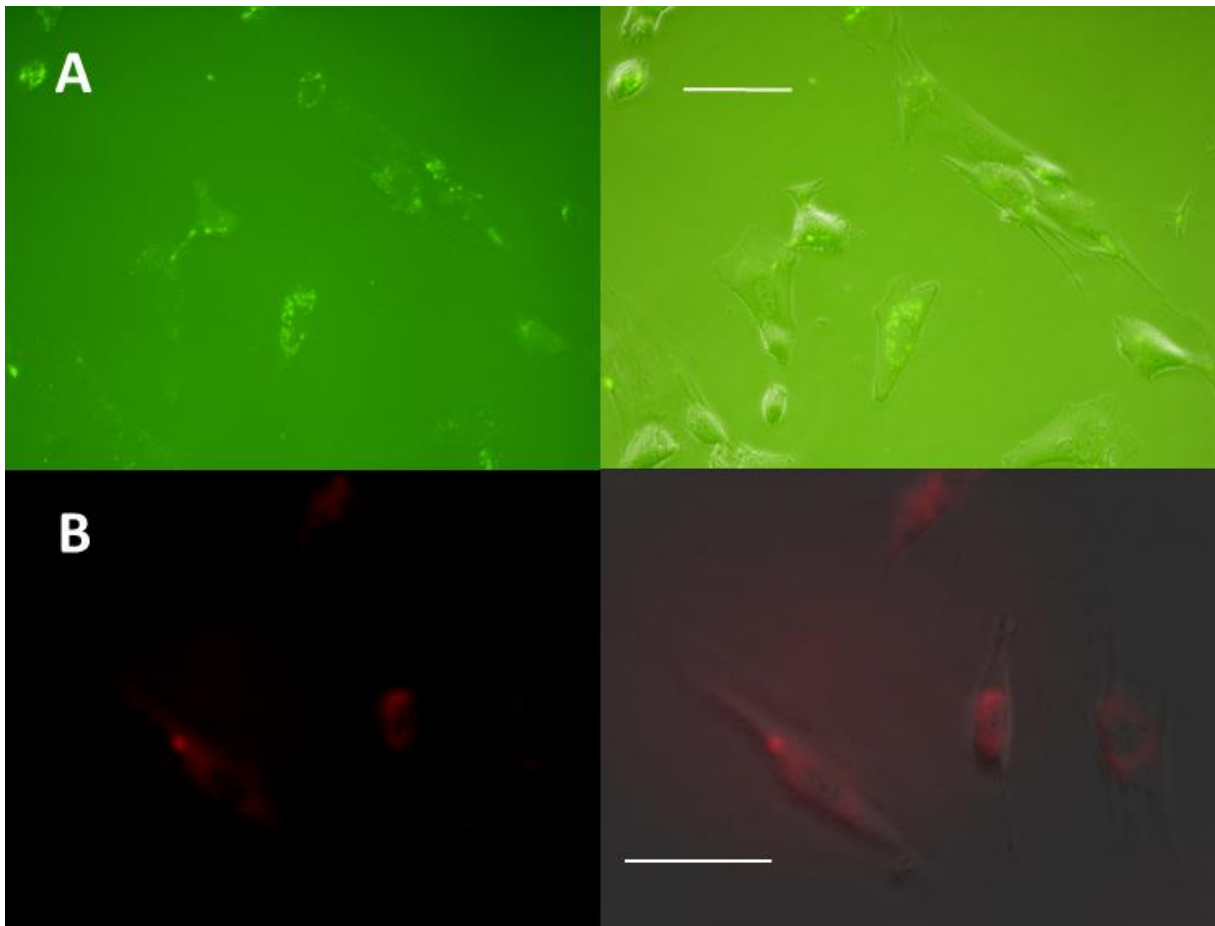


**Figure 7.4 Successful transfection of mmu-miR-181a-5p mimic and antagomiR into primary human tenocytes.** Live cell images of transfection reagent uptake 48 hours after treatment and immediately prior to processing for immunocytochemistry. **A.** Fluorescein labelled single strand RNA-23 nucleotide antagomiR treatment, **B.** Cy5 labelled mmu-miR-181a-5p mimic treatment. Bar = 50  $\mu$ m.

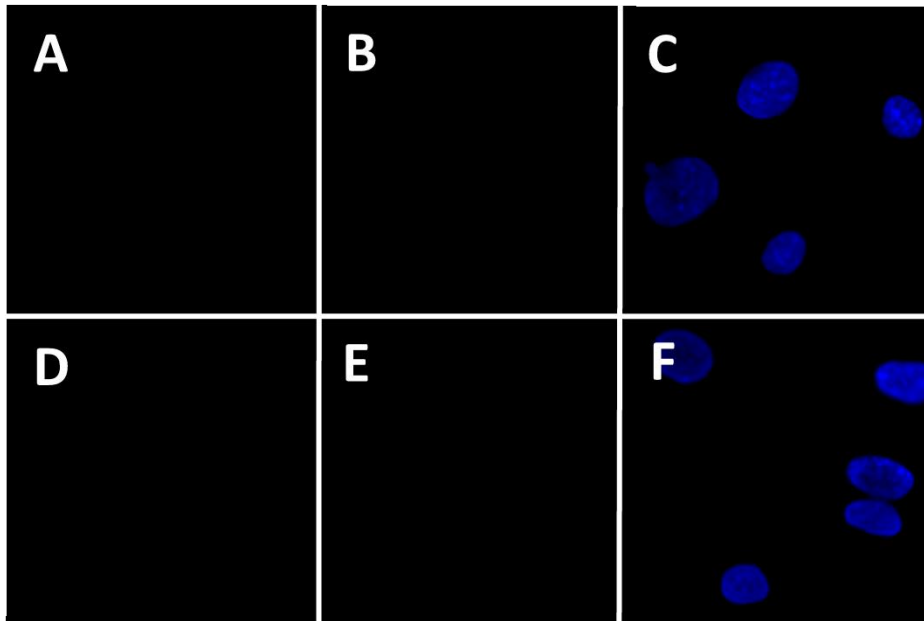


**Figure 7.5 Fluorophore-conjugated secondary anti-mouse and anti-rabbit antibodies do not generate a signal following incubation with human tenocytes in absence of primary antibody.** Tenocytes incubated for six hours with DMSO prior to fixing, permeabilisation and incubation for one hour with: **A-C** Alexa Fluor™ 488-conjugated goat anti-rabbit antibody, **D-F** Alexa Fluor 594-conjugated goat anti-mouse antibody. Images obtained at 593 nm (**A** and **D**), 510 nm (**B** and **E**), 447 nm (**C** and **F**). Nuclear counterstaining with DAPI (4',6-diamidino-2-phenylindole). DMSO = dimethyl sulfoxide.

The regulation of autophagy and mitochondrial turnover was then established by immunostaining for the proteins TOMM20, DJ-1, LC3B, P62/SQSTM1 and Parkin, as previously investigated in equine tenocytes (Chapter 5, section 5.3.3).

LC3B positive punctae are frequently regarded as specific markers of autophagosomes, representing the phosphatidylethanolamine conjugated form (LC3BII) specific to autophagosomal membranes (Runwal et al 2019). Occurrence of LC3B positive punctae has also been described when autophagosome formation is inhibited, representing LC3BI localisation to P62/SQSTM1 aggregates which accumulate secondarily to autophagy impairment (Runwal et al 2019).

In DMSO treated controls, mitochondrial networks were present in all treatment groups. LC3B positive punctae were evident in all treatment groups, distributed throughout the cells, however, miR-181a mimic treated cells showed considerably fewer punctate structures than either antagomiR or scrambled control treated cells. AntagomiR and scrambled treated groups showed a similar abundance of LC3B positive punctae, but overall these appeared to be larger and more prominent in the antagomiR treated group (Figure 7.6).

Exposure to CCCP induced mitochondrial network fragmentation in tenocytes from all treatment groups, as demonstrated by punctate TOMM20 staining pattern, indicating CCCP treatment had been successful (Figure 7.6). Markedly, increased numbers of LC3B positive punctae were apparent in both miR-181a mimic and scrambled control treated groups, whilst number appeared reduced or unchanged in the antagomiR treated group, in comparison with DMSO controls (Figure 7.6). Increase in LC3B positive punctae with CCCP treatment in mimic and scrambled groups is consistent with an increase in LC3BII positive autophagosome formation, or impaired degradation, or representative of LC3BI aggregations associated with ubiquitin and P62/SQSTM1 under autophagy deficient conditions (Runwal et al 2019). The relative lack of alteration in LC3B positive punctae number and distribution between CCCP treated tenocytes and DMSO controls in the antagomiR treated group suggests that inhibition of miR-181 activity prevents recruitment of autophagosomal membranes to dysfunctional mitochondria. Whereas immunoblotting can differentiate between LC3BI and LC3BII on the basis of different molecular weights and migration speeds in SDS-PAGE separation, fluorescent signal acquired during immunocytological imaging does not make this distinction. When considered in conjunction with the protein quantification results based on Western blot analysis above (Figure 7.3), these results suggest that miR-181 mimic treated cells are recruiting and degrading LC3BII appropriately, indicating progression of mitophagy, whilst in antagomiR treated tenocytes, the process is interrupted.

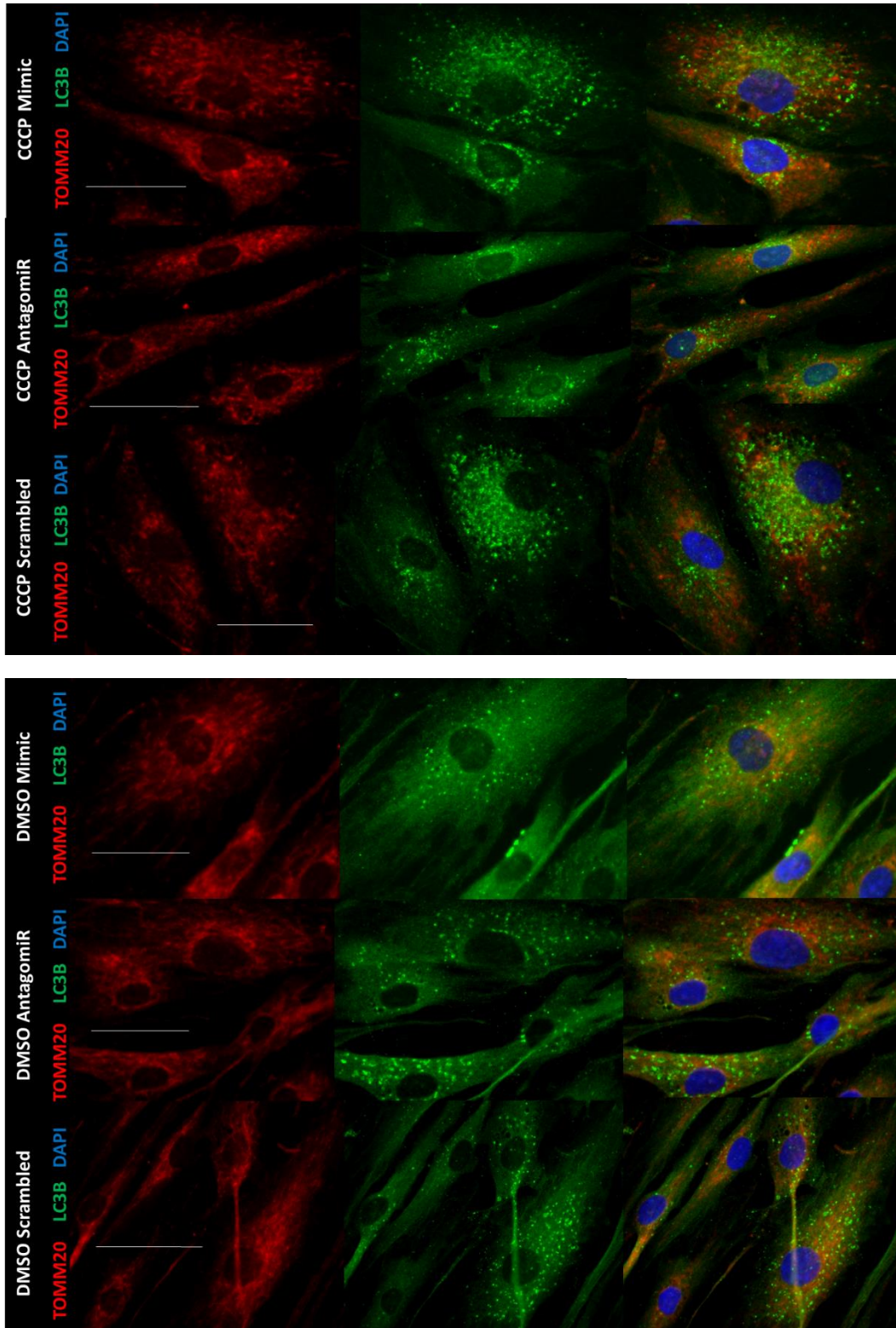


**Figure 7.6** Immunofluorescence images of miR-181a-5p mimic, antagomiR and scrambled control treated human tenocytes subjected to six hours of CCCP/DMSO exposure. TOMM20 = Translocase of outer mitochondrial membrane 20, LC3B = Microtubule-associated proteins 1A/1B light chain 3B, DAPI = 4',6-diamidino-2-phenylindole, CCCP = carbonyl cyanide m-chlorophenylhydrazone, DMSO = dimethyl sulfoxide. Images 63 x magnification, oil immersion lens, bar = 50  $\mu$ m.

We next investigated localisation of protein DJ-1, reported to localise to mitochondrial complex I under basal conditions, an effect which is rapidly enhanced under conditions of oxidative stress. Under these conditions it exerts a protective effect, becoming oxidised to maintain mitochondrial function (Hayashi et al 2009).

In DMSO controls, TOMM20 staining indicated mitochondrial networks were present, with staining more prominent in the antagomiR treated group. CCCP treatment resulted in mitochondrial disruption, as evidenced by more punctate appearance of TOMM20 staining in all treatment groups (Figure 7.7).

DMSO controls showed weak and diffuse DJ-1 staining in both miR-181a mimic and scrambled control treated cells. AntagomiR treatment resulted in greater accumulation of DJ-1 with some DJ-1 positive punctae present, suggesting DJ-1 recruitment to mitochondria (Figure 7.7). This is compatible with the observed stronger TOMM20 signal in this treatment group, suggesting preservation of mitochondrial function in these cells (McCoy and Cookson 2010).

In tenocytes incubated with CCCP, the effect of antagomiR treatment appeared to be lost, as we observed no difference in DJ-1 expression or distribution between treatment groups; miR-181a mimic, antagomiR and scrambled control treated groups all demonstrated diffuse staining without localisation to mitochondria (Figure 7.7).

These data suggest miR-181 activity may regulate DJ-1 recruitment (seen in DMSO controls), but the effect is weak in the face of widespread mitochondrial dysfunction, as this was not evident following CCCP treatment.

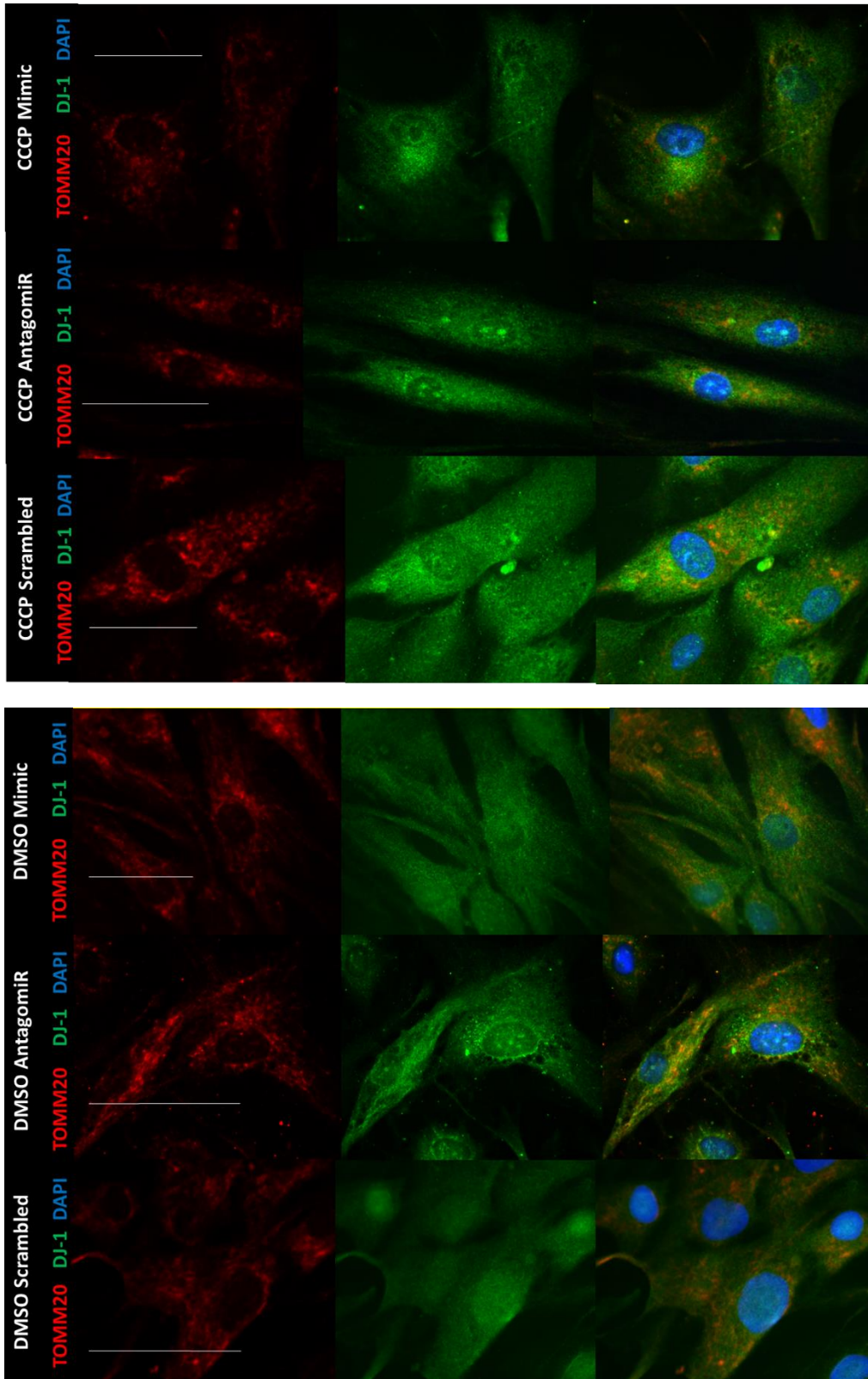


**Figure 7.7** Immunofluorescence images of miR-181a-5p mimic, antagomiR and scrambled control treated human tenocytes subjected to six hours of CCCP/DMSO exposure. TOMM20 = Translocase of outer mitochondrial membrane 20, DJ-1 = Protein deglycase DJ-1 (PARK7), DAPI = 4',6-diamidino-2-phenylindole, CCCP = carbonyl cyanide m-chlorophenylhydrazone, DMSO = dimethyl sulfoxide. Images 63 x magnification, oil immersion lens, bar = 50  $\mu$ m.

The autophagy receptor protein P62/SQSTM1 regulates formation of protein aggregates targeted for selective degradation through interactions with both ubiquitin and LC3B (Komatsu et al 2007). Similarly to LC3B, P62/SQSTM1 is also degraded during autophagy and levels can accumulate if autophagy is disrupted. However, P62/SQSTM1 accumulation can also exert a protective effect against oxidative damage by induction of the NRF2 pathway (Sánchez-Martín and Komatsu 2018), and P62/SQSTM1 has been reported to prevent CCCP-induced apoptosis (Park et al 2015).

In DMSO controls, TOMM20 staining indicated that mitochondrial networks were preserved (Figure 7.8). P62/SQSTM1 positive structures were more aggregated around the nuclei in the antagomiR treated group than others, in regions of more intense perinuclear TOMM20 staining, potentially indicative of appropriate recruitment to dysfunctional, perinuclear mitochondria, or an inappropriate accumulation due to impaired functional progression of mitophagy. Scrambled treatment showed less distinct perinuclear aggregation with a more even distribution of P62/SQSTM1 punctae. An intermediate pattern was demonstrated in miR-181a mimic treated tenocytes, with less distinct perinuclear localisation than antagomiR treated cells and punctae dispersed throughout the cell cytoplasm (Figure 7.8).

In CCCP/miR-181a mimic treated tenocytes, TOMM20 staining was punctated, with punctae distributed throughout the cytoplasm. Overall, TOMM20 staining was reduced in the miR-181a mimic treated group compared with the antagomiR and scrambled control groups (Figure 7.8). AntagomiR treated tenocytes showed a similarly punctate pattern of TOMM20 positive structures, but with a more distinct perinuclear distribution, whilst scrambled treatment showed more diffuse TOMM20 staining, with some suggestion of maintained mitochondrial networks.

P62/SQSTM1 positive aggregates were condensed in a perinuclear distribution pattern in the antagomiR and scrambled treated groups, both of which showed some degree of co-localisation with regions of more intense TOMM20 positive staining, this being more convincing in the scrambled treated group (Figure 7.8). There was a far looser perinuclear association of P62/SQSTM1 punctae demonstrated in miR-181a mimic treated cells, with punctae more widely dispersed throughout the cytoplasm, without co-localising with regions of TOMM20 positive punctae.

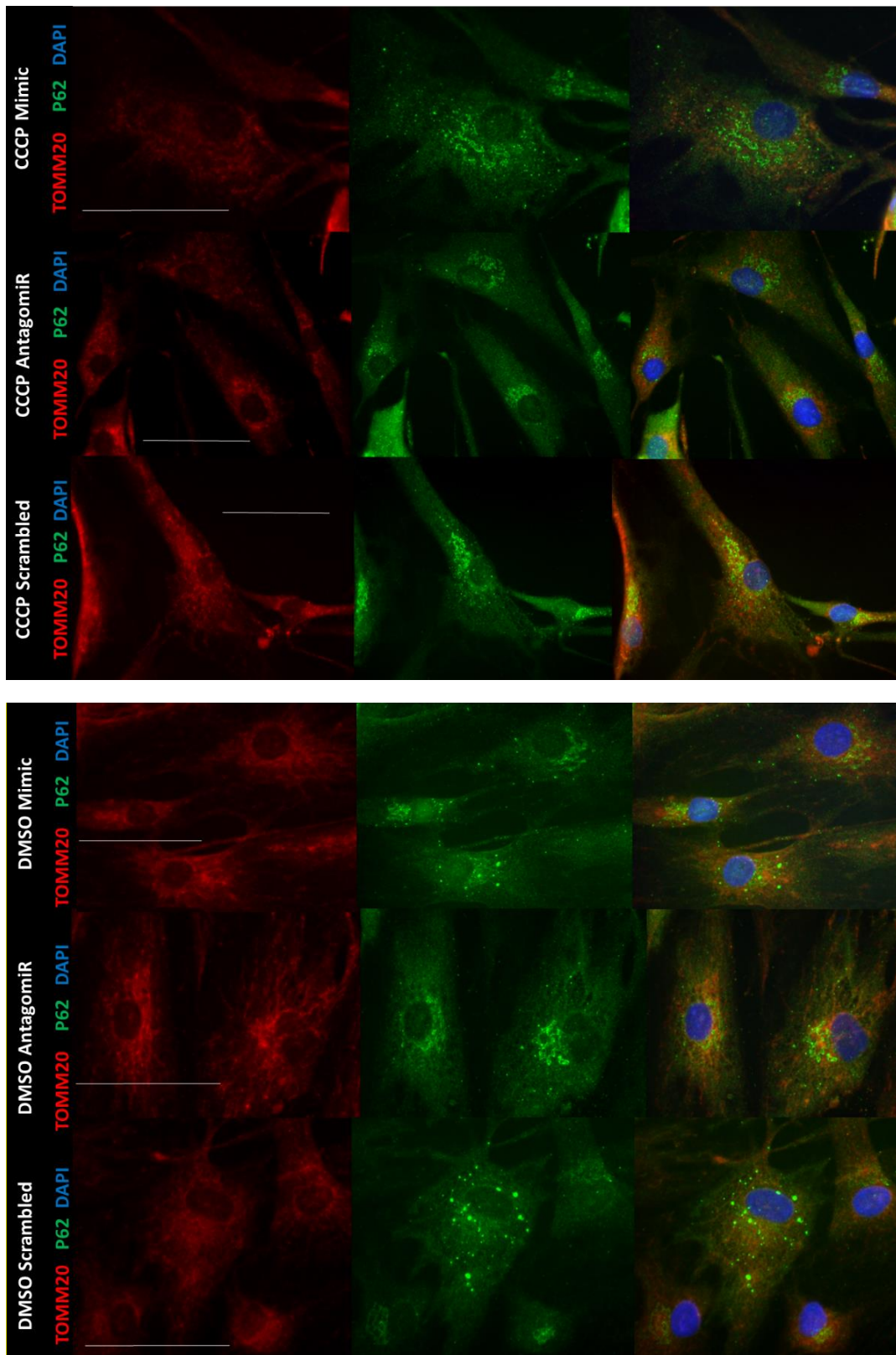


**Figure 7.8** Immunofluorescence images of miR-181a-5p mimic, antagomiR and scrambled control treated human tenocytes subjected to six hours of CCCP/DMSO exposure. TOMM20 = Translocase of outer mitochondrial membrane 20, P62 = ubiquitin-binding protein p62, DAPI = 4',6-diamidino-2-phenylindole, CCCP = carbonyl cyanide m-chlorophenylhydrazine, DMSO = dimethyl sulfoxide. Images 63 x magnification, oil immersion lens, bar = 50  $\mu$ m.

The E3 ubiquitin ligase Parkin, in concert with PINK1 is recognised as a critical component involved in the autophagic removal of depolarised mitochondria (Springer and Kahle 2011). Rapidly recruited to depolarised mitochondria, Parkin ubiquitinates outer mitochondrial membrane proteins, targeting these organelles for autophagic elimination. A parallel, but mitophagy-independent function has also been described, where Parkin recruits P62/SQSTM1 to form clusters of dysfunctional mitochondria (Narendra et al 2010). Proposed as a protective mechanism whereby surface area available for interaction with other cytosolic components is reduced, sequestration of large intracellular aggregates formed in this way may be detrimental to cell function and survival, as these are resistant to intracellular degradation (Narendra et al 2010).

In DMSO controls, TOMM20 staining revealed well defined mitochondrial networks in tenocytes in miR-181a mimic, antagomiR and scrambled control treated groups (Figure 7.9). Parkin staining was finely punctate in all treatment groups. In scrambled treated cells, Parkin signal was weak and diffusely distributed. In both miR-181a mimic and antagomiR treated cells, Parkin signal was stronger, with some areas of accumulation. No TOMM20-Parkin co-localisation was evident in any of the treatment groups (Figure 7.9).

In CCCP treated cells, mitochondrial networks were fragmented and showed a punctate staining pattern in all treatment groups (Figure 7.9). Parkin staining in mimic and antagomiR treated groups was diffuse, without evidence of co-localisation with TOMM20 positive structures. In scrambled treated cells, there were regions of Parkin accumulation, similar in appearance to those seen in the miR-181a mimic and antagomiR treated groups exposed only to DMSO. Also in the CCCP/scrambled treated group, there was a suggestion of Parkin co-localisation with regions of more densely aggregated TOMM20 positive structures, but this was not a consistent finding (Figure 7.9).

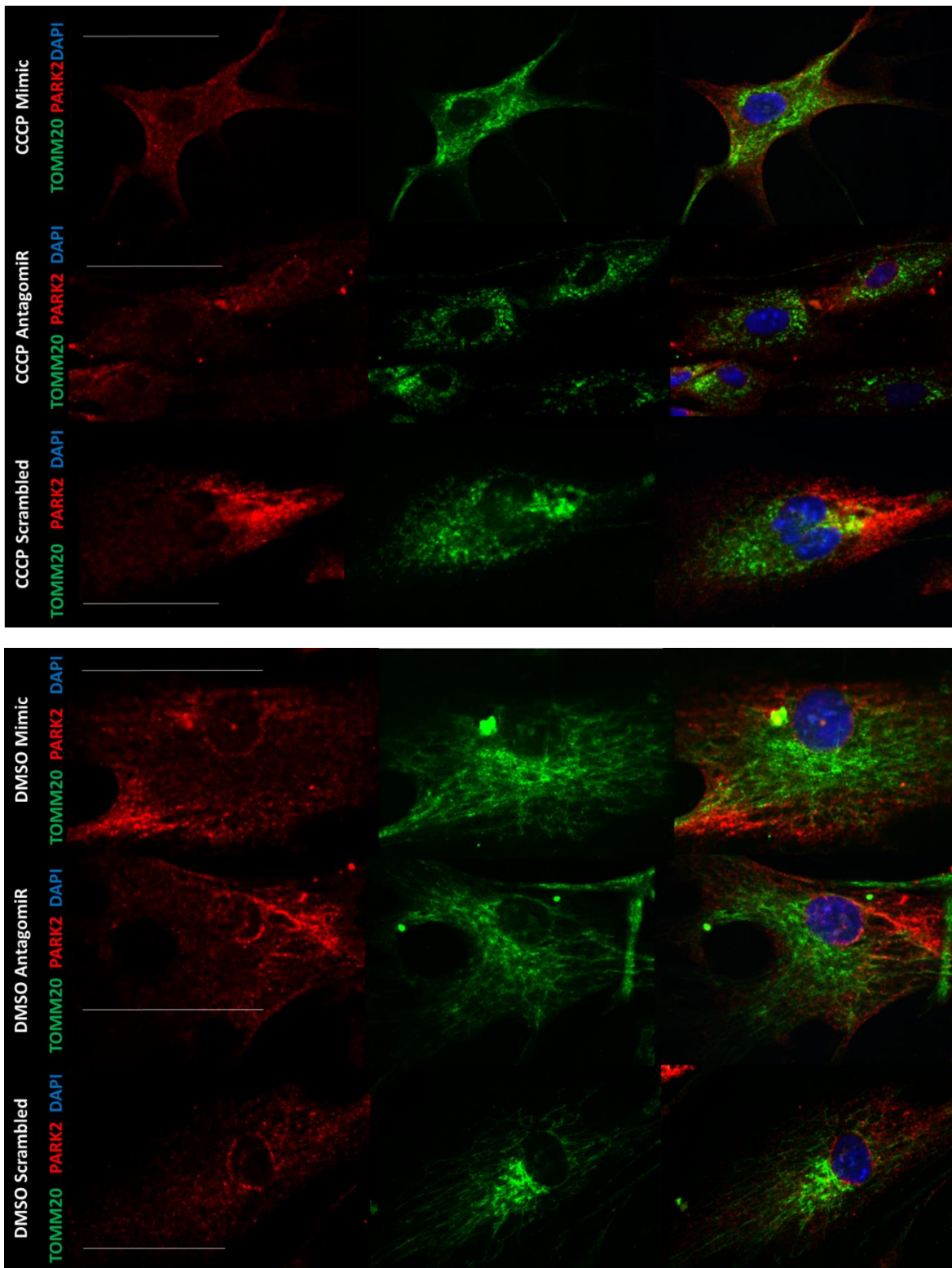


**Figure 7.9** Immunofluorescence images of miR-181a-5p mimic, antagomiR and scrambled control treated human tenocytes subjected to six hours of CCCP/DMSO exposure. TOMM20 = Translocase of outer mitochondrial membrane 20, PARK2 = Parkin, DAPI = 4',6-diamidino-2-phenylindole, CCCP = carbonyl cyanide m-chlorophenylhydrazine, DMSO = dimethyl sulfoxide. Images 63 x magnification, oil immersion lens, bar = 50  $\mu$ m.

## **7.4 Discussion**

In Chapters 5 and 6, we identified an effect of altered miR-181 activity on intracellular distribution and levels of key autophagy and mitochondrial related proteins. We additionally presented ultrastructural evidence of up regulated mitophagy subsequent to increased miR-181 levels in equine tenocytes and tendon constructs. Equine tendon has been proposed as a valid model for the study of pathophysiological processes relevant to human tendinopathy. Determination of similar mechanistic processes under equivalent conditions would substantiate this hypothesis, reinforcing the validity of this model. To this end, we have extended our investigation of overexpression and inhibition of miR-181a to human primary tenocytes in this chapter. The effect of miR-181a mimic, antagomiR and scrambled control treatments on both transcript and protein levels of selected target genes was determined in monolayer culture. We additionally utilised the CCCP-induced mitophagy model previously employed in equine tenocytes (Chapter 5, section 5.3.3) to determine the effect of miR-181 overexpression and inhibition on mitochondrial homeostasis. Our results suggest that miR-181 levels impact on autophagic processes, including mitochondrial degradation, by affecting both levels and distribution of key autophagy-associated proteins.

Treatment of tenocyte cultures with mmu-miR-181a mimic resulted in a substantial increase in total miR-181 in all cultures compared with other treatment groups. In two of the biological replicates, total miR-181 levels in miR-181a mimic treated cells were equivalent, whilst more than 10 times this level was detected in the third (Figure 7.1), recapitulating the variability in miR-181a mimic treatment effect previously observed (Chapter 5, Figure 5.2, Chapter 6, Figure 6.3). Again, miR-181b was the family member identified as being most abundant (Figure 7.1), as with miR-181a mimic treated equine tenocytes. In human tenocytes, miR-181b was responsible for 87-92% of the increase in total miR-181 levels, proportionally more than that identified in equine tenocyte monolayer culture (Chapter 5, section 5.3.2, Figure 5.2), but similar to that found in equine tendon constructs (Chapter 6, section 6.3.1, Figure 6.3). All four miR-181 family members are described in both human and murine species and each shows 100% homology between species (miRBase release 22.1, Kozomara et al 2019; Chapter 5, Table 5.3). This phenomena is therefore unlikely related to our use of human sequence directed primers in a species for which they have not been validated, but indicates that the primers used lack the sensitivity to differentiate between highly homologous short target sequences, as discussed in Chapter 5. Future work should investigate the use of locked nucleic acid oligonucleotide primers to improve sensitivity and specificity of RT-qPCR, and ideally include a greater number of biological and technical replicates, to allow selection of samples showing a more consistent treatment effect.

Total miR-181 was greater in antagomiR treated cells than in the scrambled control treated cultures in all three biological replicates. Although this was evident in some equine tenocyte cultures, in most cases antagomiR treatment of equine cells resulted in lower miR-181 levels than that expressed following scrambled control treatment (Chapter 5, section 5.3.2, Chapter 6, section 6.3.1). With equine cultures and constructs we only performed gene expression analysis in cultures where total miR-181 levels in antagomiR treated cultures was below that of the scrambled control treated group, to improve confidence in our results. This was not possible in human cultures due to the low number of biological replicates and consistent miR-181 expression pattern between all replicates. As

discussed in Chapter 5, we used a cholesterol conjugated 2'-O-Me antagomiR, modifications reported to promote miRNA degradation (Stenvang et al 2012). Accordingly, successful antagomiR treatment should have resulted in miR-181 levels being lowest in this treatment group. However, if miR-181-antagomiR interaction does not result in degradation, miR-181 will still be detected by RT-qPCR, even though in the intracellular environment it would still be susceptible to inhibition. The disparity in miR-181 levels observed between equine and human tenocytes following antagomiR treatment may reflect a difference in cellular response between the species, or a stochastic consequence of the low number of biological replicates available from human donors. Further investigation of these differences could include the use of alternative transfection protocols and culture conditions as discussed in Chapter 5. Additionally, inclusion of a greater number of biological replicates and/or increasing the number of technical replicates would be useful to determine if this is a consistent effect. Further to this, of the three biological replicates available, whilst ages were similar (within a range of eight years), two were from white British patients, one from a Chinese patient, and the cohort contained one female and two males. Ethnicity influences miRNA, and subsequently gene expression, under basal conditions in lymphoblastoid cell lines (Huang et al 2011), and in early stage breast cancer tissue (Nassar et al 2017). In human Achilles tendon, alterations in miRNA expression with ageing differs between male and female subjects (Pease et al 2017). Our results should, therefore, be interpreted with the caveat that differences in sex and ethnicity in our study cohort may have influenced our results, masking subtle changes due specifically to manipulation of miR-181 levels.

Similar to our findings with equine tenocytes in both monolayer culture (Chapter 5, Figure 5.3) and three-dimensional tissue engineered constructs (Chapter 6, Figure 6.4), we observed no difference in transcript expression of any of the target genes investigated using RT-qPCR (Figure 7.2). We did however identify significant decreases in levels of protein products of two of the genes of interest, LC3BII and TOMM20, in the miR-181a mimic treated group (Figure 7.3). The lack of significant changes in transcript expression, coupled with the identification of significant differences in the levels of these two proteins indicates that miR-181 acts through orchestrating alterations in protein translation rather than transcript stability (Soriano-Arroquia et al 2016, Bartel 2018), as discussed in Chapter 5. This is corroborated by our findings in equine tendon constructs in Chapter 6, where transcript expression of *P62/SQSTM1* and *COXIV* was unchanged, but significant differences in levels of both of these proteins were detected (Chapter 6, Figures 6.4 and 6.7).

LC3BII is the phosphatidylethanolamine-conjugated form of the ubiquitin-like LC3 protein, present on the surface of phagophores and autophagosomes (Runwal et al 2019). Nascent LC3B is rapidly converted to the soluble cytoplasmic form LC3BI by the action of the protease autophagy related 4B cysteine peptidase (ATG4B). LC3BI is then further modified by the activity of autophagy-related protein 7 (E1-like activating enzyme, ATG7), autophagy-related protein 3 (E2-like conjugating enzyme, ATG3) and conjugated to phospholipid by the ATG16L complex (E3-like ligase enzyme) to form LC3BII (Mizushima and Yoshimori 2007, Kimura et al 2009). Induction of autophagy enhances the lipidation reaction, reflecting increased autophagosome formation (Kimura et al 2009). Lysosome fusion, to create the mature autophagolysosome results in lysosomal proteases degrading LC3BII located on the inner aspect of the membrane, whilst that on the outer surface is delipidated by ATG4 to regenerate the soluble LC3BI form (Kimura et al 2009). The reduction in LC3BII observed in the miR-181a mimic treated group, with consequent reduction in LC3BII/LC3BI ratio, is therefore consistent with enhanced autophagic activity with accelerated completion of autophagolysosome

degradation, or interruption of the enzymatic lipidation of LC3BI indicating inhibition of autophagic activity (Kimura et al 2009). However, the increase in LC3B positive punctae observed in miR-181a mimic treated tenocytes following incubation with CCCP (Figure 7.6), would tend to support the former interpretation. This is substantiated by a similar response in the scrambled control treated group, as this treatment should be inert, having no impact on intrinsic intracellular processes. Equally consistent with this is lack of observed effect in the antagomiR treated group following induced mitophagy, indicating that downregulation of miR-181 activity inhibited this process (Figure 7.6).

Despite retaining an independent genome, mitochondria only derive approximately 1% of their proteins from their intrinsic genetic code (Schmidt et al 2010). This necessitates a sophisticated import system to translocate cytosolic precursor proteins across the double membrane of the organelle to the mitochondrial matrix. This is achieved by the synchronous function of the translocase of the outer membrane (TOM) and the translocase of the inner membrane (TIM) multiprotein complexes. TOMM20 is one of three preprotein receptors forming part of the TOM complex of mitochondria and is necessary for the recognition and transfer of targeted proteins through the TOM40 channel into the intermembrane space for further processing by the TIM complex (Schmidt et al 2010). TOMM20 levels are considered a reliable marker of mitochondrial mass (Song et al 2018, Buso et al 2019), with increased expression shown to correlate with increased mitochondrial mass in several types of malignant tumours (Park et al 2019). Reduction in TOMM20 levels in the miR-181a mimic treated group, concurrent with reduced LC3BII levels, suggests that miR-181 upregulation may increase mitophagic activity. In skeletal muscle, miR-181a up regulated levels of TOMM20 (encoded by the nuclear genome) and COXI and MT-ND1 (NADH-ubiquitone oxidoreductase chain 1) both encoded by the mitochondrial genome, with concurrent reduction in autophagy-associated proteins P62/SQSTM1, DJ-1 and Parkin. This indicated upregulation of both mitochondrial biogenesis and mitophagy, maintaining a functional population of morphologically normal mitochondria (Goljanek-Whysall et al 2020). Interestingly, neither TOMM20 nor LC3BII levels in tendon constructs showed alterations in response to treatment (Chapter 6, Figure 6.7).

Unfortunately, determination of protein levels in equine tenocyte monolayer culture in response to upregulation and inhibition of miR-181 activity (Chapter 5) was not performed, precluding direct comparison of effect between species. However, in tissue-engineered constructs developed using equine tenocytes, we did detect significant differences in levels of proteins NRF2, COXIV and BNIP3, which all showed higher relative levels in the miR-181a mimic treated group, and P62/SQSTM1, which showed higher levels with antagomiR treatment (Chapter 6, Figure 6.7). These differences in protein dynamics in response to miR-181 treatments may reflect differences in culture environments and temporal exposure to treatments, or species specific differences. Additionally, autophagy related proteins are tightly controlled and have a fast turnover, therefore detecting differences in levels may be problematic. Alternatively, miR-181 may regulate mitophagy further upstream than these proteins, accounting for changes in their localisation rather than levels. Further work should replicate the monolayer culture work in equine tenocytes to enable direct comparison of protein levels under equivalent conditions.

Western blots derived from human samples were of far greater quality and consistency compared to those performed on extracts from equine tenocytes, potentially reflecting the fact that primary

antibodies were validated against human proteins, but also that, with the exception of COXIV, greater mass of protein was loaded per sample for electrophoresis than with equine tenocytes.

The complete lack of detectable signal for Parkin, even with increased mass of protein loaded onto the gels, was disappointing. Although Parkin was one of the proteins visualised least successfully by Western blot immunoreactivity in equine tendon constructs, sufficient signal was obtained to enable analysis in three out of seven biological replicates, using half the amount of protein. Similar protocols were followed with human and equine tenocyte protein extracts and Ponceau staining indicated successful protein transfer to PVDF membranes with all three human biological replicates. A primary mouse monoclonal antibody directed against amino acids 399-465 at the C-terminus of the protein was used (ab77924, abcam, Cambridge, UK), identical to that used successfully for immunocytological assessment of Parkin localisation (Figure 7.9 (and Chapter 5, Figure 5.10)), although at a lower dilution (1:200 versus 1:100). Parkin has been described as a difficult protein to work with, as the structural stability and enzymatic activity are sensitive to thermal, denaturing and reducing conditions (Seirafi et al 2015). However, neither of the experimental methodologies employed here required preservation of the tertiary structure or catalytic activity, indeed Western blot analysis requires reduction and denaturation of proteins. The reason for the lack of detectable immunoreactivity following SDS-PAGE remains unclear. Further work investigating miR-181 influence on Parkin expression will require additional optimisation of this technique.

We utilised the CCCP-induced model of mitophagy previously reported with human C2C12 myoblasts and cervical adenocarcinoma HeLa cells (Kagan et al 2016, Webb et al 2017), and employed in our equine monolayer tenocyte culture work (Chapter 5). Staining for the outer mitochondrial membrane protein TOMM20 revealed a punctate staining pattern in all CCCP treated cells consistent with mitochondrial network fragmentation, indicating treatment success (Miyazono et al 2018). Consistent with reduced LC3BII protein levels in miR-181 mimic treated tenocytes (Figure 7.3), miR-181a mimic treated DMSO control cultures showed reduced LC3B positive punctae in comparison with antagomiR and scrambled control treated groups (Figure 7.6). Induction of mitophagy resulted in substantial increases in LC3B positive punctae in both miR-181a mimic and scrambled control treated groups, with little appreciable change in the antagomiR treated group (Figure 7.6). This likely represents an increase in autophagosome formation, indicating increased autophagic activity, not observed in the antagomiR treated group. Alternatively, this could represent accumulation of autophagic vesicles in miR-181a mimic and scrambled control treated cells as a result of failure of autophagosomes to progress to autolytic degradation, and/or accumulation of LC3BI aggregates in association with P62/SQSTM1, described in autophagy deficient cells (Runwal et al 2019). In equine monolayer culture, the scrambled control treated group exhibited a similar change to that apparent with human tenocytes following exposure to CCCP (Chapter 5, Figure 5.7). In miR-181a mimic treated equine tenocytes exposed to CCCP, whilst an increase in LC3B positive punctae was not observed, accumulation of LC3B immunofluorescence was evident. Again, the least change was seen in the antagomiR treated cells (Chapter 5, Figure 5.7). Thus, it appears that in both human and equine tenocytes, LC3B activity is regulated in a broadly similar fashion by miR-181.

Protein DJ-1 showed little change, either with treatment, or following CCCP exposure in human tenocytes (Figure 7.7). Equine tenocytes under similar conditions demonstrated greater numbers of DJ-1 positive punctae in all treatment groups, and changes in punctae distribution following CCCP exposure, although little effect of miR-181 treatments was found (Chapter 5, Figure 5.8). DJ-1 is

recruited to damaged mitochondria under conditions of oxidative stress, where it exerts a protective effect on mitochondrial function (McCoy and Cookson 2011). The differences in DJ-1 punctae formation and distribution observed between species may reflect differences in tenocyte susceptibility to oxidative stress under basal conditions. CCCP treatment results in rapid and complete depolarisation of the mitochondrial network, resulting in supra-physiological levels of damage (Seirafi et al 2015). Our data would suggest that the effect of miR-181 on DJ-1 is weak in both human and equine species, with any impact rendered undetectable under conditions of enhanced cellular stress.

The strikingly well demarcated, condensed perinuclear distribution of P62/SQSTM1 observed in equine tenocyte cultures in all treatment groups, incubated with DMSO (Chapter 5, Figure 5.9) was not replicated in human tenocytes under equivalent conditions (Figure 7.8). Perinuclear aggregates were observed, but these were far more fragmented and ill-defined. However, following incubation with CCCP, more distinct perinuclear accumulation was evident in antagomiR and scrambled control treated tenocytes, with a wider dispersal pattern observed in the miR-181 mimic treated group (Figure 7.8). These changes are all reminiscent of the situation observed in equine tenocytes exposed to the same conditions (Chapter 5, Figure 5.9). Therefore, under basal conditions (DMSO exposure) miR-181 activity appears to influence P62/SQSTM1 localisation to some degree, but this effect is enhanced under conditions requiring increased autophagic activity (CCCP treatment). Depolarised, ubiquitinated mitochondria cluster in perinuclear aggregates prior to degradation, a process shown to require P62/SQSTM1 recruitment in HeLa cells and mouse embryonic fibroblasts (Narendra et al 2010, Okatsu et al 2010). This is consistent with the enhanced perinuclear accumulation of P62/SQSTM1 positive aggregates observed following incubation with CCCP in antagomiR and scrambled control treated tenocytes (Figure 7.8). However, mitochondrial degradation can occur in the absence of P62/SQSTM1 (Narendra et al 2010, Okatsu et al 2010), and P62/SQSTM1 is known to function as a central signalling molecule in multiple cellular pathways in addition to being an autophagy receptor protein (Sánchez-Martín and Komatsu 2018). The more dispersed appearance of P62/SQSTM1 punctae observed in the CCCP/miR-181a mimic treated tenocytes may therefore represent involvement in autophagy of other cellular components, or processes unrelated to autophagy.

In equine tenocytes, immunocytological studies identified Parkin as one of the proteins showing greatest alteration in accumulation and co-localisation with TOMM20 punctae in antagomiR treated cells following CCCP-induced mitophagy (Chapter 5, Figure 5.10). In human tenocytes we did not observe this. Parkin staining was weak in both miR-181a mimic and antagomiR treated cells exposed to DMSO, with a suggestion of accumulation in the scrambled control group, whilst the reverse situation appeared to be evident after incubation with CCCP (Figure 7.9). Parkin levels and activity are tightly controlled within the cell, but once activated, Parkin demonstrates low substrate specificity and is itself ubiquitinated, facilitating its own degradation (Seirafi et al 2015). Mitophagy can proceed through different mechanisms, dictated by the effects of multiple signalling cascades, in turn determined by specific cellular contexts (Lemasters 2014, Palikaras et al 2018). Consequently, mitophagy can proceed through Parkin dependent and independent mechanisms. These utilise other ubiquitin E3 ligases such as SMAD specific E3 ubiquitin protein ligase 1 (SMURF1), mitochondrial E3 ubiquitin protein ligase 1 (MUL1), siah E3 ubiquitin protein ligase 1 (SIAH1), E3 ubiquitin protein ligase Autocrine Motility Factor Receptor (Gp78) and Ariadne RBR E3 ubiquitin protein ligase 1 (ARIH1) to generate ubiquitin chains, which then recruit autophagy adaptor proteins to the labelled

mitochondria (Palikaras et al 2018). Unfortunately, due to the complete lack of detectable Parkin signal generated following Western blot imaging, we were unable to use Parkin quantification to inform our interpretation of Parkin localisation determined immunocytoologically. It is possible that mitophagy in equine tenocytes is more dependent on Parkin-mediated mechanisms, with Parkin-independent mechanisms being more important in human tenocytes, although this cannot be conclusively determined from our results. Equally, the CCCP-induced mitophagy model utilised concentration and time exposure factors optimised in equine tenocytes, which we assumed would be appropriate for use in human tenocytes. However, our results suggest this protocol may engender a different response and future work should determine if the experimental methodology could be refined specifically for human tenocytes.

We have identified changes in the level of key autophagy-associated protein LC3BII in response to upregulation of miR-181 activity in association with a reduction in mitochondrial mass as determined by levels of the outer mitochondrial membrane protein TOMM20. Unlike in equine tenocytes, LC3BII was significantly lower in miR-181a mimic treated than other groups, with LC3BII/LC3BI ratio lower (a non-significant increase in LC3BII/LC3BI ratio was seen in equine tenocyte culture). Overall, our data suggest that miR-181 activity regulates mitochondrial dynamics and autophagy related proteins in both equine and human tenocytes, mechanisms fundamental to maintaining cellular functionality and adaptability and therefore critical maintaining tissue integrity and repair. Although the mechanisms may not be entirely analogous between species, and require further investigation, we believe that our data are broadly supportive of the use of equine tenocytes as a model of pathophysiological mechanisms in human cells. Further work should seek to specifically interrogate the effect of miR-181 on mitochondrial architecture and turnover. This could include using targeted delivery of a pH-sensitive fluorescent reporter protein to the mitochondrial matrix (mt-Keima; Katayama et al 2011), or a tandem GFP-mCherry pH-sensitive probe targeted to the outer mitochondrial membrane proteins (*mito*-QC; Allen et al 2013, McWilliams et al 2016), which more accurately identify lysosomal delivery of labelled mitochondria. Disruption to mitochondrial dynamics may contribute to tendon disease through ROS-induced enzymatic and non-enzymatic degradation of extracellular matrix proteins, or progression of tenocytes to a chronic pro-inflammatory senescence associated secretory phenotype, in which cell cycle arrest and further mitochondrial degradation promote continued tissue deterioration.

## **Chapter 8 – General discussion, conclusion and progression of work**

Tendon injuries represent over half of all musculoskeletal injuries sustained in UK jump racing (Williams et al 2001), the majority affecting the superficial digital flexor tendon (SDFT) of the forelimb (Ely et al 2009, Perkins et al 2005). In the general human population, incidence of tendinopathies varies between 0.3-5.5% (Littlewood et al 2013, Albers et al 2014), increasing to 11% in athletic individuals, and with a prevalence of 18.5-44.6% in some sporting disciplines (Lian et al 2005, Lopes et al 2012). Aetiology is multi-factorial and incompletely understood (Wertz et al 2013), but chronic, asymptomatic deterioration at the cellular and molecular level precedes clinically apparent disease (Sharma and Maffulli 2005, Millar et al 2010, Millar et al 2015). Altered gene expression is reported in ageing healthy (Peffer et al 2015) and chronically diseased (Ireland et al 2001) tendon, with increased expression of genes associated with apoptosis and autophagy and altered relative expression of MMPs and TIMPs reported in Achilles tendinopathy (Ireland et al 2001, Alfredson et al 2003, Jones et al 2006, Corps et al 2006). This suggests enhanced catabolism of both collagenous and non-collagenous matrix increasing the likelihood of mechanical loading resulting in tissue disruption (Peffer et al 2014). Once this occurs, mechanical integrity is never fully restored (Sharma and Maffulli 2005). There is a need to understand the mechanisms that precipitate and drive the changes that result in clinical disease. As powerful regulators of gene expression, miRNAs are likely implicated in these processes and provide an opportunity to approach tendinopathy therapeutics from a novel angle. This study has highlighted substantial changes occurring in the small non-coding RNA transcriptome associated with tendinopathy in both human and equine species, and identified some similarity between the two species.

### **8.1 Tissue sample collection**

Human tissue samples utilised in this study consisted of tendinopathic supraspinatus and posterior tibial tendon (PTT), with semitendinosus and gracilis tendon as controls. In humans a number of elastic energy storing tendons are associated with clinically important disease – rotator cuff, Achilles, PTT. Human tendon tissue samples typically only become available in the chronic stages of disease, when patients undergo surgery, therefore early stage disease samples are rarely encountered. Additionally, results presented in this study suggest that response to injury may differ between elastic energy storing tendons from different anatomical locations. Acquisition of control tissue is also problematic as there are only limited, specific tendons from which samples can be obtained, dictated by recognised reconstructive or salvage procedures being performed. Therefore, tendons from different anatomical locations with dissimilar structures and subjected to varied intensities, durations and loading regimes are often compared, introducing bias. Likewise, heterogeneity in age, sex, ethnicity, genetic and lifestyle factors of sample donors all contribute to sample variability of both diseased and control tissue.

It is extremely rare for horses to undergo surgery for tendon injury, with the exception of acute traumatic lacerations, which are not representative of the degenerative changes seen in tendinopathies. Clinically apparent tendon disease rarely results in euthanasia as conservative management is often attempted. Therefore, acquisition of tendon samples is to a large degree

opportunistic, with tendinopathic tissue often identified incidentally post-mortem. Additionally, samples are often collected from abattoir material, therefore clinical history is unavailable. Where diseased tissue is identified, however, control tissue from the same tendon, or from the analogous tendon in the contralateral limb (if disease is not bilateral) is easily obtained, enhancing the value of comparative analyses. As with human tissue though, these samples only represent the changes seen with chronic disease, although the duration of disease and prior treatment history will likely be unknown. Counteracting these problems, is the fact that the SDFT is overrepresented in equine tendon disease, making collection of a single tendon more clinically and experimentally relevant.

The method of tenocyte isolation differed between equine and human tissue in this study. Collagenase digestion of equine SDFT yielded abundant viable tenocytes which demonstrated excellent proliferative capacity. This method failed to yield any cells from human tissue samples, necessitating an alternative approach. Human tenocytes were derived through the explant method and demonstrated a more rounded appearance and slower growth characteristics than equine cells harvested by digestion. Whilst these gross differences may reflect heterogeneity in tenocyte morphology and behaviour between species, it is possible that the different methods of isolation contributed to this. Nichols and co-workers (2021) reported that explanted murine tenocytes isolated from flexor digitorum longus (FDL) tendon exhibited different morphology and reduced proliferative capacity than those obtained by digestion. Additionally, expression of *SCX*, *MKX* and *COL1A1* was reduced, whilst that of *COL3A1*, periostin, *CD248* and  $\alpha$ -smooth muscle actin was increased, compared to digestion isolated cells. Expression of tenogenic and fibroblast activation markers were also different between cells subjected to digestion and those in intact FDL tendon (Nichols et al 2021). The authors concluded that isolation by any method alters cell behaviour compared to that exhibited in intact tendon, but removal of matrix cues via digestion resulted in a different activation profile to that expressed by cells migrating out of explanted tissue. Further, application of these isolation protocols to murine tail, flexor carpi ulnaris and Achilles tendon identified that, in addition to isolation method, tendon of origin also significantly affects tendon cell population and behaviour in *in vitro* culture (Nichols et al 2021). Comparing digestion and explant methods in MSC isolation from equine SDFT, Gittel and colleagues (2013) reported similar growth characteristics and lineage differentiation capacities between methods, but higher yields and *SCX* expression following digestion isolation, suggesting this is the method of choice in equine tissue (Gittel et al 2013). The lack of tendon cell lines mandates isolation and culture of primary tendon cells, but there is no standard protocol reported for this purpose. Differences in tendon of origin and isolation techniques employed in this study may have contributed to the differences observed between species.

Whilst samples obtained from surgical or cadaveric sources may reflect the clinical population, elucidating the basic, mechanistic processes independent of the inherent confounders becomes problematic. These factors present limitations in interpretation of results derived using samples obtained in these ways, thus there remains a need to develop a suitable model in which cellular functions and behaviour can be investigated under more tightly controlled conditions.

## **8.2 Comparison of sncRNA transcriptome changes in human and equine tendinopathy**

RNA-seq of human tendon tissue generated a large, unbiased data set. The sensitivity and specificity of this technology permits differentiation of single nucleotide differences in highly similar transcripts, allows identification of small changes in expression and suffers from less technical variation than RT-qPCR. We used a targeted approach to determine miRNA expression in equine SDFT, but in future work it would be interesting to perform small RNA-seq on samples of tendinopathic and healthy equine SDFT. This would permit a more comprehensive exploration of similarities in expression profiles between species. There is obviously a cost implication in this but a larger, unbiased and more robust data set would result.

Filtering target prediction algorithms using the terms musculoskeletal and connective tissue disorders and fibroblast cell type biased the bioinformatics output, but interestingly, terms associated with cellular proliferation and survival and inflammation were prominent. Cell proliferation, differentiation or viability assays were not performed in either monolayer cell cultures or three-dimensional constructs during this study, although light and electron microscopy images indicated cell viability was maintained. Given the bioinformatics analysis prediction of increased cellular proliferation and reduced apoptotic potential, it would be interesting to further pursue this by performing cell viability and proliferation assays on tenocytes recovered from tendinopathic and control tissue, and in miR-181 mimic and antagomiR treated cultured cells in future studies. This is particularly relevant in light of the context- and family member-specific effects of miR-181 on these functions, widely reported in relation to carcinogenesis (Liu et al 2014, Pop-Bica et al 2018, Rezaei et al 2019, Yang et al 2017).

Incorporation of terminal deoxynucleotidyl transferase dUTP nick end labelling (TUNEL) staining to identify DNA fragmentation as a robust marker of apoptotic cell death (Molloy et al 2006) could be easily incorporated into future work. Likewise, cell proliferation assays which measure DNA synthesis by assimilation of bromodeoxyuridine, a thymine analogue into DNA, or overall metabolic activity within cells using fluorescent or colourimetric dyes such as luciferase or tetrazolium reduction assays (Riss et al 2013 (updated 2016)) could be employed.

Network analysis reported in this study identified expression of genes implicated in fibroblast transition to a more chondrogenic phenotype (*WNT5B* and *HOXA11*), and miR-181 is reported to regulate chondrogenic differentiation in mesenchymal stem cells (Zhao et al 2018). Ageing increases chondrogenic potential of human stem cells (Peffer et al 2016) and transition to a more chondrogenic phenotype in equine SDFT (Webbon 1978, Ali et al 2021). A more cartilaginous phenotype is also reported in collagenase induced tendinopathy (Lui et al 2009) and naturally occurring Achilles (Maffulli et al 2006) and rotator cuff (Sharma and Maffulli 2005, Yokota et al 2005) tendinopathies. Upregulation of additional chondrogenic markers such as *SOX9*, *ACAN* and *COMP* could be further explored in future work. Differential expression of collagen subtypes, principally types I, II and III would also be enlightening.

Bioinformatics analysis also identified chronic inflammation as an important process influenced by dysregulated miRNAs in both human and equine tendinopathy. This supports the theory that failure to resolve early inflammation constitutes an important driver of degenerative changes (Dakin et al

2014, Dakin et al 2018). Further research into how inflammatory pathways can be controlled is needed.

### **8.3 Development of a tendon construct model**

The lack of homogeneity between clinical samples and the reliance on those expressing chronic changes makes the prospect of experimentally induced tendinopathies attractive. This would permit investigation of early disease processes in a population of similar animals. However, there are significant anatomical differences in tendon structure in rats and mice to those of humans, and there is no universally recognised overuse model for initiating disease. Many permutations of treadmill speed, incline, frequency and duration of running have been used by different investigators, and willingness of animals to participate is also variable. Standardisation of stimulus across all experimental subjects therefore may not occur. Models have been developed to induce injury in a specific tendon, such as that developed by Soslowky and co-workers (2000) to injure rat supraspinatus tendon, based on histological and biomechanical assessment (Soslowky et al 2000). Broadly in alignment with the transcriptomic and bioinformatics analyses reported in this thesis, rats subjected to a treadmill-running regime designed to induce overuse supraspinatus tendon injury demonstrated significant DE of several apoptosis, growth, differentiation and developmental-related genes (Molloy et al 2006).

Extrapolation of one model to the study of other tendons must be viewed with caution, as changes have been shown not to occur in the Achilles tendon using Soslowky's model (Huang et al 2004). One model can even produce conflicting results on the same tendon, with the same exercise protocol used to successfully induce overuse injury in rat Achilles tendon (Glazebrook et al 2008) also reported to improve Achilles mechanical properties (Heinemeier et al 2012). Additionally, gene expression profile was different to that found in either tendinopathy (Ireland et al 2001) or following short-term loading (Heinemeier et al 2007).

Chemically induced lesions such as those produced by injection of collagenase, or surgical sectioning, do not mimic the natural disease process. Although these models have been described in horses (Watts et al 2012) and laboratory animals (Oryan et al 2008, Sugg et al 2014), they are far removed from the naturally occurring changes which precipitate tendon disease in the native population. The use of tendon explants from cadaveric material has many advantages in studying the molecular adaptations and biomechanical properties of equine tendon, however the effect of post-mortem changes (fascicular swelling) and processing techniques (non-physiological storage, freeze/thaw cycles) have not been fully quantified. Equally, it is often not possible to determine the clinical history or background to the animals from which these tendons were harvested.

*In vitro* monolayer cell culture techniques, whilst allowing investigation of large amounts of cellular material and cell products, represent a non-physiological situation, as cellular arrangement, alignment and organisation within a three-dimensional matrix are not replicated (Arnoczky et al 2007). If equine tenocytes can be demonstrated to respond biochemically in a similar manner to human tenocytes, tissue engineering can provide an alternative to live animal and cadaveric models and lends itself to testing under controlled, reproducible conditions. This study presents evidence that equine and human tenocytes do share some commonality in response to changes occurring

with tendon disease. Additionally we have successfully generated three-dimensional tissue engineered constructs using primary equine tenocytes and maintained them for 28 days in culture. The constructs used in this study were exposed to static tension, which does not replicate the normal *in vivo* situation, and utilised primary tenocytes embedded in a fibrin matrix, which bears little similarity to normal extracellular matrix. However, fibrin gels have been reported to demonstrate improved tenogenic gene expression patterns and better collagen fibril alignment compared to collagen gel-based matrices (Breidenbach et al 2015). These authors showed that murine tendon and ligament progenitor cells embedded in fibrin gel exhibited continual improvement of tenogenic marker expression over 14 days of culture. Significant upregulation of *SCX*, *TNC* and *FMOD* expression, relative to collagen gel-based constructs was demonstrated, with a temporal increase in *SCX* over 14 days followed by enhanced expression of *COL1A1*, *COL3A1*, *MKX*, *FMOD* and *TNMD* in the latter stages of culture, with a concurrent degradation of fibrin.

Subjecting three-dimensional constructs to cyclical mechanical loading programmes can mimic the mechanical stimuli to which native tendon responds, but, whilst this has been done, there is again no loading program universally recognised as physiologically appropriate or representative of overuse. Devising such a programme would be useful. A strain magnitude up to 5% and frequency of 1 Hz has been described with tendon explants (Screen et al 2005, Maeda et al 2009), and protocols have been described using tissue engineered tendon constructs subjected to cyclical 2.4% strain for up to 14 days (Nirmalanandhaan et al 2007, Breidenbach et al 2015). However, higher strains, up to 10% are reported to be required in fibrin-based constructs compared to collagen gel-based ones to increase collagen production and mechanical properties (Breidenbach et al 2015). Future work should look at developing mechanical loading programmes which mimic physiologically appropriate and overuse regimes that can be applied to tissue engineered tendon constructs.

Quantitative evaluation of tissue-engineered tendon construct phenotype requires refinement. The modified grading scheme employed in this study was not able to objectively confirm the subjective impression of differences in construct phenotype subsequent to gain or loss of miR-181 activity. Histological scoring systems for tissue-engineered tendon constructs have been described, but typically, to quantify their behaviour once implanted *in vivo* (Loppini et al 2015). These, consequently, contain elements irrelevant to the *in vitro* situation. To the author's knowledge, the only scoring matrix described relevant to purely *in vitro* tissue-engineered three-dimensional constructs is that reported by Nakanishi and co-workers (Nakanishi et al 2019). This, however, was applied to scaffold-free constructs, created using a bio-3D printer, from spontaneously formed multicellular human dermal fibroblast spheroids, a methodology very different from that utilised in this study. These authors reported statistically significant, identifiable differences between constructs matured under tension-free or tension-loaded conditions, based on cellular density, orientation and phenotype, as well as alignment and size of fibres. Nakanishi and co-workers' grading matrix was a novel, modified scoring system based on that described by Watkins (1985) to describe healing of surgically created lesions in equine SDFT (Watkins et al 1985). The grading system employed in this thesis, similarly, used elements applicable to ECM organisation and tenocyte morphology and distribution, but derived from the Movin (Movin et al 1997) and Bonar (Cook et al 2004) human tendinopathy grading systems. This did not detect differences in construct morphology resulting from over expression or inhibition of miR-181 during maturation under static tension. There remains the need to design a sensitive, objective method of quantifying histological appearance of tissue-engineered three-dimensional tendon constructs. Such schemes will likely

need precisely, quantitatively defined elements and be devised for specific construction methodologies, depending on whether or not a scaffold medium is employed, and if so, may even require to be specific for substrate type (collagen or fibrin gel).

#### **8.4 Primer specificity**

Results from this study suggest primer specificity was poor for the four hsa-miR-181 family members. Despite treatment with miR-181a-5p mimic, the highest detected levels, consistently in both equine and human studies, were for miR-181b. Discrimination between targets with very similar sequences can be problematic using PCR technology as mis-priming events, primer design, cycle parameters and reagent factors all impact on quantitative accuracy. Locked nucleic acid (LNA) technology may improve this. Since performing this study, the commercially available miR-181 primers utilised have been discontinued by the manufacturer, who now only supply LNA primers. These are purported to offer greater sensitivity in discriminating between targets with highly similar sequences, and it would be interesting to investigate this.

#### **8.5 Optimisation of miR-181 transfection protocol**

Treatment of cell cultures with miR-181a-5p mimic and the antagomiR oligonucleotide yielded inconsistent results. Whilst all mimic treated cultures demonstrated an increase in total miR-181 levels, expression levels relative to the housekeeping gene varied by between six and ten times for equine and human monolayer cultures and by up to four times in the three-dimensional equine tenocyte constructs. AntagomiR treatments resulted in more consistent relative expression of total miR-181 within experimental groups, but results were inconsistent in relation to that determined in scrambled control treated groups. The antagomiR treatment was designed to bind miR-181 transcripts, inhibiting their ability to bind endogenous targets. Additionally, cholesterol conjugated 2'-O-Me modifications, included in the design to increase oligonucleotide stability, are reported to promote miRNA degradation following binding (Stenvang et al 2012). The scrambled control oligonucleotide should have exerted no biological effect. This did not appear to be reflected in the results obtained. Although cellular uptake was confirmed by visualising intracellular fluorescence, and the activity of miR-181 transcripts should still have been inhibited by the antagomiR, alternative methods of transfection may yield more consistent results and could be explored. By reducing data variability, this would generate more homogenous samples to allow for a more robust comparison.

#### **8.6 Antibody optimisation**

In both human and equine samples, semi-quantitative evaluation of protein abundance and visualisation of their cellular distribution relied on immunological techniques. More consistent and better quality data was obtained from human than equine tenocytes. There are limited antibodies available commercially which are raised against and/or validated for use with equine-specific proteins. The use of mass spectrometry based label-free quantitative proteomics offers a highly accurate, reproducible and automated technique for direct comparison of complex protein mixtures between samples. This technique has been successfully applied to equine synovial (Anderson et al

2019) and peritoneal (Bardell et al 2019) fluid samples, with proven ability to differentiate between healthy and diseased states. Whilst liquid chromatography tandem mass spectrometry (LC-MS/MS) would be an ideal methodology to allow quantitation and differentiation of protein abundances between experimental groups and is applicable to novel species, it will not provide information on protein distributions and validation would still require use of an alternative, robust technique. Western blot results were of much better and consistent quality in human samples than those from equine tissues, indicating a limitation of available antibodies to quantitate the equine variants of the proteins of interest. Therefore, development of antibodies, such as the method described by Caterson and co-workers (1985), complementary to epitopes of equine proteins would offer a substantial advantage, both in identifying distribution changes and providing a mechanism for validation of LC-MS/MS results.

## **8.7 The role of miR-181 in autophagy and mitochondrial dynamics**

Downregulation of miR-181 was observed in equine and human tendinopathy. Our group has previously identified a role of miR-181a in regulating mitochondrial dynamics in ageing skeletal muscle (Goljanek-Whysall et al 2020). In this tissue type, downregulation of miR-181a with ageing resulted in accumulation of autophagy related proteins P62/SQSTM1, DJ-1 and Parkin, abnormal mitochondria, and reduction in functional mitochondrial mass (Goljanek-Whysall et al 2020). Using miR-181 gain and loss of function studies in both equine and human primary tenocyte cultures, including in conjunction with a model of induced mitophagy, this study has identified an effect of miR-181 on autophagy related proteins BNIP3, P62/SQSTM1, LC3B, DJ-1 and Parkin. Additionally, an effect on markers of mitochondrial dynamics and oxidative stress NRF2, TOMM20 and COXIV, in concert with ultrastructural changes in mitochondrial morphology was observed. Data presented in this thesis indicate that miR-181 regulates mitochondrial dynamics and autophagy in tenocytes. Perturbations in these processes, resulting in accumulation of defective proteins and an abnormal, dysfunctional mitochondrial population, may be important contributing factors in tendinopathy. Indeed, other authors, using different experimental methodologies, have suggested that an accumulation of partially degraded matrix proteins with ageing may contribute to mechanical weakening and subsequent failure of equine SDFT (Thorpe et al 2010). Disruption to mitochondrial dynamics may contribute to tendon disease through ROS-induced enzymatic and non-enzymatic degradation of extracellular matrix proteins, or progression of tenocytes to a chronic pro-inflammatory senescence associated secretory phenotype, in which cell cycle arrest and further mitochondrial degradation promote continued tissue deterioration. In order to fully elucidate the molecular mechanisms, further investigation of autophagy progression and mitochondrial dynamics is warranted. Refinement of the treatment protocol in tendon constructs and temporal effect of chronic exposure to altered miR-181 activity, by harvesting constructs at different time points during maturation, and by exposing mature constructs to a single treatment would also be useful. Further work should also seek to more closely examine the spatial relationship between autophagy related proteins and mitochondria. Use of dual fluorophore pH sensitive mitochondrial-targeted reporter constructs such as mt-Keima (Katayama et al 2011) or mito-QC (Allen et al 2013, McWilliams et al 2016) could accurately assess lysosomal turnover of mitochondria.

Using starvation- and rapamycin-induced models of autophagy in human breast cancer (MCF-7), hepatocarcinoma (Huh-7) and chronic myelocytic leukaemia (K562) cell lines, Tekirdag and co-workers (2013) demonstrated miR-181a directly targets *autophagy-related 5 (ATG5)*, regulating both transcript and protein levels. ATG5 is a key protein required in the progression and formation of the mature autophagic vesicle. Over expression of miR-181a reduced phagophore formation, as indicated by presence of GFP-labelled LC3BII aggregates in all three cell types, concurrent with reduced P62/SQSTM1 degradation, whilst autophagy was stimulated following transfection with miR-181a antagomiR. By this mechanism, downregulation of miR-181 levels seen in both human and equine tendinopathic samples would favour phagophore elongation and progression to mature autophagic vesicles. Inhibition of autophagy by increased miR-181a activity is also reported by Liu and co-workers (2017). These authors demonstrated downregulation of miR-181a in a human neuroblastoma cell line model of Parkinson's Disease (PD). Subsequent over expression of miR-181a altered the LC3BII/LC3BI ratio, reduced *BECLIN1* expression and decreased numbers of apoptotic neurones. These authors proposed inhibition of p38 MAPK/JNK signalling as the mechanism responsible. Downregulation of miR-181a is reported in clinical PD, and inhibition of miR-181a activity *in vitro* enhanced apoptosis in this cell type (Liu et al 2017). No apparent difference in LC3B punctae formation with miR-181 mimic or antagomiR treatment was evident in equine tenocyte monolayer culture, either under basal conditions (DMSO treatment) or following CCCP-induced mitophagy. In human tenocytes however, punctae were less abundant under basal conditions in miR-181a mimic treated tenocytes, but following CCCP treatment, LC3B positive punctae increased markedly in mimic- and scrambled-treated tenocytes, whilst no change was observed in the antagomiR treated group. This suggested autophagy was stimulated in the presence of miR-181, but inhibited in the presence of the antagomiR. Additionally, reduced LC3BII/LC3BI ratio with miR-181a mimic treatment, detected by Western blot, indicated that miR-181a may promote autophagy and LC3BII degradation, supporting Goljanek-Whysall and co-workers (2020), but contrary to the work of Tekirdag and colleagues (2013). Results however could be interpreted as miR-181 upregulating autophagy, or inhibiting autophagic flux. This requires further analysis, by inclusion of a treatment group exposed to an autophagic flux inhibitor such as bafilomycin, and using the mito-QC or mt-Keima reporter constructs which were not utilised in this study.

The most studied mechanism of mitochondrial degradation by autophagy is the PINK1:Parkin pathway (Montava-Garriga and Ganley 2020). Here, stabilisation and activation of PINK1 on the outer membrane of depolarised mitochondria recruits and activates Parkin. This accelerates ubiquitination of mitochondrial surface proteins, targeting them for degradation. However, the PINK1:Parkin pathway responds differently in the face of changes in magnitude and duration of mitochondrial depolarisation (Bowling et al 2019). This may have accounted for some of the inconsistencies observed between equine and human tenocytes exposed to CCCP-induced mitochondrial depolarisation, as both rapid and delayed autophagy have been reported (Bowling et al 2019). Additionally, other E3-ubiquitin ligases may act in concert with, or independently of, Parkin downstream of PINK1. Therefore, stabilisation of PINK1 alone, independent of Parkin activation, is sufficient to recruit autophagy receptors to dysfunctional mitochondria (Montava-Garriga and Ganley 2020). Basal level mitophagy also occurs in PINK1:Parkin deficient mice, suggesting an alternative ubiquitin-independent pathway of physiological importance (McWilliams et al 2018).

In equine tenocyte culture, Parkin demonstrated the greatest change in intracellular distribution with inhibition of miR-181 function following CCCP induced mitophagy. Distribution corresponded to

that of dysfunctional mitochondria, as indicated by TOMM20 staining, however it was not clear whether this represented an appropriate response, or interruption to autophagy progression. This effect was not, however, reproduced in human tenocytes, suggesting a different response. Unfortunately, quantification of Parkin abundance was precluded by absence of observable signal in Western blots and the reason for this requires further investigation. The BCL2 family of outer mitochondrial membrane (OMM) proteins possess the ability to recruit autophagosomal membranes by direct interaction in the absence of ubiquitin (Villa et al 2018, Montava-Garriga and Ganley 2020). Several members of this family of proteins, which have both pro- and anti-apoptotic effects, are targeted by miR-181a (Ouyang et al 2012). It may be that there are species differences in the importance of ubiquitin-dependent -independent autophagy pathways. Over expression of miR-181a in primary murine astrocytes decreased levels of the anti-apoptotic BCL2 family proteins MCL1 and BCL2, with the reverse effect seen following miR-181a antagomiR treatment (Ouyang et al 2012). No effect on BCL2 levels with over expression or inhibition of miR-181a in human cancer cell lines was seen however (Tekirdag et al 2013). Expression of the pro-apoptotic family member BNIP3 is increased during hypoxia (Zhang et al 2008). BNIP3 reduces mitochondrial membrane potential, resulting in mitochondrial swelling, increased ROS production and stimulation of hypoxia-induced mitophagy/autophagy (Liu and Frazier 2015). Significantly higher levels of BNIP3 were observed in tendon constructs treated with miR-181a mimic, where swollen mitochondria with loss of cristae were also more apparent. It would be interesting to further explore the relative activities of ubiquitin-dependent and -independent pathways in tenocytes. Levels of BNIP3 were not assessed in human tenocytes and should be performed in future work. Interestingly, elevated levels of COXIV were also detected in miR-181a mimic treated tendon constructs, consistent with increased mitochondrial biogenesis. These data combined, suggest miR-181 regulates mitochondrial turnover, not just mitophagy.

There is a limited, but growing, body of work investigating the effect of miR-181 on autophagy and mitochondrial dynamics. Results can be conflicting, or difficult to corroborate, due to different experimental methodologies, cell types, or the novel aspect of the research. Results presented in this thesis support a role of miR-181 in regulating autophagy/mitophagy in tenocytes, but precludes conclusive determination as to whether this regulation is positive or negative. Effects of miR-181a and b on mitochondrial metabolism and function are reported in primary human chondrocytes (Zheng et al 2019) and in neuro- and myo-degenerative disease models (Ouyang et al 2012, Das et al 2017, Liu et al 2017, Indrieri et al 2019, Goljanek-Whysall et al 2020). Extrapolation of these findings to the situation in tenocytes must be undertaken cautiously, given the context dependent nature of miRNA effects within and between cell types and disease processes (Das et al 2017, Yang et al 2017).

## **8.8 Concluding remarks**

This project has demonstrated substantial changes in the small non-coding RNA (sncRNA) transcriptome occur with human tendinopathy, and identified similar changes in expression of three miRNAs (miR-29a, miR-181 and miR-199a) in equine tendinopathy. This suggests commonality in processes between the two species that supports the translational value of using equine tissue in the investigation of human disease. Additionally, results from gain and loss of miR-181 function in human and equine tenocyte monolayer culture, and equine tenocytes embedded in tissue-

engineered three-dimensional constructs, indicate that miR-181 levels influence efficiency of autophagic processes, including mitochondrial degradation, by affecting both abundance and distribution of key autophagy-associated proteins. This work contributes to the understanding of the basic mechanistic processes which contribute to the disease state, therefore helping to inform how therapeutic interventions may be devised and appropriately applied.

## **Appendix 1**

**Table A1.1** Reagents, consumables and equipment utilised in this study.

Reagents	Manufacturer	Product code
6-amino-n-hexanoic acid	Sigma-Aldrich, Gillingham, UK	07260-500G
Acetone EM Grade	TAAB Laboratories Equipment Ltd, Aldermaston, UK	A018
Acid Fuchsin (1%)	BioStain ready reagents, Manchester, UK	RRBD93/X
Agarose powder	Sigma-Aldrich, Gillingham, UK	A9639-100G
Aluminium Potassium Sulphate	Acros Organics, New Jersey, USA	217485000
Amersham WB Molecular Weight Markers (17-225 kDa)	GE Healthcare Life Sciences, Little Chalfont, UK	29030735
Ammonium persulfate	Sigma-Aldrich, Gillingham, UK	A3678
Amphotericin B (250µg mL <sup>-1</sup> )	ThermoFisher Scientific, Waltham, USA	15290026
Antibodies - Primary		
BNIP3 - rabbit monoclonal to BNIP3	abcam, Cambridge, UK	ab109362
COXIV - mouse monoclonal	abcam, Cambridge, UK	ab33985
COXIV - rabbit polyclonal	abcam, Cambridge, UK	ab16056
DJ1/PARK7 - rabbit monoclonal	abcam, Cambridge, UK	ab76241
LAMP1 - rabbit polyclonal	abcam, Cambridge, UK	ab62562
LC3B - rabbit monoclonal	abcam, Cambridge, UK	ab192890
MFN1 - mouse monoclonal to Mitofusin 2 + Mitofusin 1	abcam, Cambridge, UK	ab57602
MFN2 - mouse monoclonal to Mitofusin 2	abcam, Cambridge, UK	ab56889
NRF2 C-20 - rabbit polyclonal	Santa Cruz Biotechnology, Heidelberg, Germany	sc-722
P62/SQSTM1 - mouse monoclonal	abcam, Cambridge, UK	ab56416
P62/SQSTM1 - rabbit monoclonal	abcam, Cambridge, UK	ab109012
Parkin - mouse monoclonal	abcam, Cambridge, UK	ab77924
Parkin - rabbit polyclonal	abcam, Cambridge, UK	ab15954 - withdrawn
PRDX6 - rabbit monoclonal	abcam, Cambridge, UK	ab133348
TOMM20 - mouse monoclonal	abcam, Cambridge, UK	ab56783
TOMM20 - rabbit monoclonal	abcam, Cambridge, UK	ab186734
Vinculin - mouse monoclonal	abcam, Cambridge, UK	ab130007
Antibodies - Secondary		
Green (488) - Invitrogen Goat anti-mouse conjugated to Alexa Fluor 488	ThermoFisher Scientific, Altrincham, UK	A11029
Green (488) - Invitrogen Goat anti-rabbit conjugated to Alexa Fluor 488	ThermoFisher Scientific, Altrincham, UK	A11008
Green (800) - IRDye 800CW Goat anti-Mouse IgG	LI-COR, Lincoln, USA	925-32210
Green (800) - IRDye 800CW Goat anti-Rabbit IgG	LI-COR, Lincoln, USA	926-32211
Red (532) - Invitrogen Goat anti-mouse conjugated to Alexa Fluor 532	ThermoFisher Scientific, Altrincham, UK	A11002
Red (532) - Invitrogen Goat anti-rabbit conjugated to Alexa Fluor 532	ThermoFisher Scientific, Altrincham, UK	A11009
Red (594) - Invitrogen Goat anti-mouse conjugated to Alexa Fluor 594	ThermoFisher Scientific, Altrincham, UK	A11032
Red (680) - IRDye 680RD Goat anti-Mouse IgG	LI-COR, Lincoln, USA	926-68070

Reagents (cont.)	Manufacturer	Product code
Aprotinin from bovine lung	Sigma, Welwyn Garden City, UK	A1153-10MG
Ascorbate-2-phosphate	Sigma, Welwyn Garden City, UK	A4544-25G
Borax	TAAB Laboratories Equipment Ltd, Aldermaston, UK	B021
Bovine Serum Albumin (lyophilised powder)	Sigma-Aldrich, Gillingham, UK	A2153
Bovine Serum Albumin Standards (2000, 1500, 1000, 750, 500, 250, 125 µg mL <sup>-1</sup> )	ThermoFisher, Loughborough, UK	23208
CCCP (Carbonyl cyanide 3-chlorophenylhydrazone) powder	Sigma-Aldrich, Gillingham, UK	C2759
Celestine Blue	Sigma-Aldrich, St Louis, USA	206342
Chameleon Duo Pre-stained Protein Ladder	LI-COR, Lincoln, USA	928-60000
Collagenase type II powder	Life Technologies, Warrington, UK	17101015
cOmplete ULTRA Mini EDTA-free protease inhibitor cocktail tablets	Roche, Welwyn Garden City, UK	5892791001
Custom designed ssRNA-21 mer 88 nmol	Dharmacon (GE Healthcare), Little Chalfont, Bucks	Custom designed
Custom designed ssRNA-23 mer 80 nmol	Dharmacon (GE Healthcare), Little Chalfont, Bucks	Custom designed
Custom modified miRIDIAN microRNA mimic mmu-miR-181a-5p	Dharmacon (GE Healthcare), Little Chalfont, Bucks	C-310435-05
DAPI (4',6-diamidino-2-phenylindole)	Sigma-Aldrich, Gillingham, UK	D9542-1MG
DMSO (Dimethyl sulfoxide) for molecular biology	Sigma-Aldrich, Gillingham, UK	D8418
dNTPs - 2'-Deoxyadenosine 5'-triphosphate sodium salt solution 100 mM	Sigma, Welwyn Garden City, UK	D4788-1MMO
dNTPs - 2'-Deoxycytidine 5'-triphosphate disodium salt 100 mM	Sigma, Welwyn Garden City, UK	D4913-1MMO
dNTPs - 2'-Deoxyguanosine 5'-triphosphate trisodium salt solution 100 mM	Sigma, Welwyn Garden City, UK	D5038-1MMO
dNTPs - Thymidine 5'-triphosphate sodium salt solution 100 mM	Sigma, Welwyn Garden City, UK	T9656-1MMO
DPX neutral mounting medium	Thermo Scientific, Runcorn, UK	LAMB-DPX
DTT 0.1 M	Invitrogen, Inchinnan, UK	Y00147
Dulbecco's Phosphate Buffered Saline (DPBS)	Sigma-Aldrich, Gillingham, UK	D8537
Dulbecco's Modified Eagle Medium (DMEM) 1 g L <sup>-1</sup> glucose phenol red free	Life Technologies, Paisley, UK	11880-036
Eosin Y Stain	TCS Biosciences Ltd, Botolph Claydon, UK	HS250-1L
Ethanol (absolute)	TAAB Laboratories Equipment Ltd, Aldermaston, UK	E047
Ethanol for molecular biology, ≥99.8% (absolute alcohol)	Sigma-Aldrich, Gillingham, UK	51976-500ML-F
Ferric Ammonium Sulphate	BDH Chemicals Ltd, Poole, UK	271644
Fetal Bovine Serum	Life Technologies, Paisley, UK	10270106
Fibrinogen from bovine plasma	Sigma, Welwyn Garden City, UK	F8630-1G
First Strand buffer	Invitrogen, Inchinnan, UK	Y02321
Fluoromount-G	SouthernBiotech, Birmingham, USA	0100-01
Glacial Acetic Acid	Fisher Scientific UK, Loughborough, UK	A/0360/PB17
Glutaraldehyde 25% EM Grade	TAAB Laboratories Equipment Ltd, Aldermaston, UK	G002
Glycerol	VWR International, Fontenay-sous-Bois, France	24388.295
Glycine powder for electrophoresis	Sigma-Aldrich, Gillingham, UK	G8898

Reagents (cont.)	Manufacturer	Product code
Haematoxylin 95% Monohydrate	Atom Scientific, Manchester, UK	RRBD61-X
High Sensitivity RNA Screen Tape	Agilent Technologies, Cheadle, UK	5067-5579
High Sensitivity RNA Screen Tape Ladder	Agilent Technologies, Cheadle, UK	5067-5578
High Sensitivity RNA Screen Tape Sample Buffer	Agilent Technologies, Cheadle, UK	5067-5580
Horse serum	Life Technologies, Paisley, UK	16050122
Hydromount	National Diagnostics, Hull, UK	HS-106
Intercept Blocking Buffer (PBS)	LI-COR, Lincoln, USA	927-7000
Isopropanol	Sigma-Aldrich, Gillingham, UK	I9516-500ML
Laminin	Invitrogen, Inchinnan, UK	23017-015
L-glutamine solution 200 mM	Sigma, Welwyn Garden City, UK	G7513-20ML
Light Green SF Yellowish (2%)	HD Supplies, Aylesbury, UK	HD1535
Maleic acid	TAAB Laboratories Equipment Ltd, Aldermaston, UK	M003
Marvel Original Dried Skimmed Milk P powder	Premier Foods, Thame, UK	
MEM Non-essential amino acids (100x)	Sigma, Welwyn Garden City, UK	M7145-100ML
Methanol	TAAB Laboratories Equipment Ltd, Aldermaston, UK	M023
Methanol analytical reagent grade	Fisher Scientific UK, Loughborough, UK	M/4000/15
Midori Green Direct DNA Stain	Geneflow Ltd, Lichfield, UK	S6-0016
Millers stain	HD Supplies, Aylesbury, UK	HS235-500
MirVana miRNA Isolation Kit with phenol	Life Technologies, Paisley, UK	AM1560
MirVana miRNA Isolation Kit without phenol	Life Technologies, Paisley, UK	AM1561
miScript II RT kit	Qiagen, Manchester, UK	218161
miScript SYBR Green PCR Kit	Qiagen, Manchester, UK	218073
NNN'-Tetramethylethylenediamine (TEMED)	Sigma, Welwyn Garden City, UK	T9281-100ML
Osmium tetroxide	TAAB Laboratories Equipment Ltd, Aldermaston, UK	O001
Oxalic Acid (1%)	TCS Biosciences Ltd, Botolph Claydon, UK	HK015
Paraffin wax	Solmedia Ltd, Shrewsbury, UK	WAX060
Paraformaldehyde	Sigma, Welwyn Garden City, UK	441244-1KG
Penicillin-Streptomycin 10000 units penicillin + 10 mg streptomycin mL <sup>-1</sup>	Sigma, Welwyn Garden City, UK	P4333-20ML
Phosphate buffered saline tablets	Sigma, Welwyn Garden City, UK	P4417-50TAB
Phosphomolybdic acid (1%)	Acros Organics, New Jersey, USA	206381000
Pierce Assay Reagent	ThermoFisher, Loughborough, UK	226600
Ponceau S Solution	Sigma-Aldrich, Gillingham, UK	P7170-1L
Ponceau Xylidine (1%)	HD Supplies, Aylesbury, UK	HD1800
Potassium permanganate	Sigma-Aldrich, Gillingham, UK	223468-500G
Powdered trypsin lyophilised trypsin from porcine pancreas	Sigma, Welwyn Garden City, UK	T4799-5G

Reagents (cont.)	Manufacturer	Product code
PrecisionPLUS Mastermix with SYBRgreen	Primerdesign, Chandlers Ford, UK	PrecisionPLUS-SY
Primers - miR-specific		
Hs_RNU6-2_11 miScript Primer Assay	Qiagen, Manchester, UK	18300/MS000033740
Hs_SNORD61_11 miScript Primer Assay	Qiagen, Manchester, UK	218300/MS000033705
Hs_let-7b_1 miScript Primer Assay	Qiagen, Manchester, UK	218300/MS000003122
Hs_let-7f_1 miScript Primer Assay	Qiagen, Manchester, UK	218300/MS000006489
Hs_miR-29a_1 miScript Primer Assay	Qiagen, Manchester, UK	218300/MS000003262
Hs_miR-34a_1 miScript Primer Assay	Qiagen, Manchester, UK	218300/MS000003318
Mm_miR-34b-5p_1 miScript Primer Assay	Qiagen, Manchester, UK	218300/MS000007910
Hs_miR-34b*_2 miScript Primer Assay	Qiagen, Manchester, UK	218300/MS000031780
Hs_miR-34c_1 miScript Primer Assay	Qiagen, Manchester, UK	218300/MS000003332
Hs_miR-181a_1 miScript Primer Assay	Qiagen, Manchester, UK	218300/MS000006692
Hs_miR-181a_2 miScript Primer Assay	Qiagen, Manchester, UK	218300/MS000008827
Hs_miR-181b_1 miScript Primer Assay	Qiagen, Manchester, UK	218300/MS000006699
Hs_miR-181c_2 miScript Primer Assay	Qiagen, Manchester, UK	28300/MS000008841
Hs_miR-181d_2 miScript Primer Assay	Qiagen, Manchester, UK	218300/MS000031500
Hs_miR-199a_1 miScript Primer Assay	Qiagen, Manchester, UK	218300/MS000006741
Hs_miR-199b_1 miScript Primer Assay	Qiagen, Manchester, UK	218300/MS000003731
Universal Primer Assay	Qiagen, Manchester, UK	Included with 218073
Primers - gene-specific		Sequence
IL1 $\alpha$ F	Sigma, Welwyn Garden City, UK	GGCAAAGAAATCAAGATGGCGA
IL1 $\alpha$ R	Sigma, Welwyn Garden City, UK	TTCAGAGTCTCCCGTTGGC
PARK2 F	Sigma, Welwyn Garden City, UK	AGTGAGCATGATCGTGTGTG
PARK2 R	Sigma, Welwyn Garden City, UK	TTAGCAACCGCTCCTTGAG
IL1RAP F	Primerdesign, Chandlers Ford, UK	ATGAGATTGGTGACCATTGATG
IL1RAP R	Primerdesign, Chandlers Ford, UK	CTCCATTTCATCTCTGTTAGAGTCTG
IL7 F	Primerdesign, Chandlers Ford, UK	GACCAGGGTCTGGGAGT
IL7R	Primerdesign, Chandlers Ford, UK	GGGGAGGAATCCAAAGATATACC
Insulin-like Growth Factor 1 F	Primerdesign, Chandlers Ford, UK	TCAGTTCGTGTGGAGACAG
Insulin-like Growth Factor 1 R	Primerdesign, Chandlers Ford, UK	TCCAGCCTCCTCAGATCACAG
ILGF1 receptor F	Primerdesign, Chandlers Ford, UK	GGGAATGGAGTGCTGTATGCA
ILGF1 receptor R	Primerdesign, Chandlers Ford, UK	GCTCTGGCTCATGGTGATC
Insulin receptor F	Primerdesign, Chandlers Ford, UK	CTGGATCAACCCGACAATGTC
Insulin receptor R	Primerdesign, Chandlers Ford, UK	TCGACAATCTCCAGGAAGGTC
NFKB2 F	Primerdesign, Chandlers Ford, UK	GTGATCGTGAACAGCCTAAG

Reagents (cont.)	Manufacturer	Product code
Primers - gene-specific (cont.)		
NFKB2 R	Primerdesign, Chandlers Ford, UK	GAGCACCTGGCAGTCC
p38-MAPK (MAPK14) F	Primerdesign, Chandlers Ford, UK	TGAATGAAGACTGCGAGCTGA
p38-MAPK (MAPK14) R	Primerdesign, Chandlers Ford, UK	CTGGTTGTAATGCATCCAGTTCA
P62 (SQSTM1) F	Primerdesign, Chandlers Ford, UK	TGTGAATTTCCCTCAAGAACGTAGG
P62 (SQSTM1) R	Primerdesign, Chandlers Ford, UK	CCTGGAGAGACGGAGGTCA
PARK7 F	Primerdesign, Chandlers Ford, UK	GAAGAAACAAGAAAAGAGAAAAGGC
PARK7 R	Primerdesign, Chandlers Ford, UK	TAGCCTGTGGGTGTGTGTAAC
PRDX3 F	Primerdesign, Chandlers Ford, UK	TGCTTGACAAAATGATTGTGGTC
PRDX3 R	Primerdesign, Chandlers Ford, UK	GTGCTGGGTGACGGCAG
PRDX6 F	Primerdesign, Chandlers Ford, UK	GCTCTCTCAATAGACACAGTGTGAAG
PRDX6 R	Primerdesign, Chandlers Ford, UK	AGGTTCTGATTTTATCATCAATGATG
SIRT1 F	Primerdesign, Chandlers Ford, UK	TGCTGAAGCAGTAAGAAAAGTGC
SIRT1 R	Primerdesign, Chandlers Ford, UK	CATGGAAAATGTAACGATTTGGTGG
SMAD7 F	Primerdesign, Chandlers Ford, UK	TCCAGATGCTGGCCCTCC
SMAD7 R	Primerdesign, Chandlers Ford, UK	TCTCTCCCAGTATGCCACC
TNF F	Primerdesign, Chandlers Ford, UK	TACCGAATGCCTTCCAGTCAATC
TNF R	Primerdesign, Chandlers Ford, UK	GGTTTGTACAAACATGGGCTA
TNF F	Eurogentec, Camberley, UK	CCTTCCAGTCAATCAACCCTCT
TNF R	Eurogentec, Camberley, UK	CAGCCCCACTCAGCCACT
IL1β F	Eurogentec, Camberley, UK	GCCTAAGAACTACATCCAGAGA
IL1β R	Eurogentec, Camberley, UK	GGCATTGATTAGACAACAGTGAA
GAPDH F	Eurogentec, Camberley, UK	GCATCGTGGAGGGACTCA
GAPDH R	Eurogentec, Camberley, UK	GCCACATCTCCAGAGGG
GAPDH F (human)	Sigma, Welwyn Garden City, UK	CAAGGTCATCCATGACAACCTTTG
GAPDH R (human)	Sigma, Welwyn Garden City, UK	GGCCATCCACAGTCTTCTGG
COX IV F (human )	Sigma, Welwyn Garden City, UK	TGGGAGTGTGTGAAGAGTGA
COX IV R (human.)	Sigma, Welwyn Garden City, UK	GCAGTGAAGCCGATGAAGAAC
TOMM20 F (mouse)	Sigma, Welwyn Garden City, UK	AGTCGAGCGAAGATGGTGG
TOMM20 R (mouse)	Sigma, Welwyn Garden City, UK	GCCTTTTGGGTGCGAAGTAG
PARK2 F (human)	Sigma, Welwyn Garden City, UK	CCCAGTGACCATGATAGTGTGG
PARK2 R (human)	Sigma, Welwyn Garden City, UK	TGCTGGTGCAGAAATCGACC
PARK2 F (human)	Sigma, Welwyn Garden City, UK	CCCAGTGACCATGATAGTGTGG
PARK2 R (human)	Sigma, Welwyn Garden City, UK	CCTGCGAAAATCACACGCAA
P62/SQSTM1 F (human)	Sigma, Welwyn Garden City, UK	CCGTGAAGGCCTACCTTCTG

Reagents (cont.)	Manufacturer	Product code
Primers - gene-specific (cont.)		
P62/SQSTM1 R (human)	Sigma, Welwyn Garden City, UK	CGTCTCATCGCGGTAGTG
P62/SQSTM1 F (human)	Sigma, Welwyn Garden City, UK	GTGAAGGCCTACCTTCTGGG
P62/SQSTM1 R (human)	Sigma, Welwyn Garden City, UK	GTCTCATCGCGGTAGTGC
MAP1LC3B F (human)	Sigma, Welwyn Garden City, UK	CCGCACCTTCGAACAAAGAG
MAP1LC3B R (human)	Sigma, Welwyn Garden City, UK	AGATTGGTGTGGAGACGCTG
MAP1LC3B F (human)	Sigma, Welwyn Garden City, UK	AGCATCCAACCAAAATCCCG
MAP1LC3B R (human)	Sigma, Welwyn Garden City, UK	AGCTGTAAGCGCCTTCTAAT
TOMM20 F (human)	Sigma, Welwyn Garden City, UK	GGGCTTCCAAGTTACCTGAC
TOMM20 R (human)	Sigma, Welwyn Garden City, UK	TGTCAGATGGTCTACGCCCT
TOMM20 F (human)	Sigma, Welwyn Garden City, UK	ACTTCGACCCGCAAAAAGACGA
TOMM20 R (human)	Sigma, Welwyn Garden City, UK	CTTCTCGTTCTCGAAGCCTG
COX4I1 F (human)	Sigma, Welwyn Garden City, UK	GGCAGAAGCACTATGTGTACG
COX4I1 R (human)	Sigma, Welwyn Garden City, UK	ACTGATCACAAAAGGGTTTCAGGTA
COXI F (human)	Sigma, Welwyn Garden City, UK	CTGCTATAGTGGAGGCCGGA
COXI R (human)	Sigma, Welwyn Garden City, UK	GGTGGGAGTAGTTCCTCTGC
INSR F (human)	Sigma, Welwyn Garden City, UK	GCCCTGTGACGCATGAAATC
INSR R (human)	Sigma, Welwyn Garden City, UK	GGACGTCTAAATAGTCTGCACGTA
INSR F (human)	Sigma, Welwyn Garden City, UK	TCTACGTGACAGACTATTTAGACG
INSR R (human)	Sigma, Welwyn Garden City, UK	AGTCTCGAAGGGGGTGTAT
Protein Loading Buffer (5X)	National Diagnostics, Hull, UK	EC-887
Protogel 30% w/v Acrylamide	National Diagnostics, Hull, UK	EC-890
Protogel Resolving Buffer (4X)	National Diagnostics, Hull, UK	EC-892
Protogel Stacking Buffer	National Diagnostics, Hull, UK	EC-893
PVDF Western Blotting Membrane	Roche, Welwyn Garden City, UK	3010040001
Random hexamers (50 µM)	Invitrogen, Inchinnan, UK	N8080127
Reynolds lead citrate stain (3%)	TAAB Laboratories Equipment Ltd, Aldermaston, UK	L037
Ribolock RNase Inhibitor	ThermoFisher, Loughborough, UK	EO0381
RIPA Buffer	Sigma, Welwyn Garden City, UK	R0278-50ML
RNA Later ICE Frozen Tissue Transition Solution	Life Technologies, Paisley, UK	4427575
RNA screen tape	Agilent Technologies, Cheadle, UK	5067-5576
RNA screen tape ladder	Agilent Technologies, Cheadle, UK	5067-5578
RNA screen tape sample buffer	Agilent Technologies, Cheadle, UK	5067-5577
RNAlater® Stabilisation Solution	Life Technologies, Paisley, UK	AM7021
Sodium cacodylate	TAAB Laboratories Equipment Ltd, Aldermaston, UK	S011

Reagents (cont.)	Manufacturer	Product code
Sodium dodecyl sulfate (SDS)	Sigma, Welwyn Garden City, UK	L3771-100G
Sodium iodate	Acros Organics, New Jersey, USA	201761000
Superscript II Reverse Transcriptase	Invitrogen, Inchinnan, UK	18064014
Sylgard™ 184 silicone elastomer	Dow Corning Corporation, Midland, USA	SYLG184
TAAB epoxy resin components	TAAB Laboratories Equipment Ltd, Aldermaston, UK	T001, D025, M011, D032
TAE (Tris/Acetic Acid/EDTA) Buffer	Bio-Rad, Deeside, UK	1610743
TGFβ3 Recombinant Human TGF-beta 3 protein	R&D Systems, Abingdon, UK	8420-B3-025
Thrombin from bovine plasma	Sigma, Welwyn Garden City, UK	T4648-1KU
Toluidine Blue 1%	TAAB Laboratories Equipment Ltd, Aldermaston, UK	SD211
Tris base (Trizma® base)	Sigma, Welwyn Garden City, UK	T6066-1KG
Tris-Glycine-SDS PAGE Buffer (10X)	National Diagnostics, Hull, UK	EC-870
Trypan Blue solution 0.4%	Sigma-Aldrich, Gillingham, UK	T8154
TrypLE Select Enzyme (1x) no phenol red	Life Technologies, Paisley, UK	12563029
Tween® 20	Sigma-Aldrich, Gillingham, UK	P1379
Tween20®	Sigma, Welwyn Garden City, UK	P7949-500ML
Uranyl acetate	TAAB Laboratories Equipment Ltd, Aldermaston, UK	U007
Van Giesons stain	TCS Biosciences Ltd, Botolph Claydon, UK	HS780-500
Water - Molecular Biology Reagent	Sigma, Welwyn Garden City, UK	W4502-1L
Water - RNase-free	Sigma-Aldrich, Gillingham, UK	3098
Xylene (histological grade)	Fisher Scientific UK, Loughborough, UK	X/0250/17
Plasticware	Manufacturer	Product code
10 µL Graduated Filter Tips	StarLab (UK) Ltd, Milton Keynes, UK	S1120-3810
200 µL Graduated Filter Tips	StarLab (UK) Ltd, Milton Keynes, UK	S1120-8810
1000 µL Graduated Filter Tips	StarLab (UK) Ltd, Milton Keynes, UK	S1122-1830
7 mL Bijoou Universal tubes	Greiner Bio-One, Frickenhausen, Germany	189175
30 mL Universal tubes	Scientific Laboratory Supplies, Nottingham, UK	1434362-1
60 mL Sterile Pots	Greiner Bio-One, Frickenhausen, Germany	219270
Cell culture plate - 6 well	Greiner Bio-One, Frickenhausen, Germany	657160
Cell culture plate - 12 well	Greiner Bio-One, Frickenhausen, Germany	665180
Cell culture plate - 96 well	Greiner Bio-One, Frickenhausen, Germany	655180
Cell scrapers	Sarstedt Ltd, Boston, UK	83.183
Cell Strainers (70 µm)	Fisher Scientific, Loughborough, UK	11597522
Centrifuge tubes - 15 mL	Greiner Bio-One, Frickenhausen, Germany	188261
Centrifuge tubes - 50 mL	Greiner Bio-One, Frickenhausen, Germany	227270
Chromatography Paper (3MM)	GE Healthcare Whatman, Little Chalfont, UK	3030-672

Plasticware (cont.)	Manufacturer	Product code
Cryogenic vials (1.8 mL)	StarLab (UK) Ltd, Milton Keynes, UK	E3090-6222
Embedding moulds	TAAB Laboratories Equipment Ltd, Aldermaston, UK	E095
Microseal 'B' PCR plate sealing film	Bio-Rad, Deeside, UK	MSB1001
Minisart filters 0.2 µm pore size	Sartorius, Goettingen, Germany	FC121
Optical tube strip caps (8-strip)	Agilent Technologies, Cheadle, UK	401425
Optical tube strips (8-strip)	Agilent Technologies, Cheadle, UK	401428
Pasteur pipettes	StarLab (UK) Ltd, Milton Keynes, UK	E1414-0311
PCR plates, hard shell, 96 well low profile, thin walled, skirted, clear/white	Bio-Rad, Deeside, UK	HSP9601
PCR tubes (0.2 mL 8-strip individually attached caps)	StarLab (UK) Ltd, Milton Keynes, UK	A1402-3700
Petri dishes - 60 mm	Greiner Bio-One, Frickenhausen, Germany	628160
Reaction tubes (Eppendorf tubes) - 1.5 mL	Greiner Bio-One, Frickenhausen, Germany	616201
Serological pipettes - 5 mL disposable	Greiner Bio-One, Frickenhausen, Germany	606 160
Serological pipettes - 10 mL disposable	Fisher Scientific, Loughborough, UK	13-676-10J
Serological pipettes - 25 mL disposable	Fisher Scientific, Loughborough, UK	13-676-10K
Stainless steel Minutien insect pins (1 cm x 0.2 mm)	Fine Science Tools, Linton, UK	26002-20
T75 Cell culture flask	Greiner Bio-One, Frickenhausen, Germany	658170
T175 Cell culture flask	Greiner Bio-One, Frickenhausen, Germany	660160
Tape Station loading tips	Agilent Technologies, Cheadle, UK	5067-5153
Tissue processing/embedding cassettes	Fisher Scientific, Loughborough, UK	10746851
<b>Equipment</b>	<b>Manufacturer</b>	<b>Product code</b>
200 mesh TEM thin bar copper grids	Agar Scientific, Stansted, UK	AGG2700C
Balance	OHAUS GmbH, NaniKon, Switzerland	Analytical Plus
BBraun Mikro-Dismembrator U	B. Braun Biotech International, Melsungen, Germany	8531722
Centrifuge (Cell culture)	Thermo Scientific, Runcorn, UK	Heraeus Multifuge X1
Centrifuge (for use with TapeStation)	Stuart Scientific, Stone, UK	microguge SCF2
Centrifuge (general lab work)	Grant Instruments Ltd, Cambridge, UK	PCV3000
Centrifuge (RNA extraction)	Fisher Scientific, Loughborough, UK	accuSpin Micro17R
CFX Connect Real-Time PCR detection system	Bio-Rad, Deeside, UK	1855201
Chemi Doc XRS+ Imaging System	Bio-Rad, Deeside, UK	1708265
Cover slips - 10mm diameter	VWR International, Fontenay-sous-Bois, France	631-1576
Coverslips (histology)	Fisher Scientific, Loughborough, UK	FB58670
Diatome Ultra diamond knife	Agar Scientific, Stansted, UK	AGG3397
Gel Unit (Horizontal for agarose gels)	Geneflow Ltd, Lichfield, UK	G9-0036
Heating Block (for RNA/protein extraction)	Cleaver Scientific, Rugby, UK	TCDB-01
Heating Block (for Tape Station)	Grant Instruments Ltd, Cambridge, UK	BTA

Equipment (cont.)	Manufacturer	Product code
Lint-free tissue	Kimberly-Clarke Inc, Roswell, USA	KIMTECH 34155
Mersilk 3.5 metric (size 0) braided silk suture	Ethicon, Diegem, Belgium	NW5334
Microscopes:		
Nikon Diaphot 300 (equine cytology)	Nikon UK, Surbiton, UK	
Nikon Eclipse 80i (histology)	Nikon UK, Surbiton, UK	
Nikon Eclipse Ti-E (Live cell imaging)	Nikon UK, Surbiton, UK	
Phillips EM208S Transmission Electron Microscope	ThermoFisher Scientific, Altrincham, UK	
Zeiss Axio.Vert.A1 (human cytology)	Zeiss UK, Cambridge, UK	
Zeiss AxioImager M1 (Fluorescence imaging)	Zeiss UK, Cambridge, UK	
Zeiss AxioImager M2 (Fluorescence imaging)	Zeiss UK, Cambridge, UK	
Zeiss LSM 800 Confocal microscope (Fluorescence imaging)	Zeiss UK, Cambridge, UK	
Microscope slides (cytology)	Thermo Scientific, Runcorn, UK	3808143G
Microscope slides (histology)	Solmedia Ltd, Shrewsbury, UK	MSS4511YW
Microscope slides Poly Lysine coated (histology)	Solmedia Ltd, Shrewsbury, UK	MSS61012S
Microtome (routine histology)	Leica Microsystems (UK) Ltd, Milton Keynes, UK	RM 2125 RT
Mini-PROTEAN PowerPac Basic Power Supply	Bio-Rad, Deeside, UK	1645050
Mini-PROTEAN Tetra Cell Electrophoresis System	Bio-Rad, Deeside, UK	165-8006
NanoDrop 2000	ThermoFisher Scientific, Altrincham, UK	
Odyssey CLx Imaging System	LI-COR, Lincoln, USA	9140-PRE
Orbital shaker	IKA Laboratory Equipment, Oxford, UK	Vibrax-VXR
Oven (TEM)	Genlab Ltd, Widnes, UK	MINO/4/CLAD
PowerPac Basic Power Supply	Bio-Rad, Deeside, UK	1645050
Rocker	Labnet International, Edison, USA	Rocker 35
Rocker	Stuart Scientific, Stone, UK	See-saw rocker SSL4
Rotating incubator	Scientific Industries Inc, New York, USA	Enviro-Genie
Shaking flasks for Mikro-Dismembrator U	B. Braun Biotech International, Melsungen Germany	8531803
SPECTROstar Nano microplate reader	BMG Labtech Ltd, Aylesbury, UK	
TapeStation 2200	Agilent Technologies, Cheadle, UK	
Thermal cycler (T100)	Bio-Rad, Deeside, UK	1861096
Tissue processor (routine histology)	Sakura Fintek, Torrance, USA	Tissue-Tek Vacuum Infiltration Processor
Trans-Blot Semi-Dry Transfer Cell	Bio-Rad, Deeside, UK	170-3940
Vortexer (for use with TapeStation)	IKA Laboratory Equipment, Oxford, UK	MS3 Vortexer
Vortexer (general lab work)	Scientific Industries Inc, New York, USA	Vortex Genie 2
Ultramicrotome (TEM sections)	Leica Microsystems (UK) Ltd, Milton Keynes, UK	Reichert-Jung Ultracut ultramicrotome

**Table A1.1** (*preceding 9 pages*) **Reagents, consumables and equipment utilised in this study.**

## **Appendix 2**

**Table A2.1** *Small nucleolar RNA-61 (SNORD61)* demonstrates greater stability of expression than *small nucleolar RNA-68 (SNORD68)* and *small nuclear RNA-U6 (U6)* in healthy and diseased equine superficial digital flexor tendon.

**Figure A2.1** Boxplots of regularised log counts obtained by RNA-seq for miRNA families subsequently evaluated by RT-qPCR.

**Figure A2.2** Differential expression of microRNAs used for RT-qPCR validation of human tendon RNA-seq data, according to tendon type.

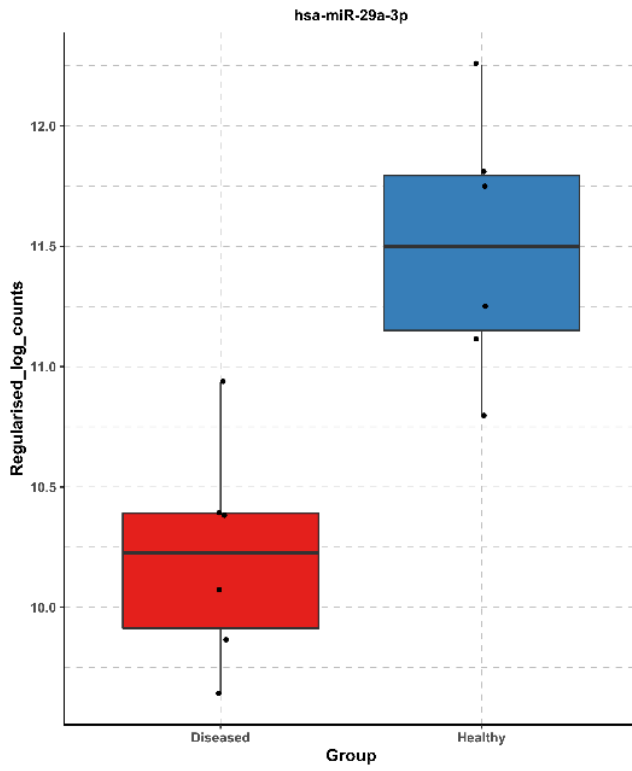
Sample Identity	Age (Years)	U6					SNORD68					SNORD61				
		Healthy		Diseased		Difference (D-H)	Healthy		Diseased		Difference (D-H)	Healthy		Diseased		Difference (D-H)
		Ct	Av Ct	Ct	Av Ct		Ct	Av Ct	Ct	Av Ct		Ct	Av Ct	Ct	Av Ct	
H1	3	23.66	23.54				32.46	32.47				22.42	22.33			
H1		23.42					32.62					22.07				
H1		24.23					32.34					22.5				
H2	25	22.51	22.74				31.6	32.11				20.59	20.63			
H2		22.66					32.07					20.58				
H2		23.04					32.67					20.72				
H3	4	20.16	20.07				29.5	29.69				20.05	20.09			
H3		20.81					29.5					20.11				
H3		19.97					30.08					20.1				
H16	3	22.02	21.99				31.13	31.3				21.94	21.84			
H16		23.28					31.54					21.69				
H16		21.96					31.22					21.89				
H18	19	21.46	21.77				30.48	30.56				19.69	19.86			
H18		21.77					30.27					19.73				
H18		22.09					30.93					20.16				
H23	6	23.58	23.61	30.01	28.91	5.3	29.57	29.77	28.75	31.7	1.93	21.21	21.29	20.89	20.83	-0.46
H23		23.64		27.9			29.7		31.66			21.1		20.75		
H23		23.61		28.83			30.05		31.74			21.56		20.85		
H24	9	18.52	18.61	27.57	27.92	9.31	28.17	28.59	32.87	32.4	3.81	21.21	21.22	21.92	21.97	0.75
H24		19.25		29.91			28.85		32.22			20.95		22.05		
H24		18.69		28.26			28.76		32.1			21.49		21.94		
H27	18	32.13	31.72				33.33	33.64				22.79	22.86			
H27		31.72					33.96					22.86				
H27		31.32					33.62					22.93				
H47	7			25.81	26.09				31.75	31.89				20.65	20.49	
H47				26.36					32.02					20.43		
H47				26.1					31.03					20.4		
H52	6			22.67	22.6				31.16	31.16				21.97	21.85	
H52				22.57					31.2					21.67		
H52				22.57					31.12					21.92		
H62	7			23.19	23.15				30.19	30.22				21.49	21.3	
H62				22.94					30.36					21.26		
H62				23.32					30.11					21.14		
Mean		23.15	23.01	25.87	25.73	2.73	31.02	31.02	31.22	31.47	0.45	21.26	21.26	21.29	21.29	0.02
SD		3.69	3.91	2.8	2.8		1.62	1.68	1.04	0.83		1.02	1.05	0.6	0.64	
Max		32.13	31.72	30.01	28.91		33.96	33.64	32.87	32.4		22.93	22.86	22.05	21.97	
Min		18.52	18.61	22.57	22.6		28.17	28.59	28.75	30.22		19.69	19.86	20.4	20.49	
Max-Min		13.61	13.12	7.44	6.31		5.79	5.04	4.12	2.18		3.24	3	1.65	1.48	

**Table A2.1 Small nucleolar RNA-61 (SNORD61) demonstrates greater stability of expression than small nucleolar RNA-68 (SNORD68) and small nuclear RNA-U6 (U6) in healthy and diseased equine superficial digital flexor tendon.** Threshold cycle (Ct) values are presented for 11 biological replicates, each run in triplicate. For two biological replicates both healthy and diseased tissue was available. Av = average (mean), D = diseased, H = healthy, SD = standard deviation, Max = maximum, Min = minimum. Values in red were excluded from analysis as they differed from technical replicates by >0.5.

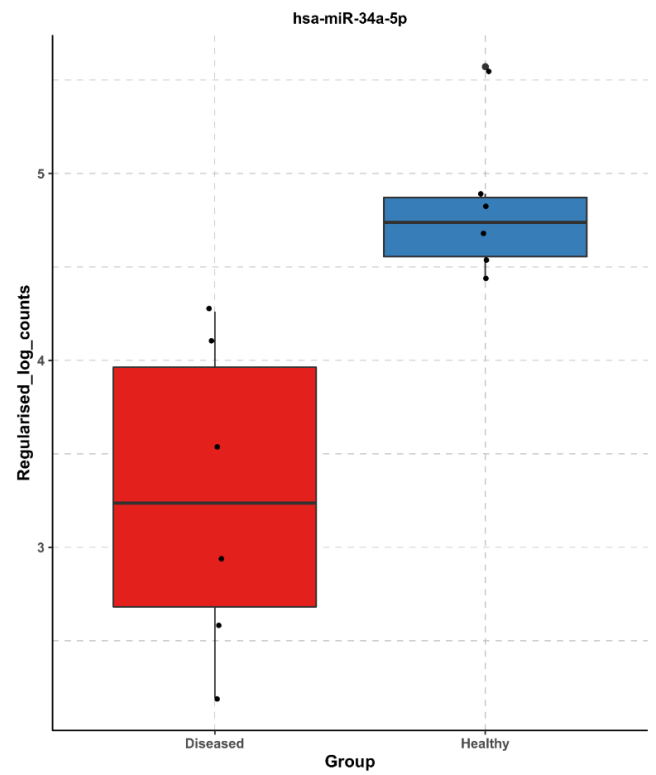
 **Diseased**

 **Healthy**

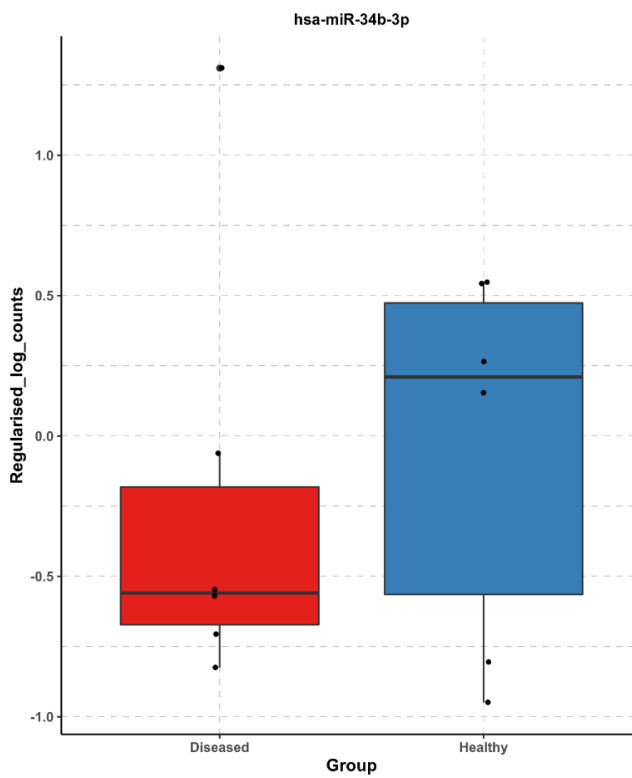
**A. miR-29a-3p**



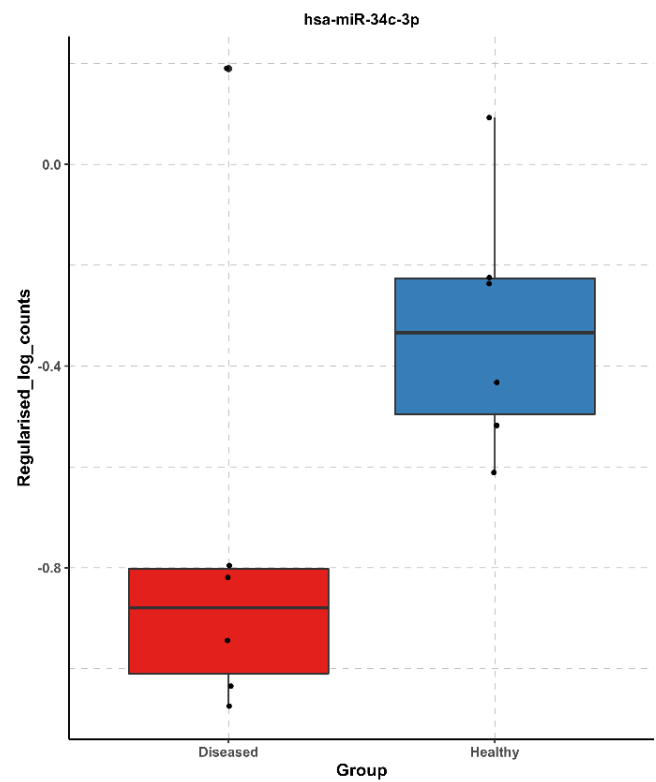
**B. miR-34a-5p**



**C. miR-34b-3p**



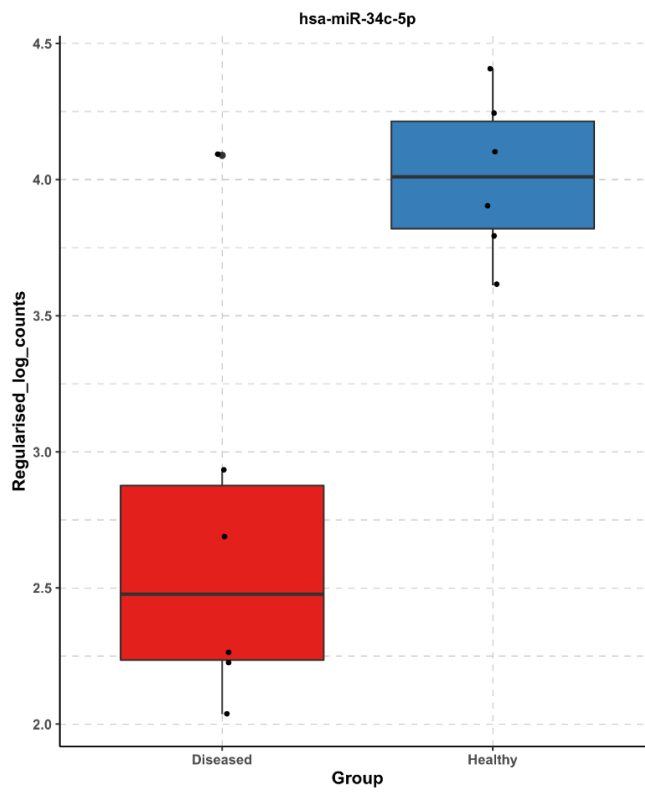
**D. miR-34c-3p**



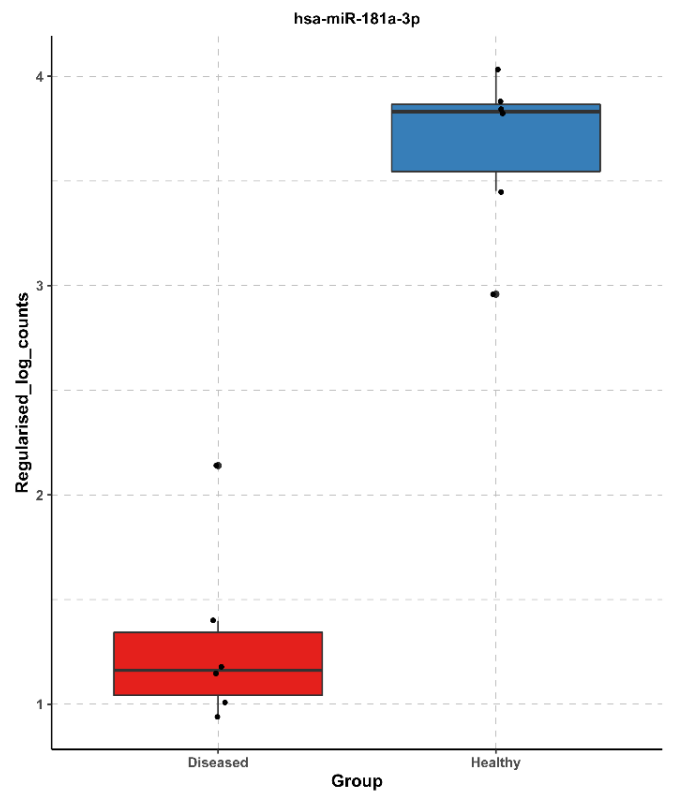
 **Diseased**

 **Healthy**

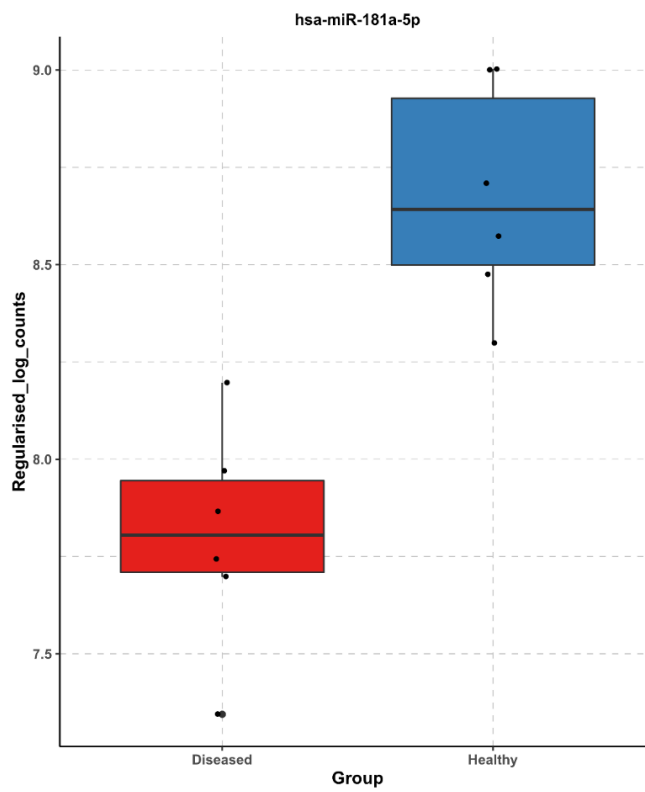
**E. miR-34c-5p**



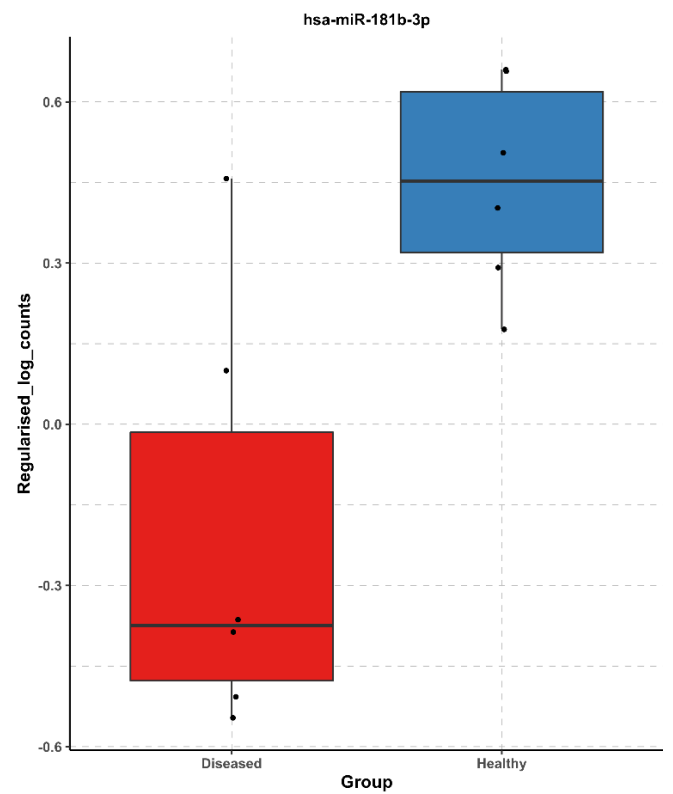
**F. miR-181a-3p**



**G. miR-181a-5p**

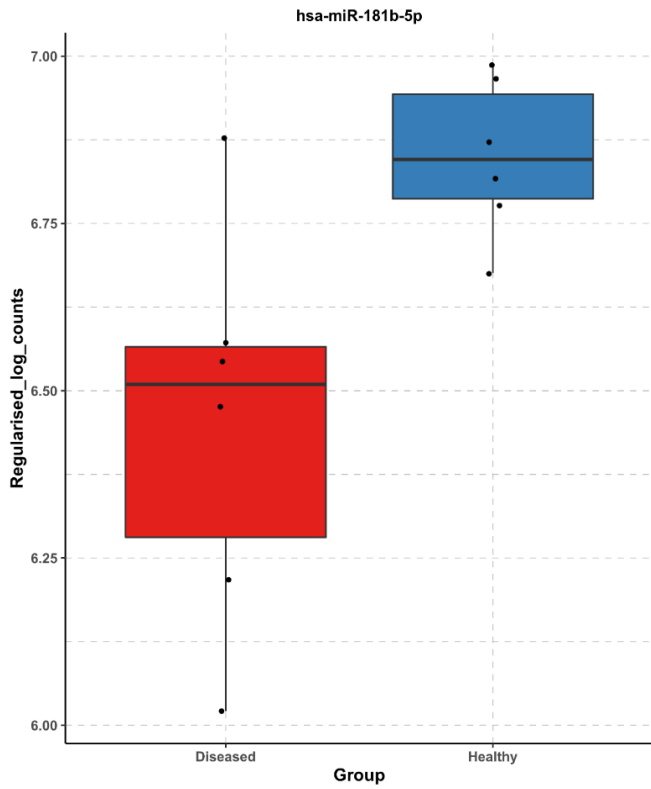


**H. miR-181b-3p**

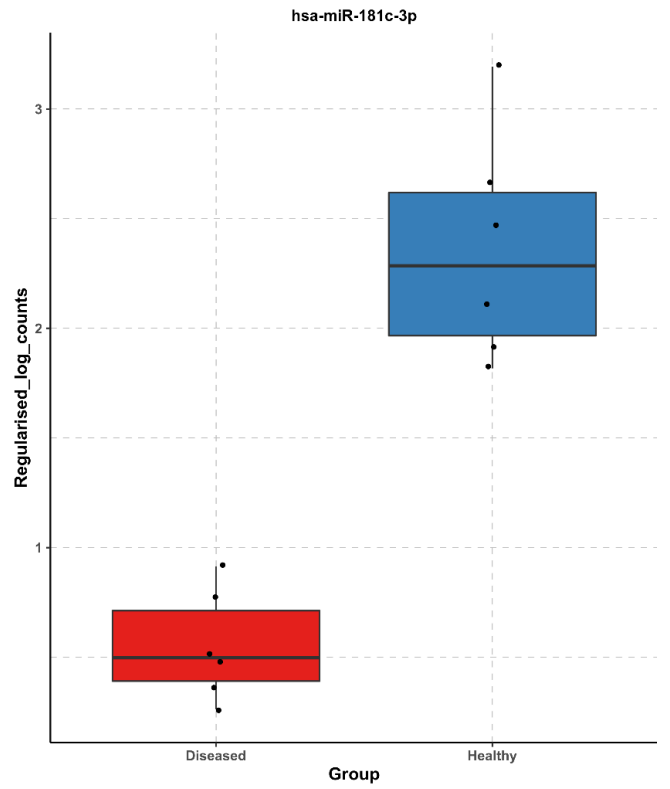


 Diseased  Healthy

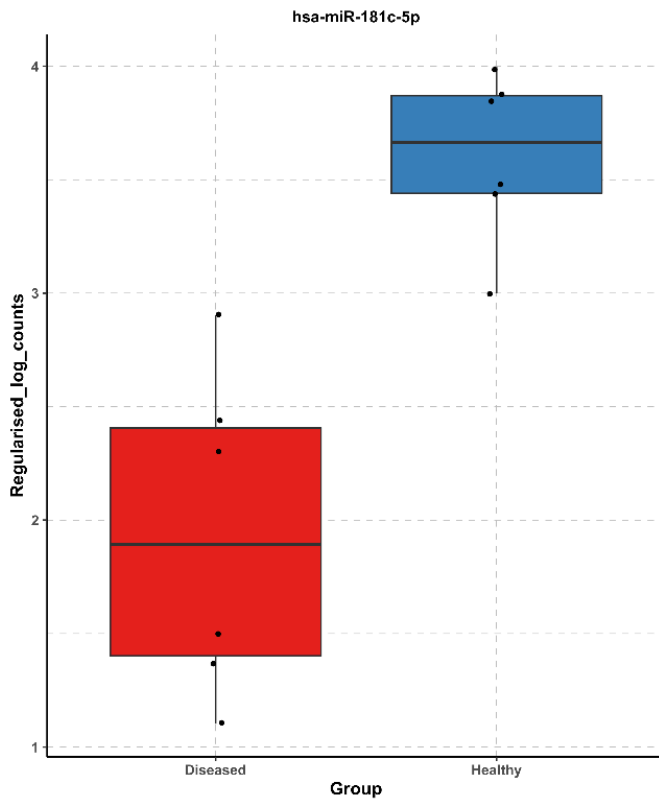
I. miR-181b-5p



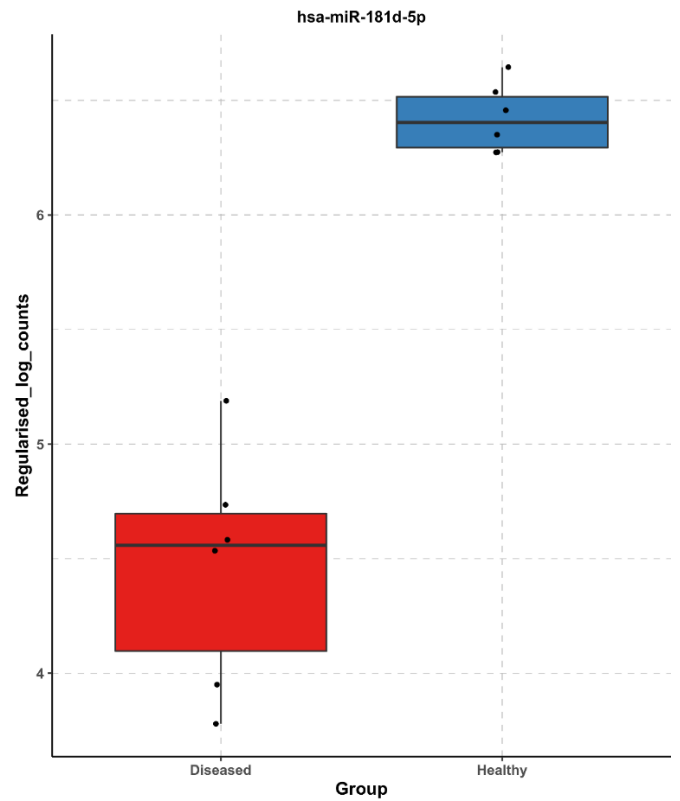
J. miR-181c-3p



K. miR-181c-5p

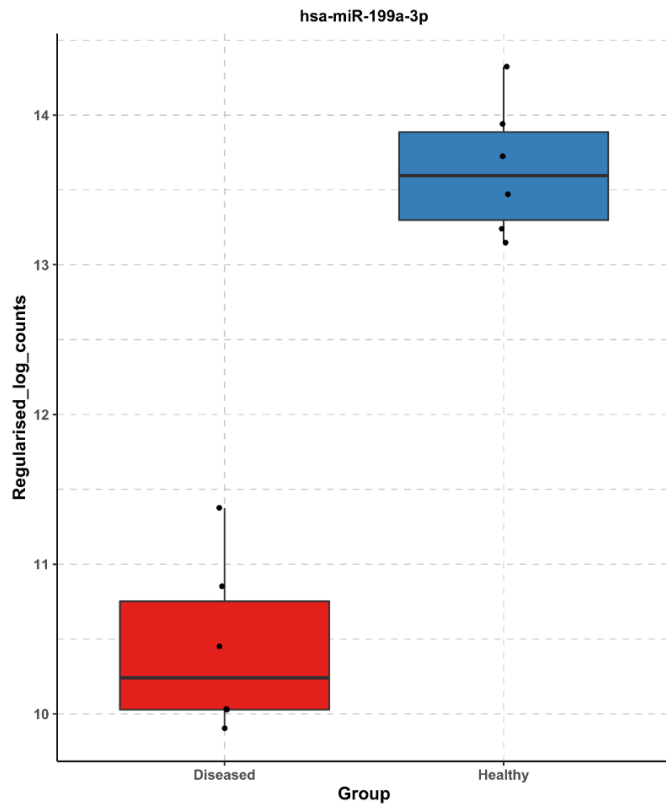


L. miR-181d-5p

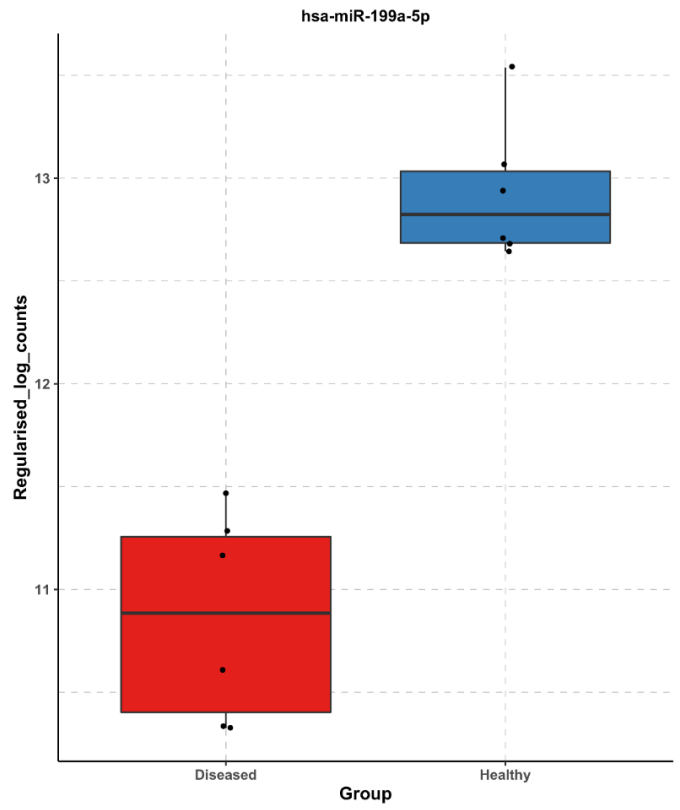




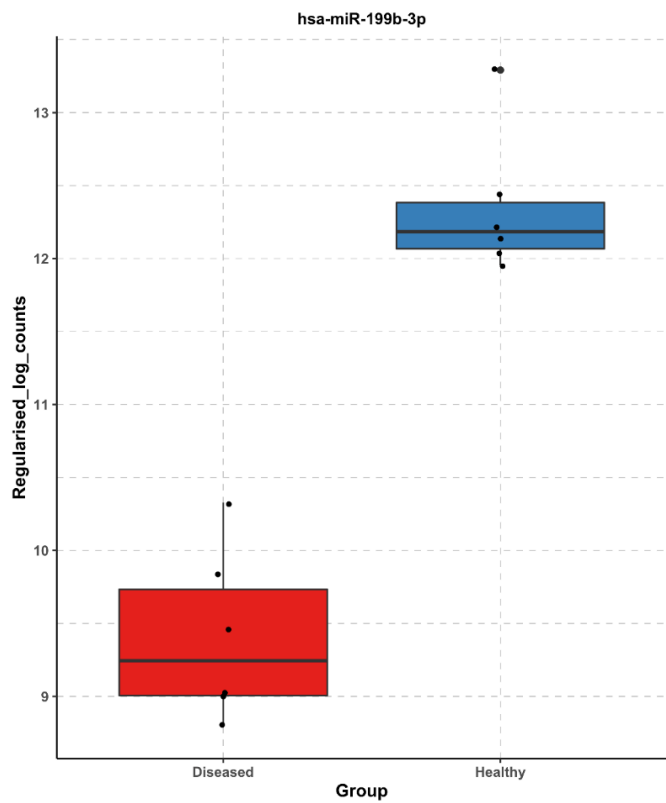
M. miR-199a-3p



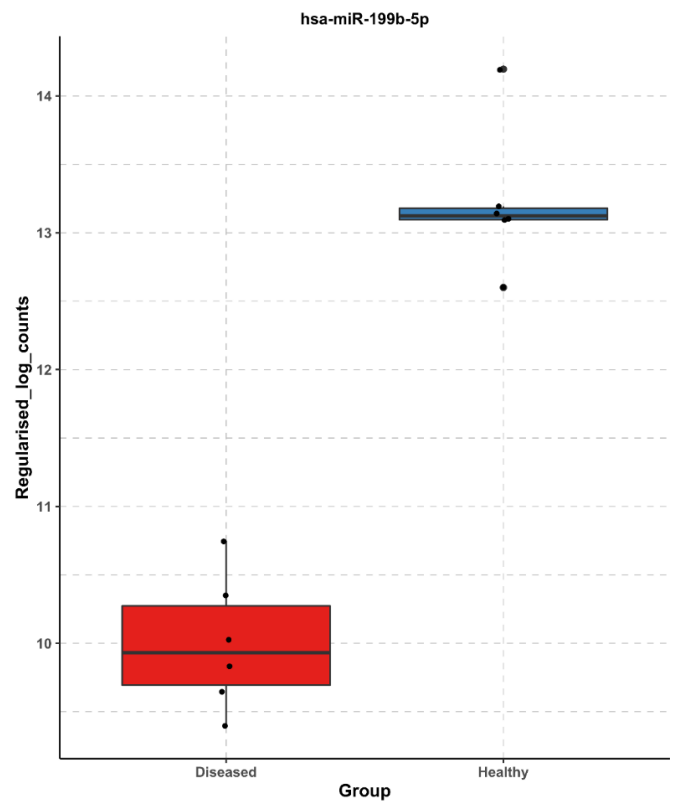
N. miR-199a-5p



O. miR-199b-3p

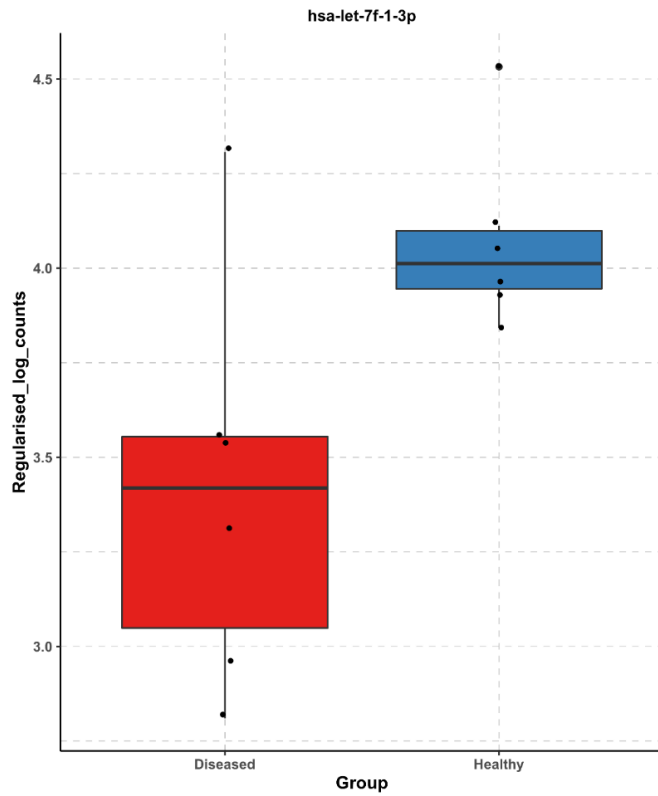


P. miR-199b-5p



 **Diseased**
 **Healthy**

**Q. miR-let-7f-3p**



**R. miR-let-7f-5p**

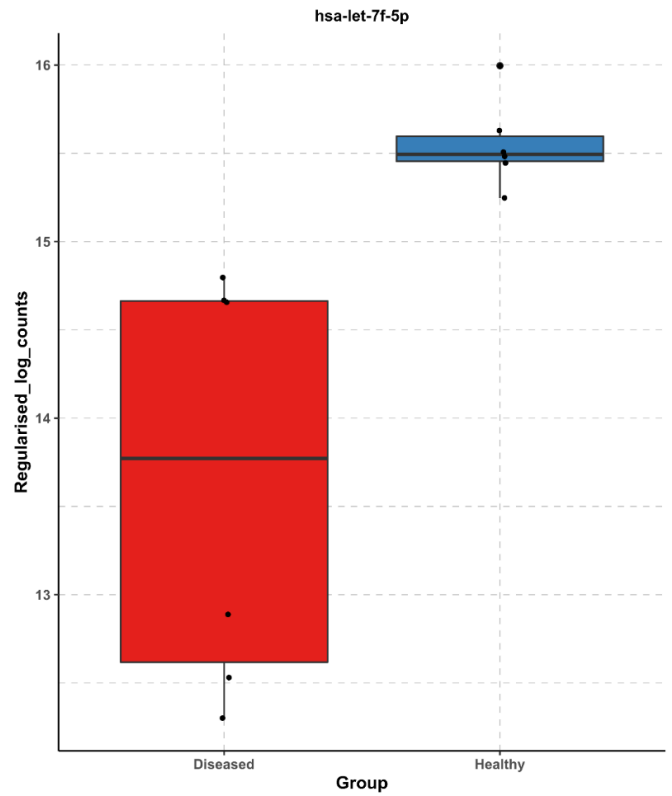
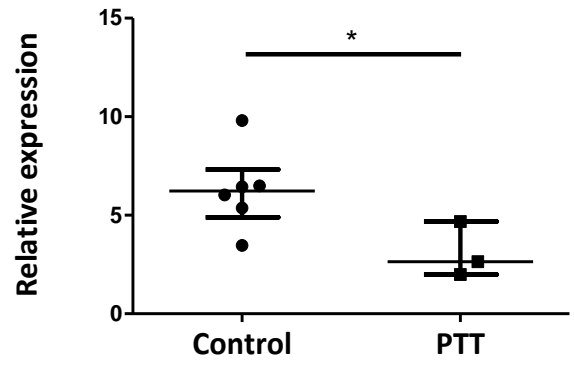
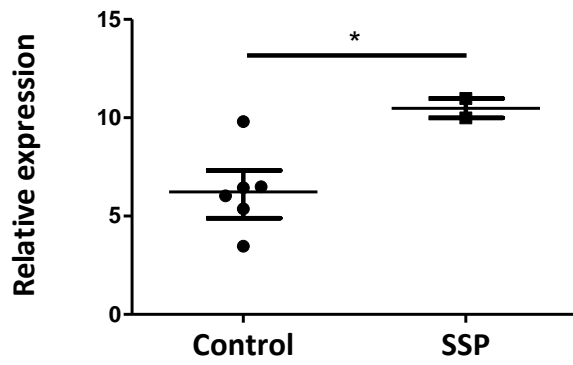
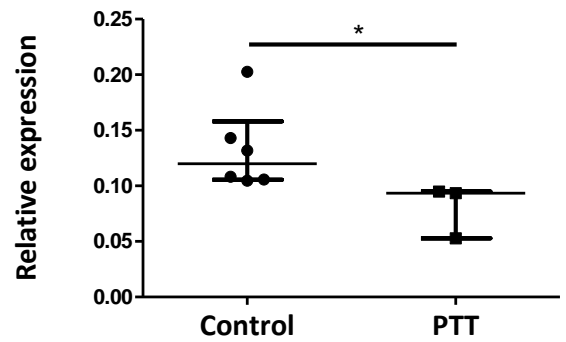
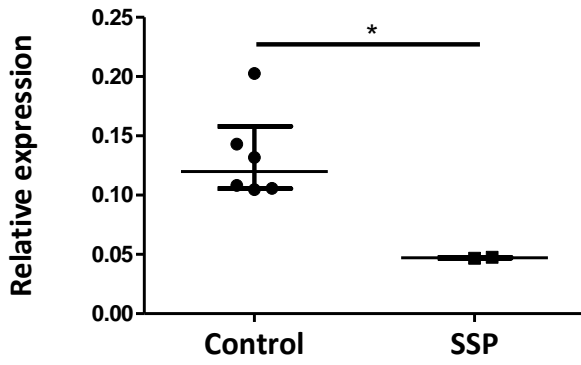


**Figure A2.1** (includes preceding 4 pages) **Boxplots of regularised log counts obtained by RNA-seq for miRNA families subsequently evaluated by RT-qPCR.** A. miR-29a-3p. B. miR-34a-5p. C. miR-34b-3p. D. miR-34c-3p. E. miR-34c-5p. F. miR-181a-3p. G. miR-181a-5p. H. miR-181b-3p. I. miR-181b-5p. J. miR-181c-3p. K. miR-181c-5p. L. miR-181d-5p. M. miR-199a-3p. N. miR-199a-5p. O. miR-199b-3p. P. miR-199b-5p. Q. miR-let-7f-3p. R. miR-let-7f-5p.

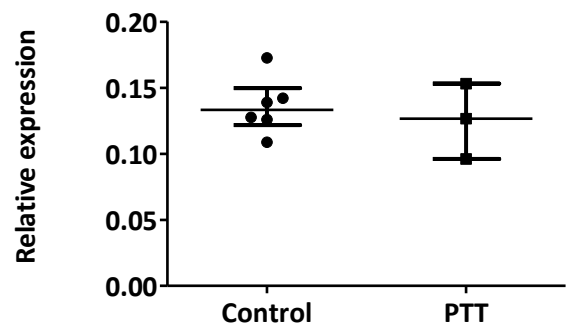
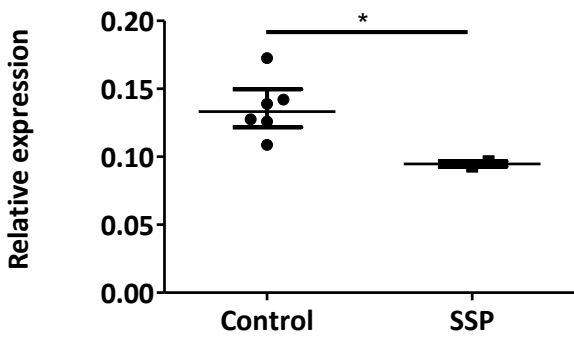
**A. miR-29a**



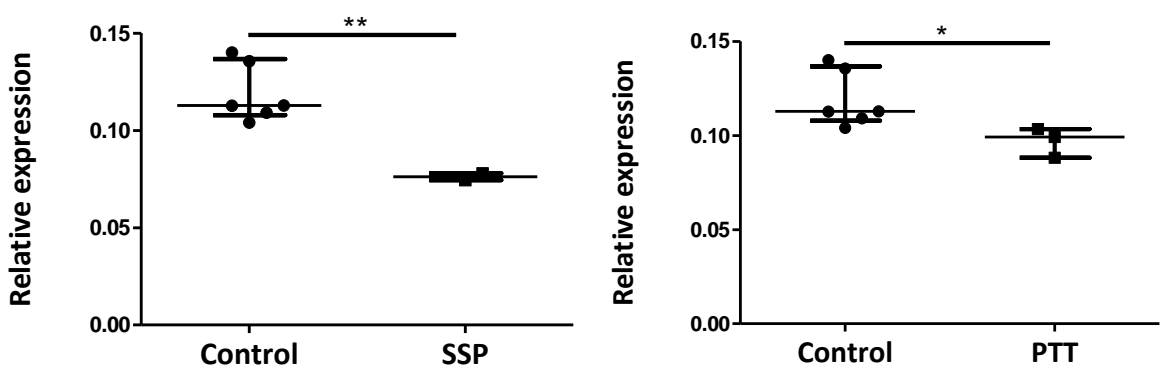
**B. miR-34a**



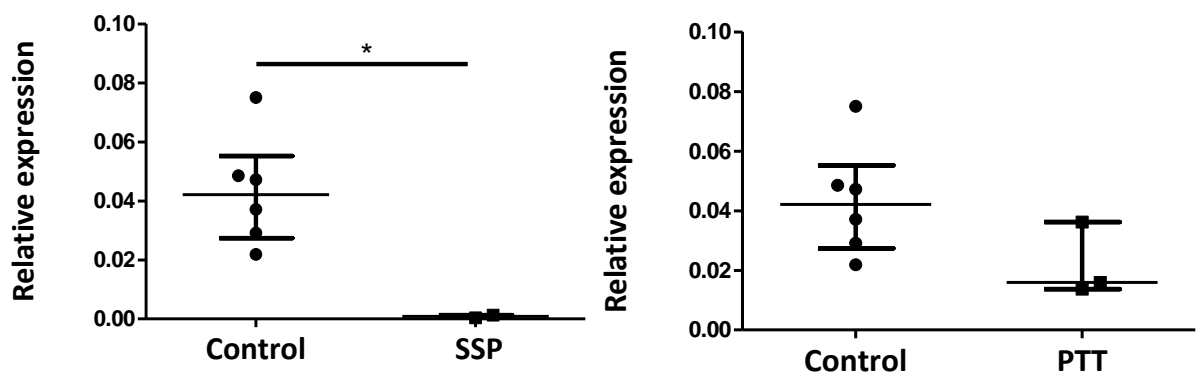
**C. miR-34b**



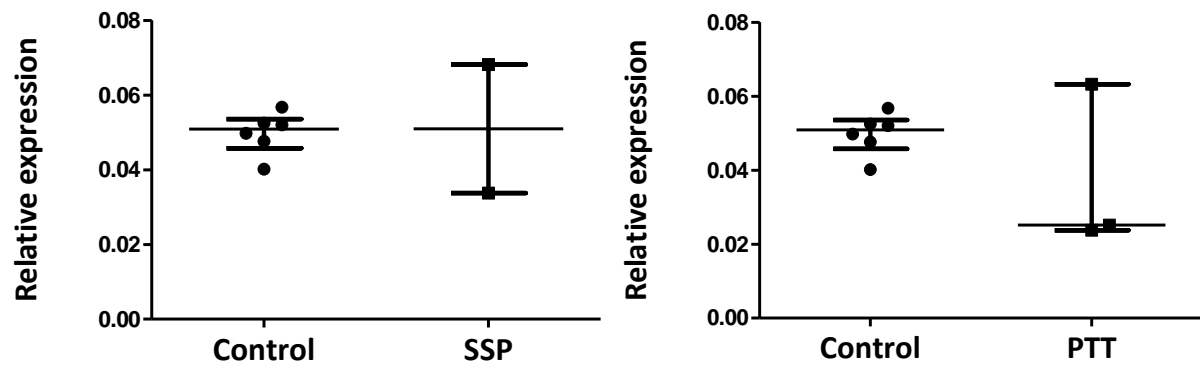
D. miR-34c



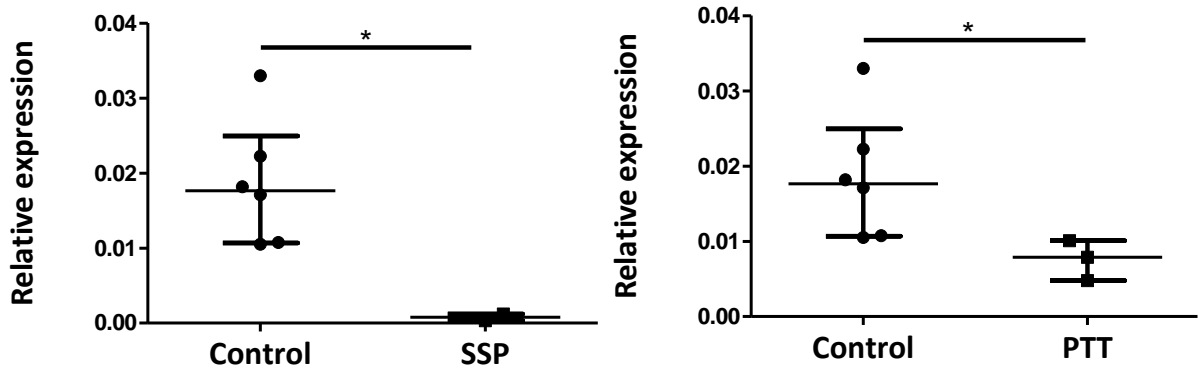
E. miR-181a



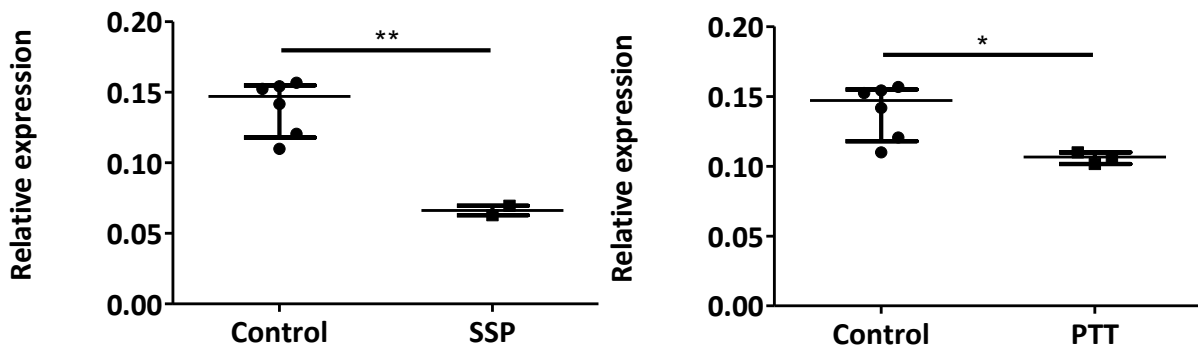
F. miR-181b



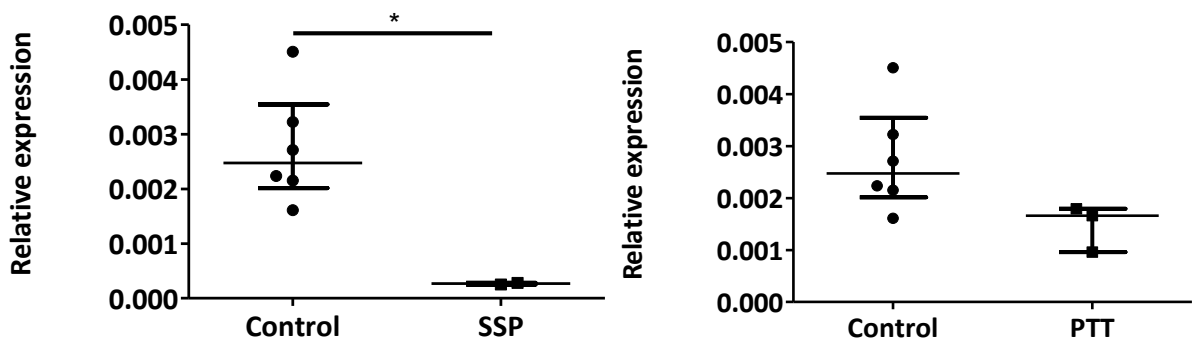
### G. miR-181c



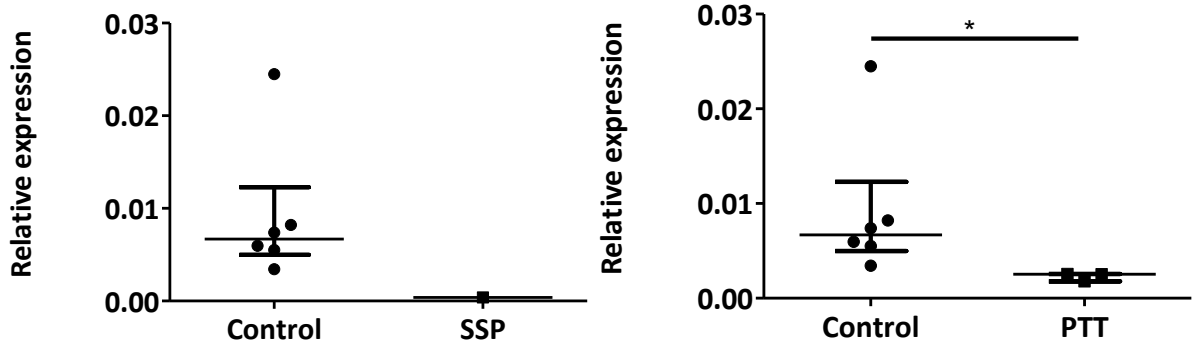
### H. miR-181d



### I. miR-199a



**J. miR-199b**



**K. miR-let-7f**

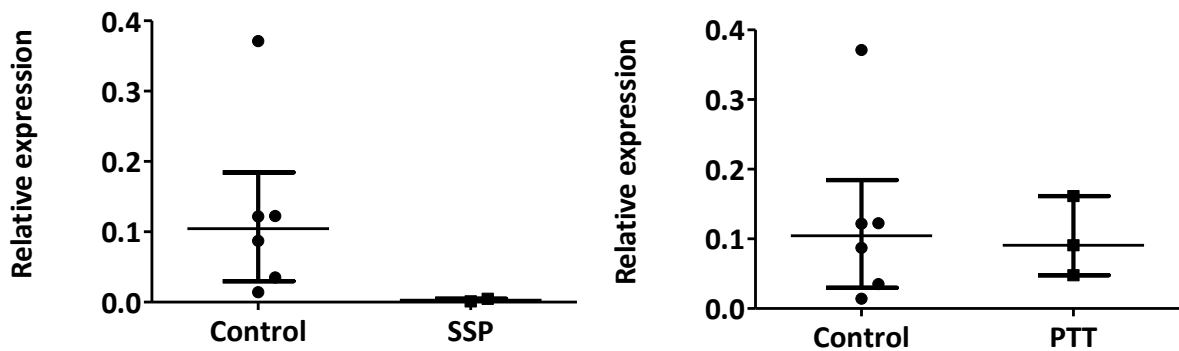


**Figure A2.2 (includes preceding 3 pages) Differential expression of microRNAs used for RT-qPCR validation of human tendon RNA-seq data, according to tendon type.** Relative expression of **A.** miR-29a, **B.** miR-34a, **C.** miR-34b, **D.** miR-34c, **E.** miR-181a, **F.** miR-181b, **G.** miR-181c, **H.** miR-181d, **I.** miR-199a, **J.** miR-199b, **K.** miR-let-7f between Control (healthy hamstring) and tendinopathic supraspinatus (SSP) and posterior tibial (PTT) tendons. Data were normalised to *SNORD61* expression. Comparisons between Control and PTT utilised Mann Whitney U test; comparisons between Control and SSP utilised Student's t-test. Graphs show median and inter-quartile range. \* =  $P < 0.05$ ; \*\* =  $P < 0.01$ .

NOTE: only 1 data point included for miR-199b expression in tendinopathic SSP cohort.

## **Appendix 3**

**Table A3.1** Differential expression profiles of non-miRNA small RNA transcripts identified by RNA-seq from six healthy and six diseased human tendon samples.

**Table A3.2** Differential expression profiles of miRNA transcripts identified by RNA-seq from six healthy and six diseased human tendon samples.

Ensembl ID	Chr	Log2 Fold Change	P (adj)	Gene	Identities from Ensembl <sup>1</sup> or Rfam <sup>2</sup>
Protein coding					
ENSG00000271043	chr5	2.66	0.000283781	MTRNR2L2	MT-RNR2 like 2 codes for protein Humanin-like 2
ENSG00000255633	chr6	2.76	0.001167647	MTRNR2L9	MT-RNR2 like 9 codes for protein Humanin-like 9
ENSG00000283274	chr14	3.67	1.35E-20	RF00002	5.8S ribosomal RNA
Vault RNA					
ENSG00000202111	chr5	2.52	4.79E-06	VTRNA1-2	Vault RNA 1-2
ENSG00000199990	chr5	0.38	0.593914457	VTRNA1-1	Vault RNA 1-1
ENSG00000202515	chr5	0.83	0.21199785	VTRNA1-3	Vault RNA 1-3
ENSG00000270123	chr5	-0.48	0.590787689	VTRNA2-1	Vault RNA 2-1
Small Cajal body-specific RNA					
ENSG00000252691	chr1	3.37	0.040366324	RF00283	Small Cajal body-specific RNA 18
ENSG00000249784	chr4	2.10	6.50E-07	SCARNA22	Small Cajal body-specific RNA 22
ENSG00000252947	chr1	-0.98	0.194007601	SCARNA1	Small Cajal body-specific RNA 1
ENSG00000252906	chr1	0.63	0.268502198	SCARNA3	Small Cajal body-specific RNA 3
ENSG00000251733	chr9	0.93	0.012113121	SCARNA8	Small Cajal body-specific RNA 8
ENSG00000251898	chr12	0.44	0.30193363	SCARNA11	Small Cajal body-specific RNA 11
ENSG00000252712	chr15	0.88	0.189361003	SCARNA14	Small Cajal body-specific RNA 14
ENSG00000252765	chr1	-1.14	0.539540229	RF00424	Small Cajal body-specific RNA 16
ENSG00000238835	chr5	-0.09	0.88347376	SCARNA18	Small Cajal body-specific RNA 18
Small nuclear RNA					
ENSG00000273727	chr1	3.37	0.000387337	RF00003	U1 small nuclear RNA
ENSG00000275291	chr1	3.28	0.000198381	RF00003	U1 small nuclear RNA
ENSG00000274428	chr1	3.07	1.81E-06	RF00003	U1 small nuclear RNA
ENSG00000274210	chr1	1.60	0.000172027	RF00003	U1 small nuclear RNA
ENSG00000283575	chr1	-2.40	0.046247508	RF00026	U6 small nuclear RNA
ENSG00000199568	chr15	-1.69	0.005784318	RNU5A-1	RNA, U5A small nuclear 1
ENSG00000200156	chr15	-2.08	0.000236663	RNU5B-1	RNA, U5B small nuclear 1
ENSG00000201558	chr1	1.62	0.000443902	RNVU1-6	RNA, variant U1 small nuclear 6
ENSG00000207349	chr1	-1.89	0.005958736	RNVU1-17	RNA, variant U1 small nuclear 17
ENSG00000278099	chr1	0.09	0.917705836	RF00003	U1 small nuclear RNA
ENSG00000277918	chr1	-0.41	0.475185356	RF00003	U1 small nuclear RNA
ENSG00000270722	chr1	-1.47	0.011406068	RF00003	U1 small nuclear RNA
ENSG00000273768	chr1	-0.47	0.393480375	RF00003	U1 small nuclear RNA
ENSG00000206828	chr1	-1.26	0.251426925	RF00003	U1 small nuclear RNA
ENSG00000273694	chr1	0.08	0.891256276	RF00004	U2 small nuclear RNA

Ensembl ID	Chr	Log2 Fold Change	P (adj)	Gene	Identities from Ensembl <sup>1</sup> or Rfam <sup>2</sup>
<b>Small nuclear RNA (cont.)</b>					
ENSG00000278234	chr3	-0.04	0.955961174	RF00004	U2 small nuclear RNA
ENSG00000278135	chr4	-0.12	0.85066227	RF00004	U2 small nuclear RNA
ENSG00000283414	chr1	-2.76	0.065378809	RF00026	U6 small nuclear RNA
ENSG00000283545	chr12	-0.77	0.45445302	RF00026	U6 small nuclear RNA
ENSG00000206652	chr1	-0.48	0.363806858	RNU1-1	RNA, U1 small nuclear 1
ENSG00000207005	chr1	-0.35	0.55039527	RNU1-2	RNA, U1 small nuclear 2
ENSG00000207513	chr1	-0.40	0.470831084	RNU1-3	RNA, U1 small nuclear 3
ENSG00000207389	chr1	-0.31	0.559056293	RNU1-4	RNA, U1 small nuclear 4
ENSG00000200795	chr12	0.65	0.293815907	RNU4-1	RNA, U4 small nuclear 1
ENSG00000202538	chr12	0.55	0.411328978	RNU4-2	RNA, U4 small nuclear 2
ENSG00000200169	chr1	-1.42	0.003568642	RNU5D-1	RNA, U5D small nuclear 1
ENSG00000199377	chr1	-0.16	0.866372984	RNU5F-1	RNA, U5F small nuclear 1
ENSG00000206625	chr15	0.90	0.007289583	RNU6-1	RNA, U6 small nuclear 1
ENSG00000264229	chr2	1.19	0.007485041	RNU4ATAC	RNA, U4atac small nuclear (U12-dependent splicing)
ENSG00000221676	chr9	-0.88	0.048176331	RNU6ATAC	RNA, U6atac small nuclear (U12-dependent splicing)
ENSG00000274450	chr1	1.73	0.100865035	RF00619	RNA, U6atac small nuclear (minor U12-type spliceosomal)
ENSG00000207340	chr1	-0.76	0.150282064	RNVU1-1	RNA, variant U1 small nuclear 1
ENSG00000201183	chr1	-2.57	0.302787792	RNVU1-3	RNA, variant U1 small nuclear 3
ENSG00000277610	chr1	0.20	0.882733863	RNVU1-4	RNA, variant U1 small nuclear 4
ENSG00000206585	chr1	0.28	0.635146853	RNVU1-7	RNA, variant U1 small nuclear 7
ENSG00000286172	chr1	-0.05	0.965348405	RNVU1-8	RNA, variant U1 small nuclear 8
ENSG00000207205	chr1	0.72	0.180528899	RNVU1-15	RNA, variant U1 small nuclear 15
ENSG00000206737	chr1	-0.37	0.509773353	RNVU1-18	RNA, variant U1 small nuclear 18
ENSG00000275538	chr1	-0.05	0.943551576	RNVU1-19	RNA, variant U1 small nuclear 19
<b>Small nucleolar RNA - H/ACA box class</b>					
ENSG00000221491	chr12	1.51	1.93E-05	SNORA2C	Small nucleolar RNA, H/ACA box 2C
ENSG00000221639	chr4	2.85	0.00694686	RF00334	Small nucleolar RNA SNORA3/SNORA45 family
ENSG00000201316	chr8	1.51	0.023365177	RF00409	Small nucleolar RNA SNORA7 (also known as ACA7)
ENSG00000206976	chr11	2.18	0.004001603	RF00409	Small nucleolar RNA SNORA7
ENSG00000206913	chr11	2.02	1.93E-08	RF00409	Small nucleolar RNA SNORA7
ENSG00000221102	chr14	1.75	0.000450182	SNORA11B	Small nucleolar RNA, H/ACA box 11B
ENSG00000201544	chr1	2.01	0.044889602	SNORA16B	Small nucleolar RNA, H/ACA box 16B
ENSG00000206649	chr8	2.70	0.002546797	RF00401	Small nucleolar RNA SNORA20 (also known as ACA20)
ENSG00000207392	chr6	1.98	0.000666487	SNORA20	Small nucleolar RNA, H/ACA box 20

Ensembl ID	Chr	Log2 Fold Change	P (adj)	Gene	Identities from Ensembl <sup>1</sup> or Rfam <sup>2</sup>
Small nucleolar RNA - H/ACA box class (cont.)					
ENSG00000207344	chr7	2.89	0.015392952	SNORA22C	Small nucleolar RNA, H/ACA box 22C
ENSG00000206755	chr16	1.79	0.011807292	SNORA30	Small nucleolar RNA, H/ACA box 30
ENSG00000252433	chr1	1.98	0.008830568	RF00322	Small nucleolar RNA SNORA31
ENSG00000252337	chr5	3.62	9.00E-06	RF00322	Small nucleolar RNA SNORA31
ENSG00000238961	chr5	2.43	5.77E-05	SNORA47	Small nucleolar RNA, H/ACA box 47
ENSG00000208892	chr12	1.70	9.60E-06	SNORA49	Small nucleolar RNA, H/ACA box 49
ENSG00000201457	chr1	1.82	6.18E-05	SNORA55	Small nucleolar RNA, H/ACA box 55
ENSG00000201003	chr1	2.92	0.026238661	RF00418	Small nucleolar RNA SNORA58
ENSG00000201229	chr3	1.91	0.000106279	SNORA63D	Small nucleolar RNA, H/ACA box 63D
ENSG00000206637	chr1	2.57	0.056826301	SNORA70H	Small nucleolar RNA, H/ACA box 70H
ENSG00000200959	chr5	1.84	0.001032975	SNORA74A	Small nucleolar RNA, H/ACA box 74A
ENSG00000222489	chr14	1.71	3.83E-05	SNORA79B	Small nucleolar RNA, H/ACA box 79B
ENSG00000239183	chr9	1.68	0.009098003	SNORA84	Small nucleolar RNA, H/ACA box 84
ENSG00000199405	chr8	0.18	0.88522411	SNORA1B	Small nucleolar RNA, H/ACA box 1B
ENSG00000206647	chr2	3.02	0.086247565	RF00410	Small nucleolar RNA SNORA2
ENSG00000206612	chr12	1.31	0.000745453	SNORA2A	Small nucleolar RNA, H/ACA box 2A
ENSG00000207313	chr12	-0.80	0.0686688	SNORA2B	Small nucleolar RNA, H/ACA box 2B
ENSG00000221148	chr12	0.35	0.74167561	RF00334	Small nucleolar RNA SNORA3/SNORA45 family
ENSG00000212607	chr11	1.45	9.97E-05	SNORA3B	Small nucleolar RNA, H/ACA box 3B
ENSG00000221719	chr16	-2.45	0.191881916	SNORA3C	Small nucleolar RNA, H/ACA box 3C
ENSG00000206838	chr7	0.19	0.754767979	SNORA5A	Small nucleolar RNA, H/ACA box 5A
ENSG00000201772	chr7	0.25	0.584738677	SNORA5C	Small nucleolar RNA, H/ACA box 5C
ENSG00000207088	chr3	1.35	4.95E-08	SNORA7B	Small nucleolar RNA, H/ACA box 7B
ENSG00000199282	chr13	-0.66	0.652639882	RF00411	Small nucleolar RNA SNORA9
ENSG00000206897	chr12	-1.10	0.272410388	SNORA9B	Small nucleolar RNA, H/ACA box 9B
ENSG00000221164	chr10	1.37	0.000511727	SNORA11F	Small nucleolar RNA, H/ACA box 11F
ENSG00000212464	chr10	0.52	0.217976655	SNORA12	Small nucleolar RNA, H/ACA box 12
ENSG00000238363	chr5	-1.01	0.081405712	SNORA13	Small nucleolar RNA, H/ACA box 13
ENSG00000201643	chr7	1.15	0.017926381	SNORA14A	Small nucleolar RNA, H/ACA box 14A
ENSG00000207181	chr1	1.38	0.0103495	SNORA14B	Small nucleolar RNA, H/ACA box 14B
ENSG00000207062	chr7	-0.19	0.867314139	SNORA15B-1	Small nucleolar RNA, H/ACA box 15B-1
ENSG00000206785	chr7	0.44	0.685479858	SNORA15B-2	Small nucleolar RNA, H/ACA box 15B-2
ENSG00000200288	chr3	-0.05	0.955961174	RF00425	Small nucleolar RNA SNORA18
ENSG00000207468	chr10	-1.60	0.261874322	SNORA19	Small nucleolar RNA, H/ACA box 19

Ensembl ID	Chr	Log2 Fold Change	P (adj)	Gene	Identities from Ensembl <sup>1</sup> or Rfam <sup>2</sup>
<b>Small nucleolar RNA - H/ACA box class (cont.)</b>					
ENSG00000206947	chr7	-0.31	0.670338886	SNORA20B	Small nucleolar RNA, H/ACA box 20B
ENSG00000206634	chr7	0.46	0.713455345	SNORA22	Small nucleolar RNA, H/ACA box 22
ENSG00000201998	chr11	0.28	0.31145409	SNORA23	Small nucleolar RNA, H/ACA box 23
ENSG00000207130	chr3	-0.02	0.991930467	RF00399	Small nucleolar RNA SNORA24
ENSG00000206903	chr15	1.52	0.067061177	SNORA24B	Small nucleolar RNA, H/ACA box 24B
ENSG00000212624	chr1	1.37	0.438926639	RF00568	Small nucleolar RNA SNORA26
ENSG00000212588	chr4	0.20	0.710682725	SNORA26	Small nucleolar RNA, H/ACA box 26
ENSG00000272533	chr14	-0.52	0.291605087	SNORA28	Small nucleolar RNA, H/ACA box 28
ENSG00000202189	chr9	1.79	0.309107735	SNORA30B	Small nucleolar RNA, H/ACA box 30B
ENSG00000199477	chr13	1.32	0.016227602	SNORA31	Small nucleolar RNA, H/ACA box 31
ENSG00000252136	chr4	-0.84	0.576051763	RF00322	Small nucleolar RNA SNORA31
ENSG00000252580	chr9	1.51	0.315220213	RF00322	Small nucleolar RNA SNORA31
ENSG00000200534	chr6	0.42	0.58133397	SNORA33	Small nucleolar RNA, H/ACA box 33
ENSG00000207016	chr2	0.22	0.787208759	SNORA36C	Small nucleolar RNA, H/ACA box 36C
ENSG00000200816	chr6	1.17	0.009003075	SNORA38	Small nucleolar RNA, H/ACA box 38
ENSG00000208308	chr2	-0.11	0.88522411	SNORA40B	Small nucleolar RNA, H/ACA box 40B
ENSG00000252840	chr1	0.78	0.279087895	RF00405	Small nucleolar RNA SNORA44
ENSG00000207008	chr11	1.41	0.00364972	SNORA54	Small nucleolar RNA, H/ACA box 54
ENSG00000249020	chr3	0.49	0.191881916	SNORA58	Small nucleolar RNA, H/ACA box 58
ENSG00000239149	chr1	-0.33	0.743490926	SNORA59A	Small nucleolar RNA, H/ACA box 59A
ENSG00000201448	chr1	0.44	0.528923005	SNORA63C	Small nucleolar RNA, H/ACA box 63C
ENSG00000201302	chr9	-0.09	0.864616452	SNORA65	Small nucleolar RNA, H/ACA box 65
ENSG00000238936	chr8	0.34	0.70506981	SNORD65B	Small nucleolar RNA, H/ACA box 65B
ENSG00000207523	chr1	0.57	0.217976655	SNORA66	Small nucleolar RNA, H/ACA box 66
ENSG00000207067	chr8	-0.83	0.142518008	SNORA72	Small nucleolar RNA, H/ACA box 72
ENSG00000201898	chr1	0.92	0.585452345	RF00139	Small nucleolar RNA SNORA72 (also known as U72)
ENSG00000207084	chr3	-0.78	0.578415275	RF00139	Small nucleolar RNA SNORA72 (also known as U72)
ENSG00000200355	chr3	-0.54	0.74960697	RF00139	Small nucleolar RNA SNORA72 (also known as U72)
ENSG00000252213	chr5	-1.29	0.049969356	SNORA74D	Small nucleolar RNA, H/ACA box 74D
ENSG00000206885	chr2	-0.32	0.621040712	SNORA75	Small nucleolar RNA, H/ACA box 75
ENSG00000206780	chr4	-1.03	0.548586071	SNORA75B	Small nucleolar RNA, H/ACA box 75B
ENSG00000221643	chr1	-0.02	0.974033927	SNORA77	Small nucleolar RNA, H/ACA box 77
ENSG00000221303	chr14	0.72	0.278103541	SNORA79	Small nucleolar RNA, H/ACA box 79
ENSG00000206633	chr2	1.76	0.067861478	SNORA80B	Small nucleolar RNA, H/ACA box 80B

Ensembl ID	Chr	Log2 Fold Change	P (adj)	Gene	Identities from Ensembl <sup>1</sup> or Rfam <sup>2</sup>
<b>Small nucleolar RNA - H/ACA box class (cont.)</b>					
ENSG00000199787	chr16	1.27	0.335355499	SNORA80C	Small nucleolar RNA, H/ACA box 80C
ENSG00000207217	chr7	1.94	0.067861478	SNORA80D	Small nucleolar RNA, H/ACA box 80D
ENSG00000207475	chr1	0.43	0.061309477	SNORA80E	Small nucleolar RNA, H/ACA box 80E
<b>Small nucleolar RNA - C/D box class</b>					
ENSG00000199436	chr14	1.50	0.012196095	SNORD9	Small nucleolar RNA, C/D box 9
ENSG00000238295	chr2	2.51	0.000196548	RF01210	Small nucleolar RNA U13 SNORD13A
ENSG00000238906	chr7	2.02	0.052947736	RF01210	Small nucleolar RNA U13, SNORD13A
ENSG00000207280	chr2	2.23	7.06E-06	SNORD20	Small nucleolar RNA, C/D box 20
ENSG00000201847	chr13	1.90	0.000731182	SNORD31B	Small nucleolar RNA, C/D box 31B
ENSG00000201330	chr6	2.29	3.38E-08	SNORD32B	Small nucleolar RNA, C/D box 32B
ENSG00000253094	chr13	1.97	0.000649506	RF00049	Small nucleolar RNA SNORD36
ENSG00000202031	chr1	1.93	1.14E-11	SNORD38A	Small nucleolar RNA, C/D box 38A
ENSG00000251830	chr6	3.03	0.049498361	RF00218	Small nucleolar RNA SNORD46
ENSG00000207031	chr12	2.82	1.11E-06	SNORD59A	Small nucleolar RNA, C/D box 59A
ENSG00000212158	chr3	1.71	5.44E-07	SNORD66	Small nucleolar RNA, C/D box 66
ENSG00000212283	chr2	1.54	0.000231782	SNORD89	Small nucleolar RNA, C/D box 89
ENSG00000221740	chr7	1.67	2.33E-05	SNORD93	Small nucleolar RNA, C/D box 93
ENSG00000206754	chr6	-2.01	0.000163528	SNORD101	Small nucleolar RNA, C/D box 101
ENSG00000239169	chr15	1.53	0.009340063	SNORD109B	Small nucleolar RNA, C/D box 109B
ENSG00000275662	chr14	-2.06	0.006045607	SNORD112	Small nucleolar RNA, C/D box 112
ENSG00000199914	chr14	-3.82	0.002247168	SNORD114-16	Small nucleolar RNA, C/D box 114-16
ENSG00000199712	chr15	3.59	0.002612135	SNORD115-2	Small nucleolar RNA, C/D box 115-2
ENSG00000199782	chr15	2.05	0.057697058	SNORD115-9	Small nucleolar RNA, C/D box 115-9
ENSG00000201943	chr15	2.55	0.017862584	SNORD115-10	Small nucleolar RNA, C/D box 115-10
ENSG00000199453	chr15	2.35	0.047026645	SNORD115-12	Small nucleolar RNA, C/D box 115-12
ENSG00000199960	chr15	3.33	0.004060463	SNORD115-14	Small nucleolar RNA, C/D box 115-14
ENSG00000201679	chr15	2.86	0.009285543	SNORD115-15	Small nucleolar RNA, C/D box 115-15
ENSG00000199833	chr15	2.60	0.03411343	SNORD115-21	Small nucleolar RNA, C/D box 115-21
ENSG00000272460	chr15	2.49	0.023611782	SNORD115-40	Small nucleolar RNA, C/D box 115-40
ENSG00000201143	chr15	2.84	0.00715716	SNORD115-42	Small nucleolar RNA, C/D box 115-42
ENSG00000212553	chr13	1.77	5.51E-06	RF00108	Small nucleolar RNA SNORD116
ENSG00000207063	chr15	2.18	8.51E-08	SNORD116-1	Small nucleolar RNA, C/D box 116-1
ENSG00000207001	chr15	1.93	2.86E-06	SNORD116-2	Small nucleolar RNA, C/D box 116-2
ENSG00000207014	chr15	1.77	1.27E-08	SNORD116-3	Small nucleolar RNA, C/D box 116-3

Ensembl ID	Chr	Log2 Fold Change	P (adj)	Gene	Identities from Ensembl <sup>1</sup> or Rfam <sup>2</sup>
Small nucleolar RNA - C/D box class (cont.)					
ENSG00000207191	chr15	2.24	3.58E-06	SNORD116-5	Small nucleolar RNA, C/D box 116-5
ENSG00000207442	chr15	1.80	9.25E-07	SNORD116-6	Small nucleolar RNA, C/D box 116-6
ENSG00000207133	chr15	2.19	3.81E-06	SNORD116-7	Small nucleolar RNA, C/D box 116-7
ENSG00000207093	chr15	1.73	7.20E-11	SNORD116-8	Small nucleolar RNA, C/D box 116-8
ENSG00000206727	chr15	1.79	4.33E-09	SNORD116-9	Small nucleolar RNA, C/D box 116-9
ENSG00000206609	chr15	1.57	2.25E-05	SNORD116-11	Small nucleolar RNA, C/D box 116-11
ENSG00000207137	chr15	1.53	4.62E-05	SNORD116-13	Small nucleolar RNA, C/D box 116-13
ENSG00000206621	chr15	1.85	0.000106279	SNORD116-14	Small nucleolar RNA, C/D box 116-14
ENSG00000207263	chr15	1.71	1.86E-06	SNORD116-16	Small nucleolar RNA, C/D Box 116-16
ENSG00000206656	chr15	1.50	6.72E-06	SNORD116-17	Small nucleolar RNA, C/D Box 116-17
ENSG00000207460	chr15	1.50	5.91E-06	SNORD116-19	Small nucleolar RNA, C/D box 116-19
ENSG00000207375	chr15	1.61	1.92E-08	SNORD116-23	Small nucleolar RNA, C/D box 116-23
ENSG00000207245	chr15	2.26	0.000978463	SNORD116-29	Small nucleolar RNA, C/D box 116-29
ENSG00000252277	chr15	1.50	0.008494721	SNORD116-30	Small nucleolar RNA, C/D box 116-30
ENSG00000201785	chr6	1.51	4.81E-05	SNORD117	Small nucleolar RNA, C/D box 117
ENSG00000212144	chr1	-2.54	3.31E-05	RF00096	U8 small nucleolar RNA (also known as SNORD118)
ENSG00000212249	chr5	-1.82	0.046247508	RF00096	U8 small nucleolar RNA (also known as SNORD118)
ENSG00000200026	chr9	-3.76	0.000127019	RF00096	U8 small nucleolar RNA (also known as SNORD118)
ENSG00000238707	chr10	-0.04	0.982647465	RF01299	Small nucleolar RNA SNORD2
ENSG00000238854	chr8	1.49	0.26055572	RF01161	Small nucleolar RNA SNORD5
ENSG00000202314	chr11	0.89	0.135472366	SNORD6	Small nucleolar RNA, C/D box 6
ENSG00000238819	chr15	-0.04	0.984743024	RF01182	Small nucleolar RNA SNORD11
ENSG00000238317	chr2	-0.57	0.162959244	SNORD11	Small nucleolar RNA, C/D box 11
ENSG00000271852	chr2	-0.69	0.242772802	SNORD11B	Small nucleolar RNA, C/D box 11B
ENSG00000239039	chr8	1.33	0.011219912	SNORD13	Small nucleolar RNA, C/D box 13
ENSG00000238902	chr3	1.30	0.195214385	RF01210	Small nucleolar RNA U13 SNORD13A
ENSG00000239035	chr15	0.59	0.706629791	SNORD13D	Small nucleolar RNA, C/D box 13D
ENSG00000272034	chr11	1.14	0.016712671	SNORD14A	Small nucleolar RNA, C/D box 14A
ENSG00000200879	chr11	1.38	6.72E-06	SNORD14E	Small nucleolar RNA, C/D box 14E
ENSG00000207445	chr11	-0.79	0.071308548	SNORD15B	Small nucleolar RNA, C/D box 15B
ENSG00000238503	chr2	-0.99	0.478605097	RF00093	Small nucleolar RNA SNORD18
ENSG00000222345	chr3	-0.44	0.508680463	SNORD19C	Small nucleolar RNA, C/D box 19C
ENSG00000277846	chr11	1.26	0.002131414	SNORD30	Small nucleolar RNA, C/D box 30
ENSG00000202440	chr4	0.57	0.189549687	RF00150	Small nucleolar RNA SNORD42

Ensembl ID	Chr	Log2 Fold Change	P (adj)	Gene	Identities from Ensembl <sup>1</sup> or Rfam <sup>2</sup>
Small nucleolar RNA - C/D box class (cont.)					
ENSG00000200051	chr5	1.22	0.015392952	RF00279	Small nucleolar RNA SNORD45
ENSG00000200706	chr6	1.58	0.123305863	RF00279	Small nucleolar RNA SNORD45
ENSG00000201009	chr7	1.19	0.024002185	RF00218	Small nucleolar RNA SNORD46
ENSG00000200913	chr1	1.23	0.017155313	SNORD46	Small nucleolar RNA, C/D box 46
ENSG00000201823	chr6	0.74	0.064622097	SNORD48	Small nucleolar RNA, C/D box 48
ENSG00000265145	chr2	1.11	0.000338	SNORD53	Small nucleolar RNA, C/D box 53
ENSG00000265706	chr2	1.30	0.001652144	SNORD53B	Small nucleolar RNA, C/D box 53B
ENSG00000212615	chr14	0.83	0.067861478	RF00151	Small nucleolar RNA SNORD58
ENSG00000199411	chr9	0.54	0.596915391	RF00153	Small nucleolar RNA SNORD62
ENSG00000235284	chr9	0.33	0.546353801	SNORD62A	Small nucleolar RNA, C/D box 62A
ENSG00000231587	chr9	0.37	0.474595206	SNORD62B	Small nucleolar RNA, C/D box 62B
ENSG00000206989	chr5	0.42	0.4398162	SNORD63	Small nucleolar RNA, C/D box 63
ENSG00000212161	chr1	-0.35	0.70506981	RF00570	Small nucleolar RNA SNORD64
ENSG00000212264	chr7	-0.17	0.898412989	SNORD65C	Small nucleolar RNA, C/D box 65C
ENSG00000212532	chr6	1.29	0.21199785	RF00572	Small nucleolar RNA SNORD66
ENSG00000212135	chr11	0.32	0.40570559	SNORD67	Small nucleolar RNA, C/D box 67
ENSG00000212452	chr3	-0.02	0.974033927	SNORD69	Small nucleolar RNA, C/D box 69
ENSG00000212534	chr2	0.92	0.012909984	SNORD70	Small nucleolar RNA, C/D box 70
ENSG00000212296	chr5	-0.15	0.834627477	SNORD72	Small nucleolar RNA, C/D box 72
ENSG00000201264	chr4	-1.63	0.137994914	SNORD73B	Small nucleolar RNA, C/D box 73B
ENSG00000200999	chr4	-0.35	0.784359794	RF00284	Small nucleolar RNA SNORD74
ENSG00000200206	chr15	0.95	0.546353801	RF00284	Small nucleolar RNA SNORD74
ENSG00000212378	chr2	-0.46	0.764546278	RF00592	Small nucleolar RNA SNORD78
ENSG00000199934	chr1	-0.27	0.682287116	RF00136	Small nucleolar RNA SNORD81
ENSG00000212278	chr5	0.32	0.845934548	RF00136	Small nucleolar RNA SNORD81
ENSG00000202023	chr7	-0.12	0.923990259	RF00136	Small nucleolar RNA SNORD81
ENSG00000202400	chr2	0.49	0.328512727	SNORD82	Small nucleolar RNA, C/D box 82
ENSG00000221611	chr12	1.38	0.017926381	RF00604	Small nucleolar RNA SNORD88
ENSG00000212447	chr9	0.59	0.295269002	SNORD90	Small nucleolar RNA, C/D box 90
ENSG00000264994	chr2	0.66	0.160804333	SNORD92	Small nucleolar RNA, C/D box 92
ENSG00000208772	chr2	1.34	8.30E-06	SNORD94	Small nucleolar RNA, C/D box 94
ENSG00000200969	chr9	0.43	0.593096342	RF00189	Small nucleolar RNA SNORD95
ENSG00000221539	chr1	0.43	0.388946724	SNORD99	Small nucleolar RNA, C/D box 99
ENSG00000221500	chr6	-0.47	0.361095038	SNORD100	Small nucleolar RNA, C/D box 100

Ensembl ID	Chr	Log2 Fold Change	P (adj)	Gene	Identities from Ensembl <sup>1</sup> or Rfam <sup>2</sup>
<b>Small nucleolar RNA - C/D box class (cont.)</b>					
ENSG00000201500	chr14	0.44	0.866372984	RF00181	Small nucleolar RNA SNORD113
ENSG00000201700	chr14	-1.38	0.004516543	SNORD113-3	Small nucleolar RNA, C/D box 113-3
ENSG00000272474	chr14	-0.47	0.608463966	SNORD113-5	Small nucleolar RNA, C/D box 113-5
ENSG00000200215	chr14	-0.23	0.651824488	SNORD113-6	Small nucleolar RNA, C/D box 113-6
ENSG00000200632	chr14	-0.15	0.824770584	SNORD113-7	Small nucleolar RNA, C/D box 113-7
ENSG00000200367	chr14	-0.19	0.690518857	SNORD113-8	Small nucleolar RNA, C/D box 113-8
ENSG00000201950	chr14	-0.90	0.072518398	SNORD113-9	Small nucleolar RNA, C/D box 113-9
ENSG00000199575	chr14	0.37	0.355924986	SNORD114-1	Small nucleolar RNA, C/D box 114-1
ENSG00000201839	chr14	0.48	0.199699614	SNORD114-3	Small nucleolar RNA, C/D box 114-3
ENSG00000199798	chr14	0.07	0.927964639	SNORD114-5	Small nucleolar RNA, C/D box 114-5
ENSG00000201240	chr14	-0.46	0.239951325	SNORD114-9	Small nucleolar RNA, C/D box 114-9
ENSG00000200279	chr14	-1.40	0.01376886	SNORD114-10	Small nucleolar RNA, C/D box 114-10
ENSG00000200608	chr14	0.13	0.769338299	SNORD114-11	Small nucleolar RNA, C/D box 114-11
ENSG00000202270	chr14	0.19	0.741874573	SNORD114-12	Small nucleolar RNA, C/D box 114-12
ENSG00000201247	chr14	-0.28	0.74863453	SNORD114-13	Small nucleolar RNA, C/D box 114-13
ENSG00000199593	chr14	0.87	0.004287113	SNORD114-14	Small nucleolar RNA, C/D box 114-14
ENSG00000201557	chr14	-0.53	0.247138216	SNORD114-15	Small nucleolar RNA, C/D box 114-15
ENSG00000201569	chr14	-0.49	0.287642087	SNORD114-17	Small nucleolar RNA, C/D box 114-17
ENSG00000202142	chr14	0.43	0.826940659	SNORD114-18	Small nucleolar RNA, C/D box 114-18
ENSG00000202048	chr14	0.03	0.982005235	SNORD114-20	Small nucleolar RNA, C/D box 114-20
ENSG00000272344	chr14	-0.19	0.714898022	SNORD114-21	Small nucleolar RNA, C/D box 114-21
ENSG00000202293	chr14	-0.25	0.685075657	SNORD114-22	Small nucleolar RNA, C/D box 114-22
ENSG00000200406	chr14	0.69	0.035342729	SNORD114-23	Small nucleolar RNA, C/D box 114-23
ENSG00000200612	chr14	-0.10	0.882733863	SNORD114-25	Small nucleolar RNA, C/D box 114-25
ENSG00000200480	chr14	0.08	0.874590657	SNORD114-28	Small nucleolar RNA, C/D box 114-28
ENSG00000201689	chr14	0.49	0.429427427	SNORD114-29	Small nucleolar RNA, C/D box 114-29
ENSG00000201831	chr15	1.74	0.169385429	SNORD115-1	Small nucleolar RNA, C/D box 115-1
ENSG00000200680	chr15	1.04	0.493354781	SNORD115-4	Small nucleolar RNA, C/D box 115-4
ENSG00000200503	chr15	1.63	0.181409036	SNORD115-5	Small nucleolar RNA, C/D box 115-5
ENSG00000200812	chr15	2.39	0.161292322	SNORD115-6	Small nucleolar RNA, C/D box 115-6
ENSG00000200726	chr15	0.92	0.670016892	SNORD115-8	Small nucleolar RNA, C/D box 115-8
ENSG00000200486	chr15	0.65	0.661776459	SNORD115-11	Small nucleolar RNA, C/D box 115-11
ENSG00000200757	chr15	-0.67	0.670338886	SNORD115-16	Small nucleolar RNA, C/D box 115-16
ENSG00000201482	chr15	1.52	0.150112475	SNORD115-17	Small nucleolar RNA, C/D box 115-17

Ensembl ID	Chr	Log2 Fold Change	P (adj)	Gene	Identities from Ensembl <sup>1</sup> or Rfam <sup>2</sup>
<b>Small nucleolar RNA - C/D box class (cont.)</b>					
ENSG00000200163	chr15	1.67	0.126402876	SNORD115-18	Small nucleolar RNA, C/D box 115-18
ENSG00000199968	chr15	1.53	0.137994914	SNORD115-19	Small nucleolar RNA, C/D box 115-19
ENSG00000201969	chr15	2.07	0.122063317	SNORD115-20	Small nucleolar RNA, C/D box 115-20
ENSG00000201326	chr15	1.74	0.122063317	SNORD115-22	Small nucleolar RNA, C/D box 115-22
ENSG00000201331	chr15	1.33	0.132755404	SNORD115-23	Small nucleolar RNA, C/D box 115-23
ENSG00000199704	chr15	0.31	0.867314139	SNORD115-29	Small nucleolar RNA, C/D box 115-29
ENSG00000200987	chr15	1.04	0.361539414	SNORD115-30	Small nucleolar RNA, C/D box 115-30
ENSG00000200949	chr15	1.29	0.178155566	SNORD115-32	Small nucleolar RNA, C/D box 115-32
ENSG00000200593	chr15	1.48	0.21199785	SNORD115-33	Small nucleolar RNA, C/D box 115-33
ENSG00000199311	chr15	1.19	0.387442875	SNORD115-34	Small nucleolar RNA, C/D box 115-34
ENSG00000201992	chr15	-0.09	0.972448285	SNORD115-35	Small nucleolar RNA, C/D box 115-35
ENSG00000202499	chr15	-0.03	0.987566079	SNORD115-36	Small nucleolar RNA, C/D box 115-36
ENSG00000200638	chr15	-1.25	0.551109514	SNORD115-37	Small nucleolar RNA, C/D box 115-37
ENSG00000201907	chr15	-1.29	0.371694817	SNORD115-38	Small nucleolar RNA, C/D box 115-38
ENSG00000200564	chr15	0.85	0.568535016	SNORD115-39	Small nucleolar RNA, C/D box 115-39
ENSG00000200478	chr15	1.35	0.429427427	SNORD115-41	Small nucleolar RNA, C/D box 115-41
ENSG00000202373	chr15	-0.11	0.955961174	SNORD115-43	Small nucleolar RNA, C/D box 115-43
ENSG00000202261	chr15	0.36	0.784239294	SNORD115-44	Small nucleolar RNA, C/D box 115-44
ENSG00000201634	chr15	2.02	0.121927546	SNORD115-48	Small nucleolar RNA, C/D box 115-48
ENSG00000202498	chr1	1.10	0.007289583	RF00108	Small nucleolar RNA SNORD116
ENSG00000207197	chr15	1.15	0.000210421	SNORD116-12	Small nucleolar RNA, C/D box 116-12
ENSG00000207174	chr15	1.44	4.95E-07	SNORD116-15	Small nucleolar RNA, C/D box 116-15
ENSG00000206688	chr15	1.18	0.556815274	SNORD116-18	Small Nucleolar RNA, C/D Box 116-18
ENSG00000207279	chr15	1.35	6.40E-06	SNORD116-24	Small nucleolar RNA, C/D box 116-24
ENSG00000252326	chr15	1.18	0.017220799	SNORD116-25	Small nucleolar RNA, C/D box 116-25
ENSG00000202537	chr2	-2.29	0.363806858	RF00096	U8 small nucleolar RNA (also known as SNORD118)
ENSG00000201398	chr3	-0.76	0.584522392	RF00096	U8 small nucleolar RNA (also known as SNORD118)
ENSG00000200496	chr11	-0.73	0.106929633	RF00096	U8 small nucleolar RNA (also known as SNORD118)
ENSG00000238886	chr9	-0.22	0.682287116	SNORD121A	Small nucleolar RNA, C/D box 121A
ENSG00000239112	chr5	-0.01	0.995646572	SNORD123	Small nucleolar RNA, C/D box 123
ENSG00000238344	chr14	1.15	0.000821911	SNORD126	Small nucleolar RNA, C/D box 126
ENSG00000239043	chr14	1.20	0.00715716	SNORD127	Small nucleolar RNA, C/D box 127

Ensembl ID	Chr	Log2 Fold Change	P (adj)	Gene	Identities from Ensembl <sup>1</sup> or Rfam <sup>2</sup>
					Y-RNA
ENSG00000202354	chr7	2.04	2.71E-08	RNY3	RNA, Ro60-associated Y3
ENSG00000200085	chr1	2.55	0.025417715	RF00019	Y RNA
ENSG00000252802	chr1	1.47	0.00882134	RF00019	Y RNA
ENSG00000199565	chr1	2.25	0.010441678	RF00019	Y RNA
ENSG00000207039	chr1	2.25	0.006419357	RF00019	Y RNA
ENSG00000206905	chr1	3.13	1.63E-07	RF00019	Y RNA
ENSG00000206640	chr1	3.83	0.025417715	RF00019	Y RNA
ENSG00000207069	chr2	2.28	1.87E-07	RF00019	Y RNA
ENSG00000202309	chr2	2.70	0.012338961	RF00019	Y RNA
ENSG00000202382	chr2	1.93	0.012805991	RF00019	Y RNA
ENSG00000207386	chr2	2.72	3.04E-12	RF00019	Y RNA
ENSG00000202137	chr2	1.64	0.028399866	RF00019	Y RNA
ENSG00000200118	chr3	2.42	0.000727202	RF00019	Y RNA
ENSG00000207481	chr4	1.84	0.003923669	RF00019	Y RNA
ENSG00000202536	chr4	2.72	9.49E-05	RF00019	Y RNA
ENSG00000200521	chr4	2.47	1.07E-12	RF00019	Y RNA
ENSG00000207293	chr5	2.89	7.83E-05	RF00019	Y RNA
ENSG00000201442	chr6	3.41	0.007485041	RF00019	Y RNA
ENSG00000200314	chr6	3.25	1.80E-20	RF00019	Y RNA
ENSG00000200847	chr7	2.74	0.027125919	RF00019	Y RNA
ENSG00000201566	chr7	2.09	0.012552841	RF00019	Y RNA
ENSG00000200769	chr7	3.00	7.54E-06	RF00019	Y RNA
ENSG00000207061	chr7	2.31	0.000210249	RF00019	Y RNA
ENSG00000199732	chr8	2.64	5.31E-07	RF00019	Y RNA
ENSG00000199667	chr8	3.11	6.44E-06	RF00019	Y RNA
ENSG00000199635	chr9	2.53	0.000385778	RF00019	Y RNA
ENSG00000200544	chr9	1.65	0.047556643	RF00019	Y RNA
ENSG00000200041	chr9	1.63	0.005958736	RF00019	Y RNA
ENSG00000199222	chr10	2.30	9.63E-09	RF00019	Y RNA
ENSG00000207024	chr11	2.41	1.01E-06	RF00019	Y RNA
ENSG00000200855	chr11	1.98	8.49E-07	RF00019	Y RNA
ENSG00000206967	chr11	1.60	0.020474773	RF00019	Y RNA
ENSG00000201228	chr12	2.37	7.49E-05	RF00019	Y RNA
ENSG00000207142	chr12	2.71	5.90E-16	RF00019	Y RNA

Ensembl ID	Chr	Log2 Fold Change	P (adj)	Gene	Identities from Ensembl <sup>1</sup> or Rfam <sup>2</sup>
Y-RNA (cont.)					
ENSG00000252660	chr12	2.31	0.004499618	RF00019	Y RNA
ENSG00000200011	chr12	3.17	0.016003662	RF00019	Y RNA
ENSG00000202368	chr12	1.82	0.04314115	RF00019	Y RNA
ENSG00000206790	chr12	2.74	0.014183243	RF00019	Y RNA
ENSG00000222601	chr12	1.58	0.029644698	RF00019	Y RNA
ENSG00000206914	chr12	1.62	0.034511212	RF00019	Y RNA
ENSG00000199291	chr14	1.53	0.000512195	RF00019	Y RNA
ENSG00000199461	chr14	2.38	4.08E-07	RF00019	Y RNA
ENSG00000200506	chr14	1.97	4.71E-07	RF00019	Y RNA
ENSG00000206846	chr15	2.10	1.60E-06	RF00019	Y RNA
ENSG00000207484	chr15	2.37	7.28E-10	RF00019	Y RNA
ENSG00000206995	chr15	1.59	0.00046294	RF00019	Y RNA
ENSG00000201098	chr7	0.45	0.120608548	RNY1	RNA, Ro60-associated Y1
ENSG00000252316	chr7	0.68	0.096485235	RNY4	RNA, Ro60-associated Y4
ENSG00000286171	chr7	0.14	0.801446869	AC073140.1	RNA, Ro60-associated Y5
ENSG00000252822	chr1	-1.46	0.354169597	RF00019	Y RNA
ENSG00000252317	chr1	0.15	0.742039684	RF00019	Y RNA
ENSG00000199241	chr1	-1.04	0.584216716	RF00019	Y RNA
ENSG00000252254	chr1	-0.50	0.578912599	RF00019	Y RNA
ENSG00000199756	chr1	0.00	0.999521291	RF00019	Y RNA
ENSG00000265961	chr1	-0.18	0.690518857	RF00019	Y RNA
ENSG00000207356	chr1	-0.56	0.720847378	RF00019	Y RNA
ENSG00000200171	chr1	0.23	0.627329956	RF00019	Y RNA
ENSG00000199459	chr1	0.27	0.88347376	RF00019	Y RNA
ENSG00000202027	chr1	0.75	0.408372132	RF00019	Y RNA
ENSG00000206651	chr1	-0.12	0.823695987	RF00019	Y RNA
ENSG00000202078	chr1	-0.26	0.740154081	RF00019	Y RNA
ENSG00000206659	chr1	1.42	0.029644698	RF00019	Y RNA
ENSG00000199840	chr1	0.17	0.939002389	RF00019	Y RNA
ENSG00000201421	chr1	1.70	0.255524438	RF00019	Y RNA
ENSG00000199349	chr1	-1.09	0.477843246	RF00019	Y RNA
ENSG00000207086	chr2	-0.53	0.368851687	RF00019	Y RNA
ENSG00000200829	chr2	0.08	0.929493402	RF00019	Y RNA
ENSG00000199936	chr2	-1.33	0.445073859	RF00019	Y RNA

Ensembl ID	Chr	Log2 Fold Change	P (adj)	Gene	Identities from Ensembl <sup>1</sup> or Rfam <sup>2</sup>
Y-RNA (cont.)					
ENSG00000207383	chr2	0.69	0.072518398	RF00019	Y RNA
ENSG00000202046	chr2	-0.44	0.787952339	RF00019	Y RNA
ENSG00000252742	chr2	0.57	0.658306897	RF00019	Y RNA
ENSG00000222394	chr2	-1.39	0.450666587	RF00019	Y RNA
ENSG00000207161	chr2	0.13	0.805339397	RF00019	Y RNA
ENSG00000222509	chr2	0.13	0.822468132	RF00019	Y RNA
ENSG00000202141	chr2	0.46	0.571109508	RF00019	Y RNA
ENSG00000199781	chr2	-0.48	0.682287116	RF00019	Y RNA
ENSG00000252759	chr2	0.54	0.276165751	RF00019	Y RNA
ENSG00000202008	chr2	0.54	0.276228326	RF00019	Y RNA
ENSG00000200764	chr2	0.65	0.663908272	RF00019	Y RNA
ENSG00000206728	chr3	0.73	0.511052266	RF00019	Y RNA
ENSG00000199591	chr3	0.39	0.578912599	RF00019	Y RNA
ENSG00000251986	chr3	1.18	0.012069842	RF00019	Y RNA
ENSG00000251811	chr3	0.13	0.867314139	RF00019	Y RNA
ENSG00000201635	chr3	0.64	0.449315178	RF00019	Y RNA
ENSG00000199476	chr3	0.32	0.74743628	RF00019	Y RNA
ENSG00000201511	chr3	1.98	0.132733217	RF00019	Y RNA
ENSG00000206721	chr3	1.26	0.45445302	RF00019	Y RNA
ENSG00000201800	chr3	1.19	0.000151498	RF00019	Y RNA
ENSG00000201031	chr3	0.90	0.066285973	RF00019	Y RNA
ENSG00000201778	chr3	0.19	0.656849915	RF00019	Y RNA
ENSG00000201343	chr3	-0.69	0.30755675	RF00019	Y RNA
ENSG00000200616	chr3	-0.64	0.690518857	RF00019	Y RNA
ENSG00000207009	chr4	-1.13	0.130456871	RF00019	Y RNA
ENSG00000238585	chr4	-0.15	0.88522411	RF00019	Y RNA
ENSG00000200998	chr4	-0.27	0.716819256	RF00019	Y RNA
ENSG00000201644	chr4	0.24	0.806724019	RF00019	Y RNA
ENSG00000207480	chr4	0.70	0.658087103	RF00019	Y RNA
ENSG00000207148	chr4	1.18	0.440796316	RF00019	Y RNA
ENSG00000201786	chr4	1.34	0.004791284	RF00019	Y RNA
ENSG00000206978	chr4	-0.24	0.682287116	RF00019	Y RNA
ENSG00000207231	chr4	-0.62	0.726251419	RF00019	Y RNA
ENSG00000207497	chr4	0.42	0.424753456	RF00019	Y RNA

Ensembl ID	Chr	Log2 Fold Change	P (adj)	Gene	Identities from Ensembl <sup>1</sup> or Rfam <sup>2</sup>
Y-RNA (cont.)					
ENSG00000252671	chr5	-0.67	0.566332019	RF00019	Y RNA
ENSG00000201370	chr5	0.81	0.66887083	RF00019	Y RNA
ENSG00000206814	chr5	-0.04	0.961757087	RF00019	Y RNA
ENSG00000207439	chr5	-0.38	0.781072606	RF00019	Y RNA
ENSG00000207404	chr5	-0.56	0.238891764	RF00019	Y RNA
ENSG00000202533	chr5	-0.68	0.374611318	RF00019	Y RNA
ENSG00000199677	chr5	-1.15	0.205652841	RF00019	Y RNA
ENSG00000274472	chr5	-1.58	0.330394671	RF00019	Y RNA
ENSG00000201277	chr5	0.26	0.754020903	RF00019	Y RNA
ENSG00000201483	chr6	-0.21	0.867314139	RF00019	Y RNA
ENSG00000199290	chr6	1.13	0.242772802	RF00019	Y RNA
ENSG00000201680	chr6	0.94	0.207746158	RF00019	Y RNA
ENSG00000201555	chr6	-0.64	0.212102831	RF00019	Y RNA
ENSG00000206717	chr6	0.43	0.541402781	RF00019	Y RNA
ENSG00000199938	chr6	0.33	0.68032418	RF00019	Y RNA
ENSG00000252891	chr6	1.93	0.085602161	RF00019	Y RNA
ENSG00000274603	chr6	0.46	0.309938225	RF00019	Y RNA
ENSG00000199303	chr6	-0.30	0.706024424	RF00019	Y RNA
ENSG00000207499	chr6	1.05	0.557563006	RF00019	Y RNA
ENSG00000238490	chr6	1.37	0.246842757	RF00019	Y RNA
ENSG00000207292	chr6	0.20	0.782285495	RF00019	Y RNA
ENSG00000202273	chr7	-0.52	0.292316752	RF00019	Y RNA
ENSG00000201774	chr7	1.65	0.138581679	RF00019	Y RNA
ENSG00000201933	chr7	-0.16	0.867314139	RF00019	Y RNA
ENSG00000251852	chr7	1.62	0.067061177	RF00019	Y RNA
ENSG00000199224	chr7	1.25	0.078304252	RF00019	Y RNA
ENSG00000199516	chr7	0.99	0.377885155	RF00019	Y RNA
ENSG00000206705	chr7	1.13	0.013784022	RF00019	Y RNA
ENSG00000206950	chr8	0.84	0.245072758	RF00019	Y RNA
ENSG00000207258	chr8	0.62	0.609281214	RF00019	Y RNA
ENSG00000207101	chr8	1.66	0.094629701	RF00019	Y RNA
ENSG00000202310	chr8	0.90	0.510319112	RF00019	Y RNA
ENSG00000201216	chr8	-1.27	0.55039527	RF00019	Y RNA
ENSG00000200834	chr9	0.43	0.504854156	RF00019	Y RNA

Ensembl ID	Chr	Log2 Fold Change	P (adj)	Gene	Identities from Ensembl <sup>1</sup> or Rfam <sup>2</sup>
Y-RNA (cont.)					
ENSG00000207032	chr9	-0.57	0.608425909	RF00019	Y RNA
ENSG00000278028	chr9	0.47	0.715695176	RF00019	Y RNA
ENSG00000238933	chr9	0.59	0.585452345	RF00019	Y RNA
ENSG00000238749	chr9	0.11	0.958502163	RF00019	Y RNA
ENSG00000275904	chr9	0.21	0.867314139	RF00019	Y RNA
ENSG00000239180	chr9	0.40	0.407406167	RF00019	Y RNA
ENSG00000201938	chr9	0.43	0.335355499	RF00019	Y RNA
ENSG00000200261	chr9	0.08	0.937240111	RF00019	Y RNA
ENSG00000201749	chr9	0.09	0.921343785	RF00019	Y RNA
ENSG00000251803	chr10	0.28	0.741874573	RF00019	Y RNA
ENSG00000199200	chr10	0.32	0.55039527	RF00019	Y RNA
ENSG00000207271	chr10	-0.17	0.752347949	RF00019	Y RNA
ENSG00000206840	chr10	0.08	0.897593717	RF00019	Y RNA
ENSG00000201548	chr10	0.63	0.682287116	RF00019	Y RNA
ENSG00000201412	chr10	0.34	0.741874573	RF00019	Y RNA
ENSG00000200737	chr10	1.23	0.135472366	RF00019	Y RNA
ENSG00000222072	chr10	-2.04	0.176361492	RF00019	Y RNA
ENSG00000207494	chr10	0.35	0.477843246	RF00019	Y RNA
ENSG00000199550	chr11	0.28	0.769338299	RF00019	Y RNA
ENSG00000201279	chr11	0.87	0.078884551	RF00019	Y RNA
ENSG00000200201	chr11	0.01	0.993132225	RF00019	Y RNA
ENSG00000200615	chr11	0.68	0.04314115	RF00019	Y RNA
ENSG00000206808	chr11	-0.39	0.68683999	RF00019	Y RNA
ENSG00000200090	chr11	1.40	8.86E-08	RF00019	Y RNA
ENSG00000202522	chr11	0.49	0.698658175	RF00019	Y RNA
ENSG00000201756	chr11	-0.26	0.752347949	RF00019	Y RNA
ENSG00000199875	chr11	-0.52	0.365107757	RF00019	Y RNA
ENSG00000206911	chr11	0.38	0.741874573	RF00019	Y RNA
ENSG00000222529	chr11	0.26	0.860779825	RF00019	Y RNA
ENSG00000206662	chr12	-1.71	0.30755675	RF00019	Y RNA
ENSG00000201788	chr12	0.62	0.664016217	RF00019	Y RNA
ENSG00000199245	chr12	0.00	0.998265009	RF00019	Y RNA
ENSG00000212448	chr12	-0.13	0.849065456	RF00019	Y RNA
ENSG00000222579	chr12	-0.22	0.834627477	RF00019	Y RNA

Ensembl ID	Chr	Log2 Fold Change	P (adj)	Gene	Identities from Ensembl <sup>1</sup> or Rfam <sup>2</sup>
ENSG00000200309	chr12	-0.05	0.974033927	RF00019	Y RNA
ENSG00000200428	chr12	0.05	0.955961174	RF00019	Y RNA
ENSG00000238443	chr12	0.59	0.70506981	RF00019	Y RNA
ENSG00000199584	chr12	1.17	0.089865396	RF00019	Y RNA
ENSG00000206850	chr12	0.54	0.219677919	RF00019	Y RNA
ENSG00000252655	chr14	0.15	0.900800888	RF00019	Y RNA
ENSG00000201351	chr14	0.46	0.590836827	RF00019	Y RNA
ENSG00000212335	chr14	0.63	0.477076409	RF00019	Y RNA
ENSG00000202402	chr14	0.55	0.68032418	RF00019	Y RNA
ENSG00000202306	chr14	-0.68	0.348034527	RF00019	Y RNA
ENSG00000199285	chr14	0.00	0.993132225	RF00019	Y RNA
ENSG00000252919	chr14	1.05	0.121927546	RF00019	Y RNA
ENSG00000251792	chr14	0.81	0.03411343	RF00019	Y RNA
ENSG00000201573	chr14	-1.50	0.302405911	RF00019	Y RNA
ENSG00000201820	chr14	1.09	0.374611318	RF00019	Y RNA
ENSG00000200742	chr14	1.09	0.218624973	RF00019	Y RNA
ENSG00000252198	chr14	0.05	0.982005235	RF00019	Y RNA
ENSG00000206822	chr14	0.30	0.669508161	RF00019	Y RNA
ENSG00000202182	chr14	1.58	0.180754273	RF00019	Y RNA
ENSG00000201529	chr14	0.47	0.361512786	RF00019	Y RNA
ENSG00000206676	chr15	1.34	0.171192342	RF00019	Y RNA
ENSG00000200305	chr15	0.90	0.466325611	RF00019	Y RNA
ENSG00000202211	chr15	-0.35	0.867314139	RF00019	Y RNA
ENSG00000238845	chr15	0.01	0.991015284	RF00019	Y RNA
ENSG00000252171	chr15	0.23	0.640689601	RF00019	Y RNA
ENSG00000200419	chr15	0.08	0.944644577	RF00019	Y RNA
ENSG00000202542	chr15	-0.04	0.978208228	RF00019	Y RNA
ENSG00000200605	chr15	0.23	0.70506981	RF00019	Y RNA
ENSG00000201071	chr15	0.38	0.528617995	RF00019	Y RNA
ENSG00000207223	chr15	2.51	0.073209557	RF00019	Y RNA
ENSG00000252217	chr15	-0.31	0.85769577	RF00019	Y RNA
ENSG00000199580	chr15	-0.75	0.104509445	RF00019	Y RNA
ENSG00000200142	chr15	0.82	0.459273255	RF00019	Y RNA
ENSG00000201724	chr15	1.04	0.156054735	RF00019	Y RNA

Ensembl ID	Chr	Log2 Fold Change	P (adj)	Gene	Identities from Ensembl <sup>1</sup> or Rfam <sup>2</sup>
Y-RNA (cont.)					
ENSG00000212306	chr15	0.41	0.403484062	RF00019	Y RNA
ENSG00000201034	chr16	0.28	0.810461654	RF00019	Y RNA
ENSG00000202476	chr16	0.42	0.480041749	RF00019	Y RNA
ENSG00000222701	chr16	2.68	0.080622167	RF00019	Y RNA
Pseudogenes - Small nuclear pseudogenes					
ENSG00000201699	chr1	1.88	0.016398086	RNU1-59P	RNA, U1 small nuclear 59, pseudogene
ENSG00000200885	chr12	-2.18	0.020845505	RNU1-146P	RNA, U1 small nuclear 146, pseudogene
ENSG00000222293	chr9	-2.35	6.97E-06	RNU2-36P	RNA, U2 small nuclear 36, pseudogene
ENSG00000222627	chr3	-1.61	0.001237054	RNU2-37P	RNA, U2 small nuclear 37, pseudogene
ENSG00000221601	chr5	2.55	0.001876899	RNU4ATAC2P	RNA, U4atac small nuclear 2, pseudogene
ENSG00000221439	chr12	2.03	0.0103495	RNU4ATAC16P	RNA, U4atac small nuclear 16, pseudogene
ENSG00000207065	chr4	-1.85	0.001239373	RNU5A-2P	RNA, U5A small nuclear 2, pseudogene
ENSG00000200972	chr1	-2.02	0.000283076	RNU5A-8P	RNA, U5A small nuclear 8, pseudogene
ENSG00000199906	chr3	-3.30	3.34E-05	RNU5B-2P	RNA, U5B small nuclear 2, pseudogene
ENSG00000201801	chr1	-1.75	0.000655114	RNU5E-4P	RNA, U5E small nuclear 4, pseudogene
ENSG00000200376	chr11	-2.78	0.001025486	RNU5E-10P	RNA, U5E small nuclear 10, pseudogene
ENSG00000252390	chr12	-2.41	0.000163766	RNU5F-4P	RNA, U5F small nuclear 4, pseudogene
ENSG00000206975	chr8	-2.61	0.001902149	RNU6-13P	RNA, U6 small nuclear 13, pseudogene
ENSG00000201474	chr5	-2.88	0.028350344	RNU6-164P	RNA, U6 small nuclear 164, pseudogene
ENSG00000207256	chr1	-2.53	0.029612718	RNU6-880P	RNA, U6 small nuclear 880, pseudogene
ENSG00000251905	chr2	-2.62	0.006228969	RNU7-2P	RNA, U7 small nuclear 2, pseudogene
ENSG00000252244	chr6	-2.19	0.000654304	RNU7-3P	RNA, U7 small nuclear 3, pseudogene
ENSG00000238782	chr2	-3.28	0.017418293	RNU7-9P	RNA, U7 small nuclear 9, pseudogene
ENSG00000238959	chr3	-2.79	0.002065876	RNU7-19P	RNA, U7 small nuclear 19, pseudogene
ENSG00000206702	chr6	-0.39	0.517584938	RNU1-11P	RNA, U1 small nuclear 11, pseudogene
ENSG00000238825	chr1	0.86	0.291605087	RNU1-13P	RNA, U1 small nuclear 13, pseudogene
ENSG00000199629	chr7	-0.72	0.741874573	RNU1-14P	RNA, U1 small nuclear 14, pseudogene
ENSG00000202347	chr13	2.01	0.176361492	RNU1-16P	RNA, U1 small nuclear 16, pseudogene
ENSG00000199932	chr6	0.69	0.305346649	RNU1-18P	RNA, U1 small nuclear 18, pseudogene
ENSG00000200176	chr10	0.44	0.452200962	RNU1-19P	RNA, U1 small nuclear 19, pseudogene
ENSG00000200184	chr3	-2.12	0.212435587	RNU1-20P	RNA, U1 small nuclear 20, pseudogene
ENSG00000200197	chr11	0.96	0.593914457	RNU1-21P	RNA, U1 small nuclear 21, pseudogene
ENSG00000200204	chr16	-1.03	0.226883539	RNU1-22P	RNA, U1 small nuclear 22, pseudogene
ENSG00000206596	chr14	-0.23	0.690518857	RNU1-27P	RNA, U1 small nuclear 27, pseudogene

Ensembl ID	Chr	Log2 Fold Change	P (adj)	Gene	Identities from Ensembl <sup>1</sup> or Rfam <sup>2</sup>
<b>Pseudogenes - Small nuclear pseudogenes (cont.)</b>					
ENSG00000206588	chr14	-0.20	0.731561139	RNUJ1-28P	RNA, U1 small nuclear 28, pseudogene
ENSG00000271739	chr7	2.19	0.072169209	RNUJ1-29P	RNA, U1 small nuclear 29, pseudogene
ENSG00000201291	chr6	-0.43	0.718174278	RNUJ1-34P	RNA, U1 small nuclear 34, pseudogene
ENSG00000199652	chr8	0.53	0.720847378	RNUJ1-35P	RNA, U1 small nuclear 35, pseudogene
ENSG00000207182	chr4	0.64	0.70936573	RNUJ1-44P	RNA, U1 small nuclear 44, pseudogene
ENSG00000199469	chr3	-2.07	0.168056931	RNUJ1-62P	RNA, U1 small nuclear 62, pseudogene
ENSG00000206629	chr4	0.49	0.617260054	RNUJ1-63P	RNA, U1 small nuclear 63, pseudogene
ENSG00000194297	chr1	1.54	0.246842757	RNUJ1-75P	RNA, U1 small nuclear 75, pseudogene
ENSG00000212170	chr15	0.14	0.902927747	RNUJ1-77P	RNA, U1 small nuclear 77, pseudogene
ENSG00000212550	chr15	-1.55	0.377885155	RNUJ1-78P	RNA, U1 small nuclear 78, pseudogene
ENSG00000212153	chr7	-0.92	0.302787792	RNUJ1-82P	RNA, U1 small nuclear 82, pseudogene
ENSG00000200296	chr12	-1.05	0.232998302	RNUJ1-83P	RNA, U1 small nuclear 83, pseudogene
ENSG00000202317	chr11	-2.10	0.194046438	RNUJ1-84P	RNA, U1 small nuclear 84, pseudogene
ENSG00000238554	chr6	-0.40	0.636443882	RNUJ1-88P	RNA, U1 small nuclear 88, pseudogene
ENSG00000207322	chr4	0.04	0.957807697	RNUJ1-89P	RNA, U1 small nuclear 89, pseudogene
ENSG00000253089	chr12	0.96	0.429427427	RNUJ1-104P	RNA, U1 small nuclear 104, pseudogene
ENSG00000207110	chr8	0.01	0.989132846	RNUJ1-106P	RNA, U1 small nuclear 106, pseudogene
ENSG00000252850	chr12	-0.97	0.235087431	RNUJ1-117P	RNA, U1 small nuclear 117, pseudogene
ENSG00000199879	chr1	-0.39	0.710272916	RNUJ1-120P	RNA, U1 small nuclear 120, pseudogene
ENSG00000202408	chr1	1.11	0.328512727	RNUJ1-122P	RNA, U1 small nuclear 122, pseudogene
ENSG00000201170	chr1	-0.06	0.975841336	RNUJ1-132P	RNA, U1 small nuclear 132, pseudogene
ENSG00000206908	chr6	0.36	0.696517526	RNUJ1-136P	RNA, U1 small nuclear 136, pseudogene
ENSG00000206820	chr4	0.60	0.3965295	RNUJ1-138P	RNA, U1 small nuclear 138, pseudogene
ENSG00000207201	chr8	1.00	0.238851051	RNUJ1-148P	RNA, U1 small nuclear 148, pseudogene
ENSG00000222076	chr15	-0.67	0.255269425	RNUJ2-3P	RNA, U2 small nuclear 3, pseudogene
ENSG00000222465	chr9	0.10	0.883579995	RNUJ2-5P	RNA, U2 small nuclear 5, pseudogene
ENSG00000223336	chr13	-0.19	0.779295524	RNUJ2-6P	RNA, U2 small nuclear 6, pseudogene
ENSG00000222726	chr13	-0.96	0.152188715	RNUJ2-7P	RNA, U2 small nuclear 7, pseudogene
ENSG00000251718	chr2	-0.22	0.70506981	RNUJ2-13P	RNA, U2 small nuclear 13, pseudogene
ENSG00000222985	chr14	0.53	0.439426813	RNUJ2-14P	RNA, U2 small nuclear 14, pseudogene
ENSG00000222624	chr1	-1.92	0.31099422	RNUJ2-15P	RNA, U2 small nuclear 15, pseudogene
ENSG00000222644	chr4	-0.03	0.974794797	RNUJ2-16P	RNA, U2 small nuclear 16, pseudogene
ENSG00000222222	chr1	0.27	0.690518857	RNUJ2-17P	RNA, U2 small nuclear 17, pseudogene
ENSG00000223156	chr10	-0.40	0.593914457	RNUJ2-18P	RNA, U2 small nuclear 18, pseudogene

Ensembl ID	Chr	Log2 Fold Change	P (adj)	Gene	Identities from Ensembl <sup>1</sup> or Rfam <sup>2</sup>
<b>Pseudogenes - Small nuclear pseudogenes (cont.)</b>					
ENSG00000253097	chr1	-1.47	0.354169597	RNU2-19P	RNA, U2 small nuclear 19, pseudogene
ENSG00000222477	chr11	-0.01	0.984743024	RNU2-23P	RNA, U2 small nuclear 23, pseudogene
ENSG00000222973	chr9	0.43	0.547790544	RNU2-25P	RNA, U2 small nuclear 25, pseudogene
ENSG00000222389	chr3	0.02	0.980574994	RNU2-28P	RNA, U2 small nuclear 28, pseudogene
ENSG00000222355	chr7	1.33	0.105828607	RNU2-29P	RNA, U2 small nuclear 29, pseudogene
ENSG00000252018	chr1	-0.30	0.637462789	RNU2-30P	RNA, U2 small nuclear 30, pseudogene
ENSG00000222276	chr14	-0.67	0.233662601	RNU2-33P	RNA, U2 small nuclear 33, pseudogene
ENSG00000252343	chr4	-0.25	0.867314139	RNU2-34P	RNA, U2 small nuclear 34, pseudogene
ENSG00000252255	chr11	0.22	0.87603684	RNU2-35P	RNA, U2 small nuclear 35, pseudogene
ENSG00000222788	chr1	0.41	0.496215336	RNU2-38P	RNA, U2 small nuclear 38, pseudogene
ENSG00000222536	chr2	0.97	0.106874278	RNU2-39P	RNA, U2 small nuclear 39, pseudogene
ENSG00000222923	chr2	0.25	0.70506981	RNU2-41P	RNA, U2 small nuclear 41, pseudogene
ENSG00000222238	chr10	0.66	0.229153626	RNU2-43P	RNA, U2 small nuclear 43, pseudogene
ENSG00000252847	chr9	0.25	0.710272916	RNU2-46P	RNA, U2 small nuclear 46, pseudogene
ENSG00000222626	chr5	0.44	0.499474829	RNU2-48P	RNA, U2 small nuclear 48, pseudogene
ENSG00000222598	chr5	-0.57	0.752347949	RNU2-49P	RNA, U2 small nuclear 49, pseudogene
ENSG00000222426	chr9	-0.42	0.693024098	RNU2-50P	RNA, U2 small nuclear 50, pseudogene
ENSG00000222640	chr14	0.69	0.142024063	RNU2-51P	RNA, U2 small nuclear 51, pseudogene
ENSG00000252066	chr15	-1.14	0.521645585	RNU2-53P	RNA, U2 small nuclear 53, pseudogene
ENSG00000222414	chr10	-0.83	0.072169209	RNU2-59P	RNA, U2 small nuclear 59, pseudogene
ENSG00000223001	chr6	-0.81	0.070497333	RNU2-61P	RNA, U2 small nuclear 61, pseudogene
ENSG00000222800	chr6	1.55	0.309107735	RNU2-62P	RNA, U2 small nuclear 62, pseudogene
ENSG00000222724	chr2	0.80	0.132733217	RNU2-63P	RNA, U2 small nuclear 63, pseudogene
ENSG00000223247	chr3	0.93	0.186491024	RNU2-64P	RNA, U2 small nuclear 64, pseudogene
ENSG00000222582	chr4	-0.38	0.675950695	RNU2-66P	RNA, U2 small nuclear 66, pseudogene
ENSG00000222650	chr1	-0.61	0.142518008	RNU2-70P	RNA, U2 small nuclear 70, pseudogene
ENSG00000223107	chr10	-1.38	0.299243799	RNU2-72P	RNA, U2 small nuclear 72, pseudogene
ENSG00000252955	chr4	0.11	0.957807697	RNU4ATAC9P	RNA, U4atac small nuclear 9, pseudogene
ENSG00000252013	chr14	0.41	0.744481397	RNU4ATAC14P	RNA, U4atac small nuclear 14, pseudogene
ENSG00000251988	chr6	1.36	0.221109604	RNU4ATAC18P	RNA, U4atac small nuclear 18, pseudogene
ENSG00000201458	chr3	-1.89	0.058912522	RNU4-4P	RNA, U4 small nuclear 4, pseudogene
ENSG00000201628	chr6	-1.37	0.361850434	RNU4-7P	RNA, U4 small nuclear 7, pseudogene
ENSG00000201806	chr2	2.01	0.224389516	RNU4-8P	RNA, U4 small nuclear 8, pseudogene
ENSG00000199709	chr11	-1.64	0.251426925	RNU4-23P	RNA, U4 small nuclear 23, pseudogene

Ensembl ID	Chr	Log2 Fold Change	P (adj)	Gene	Identities from Ensembl <sup>1</sup> or Rfam <sup>2</sup>
<b>Pseudogenes - Small nuclear pseudogenes (cont.)</b>					
ENSG00000201231	chr8	-0.33	0.870953484	RNU4-50P	RNA, U4 small nuclear 50, pseudogene
ENSG00000252237	chr12	-1.02	0.540808929	RNU4-54P	RNA, U4 small nuclear 54, pseudogene
ENSG00000201317	chr1	-1.43	0.256389703	RNU4-59P	RNA, U4 small nuclear 59, pseudogene
ENSG00000201439	chr12	0.08	0.973422303	RNU4-67P	RNA, U4 small nuclear 67, pseudogene
ENSG00000199313	chr9	1.96	0.145020206	RNU4-82P	RNA, U4 small nuclear 82, pseudogene
ENSG00000201070	chr2	0.19	0.915871996	RNU4-84P	RNA, U4 small nuclear 84, pseudogene
ENSG00000201648	chr3	0.86	0.294442513	RNU4-91P	RNA, U4 small nuclear 91, pseudogene
ENSG00000254172	chr8	-1.72	0.19361305	RNU5A-3P	RNA, U5A small nuclear 3, pseudogene
ENSG00000200378	chr5	-2.18	0.129005094	RNU5B-4P	RNA, U5B small nuclear 4, pseudogene
ENSG00000252574	chr10	-1.72	0.202273927	RNU5B-6P	RNA, U5B small nuclear 6, pseudogene
ENSG00000252521	chr9	-1.33	0.000295403	RNU5D-2P	RNA, U5D small nuclear 2, pseudogene
ENSG00000223096	chr2	-1.74	0.053143319	RNU5E-9P	RNA, U5E small nuclear 9, pseudogene
ENSG00000210678	chr5	-0.59	0.40570559	RNU6ATAC2P	RNA, U6atac small nuclear 2, pseudogene
ENSG00000221562	chr5	-0.65	0.36694033	RNU6ATAC10P	RNA, U6atac small nuclear 10, pseudogene
ENSG00000251835	chr8	-0.19	0.897593717	RNU6ATAC32P	RNA, U6atac small nuclear 32, pseudogene
ENSG00000206932	chr3	0.13	0.792861954	RNU6-4P	RNA, U6 small nuclear 4, pseudogene
ENSG00000206965	chr2	0.64	0.176361492	RNU6-5P	RNA, U6 small nuclear 5, pseudogene
ENSG00000272055	chr10	0.77	0.067913446	RNU6-6P	RNA, U6 small nuclear 6, pseudogene
ENSG00000201654	chr14	0.04	0.943551576	RNU6-7	RNA, U6 small nuclear 7, pseudogene
ENSG00000202337	chr14	0.50	0.258209225	RNU6-8	RNA, U6 small nuclear 8, pseudogene
ENSG00000206763	chr7	-0.65	0.64084427	RNU6-10P	RNA, U6 small nuclear 10, pseudogene
ENSG00000201104	chr7	0.33	0.593914457	RNU6-11P	RNA, U6 small nuclear 11, pseudogene
ENSG00000207334	chr8	-1.39	0.062578427	RNU6-12P	RNA, U6 small nuclear 12, pseudogene
ENSG00000207360	chr9	-0.82	0.53438665	RNU6-14P	RNA, U6 small nuclear 14, pseudogene
ENSG00000207264	chr10	0.31	0.611762436	RNU6-15P	RNA, U6 small nuclear 15, pseudogene
ENSG00000207113	chr11	0.24	0.70506981	RNU6-16P	RNA, U6 small nuclear 16, pseudogene
ENSG00000206972	chr15	-0.77	0.410559728	RNU6-17P	RNA, U6 small nuclear 17, pseudogene
ENSG00000207257	chr15	-1.34	0.142518008	RNU6-18P	RNA, U6 small nuclear 18, pseudogene
ENSG00000206600	chr3	-0.28	0.68032418	RNU6-25P	RNA, U6 small nuclear 25, pseudogene
ENSG00000207116	chr2	-1.99	0.296452573	RNU6-31P	RNA, U6 small nuclear 31, pseudogene
ENSG00000206675	chr4	-0.61	0.593914457	RNU6-32P	RNA, U6 small nuclear 32, pseudogene
ENSG00000207524	chr4	-0.33	0.556815274	RNU6-33P	RNA, U6 small nuclear 33, pseudogene
ENSG00000201744	chr4	-1.59	0.361095038	RNU6-34P	RNA, U6 small nuclear 34, pseudogene
ENSG00000206899	chr12	-0.10	0.867314139	RNU6-36P	RNA, U6 small nuclear 36, pseudogene

Ensembl ID	Chr	Log2 Fold Change	P (adj)	Gene	Identities from Ensembl <sup>1</sup> or Rfam <sup>2</sup>
<b>Pseudogenes - Small nuclear pseudogenes (cont.)</b>					
ENSG00000199562	chr1	0.15	0.769338299	RNU6-37P	RNA, U6 small nuclear 37, pseudogene
ENSG00000206981	chr1	-0.92	0.574031515	RNU6-40P	RNA, U6 small nuclear 40, pseudogene
ENSG00000207472	chr1	-1.09	0.363806858	RNU6-41P	RNA, U6 small nuclear 41, pseudogene
ENSG00000206892	chr3	-0.08	0.93535566	RNU6-42P	RNA, U6 small nuclear 42, pseudogene
ENSG00000207029	chr10	-1.74	0.284837843	RNU6-43P	RNA, U6 small nuclear 43, pseudogene
ENSG00000207200	chr11	-1.09	0.511098978	RNU6-45P	RNA, U6 small nuclear 45, pseudogene
ENSG00000206593	chr5	-0.32	0.836063033	RNU6-47P	RNA, U6 small nuclear 47, pseudogene
ENSG00000206888	chr1	-1.16	0.078107929	RNU6-48P	RNA, U6 small nuclear 48, pseudogene
ENSG00000252247	chr13	-2.12	0.152188715	RNU6-70P	RNA, U6 small nuclear 70, pseudogene
ENSG00000207330	chr13	-1.89	0.218956504	RNU6-73P	RNA, U6 small nuclear 73, pseudogene
ENSG00000252373	chr5	-2.38	0.084465338	RNU6-358P	RNA, U6 small nuclear 358, pseudogene
ENSG00000207052	chr5	-0.70	0.682287116	RNU6-378P	RNA, U6 small nuclear 378, pseudogene
ENSG00000207336	chr5	-1.90	0.32865529	RNU6-658P	RNA, U6 small nuclear 658, pseudogene
ENSG00000207261	chr5	-1.44	0.414012086	RNU6-738P	RNA, U6 small nuclear 738, pseudogene
ENSG00000206875	chr6	-0.73	0.494749205	RNU6-761P	RNA, U6 small nuclear 761, pseudogene
ENSG00000207000	chr9	-2.73	0.067811003	RNU6-820P	RNA, U6 small nuclear 820, pseudogene
ENSG00000238941	chr15	-2.44	0.180528899	RNU6-953P	RNA, U6 small nuclear 953, pseudogene
ENSG00000199664	chr10	-1.58	0.332691151	RNU6-1266P	RNA, U6 small nuclear 1266, pseudogene
ENSG00000202534	chr12	-0.15	0.938403518	RNU6-1329P	RNA, U6 small nuclear 1329, pseudogene
ENSG00000206832	chr1	-1.27	0.438005723	RNU6V	RNA, U6 small nuclear variant sequence with SNRPE pseudogene sequence
ENSG00000252770	chr12	-1.41	0.433722546	RNU7-4P	RNA, U7 small nuclear 4 pseudogene
ENSG00000251767	chr1	-2.46	0.145385518	RNU7-8P	RNA, U7 small nuclear 8 pseudogene
ENSG00000252796	chr4	-1.76	0.444633771	RNU7-11P	RNA, U7 small nuclear 11 pseudogene
ENSG00000251839	chr10	-2.59	0.216300936	RNU7-12P	RNA, U7 small nuclear 12 pseudogene
ENSG00000251712	chr7	-2.30	0.115434093	RNU7-20P	RNA, U7 small nuclear 20 pseudogene
ENSG00000238610	chr6	-2.62	0.097730439	RNU7-26P	RNA, U7 small nuclear 26 pseudogene
ENSG00000252369	chr14	-2.61	0.14522725	RNU7-51P	RNA, U7 small nuclear 51 pseudogene
ENSG00000252057	chr8	-2.58	0.11149042	RNU7-174P	RNA, U7 small nuclear 174 pseudogene
<b>Pseudogenes - Small nucleolar pseudogenes</b>					
ENSG00000239128	chr3	1.12	0.023365177	SNORD13P3	Small nucleolar RNA, C/D box 13 pseudogene 3
<b>Pseudogenes - Y-RNA pseudogenes</b>					
ENSG00000201900	chr1	2.24	0.000146757	RNY1P13	RNY1 pseudogene 13
ENSG00000201955	chr5	1.74	0.000193014	RNY3P1	RNY3 pseudogene 1
ENSG00000199788	chr13	1.62	0.011145955	RNY3P2	RNY3 pseudogene 2

Ensembl ID	Chr	Log2 Fold Change	P (adj)	Gene	Identities from Ensembl <sup>1</sup> or Rfam <sup>2</sup>
Pseudogenes - Y-RNA pseudogenes (cont.)					
ENSG00000223298	chr13	2.14	3.57E-05	RNY3P8	RNY3 pseudogene 8
ENSG00000202412	chr3	-2.79	0.04314115	RNY3P13	RNY3 pseudogene 13
ENSG00000200064	chr13	1.47	0.051086609	RNY4P9	RNY4 pseudogene 9
ENSG00000206617	chr13	-0.45	0.689403951	RNY1P5	RNY1 pseudogene 5
ENSG00000207474	chr13	0.87	0.346282319	RNY1P7	RNY1 pseudogene 7
ENSG00000200629	chr7	1.67	0.127356735	RNY1P11	RNY1 pseudogene 11
ENSG00000201121	chr3	-0.02	0.979135537	RNY1P12	RNY1 pseudogene 12
ENSG00000207157	chr13	1.62	0.358584702	RNY3P4	RNY3 pseudogene 4
ENSG00000206854	chr13	1.48	0.218956504	RNY3P5	RNY3 pseudogene 5
ENSG00000200537	chr11	0.85	0.066098668	RNY4P6	RNY4 pseudogene 6
ENSG00000201470	chr2	0.21	0.66887083	RNY4P7	RNY4 pseudogene 7
ENSG00000202441	chr6	0.56	0.168056931	RNY4P10	RNY4 pseudogene 10
ENSG00000200526	chr13	1.06	0.186035782	RNY4P14	RNY4 pseudogene 14
ENSG00000201638	chr1	1.16	0.277925598	RNY4P16	RNY4 pseudogene 16
ENSG00000201818	chr4	0.34	0.492967802	RNY4P17	RNY4 pseudogene 17
ENSG00000212409	chr9	-0.31	0.593914457	RNY4P18	RNY4 pseudogene 18
ENSG00000252487	chr6	0.75	0.120010034	RNY4P20	RNY4 pseudogene 20
ENSG00000199605	chr13	1.45	0.092809222	RNY4P24	RNY4 pseudogene 24
ENSG00000238711	chr1	0.19	0.698658175	RNY4P25	RNY4 pseudogene 25
ENSG00000200211	chr13	0.47	0.260492679	RNY4P27	RNY4 pseudogene 27
ENSG00000202151	chr13	1.53	0.092429397	RNY4P28	RNY4 pseudogene 28
ENSG00000201649	chr2	1.09	0.292548426	RNY4P34	RNY4 pseudogene 34
Pseudogenes - miscellaneous					
ENSG00000249774	chr5	2.12	0.006299575	AC025458.1	Translocase of outer mitochondrial membrane 7 homolog (yeast) (TOMM7) pseudogene
ENSG00000256148	chr11	3.19	0.00033091	AP000763.2	Mitochondrially encoded cytochrome c oxidase I (MT-COI) pseudogene
ENSG00000180389	chr13	2.08	0.01713873	ATP5F1EP2	ATP synthase F1 subunit epsilon pseudogene 2
ENSG00000231884	chr3	3.17	0.000876071	NDUFB1P1	NADH:ubiquinone oxidoreductase subunit B1 pseudogene 1
ENSG00000249072	chr4	1.59	0.016625071	AC114801.3	Novel pseudogene
ENSG00000187653	chr4	2.32	0.000182926	TMSB4XP8	TMSB4X pseudogene 8 (Thymosin Beta 4 X-Linked)
ENSG00000234594	chr3	1.13	0.315220213	AC008134.1	Pseudogene similar to part of mitochondrially encoded cytochrome c oxidase I MT-CO1
ENSG00000233648	chr2	1.80	0.320082983	AC010095.1	Cytochrome c oxidase subunit VIIb (COX7B) pseudogene
ENSG00000253683	chr5	1.83	0.131109597	AC027309.2	Coiled-coil domain containing 72 (CCDC72) pseudogene
ENSG00000235449	chr1	0.40	0.741874573	AC098934.3	Cytochrome c oxidase subunit VIIIc (COX7C) pseudogene
ENSG00000234604	chr1	1.96	0.070331593	AL021068.2	ATP synthase 6 (MTATP6) pseudogene

Ensembl ID	Chr	Log2 Fold Change	P (adj)	Gene	Identities from Ensembl <sup>1</sup> or Rfam <sup>2</sup>
<b>Pseudogenes -miscellaneous (cont.)</b>					
ENSG00000232296	chr1	2.20	0.156189437	AL691482.1	LSM3 homolog, U6 small nuclear RNA associated pseudogene
ENSG00000205105	chr13	0.82	0.542149768	COX17P1	COX17 pseudogene 1
ENSG00000235957	chr13	1.14	0.356314148	COX7CP1	Cytochrome c oxidase subunit 7C pseudogene 1
ENSG00000183586	chr1	1.27	0.438005723	HMG3P1	High mobility group nucleosomal binding domain 3 pseudogene 1
ENSG00000162840	chr4	0.52	0.693024098	MT2P1	Metallothionein 2 pseudogene 1
ENSG00000233929	chr1	0.81	0.541217308	MT1XP1	Metallothionein 1X pseudogene 1
ENSG00000249192	chr5	1.93	0.072080424	MTND3P25	MT-ND3 pseudogene 25
ENSG00000235912	chr1	-1.34	0.472257209	AL031729.1	Novel pseudogene
ENSG00000250273	chr5	1.44	0.216121605	PSMC1P5	Proteasome 26S subunit, ATPase 1 pseudogene 5
ENSG00000227850	chr1	0.57	0.651120006	SEPT2P1	Septin 2 pseudogene 1
ENSG00000218512	chr6	0.03	0.991015284	SPTLC1P2	Serine palmitoyltransferase long chain base subunit 1 pseudogene 2
ENSG00000228499	chr2	1.03	0.438484363	TMSB10P1	Thymosin beta 10 pseudogene 1
ENSG00000236876	chr1	-0.97	0.181634456	TMSB4XP1	TMSB4X pseudogene 1 (Thymosin Beta 4 X-Linked)

**Table A3.1** (includes preceding 21 pages) **Differential expression profiles of non-miRNA small RNA transcripts identified by RNA-seq from six healthy and six diseased human tendon samples.** RNA species achieving statistically significant differential expression (Log2 Fold Change  $\geq 1.5$  with Benjamin-Hochberg adjusted P-value (P adj)  $< 0.05$ ) between healthy and diseased cohorts are given in **bold type** at the top of each subsection. Chr = chromosome.

1 - Yates et al. (2020).

2 - Kalvari et al. (2018).

Ensembl ID	Chr	Log2 Fold Change	P (adj)	Gene
MIMAT0004481	chr22;chr9	-2.57	9.06E-07	hsa-let-7a-3p
MIMAT0026472	chr21	-3.40	1.75E-07	hsa-let-7c-3p
MIMAT0000067	chr9;chrX	-2.11	0.00715716	hsa-let-7f-5p
MIMAT0031892	chr20	-2.84	0.014948579	hsa-miR-1-5p
MIMAT0004553	chr9	-3.75	0.001763863	hsa-miR-7-1-3p
MIMAT0000252	chr15;chr19;chr9	-3.60	3.05E-10	hsa-miR-7-5p
MIMAT0000441	chr1;chr15;chr5	-3.41	0.000340162	hsa-miR-9-5p
MIMAT0000253	chr17	-1.74	0.007508314	hsa-miR-10a-5p
MIMAT0004556	chr2	-3.05	9.97E-05	hsa-miR-10b-3p
MIMAT0000254	chr2	-3.12	3.62E-07	hsa-miR-10b-5p
MIMAT0000068	chr13	-4.62	1.86E-05	hsa-miR-15a-5p
MIMAT0000417	chr3	-2.13	0.002220854	hsa-miR-15b-5p
MIMAT0000069	chr13;chr3	-5.05	1.33E-17	hsa-miR-16-5p
MIMAT0004518	chr3	-3.30	1.08E-05	hsa-miR-16-2-3p
MIMAT0000070	chr13	-4.52	3.17E-16	hsa-miR-17-5p
MIMAT0000072	chr13	-3.48	0.023365177	hsa-miR-18a-5p
MIMAT0000073	chr13	-5.01	1.10E-06	hsa-miR-19a-3p
MIMAT0000074	chr13;chrX	-6.57	7.27E-08	hsa-miR-19b-3p
MIMAT0000075	chr13	-4.27	5.06E-11	hsa-miR-20a-5p
MIMAT0001413	chrX	-4.39	0.00021927	hsa-miR-20b-5p
MIMAT0000076	chr17	-4.85	1.77E-24	hsa-miR-21-5p
MIMAT0000077	chr17	-3.66	3.86E-10	hsa-miR-22-3p
MIMAT0000078	chr19	-3.64	8.84E-11	hsa-miR-23a-3p
MIMAT0000079	chr9	-2.62	2.93E-05	hsa-miR-24-1-5p
MIMAT0000080	chr19;chr9	-2.70	1.49E-09	hsa-miR-24-3p
MIMAT0004497	chr19	-3.71	1.22E-15	hsa-miR-24-2-5p
MIMAT0000082	chr12;chr3	-2.47	6.34E-08	hsa-miR-26a-5p
MIMAT0004681	chr12	-2.23	0.003354372	hsa-miR-26a-2-3p
MIMAT0000083	chr2	-3.77	5.48E-13	hsa-miR-26b-5p
MIMAT0000084	chr19	-2.46	0.000692675	hsa-miR-27a-3p
MIMAT0004501	chr19	-2.79	5.51E-09	hsa-miR-27a-5p
MIMAT0000419	chr9	-2.16	1.54E-07	hsa-miR-27b-3p
MIMAT0004502	chr3	-1.65	0.000319068	hsa-miR-28-3p
MIMAT0000085	chr3	-3.12	2.30E-07	hsa-miR-28-5p
MIMAT0000086	chr7	-1.91	7.22E-05	hsa-miR-29a-3p
MIMAT0000100	chr1;chr7	-3.77	1.07E-15	hsa-miR-29b-3p
MIMAT0004515	chr1	-1.52	0.032213347	hsa-miR-29b-2-5p
MIMAT0000681	chr1	-1.99	0.000171117	hsa-miR-29c-3p
MIMAT0000087	chr6	-2.95	8.44E-07	hsa-miR-30a-5p
MIMAT0000420	chr8	-3.45	2.72E-07	hsa-miR-30b-5p
MIMAT0004551	chr8	-5.27	4.42E-07	hsa-miR-30d-3p
MIMAT0000245	chr8	-1.59	3.66E-05	hsa-miR-30d-5p
MIMAT0000693	chr1	-1.60	0.031058981	hsa-miR-30e-3p
MIMAT0000692	chr1	-4.22	2.28E-13	hsa-miR-30e-5p
MIMAT0000090	chr9	-5.97	2.50E-12	hsa-miR-32-5p
MIMAT0000255	chr1	-2.03	0.002151014	hsa-miR-34a-5p
MIMAT0000686	chr11	-1.66	0.014910912	hsa-miR-34c-5p
MIMAT0000093	chr7	-2.56	3.40E-06	hsa-miR-93-5p
MIMAT0000095	chr7	-3.18	0.012041173	hsa-miR-96-5p
MIMAT0000096	chrX	-2.53	5.35E-05	hsa-miR-98-5p
MIMAT0000097	chr21	-2.99	1.35E-15	hsa-miR-99a-5p

Ensembl ID	Chr	Log2 Fold Change	P (adj)	Gene
MIMAT0000098	chr11	-2.97	1.41E-12	hsa-miR-100-5p
MIMAT0000099	chr1;chr9	-6.35	3.38E-29	hsa-miR-101-3p
MIMAT0004513	chr1	-4.23	0.000353944	hsa-miR-101-5p
MIMAT0037312	chr9	-3.76	0.022552453	hsa-miR-101-2-5p
MIMAT0000101	chr20;chr5	-2.55	1.87E-07	hsa-miR-103a-3p
MIMAT0000103	chrX	-4.64	0.000622224	hsa-miR-106a-5p
MIMAT0000680	chr7	-3.21	2.12E-06	hsa-miR-106b-5p
MIMAT0000104	chr10	-2.70	4.35E-05	hsa-miR-107
MIMAT0004592	chr11	-2.29	1.69E-07	hsa-miR-125b-1-3p
MIMAT0004603	chr21	-2.31	1.00E-10	hsa-miR-125b-2-3p
MIMAT0000423	chr11;chr21	-2.98	4.71E-20	hsa-miR-125b-5p
MIMAT0000445	chr9	-3.17	1.51E-06	hsa-miR-126-3p
MIMAT0000444	chr9	-1.92	0.002065876	hsa-miR-126-5p
MIMAT0004604	chr14	-4.50	1.22E-09	hsa-miR-127-5p
MIMAT0000425	chr11	-5.79	8.79E-09	hsa-miR-130a-3p
MIMAT0000426	chr17	-1.96	0.000500724	hsa-miR-132-3p
MIMAT0000447	chr14	-1.60	0.000478835	hsa-miR-134-5p
MIMAT0004606	chr14	-4.84	6.14E-11	hsa-miR-136-3p
MIMAT0000448	chr14	-4.75	1.02E-10	hsa-miR-136-5p
MIMAT0004597	chr16	-2.76	2.12E-06	hsa-miR-140-3p
MIMAT0000431	chr16	-5.37	1.10E-30	hsa-miR-140-5p
MIMAT0000434	chr17	-5.42	5.47E-11	hsa-miR-142-3p
MIMAT0000433	chr17	-4.46	0.000283781	hsa-miR-142-5p
MIMAT0000435	chr5	-4.76	1.41E-13	hsa-miR-143-3p
MIMAT0004599	chr5	-2.40	0.000223936	hsa-miR-143-5p
MIMAT0004600	chr17	-6.32	3.82E-08	hsa-miR-144-5p
MIMAT0004601	chr5	-2.88	6.72E-06	hsa-miR-145-3p
MIMAT0000437	chr5	-1.54	0.009340063	hsa-miR-145-5p
MIMAT0000449	chr5	-2.81	1.26E-06	hsa-miR-146a-5p
MIMAT0002809	chr10	-3.25	2.66E-10	hsa-miR-146b-5p
MIMAT0000243	chr7	-4.33	2.29E-18	hsa-miR-148a-3p
MIMAT0000759	chr12	-1.78	0.00348891	hsa-miR-148b-3p
MIMAT0004699	chr12	-2.65	8.30E-06	hsa-miR-148b-5p
MIMAT0000757	chr8	-1.71	0.001032975	hsa-miR-151a-3p
MIMAT0004697	chr8	-2.59	1.68E-05	hsa-miR-151a-5p
MIMAT0000438	chr17	-3.02	1.81E-06	hsa-miR-152-3p
MIMAT0000452	chr14	-2.31	0.005239835	hsa-miR-154-5p
MIMAT0000270	chr1	-4.28	9.25E-07	hsa-miR-181a-3p
MIMAT0004559	chr19	-4.12	0.000196064	hsa-miR-181c-3p
MIMAT0000258	chr19	-2.59	0.000196613	hsa-miR-181c-5p
MIMAT0002821	chr19	-2.82	6.14E-11	hsa-miR-181d-5p
MIMAT0000259	chr7	-3.17	0.000810915	hsa-miR-182-5p
MIMAT0000455	chr22	-3.52	3.93E-07	hsa-miR-185-5p
MIMAT0000456	chr1	-2.72	4.95E-08	hsa-miR-186-5p
MIMAT0000458	chr15	-3.67	0.009003075	hsa-miR-190a-5p
MIMAT0000222	chr11	-2.59	0.002013938	hsa-miR-192-5p
MIMAT0004767	chr16	2.18	0.007485041	hsa-miR-193b-5p
MIMAT0000460	chr1;chr11	-4.16	1.60E-06	hsa-miR-194-5p
MIMAT0000461	chr17	-4.97	3.34E-11	hsa-miR-195-5p
MIMAT0000226	chr12;chr17	-4.31	2.92E-15	hsa-miR-196a-5p
MIMAT0001080	chr7	-1.69	4.61E-06	hsa-miR-196b-5p

Ensembl ID	Chr	Log2 Fold Change	P (adj)	Gene
MIMAT0000232	chr1;chr19	-4.69	3.36E-18	hsa-miR-199a-3p
MIMAT0000231	chr1;chr19	-2.98	1.68E-11	hsa-miR-199a-5p
MIMAT0004563	chr9	-4.31	3.09E-15	hsa-miR-199b-3p
MIMAT0000263	chr9	-4.86	4.30E-21	hsa-miR-199b-5p
MIMAT0000682	chr1	-3.07	0.027415471	hsa-miR-200a-3p
MIMAT0000318	chr1	-3.95	2.91E-07	hsa-miR-200b-3p
MIMAT0000264	chr14	-4.71	0.000107844	hsa-miR-203a-3p
MIMAT0000266	chr1	-4.25	0.006652449	hsa-miR-205-5p
MIMAT0004960	chr14	-3.73	0.005264697	hsa-miR-208b-3p
MIMAT0000271	chr1	-1.95	2.62E-06	hsa-miR-214-3p
MIMAT0004564	chr1	-1.96	1.81E-05	hsa-miR-214-5p
MIMAT0000272	chr1	-3.82	0.000138578	hsa-miR-215-5p
MIMAT0000275	chr4;chr5	-3.50	8.85E-21	hsa-miR-218-5p
MIMAT0000278	chrX	-1.64	0.002641838	hsa-miR-221-3p
MIMAT0004568	chrX	-2.44	8.34E-05	hsa-miR-221-5p
MIMAT0000280	chrX	-2.08	0.000276512	hsa-miR-223-3p
MIMAT0004570	chrX	-3.50	3.96E-08	hsa-miR-223-5p
MIMAT0022696	chr17	-2.91	0.00542813	hsa-miR-301a-5p
MIMAT0000761	chr17	-1.62	0.04689793	hsa-miR-324-5p
MIMAT0001629	chr14;chr14	-2.91	0.00057691	hsa-miR-329-3p
MIMAT0000765	chr7	-5.88	3.17E-16	hsa-miR-335-5p
MIMAT0000754	chr14	-1.88	0.0103495	hsa-miR-337-3p
MIMAT0004702	chr7	-1.63	0.006299575	hsa-miR-339-3p
MIMAT0000750	chr5	-1.85	0.001345583	hsa-miR-340-3p
MIMAT0004692	chr5	-5.66	3.21E-28	hsa-miR-340-5p
MIMAT0004682	chrX	-1.66	1.57E-05	hsa-miR-361-3p
MIMAT0000703	chrX	-2.87	7.13E-10	hsa-miR-361-5p
MIMAT0000707	chrX	-2.07	0.000318207	hsa-miR-363-3p
MIMAT0000710	chr16	-2.04	1.54E-05	hsa-miR-365a-3p
MIMAT0001621	chr14	-3.29	0.01184179	hsa-miR-369-5p
MIMAT0000724	chr19	-4.43	0.001677136	hsa-miR-372-3p
MIMAT0004688	chrX	-6.76	2.92E-17	hsa-miR-374a-3p
MIMAT0000727	chrX	-5.34	1.09E-20	hsa-miR-374a-5p
MIMAT0004956	chrX	-5.20	5.04E-07	hsa-miR-374b-3p
MIMAT0004955	chrX	-4.25	8.80E-05	hsa-miR-374b-5p
MIMAT0000730	chr14	-4.22	0.000704663	hsa-miR-377-3p
MIMAT0000733	chr14	-2.36	0.011406068	hsa-miR-379-5p
MIMAT0000736	chr14	-3.09	5.93E-07	hsa-miR-381-3p
MIMAT0022697	chr14	-5.13	5.39E-09	hsa-miR-382-3p
MIMAT0000737	chr14	-1.52	0.000415788	hsa-miR-382-5p
MIMAT0000738	chr8	-5.65	3.81E-05	hsa-miR-383-5p
MIMAT0001638	chr14	-3.33	8.74E-09	hsa-miR-409-5p
MIMAT0003329	chr14	-3.94	2.36E-08	hsa-miR-411-5p
MIMAT0003339	chrX	-2.79	4.57E-05	hsa-miR-421
MIMAT0001343	chr3	-1.65	0.01635651	hsa-miR-425-3p
MIMAT0003393	chr3	-2.25	1.81E-06	hsa-miR-425-5p
MIMAT0001545_1	chrX	-3.34	0.012196095	hsa-miR-450a-5p
MIMAT0004909	chrX	-4.72	5.35E-05	hsa-miR-450b-5p
MIMAT0001631	chr17	-7.15	1.63E-14	hsa-miR-451a
MIMAT0001636	chrX	-4.36	1.77E-05	hsa-miR-452-3p
MIMAT0001635	chrX	-2.16	0.030824214	hsa-miR-452-5p

Ensembl ID	Chr	Log2 Fold Change	P (adj)	Gene
MIMAT0003885	chr17	-5.12	5.52E-08	hsa-miR-454-3p
MIMAT0003150	chr9	-4.44	7.53E-14	hsa-miR-455-5p
MIMAT0002173	chr11	-2.90	0.000399289	hsa-miR-483-3p
MIMAT0003180	chr14	-2.06	7.71E-05	hsa-miR-487b-3p
MIMAT0002805	chr7	-2.82	0.043943152	hsa-miR-489-3p
MIMAT0003161	chr14	-2.50	2.56E-06	hsa-miR-493-3p
MIMAT0002813	chr14	-2.49	0.001186299	hsa-miR-493-5p
MIMAT0002816	chr14	-4.69	3.45E-13	hsa-miR-494-3p
MIMAT0002817	chr14	-2.98	0.000463808	hsa-miR-495-3p
MIMAT0002820	chr17	-3.58	4.01E-11	hsa-miR-497-5p
MIMAT0002871	chrX	-3.63	3.19E-18	hsa-miR-500a-3p
MIMAT0004774	chrX	-1.67	6.68E-05	hsa-miR-501-3p
MIMAT0004775	chrX	-2.89	9.47E-08	hsa-miR-502-3p
MIMAT0004975	chrX	-3.92	0.002437028	hsa-miR-509-3-5p
MIMAT0026606	chr10	-3.01	0.028735277	hsa-miR-511-3p
MIMAT0002859	chr19;chr19	-2.48	0.014594778	hsa-miR-516b-5p
MIMAT0002888	chrX	-2.16	1.66E-07	hsa-miR-532-5p
MIMAT0022705	chr14	-4.85	1.25E-05	hsa-miR-539-3p
MIMAT0003389	chrX	-3.77	0.003068131	hsa-miR-542-3p
MIMAT0005874	chr10	-3.01	0.023254097	hsa-miR-548e-3p
MIMAT0003241	chr4	-3.78	3.39E-07	hsa-miR-576-5p
MIMAT0004797	chr5	-3.36	0.001032975	hsa-miR-582-3p
MIMAT0003250	chr5	-2.28	0.003205365	hsa-miR-585-3p
MIMAT0004801	chr7	-3.58	0.007500461	hsa-miR-590-3p
MIMAT0003266	chr8	-5.53	1.74E-06	hsa-miR-598-3p
MIMAT0003280	chr11	2.86	0.028222836	hsa-miR-612
MIMAT0004808	chr14	-2.07	0.00542813	hsa-miR-625-3p
MIMAT0004809	chr15	-1.98	0.003144318	hsa-miR-628-5p
MIMAT0003302	chr17	2.50	6.48E-07	hsa-miR-632
MIMAT0003321	chrX	-3.32	0.006652116	hsa-miR-651-5p
MIMAT0003322	chrX	-2.18	0.006697667	hsa-miR-652-3p
MIMAT0003328	chr7	-5.22	3.62E-07	hsa-miR-653-5p
MIMAT0004814	chr14	-1.81	0.000283076	hsa-miR-654-3p
MIMAT0003331	chr14	-4.17	4.57E-05	hsa-miR-655-3p
MIMAT0003338	chrX	-5.85	1.04E-21	hsa-miR-660-5p
MIMAT0005949	chr1	-1.89	3.09E-05	hsa-miR-664a-3p
MIMAT0003880	chr7	-4.71	8.86E-08	hsa-miR-671-5p
MIMAT0004927	chr11	-3.93	0.002151014	hsa-miR-708-3p
MIMAT0004926	chr11	-4.16	2.29E-18	hsa-miR-708-5p
MIMAT0003879	chr14	-2.13	0.009831129	hsa-miR-758-3p
MIMAT0003886	chr19	-2.48	7.86E-06	hsa-miR-769-5p
MIMAT0004951	chr5	-2.08	0.04689793	hsa-miR-887-3p
MIMAT0004921	chr14	-4.18	0.0001279	hsa-miR-889-3p
MIMAT0004987	chr3	-2.67	0.01635651	hsa-miR-944
MIMAT0022838	chr14	-3.26	0.016722514	hsa-miR-1185-1-3p
MIMAT0005901	chr22	-2.39	0.017926381	hsa-miR-1249-3p
MIMAT0005906	chr4	-2.70	0.019068302	hsa-miR-1255a
MIMAT0005936	chr1	-3.73	0.003688757	hsa-miR-1278
MIMAT0005878	chr10	-2.06	0.001242288	hsa-miR-1287-5p
MIMAT0005881	chr12	1.90	4.08E-07	hsa-miR-1291
MIMAT0010133	chr10	2.05	2.59E-05	hsa-miR-2110

Ensembl ID	Chr	Log2 Fold Change	P (adj)	Gene
MIMAT0015066	chr17	-3.72	0.003764746	hsa-miR-3065-5p
MIMAT0017991	chr13	-4.32	0.000138811	hsa-miR-3613-3p
MIMAT0017990	chr13	-5.92	7.49E-19	hsa-miR-3613-5p
MIMAT0018072	chr12	2.93	0.003390836	hsa-miR-3652
MIMAT0018074	chr7	2.38	0.020231885	hsa-miR-3654
MIMAT0018075	chr5	1.78	0.007443976	hsa-miR-3655
MIMAT0018191	chr1	2.64	0.000821911	hsa-miR-3917
MIMAT0019019	chr11	3.73	0.005572547	hsa-miR-4485-3p
MIMAT0019731	chr8	-4.75	2.85E-05	hsa-miR-4662a-5p
MIMAT0019744	chr9	3.90	0.019236461	hsa-miR-4667-3p
MIMAT0019761	chr1	-3.26	0.013506776	hsa-miR-4677-3p
MIMAT0019970	chr3	-3.16	0.041643603	hsa-miR-4796-5p
MIMAT0022472	chr6	-4.99	0.000201776	hsa-miR-5683
MIMAT0024598	chr12	1.67	0.008723689	hsa-miR-6125
MIMAT0025470	chr10	-4.27	0.000308331	hsa-miR-6507-5p
MIMAT0025856	chr21;chr21;chr21;chr21	4.00	1.16E-06	hsa-miR-6724-5p
MIMAT0041615	chr11	2.12	0.000215017	hsa-miR-10392-5p
MIMAT0041620	chr19	1.77	0.044227164	hsa-miR-10394-3p
MIMAT0049032	chr1	2.14	0.01825495	hsa-miR-12136
MIMAT0000062	chr9;chr11;chr22	-0.48	0.413965287	hsa-let-7a-5p
MIMAT0004482	chr22	-0.32	0.597128339	hsa-let-7b-3p
MIMAT0000063	chr22	0.24	0.682287116	hsa-let-7b-5p
MIMAT0000064	chr21	-0.33	0.492557966	hsa-let-7c-5p
MIMAT0004484	chr9	1.01	0.022552453	hsa-let-7d-3p
MIMAT0000065	chr9	-0.22	0.757174192	hsa-let-7d-5p
MIMAT0004485	chr19	-0.41	0.682287116	hsa-let-7e-3p
MIMAT0000066	chr19	0.59	0.279087895	hsa-let-7e-5p
MIMAT0004486	chr9	-0.86	0.130731986	hsa-let-7f-1-3p
MIMAT0004487	chrX	0.94	0.405841352	hsa-let-7f-2-3p
MIMAT0000414	chr3	0.00	0.998265009	hsa-let-7i-3p
MIMAT0004585	chr12	-0.97	0.09972312	hsa-let-7g-5p
MIMAT0000415	chr12	-0.86	0.016625071	hsa-let-7i-5p
MIMAT0000416	chr18;chr20	-3.01	0.06866688	hsa-miR-1-3p
MIMAT0000442_1	chr15	-2.51	0.321055779	hsa-miR-9-3p
MIMAT0004555	chr17	-1.04	0.652478678	hsa-miR-10a-3p
MIMAT0004488	chr13	-2.31	0.357464214	hsa-miR-15a-3p
MIMAT0004586	chr3	-2.79	0.059258826	hsa-miR-15b-3p
MIMAT0002891	chr13	0.58	0.633106555	hsa-miR-18a-3p
MIMAT0004494	chr17	-1.18	0.283713611	hsa-miR-21-3p
MIMAT0004495	chr17	-1.79	0.075724601	hsa-miR-22-5p
MIMAT0004496	chr19	1.04	0.383280593	hsa-miR-23a-5p
MIMAT0000418	chr9	-1.12	0.005404021	hsa-miR-23b-3p
MIMAT0004587	chr9	0.69	0.332851698	hsa-miR-23b-5p
MIMAT0000081	chr7	-1.31	0.002013938	hsa-miR-25-3p
MIMAT0004498	chr7	0.57	0.291605087	hsa-miR-25-5p
MIMAT0004500	chr2	0.13	0.896016639	hsa-miR-26b-3p
MIMAT0004588	chr9	-1.29	0.080771694	hsa-miR-27b-5p
MIMAT0004514	chr7	0.76	0.472257209	hsa-miR-29b-1-5p
MIMAT0004673	chr1	-1.14	0.022552453	hsa-miR-29c-5p
MIMAT0000088	chr6	-0.42	0.658966639	hsa-miR-30a-3p
MIMAT0004589	chr8	0.06	0.944644577	hsa-miR-30b-3p

Ensembl ID	Chr	Log2 Fold Change	P (adj)	Gene
MIMAT0004550	chr6	-1.28	0.044845342	hsa-miR-30c-2-3p
MIMAT0004674	chr1	-1.65	0.101003672	hsa-miR-30c-1-3p
MIMAT0000244	chr1;chr6	-0.56	0.334727096	hsa-miR-30c-5p
MIMAT0004506	chr22	1.88	0.199699614	hsa-miR-33a-3p
MIMAT0004676	chr11	-0.14	0.948855971	hsa-miR-34b-3p
MIMAT0004677	chr11	-1.17	0.500440987	hsa-miR-34c-3p
MIMAT0000092	chr13;chrX	-0.53	0.09758533	hsa-miR-92a-3p
MIMAT0004507	chr13	0.96	0.256119449	hsa-miR-92a-1-5p
MIMAT0003218	chr1	-0.17	0.800739207	hsa-miR-92b-3p
MIMAT0004792	chr1	0.48	0.593914457	hsa-miR-92b-5p
MIMAT0004509	chr7	-1.15	0.150282064	hsa-miR-93-3p
MIMAT0000094	chr4	-1.10	0.273151351	hsa-miR-95-3p
MIMAT0022842	chrX	1.78	0.202677653	hsa-miR-98-3p
MIMAT0004511	chr21	-0.97	0.161292322	hsa-miR-99a-3p
MIMAT0004678	chr19	0.35	0.472456379	hsa-miR-99b-3p
MIMAT0000689	chr19	0.07	0.860879455	hsa-miR-99b-5p
MIMAT0004512	chr11	0.17	0.93535566	hsa-miR-100-3p
MIMAT0009196	chr20	-3.14	0.094573	hsa-miR-103a-2-5p
MIMAT0004672	chr7	-1.13	0.000633555	hsa-miR-106b-3p
MIMAT0000421	chr18	-1.33	0.263628621	hsa-miR-122-5p
MIMAT0019876	chr18	-0.19	0.90215418	hsa-miR-122b-5p
MIMAT0004602	chr19	-3.13	0.071518821	hsa-miR-125a-3p
MIMAT0000443	chr19	-0.70	0.074494388	hsa-miR-125a-5p
MIMAT0000446	chr14	-1.42	5.78E-07	hsa-miR-127-3p
MIMAT0026477	chr2	0.94	0.593096342	hsa-miR-128-1-5p
MIMAT0000424	chr2;chr3	-0.17	0.898412989	hsa-miR-128-3p
MIMAT0004593	chr11	-1.87	0.15848136	hsa-miR-130a-5p
MIMAT0004680	chr22	0.15	0.823241614	hsa-miR-130b-5p
MIMAT0004594	chr17	-0.81	0.217976655	hsa-miR-132-5p
MIMAT0000427	chr18;chr20	-1.21	0.357252812	hsa-miR-133a-3p
MIMAT0026478	chr18;chr20	-1.08	0.426562915	hsa-miR-133a-5p
MIMAT0000770	chr6	-1.67	0.174919198	hsa-miR-133b
MIMAT0004552	chr11	0.60	0.230917505	hsa-miR-139-3p
MIMAT0000250	chr11	0.38	0.537384939	hsa-miR-139-5p
MIMAT0004608	chr5	-0.71	0.633106555	hsa-miR-146a-3p
MIMAT0004766	chr10	-0.76	0.477843246	hsa-miR-146b-3p
MIMAT0004549	chr7	-1.46	0.012069842	hsa-miR-148a-5p
MIMAT0000450	chr2	0.72	0.158435987	hsa-miR-149-5p
MIMAT0004610	chr19	0.36	0.808486171	hsa-miR-150-3p
MIMAT0000451	chr19	-0.14	0.772574778	hsa-miR-150-5p
MIMAT0026479	chr17	-1.14	0.032498843	hsa-miR-152-5p
MIMAT0000646	chr21	0.00	0.995646572	hsa-miR-155-5p
MIMAT0004558	chr9	0.52	0.504854156	hsa-miR-181a-2-3p
MIMAT0000256	chr1;chr9	-1.31	1.07E-05	hsa-miR-181a-5p
MIMAT0022692	chr1	-1.55	0.268502198	hsa-miR-181b-3p
MIMAT0000257	chr1;chr9	-1.02	0.000198381	hsa-miR-181b-5p
MIMAT0000261	chr7	-1.33	0.069836531	hsa-miR-183-5p
MIMAT0000454	chr15	1.22	0.452200962	hsa-miR-184
MIMAT0004929	chr1	1.63	0.107292608	hsa-miR-190b-5p
MIMAT0000440	chr3	-1.23	0.001334452	hsa-miR-191-5p
MIMAT0000459	chr17	-1.21	0.46279592	hsa-miR-193a-3p

Ensembl ID	Chr	Log2 Fold Change	P (adj)	Gene
MIMAT0004614	chr17	0.75	0.068543836	hsa-miR-193a-5p
MIMAT0002819	chr16	0.38	0.576818875	hsa-miR-193b-3p
MIMAT0004615	chr17	-0.20	0.664016217	hsa-miR-195-3p
MIMAT0009201	chr7	0.44	0.793351372	hsa-miR-196b-3p
MIMAT0000227	chr1	-0.03	0.958502163	hsa-miR-197-3p
MIMAT0022691	chr1	1.55	0.346933234	hsa-miR-197-5p
MIMAT0000228	chr3	1.68	0.10336532	hsa-miR-198
MIMAT0000617	chr12	-0.99	0.09395942	hsa-miR-200c-3p
MIMAT0022693	chr9	0.27	0.869087749	hsa-miR-204-3p
MIMAT0000265	chr9	-1.30	0.021160598	hsa-miR-204-5p
MIMAT0000462	chr6	-0.80	0.585452345	hsa-miR-206
MIMAT0000267	chr11	-1.49	0.002437028	hsa-miR-210-3p
MIMAT0026475	chr11	-0.30	0.88347376	hsa-miR-210-5p
MIMAT0000269	chr17	-1.39	0.256389703	hsa-miR-212-3p
MIMAT0022695	chr17	-0.20	0.764013058	hsa-miR-212-5p
MIMAT0004565	chr4	-2.70	0.175850826	hsa-miR-218-1-3p
MIMAT0000279	chrX	-0.20	0.711266313	hsa-miR-222-3p
MIMAT0009198	chrX	-2.16	0.14113579	hsa-miR-224-3p
MIMAT0000281	chrX	-0.19	NA	hsa-miR-224-5p
MIMAT0004679	chr20	-1.33	0.418927415	hsa-miR-296-3p
MIMAT0000687	chr14	-3.21	0.059792404	hsa-miR-299-3p
MIMAT0002890	chr14	-1.77	0.094161579	hsa-miR-299-5p
MIMAT0000683	chr4	-0.43	0.825161988	hsa-miR-302a-5p
MIMAT0000510	chr8	0.42	0.444745895	hsa-miR-320a-3p
MIMAT0037311	chr8	1.25	0.222733975	hsa-miR-320a-5p
MIMAT0005792	chr1;chr1	1.04	0.206260688	hsa-miR-320b
MIMAT0000755	chr14	-0.82	0.134660597	hsa-miR-323a-3p
MIMAT0000752	chr16	1.01	0.0103495	hsa-miR-328-3p
MIMAT0000751	chr19	-0.18	0.754020903	hsa-miR-330-3p
MIMAT0004693	chr19	-1.69	0.315220213	hsa-miR-330-5p
MIMAT0000760	chr12	0.04	0.978208228	hsa-miR-331-3p
MIMAT0004700	chr12	-1.70	0.052924829	hsa-miR-331-5p
MIMAT0004703	chr7	-1.33	NA	hsa-miR-335-3p
MIMAT0000764	chr7	-1.32	0.061164623	hsa-miR-339-5p
MIMAT0000753	chr14	-0.80	0.052379399	hsa-miR-342-3p
MIMAT0004694	chr14	1.48	0.004268322	hsa-miR-342-5p
MIMAT0000772	chr14	-0.29	0.603761139	hsa-miR-345-5p
MIMAT0000773	chr10	-0.96	0.593096342	hsa-miR-346
MIMAT0000705	chrX	-1.06	0.164733517	hsa-miR-362-5p
MIMAT0009199	chr16	1.24	0.011406068	hsa-miR-365a-5p
MIMAT0022834	chr17	-1.24	0.001583584	hsa-miR-365b-3p
MIMAT0022833	chr17	-0.59	0.491508778	hsa-miR-365b-5p
MIMAT0000721	chr14	-3.05	0.059275773	hsa-miR-369-3p
MIMAT0000722	chr14	-0.57	0.161848728	hsa-miR-370-3p
MIMAT0026483	chr14	-1.88	0.200661286	hsa-miR-370-5p
MIMAT0000729	chr14;chr14	-2.64	0.13134623	hsa-miR-376a-3p
MIMAT0002172	chr14	0.45	0.724586755	hsa-miR-376b-3p
MIMAT0000720	chr14	-2.56	0.191297903	hsa-miR-376c-3p
MIMAT0022861	chr14	-1.10	0.556815274	hsa-miR-376c-5p
MIMAT0004689	chr14	-2.00	0.142518008	hsa-miR-377-5p
MIMAT0000732	chr5	-1.34	0.21199785	hsa-miR-378a-3p

Ensembl ID	Chr	Log2 Fold Change	P (adj)	Gene
MIMAT0000731	chr5	-0.85	0.472257209	hsa-miR-378a-5p
MIMAT0019074	chr22	-0.90	0.652478678	hsa-miR-378i
MIMAT0001639	chr14	-0.21	0.579231772	hsa-miR-409-3p
MIMAT0026557	chr14	-0.98	0.593914457	hsa-miR-412-5p
MIMAT0001340	chr17	0.76	0.001025486	hsa-miR-423-3p
MIMAT0004748	chr17	0.84	0.036836424	hsa-miR-423-5p
MIMAT0004749	chrX	0.77	0.482222709	hsa-miR-424-3p
MIMAT0004757	chr14	-0.87	0.359107228	hsa-miR-431-3p
MIMAT0002814	chr14	0.56	0.30755675	hsa-miR-432-5p
MIMAT0001627	chr14	-0.84	0.023485045	hsa-miR-433-3p
MIMAT0010251	chr5	-0.13	0.938403518	hsa-miR-449c-5p
MIMAT0003884	chr17	-0.95	0.418743893	hsa-miR-454-5p
MIMAT0004784	chr9	0.07	0.920598316	hsa-miR-455-3p
MIMAT0004761	chr11	0.02	0.982647465	hsa-miR-483-5p
MIMAT0002174	chr16	-0.76	0.162829738	hsa-miR-484
MIMAT0002176	chr14	0.59	0.49317228	hsa-miR-485-3p
MIMAT0002175	chr14	-0.66	0.1401763	hsa-miR-485-5p
MIMAT0004762	chr8;chr8	0.66	0.652478678	hsa-miR-486-3p
MIMAT0002177	chr8;chr8	0.81	0.335355499	hsa-miR-486-5p
MIMAT0026559	chr14	-0.50	0.472567494	hsa-miR-487a-5p
MIMAT0002807	chr9	-0.56	0.580124105	hsa-miR-491-5p
MIMAT0004772	chr20	2.75	0.277879228	hsa-miR-499a-3p
MIMAT0002870	chr20	-1.24	0.504108054	hsa-miR-499a-5p
MIMAT0004773	chrX	-0.55	0.667775057	hsa-miR-500a-5p
MIMAT0027032	chrX	-1.77	0.368851687	hsa-miR-500b-3p
MIMAT0016925	chrX	-1.50	0.223487963	hsa-miR-500b-5p
MIMAT0002872	chrX	-0.47	0.525656503	hsa-miR-501-5p
MIMAT0002875	chrX	-0.60	0.328713718	hsa-miR-504-5p
MIMAT0002876	chrX	-0.35	0.49317228	hsa-miR-505-3p
MIMAT0004776	chrX	0.86	0.266119624	hsa-miR-505-5p
MIMAT0002878	chrX	0.48	0.764822298	hsa-miR-506-3p
MIMAT0002880	chrX	-2.59	0.21199785	hsa-miR-508-3p
MIMAT0002808	chr10	0.10	0.915915476	hsa-miR-511-5p
MIMAT0002858	chr19	-2.38	0.253695548	hsa-miR-520g-3p
MIMAT0002835	chr19	-1.61	0.354169597	hsa-miR-526b-5p
MIMAT0004780	chrX	-0.31	0.662587171	hsa-miR-532-3p
MIMAT0003163	chr14	-1.79	0.064947861	hsa-miR-539-5p
MIMAT0004920	chr14	-1.35	0.438926639	hsa-miR-541-3p
MIMAT0004954	chr14	-0.43	0.363806858	hsa-miR-543
MIMAT0022471	chr9	-3.01	0.142532723	hsa-miR-548aw
MIMAT0005875	chr22	-0.44	0.802633622	hsa-miR-548j-5p
MIMAT0005882	chr11	-2.45	0.079915648	hsa-miR-548k
MIMAT0005919	chr7;chr20	-0.77	0.521247118	hsa-miR-548o-3p
MIMAT0004800	chr7	-0.57	0.765686567	hsa-miR-550a-5p
MIMAT0003239	chr4	0.17	0.830674136	hsa-miR-574-3p
MIMAT0004795	chr4	-0.25	0.779295524	hsa-miR-574-5p
MIMAT0004796	chr4	-2.18	0.168033042	hsa-miR-576-3p
MIMAT0003246	chr5	-1.62	0.355924986	hsa-miR-581
MIMAT0003247	chr5	-1.71	0.472257209	hsa-miR-582-5p
MIMAT0003249	chr5	-0.53	0.690518857	hsa-miR-584-5p
MIMAT0004799	chr7	0.66	0.200661286	hsa-miR-589-5p

Ensembl ID	Chr	Log2 Fold Change	P (adj)	Gene
MIMAT0026619	chr8	-1.71	0.336535771	hsa-miR-597-3p
MIMAT0026621	chr10	-0.52	0.817038348	hsa-miR-605-3p
MIMAT0003283	chr12	-0.23	0.762993824	hsa-miR-615-3p
MIMAT0004804	chr12	-0.66	0.691512693	hsa-miR-615-5p
MIMAT0004805	chr12	-1.56	0.296452573	hsa-miR-616-3p
MIMAT0003287	chr12	0.37	0.669508161	hsa-miR-618
MIMAT0003297	chr15	-1.30	0.061164623	hsa-miR-628-3p
MIMAT0004810	chr15	-1.64	0.051478918	hsa-miR-629-5p
MIMAT0003309	chr19	0.42	0.745641731	hsa-miR-639
MIMAT0003311	chr19	-1.36	0.115712485	hsa-miR-641
MIMAT0003330	chr14	-0.97	0.021406543	hsa-miR-654-5p
MIMAT0022710	chr22	-2.01	0.072518398	hsa-miR-659-5p
MIMAT0005867	chr2	-1.14	0.559056293	hsa-miR-663b
MIMAT0005948	chr1	-0.48	0.509049413	hsa-miR-664a-5p
MIMAT0022272	chrX	1.20	0.133736071	hsa-miR-664b-3p
MIMAT0022271	chrX	1.41	0.000128008	hsa-miR-664b-5p
MIMAT0003881	chr14	2.23	0.18770723	hsa-miR-668-3p
MIMAT0004819	chr7	1.23	0.017266595	hsa-miR-671-3p
MIMAT0006790	chr11	-0.42	0.652478678	hsa-miR-675-3p
MIMAT0004284	chr11	-0.96	0.354738471	hsa-miR-675-5p
MIMAT0018204	chrX	-0.85	0.572378395	hsa-miR-676-3p
MIMAT0004946	chr17	0.83	0.497029229	hsa-miR-744-3p
MIMAT0004945	chr17	-0.46	0.277285584	hsa-miR-744-5p
MIMAT0004957	chr1	2.18	0.096755139	hsa-miR-760
MIMAT0003888	chrX	-0.17	0.883918735	hsa-miR-766-3p
MIMAT0022714	chrX	0.02	0.991930467	hsa-miR-766-5p
MIMAT0003887	chr19	-0.43	0.762533052	hsa-miR-769-3p
MIMAT0004911	chr5	-0.58	0.188777325	hsa-miR-874-3p
MIMAT0004949	chr6	1.70	0.138236968	hsa-miR-877-5p
MIMAT0004947	chr3	-0.48	0.694673039	hsa-miR-885-5p
MIMAT0026720	chr5	-1.17	0.245072758	hsa-miR-887-5p
MIMAT0004916	chrX	-2.35	0.19644372	hsa-miR-888-5p
MIMAT0004902	chrX	-0.26	0.882733863	hsa-miR-891a-5p
MIMAT0004978	chr19	-0.14	0.923553741	hsa-miR-935
MIMAT0004984	chr20;chr20;chr20;chr20;chr20	-0.83	0.03509809	hsa-miR-941
MIMAT0004985	chr1	0.03	0.982005235	hsa-miR-942-5p
MIMAT0005825	chr17	0.35	0.459273255	hsa-miR-1180-3p
MIMAT0005826	chr19	0.48	0.805339397	hsa-miR-1181
MIMAT0005573	chr16	0.33	0.742039684	hsa-miR-1225-3p
MIMAT0005572	chr16	0.96	0.478605097	hsa-miR-1225-5p
MIMAT0005583	chr12	-0.29	0.866372984	hsa-miR-1228-3p
MIMAT0005582	chr12	-2.37	0.206260688	hsa-miR-1228-5p
MIMAT0005896_2	chr2;chr5	1.15	0.403818715	hsa-miR-1244
MIMAT0005899	chr14	0.81	0.448238261	hsa-miR-1247-5p
MIMAT0005900	chr3	0.34	0.477076409	hsa-miR-1248
MIMAT0005914	chr1	-0.79	0.524367053	hsa-miR-1262
MIMAT0005924	chr19	-2.38	0.185804054	hsa-miR-1270
MIMAT0005796	chr5	-0.81	0.316849757	hsa-miR-1271-5p
MIMAT0005943	chr20	0.02	0.98509882	hsa-miR-1292-5p
MIMAT0005884	chr5	-2.55	0.070497333	hsa-miR-1294
MIMAT0005794	chr10	-0.56	0.26577278	hsa-miR-1296-5p

Ensembl ID	Chr	Log2 Fold Change	P (adj)	Gene
MIMAT0005797	chr2	0.25	0.741874573	hsa-miR-1301-3p
MIMAT0005891	chr5	0.09	0.951447935	hsa-miR-1303
MIMAT0005892	chr11	-0.40	0.806724019	hsa-miR-1304-5p
MIMAT0005950	chr22	1.21	0.442650954	hsa-miR-1306-3p
MIMAT0022726	chr22	-0.15	0.916236624	hsa-miR-1306-5p
MIMAT0005951	chr10	0.74	0.022552453	hsa-miR-1307-3p
MIMAT0022727	chr10	-0.43	0.689403951	hsa-miR-1307-5p
MIMAT0005795	chr19	-2.68	0.096485235	hsa-miR-1323
MIMAT0019776	chr11	-0.40	0.866372984	hsa-miR-1343-3p
MIMAT0006789	chrX	0.38	0.631529448	hsa-miR-1468-5p
MIMAT0039764	chr1	0.28	0.636443882	hsa-miR-1843
MIMAT0009451	chr1	0.60	0.762533052	hsa-miR-1976
MIMAT0017352	chr5	-1.22	0.35863189	hsa-miR-2277-5p
MIMAT0017950	chr2	-0.88	0.578415275	hsa-miR-2355-3p
MIMAT0019865	chr17	-0.70	0.709744638	hsa-miR-3064-3p
MIMAT0019864	chr17	0.67	0.383280593	hsa-miR-3064-5p
MIMAT0048635	chr10	1.96	0.439426813	hsa-miR-3085-5p
MIMAT0014986	chr1	-1.34	0.460343358	hsa-miR-3124-5p
MIMAT0014988	chr2	-1.01	0.690626022	hsa-miR-3125
MIMAT0014990	chr2	1.09	0.593096342	hsa-miR-3127-5p
MIMAT0014992	chr2	-2.74	0.08569919	hsa-miR-3129-5p
MIMAT0015038	chr11	0.30	0.869087749	hsa-miR-3164
MIMAT0019214	chr14	-0.71	0.611762436	hsa-miR-3173-5p
MIMAT0015070	chr19	-0.08	0.974698976	hsa-miR-3188
MIMAT0015084	chr22;chr22	-1.66	0.120559211	hsa-miR-3199
MIMAT0015085	chr22	-1.57	0.322011301	hsa-miR-3200-3p
MIMAT0018004	chr8	0.73	0.70506981	hsa-miR-3622a-3p
MIMAT0018003	chr8	-0.68	0.490504252	hsa-miR-3622a-5p
MIMAT0018006	chr8	-1.82	0.26055572	hsa-miR-3622b-3p
MIMAT0017982	chr1	1.38	0.151083919	hsa-miR-3605-3p
MIMAT0017981	chr1	-0.41	0.66142723	hsa-miR-3605-5p
MIMAT0022965	chr2	0.07	0.979007216	hsa-miR-3606-3p
MIMAT0017986	chr7	1.45	1.66E-07	hsa-miR-3609
MIMAT0017987	chr8	1.31	0.247138216	hsa-miR-3610
MIMAT0017989	chr12	-2.25	0.242772802	hsa-miR-3612
MIMAT0017992	chr17	-0.09	0.962870291	hsa-miR-3614-5p
MIMAT0017994	chr17	-1.29	0.088646747	hsa-miR-3615
MIMAT0018071	chr9	1.12	0.096766384	hsa-miR-3651
MIMAT0018183	chr22	-0.70	0.300156646	hsa-miR-3909
MIMAT0018187	chr12;chr12	-2.77	0.151083919	hsa-miR-3913-5p
MIMAT0018205	chr22	-1.37	0.333947059	hsa-miR-3928-3p
MIMAT0018349	chr6	0.89	0.483574147	hsa-miR-3934-5p
MIMAT0016888	chr20	-0.61	0.608822481	hsa-miR-4326
MIMAT0018941	chr1	1.26	0.296452573	hsa-miR-4426
MIMAT0018962	chr2;chr3	1.08	0.247595571	hsa-miR-4444
MIMAT0018968	chr4	1.89	0.28398691	hsa-miR-4449
MIMAT0019000	chr9	0.87	0.53316431	hsa-miR-4473
MIMAT0032116	chr11	3.24	0.065695892	hsa-miR-4485-5p
MIMAT0019058	chr17	0.59	0.246764647	hsa-miR-4521
MIMAT0019706	chr6	-1.85	0.293940343	hsa-miR-4645-3p
MIMAT0019711	chr7	-2.72	0.173749478	hsa-miR-4649-5p

Ensembl ID	Chr	Log2 Fold Change	P (adj)	Gene
MIMAT0019729	chr8	0.96	0.553584851	hsa-miR-4661-5p
MIMAT0019750	chr9	-2.05	0.24978591	hsa-miR-4670-5p
MIMAT0019764	chr10	0.89	0.682287116	hsa-miR-4680-5p
MIMAT0019768	chr10	0.79	0.289222123	hsa-miR-4683
MIMAT0019805	chr13	-2.97	0.14887605	hsa-miR-4705
MIMAT0019812	chr14	-1.02	0.38236541	hsa-miR-4709-3p
MIMAT0019811	chr14	0.78	0.405841352	hsa-miR-4709-5p
MIMAT0019855	chr17	-0.68	0.709744638	hsa-miR-4732-5p
MIMAT0019931	chr2	-0.05	0.984012474	hsa-miR-4775
MIMAT0019957	chr3	1.87	0.135822284	hsa-miR-4787-3p
MIMAT0021017	chr19	0.96	0.764822298	hsa-miR-4999-5p
MIMAT0021021	chr2	2.44	0.115416148	hsa-miR-5001-5p
MIMAT0021041	chr15	-1.61	0.394098292	hsa-miR-5009-5p
MIMAT0021044	chr17	-0.62	0.531107557	hsa-miR-5010-3p
MIMAT0021083	chr4	0.65	0.606667135	hsa-miR-5091
MIMAT0022491	chr1	1.66	0.428905534	hsa-miR-5698
MIMAT0022496	chr2	2.38	0.205388823	hsa-miR-5703
MIMAT0025458	chr21	-2.74	0.167665663	hsa-miR-6501-5p
MIMAT0025467	chr12	1.55	0.228121556	hsa-miR-6505-3p
MIMAT0025466	chr12	-1.43	0.260492679	hsa-miR-6505-5p
MIMAT0025468	chr16	0.70	0.682287116	hsa-miR-6506-5p
MIMAT0025479	chr16;chr16;chr16;chr16	2.34	0.138421742	hsa-miR-6511a-3p
MIMAT0025848	chr16;chr16	-0.51	0.631412567	hsa-miR-6511b-3p
MIMAT0025484	chr11	-0.13	0.945527201	hsa-miR-6514-5p
MIMAT0025487	chr19	-2.09	0.126767602	hsa-miR-6515-3p
MIMAT0030418	chr17	-1.05	0.052379399	hsa-miR-6516-3p
MIMAT0030417	chr17	-0.93	0.085602161	hsa-miR-6516-5p
MIMAT0025845	chr11	1.33	0.157126867	hsa-miR-6716-3p
MIMAT0025852	chr6	1.51	0.311852909	hsa-miR-6721-5p
MIMAT0027370	chr1	-0.36	0.874590657	hsa-miR-6734-3p
MIMAT0027369	chr1	0.73	0.70506981	hsa-miR-6734-5p
MIMAT0027513	chr19	1.06	0.489704077	hsa-miR-6806-3p
MIMAT0027537	chr22	0.26	0.898412989	hsa-miR-6818-3p
MIMAT0027554	chr3	-2.03	0.150112475	hsa-miR-6827-5p
MIMAT0027587	chr8	0.38	0.78186664	hsa-miR-6842-3p
MIMAT0027588	chr8	-0.86	0.504854156	hsa-miR-6843-3p
MIMAT0027605	chr9	-0.33	0.837080115	hsa-miR-6852-3p
MIMAT0027633	chr17	1.65	0.324176569	hsa-miR-6866-3p
MIMAT0027632	chr17	-1.48	0.067811003	hsa-miR-6866-5p
MIMAT0028120	chr6	2.80	0.088744721	hsa-miR-7111-3p
MIMAT0030020	chr8	-0.79	0.691512693	hsa-miR-7705
MIMAT0030021	chr15	0.60	0.27180229	hsa-miR-7706
MIMAT0030419	chr12	2.75	0.154755793	hsa-miR-7844-5p
MIMAT0030421	chr1	-0.72	0.690843217	hsa-miR-7846-3p
MIMAT0030999	chr12	0.31	0.823241614	hsa-miR-8072
MIMAT0041618	chr15	0.21	0.690518857	hsa-miR-10393-3p
MIMAT0041617	chr15	0.39	0.410559728	hsa-miR-10393-5p
MIMAT0041619	chr19	1.35	0.377885155	hsa-miR-10394-5p
MIMAT0041622	chr19	1.24	1.60E-06	hsa-miR-10395-3p
MIMAT0041621	chr19	1.24	1.50E-06	hsa-miR-10395-5p
MIMAT0041626	chr5	0.70	0.5586295	hsa-miR-10397-3p

Ensembl ID	Chr	Log2 Fold Change	P (adj)	Gene
MIMAT0041625	chr5	1.02	0.444966557	hsa-miR-10397-5p
MIMAT0041630	chr7	0.43	0.632133916	hsa-miR-10399-3p
MIMAT0041633_3	chr21	2.85	0.085602161	hsa-miR-10401-5p
MIMAT0041997	chr12	-0.27	0.741798201	hsa-miR-10527-5p

**Table A3.2** (includes preceding 11 pages) **Differential expression profiles of miRNA transcripts identified by RNA-seq from six healthy and six diseased human tendon samples.** miRNAs achieving statistically significant differential expression (Log2 Fold Change  $\geq 1.5$  with Bejaminin-Hochberg adjusted *P*-value (*P* adj)  $< 0.05$ ) between healthy and diseased cohorts are given in **bold type** at the top of the table. Chr = chromosome.

Red ground colour	= Negative fold change
Blue ground colour	= Positive fold change
Uncoloured cells	= No change

## **Appendix 4**

**Table A4.1** Predicted mRNA targets of miRNAs significantly differentially expressed in human tendinopathy.

**Table A4.2** Predicted mRNA targets of miRNAs identified as significantly differentially expressed in both human and equine tendinopathy.

Gene Symbol	Gene Name	miRNAs Targeting Gene	Confidence
ACE2	Angiotensin I converting enzyme 2	hsa-miR-200b-3p (and other miRNAs w/seed AAUACUG) hsa-miR-4677-3p (miRNAs w/seed CUGUGAG)	Experimentally Observed High (pre dicted)
ACTA2	Actin alpha 2, smooth muscle	hsa-miR-21-5p (and other miRNAs w/seed AGCUUUAU) hsa-miR-27a-3p (and other miRNAs w/seed UCACAGU)	Experimentally Observed High (pre dicted)
ACTB	Actin beta	hsa-miR-145-5p (and other miRNAs w/seed UCCA GUU)	High (pre dicted)
ACVR1	Activin A receptor type 1	hsa-miR-30e-5p (and other miRNAs w/seed GUAACA) hsa-miR-130a-3p (and other miRNAs w/seed AUGGCAA) hsa-miR-365a-3p (and other miRNAs w/seed AAUGCCC)	Experimentally Observed High (pre dicted) High (pre dicted)
ADAMTS1	ADAM metalloproteinase with thrombospondin type 1 motif 1	hsa-miR-125b-5p (and other miRNAs w/seed CCCUGAG)	Experimentally Observed
ADAMTS14	ADAM metalloproteinase with thrombospondin type 1 motif 14	hsa-miR-29b-3p (and other miRNAs w/seed AGACCA) hsa-miR-30e-5p (and other miRNAs w/seed GUAACA) hsa-miR-30e-5p (and other miRNAs w/seed GUAACA) hsa-miR-98-5p (and other miRNAs w/seed GAGGUAG)	Experimentally Observed Experimentally Observed Experimentally Observed Experimentally Observed
ADAMTS2	ADAM metalloproteinase with thrombospondin type 1 motif 2	hsa-miR-339-3p (miRNAs w/seed GAGCGCC) hsa-miR-1291 (and other miRNAs w/seed GGCCUUG)	High (pre dicted) High (pre dicted)
ADAMTS20	ADAM metalloproteinase with thrombospondin type 1 motif 20	hsa-miR-29b-3p (and other miRNAs w/seed AGACCA)	Experimentally Observed
ADAMTS3	ADAM metalloproteinase with thrombospondin type 1 motif 3	hsa-miR-30e-5p (and other miRNAs w/seed GUAACA) hsa-miR-98-5p (and other miRNAs w/seed GAGGUAG) hsa-miR-29b-3p (and other miRNAs w/seed AGACCA)	Experimentally Observed Experimentally Observed High (pre dicted)
ADAMTS9	ADAM metalloproteinase with thrombospondin type 1 motif 9	hsa-miR-199a-3p (and other miRNAs w/seed CAGUAGU) hsa-miR-502-3p (and other miRNAs w/seed AUGCACC)	High (pre dicted) High (pre dicted)
ADCY6	Adenylate cyclase 6	hsa-miR-29b-3p (and other miRNAs w/seed AGACCA) hsa-miR-96-5p (and other miRNAs w/seed UUGGCAC) hsa-miR-182-5p (and other miRNAs w/seed UUGGCAA) hsa-miR-4667-3p (miRNAs w/seed CCCUCCU)	Experimentally Observed Experimentally Observed Experimentally Observed High (pre dicted)
ADH1B	Alcohol dehydrogenase 1B (class I), beta polypeptide	hsa-miR-511-3p (miRNAs w/seed AUGUGUA)	High (pre dicted)
ADIPOR2	Adiponectin receptor 2	hsa-miR-218-5p (and other miRNAs w/seed UGUGCUU)	High (pre dicted)
ADORA2B	Adenosine A2b receptor	hsa-miR-27a-3p (and other miRNAs w/seed UCACAGU)	Experimentally Observed
ADRA1A	Adrenoreceptor alpha 1A	hsa-miR-340-3p (and other miRNAs w/seed CCGUCUC)	High (pre dicted)
ADRA1D	Adrenoreceptor alpha 1D	hsa-miR-34a-5p (and other miRNAs w/seed GGCA GUG)	High (pre dicted)
ADRB2	Adrenoreceptor beta 2	hsa-miR-98-5p (and other miRNAs w/seed GAGGUAG)	High (pre dicted)
AGTR1	Angiotensin II receptor type 1	hsa-miR-34a-5p (and other miRNAs w/seed GGCA GUG)	High (pre dicted)
AGTR2	Angiotensin II receptor type 2	hsa-miR-708-5p (and other miRNAs w/seed AGGAGCU)	High (pre dicted)
AIRE	Autoimmune regulator	hsa-miR-34a-5p (and other miRNAs w/seed GGCA GUG)	High (pre dicted)
AKT1	AKT serine/threonine kinase 1	hsa-miR-185-5p (and other miRNAs w/seed GGAGAGA)	Experimentally Observed
AKT2	AKT serine/threonine kinase 2	hsa-miR-151a-5p (and other miRNAs w/seed CGAGGAG) hsa-miR-612 (and other miRNAs w/seed CUGGGCA)	High (pre dicted) Experimentally Observed
AKT3	AKT serine/threonine kinase 3	hsa-miR-16-5p (and other miRNAs w/seed AGCAGCA) hsa-miR-22-3p (miRNAs w/seed AGCUGCC)	High (pre dicted) High (pre dicted)

Gene Symbol	Gene Name	miRNAs Targeting Gene	Confidence
ALDH18A1	Aldehyde dehydrogenase 18 family member A1	hsa-miR-181a-3p (and other miRNAs w/seed CCAUCGA) hsa-miR-539-3p (and other miRNAs w/seed UCAUACA)	High (predicted) High (predicted)
ALDH1A2	Aldehyde dehydrogenase 1 family member A2	hsa-miR-221-5p (and other miRNAs w/seed CCUGGCA) hsa-miR-542-3p (miRNAs w/seed GUGACAG) hsa-miR-632 (and other miRNAs w/seed UGUCUGC)	High (predicted) High (predicted) High (predicted)
ALG8	ALG8 alpha-1,3-glucosyltransferase	hsa-miR-24-2-5p (and other miRNAs w/seed GCCUACU) hsa-miR-221-5p (and other miRNAs w/seed CCUGGCA)	High (predicted) High (predicted)
AOC3	Amine oxidase copper containing 3	hsa-miR-425-3p (miRNAs w/seed UCGGGAA) hsa-miR-660-5p (and other miRNAs w/seed ACCCAUU) hsa-miR-1255a (and other miRNAs w/seed GGAUGAG) hsa-miR-3652 (and other miRNAs w/seed GCGUGGA)	High (predicted) High (predicted) High (predicted) High (predicted)
AP3B1	Adaptor related prote in complex 3 subunit beta 1	hsa-miR-9-5p (and other miRNAs w/seed CUUUGGU)	High (predicted)
AP3S2	Adaptor related prote in complex 3 subunit sigma 2	hsa-miR-18a-5p (and other miRNAs w/seed AAGGUGC) hsa-miR-34a-5p (and other miRNAs w/seed GGCAGUG)	High (predicted) High (predicted)
APBB1	Amyloid beta precursor protein binding family B member 1	hsa-miR-144-5p (miRNAs w/seed GAUAUCA) hsa-miR-199b-5p (and other miRNAs w/seed CCAAGUGU)	High (predicted) High (predicted)
APP	Amyloid beta precursor protein	hsa-miR-101-3p (and other miRNAs w/seed ACAGUAC) hsa-miR-106a-5p (and other miRNAs w/seed AAAAGUGC) hsa-miR-372-3p (and other miRNAs w/seed AAGUGCU) hsa-miR-3917 (miRNAs w/seed CUGGGAC)	Experimentally Observed Experimentally Observed Experimentally Observed High (predicted)
APTX	Aprataxin	hsa-miR-28-3p (and other miRNAs w/seed ACUAGAU)	Experimentally Observed
AR	Androgen receptor	hsa-miR-223-5p (miRNAs w/seed GUGUAUU) hsa-miR-381-3p (and other miRNAs w/seed AUA CAAG) hsa-miR-502-3p (and other miRNAs w/seed AUGCACC)	Experimentally Observed High (predicted) Experimentally Observed
ATF6	Activating transcription factor 6	hsa-miR-16-5p (and other miRNAs w/seed AGCAGCA)	Experimentally Observed
ATP2A2	ATPase sarcoplasmic/endoplasmic reticulum Ca2+ transporting 2	hsa-miR-30e-5p (and other miRNAs w/seed GUAAACA) hsa-miR-329-3p (and other miRNAs w/seed ACACACC)	Experimentally Observed High (predicted)
ATP7A	ATPase copper transporting alpha	hsa-miR-16-2-3p (and other miRNAs w/seed CAAUAUU) hsa-miR-223-3p (miRNAs w/seed GUCAGUU)	High (predicted) High (predicted)
AXL	AXL receptor tyrosine kinase	hsa-miR-34a-5p (and other miRNAs w/seed GGCAGUG)	High (predicted)
B2M	Beta-2-microglobulin	hsa-miR-16-2-3p (and other miRNAs w/seed CAAUAUU)	High (predicted)
B3GALT4	Beta-1,3-galactosyltransferase 4	hsa-miR-107 (and other miRNAs w/seed GCAGCAU) hsa-miR-125b-5p (and other miRNAs w/seed CCCUGAG)	High (predicted) Experimentally Observed
BARD1	BRCA1 associated RING domain 1	hsa-miR-3613-3p (miRNAs w/seed CAAAAA)	High (predicted)
BBC3	BCL2 binding component 3	hsa-miR-24-3p (and other miRNAs w/seed GGCUCAG) hsa-miR-27a-3p (and other miRNAs w/seed UCA CAGU) hsa-miR-221-3p (and other miRNAs w/seed GCUACAU) hsa-miR-483-3p (miRNAs w/seed CACUCCU) hsa-miR-3652 (and other miRNAs w/seed GCGUGGA)	Experimentally Observed Experimentally Observed Experimentally Observed Experimentally Observed High (predicted)

Gene Symbol	Gene Name	miRNAs Targeting Gene	Confidence
BCL2	BCL2 apoptosis regulator	hsa-miR-16-5p (and other miRNAs w/seed AGCAGCA) hsa-miR-34a-5p (and other miRNAs w/seed GGCAGUG) hsa-miR-106a-5p (and other miRNAs w/seed AAAGUGC) hsa-miR-140-3p (and other miRNAs w/seed ACCACAG) hsa-miR-143-3p (and other miRNAs w/seed GAGAUGA) hsa-miR-181d-5p (and other miRNAs w/seed ACAUUCA) hsa-miR-493-5p (miRNAs w/seed UGUACA U)	Experimentally Observed Experimentally Observed Experimentally Observed High (predicted) Experimentally Observed Experimentally Observed High (predicted)
BDNF	Brain derived ne urotrophic factor	hsa-miR-10b-5p (and other miRNAs w/seed ACCUUGU) hsa-miR-16-5p (and other miRNAs w/seed AGCAGCA) hsa-miR-107 (and other miRNAs w/seed GCAGCAU) hsa-miR-340-5p (miRNAs w/seed UAUAAG) hsa-miR-516b-5p (miRNAs w/seed UCUGGAG) hsa-miR-3652 (and other miRNAs w/seed GGCUGGA) hsa-miR-193b-5p (miRNAs w/seed GGGGUUU) hsa-miR-142-3p (and other miRNAs w/seed GUAGUGU) hsa-miR-22-3p (miRNAs w/seed AGCUGCC) hsa-miR-3613-3p (miRNAs w/seed CAAAAA)	High (predicted) Experimentally Observed High (predicted) High (predicted) High (predicted) High (predicted) High (predicted) High (predicted) High (predicted) Experimentally Observed High (predicted)
BGLAP	Bone gamma-carboxyglutamate protein	hsa-miR-125b-5p (and other miRNAs w/seed CCCUGAG) hsa-miR-182-5p (and other miRNAs w/seed UUGGCAA)	Experimentally Observed High (predicted)
BGN	Biglycan	hsa-miR-19b-3p (and other miRNAs w/seed GUGCAAA) hsa-miR-21-5p (and other miRNAs w/seed AGCUUAU)	Experimentally Observed Experimentally Observed
BMP2	Bone morphogenetic protein 2	hsa-miR-32-5p (and other miRNAs w/seed AUUGCAC) hsa-miR-106a-5p (and other miRNAs w/seed AAAGUGC)	Experimentally Observed Experimentally Observed
BMP4	Bone morphogenetic protein 4	hsa-miR-186-5p (miRNAs w/seed AAAGAAU)	High (predicted)
BMP7	Bone morphogenetic protein 7	hsa-miR-205-5p (and other miRNAs w/seed CCUJCAU) hsa-miR-24-2-5p (and other miRNAs w/seed GCCUACU)	High (predicted) High (predicted)
BMPR1A	Bone morphogenetic protein receptor type 1A	hsa-miR-361-3p (miRNAs w/seed CCCCAG)	High (predicted)
BMPR1B	Bone morphogenetic protein receptor type 1B	hsa-miR-27a-5p (miRNAs w/seed GGGCUUA) hsa-miR-29b-3p (and other miRNAs w/seed AGCACCA) hsa-miR-4662a-5p (miRNAs w/seed UAGCCAA)	High (predicted) High (predicted) High (predicted)
BMPR2	Bone morphogenetic protein receptor type 2	hsa-miR-29b-2-5p (and other miRNAs w/seed UGGUUUC) hsa-miR-107 (and other miRNAs w/seed GCAGCAU)	High (predicted) High (predicted)
CALCL	Calcitonin receptor like receptor	hsa-miR-324-5p (miRNAs w/seed GCAUCCC)	High (predicted)
CALD1	Caldesmon 1	hsa-miR-374a-5p (and other miRNAs w/seed UAUAUA) hsa-miR-664a-3p (and other miRNAs w/seed AUUCAUU)	High (predicted) High (predicted)
CAMK2B	Calcium/calmodulin dependent protein kinase II beta	hsa-miR-3065-5p (and other miRNAs w/seed CAACAAA)	High (predicted)
CASP8	Caspase 8		
CCL11	C-C motif chemokine ligand 11		
CCL13	C-C motif chemokine ligand 13		
CCL2	C-C motif chemokine ligand 2		

Gene Symbol	Gene Name	miRNAs Targeting Gene	Confidence
CCL5	C-C motif chemokine ligand 5	hsa-miR-146b-5p (and other miRNAs w/seed GAGAAU)	High (predicted)
		hsa-miR-193b-5p (miRNAs w/seed GGGUUUU)	High (predicted)
		hsa-miR-2110 (and other miRNAs w/seed UGGGAA)	High (predicted)
		hsa-miR-3652 (and other miRNAs w/seed GGCUGGA)	High (predicted)
		hsa-miR-6724-5p (and other miRNAs w/seed UGGGCC)	High (predicted)
CCN1	Cellular communication network factor 1	hsa-miR-22-3p (miRNAs w/seed AGCUGCC)	High (predicted)
CCN2	Cellular communication network factor 2	hsa-miR-30d-3p (and other miRNAs w/seed UUUCAU)	Experimentally Observed
		hsa-miR-18a-5p (and other miRNAs w/seed AAGGUG)	Experimentally Observed
		hsa-miR-19b-3p (and other miRNAs w/seed GUGCAA)	Experimentally Observed
		hsa-miR-30e-5p (and other miRNAs w/seed GUAAACA)	Experimentally Observed
		hsa-miR-361-3p (miRNAs w/seed CCCCAG)	High (predicted)
CCN5	Cellular communication network factor 5	hsa-miR-383-5p (miRNAs w/seed GAUCAGA)	High (predicted)
CCND1	Cyclin D1	hsa-miR-34a-5p (and other miRNAs w/seed GGCAGUG)	Experimentally Observed
		hsa-miR-16-5p (and other miRNAs w/seed AGCAGCA)	Experimentally Observed
		hsa-miR-19b-3p (and other miRNAs w/seed GUGCAA)	Experimentally Observed
		hsa-miR-34a-5p (and other miRNAs w/seed GGCAGUG)	Experimentally Observed
		hsa-miR-98-5p (and other miRNAs w/seed GAGGUAG)	Experimentally Observed
		hsa-miR-106a-5p (and other miRNAs w/seed AAAGUG)	Experimentally Observed
		hsa-miR-221-5p (and other miRNAs w/seed CCUGGCA)	High (predicted)
		hsa-miR-372-3p (and other miRNAs w/seed AAGUGCU)	Experimentally Observed
		hsa-miR-16-5p (and other miRNAs w/seed AGCAGCA)	Experimentally Observed
		hsa-miR-34a-5p (and other miRNAs w/seed GGCAGUG)	High (predicted)
		hsa-miR-193b-5p (miRNAs w/seed GGGUUU)	High (predicted)
		hsa-miR-502-3p (and other miRNAs w/seed AUGCACC)	High (predicted)
		hsa-miR-628-5p (and other miRNAs w/seed UGCUGAC)	High (predicted)
		hsa-miR-27a-5p (miRNAs w/seed GGGUUU)	High (predicted)
		hsa-miR-125b-5p (and other miRNAs w/seed CCUGAG)	Experimentally Observed
CCND3	Cyclin D3	hsa-miR-4667-3p (miRNAs w/seed CCUCU)	High (predicted)
CCR1	C-C motif chemokine receptor 1	hsa-miR-493-3p (miRNAs w/seed GAAAGGU)	High (predicted)
		hsa-miR-539-3p (and other miRNAs w/seed UCAUACA)	High (predicted)
		hsa-miR-16-5p (and other miRNAs w/seed AGCAGCA)	High (predicted)
		hsa-miR-146b-5p (and other miRNAs w/seed GAGAAU)	Experimentally Observed
		hsa-miR-361-3p (miRNAs w/seed CCCCAG)	High (predicted)
CD36	CD36 molecule	hsa-miR-6125 (miRNAs w/seed CGGAAGG)	High (predicted)
CD40	CD40 molecule	hsa-miR-185-5p (and other miRNAs w/seed GGAGAGA)	High (predicted)
CD40LG	CD40 ligand	hsa-miR-208b-3p (and other miRNAs w/seed UAAGACG)	Experimentally Observed
		hsa-miR-4485-3p (miRNAs w/seed AACGGCC)	High (predicted)

Gene Symbol	Gene Name	miRNAs Targeting Gene	Confidence
CD44	CD44 molecule	hsa-miR-199a-3p (and other miRNAs w/seed CAGUAGU)	Experimentally Observed
		hsa-miR-372-3p (and other miRNAs w/seed AAGUGCU)	Experimentally Observed
		hsa-miR-6724-5p (and other miRNAs w/seed UGGGCC)	High (predicted)
CD47	CD47 molecule	hsa-miR-34a-5p (and other miRNAs w/seed GGCAAGUG)	Experimentally Observed
		hsa-miR-16-5p (and other miRNAs w/seed AGCAGCA)	High (predicted)
CD80	CD80 molecule	hsa-miR-22-3p (miRNAs w/seed AGCUGCC)	High (predicted)
		hsa-miR-107 (and other miRNAs w/seed GCAGCAU)	High (predicted)
CD9	CD9 molecule	hsa-miR-200a-3p (and other miRNAs w/seed AACACUG)	High (predicted)
		hsa-miR-628-5p (and other miRNAs w/seed UGCUGAC)	High (predicted)
CD99	CD99 molecule	hsa-miR-16-2-3p (and other miRNAs w/seed CAAUAUU)	High (predicted)
		hsa-miR-495-3p (and other miRNAs w/seed AACAAAC)	High (predicted)
CDH1	Cadherin 1	hsa-miR-3065-5p (and other miRNAs w/seed CAACAAA)	High (predicted)
		hsa-miR-29b-2-5p (and other miRNAs w/seed UGGUUUC)	High (predicted)
CDH11	Cadherin 11	hsa-miR-30e-5p (and other miRNAs w/seed GUAACA)	High (predicted)
		hsa-miR-193b-5p (miRNAs w/seed GGGUUUU)	High (predicted)
CDKN1A	Cyclin dependent kinase inhibitor 1A	hsa-miR-576-5p (miRNAs w/seed UUCUAAU)	High (predicted)
		hsa-miR-9-5p (and other miRNAs w/seed CUUUGGU)	Experimentally Observed
CDKN2A	Cyclin dependent kinase inhibitor 2A	hsa-miR-612 (and other miRNAs w/seed CUGGCA)	High (predicted)
		hsa-miR-7c-3p (and other miRNAs w/seed UGUACAA)	High (predicted)
CFTR	CF transmembrane conductance regulator	hsa-miR-205-5p (and other miRNAs w/seed CCUUCAU)	High (predicted)
		hsa-miR-18a-5p (and other miRNAs w/seed AAGGUGC)	Experimentally Observed
CHAD	Chondroaderin	hsa-miR-21-5p (and other miRNAs w/seed AGCUUAU)	Experimentally Observed
		hsa-miR-32-5p (and other miRNAs w/seed AUUGCAC)	Experimentally Observed
CFTR	CF transmembrane conductance regulator	hsa-miR-98-5p (and other miRNAs w/seed GAGGUAG)	High (predicted)
		hsa-miR-106a-5p (and other miRNAs w/seed AAAGUGC)	Experimentally Observed
CHAD	Chondroaderin	hsa-miR-365a-3p (and other miRNAs w/seed AAUGCCC)	High (predicted)
		hsa-miR-372-3p (and other miRNAs w/seed AAGUGCU)	Experimentally Observed
CFTR	CF transmembrane conductance regulator	hsa-miR-708-5p (and other miRNAs w/seed AGGAGCU)	High (predicted)
		hsa-miR-1255a (and other miRNAs w/seed GGAUGAG)	High (predicted)
CHAD	Chondroaderin	hsa-miR-24-3p (and other miRNAs w/seed GGCUCAG)	Experimentally Observed
		hsa-miR-125b-5p (and other miRNAs w/seed CCCUGAG)	Experimentally Observed
CFTR	CF transmembrane conductance regulator	hsa-miR-500a-3p (miRNAs w/seed UGCACCU)	High (predicted)
		hsa-miR-1291 (and other miRNAs w/seed GGCCUUG)	High (predicted)
CHAD	Chondroaderin	hsa-miR-377-3p (miRNAs w/seed UCACACA)	High (predicted)
		hsa-miR-379-5p (and other miRNAs w/seed GGUA GAC)	High (predicted)
CHAD	Chondroaderin	hsa-miR-107 (and other miRNAs w/seed GCAGCAU)	High (predicted)

Gene Symbol	Gene Name	miRNAs Targeting Gene	Confidence
CHMP1A	Charged multivesicular body protein 1A	hsa-miR-151a-5p (and other miRNAs w/seed CGAGGAG)	High (predicted)
		hsa-miR-182-5p (and other miRNAs w/seed UUGGCAA)	High (predicted)
		hsa-miR-361-3p (miRNAs w/seed CCCCAG)	High (predicted)
		hsa-miR-671-5p (miRNAs w/seed GGAAAGCC)	High (predicted)
		hsa-miR-6724-5p (and other miRNAs w/seed UGGGCC)	High (predicted)
CHUK	Component of inhibitor of nuclear factor kappa B kinase complex	hsa-miR-146b-5p (and other miRNAs w/seed GAGAACU)	Experimentally Observed
CNR1	Cannabinoid receptor 1	hsa-miR-19b-3p (and other miRNAs w/seed GUGCAAA)	High (predicted)
		hsa-miR-27a-5p (miRNAs w/seed GGCCUUA)	High (predicted)
		hsa-miR-29b-3p (and other miRNAs w/seed AGCACCA)	High (predicted)
		hsa-miR-193b-5p (miRNAs w/seed GGGUUU)	High (predicted)
		hsa-miR-214-3p (and other miRNAs w/seed CAGCAGG)	High (predicted)
		hsa-miR-409-5p (and other miRNAs w/seed GGUUACC)	High (predicted)
		hsa-miR-494-3p (miRNAs w/seed GAAACAU)	High (predicted)
		hsa-miR-509-3-5p (and other miRNAs w/seed ACUGCAG)	High (predicted)
		hsa-miR-539-3p (and other miRNAs w/seed UCAUACA)	High (predicted)
		hsa-miR-655-3p (and other miRNAs w/seed UAAUACA)	High (predicted)
		hsa-miR-1185-1-3p (and other miRNAs w/seed UAUACAG)	High (predicted)
		hsa-miR-4677-3p (miRNAs w/seed CUGUGAG)	High (predicted)
		hsa-miR-29b-3p (and other miRNAs w/seed AGCACCA)	Experimentally Observed
		hsa-miR-30e-5p (and other miRNAs w/seed GUAAACA)	Experimentally Observed
hsa-miR-98-5p (and other miRNAs w/seed GAGGUAG)	Experimentally Observed		
hsa-miR-218-5p (and other miRNAs w/seed UGUGUUU)	Experimentally Observed		
COL1A2	Collagen type I alpha 2 chain	hsa-miR-29b-3p (and other miRNAs w/seed AGCACCA)	Experimentally Observed
		hsa-miR-30e-5p (and other miRNAs w/seed GUAAACA)	Experimentally Observed
COL3A1	Collagen type III alpha 1 chain	hsa-miR-29b-3p (and other miRNAs w/seed AGCACCA)	Experimentally Observed
COL6A3	Collagen type VI alpha 3 chain	hsa-miR-29b-3p (and other miRNAs w/seed AGCACCA)	High (predicted)
COLEC12	Collectin subfamily member 12	hsa-miR-7-5p (and other miRNAs w/seed GGAAGAC)	High (predicted)
		hsa-miR-30d-3p (and other miRNAs w/seed UUUACAGU)	High (predicted)
CPQ	Carboxypeptidase Q	hsa-miR-632 (and other miRNAs w/seed UGUCUGC)	High (predicted)
CPT1A	Carnitine palmitoyltransferase 1A	hsa-miR-145-3p (miRNAs w/seed GAUUCUU)	High (predicted)
		hsa-miR-218-5p (and other miRNAs w/seed UGUGUUU)	High (predicted)
CPT2	Carnitine palmitoyltransferase 2	hsa-miR-324-5p (miRNAs w/seed GCAUCCC)	High (predicted)
		hsa-miR-365a-3p (and other miRNAs w/seed AAUGCCC)	High (predicted)
CSF1	Colony stimulating factor 1	hsa-miR-365a-3p (and other miRNAs w/seed AAUGCCC)	High (predicted)
		hsa-miR-130a-3p (and other miRNAs w/seed AGUGCAA)	Experimentally Observed
CSF1R	Colony stimulating factor 1 receptor	hsa-miR-3652 (and other miRNAs w/seed GGCUGGA)	High (predicted)
		hsa-miR-22-3p (miRNAs w/seed AGUGGCC)	High (predicted)
		hsa-miR-4677-3p (miRNAs w/seed CUGUGAG)	High (predicted)

Gene Symbol	Gene Name	miRNAs Targeting Gene	Confidence
CSF3	Colony stimulating factor 3	hsa-miR-542-3p (miRNAs w/seed GUGACAG)	High (predicted)
CSRP2	Cysteine and glycine rich protein 2	hsa-miR-27a-3p (and other miRNAs w/seed UCACAGU)	High (predicted)
		hsa-miR-101-3p (and other miRNAs w/seed ACAGUAC)	High (predicted)
		hsa-miR-199a-3p (and other miRNAs w/seed CAGUAGU)	High (predicted)
CST3	Cystatin C	hsa-miR-107 (and other miRNAs w/seed GCAGCAU)	High (predicted)
		hsa-miR-154-5p (miRNAs w/seed AGGUUUAU)	High (predicted)
CTF1	Cardiotrophin 1	hsa-miR-185-5p (and other miRNAs w/seed GGAGAGA)	High (predicted)
		hsa-miR-379-5p (and other miRNAs w/seed GGUAGAC)	High (predicted)
		hsa-miR-6125 (miRNAs w/seed CGGAAGG)	High (predicted)
CTN1B1	Catenin beta 1	hsa-miR-200a-3p (and other miRNAs w/seed AACACUG)	Experimentally Observed
CTSD	Cathepsin D	hsa-miR-24-3p (and other miRNAs w/seed GGCUCAG)	High (predicted)
CTSK	Cathepsin K	hsa-miR-7-5p (and other miRNAs w/seed GGAAGAC)	High (predicted)
		hsa-miR-106a-5p (and other miRNAs w/seed AAAGUGC)	High (predicted)
CTSL	Cathepsin L	hsa-miR-185-5p (and other miRNAs w/seed GGAGAGA)	High (predicted)
		hsa-miR-379-5p (and other miRNAs w/seed GGUAGAC)	High (predicted)
CXCL1	C-X-C motif chemokine ligand 1	hsa-miR-372-3p (and other miRNAs w/seed AAGUGCU)	High (predicted)
CXCL11	C-X-C motif chemokine ligand 11	hsa-miR-532-5p (and other miRNAs w/seed AUGCCUU)	High (predicted)
		hsa-miR-9-5p (and other miRNAs w/seed CUUUGGU)	High (predicted)
		hsa-miR-199a-3p (and other miRNAs w/seed CAGUAGU)	High (predicted)
		hsa-miR-221-3p (and other miRNAs w/seed GCUACAU)	High (predicted)
		hsa-miR-223-5p (miRNAs w/seed GUGUUAU)	High (predicted)
		hsa-miR-379-5p (and other miRNAs w/seed GGUAGAC)	High (predicted)
		hsa-miR-2110 (and other miRNAs w/seed UGGGGAA)	High (predicted)
CXCL12	C-X-C motif chemokine ligand 12	hsa-miR-23a-3p (and other miRNAs w/seed UCACAUU)	Experimentally Observed
		hsa-miR-140-5p (and other miRNAs w/seed AGUGGUU)	Experimentally Observed
CXCL16	C-X-C motif chemokine ligand 16	hsa-miR-185-5p (and other miRNAs w/seed GGAGAGA)	High (predicted)
		hsa-miR-340-3p (and other miRNAs w/seed CCGUCUC)	High (predicted)
		hsa-miR-451a (and other miRNAs w/seed AACCGUU)	High (predicted)
		hsa-miR-3652 (and other miRNAs w/seed GGCUUGGA)	High (predicted)
CXCL6	C-X-C motif chemokine ligand 6	hsa-miR-101-3p (and other miRNAs w/seed ACAGUAC)	High (predicted)
		hsa-miR-101-5p (miRNAs w/seed AGUUAUC)	High (predicted)
		hsa-miR-106a-5p (and other miRNAs w/seed AAAGUGC)	High (predicted)
		hsa-miR-337-3p (miRNAs w/seed UCCUAUA)	High (predicted)
		hsa-miR-425-5p (and other miRNAs w/seed AUGACAC)	High (predicted)
CXCL8	C-X-C motif chemokine ligand 8	hsa-miR-106a-5p (and other miRNAs w/seed AAAGUGC)	Experimentally Observed
		hsa-miR-146b-5p (and other miRNAs w/seed GAGAAUCU)	Experimentally Observed
		hsa-miR-493-5p (miRNAs w/seed UGUACAUCU)	High (predicted)
		hsa-miR-889-3p (miRNAs w/seed UAAUAUC)	High (predicted)
CXCR4	C-X-C motif chemokine receptor 4	hsa-miR-146b-5p (and other miRNAs w/seed GAGAAUCU)	Experimentally Observed

Gene Symbol	Gene Name	miRNAs Targeting Gene	Confidence
CYP19A1	Cytochrome P450 family 19 subfamily A member 1	hsa-miR-98-5p (and other miRNAs w/seed GAGGUAG) hsa-miR-361-3p (miRNAs w/seed CCCCCAG) hsa-miR-125ba (and other miRNAs w/seed GGAUGAG)	High (predicted) High (predicted) High (predicted)
CYP11A1	Cytochrome P450 family 1 subfamily A member 1	hsa-miR-125b-5p (and other miRNAs w/seed CCUCGAG) hsa-miR-1291 (and other miRNAs w/seed GGCCUCUG)	Experimentally Observed High (predicted)
CYP11B1	Cytochrome P450 family 1 subfamily B member 1	hsa-miR-27a-3p (and other miRNAs w/seed UCACAGU) hsa-miR-154-5p (miRNAs w/seed AGGUUUAU)	Experimentally Observed High (predicted)
CYP27A1	Cytochrome P450 family 27 subfamily A member 1	hsa-miR-200a-3p (and other miRNAs w/seed AACACUG) hsa-miR-377-3p (miRNAs w/seed UCACACA)	Experimentally Observed High (predicted)
CYP51A1	Cytochrome P450 family 51 subfamily A member 1	hsa-miR-6724-5p (and other miRNAs w/seed UGGGCCCC) hsa-miR-4667-3p (miRNAs w/seed CCCUCCU)	High (predicted) High (predicted)
CYSLTR1	Cysteinyl leukotriene receptor 1	hsa-miR-199b-5p (and other miRNAs w/seed CCAGUGU) hsa-miR-130a-3p (and other miRNAs w/seed AGUGCAA)	High (predicted) High (predicted)
DCLRE1C	DNA cross-link repair 1C	hsa-miR-98-5p (and other miRNAs w/seed GAGGUAG) hsa-miR-452-5p (and other miRNAs w/seed ACUGUUU)	High (predicted) High (predicted)
DCN	Decorin	hsa-miR-1278 (miRNAs w/seed AGUACUG) hsa-miR-3654 (miRNAs w/seed ACUGGAC)	High (predicted) High (predicted)
DDIT3	DNA damage inducible transcript 3	hsa-miR-96-5p (and other miRNAs w/seed UUGGCAC) hsa-miR-185-5p (and other miRNAs w/seed GGAGAGA)	High (predicted) Experimentally Observed
DDR1	Discoidin domain receptor tyrosine kinase 1	hsa-miR-769-5p (miRNAs w/seed GAGACCU) hsa-miR-145-5p (and other miRNAs w/seed UCCAGUU) hsa-miR-199b-5p (and other miRNAs w/seed CCAGUGU)	High (predicted) Experimentally Observed High (predicted)
DIO3	Iodothyronine deiodinase 3	hsa-miR-361-3p (miRNAs w/seed CCCCCAG) hsa-miR-6724-5p (and other miRNAs w/seed UGGGCCCC)	High (predicted) High (predicted)
DKK1	Dickkopf WNT signaling pathway inhibitor 1	hsa-miR-125b-5p (and other miRNAs w/seed CCUCGAG) hsa-miR-372-3p (and other miRNAs w/seed AAGUGCU) hsa-miR-493-3p (miRNAs w/seed GAAGGUC)	Experimentally Observed Experimentally Observed High (predicted)
DKK3	Dickkopf WNT signaling pathway inhibitor 3	hsa-miR-32-5p (and other miRNAs w/seed AUUGCAC) hsa-miR-16-5p (and other miRNAs w/seed AGCAGCA)	High (predicted) High (predicted)
DLL1	Delta like canonical Notch ligand 1	hsa-miR-34a-5p (and other miRNAs w/seed GGACGUG) hsa-miR-452-3p (miRNAs w/seed UCAUCUG)	Experimentally Observed High (predicted)
DMD	Dystrophin	hsa-miR-10394-3p (and other miRNAs w/seed GGGCGCG) hsa-miR-24-3p (and other miRNAs w/seed GGCUCAG)	High (predicted) High (predicted)
DMPK	DM1 protein kinase	hsa-miR-148a-3p (and other miRNAs w/seed CAGUGCA) hsa-miR-98-5p (and other miRNAs w/seed GAGGUAG)	High (predicted) Experimentally Observed
DNASE1L3	Deoxyribonuclease 1 like 3	hsa-miR-24-3p (and other miRNAs w/seed GGCUCAG) hsa-miR-148a-3p (and other miRNAs w/seed CAGUGCA)	High (predicted) High (predicted)
DPP4	Dipeptidyl peptidase 4	hsa-miR-98-5p (and other miRNAs w/seed GAGGUAG) hsa-miR-24-3p (and other miRNAs w/seed GGCUCAG)	Experimentally Observed High (predicted)
DRD3	Dopamine receptor D3	hsa-miR-101-3p (and other miRNAs w/seed ACAGUAC) hsa-miR-148a-3p (and other miRNAs w/seed CAGUGCA)	High (predicted) Experimentally Observed
DUSP1	Dual specificity phosphatase 1	hsa-miR-425-3p (miRNAs w/seed UCGGAA)	High (predicted)

Gene Symbol	Gene Name	miRNAs Targeting Gene	Confidence
DUSP6	Dual specificity phosphatase 6	hsa-miR-145-5p (and other miRNAs w/seed UCCAGUU) hsa-miR-1185-1-3p (and other miRNAs w/seed UAUACAG)	High (predicted) High (predicted)
DYM	Dymeclin	hsa-miR-29b-3p (and other miRNAs w/seed AGCACCA) hsa-miR-450a-5p (and other miRNAs w/seed UUUUGCGA) hsa-miR-455-5p (and other miRNAs w/seed AUGUGCC) hsa-miR-612 (and other miRNAs w/seed CUGGCGA) hsa-miR-3652 (and other miRNAs w/seed GGCUGGA)	High (predicted) High (predicted) High (predicted) High (predicted) High (predicted)
E2F1	E2F transcription factor 1	hsa-miR-18a-5p (and other miRNAs w/seed AAGGUGC) hsa-miR-106a-5p (and other miRNAs w/seed AAAAGUGC)	Experimentally Observed Experimentally Observed
EDN1	Endothelin 1	hsa-miR-98-5p (and other miRNAs w/seed GAGGUAG) hsa-miR-134-5p (and other miRNAs w/seed GUGACUG) hsa-miR-671-5p (miRNAs w/seed GGAAAGCC)	High (predicted) High (predicted) High (predicted)
EFNB1	Ephrin B1	hsa-miR-34a-5p (and other miRNAs w/seed GGCAGUG)	High (predicted)
EFNB2	Ephrin B2	hsa-miR-19b-3p (and other miRNAs w/seed GUGCAAA) hsa-miR-151a-5p (and other miRNAs w/seed CGAGGAG)	High (predicted) High (predicted)
EFNB3	Ephrin B3	hsa-miR-3652 (and other miRNAs w/seed GGCUGGA)	High (predicted)
EGFR	Epidermal growth factor receptor	hsa-miR-7-5p (and other miRNAs w/seed GGAAGAC) hsa-miR-16-5p (and other miRNAs w/seed AGCAGCA) hsa-miR-134-5p (and other miRNAs w/seed GUGACUG) hsa-miR-218-5p (and other miRNAs w/seed UGUGCUU) hsa-miR-29b-3p (and other miRNAs w/seed AGCACCA)	Experimentally Observed Experimentally Observed High (predicted) Experimentally Observed High (predicted)
ELN	Elastin	hsa-miR-29b-3p (and other miRNAs w/seed AGCACCA)	High (predicted)
ENPP1	Ectonucleotide pyrophosphatase/phosphodiesterase 1	hsa-miR-3613-3p (miRNAs w/seed CAAAAA)	High (predicted)
ENTPD1	Ectonucleoside triphosphate diphosphohydrolase 1	hsa-miR-24-2-5p (and other miRNAs w/seed GCCUACU) hsa-miR-125b-5p (and other miRNAs w/seed CCCUGAG) hsa-miR-758-3p (miRNAs w/seed UUGUGAC)	High (predicted) High (predicted) High (predicted)
EPHA2	EPH receptor A2	hsa-miR-26b-5p (and other miRNAs w/seed UCAAGUA)	Experimentally Observed
EPHB3	EPH receptor B3	hsa-miR-6724-5p (and other miRNAs w/seed UGGGCC)	High (predicted)
EPHB4	EPH receptor B4	hsa-miR-6724-5p (and other miRNAs w/seed UGGGCC)	High (predicted)
ERBB2	ErbB2 receptor tyrosine kinase 2	hsa-miR-125b-5p (and other miRNAs w/seed CCCUGAG)	Experimentally Observed
ERCC5	ERCC excision repair 5, endonuclease	hsa-miR-450a-5p (and other miRNAs w/seed UUUUGCGA)	High (predicted)
ESR1	Estrogen receptor 1	hsa-miR-18a-5p (and other miRNAs w/seed AAGGUGC) hsa-miR-19b-3p (and other miRNAs w/seed GUGCAAA) hsa-miR-22-3p (miRNAs w/seed AGCUGCC) hsa-miR-106a-5p (and other miRNAs w/seed AAAAGUGC) hsa-miR-130a-3p (and other miRNAs w/seed AGUGCAA)	Experimentally Observed Experimentally Observed Experimentally Observed Experimentally Observed High (predicted)
		hsa-miR-181d-5p (and other miRNAs w/seed ACAUUCA) hsa-miR-221-3p (and other miRNAs w/seed GCUACAU) hsa-miR-372-3p (and other miRNAs w/seed AAGUCU)	Experimentally Observed Experimentally Observed Experimentally Observed
ESR2	Estrogen receptor 2	hsa-miR-140-3p (and other miRNAs w/seed ACCACAG)	High (predicted)

Gene Symbol	Gene Name	miRNAs Targeting Gene	Confidence
ETS1	ETS proto-oncogene 1, transcription factor	hsa-miR-148a-3p (and other miRNAs w/seed CAGUGCA)	High (predicted)
		hsa-miR-148b-5p (and other miRNAs w/seed AGUUCUG)	High (predicted)
		hsa-miR-199b-5p (and other miRNAs w/seed CCAGUGU)	Experimentally Observed
		hsa-miR-208b-3p (and other miRNAs w/seed UAAGACG)	Experimentally Observed
		hsa-miR-324-5p (miRNAs w/seed GCAUCCC)	High (predicted)
F2R	Coagulation factor II thrombin receptor	hsa-miR-377-3p (miRNAs w/seed LCAACACA)	High (predicted)
		hsa-miR-1255a (and other miRNAs w/seed GGAUGAG)	High (predicted)
		hsa-miR-144-5p (miRNAs w/seed GAUAUCA)	High (predicted)
		hsa-miR-190a-5p (and other miRNAs w/seed GAUAUGU)	High (predicted)
		hsa-miR-769-5p (miRNAs w/seed GAGACCU)	High (predicted)
F3	Coagulation factor III, tissue factor	hsa-miR-18a-5p (and other miRNAs w/seed AAGGUGC)	High (predicted)
		hsa-miR-19b-3p (and other miRNAs w/seed GUGCAAA)	High (predicted)
		hsa-miR-106a-5p (and other miRNAs w/seed AAAGUGC)	High (predicted)
		hsa-miR-340-3p (and other miRNAs w/seed CCGUCUC)	High (predicted)
		hsa-miR-324-5p (miRNAs w/seed GCAUCCC)	High (predicted)
F7	Coagulation factor VII	hsa-miR-4667-3p (miRNAs w/seed CCCUCCU)	High (predicted)
		hsa-miR-98-5p (and other miRNAs w/seed GAGGUAG)	Experimentally Observed
FADS2	Fatty acid desaturase 2	hsa-miR-3917 (miRNAs w/seed CUCGGAC)	High (predicted)
		hsa-miR-4667-3p (miRNAs w/seed CCCUCCU)	High (predicted)
FASLG	Fas ligand	hsa-miR-21-5p (and other miRNAs w/seed AGCUJAU)	Experimentally Observed
		hsa-miR-24-3p (and other miRNAs w/seed GGCUCAG)	High (predicted)
FBLN1	Fibulin 1	hsa-miR-98-5p (and other miRNAs w/seed GAGGUAG)	High (predicted)
		hsa-miR-24-3p (and other miRNAs w/seed GGCUCAG)	High (predicted)
FBN1	Fibrillin 1	hsa-miR-9-5p (and other miRNAs w/seed CUUUUGU)	High (predicted)
		hsa-miR-29b-3p (and other miRNAs w/seed AGCACCA)	Experimentally Observed
FCGRT	Fc fragment of IgG receptor and transporter	hsa-miR-374b-3p (miRNAs w/seed UUAAGCAG)	High (predicted)
FGF1	Fibroblast growth factor 1	hsa-miR-143-5p (and other miRNAs w/seed GUGCAGU)	High (predicted)
FGF2	Fibroblast growth factor 2	hsa-miR-16-5p (and other miRNAs w/seed AGCAGCA)	Experimentally Observed
FGF5	Fibroblast growth factor 5	hsa-miR-30d-3p (and other miRNAs w/seed UJUACAGU)	High (predicted)
		hsa-miR-145-5p (and other miRNAs w/seed UCCAGUU)	High (predicted)
FGF7	Fibroblast growth factor 7	hsa-miR-16-5p (and other miRNAs w/seed AGCAGCA)	Experimentally Observed
		hsa-miR-34a-5p (and other miRNAs w/seed GGCAGUG)	High (predicted)
		hsa-miR-199a-3p (and other miRNAs w/seed CAGUAGU)	High (predicted)
		hsa-miR-215-5p (and other miRNAs w/seed UGACCUA)	High (predicted)
		hsa-miR-223-5p (miRNAs w/seed GUGUJAUU)	High (predicted)
FGF9	Fibroblast growth factor 9	hsa-miR-511-3p (miRNAs w/seed AUGUGUA)	High (predicted)
		hsa-miR-140-5p (and other miRNAs w/seed AGUGGUU)	High (predicted)
FGFR1	Fibroblast growth factor receptor 1	hsa-miR-383-5p (miRNAs w/seed GAUCAGA)	High (predicted)
		hsa-miR-16-5p (and other miRNAs w/seed AGCAGCA)	Experimentally Observed

Gene Symbol	Gene Name	miRNAs Targeting Gene	Confidence
FLI1	Fli-1 proto-oncogene, ETS transcription factor	hsa-miR-145-5p (and other miRNAs w/seed UCCAGUU) hsa-miR-200b-3p (and other miRNAs w/seed AAUACUG) hsa-miR-1291 (and other miRNAs w/seed GGCCUCG)	Experimentally Observed High (predicted) High (predicted)
FLT3LG	Fms related receptor tyrosine kinase 3 ligand	hsa-miR-1287-5p (miRNAs w/seed GCUGGAU)	High (predicted)
FMN1	Formin 1	hsa-miR-205-5p (and other miRNAs w/seed CCUUCAU)	High (predicted)
FMOD	Fibromodulin	hsa-miR-612 (and other miRNAs w/seed CUGGGCA)	High (predicted)
FN1	Fibronectin 1	hsa-miR-199a-3p (and other miRNAs w/seed CAGUAGU) hsa-miR-425-3p (miRNAs w/seed UCGGGAA)	Experimentally Observed High (predicted)
FOS	Fos proto-oncogene, AP-1 transcription factor subunit	hsa-miR-7-5p (and other miRNAs w/seed GGAAGAC)	Experimentally Observed
FOSL1	FOS like 1, AP-1 transcription factor subunit	hsa-miR-101-3p (and other miRNAs w/seed ACAGUAC) hsa-miR-221-3p (and other miRNAs w/seed GCUACAU)	High (predicted) Experimentally Observed
FOSL2	FOS like 2, AP-1 transcription factor subunit	hsa-miR-34a-5p (and other miRNAs w/seed GGCAGUG) hsa-miR-130a-3p (and other miRNAs w/seed AGUGCAA)	High (predicted) High (predicted)
FOXF1	Forkhead box F1	hsa-miR-143-3p (and other miRNAs w/seed GGAUGA) hsa-miR-361-3p (miRNAs w/seed CCCCAG)	High (predicted) High (predicted)
FPR1	Formyl peptide receptor 1	hsa-miR-3917 (miRNAs w/seed CUCGGAC)	High (predicted)
FZD8	Frizzled class receptor 8	hsa-miR-4667-3p (miRNAs w/seed CCCUCCU)	High (predicted)
GAS1	Growth arrest specific 1	hsa-miR-99a-5p (and other miRNAs w/seed ACCCGUA) hsa-miR-34a-5p (and other miRNAs w/seed GGCAGUG)	High (predicted) High (predicted)
GAS6	Growth arrest specific 6	hsa-miR-493-5p (miRNAs w/seed UGUACA U) hsa-miR-4796-5p (miRNAs w/seed GUCUAUA)	High (predicted) High (predicted)
GBA	Glucosylceramidase beta	hsa-miR-3917 (miRNAs w/seed CUCGGAC) hsa-miR-22-3p (miRNAs w/seed AGCUGCC)	High (predicted) High (predicted)
GFRA2	GDNF family receptor alpha 2	hsa-miR-1291 (and other miRNAs w/seed GGCCUCG)	High (predicted)
GHR	Growth hormone receptor	hsa-miR-2110 (and other miRNAs w/seed UGGGAA) hsa-miR-3652 (and other miRNAs w/seed GGUGGA)	High (predicted) High (predicted)
GJA1	Gap junction protein alpha 1	hsa-miR-6724-5p (and other miRNAs w/seed UGGGCC) hsa-miR-632 (and other miRNAs w/seed UGUCUGC)	High (predicted) High (predicted)
GJA5	Gap junction protein alpha 5	hsa-miR-3613-3p (miRNAs w/seed CAAAAA)	High (predicted)
GJC1	Gap junction protein gamma 1	hsa-miR-19b-3p (and other miRNAs w/seed GUGCAA) hsa-miR-101-3p (and other miRNAs w/seed ACAGUAC) hsa-miR-130a-3p (and other miRNAs w/seed AGUGCAA)	High (predicted) High (predicted) High (predicted)
GLP1R	Glucagon like peptide 1 receptor	hsa-miR-483-3p (miRNAs w/seed CACUCCU) hsa-miR-199b-5p (and other miRNAs w/seed CCAGUGU) hsa-miR-7-5p (and other miRNAs w/seed GGAAGAC)	Experimentally Observed High (predicted) High (predicted)
		hsa-miR-125b-5p (and other miRNAs w/seed CCUGAG) hsa-miR-612 (and other miRNAs w/seed CUGGGCA)	High (predicted) High (predicted)
		hsa-miR-2110 (and other miRNAs w/seed UGGGAA)	High (predicted)

Gene Symbol	Gene Name	miRNAs Targeting Gene	Confidence
ONE	Glucosamine (UDP-N-acetyl)-2-epimerase/N-acetylmannosamine kinase	hsa-miR-24-3p (and other miRNAs w/seed GGCUCAG) hsa-miR-96-5p (and other miRNAs w/seed UUGGCAC) hsa-miR-493-3p (miRNAs w/seed GAA GGUC)	High (predicted) High (predicted) High (predicted)
GRB2	Growth factor receptor bound protein 2	hsa-miR-16-5p (and other miRNAs w/seed AGCAGCA) hsa-miR-27a-3p (and other miRNAs w/seed UCACAGU) hsa-miR-223-5p (miRNAs w/seed GUGUAUU) hsa-miR-516b-5p (miRNAs w/seed UCUGGAG)	Experimentally Observed Experimentally Observed High (predicted) High (predicted)
GREM1	Gremlin 1, DAN family BMP antagonist	hsa-miR-30d-3p (and other miRNAs w/seed UUUUCAGU) hsa-miR-151a-3p (and other miRNAs w/seed UAAGACUG) hsa-miR-190a-5p (and other miRNAs w/seed GAUAUGU) hsa-miR-199a-3p (and other miRNAs w/seed CAGUAGU) hsa-miR-218-5p (and other miRNAs w/seed UGUGCUU) hsa-miR-455-5p (and other miRNAs w/seed AUGUGCC) hsa-miR-4485-3p (miRNAs w/seed AACGGCC)	High (predicted) High (predicted) High (predicted) High (predicted) High (predicted) High (predicted) High (predicted)
GRPR	Gastrin releasing peptide receptor	hsa-miR-125b-2-3p (and other miRNAs w/seed CACAAAGU)	High (predicted)
GUCY1A1	Guanylate cyclase 1 soluble subunit alpha 1	hsa-miR-106a-5p (and other miRNAs w/seed AAAGUGC) hsa-miR-372-3p (and other miRNAs w/seed AAGUGCU)	High (predicted) High (predicted)
GUCY1B1	Guanylate cyclase 1 soluble subunit beta 1	hsa-miR-24-2-5p (and other miRNAs w/seed GCCUACU) hsa-miR-190a-5p (and other miRNAs w/seed GAUAUGU)	High (predicted) High (predicted)
HAS2	Hyaluronan synthase 2	hsa-miR-96-5p (and other miRNAs w/seed UUGGCAC) hsa-miR-182-5p (and other miRNAs w/seed UUGGCAA) hsa-miR-4485-3p (miRNAs w/seed AACGGCC)	High (predicted) High (predicted) High (predicted)
HBEGF	Heparin binding EGF like growth factor	hsa-miR-27a-3p (and other miRNAs w/seed UCACAGU) hsa-miR-96-5p (and other miRNAs w/seed UUGGCAC) hsa-miR-181c-3p (miRNAs w/seed ACCAUCG) hsa-miR-182-5p (and other miRNAs w/seed UUGGCAA) hsa-miR-193b-5p (miRNAs w/seed GGGGUUU)	High (predicted) High (predicted) High (predicted) High (predicted) High (predicted)
HDAC1	Histone deacetylase 1	hsa-miR-34a-5p (and other miRNAs w/seed GGCAGUG) hsa-miR-214-3p (and other miRNAs w/seed CAGCAGG) hsa-miR-2110 (and other miRNAs w/seed UGGGGAA)	Experimentally Observed High (predicted) High (predicted)
HIF1A	Hypoxia inducible factor 1 subunit alpha	hsa-miR-18a-5p (and other miRNAs w/seed AAGGUGC) hsa-miR-143-5p (and other miRNAs w/seed GUGCAGU)	Experimentally Observed High (predicted)
HMCN1	Hemichentin 1	hsa-miR-199b-5p (and other miRNAs w/seed CCAGUGU) hsa-miR-660-5p (and other miRNAs w/seed ACCCAUU) hsa-miR-29b-3p (and other miRNAs w/seed AGCACA) hsa-miR-199b-5p (and other miRNAs w/seed CCAGUGU)	Experimentally Observed High (predicted) High (predicted) Experimentally Observed

Gene Symbol	Gene Name	miRNAs Targeting Gene	Confidence
HMOX1	Heme oxygenase 1	hsa-miR-16-5p (and other miRNAs w/seed AGCAGCA)	Experimentally Observed
		hsa-miR-98-5p (and other miRNAs w/seed GAGGUAG)	Experimentally Observed
		hsa-miR-377-3p (miRNAs w/seed UCACACA)	High (predicted)
		hsa-miR-494-3p (miRNAs w/seed GAAACAU)	Experimentally Observed
HOXA13	Homeobox A13	hsa-miR-1291 (and other miRNAs w/seed GGCCCUUG)	High (predicted)
		hsa-miR-2110 (and other miRNAs w/seed UGGGGAA)	High (predicted)
		hsa-miR-34a-5p (and other miRNAs w/seed GGCAGUG)	High (predicted)
		hsa-miR-612 (and other miRNAs w/seed CUGGGCA)	High (predicted)
HPRT1	Hypoxanthine phosphoribosyltransferase 1	hsa-miR-1278 (miRNAs w/seed AGUACUG)	High (predicted)
		hsa-miR-130a-3p (and other miRNAs w/seed AGUGCAA)	High (predicted)
		hsa-miR-450a-5p (and other miRNAs w/seed UUUGCCGA)	High (predicted)
		hsa-miR-671-5p (miRNAs w/seed GGAAGCC)	High (predicted)
HS6ST1	Heparan sulfate 6-O-sulfotransferase 1	hsa-miR-6724-5p (and other miRNAs w/seed UGGGGCCC)	High (predicted)
		hsa-miR-126-5p (and other miRNAs w/seed AUUAUUA)	High (predicted)
		hsa-miR-142-5p (and other miRNAs w/seed AUAAAAGU)	High (predicted)
		hsa-miR-214-5p (miRNAs w/seed GCCUGUC)	High (predicted)
HTR2C	5-hydroxytryptamine receptor 2C	hsa-miR-34a-5p (and other miRNAs w/seed GGCAAGUG)	High (predicted)
		hsa-miR-409-5p (and other miRNAs w/seed GGUUACC)	High (predicted)
		hsa-miR-16-5p (and other miRNAs w/seed AGCAGCA)	Experimentally Observed
		hsa-miR-221-3p (and other miRNAs w/seed GCUACAU)	Experimentally Observed
HYAL3	Hyaluronidase 3	hsa-miR-19b-3p (and other miRNAs w/seed GUGCAAA)	High (predicted)
		hsa-miR-125b-5p (and other miRNAs w/seed CCCUGAG)	Experimentally Observed
		hsa-miR-1185-1-3p (and other miRNAs w/seed UAUACAG)	High (predicted)
		hsa-miR-7-5p (and other miRNAs w/seed GGAAGAC)	High (predicted)
IGF1	Insulin like growth factor 1	hsa-miR-16-5p (and other miRNAs w/seed AGCAGCA)	Experimentally Observed
		hsa-miR-27a-3p (and other miRNAs w/seed UCACAGU)	Experimentally Observed
		hsa-miR-130a-3p (and other miRNAs w/seed AGUGCAA)	High (predicted)
		hsa-miR-483-3p (miRNAs w/seed CACUCCU)	Experimentally Observed
IGF1R	Insulin like growth factor 1 receptor	hsa-miR-16-5p (and other miRNAs w/seed AGCAGCA)	Experimentally Observed
		hsa-miR-98-5p (and other miRNAs w/seed GAGGUAG)	High (predicted)
		hsa-miR-99a-5p (and other miRNAs w/seed ACCCGUA)	Experimentally Observed
		hsa-miR-145-5p (and other miRNAs w/seed UCCAGUU)	Experimentally Observed
IGF2	Insulin like growth factor 2	hsa-miR-182-5p (and other miRNAs w/seed UUGGCAA)	Experimentally Observed
		hsa-miR-218-5p (and other miRNAs w/seed UGUUCUU)	High (predicted)
		hsa-miR-425-3p (miRNAs w/seed UCGGGAA)	High (predicted)
		hsa-miR-2110 (and other miRNAs w/seed UGGGGAA)	High (predicted)
		hsa-miR-4662a-5p (miRNAs w/seed UAGCCAA)	High (predicted)

Gene Symbol	Gene Name	miRNAs Targeting Gene	Confidence
IGFBP3	Insulin like growth factor binding protein 3	hsa-miR-19b-3p (and other miRNAs w/seed GUGCAAA)	High (predicted)
		hsa-miR-125b-5p (and other miRNAs w/seed CCUGAG)	Experimentally Observed
		hsa-miR-628-5p (and other miRNAs w/seed UGUGAC)	High (predicted)
IGFBP4	Insulin like growth factor binding protein 4	hsa-miR-1255a (and other miRNAs w/seed GGAUGAG)	High (predicted)
		hsa-miR-3652 (and other miRNAs w/seed GGCUUGA)	High (predicted)
IGFBP5	Insulin like growth factor binding protein 5	hsa-miR-140-5p (and other miRNAs w/seed AGUGGUU)	Experimentally Observed
IGFBP6	Insulin like growth factor binding protein 6	hsa-miR-143-3p (and other miRNAs w/seed GAGAUGA)	Experimentally Observed
		hsa-miR-1291 (and other miRNAs w/seed GGCCUG)	High (predicted)
IKKB	Inhibitor of nuclear factor kappa B kinase subunit beta	hsa-miR-16-5p (and other miRNAs w/seed AGCAGCA)	High (predicted)
		hsa-miR-196a-5p (and other miRNAs w/seed AGGUAGU)	Experimentally Observed
		hsa-miR-214-3p (and other miRNAs w/seed CAGCAGG)	High (predicted)
		hsa-miR-708-5p (and other miRNAs w/seed AGGAGCU)	High (predicted)
		hsa-miR-4677-3p (miRNAs w/seed CUGUGAG)	High (predicted)
		hsa-miR-98-5p (and other miRNAs w/seed GAGGUAG)	High (predicted)
		hsa-miR-146b-5p (and other miRNAs w/seed GAGAAUCU)	Experimentally Observed
		hsa-miR-425-5p (and other miRNAs w/seed AUGACAC)	High (predicted)
		hsa-miR-142-5p (and other miRNAs w/seed AUAAGU)	High (predicted)
		hsa-miR-144-5p (miRNAs w/seed GAUAUCA)	High (predicted)
IL19	Interleukin 19	hsa-miR-140-3p (and other miRNAs w/seed ACCACAG)	High (predicted)
		hsa-miR-24-3p (and other miRNAs w/seed GGCUCAG)	High (predicted)
IL1A	Interleukin 1 alpha	hsa-miR-365a-3p (and other miRNAs w/seed AAUGCCC)	High (predicted)
		hsa-miR-532-5p (and other miRNAs w/seed AUGCCUU)	High (predicted)
IL1B	Interleukin 1 beta	hsa-miR-30d-3p (and other miRNAs w/seed UUUUCAGU)	High (predicted)
		hsa-miR-125b-1-3p (miRNAs w/seed CGGGUUA)	Experimentally Observed
IL1RL2	Interleukin 1 receptor like 2	hsa-miR-1291 (and other miRNAs w/seed GGCCUG)	High (predicted)
		hsa-miR-146b-5p (and other miRNAs w/seed GAGAAUCU)	Experimentally Observed
IL2	Interleukin 2	hsa-miR-361-3p (miRNAs w/seed CCCCAG)	High (predicted)
		hsa-miR-181d-5p (and other miRNAs w/seed ACAUUCA)	High (predicted)
IL20RB	Interleukin 20 receptor subunit beta	hsa-miR-190a-5p (and other miRNAs w/seed GAUAUGU)	High (predicted)
		hsa-miR-421 (and other miRNAs w/seed UCAACAG)	High (predicted)
		hsa-miR-6507-5p (miRNAs w/seed AAGAAUA)	High (predicted)
IL24	Interleukin 24	hsa-miR-1291 (and other miRNAs w/seed GGCCUG)	High (predicted)
		hsa-miR-29b-3p (and other miRNAs w/seed AGCACCA)	High (predicted)
IL2RB	Interleukin 2 receptor subunit beta	hsa-miR-203a-3p (and other miRNAs w/seed UGAAUUG)	High (predicted)
		hsa-miR-214-3p (and other miRNAs w/seed CAGCAGG)	High (predicted)



Gene Symbol	Gene Name	miRNAs Targeting Gene	Confidence
JAZF1	JAZF zinc finger 1	hsa-miR-19b-3p (and other miRNAs w/seed GUGCAAA) hsa-miR-96-5p (and other miRNAs w/seed UUGGCAC)	High (predicted) High (predicted)
JUN	Jun proto-oncogene, AP-1 transcription factor subunit	hsa-miR-16-5p (and other miRNAs w/seed AGCAGCA) hsa-miR-30e-5p (and other miRNAs w/seed GUAACA) hsa-miR-3917 (miRNAs w/seed CUCGGAC) hsa-miR-4667-3p (miRNAs w/seed CCCUCCU) hsa-miR-377-3p (miRNAs w/seed UCACACA)	Experimentally Observed Experimentally Observed High (predicted) High (predicted) High (predicted)
KAZN	Kazrin, periplakin interacting protein	hsa-miR-34a-5p (and other miRNAs w/seed GGCAGUG) hsa-miR-221-3p (and other miRNAs w/seed GCUACAU)	High (predicted) Experimentally Observed
KIT	KIT proto-oncogene, receptor tyrosine kinase	hsa-miR-335-5p (and other miRNAs w/seed CAAGAGC) hsa-miR-494-3p (miRNAs w/seed GAAACAU) hsa-miR-671-5p (miRNAs w/seed GGAAGCC) hsa-miR-4485-3p (miRNAs w/seed AACGGCC)	Experimentally Observed Experimentally Observed High (predicted) High (predicted)
KITLG	KIT ligand	hsa-miR-16-5p (and other miRNAs w/seed AGCAGCA) hsa-miR-27a-3p (and other miRNAs w/seed UCACAGU) hsa-miR-182-5p (and other miRNAs w/seed UUGGCAA)	Experimentally Observed High (predicted) High (predicted)
KLF2	Kruppel like factor 2	hsa-miR-32-5p (and other miRNAs w/seed AUUGCAC) hsa-miR-101-3p (and other miRNAs w/seed ACAGUAC)	High (predicted) High (predicted)
KLF4	Kruppel like factor 4	hsa-miR-7-5p (and other miRNAs w/seed GGAAAGC) hsa-miR-10b-5p (and other miRNAs w/seed ACCUGU) hsa-miR-29b-3p (and other miRNAs w/seed AGACCA) hsa-miR-32-5p (and other miRNAs w/seed AUUGCAC) hsa-miR-34a-5p (and other miRNAs w/seed GGCAGUG) hsa-miR-145-5p (and other miRNAs w/seed UCCAGUU)	High (predicted) Experimentally Observed Experimentally Observed High (predicted) High (predicted) High (predicted) Experimentally Observed
KRAS	KRAS proto-oncogene, GTPase	hsa-miR-98-5p (and other miRNAs w/seed GAGGUAG) hsa-miR-143-3p (and other miRNAs w/seed GAGUAGA) hsa-miR-181d-5p (and other miRNAs w/seed ACAUUCA) hsa-miR-532-5p (and other miRNAs w/seed AUGCCUU) hsa-miR-19b-3p (and other miRNAs w/seed GUGCAAA) hsa-miR-130a-3p (and other miRNAs w/seed AGUGCAA) hsa-miR-148a-3p (and other miRNAs w/seed CAGUGCA) hsa-miR-221-5p (and other miRNAs w/seed CCUGGCA)	Experimentally Observed Experimentally Observed Experimentally Observed High (predicted) High (predicted) High (predicted) High (predicted) High (predicted)
LDLR	Low density lipoprotein receptor	hsa-miR-9-5p (and other miRNAs w/seed CUUUGGU) hsa-miR-6724-5p (and other miRNAs w/seed UGGGCC) hsa-miR-22-3p (miRNAs w/seed AGCUGCC)	High (predicted) High (predicted) High (predicted)
LDLRAP1	Low density lipoprotein receptor adaptor protein 1	hsa-miR-151a-5p (and other miRNAs w/seed CGAGGAG) hsa-miR-493-3p (miRNAs w/seed GAAAGGUC) hsa-miR-671-5p (miRNAs w/seed GGAAGCC)	High (predicted) High (predicted) High (predicted)
LGALS1	Galectin 1		
LGALS3BP	Galectin 3 binding protein		



Gene Symbol	Gene Name	miRNAs Targeting Gene	Confidence
MICA	MHC class I polypeptide-related sequence A	hsa-miR-106a-5p (and other miRNAs w/seed AAAGUGC) hsa-miR-372-3p (and other miRNAs w/seed AAGUGCU)	Experimentally Observed Experimentally Observed
MK167	Marker of proliferation Ki-67	hsa-miR-483-3p (miRNAs w/seed CACUCCU)	Experimentally Observed
MMP1	Matrix metalloproteinase 1	hsa-miR-145-5p (and other miRNAs w/seed UCCAGUU) hsa-miR-221-3p (and other miRNAs w/seed GCUACAU)	Experimentally Observed Experimentally Observed
MMP11	Matrix metalloproteinase 11	hsa-miR-1291 (and other miRNAs w/seed GGCCUUG)	High (predicted)
MMP13	Matrix metalloproteinase 13	hsa-miR-1-5p (and other miRNAs w/seed CAUACUU)	High (predicted)
MMP14	Matrix metalloproteinase 14	hsa-miR-27a-3p (and other miRNAs w/seed UCACAGU)	Experimentally Observed
MMP16	Matrix metalloproteinase 16	hsa-miR-181d-5p (and other miRNAs w/seed ACAUUA) hsa-miR-146b-5p (and other miRNAs w/seed GAGAAACU)	Experimentally Observed Experimentally Observed
MMP19	Matrix metalloproteinase 19	hsa-miR-3613-3p (miRNAs w/seed CAAAAA)	High (predicted)
MMP3	Matrix metalloproteinase 3	hsa-miR-130a-3p (and other miRNAs w/seed AGUGCAA) hsa-miR-106a-5p (and other miRNAs w/seed AAAGUGC)	High (predicted) Experimentally Observed
MMP8	Matrix metalloproteinase 8	hsa-miR-421 (and other miRNAs w/seed UCAACAG)	High (predicted)
MNT	MAX network transcriptional repressor	hsa-miR-24-3p (and other miRNAs w/seed GGCUCAG) hsa-miR-3652 (and other miRNAs w/seed GGCUGGA)	High (predicted) High (predicted)
MRC1	Mannose receptor C-type 1	hsa-miR-23a-3p (and other miRNAs w/seed UCACAUU)	High (predicted)
MSR1	Macrophage scavenger receptor 1	hsa-miR-655-3p (and other miRNAs w/seed UAAUACA) hsa-miR-1278 (miRNAs w/seed AGUACUG)	High (predicted) High (predicted)
MSX1	Msh homeobox 1	hsa-miR-3652 (and other miRNAs w/seed GGCUGGA)	High (predicted)
MSX2	Msh homeobox 2	hsa-miR-1291 (and other miRNAs w/seed GGCCUUG)	High (predicted)
MT-ND5	Mitochondrially encoded NADH:ubiquinone oxidoreductase core subunit 5	hsa-miR-140-5p (and other miRNAs w/seed AGUGGUU) hsa-miR-585-3p (miRNAs w/seed GGGCGUA)	High (predicted) High (predicted)
MTOR	Mechanistic target of rapamycin kinase	hsa-miR-96-5p (and other miRNAs w/seed UUGGCAC) hsa-miR-99a-5p (and other miRNAs w/seed ACCCGUA) hsa-miR-199a-3p (and other miRNAs w/seed CAGUAGU)	High (predicted) Experimentally Observed Experimentally Observed
MYB	MYB proto-oncogene, transcription factor	hsa-miR-16-5p (and other miRNAs w/seed AGCAGCA) hsa-miR-34a-5p (and other miRNAs w/seed GGCAGUG) hsa-miR-140-3p (and other miRNAs w/seed ACCACAG)	Experimentally Observed Experimentally Observed High (predicted)
MYC	MYC proto-oncogene, bHLH transcription factor	hsa-miR-24-3p (and other miRNAs w/seed GGCUCAG) hsa-miR-34a-5p (and other miRNAs w/seed GGCAGUG) hsa-miR-98-5p (and other miRNAs w/seed GAGGUAG) hsa-miR-145-5p (and other miRNAs w/seed UCCAGUU)	Experimentally Observed Experimentally Observed Experimentally Observed Experimentally Observed
MYD88	MYD88 innate immune signal transduction adaptor	hsa-miR-125b-5p (and other miRNAs w/seed CCCUGAG) hsa-miR-126-5p (and other miRNAs w/seed AUUAUUA)	Experimentally Observed High (predicted)
MYH1	Myosin heavy chain 1	hsa-miR-9-5p (and other miRNAs w/seed CUUUGGU)	High (predicted)
MYH2	Myosin heavy chain 2	hsa-miR-23a-3p (and other miRNAs w/seed UCACAUU) hsa-miR-214-5p (miRNAs w/seed GCCUGUC)	High (predicted) High (predicted)

Gene Symbol	Gene Name	miRNAs Targeting Gene	Confidence
MYLK	Myosin light chain kinase	hsa-miR-16-5p (and other miRNAs w/seed AGCAGCA) hsa-miR-142-3p (and other miRNAs w/seed GUAGUGU)	High (predicted) High (predicted)
MYO1C	Myosin IC	hsa-miR-337-3p (miRNAs w/seed UCCUAUA) hsa-miR-585-3p (miRNAs w/seed GGGCGUA)	High (predicted) High (predicted)
MYO11	Myogenic differentiation 1	hsa-miR-10394-3p (and other miRNAs w/seed GGGCGCG) hsa-miR-1255a (and other miRNAs w/seed GGAUGAG)	High (predicted) High (predicted)
MYOG	Myogenin	hsa-miR-101-3p (and other miRNAs w/seed ACAGUAC)	High (predicted)
NAGLU	N-acetyl-alpha-glucosaminidase	hsa-miR-532-5p (and other miRNAs w/seed AUGCCUU)	High (predicted)
NCF2	Neutrophil cytosolic factor 2	hsa-miR-374a-5p (and other miRNAs w/seed UAUAAUA)	High (predicted)
NCK1	NCK adaptor protein 1	hsa-miR-10b-5p (and other miRNAs w/seed ACCUCUG)	High (predicted)
NCOR2	Nuclear receptor corepressor 2	hsa-miR-27a-3p (and other miRNAs w/seed UCACAGU)	High (predicted)
NDUFS4	NADH:ubiquinone oxidoreductase subunit S4	hsa-miR-339-3p (miRNAs w/seed GAGCGCC)	High (predicted)
NDUFS7	NADH:ubiquinone oxidoreductase core subunit S7	hsa-miR-361-3p (miRNAs w/seed CCCCAG)	High (predicted)
NECTIN1	Nectin cell adhesion molecule 1	hsa-miR-34a-5p (and other miRNAs w/seed GGCAGUG) hsa-miR-214-3p (and other miRNAs w/seed CAGCAGG) hsa-miR-221-3p (and other miRNAs w/seed GCUACAU) hsa-miR-612 (and other miRNAs w/seed CUGGGCA) hsa-miR-2110 (and other miRNAs w/seed UGGGGAA)	High (predicted) High (predicted) High (predicted) High (predicted) High (predicted)
NF1	Neurofibromin 1	hsa-miR-10b-5p (and other miRNAs w/seed ACCUCUG) hsa-miR-107 (and other miRNAs w/seed GCAGCAU)	Experimentally Observed High (predicted)
NFE2L3	Nuclear factor, erythroid 2 like 3	hsa-miR-99a-5p (and other miRNAs w/seed ACCCGUA) hsa-miR-148a-3p (and other miRNAs w/seed CAGUGCA)	High (predicted) High (predicted)
NFIA	Nuclear factor I A	hsa-miR-16-5p (and other miRNAs w/seed AGCAGCA) hsa-miR-19b-3p (and other miRNAs w/seed GUGCAAA) hsa-miR-29b-3p (and other miRNAs w/seed AGCACC) hsa-miR-32-5p (and other miRNAs w/seed AUUGCAC) hsa-miR-107 (and other miRNAs w/seed GCAGCAU) hsa-miR-130a-3p (and other miRNAs w/seed AGUGCAA) hsa-miR-223-3p (miRNAs w/seed GUCAGUU) hsa-miR-3065-5p (and other miRNAs w/seed CAACAAA) hsa-miR-3613-3p (miRNAs w/seed CAAAAA)	Experimentally Observed High (predicted) High (predicted) High (predicted) Experimentally Observed High (predicted) Experimentally Observed High (predicted) High (predicted)
NFIB	Nuclear factor I B	hsa-miR-19b-3p (and other miRNAs w/seed GUGCAAA) hsa-miR-21-5p (and other miRNAs w/seed AGCUUAU) hsa-miR-30e-5p (and other miRNAs w/seed GUAAACA) hsa-miR-32-5p (and other miRNAs w/seed AUUGCAC) hsa-miR-365a-3p (and other miRNAs w/seed AAUGCCC) hsa-miR-372-3p (and other miRNAs w/seed AAGUGCU) hsa-miR-3613-3p (miRNAs w/seed CAAAAA) hsa-miR-3652 (and other miRNAs w/seed GCGUGGA)	High (predicted) Experimentally Observed High (predicted) High (predicted) High (predicted) High (predicted) High (predicted) High (predicted)

Gene Symbol	Gene Name	miRNAs Targeting Gene	Confidence
NFKBIA	NFKB inhibitor alpha	hsa-let-7c-3p (and other miRNAs w/seed UGUUCAA)	High (predicted)
NOD2	Nucleotide binding oligomerization domain containing 2	hsa-miR-4485-3p (miRNAs w/seed AACGGCC)	High (predicted)
NOS1	Nitric oxide synthase 1	hsa-miR-516b-5p (miRNAs w/seed UCUGGAG) hsa-miR-585-3p (miRNAs w/seed GGGCGUA)	High (predicted) High (predicted)
NOS2	Nitric oxide synthase 2	hsa-miR-2110 (and other miRNAs w/seed UGGGAA) hsa-miR-136-5p (miRNAs w/seed CUCAUU)	High (predicted) High (predicted)
NOTCH1	Notch receptor 1	hsa-miR-146b-5p (and other miRNAs w/seed GAGAACU) hsa-miR-23a-3p (and other miRNAs w/seed UCACAUU) hsa-miR-24-3p (and other miRNAs w/seed GGCUCAG) hsa-miR-27a-3p (and other miRNAs w/seed UCACAGU) hsa-miR-34a-5p (and other miRNAs w/seed GGCAGUG) hsa-miR-221-5p (and other miRNAs w/seed CCUGGCA)	Experimentally Observed Experimentally Observed Experimentally Observed Experimentally Observed Experimentally Observed High (predicted)
NPPC	Natriuretic peptide C	hsa-miR-374a-5p (and other miRNAs w/seed UAUAAUA)	High (predicted)
NR3C2	Nuclear receptor subfamily 3 group C member 2	hsa-miR-365a-3p (and other miRNAs w/seed AAUGCCC)	High (predicted)
NRF1	Nuclear respiratory factor 1	hsa-miR-377-3p (miRNAs w/seed UCACACA) hsa-miR-409-5p (and other miRNAs w/seed GGUUACC) hsa-miR-500a-3p (miRNAs w/seed UGCACCU)	High (predicted) High (predicted) High (predicted)
NRP1	Neuropilin 1	hsa-miR-539-3p (and other miRNAs w/seed UCAUACA) hsa-miR-148a-3p (and other miRNAs w/seed CAGUGCA) hsa-miR-185-5p (and other miRNAs w/seed GGAGAGA)	High (predicted) High (predicted) High (predicted)
NTSE	5,-nucleotidase ecto	hsa-miR-30e-5p (and other miRNAs w/seed GUAAAACA)	Experimentally Observed
NTF3	Neurotrophin 3	hsa-miR-21-5p (and other miRNAs w/seed AGCUUUAU) hsa-miR-200b-3p (and other miRNAs w/seed AAUACUG) hsa-miR-221-3p (and other miRNAs w/seed GCUACA U) hsa-miR-374a-5p (and other miRNAs w/seed UAUAAUA)	High (predicted) High (predicted) High (predicted) High (predicted)
NTN1	Netrin 1	hsa-miR-598-3p (miRNAs w/seed ACGUCAU)	High (predicted)
NTRK2	Neurotrophic receptor tyrosine kinase 2	hsa-miR-22-3p (miRNAs w/seed AGCUGCC)	High (predicted)
NTRK3	Neurotrophic receptor tyrosine kinase 3	hsa-miR-185-5p (and other miRNAs w/seed GGAGAGA) hsa-miR-9-5p (and other miRNAs w/seed CUUUGGU) hsa-miR-34a-5p (and other miRNAs w/seed GGCAGUG) hsa-miR-99a-5p (and other miRNAs w/seed ACCGUA) hsa-miR-539-3p (and other miRNAs w/seed UCAUACA)	High (predicted) Experimentally Observed High (predicted) High (predicted) Experimentally Observed
NTSR1	Neurotensin receptor 1	hsa-miR-1291 (and other miRNAs w/seed GGCCUUG)	High (predicted)
OCLN	Occludin	hsa-miR-377-3p (miRNAs w/seed UCACACA) hsa-miR-3613-3p (miRNAs w/seed CAAAAA)	High (predicted) High (predicted)
OGG1	8-oxoguanine DNA glycosylase	hsa-miR-1255a (and other miRNAs w/seed GGAUGAG) hsa-miR-3652 (and other miRNAs w/seed GGCUGGA)	High (predicted) High (predicted)



Gene Symbol	Gene Name	miRNAs Targeting Gene	Confidence
PLS3	Plastin 3	hsa-miR-421 (and other miRNAs w/seed UCAACAG)	High (predicted)
POU5F1	POU class 5 homeobox 1	hsa-miR-335-5p (and other miRNAs w/seed CAAGAGC)	High (predicted)
PPARA	Peroxisome proliferator activated receptor alpha	hsa-miR-22-3p (miRNAs w/seed AGCUGCC)	Experimentally Observed
PPARD	Peroxisome proliferator activated receptor delta	hsa-miR-1291 (and other miRNAs w/seed GGCCUUG)	High (predicted)
PPARG	Peroxisome proliferator activated receptor gamma	hsa-miR-24-3p (and other miRNAs w/seed GGCUCAG)	High (predicted)
		hsa-miR-27a-3p (and other miRNAs w/seed UCACAGU)	Experimentally Observed
		hsa-miR-34a-5p (and other miRNAs w/seed GGCAGUG)	High (predicted)
		hsa-miR-106a-5p (and other miRNAs w/seed AAAGUGC)	Experimentally Observed
		hsa-miR-130a-3p (and other miRNAs w/seed AGUGCAA)	High (predicted)
		hsa-miR-516b-5p (miRNAs w/seed UCUGGAG)	High (predicted)
PRDM16	PR/SET domain 16	hsa-miR-125b-1-3p (miRNAs w/seed CGGGUUA)	High (predicted)
		hsa-miR-200b-3p (and other miRNAs w/seed AAUACUG)	High (predicted)
PRKCA	Protein kinase C alpha	hsa-miR-142-3p (and other miRNAs w/seed GUAGUGU)	Experimentally Observed
		hsa-miR-203a-3p (and other miRNAs w/seed UGAAAUUG)	Experimentally Observed
PROCR	Protein C receptor	hsa-miR-361-5p (miRNAs w/seed UAUACAGA)	High (predicted)
PSAP	Prosaposin	hsa-miR-361-3p (miRNAs w/seed CCCCCAG)	High (predicted)
PSEN1	Presenilin 1	hsa-miR-22-3p (miRNAs w/seed AGCUGCC)	High (predicted)
PSEN2	Presenilin 2	hsa-miR-483-3p (miRNAs w/seed CACUCCU)	Experimentally Observed
PTAFR	Platelet activating factor receptor	hsa-miR-98-5p (and other miRNAs w/seed GAGGUAG)	High (predicted)
		hsa-miR-146b-5p (and other miRNAs w/seed GAGAACU)	Experimentally Observed
		hsa-miR-193b-5p (miRNAs w/seed GGGGUUU)	High (predicted)
		hsa-miR-361-3p (miRNAs w/seed CCCCCAG)	High (predicted)
		hsa-miR-671-5p (miRNAs w/seed GGAAGCC)	High (predicted)
PTGER4	Prostaglandin E receptor 4	hsa-miR-32-5p (and other miRNAs w/seed AUUGCAC)	High (predicted)
PTGES	Prostaglandin E synthase	hsa-miR-329-3p (and other miRNAs w/seed ACACACC)	High (predicted)
PTGIR	Prostaglandin I2 receptor	hsa-miR-208b-3p (and other miRNAs w/seed UAAAGACC)	Experimentally Observed
		hsa-miR-598-3p (miRNAs w/seed ACGUCAU)	High (predicted)
PTGS1	Prostaglandin-endoperoxide synthase 1	hsa-miR-340-3p (and other miRNAs w/seed CCGUCUC)	High (predicted)
		hsa-miR-516b-5p (miRNAs w/seed UCUGGAG)	High (predicted)
PTGS2	Prostaglandin-endoperoxide synthase 2	hsa-miR-16-5p (and other miRNAs w/seed AGCAGCA)	Experimentally Observed
		hsa-miR-26b-5p (and other miRNAs w/seed UCAAGUA)	Experimentally Observed
		hsa-miR-98-5p (and other miRNAs w/seed GAGGUAG)	Experimentally Observed
		hsa-miR-101-3p (and other miRNAs w/seed ACAGUAC)	Experimentally Observed
		hsa-miR-199a-3p (and other miRNAs w/seed CAGUAGU)	Experimentally Observed
		hsa-miR-542-3p (miRNAs w/seed GUGACAG)	Experimentally Observed

Gene Symbol	Gene Name	miRNAs Targeting Gene	Confidence
PTH LH	Parathyroid hormone like hormone	hsa-miR-29b-3p (and other miRNAs w/seed AGCACCA)	High (predicted)
		hsa-miR-106a-5p (and other miRNAs w/seed AAAGUGC)	High (predicted)
		hsa-miR-143-5p (and other miRNAs w/seed GUGCAGU)	High (predicted)
		hsa-miR-190a-5p (and other miRNAs w/seed GAUAUGU)	High (predicted)
		hsa-miR-200b-3p (and other miRNAs w/seed AAUACUG)	High (predicted)
RAB6A	RAB6A, member RAS oncogene family	hsa-miR-576-5p (miRNAs w/seed UUCUAAU)	High (predicted)
RAC1	Rac family small GTPase 1	hsa-miR-215-5p (and other miRNAs w/seed UGACCUA)	High (predicted)
		hsa-miR-142-3p (and other miRNAs w/seed GUAGUGU)	High (predicted)
RAD51	RAD51 recombinase	hsa-miR-182-5p (and other miRNAs w/seed UUGGCAA)	High (predicted)
		hsa-miR-200a-3p (and other miRNAs w/seed AACACUG)	Experimentally Observed
		hsa-miR-425-3p (miRNAs w/seed UCGGGAA)	High (predicted)
		hsa-miR-221-5p (and other miRNAs w/seed CCUGGCA)	High (predicted)
		hsa-miR-758-3p (miRNAs w/seed UUGUGAC)	High (predicted)
RARβ	Retinoic acid receptor beta	hsa-miR-30e-5p (and other miRNAs w/seed GUAAACA)	High (predicted)
		hsa-miR-379-5p (and other miRNAs w/seed GGUGAC)	High (predicted)
RARG	Retinoic acid receptor gamma	hsa-miR-30e-5p (and other miRNAs w/seed GUAAACA)	High (predicted)
		hsa-miR-96-5p (and other miRNAs w/seed UUGGCAC)	High (predicted)
RB1	RB transcriptional corepressor 1	hsa-miR-182-5p (and other miRNAs w/seed UUGGCAA)	Experimentally Observed
		hsa-miR-26b-5p (and other miRNAs w/seed UCAAGUA)	Experimentally Observed
		hsa-miR-106a-5p (and other miRNAs w/seed AAAGUGC)	Experimentally Observed
		hsa-miR-132-3p (and other miRNAs w/seed AACAGUC)	Experimentally Observed
		hsa-miR-27a-3p (and other miRNAs w/seed UCACAGU)	High (predicted)
RCAN2	Regulator of calcineurin 2	hsa-miR-3652 (and other miRNAs w/seed GCGUGGA)	High (predicted)
REV3L	REV3 like, DNA directed polymerase zeta catalytic subunit	hsa-miR-4677-3p (miRNAs w/seed CUGUGAG)	High (predicted)
		hsa-miR-29b-3p (and other miRNAs w/seed AGCACCA)	High (predicted)
		hsa-miR-32-5p (and other miRNAs w/seed AUUGCAC)	High (predicted)
		hsa-miR-30e-5p (and other miRNAs w/seed GUAAACA)	Experimentally Observed
		hsa-miR-203a-3p (and other miRNAs w/seed UGAAAUG)	Experimentally Observed
RXRA	Retinoid X receptor alpha	hsa-miR-218-5p (and other miRNAs w/seed UGUGCUU)	Experimentally Observed
SCX	Scleraxis bHLH transcription factor	hsa-miR-27a-3p (and other miRNAs w/seed UCACAGU)	Experimentally Observed
		hsa-let-7a-3p (and other miRNAs w/seed UAUACAA)	High (predicted)
SDC1	Syndecan 1	hsa-miR-361-3p (miRNAs w/seed CCCCCAG)	High (predicted)
		hsa-miR-452-5p (and other miRNAs w/seed ACUGUUU)	High (predicted)
		hsa-miR-10b-5p (and other miRNAs w/seed ACCCUGU)	High (predicted)
		hsa-miR-185-5p (and other miRNAs w/seed GGAGAGA)	High (predicted)
		hsa-miR-107 (and other miRNAs w/seed GCAGCAU)	High (predicted)
SDCBP	Syndecan binding protein	hsa-miR-361-5p (miRNAs w/seed UAUACAGA)	High (predicted)

Gene Symbol	Gene Name	miRNAs Targeting Gene	Confidence
SEPTIN6	Septin 6	hsa-miR-107 (and other miRNAs w/seed GCAGCAU) hsa-miR-3652 (and other miRNAs w/seed GGCUGGA) hsa-miR-10394-3p (and other miRNAs w/seed GGGCGCG) hsa-miR-182-5p (and other miRNAs w/seed UUGGCAA)	High (predicted) High (predicted) High (predicted) High (predicted)
SERPINB2	Serpin family B member 2	hsa-miR-21-5p (and other miRNAs w/seed AGCUUUAU)	Experimentally Observed
SERPINB5	Serpin family B member 5	hsa-let-7c-3p (and other miRNAs w/seed UGUJACAA)	High (predicted)
SERPINE2	Serpin family E member 2	hsa-miR-16-5p (and other miRNAs w/seed AGCAGCA) hsa-miR-199a-3p (and other miRNAs w/seed CAGUAGU) hsa-miR-671-5p (miRNAs w/seed GGAAGCC)	Experimentally Observed High (predicted) High (predicted)
SFRP1	Secreted frizzled related protein 1	hsa-miR-4677-3p (miRNAs w/seed CUGUGAG)	High (predicted)
SGMS2	Sphingomyelin synthase 2	hsa-miR-1-5p (and other miRNAs w/seed CAUACUU) hsa-miR-9-5p (and other miRNAs w/seed CUUUGGU) hsa-miR-29b-3p (and other miRNAs w/seed AGCACCA) hsa-miR-96-5p (and other miRNAs w/seed UUGGCAC) hsa-miR-182-5p (and other miRNAs w/seed UUGGCAA) hsa-miR-3613-3p (miRNAs w/seed CAAAAA)	High (predicted) High (predicted) High (predicted) High (predicted) High (predicted) High (predicted)
SH3BP4	SH3 domain binding protein 4	hsa-miR-18a-5p (and other miRNAs w/seed AAGGUGC) hsa-miR-107 (and other miRNAs w/seed GCAGCAU) hsa-miR-125b-5p (and other miRNAs w/seed CCCUGAG) hsa-miR-151a-5p (and other miRNAs w/seed CGAGGAG) hsa-miR-32-5p (and other miRNAs w/seed AUUGCAC) hsa-miR-340-3p (and other miRNAs w/seed CCGUCUC)	High (predicted) High (predicted) Experimentally Observed High (predicted) High (predicted) High (predicted)
SLC20A1	Solute carrier family 20 member 1	hsa-miR-125b-2-3p (and other miRNAs w/seed CACAAGU) hsa-miR-200a-3p (and other miRNAs w/seed AACACUG)	High (predicted) High (predicted)
SLC2A1	Solute carrier family 2 member 1	hsa-miR-148a-3p (and other miRNAs w/seed CAGUGCA) hsa-miR-1291 (and other miRNAs w/seed GGCCUUG) hsa-miR-3652 (and other miRNAs w/seed GGCUGGA)	High (predicted) High (predicted) High (predicted)
SLC46A1	Solute carrier family 46 member 1	hsa-miR-4667-3p (miRNAs w/seed CCUCU)	High (predicted)
SLC9A1	Solute carrier family 9 member A1	hsa-miR-214-3p (and other miRNAs w/seed CAGCAGG)	High (predicted)
SLC9A2	Solute carrier family 9 member A2	hsa-miR-96-5p (and other miRNAs w/seed UUGGCAC)	High (predicted)
SLIT2	Slit guidance ligand 2	hsa-miR-16-5p (and other miRNAs w/seed AGCAGCA) hsa-miR-489-3p (miRNAs w/seed UGACAUC) hsa-miR-516b-5p (miRNAs w/seed UCUGGAG) hsa-miR-628-5p (and other miRNAs w/seed UGCUGAC)	High (predicted) High (predicted) High (predicted) High (predicted)
SMAD1	SMAD family member 1	hsa-miR-26b-5p (and other miRNAs w/seed UCAAAGUA) hsa-miR-30e-5p (and other miRNAs w/seed GUAAACA) hsa-miR-199a-3p (and other miRNAs w/seed CAGUAGU) hsa-miR-582-3p (miRNAs w/seed AACUGGU)	Experimentally Observed High (predicted) Experimentally Observed High (predicted)

Gene Symbol	Gene Name	miRNAs Targeting Gene	Confidence
SMAD4	SMAD family member 4	hsa-miR-23a-3p (and other miRNAs w/seed UCACAUU)	Experimentally Observed
		hsa-miR-24-3p (and other miRNAs w/seed GGCUCAG)	Experimentally Observed
		hsa-miR-27a-3p (and other miRNAs w/seed UCACAGU)	Experimentally Observed
		hsa-miR-130a-3p (and other miRNAs w/seed AGUGCAA)	Experimentally Observed
SMAD7	SMAD family member 7	hsa-miR-483-3p (miRNAs w/seed CACUCCU)	Experimentally Observed
		hsa-miR-16-5p (and other miRNAs w/seed AGCAGCA)	High (predicted)
SMARCD1	SWI/SNF-related, matrix-associated actin-dependent regulator of chromatin, subfamily a, containing DEAD/H box 1	hsa-miR-21-5p (and other miRNAs w/seed AGCUUUAU)	High (predicted)
		hsa-miR-98-5p (and other miRNAs w/seed GAGGUJAG)	High (predicted)
SNAI1	Snail family transcriptional repressor 1	hsa-miR-22-3p (miRNAs w/seed AGCUGCC)	High (predicted)
		hsa-miR-30e-5p (and other miRNAs w/seed GUAAACA)	High (predicted)
		hsa-miR-34a-5p (and other miRNAs w/seed GGCAGUG)	High (predicted)
		hsa-miR-199b-5p (and other miRNAs w/seed CCAGUGU)	High (predicted)
		hsa-miR-6724-5p (and other miRNAs w/seed UGGGCC)	High (predicted)
		hsa-miR-16-5p (and other miRNAs w/seed AGCAGCA)	High (predicted)
		hsa-miR-24-2-5p (and other miRNAs w/seed GCCUACU)	High (predicted)
		hsa-miR-34a-5p (and other miRNAs w/seed GGCAGUG)	High (predicted)
		hsa-miR-218-5p (and other miRNAs w/seed UGUGCUU)	High (predicted)
		hsa-miR-372-3p (and other miRNAs w/seed AAGUGCU)	High (predicted)
SOD1	Superoxide dismutase 1	hsa-miR-374a-3p (miRNAs w/seed UUAUCAG)	High (predicted)
		hsa-miR-221-3p (and other miRNAs w/seed GCUACAU)	Experimentally Observed
		hsa-miR-21-5p (and other miRNAs w/seed AGCUUUAU)	Experimentally Observed
SOD2	Superoxide dismutase 2	hsa-miR-339-3p (miRNAs w/seed GAGGCC)	High (predicted)
		hsa-miR-769-5p (miRNAs w/seed GAGACCU)	High (predicted)
SOD3	Superoxide dismutase 3	hsa-let-7a-3p (and other miRNAs w/seed UAUACAA)	High (predicted)
		hsa-miR-145-5p (and other miRNAs w/seed UCCAGUU)	Experimentally Observed
SOX9	SRY-box transcription factor 9	hsa-miR-1249-3p (and other miRNAs w/seed CGCCUUU)	High (predicted)
		hsa-miR-3613-3p (miRNAs w/seed CAAAAA)	High (predicted)
		hsa-miR-27a-5p (miRNAs w/seed GGCCUUA)	High (predicted)
		hsa-miR-29b-3p (and other miRNAs w/seed AGCACA)	Experimentally Observed
SPARC	Secreted protein acidic and cysteine rich	hsa-miR-30e-5p (and other miRNAs w/seed GUAAACA)	Experimentally Observed
		hsa-miR-98-5p (and other miRNAs w/seed GAGGUJAG)	Experimentally Observed
		hsa-miR-221-5p (and other miRNAs w/seed CCUGGCA)	High (predicted)
		hsa-miR-203a-3p (and other miRNAs w/seed UGAAAUG)	Experimentally Observed
SREBF2	Sterol regulatory element binding transcription factor 2	hsa-miR-185-5p (and other miRNAs w/seed GGAGAGA)	High (predicted)
		hsa-miR-146b-5p (and other miRNAs w/seed GAGAACU)	Experimentally Observed
STAT1	Signal transducer and activator of transcription 1	hsa-miR-769-5p (miRNAs w/seed GAGACCU)	High (predicted)
		hsa-miR-9-5p (and other miRNAs w/seed CUUUGGU)	High (predicted)
STK3	Serine/threonine kinase 3	hsa-miR-140-5p (and other miRNAs w/seed AGUGGUU)	High (predicted)

Gene Symbol	Gene Name	miRNAs Targeting Gene	Confidence
STK4	Serine/threonine kinase 4	hsa-miR-340-3p (and other miRNAs w/seed CCGUCUC) hsa-miR-372-3p (and other miRNAs w/seed AAGUGCU)	High (predicted) Experimentally Observed
SYNE1	Spectrin repeat containing nuclear envelope protein 1	hsa-miR-7-5p (and other miRNAs w/seed GGAAGAC) hsa-miR-22-3p (miRNAs w/seed AGCUGCC)	Experimentally Observed High (predicted)
SYVN1	Synoviolin 1	hsa-miR-125b-5p (and other miRNAs w/seed CCUGAG)	High (predicted)
TAC1	Tachykinin precursor 1	hsa-miR-96-5p (and other miRNAs w/seed UUGGCAC) hsa-miR-130a-3p (and other miRNAs w/seed AGUGCAA) hsa-miR-200a-3p (and other miRNAs w/seed AACACUG)	High (predicted) Experimentally Observed High (predicted)
TFE3	Transcription factor binding to IGHM enhancer 3	hsa-miR-361-3p (miRNAs w/seed CCCCAG) hsa-miR-612 (and other miRNAs w/seed CUGGGCA)	High (predicted) High (predicted)
TFPI	Tissue factor pathway inhibitor	hsa-miR-127-5p (miRNAs w/seed UGAAGCU) hsa-miR-199b-5p (and other miRNAs w/seed CCAGUGU) hsa-miR-411-5p (and other miRNAs w/seed AGUAGAC)	High (predicted) High (predicted) High (predicted)
TFPI2	Tissue factor pathway inhibitor 2	hsa-miR-494-3p (miRNAs w/seed GAAACAU)	High (predicted)
TFPI2	Tissue factor pathway inhibitor 2	hsa-miR-16-5p (and other miRNAs w/seed AGCAGCA) hsa-miR-379-5p (and other miRNAs w/seed GGUAGAC)	High (predicted) High (predicted)
TGFB2	Transforming growth factor beta 2	hsa-miR-132-3p (and other miRNAs w/seed AACAGUC) hsa-miR-136-3p (miRNAs w/seed AUCAUCG) hsa-miR-199b-5p (and other miRNAs w/seed CCAGUGU) hsa-miR-200a-3p (and other miRNAs w/seed AACACUG)	High (predicted) High (predicted) High (predicted) Experimentally Observed
TGFB3	Transforming growth factor beta 3	hsa-miR-1-5p (and other miRNAs w/seed CAUACUU)	High (predicted)
TGFB1	Transforming growth factor beta receptor 1	hsa-miR-29b-3p (and other miRNAs w/seed AGCACCA) hsa-miR-30e-5p (and other miRNAs w/seed AGCACCA) hsa-miR-98-5p (and other miRNAs w/seed GAGGUAG) hsa-miR-101-3p (and other miRNAs w/seed ACAGUAC)	Experimentally Observed Experimentally Observed Experimentally Observed High (predicted)
TGFB2	Transforming growth factor beta receptor 2	hsa-miR-19b-3p (and other miRNAs w/seed GUGCAAA) hsa-miR-21-5p (and other miRNAs w/seed AGCUUAU) hsa-miR-26b-5p (and other miRNAs w/seed UCAAGUA) hsa-miR-29b-3p (and other miRNAs w/seed AGCACCA) hsa-miR-30e-5p (and other miRNAs w/seed GUAAACA) hsa-miR-98-5p (and other miRNAs w/seed GAGGUAG) hsa-miR-106a-5p (and other miRNAs w/seed AAAGUGC) hsa-miR-107 (and other miRNAs w/seed GCAGCAU)	High (predicted) Experimentally Observed Experimentally Observed Experimentally Observed Experimentally Observed Experimentally Observed Experimentally Observed
TGFB3	Transforming growth factor beta receptor 3	hsa-miR-130a-3p (and other miRNAs w/seed AGUGCAA) hsa-miR-372-3p (and other miRNAs w/seed AAGUGCU) hsa-let-7a-3p (and other miRNAs w/seed UAUACAA) hsa-miR-98-5p (and other miRNAs w/seed GAGGUAG)	High (predicted) High (predicted) High (predicted) High (predicted)
TH	Tyrosine hydroxylase	hsa-miR-140-3p (and other miRNAs w/seed ACCACAG)	High (predicted)

Gene Symbol	Gene Name	miRNAs Targeting Gene	Confidence
THBS1	Thrombospondin 1	hsa-miR-18a-5p (and other miRNAs w/seed AAGGUGC)	Experimentally Observed
		hsa-miR-19b-3p (and other miRNAs w/seed GUGCAA)	Experimentally Observed
		hsa-miR-30d-3p (and other miRNAs w/seed UUUUCAGU)	Experimentally Observed
		hsa-miR-98-5p (and other miRNAs w/seed GAGGUAG)	Experimentally Observed
THY1	Thy-1 cell surface antigen	hsa-miR-143-5p (and other miRNAs w/seed GUGCAGU)	High (predicted)
TIMP2	TIMP metalloproteinase inhibitor 2	hsa-miR-1255a (and other miRNAs w/seed GGAUGAG)	High (predicted)
TIMP3	TIMP metalloproteinase inhibitor 3	hsa-miR-21-5p (and other miRNAs w/seed AGCUUUAU)	Experimentally Observed
		hsa-miR-181d-5p (and other miRNAs w/seed ACAUUA)	Experimentally Observed
		hsa-miR-221-3p (and other miRNAs w/seed GCUACA)	Experimentally Observed
		hsa-miR-223-5p (miRNAs w/seed GUGUAU)	High (predicted)
TIMP4	TIMP metalloproteinase inhibitor 4	hsa-miR-452-3p (miRNAs w/seed UCAUCUG)	High (predicted)
TIRAP	TIR domain containing adaptor protein	hsa-miR-193b-5p (miRNAs w/seed GGGUUU)	High (predicted)
TJP1	Tight junction protein 1	hsa-miR-671-5p (miRNAs w/seed GGAAGCC)	High (predicted)
TLR1	Toll like receptor 1	hsa-miR-132-3p (and other miRNAs w/seed AACAGUC)	Experimentally Observed
TLR2	Toll like receptor 2	hsa-miR-146b-5p (and other miRNAs w/seed GAGAAUCU)	Experimentally Observed
TLR3	Toll like receptor 3	hsa-miR-654-3p (and other miRNAs w/seed AUGUCUG)	High (predicted)
TLR4	Toll like receptor 4	hsa-miR-495-3p (and other miRNAs w/seed AACAAAC)	High (predicted)
		hsa-miR-98-5p (and other miRNAs w/seed GAGGUAG)	Experimentally Observed
TLR7	Toll like receptor 7	hsa-miR-146b-5p (and other miRNAs w/seed GAGAAUCU)	Experimentally Observed
		hsa-miR-106a-5p (and other miRNAs w/seed AAAAGUGC)	Experimentally Observed
TLR8	Toll like receptor 8	hsa-miR-1255a (and other miRNAs w/seed GGAUGAG)	High (predicted)
		hsa-miR-22-3p (miRNAs w/seed AGCUGCC)	High (predicted)
TMEM176B	Transmembrane protein 176B	hsa-miR-652-3p (miRNAs w/seed AUGGCGC)	High (predicted)
		hsa-miR-516b-5p (miRNAs w/seed UCUGGAG)	High (predicted)
TNC	Tenascin C	hsa-miR-9-5p (and other miRNAs w/seed CUUUGGU)	High (predicted)
		hsa-miR-218-5p (and other miRNAs w/seed UGUGCUU)	High (predicted)
TNF	Tumor necrosis factor	hsa-miR-21-5p (and other miRNAs w/seed AGCUUUAU)	Experimentally Observed
		hsa-miR-106a-5p (and other miRNAs w/seed AAAAGUGC)	Experimentally Observed
		hsa-miR-125b-1-3p (miRNAs w/seed CGGGUUA)	Experimentally Observed
		hsa-miR-125b-2-3p (and other miRNAs w/seed CACAAGU)	High (predicted)
		hsa-miR-140-5p (and other miRNAs w/seed AGUGGUU)	High (predicted)
		hsa-miR-361-3p (miRNAs w/seed CCCCAG)	High (predicted)
		hsa-miR-452-3p (miRNAs w/seed UCAUCUG)	High (predicted)
		hsa-miR-516b-5p (miRNAs w/seed UCUGGAG)	High (predicted)
		hsa-miR-23a-3p (and other miRNAs w/seed UCACAUU)	High (predicted)
		hsa-miR-142-5p (and other miRNAs w/seed AUAAAGU)	High (predicted)
		hsa-miR-337-3p (miRNAs w/seed UCCUUAU)	High (predicted)
		hsa-miR-30e-5p (and other miRNAs w/seed GUAAACA)	Experimentally Observed
hsa-miR-126-3p (and other miRNAs w/seed CGUACCG)	High (predicted)		

Gene Symbol	Gene Name	miRNAs Targeting Gene	Confidence
TNFRSF10D	TNF receptor superfamily member 10d	hsa-miR-22-3p (miRNAs w/seed AGCUGCC)	High (predicted)
TNFRSF11A	TNF receptor superfamily member 11a	hsa-miR-125b-1-3p (miRNAs w/seed CGGGUUA)	High (predicted)
TNFRSF11B	TNF receptor superfamily member 11b	hsa-miR-181d-5p (and other miRNAs w/seed ACAUUA) hsa-miR-193b-5p (miRNAs w/seed GGGUUU)	High (predicted) High (predicted)
TNFRSF1A	TNF receptor superfamily member 1A	hsa-miR-29b-3p (and other miRNAs w/seed A GCACCA)	High (predicted)
TNFRSF1B	TNF receptor superfamily member 1B	hsa-miR-193b-5p (miRNAs w/seed GGGUUU)	High (predicted)
TNFSF11	TNF superfamily member 11	hsa-miR-495-3p (and other miRNAs w/seed ACAAAC) hsa-miR-329-3p (and other miRNAs w/seed ACACACC)	High (predicted) High (predicted)
TNFSF15	TNF superfamily member 15	hsa-miR-654-3p (and other miRNAs w/seed AUGUCUG) hsa-miR-27a-5p (miRNAs w/seed GGGUUU)	High (predicted) High (predicted)
TOB1	Transducer of ERBB2, 1	hsa-miR-6724-5p (and other miRNAs w/seed UGGGCC) hsa-miR-26b-5p (and other miRNAs w/seed UCAAGUA)	High (predicted) High (predicted)
TOLLIP	Toll interacting protein	hsa-miR-32-5p (and other miRNAs w/seed AUUGCAC) hsa-miR-218-5p (and other miRNAs w/seed UGUUCUU) hsa-miR-6724-5p (and other miRNAs w/seed UGGGCC)	High (predicted) High (predicted) High (predicted)
TP53	Tumor protein p53	hsa-miR-339-3p (miRNAs w/seed GAGGCC) hsa-miR-30e-5p (and other miRNAs w/seed GUAAACA) hsa-miR-34a-5p (and other miRNAs w/seed GGCAGUG) hsa-miR-98-5p (and other miRNAs w/seed GAGGUAG)	Experimentally Observed Experimentally Observed Experimentally Observed Experimentally Observed
TRAPPC2	Trafficking protein particle complex 2	hsa-miR-125b-5p (and other miRNAs w/seed CCUGAG) hsa-miR-612 (and other miRNAs w/seed CUGGCA) hsa-miR-3652 (and other miRNAs w/seed GGCUGGA)	Experimentally Observed Experimentally Observed High (predicted)
TSLP	Thymic stromal lymphopoietin	hsa-miR-21-5p (and other miRNAs w/seed AGCUUUAU) hsa-miR-26b-5p (and other miRNAs w/seed UCAAGUA)	High (predicted) High (predicted)
TWIST1	Twist family bHLH transcription factor 1	hsa-miR-377-3p (miRNAs w/seed UCACACA) hsa-miR-542-3p (miRNAs w/seed GUGACAG) hsa-miR-3613-3p (miRNAs w/seed CAAAAA)	High (predicted) High (predicted) High (predicted)
TXN	Thioredoxin	hsa-miR-27a-3p (and other miRNAs w/seed UCACAGU)	High (predicted)
TYR	Tyrosinase	hsa-miR-96-5p (and other miRNAs w/seed UJGGCAC) hsa-miR-186-5p (miRNAs w/seed AAAGAAU)	High (predicted) Experimentally Observed
UCP2	Uncoupling protein 2	hsa-miR-4662a-5p (miRNAs w/seed UAGCCAA) hsa-miR-27a-5p (miRNAs w/seed GGGUUU)	High (predicted) High (predicted)
VAMP1	Vesicle associated membrane protein 1	hsa-miR-145-5p (and other miRNAs w/seed UCCAGUU) hsa-miR-16-5p (and other miRNAs w/seed AGCAGCA) hsa-miR-6125 (miRNAs w/seed CGGAAGG)	Experimentally Observed Experimentally Observed High (predicted)
		hsa-miR-612 (and other miRNAs w/seed CUGGGCA)	High (predicted)

Gene Symbol	Gene Name	miRNAs Targeting Gene	Confidence
VAMP2	Vesicle associated membrane protein 2	hsa-miR-34a-5p (and other miRNAs w/seed GGCAGUG)	High (predicted)
		hsa-miR-185-5p (and other miRNAs w/seed GGAGAGA)	High (predicted)
		hsa-miR-493-5p (miRNAs w/seed UGUACAU)	High (predicted)
		hsa-miR-612 (and other miRNAs w/seed CUGGGCA)	High (predicted)
		hsa-miR-1291 (and other miRNAs w/seed GGCCUCUG)	High (predicted)
		hsa-miR-2110 (and other miRNAs w/seed UGGGGAA)	High (predicted)
VASH1	Vasohibin 1	hsa-miR-29b-3p (and other miRNAs w/seed AGCACCA)	High (predicted)
		hsa-miR-221-5p (and other miRNAs w/seed CCUGGCA)	High (predicted)
		hsa-miR-324-5p (miRNAs w/seed GCAUCCC)	High (predicted)
		hsa-miR-361-3p (miRNAs w/seed CCCCCAG)	High (predicted)
		hsa-miR-1291 (and other miRNAs w/seed GGCCUCUG)	High (predicted)
		hsa-miR-3652 (and other miRNAs w/seed GGCUGGA)	High (predicted)
		hsa-miR-4485-3p (miRNAs w/seed AACGGCC)	High (predicted)
		hsa-miR-29b-3p (and other miRNAs w/seed AGCACCA)	Experimentally Observed
		hsa-miR-30e-5p (and other miRNAs w/seed GUAAACA)	Experimentally Observed
		hsa-miR-98-5p (and other miRNAs w/seed GAGGUAG)	Experimentally Observed
VCAN	Versican	hsa-miR-107 (and other miRNAs w/seed GCAGCAU)	High (predicted)
		hsa-miR-199a-3p (and other miRNAs w/seed CAGUAGU)	Experimentally Observed
		hsa-miR-214-3p (and other miRNAs w/seed CAGCAGG)	High (predicted)
		hsa-miR-16-5p (and other miRNAs w/seed AGCAGCA)	Experimentally Observed
		hsa-miR-29b-3p (and other miRNAs w/seed AGCACCA)	High (predicted)
		hsa-miR-34a-5p (and other miRNAs w/seed GGCAGUG)	Experimentally Observed
		hsa-miR-106a-5p (and other miRNAs w/seed AAAGUGC)	Experimentally Observed
		hsa-miR-126-3p (and other miRNAs w/seed CGUACCG)	Experimentally Observed
		hsa-miR-140-5p (and other miRNAs w/seed AGUGGUU)	Experimentally Observed
		hsa-miR-205-5p (and other miRNAs w/seed CCUUCAU)	Experimentally Observed
		hsa-miR-372-3p (and other miRNAs w/seed AAGUGCU)	Experimentally Observed
		hsa-miR-7-5p (and other miRNAs w/seed GGAA GAC)	High (predicted)
		hsa-miR-28-3p (and other miRNAs w/seed ACUAGAU)	High (predicted)
		hsa-miR-30e-5p (and other miRNAs w/seed GUAAACA)	High (predicted)
hsa-miR-98-5p (and other miRNAs w/seed GAGGUAG)	Experimentally Observed		
VEGFA	Vascular endothelial growth factor A	hsa-miR-106a-5p (and other miRNAs w/seed AAAGUGC)	Experimentally Observed
		hsa-miR-126-3p (and other miRNAs w/seed CGUACCG)	Experimentally Observed
		hsa-miR-140-5p (and other miRNAs w/seed AGUGGUU)	Experimentally Observed
		hsa-miR-205-5p (and other miRNAs w/seed CCUUCAU)	Experimentally Observed
		hsa-miR-372-3p (and other miRNAs w/seed AAGUGCU)	Experimentally Observed
		hsa-miR-7-5p (and other miRNAs w/seed GGAA GAC)	High (predicted)
VEGFD	Vascular endothelial growth factor D	hsa-miR-28-3p (and other miRNAs w/seed ACUAGAU)	High (predicted)
		hsa-miR-30e-5p (and other miRNAs w/seed GUAAACA)	High (predicted)
		hsa-miR-98-5p (and other miRNAs w/seed GAGGUAG)	Experimentally Observed
		hsa-miR-106a-5p (and other miRNAs w/seed AAAGUGC)	Experimentally Observed
		hsa-miR-223-3p (miRNAs w/seed GUCAGUU)	Experimentally Observed
		hsa-miR-382-5p (miRNAs w/seed AAGUUGU)	Experimentally Observed
		hsa-miR-708-3p (miRNAs w/seed AACUAGA)	High (predicted)
		hsa-miR-140-3p (and other miRNAs w/seed ACCACAG)	High (predicted)
		hsa-miR-539-3p (and other miRNAs w/seed UCAUACA)	High (predicted)
		hsa-miR-34a-5p (and other miRNAs w/seed GGCAGUG)	Experimentally Observed
WNT1	Wnt family member 1	hsa-miR-98-5p (and other miRNAs w/seed GAGGUAG)	Experimentally Observed
		hsa-miR-98-5p (and other miRNAs w/seed GAGGUAG)	Experimentally Observed

Gene Symbol	Gene Name	miRNAs Targeting Gene	Confidence
WNT16	Wnt family member 16	hsa-miR-107 (and other miRNAs w/seed GCAGCAU) hsa-miR-200b-3p (and other miRNAs w/seed AAUACUG) hsa-miR-383-5p (miRNAs w/seed GAUCAGA)	High (predicted) High (predicted) High (predicted)
WNT3	Wnt family member 3	hsa-miR-509-3-5p (and other miRNAs w/seed ACUGCAG)	High (predicted)
WNT5A	Wnt family member 5A	hsa-miR-30e-5p (and other miRNAs w/seed GUAACA) hsa-miR-2110 (and other miRNAs w/seed UGGGAA)	Experimentally Observed High (predicted)
WNT5B	Wnt family member 5B	hsa-miR-708-5p (and other miRNAs w/seed AGGAGCU)	High (predicted)
XYLT1	Xylosyltransferase 1	hsa-miR-34a-5p (and other miRNAs w/seed GGCAGUG)	High (predicted)
ZFP36	ZFP36 ring finger protein	hsa-miR-361-3p (miRNAs w/seed CCCCAG)	High (predicted)

**Table A4.1 (includes preceding 29 pages) Predicted mRNA targets of miRNAs significantly differentially expressed in human tendinopathy.** Target prediction performed using Ingenuity Pathway Analysis (IPA; <https://www.qiagenbioinformatics.com/products/ingenuity-pathway-analysis>) microRNA Target Filter function. Following application of filters: Confidence of prediction (Experimentally Observed and High), Disease (Connective Tissue Disorders and Skeletal and Muscular Disorders) and Tissue/Cell Line (Tissues and Primary Cells and Fibroblasts), 167 miRNAs targeting 464 genes were identified. NB. IPA microRNA Target Filter clusters miRNAs on the basis of common seed sequences (see text for details).

Gene Symbol	Gene Name	miRNAs Targeting Gene	Confidence
ADAMTS14	ADAM metalloproteinase with thrombospondin type 1 motif 14	miR-29b-3p (and other miRNAs w/seed AGCACCA)	Experimentally Observed
ADAMTS2	ADAM metalloproteinase with thrombospondin type 1 motif 2	miR-29b-3p (and other miRNAs w/seed AGCACCA)	Experimentally Observed
ADAMTS20	ADAM metalloproteinase with thrombospondin type 1 motif 20	miR-29b-3p (and other miRNAs w/seed AGCACCA)	High (predicted)
ADAMTS9	ADAM metalloproteinase with thrombospondin type 1 motif 9	miR-29b-3p (and other miRNAs w/seed AGCACCA)	High (predicted)
APBB1	Amyloid beta precursor protein binding family B member 1	miR-199a-5p (and other miRNAs w/seed CCAGUGU)	High (predicted)
BCL2	BCL2 apoptosis regulator	miR-181a-5p (and other miRNAs w/seed ACAUUA)	Experimentally Observed
CASP8	Caspase 8	miR-29b-3p (and other miRNAs w/seed AGCACCA)	High (predicted)
CNR1	Cannabinoid receptor 1	miR-29b-3p (and other miRNAs w/seed AGCACCA)	High (predicted)
COL1A1	Collagen type I alpha 1 chain	miR-29b-3p (and other miRNAs w/seed AGCACCA)	Experimentally Observed
COL1A2	Collagen type I alpha 2 chain	miR-29b-3p (and other miRNAs w/seed AGCACCA)	Experimentally Observed
COL3A1	Collagen type III alpha 1 chain	miR-29b-3p (and other miRNAs w/seed AGCACCA)	Experimentally Observed
COL6A3	Collagen type VI alpha 3 chain	miR-29b-3p (and other miRNAs w/seed AGCACCA)	High (predicted)
CYP51A1	Cytochrome P450 family 51 subfamily A member 1	miR-199a-5p (and other miRNAs w/seed CCAGUGU)	High (predicted)
DDR1	Discoidin domain receptor tyrosine kinase 1	miR-199a-5p (and other miRNAs w/seed CCAGUGU)	High (predicted)
DYM	Dymeclin	miR-29b-3p (and other miRNAs w/seed AGCACCA)	High (predicted)
ELN	Elastin	miR-29b-3p (and other miRNAs w/seed AGCACCA)	High (predicted)
ESR1	Estrogen receptor 1	miR-181a-5p (and other miRNAs w/seed ACAUUA)	Experimentally Observed
ETS1	ETS proto-oncogene 1, transcription factor	miR-199a-5p (and other miRNAs w/seed CCAGUGU)	Experimentally Observed
FBN1	Fibrillin 1	miR-29b-3p (and other miRNAs w/seed AGCACCA)	Experimentally Observed
GJA5	Gap junction protein alpha 5	miR-199a-5p (and other miRNAs w/seed CCAGUGU)	High (predicted)
HIF1A	Hypoxia inducible factor 1 subunit alpha	miR-199a-5p (and other miRNAs w/seed CCAGUGU)	Experimentally Observed
HMCN1	Hemicentin 1	miR-199a-5p (and other miRNAs w/seed CCAGUGU)	High (predicted)
IL2	Interleukin 2	miR-29b-3p (and other miRNAs w/seed AGCACCA)	High (predicted)
IL24	Interleukin 24	miR-181a-5p (and other miRNAs w/seed ACAUUA)	High (predicted)
KLF4	Kruppel like factor 4	miR-29b-3p (and other miRNAs w/seed AGCACCA)	High (predicted)
KRAS	KRAS proto-oncogene, GTPase	miR-29b-3p (and other miRNAs w/seed AGCACCA)	Experimentally Observed
MMP14	Matrix metalloproteinase 14	miR-181a-5p (and other miRNAs w/seed ACAUUA)	Experimentally Observed
NFIA	Nuclear factor I A	miR-29b-3p (and other miRNAs w/seed AGCACCA)	High (predicted)
PDGFA	Platelet derived growth factor subunit A	miR-29b-3p (and other miRNAs w/seed AGCACCA)	Experimentally Observed
PDGFC	Platelet derived growth factor C	miR-29b-3p (and other miRNAs w/seed AGCACCA)	High (predicted)
PIK3R1	Phosphoinositide-3-kinase regulatory subunit 1	miR-29b-3p (and other miRNAs w/seed AGCACCA)	Experimentally Observed
PLEC	Plectin	miR-29b-3p (and other miRNAs w/seed AGCACCA)	Experimentally Observed
PTH1H	Parathyroid hormone like hormone	miR-29b-3p (and other miRNAs w/seed AGCACCA)	High (predicted)
REV3L	REV3 like, DNA directed polymerase zeta catalytic subunit	miR-29b-3p (and other miRNAs w/seed AGCACCA)	High (predicted)

Gene Symbol	Gene Name	miRNAs Targeting Gene	Confidence
SGMS2	Sphingomyelin synthase 2	miR-29b-3p (and other miRNAs w/seed AGCACCA)	High (predicted)
SNAI1	Snail family transcriptional repressor 1	miR-199a-5p (and other miRNAs w/seed CCAGUGU)	High (predicted)
SPARC	Secreted protein acidic and cysteine rich	miR-29b-3p (and other miRNAs w/seed AGCACCA)	Experimentally Observed
TFPI	Tissue factor pathway inhibitor	miR-199a-5p (and other miRNAs w/seed CCAGUGU)	High (predicted)
TGFB2	Transforming growth factor beta 2	miR-199a-5p (and other miRNAs w/seed CCAGUGU)	High (predicted)
TGFB3	Transforming growth factor beta 3	miR-29b-3p (and other miRNAs w/seed AGCACCA)	Experimentally Observed
TGFBR1	Transforming growth factor beta receptor 1	miR-29b-3p (and other miRNAs w/seed AGCACCA)	Experimentally Observed
TGFBR2	Transforming growth factor beta receptor 2	miR-29b-3p (and other miRNAs w/seed AGCACCA)	Experimentally Observed
TIMP3	TIMP metalloproteinase inhibitor 3	miR-181a-5p (and other miRNAs w/seed ACAUUCA)	Experimentally Observed
TNFRSF11B	TNF receptor superfamily member 11b	miR-181a-5p (and other miRNAs w/seed ACAUUCA)	High (predicted)
TNFRSF1A	TNF receptor superfamily member 1A	miR-29b-3p (and other miRNAs w/seed AGCACCA)	High (predicted)
VASH1	Vasohibin 1	miR-29b-3p (and other miRNAs w/seed AGCACCA)	High (predicted)
VCAN	Versican	miR-29b-3p (and other miRNAs w/seed AGCACCA)	Experimentally Observed
VEGFA	Vascular endothelial growth factor A	miR-29b-3p (and other miRNAs w/seed AGCACCA)	High (predicted)

**Table A4.2 (includes preceding page) Predicted mRNA targets of miRNAs identified as significantly differentially expressed in both human and equine tendinopathy.** Target prediction performed using Ingenuity Pathway Analysis (IPA); <https://www.qiagenbioinformatics.com/products/ingenuity-pathway-analysis> microRNA Target Filter function.

NB. IPA microRNA Target Filter clusters miRNAs on the basis of common seed sequences (see text for details).

## **Appendix 5**

**Table A5.1** *Small nucleolar RNA-61 (SNORD61)* expression in equine primary tenocytes is unaffected by treatment with miR-181a-5p mimic, antagomiR or scrambled control sequence oligonucleotides.

**Table A5.2** *Glyceraldehyde 3-phosphate dehydrogenase (GAPDH)* expression in equine primary tenocytes is unaffected by treatment with miR-181a-5p mimic, antagomiR or scrambled control oligonucleotides.

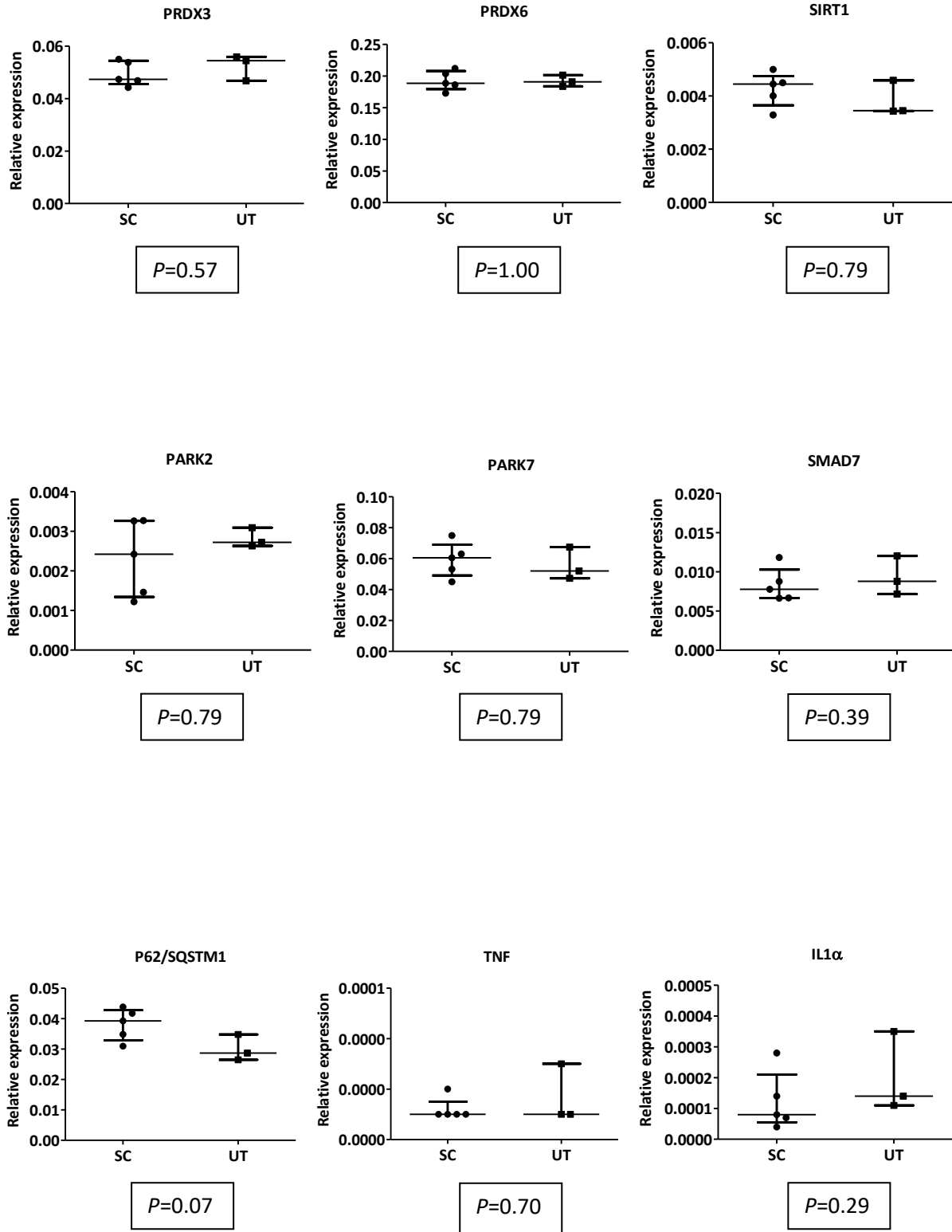
**Figure A5.1** Expression of selected target genes does not differ between scrambled control sequence (SC) treated and untreated (UT) equine tenocytes.

Donor Identity (Passage number)	Mimic treated		AntagomiR treated		Ct Values Scrambled control treated		Untreated control		Max	Min	Max - Min
	Replicates	Average	Replicates	Average	Replicates	Average	Replicates	Average			
EqDB5-5(P4)	28.61	28.86	28.31	28.79	29.73	29.97	30.22	30.49	30.49	28.79	1.70
EqDB5-5(P4)	28.97		28.87		30.22		30.37				
EqDB5-5(P4)	29.01		29.18		29.97		30.87				
EqDB30-3(P2)	30.18	30.13	29.11	30.03	29.43	29.91	29.35	29.81	30.13	29.81	0.32
EqDB30-3(P2)	30.27		30.64		30.35		30.07				
EqDB30-3(P2)	29.94		30.34		29.94		30				
EqDB7-5(P2)	27.36	27.31	27.06	27.89	28.82	29.04	29.13	29.18	29.18	27.31	1.88
EqDB7-5(P2)	27.45		28.49		28.92		29.18				
EqDB7-5(P2)	27.11		28.11		29.39		29.24				
EqDB9-12(P4)	27.88	27.85	29.34	29.20	28.62	29.28	27.4	27.31	29.28	27.31	1.97
EqDB9-12(P4)	27.64		28.86		29.86		27.31				
EqDB9-12(P4)	28.03		29.41		29.37		27.22				
EqDB10-18(P3)	28.26	28.21	28.82	29.06	30.12	29.67			29.67	28.21	1.46
EqDB10-18(P3)	27.98		29.09		29.31						
EqDB10-18(P3)	28.4		29.28		29.59						
EqDB11-3(P2)	29.58	29.47	30.1	29.69	28.06	28.11	28.57	28.69	29.69	28.11	1.58
EqDB11-3(P2)	29.47		29.4		28.2		29.16				
EqDB11-3(P2)	29.37		29.58		28.08		28.35				
EqDB12-8(P3)	28.45	28.27	28.28	28.31	29.23	28.76			28.76	28.27	0.49
EqDB12-8(P3)	28.23		28.48		28.16						
EqDB12-8(P3)	28.13		28.18		28.88						
EqDB18-9(P4)	28.32	28.03	30.64	29.44	29.69	29.42	28.11	28.34	29.44	28.03	1.41
EqDB18-9(P4)	28.03		29.23		30.1		28.4				
EqDB18-9(P4)	27.74		28.46		28.47		28.5				
<b>Mean</b>	<b>28.52</b>	<b>28.52</b>	<b>29.05</b>	<b>29.05</b>	<b>29.27</b>	<b>29.27</b>	<b>28.97</b>	<b>28.97</b>	<b>29.27</b>	<b>28.52</b>	<b>0.75</b>
<b>SD</b>	<b>0.90</b>	<b>0.92</b>	<b>0.84</b>	<b>0.71</b>	<b>0.73</b>	<b>0.63</b>	<b>1.08</b>	<b>1.12</b>	<b>1.12</b>	<b>0.63</b>	<b>0.50</b>
<b>Max</b>	<b>30.27</b>	<b>30.13</b>	<b>30.64</b>	<b>30.03</b>	<b>30.35</b>	<b>29.97</b>	<b>30.87</b>	<b>30.49</b>	<b>30.49</b>	<b>29.97</b>	<b>0.51</b>
<b>Min</b>	<b>27.11</b>	<b>27.31</b>	<b>27.06</b>	<b>27.89</b>	<b>28.06</b>	<b>28.11</b>	<b>27.22</b>	<b>27.31</b>	<b>28.11</b>	<b>27.31</b>	<b>0.81</b>
<b>Max - Min</b>	<b>3.16</b>	<b>2.82</b>	<b>3.58</b>	<b>2.14</b>	<b>2.29</b>	<b>1.86</b>	<b>3.65</b>	<b>3.18</b>	<b>3.18</b>	<b>1.86</b>	<b>1.32</b>

**Table A5.1 Small nucleolar RNA-61 (SNORD61) expression in equine primary tenocytes is unaffected by treatment with miR-181a-5p mimic, antagomiR or scrambled control sequence oligonucleotides.** Threshold cycle (Ct) values are presented for eight biological replicates, each run in triplicate. Untreated controls were not performed for two biological replicates. Columns demonstrate variation between biological replicates, rows demonstrate variation with treatment. Max = maximum, Min = minimum, SD = standard deviation.

Donor Identity (Passage number)	Mimic treated		AntagomiR treated		Ct values Scrambled control treated		Untreated control		Max	Min	Max - Min
	Replicates	Average	Replicates	Average	Replicates	Average	Replicates	Average			
EqDB5-5(P4)	16.54	16.46	16.83	16.80	16.73	16.69	16.77	16.75	16.80	16.46	0.34
EqDB5-5(P4)	16.44		16.53		16.73		16.69				
EqDB5-5(P4)	16.41		17.04		16.62		16.80				
EqDB30-3(P2)	17.37	17.36	17.15	17.12	17.19	17.09	16.54	16.64	17.36	16.64	0.72
EqDB30-3(P2)	17.42		17.10		17.01		16.59				
EqDB30-3(P2)	17.29		17.10		17.08		16.78				
EqDB7-5(P2)	16.64	16.80	16.40	16.49	17.09	17.11	16.74	16.91	17.11	16.49	0.62
EqDB7-5(P2)	16.79		16.38		17.24		17.12				
EqDB7-5(P2)	16.96		16.69		17.01		16.87				
EqDB9-12(P4)	16.09	16.03	16.45	16.46	16.36	16.30	16.46	16.45	16.46	16.03	0.43
EqDB9-12(P4)	15.86		16.50		16.32		16.46				
EqDB9-12(P4)	16.14		16.44		16.22		16.43				
EqDB10-18(P3)	16.05	16.22	16.11	16.10	16.07	15.93			16.22	15.93	0.28
EqDB10-18(P3)	16.29		16.09		15.69						
EqDB10-18(P3)	16.31		16.11		16.04						
EqDB11-3(P2)	16.97	17.04	16.52	16.63	16.20	16.40	16.64	16.66	17.04	16.40	0.64
EqDB11-3(P2)	17.11		16.61		16.52		16.66				
EqDB11-3(P2)	17.03		16.77		16.47		16.68				
EqDB12-8(P3)	16.02	15.86	16.06	16.04	15.86	16.02			16.04	15.86	0.18
EqDB12-8(P3)	15.99		16.07		15.95						
EqDB12-8(P3)	15.57		15.98		16.26						
EqDB18-9(P4)	15.60	15.80	17.22	17.17	16.60	16.69	16.44	16.36	17.17	15.80	1.37
EqDB18-9(P4)	15.95		17.15		16.58		16.34				
EqDB18-9(P4)	15.86		17.14		16.89		16.30				
<b>Mean</b>	<b>16.45</b>	<b>16.45</b>	<b>16.60</b>	<b>16.60</b>	<b>16.53</b>	<b>16.53</b>	<b>16.63</b>	<b>16.63</b>	<b>16.63</b>	<b>16.45</b>	<b>0.18</b>
<b>SD</b>	<b>0.56</b>	<b>0.57</b>	<b>0.41</b>	<b>0.42</b>	<b>0.44</b>	<b>0.45</b>	<b>0.21</b>	<b>0.20</b>	<b>0.57</b>	<b>0.20</b>	<b>0.37</b>
<b>Max</b>	<b>17.42</b>	<b>17.36</b>	<b>17.22</b>	<b>17.17</b>	<b>17.24</b>	<b>17.11</b>	<b>17.12</b>	<b>16.91</b>	<b>17.36</b>	<b>16.91</b>	<b>0.45</b>
<b>Min</b>	<b>15.57</b>	<b>15.80</b>	<b>15.98</b>	<b>16.04</b>	<b>15.69</b>	<b>15.93</b>	<b>16.30</b>	<b>16.36</b>	<b>16.36</b>	<b>15.80</b>	<b>0.56</b>
<b>Max - Min</b>	<b>1.85</b>	<b>1.56</b>	<b>1.24</b>	<b>1.13</b>	<b>1.55</b>	<b>1.18</b>	<b>0.82</b>	<b>0.55</b>	<b>1.56</b>	<b>0.55</b>	<b>1.01</b>

**Table A5.2 Glyceraldehyde 3-phosphate dehydrogenase (GAPDH) expression in equine primary tenocytes is unaffected by treatment with miR-181a-5p mimic, antagomiR or scrambled control oligonucleotides.** Threshold cycle (Ct) values are presented for eight biological replicates, each run in triplicate. Untreated controls were not performed for two biological replicates. Columns demonstrate variation between biological replicates, rows demonstrate variation with treatment. Max = maximum, Min = minimum, SD = standard deviation.



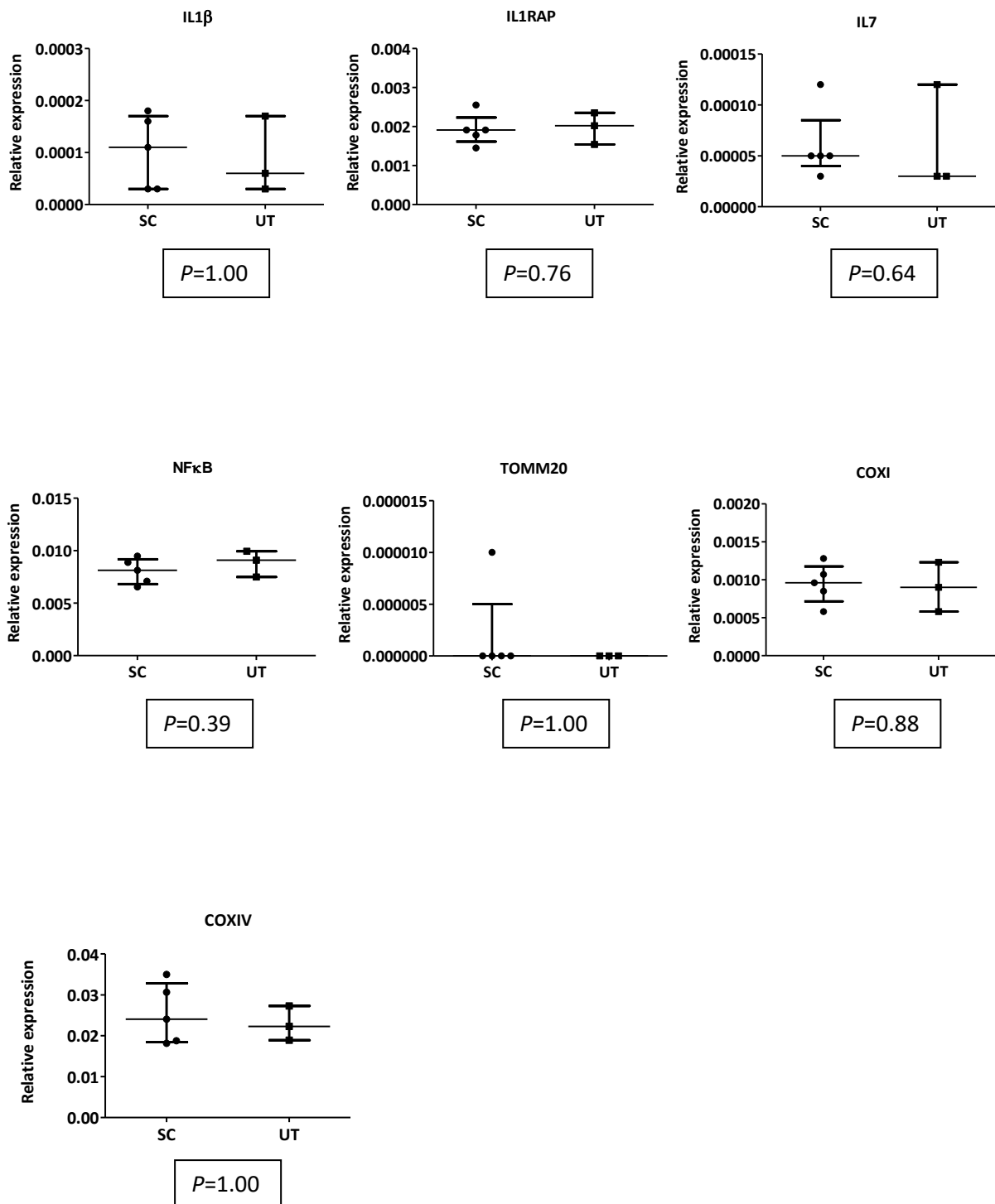


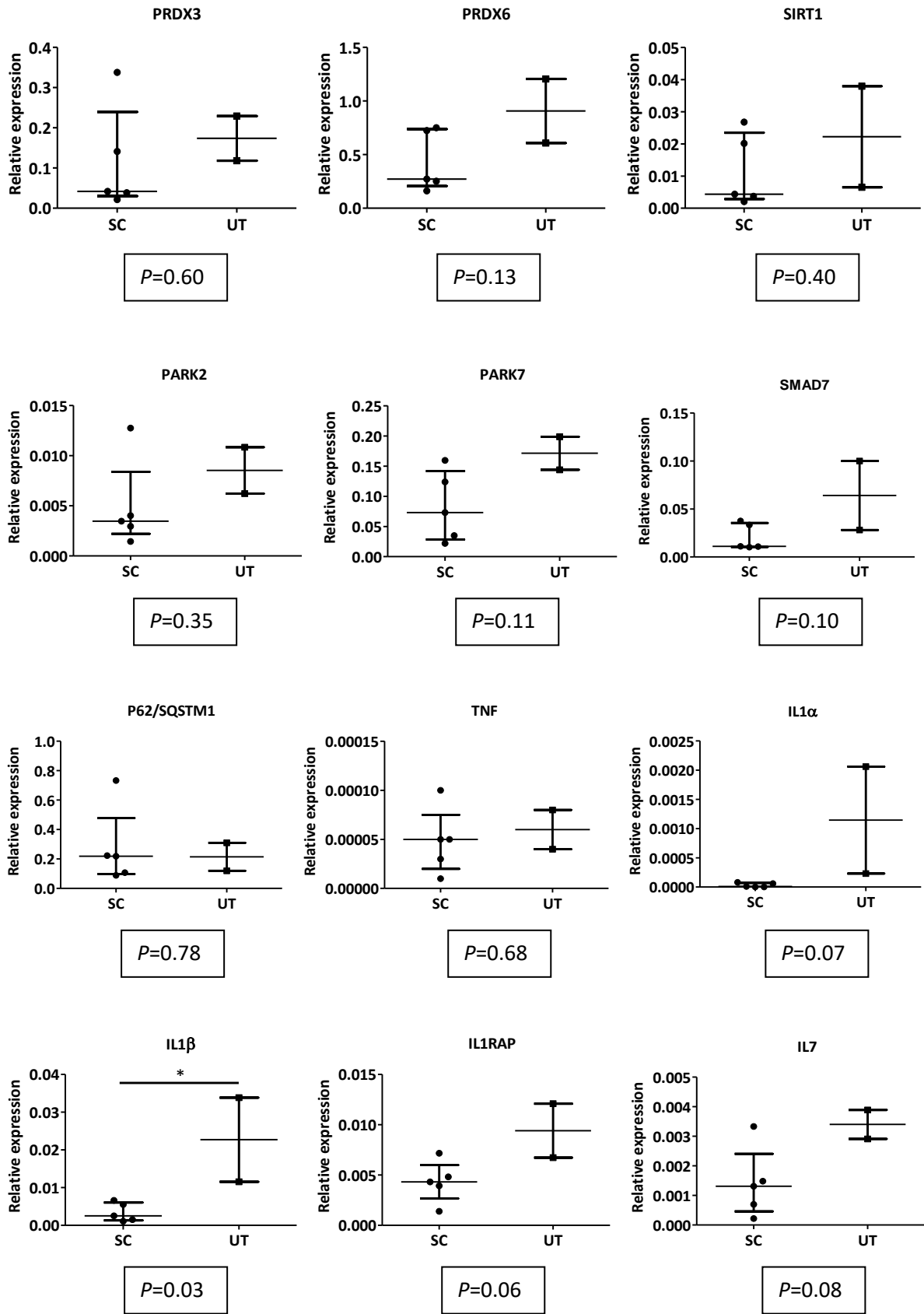
**Figure A5.1** (includes preceding page) Expression of selected target genes does not differ between scrambled control sequence (SC) treated and untreated (UT) equine tenocytes. Y-axis values represent expression relative to *glyceraldehyde 3-phosphate dehydrogenase (GAPDH)*. P-values calculated from delta Ct values, using the Mann-Whitney test. Graphs show median and interquartile range.

## **Appendix 6**

**Figure A6.1** Comparison between scrambled control (SC) treated and untreated (UT) equine tendon constructs on the expression of selected target genes.

**Figure A6.2** Western blot images from mmu-miR-181a-5p mimic (M), antagomiR (AM) and scrambled control (SC) treated equine tendon constructs.

**Figure A6.3** Comparison between scrambled control (SC) treated and untreated (UT) equine tendon constructs on histological scoring of H&E and Masson's Trichrome stained sections.



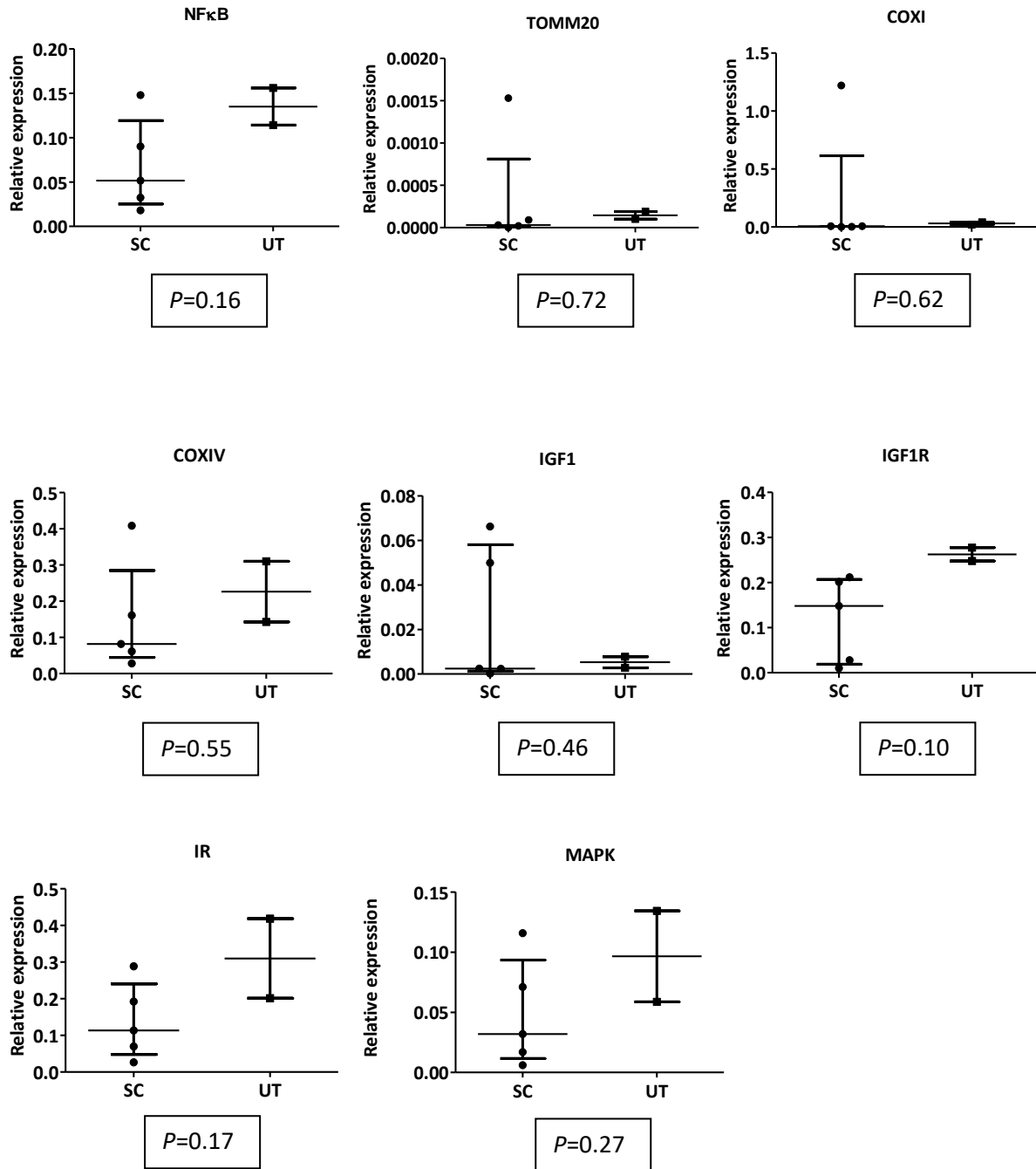
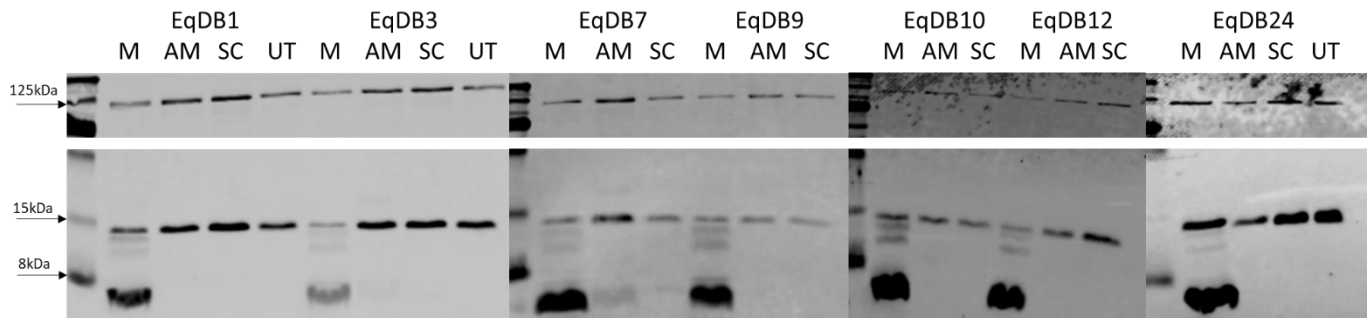


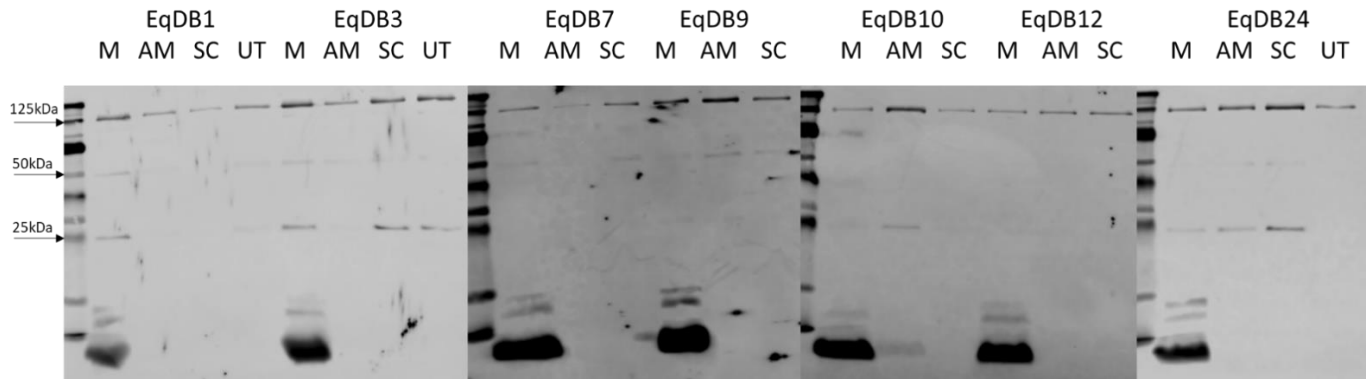
**Figure A6.1** (includes preceding page) Comparison between scrambled control (SC) treated and untreated (UT) equine tendon constructs on the expression of selected target genes. Y-axis values represent expression relative to *glyceraldehyde 3-phosphate dehydrogenase (GAPDH)*. P-values calculated from delta Ct values, using Student-t test. Graphs show median and interquartile range.

**A. TOMM20 and Vinculin**



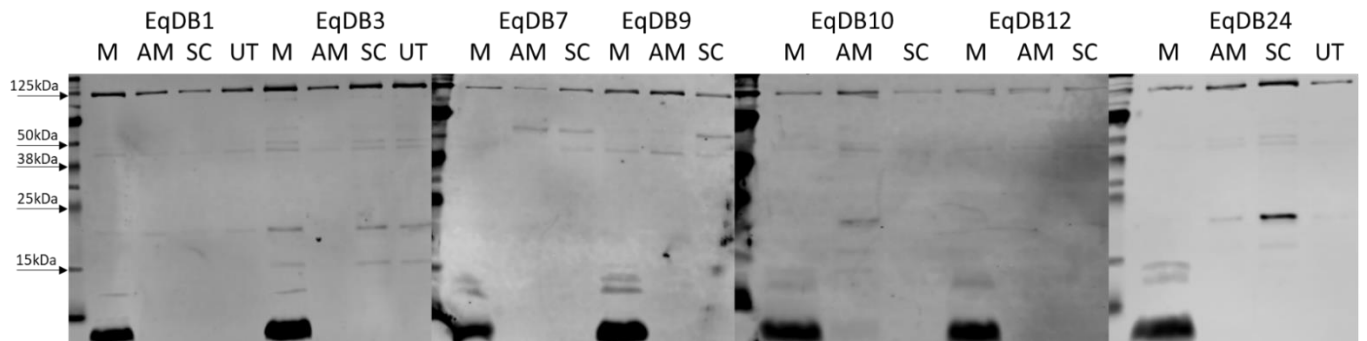
TOMM20 = translocase of outer mitochondrial membrane 20, predicted molecular weight 16 kDa.

**B. BNIP3 and Vinculin**



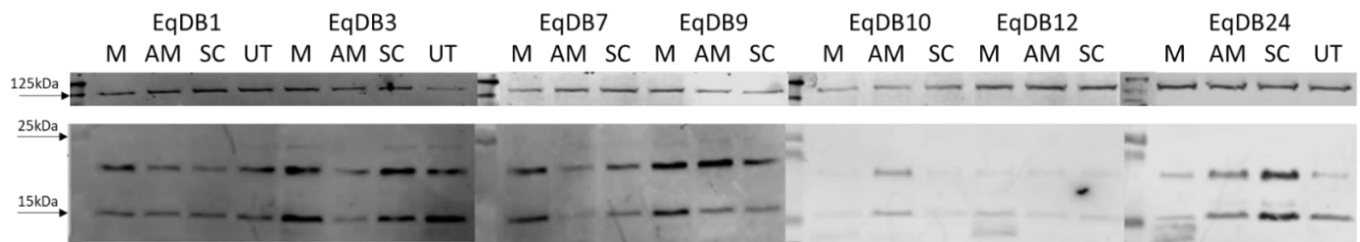
BNIP3 = Bcl-2 interacting protein 3, predicted molecular weight 22 kDa.

**C. LAMP1 and Vinculin**



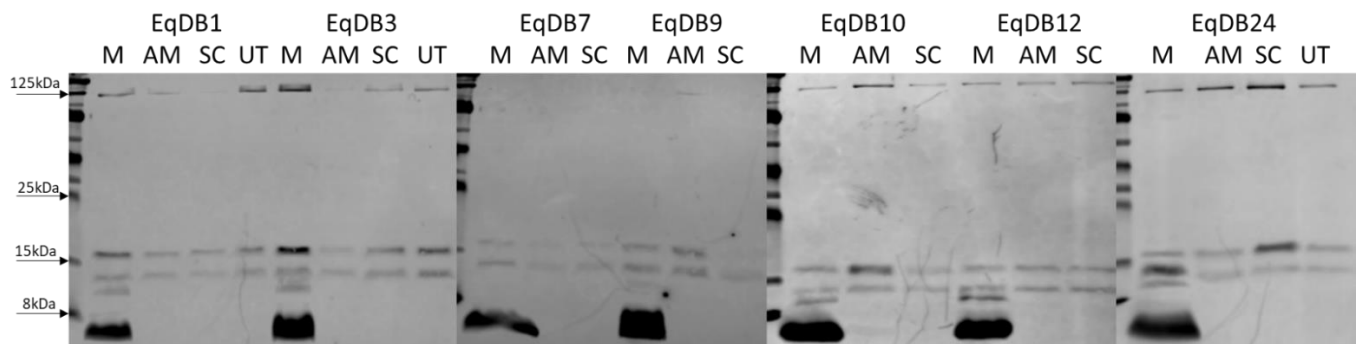
LAMP1 = lysosomal-associated membrane protein 1, predicted molecular weight 45 kDa.

#### D. COXIV and Vinculin



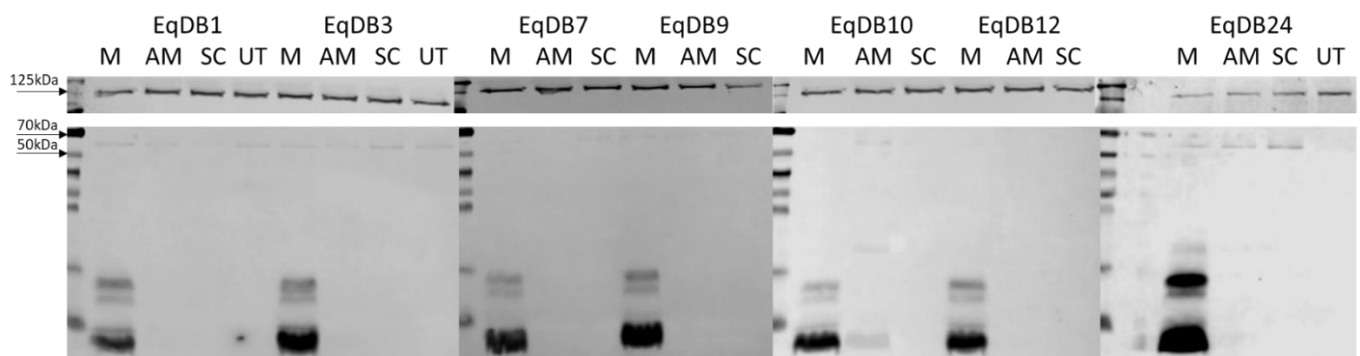
COXIV = cytochrome c oxidase subunit 4, predicted molecular weight 17 kDa.

#### E. LC3B and Vinculin



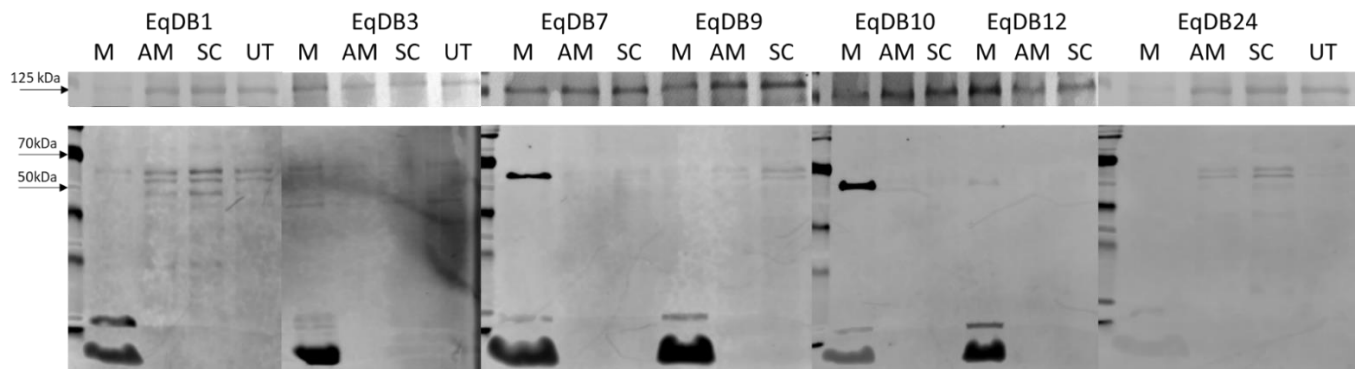
LC3B = microtubule-associated proteins 1A/1B light chain 3B, predicted molecular weight 15 kDa.

#### F. P62/SQSTM1 and Vinculin



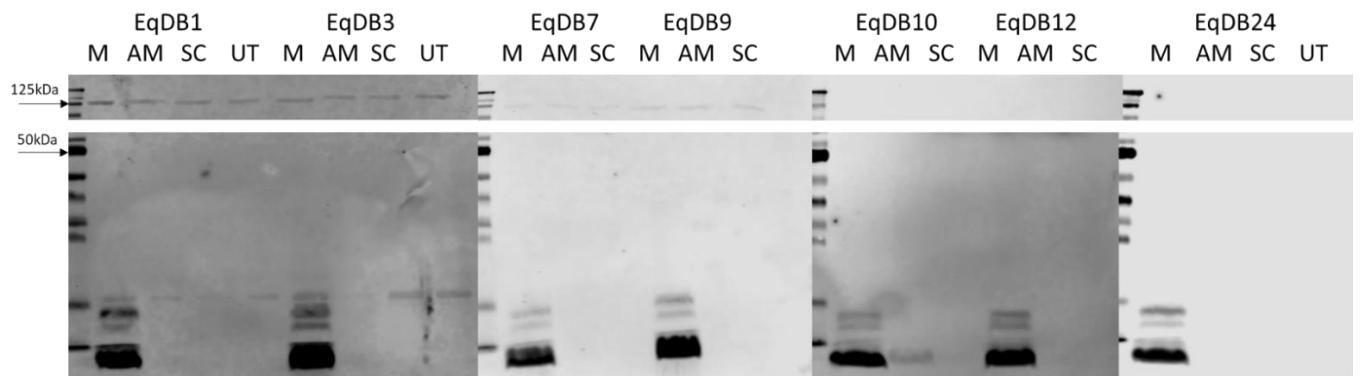
P62/SQSTM1 = ubiquitin-binding protein p62, predicted molecular weight 61 kDa.

### G. NRF2 and Vinculin



NRF2 = nuclear factor erythroid 2, predicted molecular weight 61 kDa.

### H. Parkin and Vinculin



Parkin predicted molecular weight 52 kDa.

**Figure A6.2** (includes preceding 2 pages) Western blot images from mmu-miR-181a-5p mimic (M), antagomiR (AM) and scrambled control (SC) treated equine tendon constructs. Vinculin used as loading control, predicted molecular weight 124 kDa. UT = untreated. Images acquired using LI-COR Odyssey CLx Imaging System at emission wavelengths 700 nm (for vinculin) and 800 nm (all other targets).



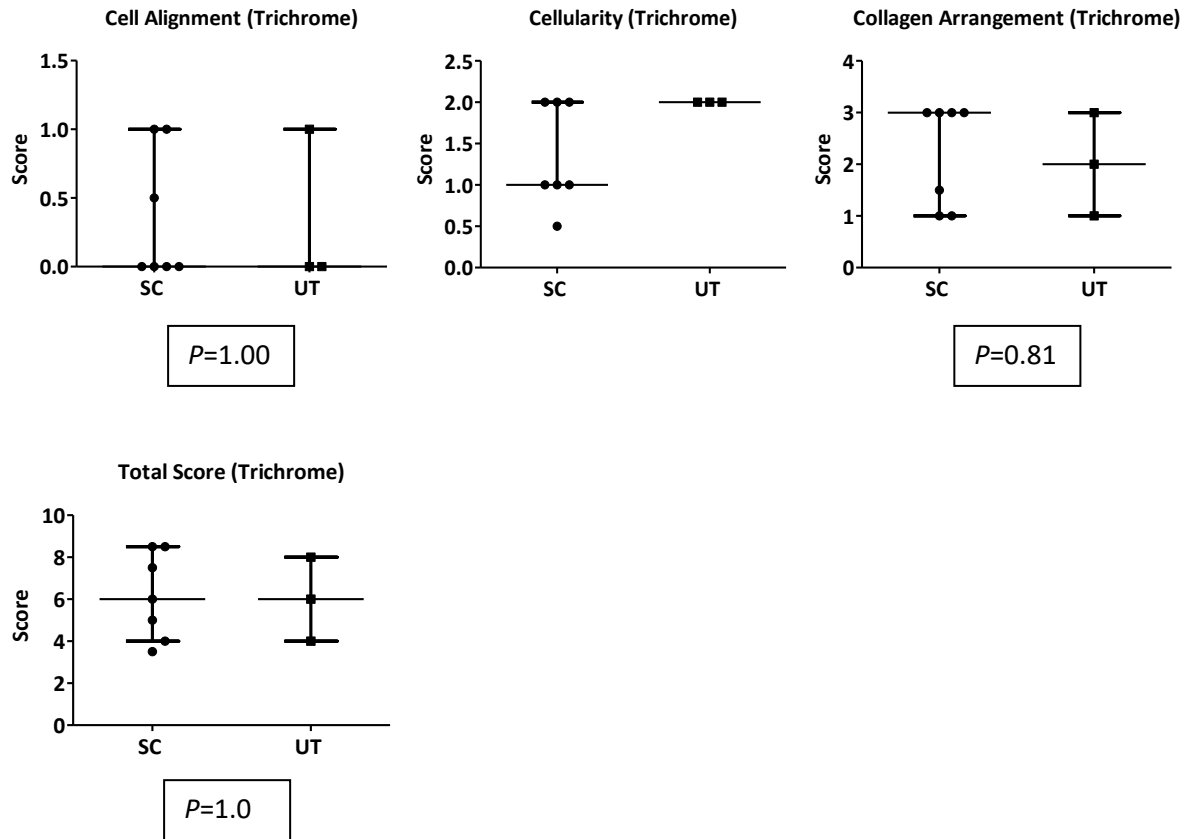


**Figure A6.3** (includes preceding page) Comparison between scrambled control (SC) treated and untreated (UT) equine tendon constructs on histological scoring of haematoxylin and eosin (H&E) and Masson's Trichrome stained sections. Results show average of two consecutive blinded gradings by the same operator (First grader). *P*-values obtained using Mann Whitney test. *P*-values are not calculable where all values in one group are identical. Graphs show median and interquartile range.

## **Appendix 7**

**Table A7.1** *Small nucleolar RNA-61 (SNORD61)* expression in human primary tenocytes is unaffected by treatment with miR-181a-5p mimic, antagomiR or scrambled control sequence oligonucleotides.

**Table A7.2** *Glyceraldehyde 3-phosphate dehydrogenase (GAPDH)* expression in human primary tenocytes is unaffected by treatment with miR-181a-5p mimic, antagomiR or scrambled control oligonucleotides.

**Figure A7.1** Comparison between scrambled control (SC) treated and untreated (UT) human tenocytes on the expression of selected target genes.

**Figure A7.2** Western blot images from mmu-miR-181a-5p mimic (M), antagomiR (AM) and scrambled control (SC) treated human tenocytes for three biological replicates.

**Figure A7.3** Comparison between scrambled control (SC) treated and untreated (UT) human tenocytes on the levels of selected target proteins.

Donor Identity	Ct Values										
	Mimic treated		AntagomiR treated		Scrambled control treated		Untreated control		Max	Min	Max - Min
	Replicates	Average	Replicates	Average	Replicates	Average	Replicates	Average			
LMB-JL-280	29.9	29.47	28.57	28.55	28.54	28.31	28.38	28.50	29.47	28.31	1.17
LMB-JL-280	29.39		28.4		28.19		28.67				
LMB-JL-280	29.13		28.67		28.19		28.44				
LMB-SF-282	28.98	28.70	27.94	28.75	27.92	28.27	29.12	29.79	29.79	28.27	1.52
LMB-SF-282	28.51		29.04		28.15		30.01				
LMB-SF-282	28.61		29.28		28.73		30.23				
LMB-RL-286	28.56	28.64	28.27	28.35	28.2	28.32	28.73	28.76	28.76	28.32	0.44
LMB-RL-286	28.7		28.45		28.27		28.73				
LMB-RL-286	28.66		28.34		28.49		28.83				
Mean	28.94	28.94	28.55	28.55	28.30	28.30	29.02	29.02	29.02	28.30	0.72
SD	0.47	0.46	0.41	0.20	0.25	0.03	0.66	0.68	0.68	0.03	0.65
Max	29.90	29.47	29.28	28.75	28.73	28.32	30.23	29.79	29.79	28.32	1.47
Min	28.51	28.64	27.94	28.35	27.92	28.27	28.38	28.50	28.64	28.27	0.37
Max - Min	1.39	0.83	1.34	0.40	0.81	0.05	1.85	1.29	1.29	0.05	1.24

**Table A7.1 *Small nucleolar RNA-61 (SNORD61)* expression in human primary tenocytes is unaffected by treatment with miR-181a-5p mimic, antagomiR or scrambled control sequence oligonucleotides.** Threshold cycle (Ct) values are presented for three biological replicates, each run in triplicate. Columns demonstrate variation between biological replicates, rows demonstrate variation with treatment. Max = maximum, Min = minimum, SD = standard deviation.

Donor Identity	Ct Values										
	Mimic treated		AntagomiR treated		Scrambled control treated		Untreated control		Max	Min	Max - Min
	Replicates	Average	Replicates	Average	Replicates	Average	Replicates	Average			
LMB-JL-280	20.65	20.64	20.15	20.18	20.43	20.41	20.28	20.27	20.64	20.18	0.46
LMB-JL-280	20.68		20.2		20.42		20.27				
LMB-JL-280	20.6		20.19		20.38		20.27				
LMB-SF-282	20.4	20.43	20.55	20.60	21.02	21.01	21.18	21.23	21.23	20.43	0.79
LMB-SF-282	20.46		20.65		21.01		21.3				
LMB-SF-282	20.44		20.61		21		21.2				
LMB-RL-286	20.19	20.09	20.37	20.48	20.31	20.31	20.41	20.43	20.48	20.09	0.39
LMB-RL-286	20.08		20.69		20.3		20.46				
LMB-RL-286	19.99		20.37		20.32		20.42				
Mean	20.39	20.39	20.42	20.42	20.58	20.58	20.64	20.64	20.64	20.39	0.26
SD	0.25	0.28	0.21	0.22	0.33	0.38	0.44	0.51	0.51	0.22	0.29
Max	20.68	20.64	20.69	20.60	21.02	21.01	21.30	21.23	21.23	20.60	0.62
Min	19.99	20.09	20.15	20.18	20.30	20.31	20.27	20.27	20.31	20.09	0.22
Max - Min	0.69	0.56	0.54	0.42	0.72	0.70	1.03	0.95	0.95	0.42	0.53

**Table A7.2 *Glyceraldehyde 3-phosphate dehydrogenase (GAPDH)* expression in human primary tenocytes is unaffected by treatment with miR-181a-5p mimic, antagomiR or scrambled control oligonucleotides.** Threshold cycle (Ct) values are presented for three biological replicates, each run in triplicate. Columns demonstrate variation between biological replicates, rows demonstrate variation with treatment. Max = maximum, Min = minimum, SD = standard deviation.

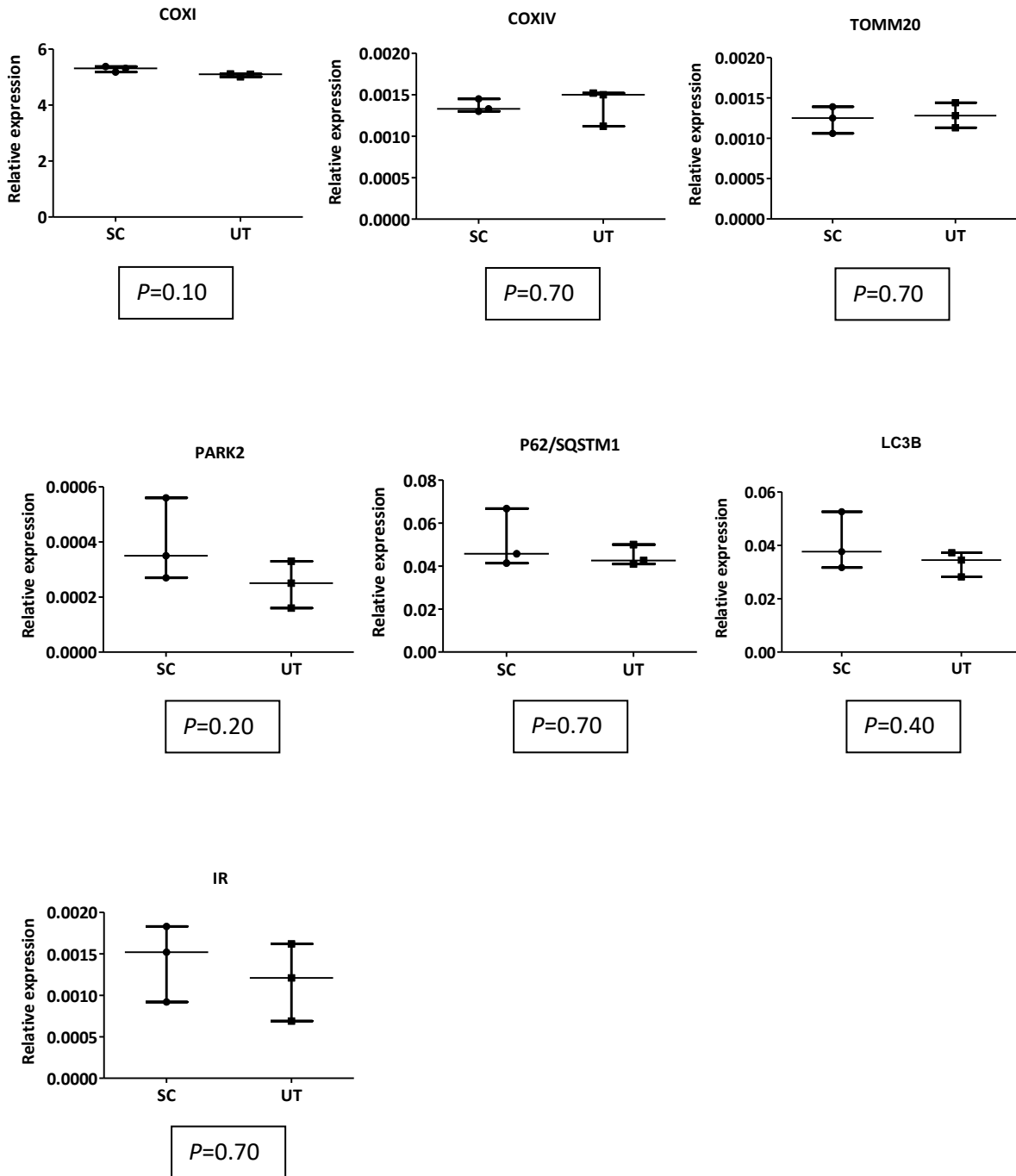
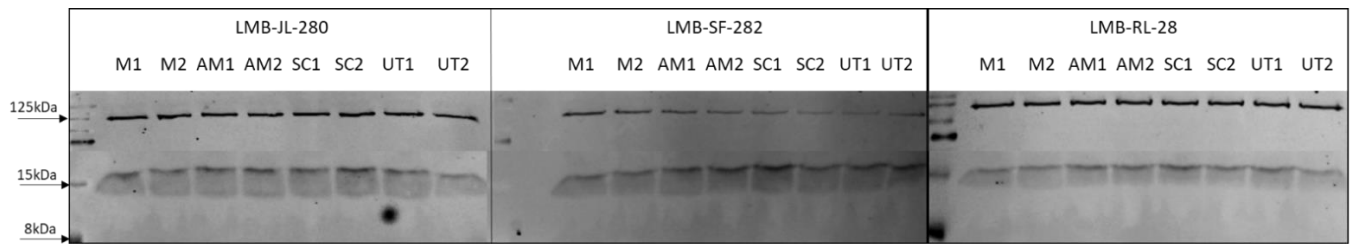


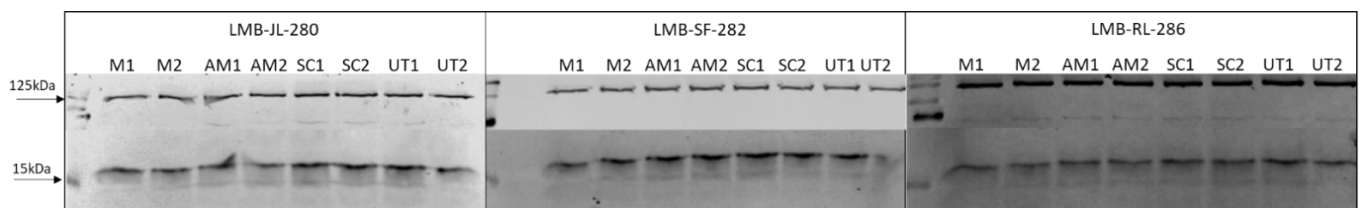
**Figure A7.1 Comparison between scrambled control (SC) treated and untreated (UT) human tenocytes on the expression of selected target genes.** Y-axis values represent expression relative to *glyceraldehyde 3-phosphate dehydrogenase* (GAPDH). P-values calculated from delta Ct values, using Mann-Whitney test. Graphs show median and interquartile range.

### A. TOMM20 and Vinculin



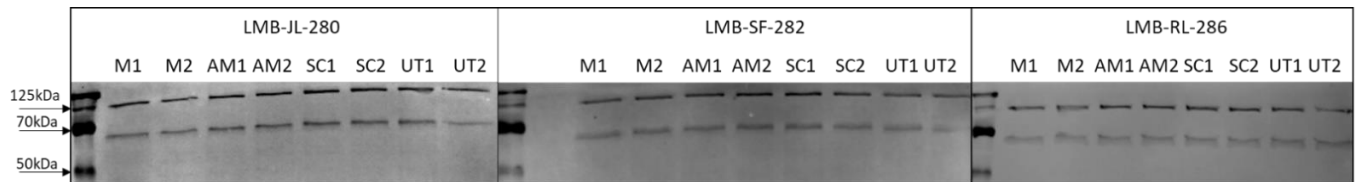
TOMM20 = translocase of outer mitochondrial membrane 20, predicted molecular weight 16 kDa.

### B. LC3B and Vinculin



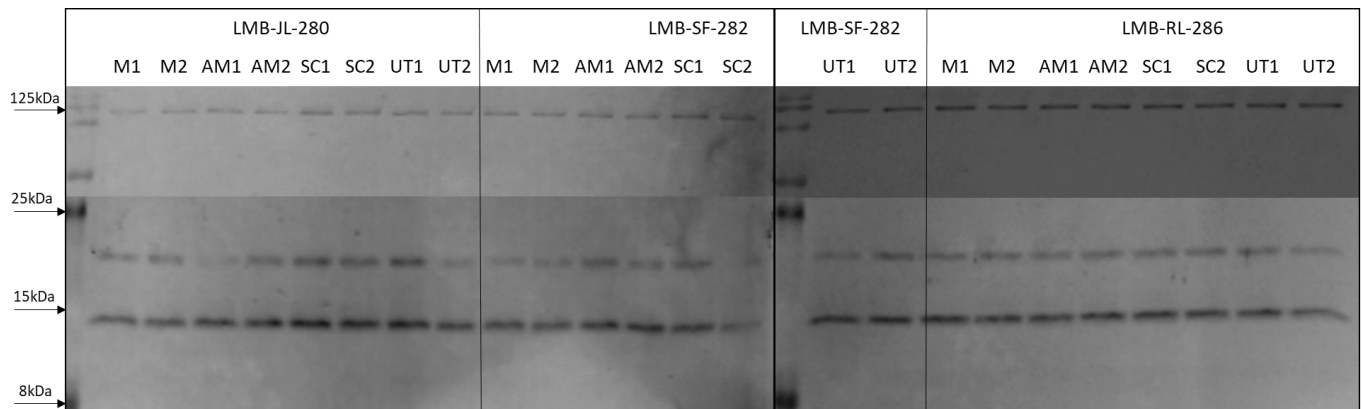
LC3B = microtubule-associated proteins 1A/1B light chain 3B, predicted molecular weight 15 kDa.

### C. P62/SQSTM1 and Vinculin



P62/SQSTM1 = ubiquitin-binding protein p62, predicted molecular weight 61 kDa.

### D. COXIV and Vinculin



COXIV = cytochrome c oxidase subunit 4, predicted molecular weight 17 kDa.

**Figure A7.2** (*preceding page*) **Western blot images from mmu-miR-181a-5p mimic (M), antagomiR (AM) and scrambled control (SC) treated human tenocytes for three biological replicates.** Vinculin used as loading control, predicted molecular weight 124 kDa. UT = untreated. Images acquired using LI-COR Odyssey CLx Imaging System at emission wavelengths 700 nm (vinculin) and 800 nm (all other targets).

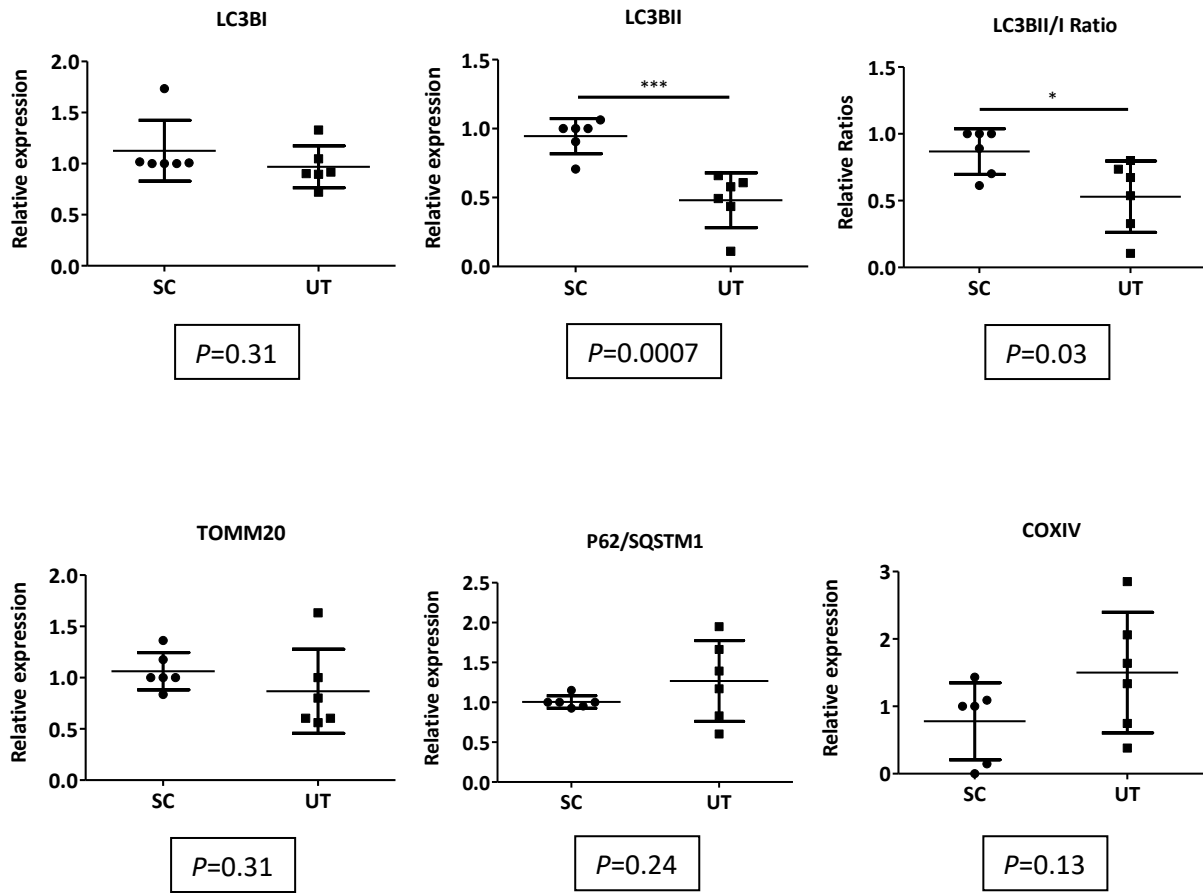


**Figure A7.3 Comparison between scrambled control (SC) treated and untreated (UT) human tenocytes on the levels of selected target proteins.** Protein levels calculated using densitometric analysis in ImageJ 1.52 software (<https://imagej.nih.gov/ij/>, 1997-2018), normalised to vinculin as loading control. P-values calculated using Student-t test. \* =  $P < 0.05$ , \*\*\* =  $P < 0.001$ . Graphs show mean and standard deviation.

## **References**

- Abrahams, Y., Laguette, M.-J., Prince, S., Collins, M. (2013) Polymorphisms within the COL5A1 3'-UTR that alters mRNA structure and the MIR608 gene are associated with Achilles tendinopathy. *Ann Human Genet* 77; 204-214.
- Abraham, A.C., Shah, S.A., Golman, M., Song, L., Li, X., Kurtaliaj, I., Akbar, M., Millar, N.L., Abu-Amer, Y., Galatz, L.M., Thomopoulos, S. (2019) Targeting the NF- $\kappa$ B signalling pathway in chronic tendon disease. *Sci Transl Med* 11; eaav4319. doi:10.1126/scitranslmed.aav4319.
- Agarwal, V., Bell, G.W., Nam, J., Bartel, D.P. (2015) Predicting effective microRNA target sites in mammalian mRNAs. *eLife* 4; e05005.
- Albers, S., Zwerver, J., van den Akker-Scheek, I. (2014). Incidence and prevalence of lower extremity tendinopathy in the general population. *Br J Sports Med* 48 (Suppl 2); A5. doi:10.1136/bjsports-2014-094114.7.
- Alfredson, H., Lorentzon, M., Bäckman, S., Bäckman, A., Lerner, U.H. (2003) cDNA-arrays and real-time quantitative PCR techniques in the investigation of chronic Achilles tendinosis. *J Orthop Res* 21; 970-975.
- Ali, O.J., Comerford, E.J., Clegg, P.D., Canty-Laird, E.G. (2018) Variations during ageing in the three-dimensional anatomical arrangement of fascicles within the equine superficial digital flexor tendon. *Eur Cells Materials* 35; 87-102. doi:10.22203/eCM.v035a07.
- Ali, O.J., Ehrle, A., Comerford, E.J., Canty-Laird, E.G., Mead, A., Clegg, P.D., Maddox, T.W. (2021) Intrafascicular chondroid-like bodies in the ageing equine superficial digital flexor tendon comprise glycosaminoglycans and type II collagen. *J Orthop Res* Epub ahead of print. doi:10.1002/jor.25002.
- Allen, G.F.G., Toth, R., James, J., Ganley, I.G. (2013) Loss of iron triggers PINK/Parkin-independent mitophagy. *EMBO Reports* 14; 1127-1135.
- Alles, J., Fehlmann, T., Fischer, U., Backes, C., Galata, V., Minet, M., Hart, M., Abu-Halima, M., Grässer, F.A., Lenhof, H-P., Keller, A., Meese, E. (2019) An estimate of the total number of true human miRNAs. *Nucleic Acids Res* 47; 3353-3364.
- Amort, M., Nachbauer, B., Tuzlak, S., Kieser, A., Schepers, A., Villunger, A., Polacek, N. (2015) Expression of the vault RNA protects cells from undergoing apoptosis. *Nat Commun* 6; 7030. doi:10.1038/ncomms8030.
- Anderson, J.R., Smagul, A., Simpson, D., Clegg, P.D., Rubio-Martinez, L., Peffers, M.J. (2019) The synovial fluid proteome differs between septic and non-septic articular pathologies. *J Proteomics* 202; 103370. doi:10.1016/j.jprot.2019.04.020.
- Andrejewski, N., Punnonen, E-L., Guhde, G., Tanaka, Y., Lüllmann-Rauch, R., Hartmann, D., von Figura, K., Saftig, P. (1999) Normal lysosomal morphology and function in LAMP-1-deficient mice. *J Biol Chem* 274; 12692-12701.

- Archambault, J., Jelinsky, S.A., Lake, S.P., Hill, A.A., Glaser, D.L., Soslowsky, L.J. (2007) Rat supraspinatus tendon expresses cartilage markers with overuse. *J Orthop Res* 25; 617-624.
- Archer, S.L. (2013) Mitochondrial dynamics – mitochondrial fission and fusion in human diseases. *N Engl J Med* 369; 2236-2251.
- Arndt, A.N., Komi, P.V., Bruggemann, G.P., Lukkariniemi, J. (1998) Individual muscle contributions to the in vivo Achilles tendon force. *Clin Biomech* 13; 532-541.
- Arnoczky, S.P., Lavagnino, M., Egerbacher, M. (2007). The mechanobiological aetiopathogenesis of tendinopathy: is it the over-stimulation or the under-stimulation of tendon cells? *Int J Exp Path* 88; 217-226.
- Asirvatham, A.J., Magner, W.J., Tomasi, T.B. (2009) miRNA regulation of cytokine genes. *Cytokine* 45; 58-69.
- Astrom, M. (2000) Laser Doppler flowmetry in the assessment of tendon blood flow. *Scand J Med Sci Sports* 10; 365-367.
- Avery, N.C., Bailey, A.J. (2006) The effects of the Maillard reaction on the physical properties and cell interactions of collagen. *Pathol Biol* 54; 387-395.
- Backes, C., Fehlmann, T., Kern, F., Kehl, T., Lenhof, H-P., Meese, E., Keller, A. (2018) miRCarta: a central repository for collecting miRNA candidates. *Nucleic Acids Res* 46; D160-D167. doi:10.1093/nar/gkx851.
- Backman, C., Boquist, L., Friden, J., Lorentzon, R., Toolanen, G. (1990) Chronic Achilles paratenonitis and tendinosis: an experimental model in the rabbit. *J Orthop Res* 8; 541-547.
- Bader, B.L., Smyth, N., Nedbal, S., Miosge, N., Baranowsky, A., Mokkapati, S., Murshed, M., Nischt, R. (2005) Compound genetic ablation of nidogen 1 and 2 causes basement membrane defects and perinatal lethality in mice. *Mol Cell Biol* 25; 6846-6856. doi:10.1128/MCB.24.15.6846.6856.2005.
- Barbe, M.F., Barr, A.E., Gorzelany, I., Amin, M., Gaughan, J.P., Safadi, F.F. (2003) Chronic repetitive reaching and grasping results in decreased motor performance and widespread tissue responses in a rat model of MSD. *J Orthop Res* 21; 167-176.
- Bardell, D., Peffers, M.J., Clegg, P.D., Molloy, A., Goljanek-Whysall, K. (2018) The role of microRNAs in tendon dysfunction. *Osteoarthritis and Cartilage* 26; S165-166. doi:10.1016/j.joca.2018.02.361.
- Bardell, D., Milner, P., Goljanek-Whysall, K., Peffers, M. (2019) Differences in plasma and peritoneal fluid proteomes identifies potential biomarkers associated with survival following strangulating small intestinal disease. *Equine Vet J* 51; 727-732. doi:10.1111/evj.13094.
- Bartel, D.P. (2004) microRNAs: genomics, biogenesis, mechanism and function. *Cell* 116; 281-297.
- Bartel, D.P. (2009) microRNAs: target recognition and regulatory functions. *Cell* 136; 215-233.
- Bartel, D.P. (2018) Metazoan microRNAs. *Cell* 173; 20-51.
- Batson, E.L., Paramour, R.J., Smith, T.J., Birch, H.L., Patterson-Kane, J.C., Goodship, A.E. (2003) Are the material properties and matrix composition of equine flexor and extensor tendons determined by their functions? *Equine Vet J* 35; 314-318.

- Bavin, E.P., Atkinson, F., Barsby, T., Guest, D.J. (2017) Scleraxis is essential for tendon differentiation by equine embryonic stem cells and in equine fetal tenocytes. *Stem Cell Dev* 26; 441-450. doi:10.1089/scd.2016.0279.
- Benson, R.T., McDonnell, S.M., Knowles, H.J., Rees, J.L., Carr, A.J., Hulley, P.A. (2010) Tendinopathy and tears of the rotator cuff are associated with hypoxia and apoptosis. *J Bone Joint Surg (Br)* 92-B; 448-453.
- Bentwich, I. (2005) Prediction and validation of microRNAs and their targets. *FEBS Letters* 579; 5904-5910.
- Bernard-Beaubois, K., Hecquet, C., Hayem, G., Rat, P., Adolphe, M. (1998) In vitro study of cytotoxicity of quinolones on rabbit tenocytes. *Cell Biol Toxicol* 14; 283-292.
- Bi, Y., Ehrchiou, D., Kilts, T.M., Inkson, C.A., Embree, M.C., Sonoyama, W., Li, L., Leet, A.I., Seo, B-M., Zhang, L., Shi, S., Young, M.F. (2007) Identification of tendon stem/progenitor cells and the role of the extracellular matrix in their niche. *Nat Med* 13; 1219-1227.
- Bignotti, E., Calza, S., Tassi, R.A., Zanotti, L., Bandiera, E., Sartori, E., Odicino, F.E., Ravaggi, A., Todeschini, P., Romani, C. (2016) Identification of stably expressed reference small non-coding RNAs for microRNA quantification in high-grade serous ovarian carcinoma tissues. *J Cell Mol Med* 20; 2341-2348.
- Birch, H.L., Rutter, G.A., Goodship, A.E. (1997) Oxidative energy metabolism in equine tendon cells. *Res Vet Sci* 62; 93-97.
- Birch, H.L., Bailey, A.J., Goodship, A.E. (1998) Macroscopic 'degeneration' of equine superficial digital flexor tendon is accompanied by a change in extracellular matrix composition. *Equine Vet J* 30; 534-539.
- Birch, H.L., Bailey, J.V.B., Bailey, A.J., Goodship, A.E. (1999) Age-related changes to the molecular and cellular components of equine flexor tendons. *Equine Vet J* 31; 391-396.
- Birch, H.L., Smith, T.J., Poulton, C., Peiffer, D., Goodship, A.E. (2002) Do regional variations in flexor tendons predispose to site-specific injuries? *Equine Vet J Suppl* 34; 288-292.
- Birch, H.L. (2007) Tendon matrix composition and turnover in relation to functional requirements. *Int J Exp Path* 88; 241-248.
- Birch, H.L., Worboys, S., Eissa, S., Jackson, B., Strassburg, S., Clegg, P.D. (2008a) Matrix metabolism rate differs in functionally distinct tendons. *Matrix Biology* 27; 182-189.
- Birch, H.L., Wilson, A.M., Goodship, A.E. (2008b) Physical activity: does long-term, high-intensity exercise in horses result in tendon degeneration? *J Appl Physiol* 105; 1927-1933.
- Birk, D.E. (2001) Type V collagen: heterotypic type I/V collagen interactions in the regulation of fibril assembly. *Micron* 32; 223-237.
- Bowling, J.L., Skolfield, M.C., Riley, W.A., Nolin, A.P., Wolf, L.C., Nelson, D.E. (2019) Temporal integration of mitochondrial stress signals by the PINK1:Parkin pathway. *BMC Mol Cell Biol* 20; 33. doi:10.1186/s12860-019-0220-5.

- Boyle, B., Dallaire, N., MacKay, J. (2009) Evaluation of the impact of single nucleotide polymorphisms and primer mismatches on quantitative PCR. *BMC Biotech* 9; 75. doi:10.1186/1472-6750-9-75.
- Breidenbach, A.P., Dymont, N.A., Lu, Y., Rao, M., Shearn, J.T., Rowe, D.W., Kadler, K.E., Butler, D.L. (2015) Structural and mechanical properties compared with collagen gels in cell-based tendon tissue-engineered constructs. *Tissue Engineering Part A* 21: 438-450. doi:10.1089/ten.tea.2013.0768.
- Brown, D.M., Goljanek-Whysall, K. (2015) microRNAs: modulators of the underlying pathophysiology of sarcopaenia? *Ageing Res Rev* 24; 263-273.
- Buso, A., Comelli, M., Picco, R., Isola, M., Magnesa, B., Pišot, R., Rittweger, J., Salvadego, D., Šimunič, B., Grassi, B., Mavelli, I. (2019) Mitochondrial adaptations in elderly and young men skeletal muscle following 2 weeks of bed rest and rehabilitation. *Front Physiol* 10; 474. doi:10.3389/fphys.2019.00474.
- Butcher, M.T., Hermanson, J.W., Ducharme, N.G., Mitchell, L.M., Soderholm, L.V., Bertram, J.E.A. (2007) Superficial digital flexor tendon lesions in racehorses as a sequela to muscle fatigue: a preliminary study. *Equine Vet J* 39; 540-545.
- Canty, E.G., Lu, Y., Meadows, R.S., Shaw, M.K., Holmes, D.F., Kadler, K.E. (2004) Coalignment of plasma membrane channels and protrusions (fibripositors) specifies the parallelism of tendon. *J Cell Biol* 165; 553-563.
- Carroll, A.P., Tooney, P.A., Cairns, M.J. (2013) Context-specific microRNA function in developmental complexity. *J Mol Cell Biol* 5; 73-84.
- Caterson, B., Baker, J.R., Christner, J.E., Lee, Y., Lentz, M. (1985) Monoclonal antibodies as probes for determining the microheterogeneity of the link proteins of cartilage proteoglycan. *J Biol Chem* 260; 11348-11356.
- Chapman, J., Fielder, E., Passos, J.F. (2019) Mitochondrial dysfunction and cell senescence: deciphering a complex relationship. *FEBS Letters* 593; 1566-1579.
- Chatterjee, S., Grosshans, H. (2009) Active turnover modulates microRNA activity in *Caenorhabditis elegans*. *Nature* 461; 546-549.
- Cheloufi, S., Dos Santos, C.O., Chong, M.M., Hannon, G.J. (2010) A Dicer-independent miRNA biogenesis pathway that requires Ago catalysis. *Nature* 465; 584-589.
- Chen, H., Detmer, S.A., Ewald, A.J., Griffin, E.E., Fraser, S.E., Chan, D.C. (2003) Mitofusins Mfn1 and Mfn2 coordinately regulate mitochondrial fusion and are essential for embryonic development. *J Cell Biol* 160; 189-200.
- Chen, J., Bardes, E.E., Aronow, B.J., Jegga, A.G. (2009) ToppGene Suite for gene list enrichment analysis and candidate gene prioritization. *Nucleic Acids Res* 37; W305-W311. doi:10.1093/nar/gkp427.
- Chen, C., Zhang, Y., Zhang, L., Weakley, S.M., Yao, Q. (2011) MicroRNA-196: critical roles and clinical applications in development and cancer. *J Cell Mol Med* 15; 14-23.
- Chen, L., Liu, J., Tao, X., Wang, G., Wang, Q., Liu, X. (2015a) The role of Pin1 protein in aging of human tendon stem/progenitor cells. *Biochem Biophys Res Commun* 464; 487-492.

- Chen, L., Wang, G-D., Liu, J-P., Wang, H-S., Liu, X-M., Wang, Q., Cai, X-H. (2015b) MiR-135a modulates tendon stem/progenitor cell senescence via suppressing ROCK1. *Bone* 71; 210–216.
- Chen, P., Pan, J., Zhang, X., Shi, Z., Yang, X. (2018) The role of micro-RNA-181a in myocardial fibrosis following myocardial infarction in a rat model. *Med Sci Monit* 24; 4121-4127.
- Chen, C., Turnbull, D.M., Reeve, A.K. (2019) Mitochondrial dysfunction in Parkinson’s Disease – cause or consequence? *Biology* 8; 38. doi:10.3390/biology8020038.
- Cheng, V.W.T., Screen, H.R.C. (2007) The micro-structural strain response of tendon. *J Mater Sci* 42; 8957-8965.
- Chiang, H.R., Schoenfeld, L.W., Ruby, J.G., Auyeung, V.C., Spies, N. Baek, D., Johnston, W.K., Russ, C., Luo, S., Babiarz, J.E., Blelloch, R., Schroth, G.P., Nusbaum, C., Bartel, D.P. (2010) Mammalian microRNAs: experimental evaluation of novel and previously annotated genes. *Genes Dev* 24; 992-1009.
- Chisari, E., Rehak, L., Khan, W.S., Maffulli, N. (2019) Tendon healing in presence of chronic low-level inflammation: a systematic review. *Br Med Bull* 132; 97-116. doi:10.1093/bmb/ldz035.
- Chou, C-H., Shrestha, S., Yang, C-D., Chang, N-W., Lin, Y-L., Liao, K-W., Huang, W-C., Sun, T-H., Tu, S-J., Lee, W-H., Chiew, M-Y., Tai, C-S., Wei, T-Y., Tsai, T-R., Huang, H-T., Wang, C-Y., Wu, H-Y., Ho, S-Y., Chen, P-R., Chuang, C-H., Hsieh, P-J., Wu, T-S., Chen, W-L., Li, M-J., Wu, Y-C., Huang, X-Y., Ng, F.L., Buddhakosai, W., Huang, P-C., Lan, K-C., Huang, C-Y., Weng, S-L., Cheng, Y-N., Liang, C., Hsu, W-L., Huang, H-D. (2018) miRTarBase update 2018: a resource for experimentally validated microRNA-target interactions. *Nucleic Acids Res* 46; D296-D302. doi:10.1093/nar/gkx1067.
- Chuen, F.S., Chuk, C.Y., Ping, W.Y., Nar, W.W., Kim, H.L., Ming, C.K. (2004) Immunohistochemical characterisation of cells in adult human patellar tendons. *J Histochem Cytochem* 52; 1151-1157.
- Ciechomska, M., O’Reilly, S., Suwara, M., Bogunia-Kubik, K., van Laar, J.M. (2014) mir-29a reduces TIMP-1 production by dermal fibroblasts via targeting TGF- $\beta$  activated kinase 1 binding protein 1, implications for systemic sclerosis. *PLoS ONE* 9; e115596. doi:10.1371/journal.pone.0115596.
- Clarke-Cornwell, A., Jordan, K., Croft, P., Symmons, D.P. (2006). Variation of musculoskeletal consultation prevalence by practice and social deprivation category: data from the general practice research database. *Rheumatol* 45 (Suppl 1); 127-130.
- Comeau, J.W.D., Costantino, S., Wiseman, P.W. (2006) A guide to accurate fluorescence microscopy colocalization measurements. *Biophys J* 91; 4611-4622.
- Cook, J.L., Feller, J.A., Bonar, S.F., Khan, K.M. (2004) Abnormal tenocyte morphology is more prevalent than collagen disruption in asymptomatic athletes’ patellar tendons. *J Orthop Res* 22; 334-338.
- Corps, A.N., Robinson, A.H.N., Movin, T., Costa, M.L., Hazleman, B.L., Riley, G.P. (2006) Increased expression of aggrecan and biglycan mRNA in Achilles tendinopathy. *Rheumatol* 45; 291-294.
- da Costa Martins, P.A., Salic, K., Gladka, M.M., Armand, A-S., Leptidis, S., el Azzouzi, H., Hansen, A., Coenen-de Roo, C.J., Bierhuizen, M.F., van der Nagel, R., van Kuik, J., de Weger, R., de Bruin, A., Condorelli, G., Arbones, M.L., Eschenhagen, T., de Windt, L.J. (2010) microRNA-199b targets the

- nuclear kinase Dyrk1a in an auto-amplification loop promoting calcineurin/NFAT signalling. *Nat Cell Biol* 12; 1220-1227. doi:10.1038/ncb2126.
- Couppé, C., Hansen, P., Kongsgaard, M., Kovanen, V., Suetta, C., Aagaard, P., Kjær, M., Magnusson, S.P. (2009) Mechanical properties and collagen cross-linking of the patellar tendon in old and young men. *J Appl Physiol* 107; 880-886.
- Cui, H., Ge, J., Xie, N., Banerjee, S., Zhou, Y., Liu, R-M., Thannickal, V.J., Liu, G. (2017) miR-34a promotes fibrosis in aged lungs by inducing alveolarepithelial dysfunctions. *Am J Physiol Cell Mol Physiol* 312; L415-L424. doi:10.1152/ajplung.00335.2016.
- Cummins, E.J., Anson, B.J., Carr, B.W., Wright, R.R., Hauser, E.D. (1946) The structure of the calcaneal (Achilles) tendon in relation to orthopaedic surgery. *Surg Gynaecol Obstet* 83; 107-116.
- Dahlgren, L.A., van der Meulen, M., Bertram, J.E.A., Starrak, G.S., Nixon, A.J. (2002) Insulin-like growth factor-I improves cellular and molecular aspects of healing in a collagenase-induced model of flexor tendinitis. *J Orthop Res* 20; 910-919.
- Dakin, S.G., Werling, D., Hibbert, A., Abayasekara, D.R.E., Young, N.J., Smith, R.K.W., Dudhia, J. (2012) Macrophage sub-populations and the Lipoxin A<sub>4</sub> receptor implicate active inflammation during equine tendon repair. *PLoS ONE* 7; e32333. doi:10.1371/journal.pone.0032333.
- Dakin, S.G., Dudhia, J., Smith, R.K.W. (2014) Resolving an inflammatory concept: the importance of inflammation and resolution in tendinopathy. *Vet Immunol Immunopathol* 158; 121-127. doi:10.1016/j.vetimm.2014.01.007.
- Dakin, S.G., Newton, J., Martinez, F.O., Hedley, R., Gwilym, S., Jones, N., Reid, H.A.B., Wood, S., Wells, G., Appleton, L., Wheway, K., Watkins, B., Carr, A.J. (2018) Chronic inflammation is a feature of Achilles tendinopathy and rupture. *Br J Sports Med* 52; 359-367.
- Das, S., Kohr, M., Dunkerly-Eyring, B., Lee, D.I., Bedja, D., Kent, O.A., Leung, A.K.L., Henao-Mejia, J.H., Flavell, R.A., Steenbergen, C. (2017) Divergent effects of miR-181 family members on myocardial function through protective cytosolic and detrimental mitochondrial microRNA targets. *J Am Heart Assoc* 6; e004694.
- Davis, B.N., Hilyard, A.C., Nguyen, P.H., Lagna, G., Hata, A. (2010) SMAD proteins bind a conserved RNA sequence to promote microRNA maturation by Drosha. *Mol Cell* 39; 373-384. doi:10.1016/j.molcel.2010.07.011.
- de la Mata, M., Gaidatzis, D., Vitanescu, M., Stadler, M.B., Wentzel, C., Scheiffele, P., Filipowicz, W., Grosshans, H. (2015) Potent degradation of neuronal miRNAs induced by highly complementary targets. *EMBO Reports* 16; 500-511.
- Dikic, I., Elazar, Z. (2018) Mechanism and medical implications of mammalian autophagy. *Nat Rev Mol Cell Biol* 19; 349-364.
- Dillies, M-A., Tau, A., Aubert, J., Hennequet-Antier, C., Jeanmougin, M., Servant, N., Keime, C., Marot, G., Castel, D., Estelle, J., Guernec, G., Jagla, B., Jouneau, I., Laloë, D., le Gall, C., Schaëffer, B., le Crom, S., Guedj, M., Jaffrézic, F. (2012) A comprehensive evaluation of normalization methods for Illumina high-throughput RNA sequencing data analysis. *Briefings Bioinformatics* 14; 671-683. doi:10.1093/bib/bbs046.

- Disser, N.P., Sugg, K.B., Talarek, J.R., Sarver, D.C., Rourke, B.J., Mendias, C.L. (2019) Insulin-like growth factor 1 signalling in tenocytes is required for adult tendon growth. *FASEB J* 33; 12680-12695.
- Doroski, D.M., Brink, K.S., Temenoff, J.S. (2007) Techniques for biological characterisation of tissue-engineered tendon and ligament. *Biomater* 28; 187-202.
- Dowling, B.A., Dart, A.J. (2005) Mechanical and functional properties of the equine superficial digital flexor tendon. *Vet J* 170; 184-192.
- Dudhia, J., Scott, C.M., Draper, E.R.C., Heinegard, D., Pitsillides, A.A., Smith, R.K. (2007) Aging enhances a mechanically-induced reduction in tendon strength by an active process involving matrix metalloproteinase activity. *Aging Cell* 6; 547-556.
- Dyson, S.J. (2004) Medical management of superficial digital flexor tendonitis: a comparative study in 219 horses (1992-2000). *Equine Vet J* 36; 415-419.
- Egerbacher, M., Gabner, S., Battisti, S., Handschuh, S. (2020) Tenocytes form a 3-D network and are connected via nanotubes. *J Anat* 236; 165-170.
- Eichhorn, S.W., Guo, H., McGearry, S.E., Rodriguez-Mias, R.A., Shin, C., Baek, D., Hsu, S.H., Ghoshal, K., Villén, J., Bartel, D.P. (2014) mRNA destabilisation is the dominant effect of mammalian microRNAs by the time substantial repression ensues. *Mol Cell* 56; 104-115.
- Ely, E.R., Avella, C.S., Price, J.S., Smith, R.K.W., Wood, J.L.N., Verheyen, K.L.P. (2009) Descriptive epidemiology of fracture, tendon and suspensory ligament injuries in National Hunt racehorses in training. *Equine Vet J* 41; 372-378.
- Erhard, F., Haas, J., Lieber, D., Malterer, G., Jaskiewicz, L., Zavolan, M., Dölken, L., Zimmer, R. (2014) Widespread context dependency of microRNA-mediated regulation. *Genome Res* 24; 906-919.
- Eskelinen, E-L. (2006) Roles of LAMP-1 and LAMP-2 in lysosome biogenesis and autophagy. *Mol Aspects Med* 27; 495-502.
- Essen, B., Jansson, E., Henriksson, J., Taylor, A.W., Saltin, B. (1975). Metabolic characteristics of fibre types in human skeletal muscle. *Acta Physiol Scand* 95; 153-165.
- Esteller, M. (2011) Non-coding RNAs in human disease. *Nature Rev Genet* 12; 861-874.
- Fabbri, M. (2012) TLRs as miRNA receptors. *Cancer Res* 72; 6333-6337.
- Fang, E.F., Waltz, T.B., Kassahun, H., Lu, Q., Kerr, J.S., Morevati, M., Fivenson, E.M., Wollman, B.N., Marosi, K., Wilson, M.A., Iser, W.B., Eckley, D.M., Zhang, Y., Lehrmann, E., Goldberg, I.G., Scheibye-Knudsen, M., Mattson, M.P., Nilsen, H., Bohr, V.A., Becker, K.G. (2017) Tomatidine enhances lifespan and healthspan in *C. elegans* through mitophagy induction via the SKN-1/Nrf2 pathway. *Sci Rep* 7; 46208. doi:10.1038/srep46208.
- Farquharson, C., Robins, S.P. (1989) Immunolocalisation of collagen types I and III in the arterial wall of the rat. *Histochem J* 21; 172-1778.
- Fehlmann, T., Backes, C., Kahraman, M., Haas, J., Ludwig, N., Posch, A.E., Würstle, M.L., Hübenthal, M., Franke, A., Meder, B., Meese, E., Keller, A. (2017) Web-based NGS data analysis using

- miRMaster: a large-scale meta-analysis of human miRNAs. *Nucleic Acids Res* 45; 8731-8744. doi:10.1093/nar/gkx595.
- Filipowicz, W., Bhattacharyya, S.N., Sonenberg, N. (2008) Mechanisms of post-translational regulation by microRNAs: are the answers in sight? *Nat Rev Genet* 9; 102-114.
- Frey, C., Shereff, M., Greenidge, N. (1990) Vascularity of the posterior tibial tendon. *J Bone Joint Surg* 72-A; 884-888.
- Friedländer, M.R., Chen, W., Adamidi, C., Maaskola, J., Einspanier, R., Knespel, S., Rajewsky, N. (2008) Discovering microRNAs from deep sequencing data using miRDeep. *Nat Biotechnol* 26; 407-415. doi:10.1038/nbt1394.
- Friedman, R.C., Farh, K.K-H., Burge, C.B., Bartel, D.P. (2009) Most mammalian mRNAs are conserved targets of microRNAs. *Genome Res* 19; 92-105. doi:10.1101/gr.082701.108.
- Fromm, B., Domanska, D., Høy, E., Ovchinnikov, V., Kang, W., Aparicio-Puerta, E., Johansen, M., Flatmark, K., Mathelier, A., Hovig, E., Hackenberg, M., Friedländer, M.R., Peterson, K.J. (2020) MirGeneDB 2.0: the metazoan microRNA complement. *Nucleic Acids Res* 48; D132-D141. doi:10.1093/nar/gkz885.
- Gajhede-Knudsen, M., Ekstrand, J., Magnusson, H., Maffulli, N. (2013) Recurrence of Achilles tendon injuries in elite male football players is more common after early return to play: an 11-year follow-up of the UEFA Champions League injury study. *Br J Sports Med* 47; 763-768.
- Galicia, J., Naqvi, A., Ko, C-C., Nares, S., Khan, A.A. (2014) MiRNA-181a regulates Toll-like receptor agonist-induced inflammatory response in human fibroblasts. *Genes Immun* 15; 333-337. doi:10.1038/gene.2014.24.
- Gaut, L., Duprez, D. (2016) Tendon development and disease. *WIREs Dev Biol* 5; 5-23. doi:10.1002/wdev.201.
- Gebetsberger, J., Fricker, R., Polacek, N. (2015) cDNA library preparation for the analysis of small RNAs by high-throughput sequencing. Chapter 13, In Rederstorff, M. (Ed) *Small Non-Coding RNAs – Methods and Protocols, Methods in Molecular Biology* 1296; 139-149. doi:10.1007/978-1-4939-2547-6\_13. Springer Science+Business Media New York.
- Geisert, E.E., Yang, L-J., Irwin, M.H. (1996) Astrocyte growth, reactivity and the target of the antiproliferative antibody, TAPA. *J Neurosci* 16; 5478-5487.
- Gittel, C., Brehm, W., Burk, J., Juelke, H., Staszky, C., Ribitsch, I. (2013) Isolation of equine multipotent mesenchymal stromal cells by enzymatic tissue digestion or explant technique: comparison of cellular properties. *BMC Vet Res* 9; 221.
- Glazebrook, M.A., Wright, J.R., Langman, M., Staans, W.D., Lee, J.M. (2008) Histological analysis of Achilles tendons in an overuse rat model. *J Orthop Res* 26; 840-846.
- Goljanek-Whysall, K., Sweetman, D., Münsterberg, A.E. (2012) microRNAs in skeletal muscle differentiation and disease. *Clin Sci* 123; 611-625.

- Goljanek-Whysall, K., Soriano-Arroquia, A., McCormick, R., Chinda, C., McDonagh, B. (2020) miR-181a regulates p62/SQSTM1, Parkin and Protein DJ-1 promoting mitochondrial dynamics in skeletal muscle aging. *Aging Cell* 19; e13140. doi:10.1111/accel.13140.
- Gross, S., Krause, Y., Wuelling, M., Vortkamp, A. (2012) Hoxa11 and Hoxd11 regulate chondrocyte differentiation upstream of Runx2 and Shox2 in mice. *PLoS ONE* 7:e43553. doi:10.1371/journal.pone.0043553.
- Gustafsson, Å.B. (2011) BNIP3 as a dual regulator of mitochondrial turnover and cell death in the myocardium. *Pediatr Cardiol* 32; 267-274.
- Han, W., Wang, B., Liu, J., Chen, L. (2017) The p16/miR-217/EGR1 pathway modulates age-related tenogenic differentiation in tendon stem/progenitor cells. *Acta Biochim Biophys Sin* 49; 1015–1021.
- Hanna, J., Hossain, G.S., Kocerha, J. (2019) The potential for microRNA therapeutics and clinical research. *Front Genet* 10; 478. doi:10.3389/fgene.2019.00478.
- Hansson, H-A., Engström, A.M.C., Holm, S., Rosenqvist, A-I. (1988) Somatomedin C immunoreactivity in the Achilles tendon varies in a dynamic manner with the mechanical load. *Acta Physiol Scand* 134; 199-208.
- Hao, Y-H., Zhang, J., Wang, H., Wang, H-Y., Dong, J., Xu, X-P., Yao, B-W., Wang, L-F., Zhou, H-M., Zhao, L., Peng, R-Y. (2018) HIF-1 $\alpha$  regulates COXIV subunits, a potential mechanism of self-protective response to microwave induced mitochondrial damages in neurons. *Sci Rep* 8; 10403. doi:10.1038/s41598-018-28427-5.
- Harada, S., Yamamura, M., Okamoto, H., Morita, Y., Kawashima, M., Aita, T., Makino, H. (1999) Production of interleukin-7 and interleukin-15 by fibroblast-like synoviocytes from patients with rheumatoid arthritis. *Arthritis Rheum* 42; 1508-1516.
- Hart, L. (2011) Corticosteroid and other injections in the management of tendinopathies: a review. *Clin J Sports Med* 21; 540-541.
- Harvie, P., Ostlere, S.J., Teh, J., McNally, E.G., Clipsham, K., Burston, B.J., Pollard, T.C.B., Carr, A.J. (2004) Genetic influences in the aetiology of tears of the rotator cuff. *J Bone Joint Surg (Br)* 86-B; 696-700.
- Hayashi, T., Ishimori, C., Takahashi-Niki, K., Taira, T., Kim, Y-C., Maita, H., Maita, C., Ariga, H., Iguchi-Ariga, S.M.M. (2009) DJ-1 binds to mitochondrial complex I and maintains its activity. *Biochem Biophys Res Comm* 390; 667-672.
- He, L., He, X., Lim, L.P., de Stanchina, E., Xuan, Z., Liang, Y., Xue, W., Zender, L., Magnus, J., Ridzon, D., Jackson, A.L., Linsley, P.S., Chen, C., Lowe, S.W., Cleary, M.A., Hannon, G.J. (2007) A microRNA component of the p53 tumour suppressor network. *Nature* 447; 1130-1134. doi:10.1038/nature05939.
- Hecht, J.T., Nelson, L.D., Crowder, E., Wang, Y., Elder, F.F.B., Harrison, W.R., Francomano, C.A., Prange, C.K., Lennon, G.C., Deere, M., Lawler, J. (1995) Mutations in exon 17B of cartilage oligomeric matrix protein (COMP) cause pseudoachondroplasia. *Nat Genet* 10; 325-329.

- Heinemeier, K.M., Olesen, J.L., Haddad, F., Langberg, H., Kjær, M., Baldwin, K.M., Schjerling, P. (2007) Expression of collagen and related growth factors in rat tendon and skeletal muscle in response to specific contraction types. *J Physiol* 582; 1303-1326.
- Heinemeier, K.M., Kjær, M. (2011) In vivo investigation of tendon responses to mechanical loading. *J Musculoskelet Neuronal Interact* 11; 115-123.
- Heinemeier, K.M., Skovgaard, D., Bayer, M.L., Qvortrup, K., Kjaer, A., Magnusson, S.P., Kongsgaard, M. (2012) Uphill running improves rat Achilles tendon tissue mechanical properties and alters gene expression without inducing pathological changes. *J Appl Physiol* 113; 827-836.
- Heinemeier, K.M., Schjerling, P., Heinemeier, J., Magnusson, S.P., Kjær, M. (2013) Lack of tissue renewal in human adult Achilles tendon is revealed by nuclear bomb <sup>14</sup>C. *FASEB J* 27; 2074-2079.
- Hernández, J.M., Giner, P., Hernández-Yago, J. (1999) Gene structure of the human mitochondrial outer membrane receptor Tom20 and evolutionary study of its family of processed pseudogenes. *Gene* 239; 283-291.
- Hernanz, A., Medina, S., de Miguel, E., Martín-Mola, E. (2003) Effect of calcitonin gene-related peptide, neuropeptide Y, substance P and vasoactive intestinal peptide on interleukin-1 $\beta$ , interleukin-6 and tumour necrosis factor-alpha production by peripheral whole blood cells from rheumatoid arthritis and osteoarthritis patients. *Regulatory Peptides* 115; 19-24.
- Hess, G.W. (2010) Achilles tendon rupture. A review of etiology, population, anatomy, risk factors and injury prevention. *Foot Ankle Spec* 3; 29-32.
- 't Hoen, P.A.C., Ariyurek, Y., Thygesen, H.H., Vreugdenhil, E., Vossen, R.H.A.M., de Menezes, R.X., Boer, J.M., van Ommen, G-J.B., den Dunnen, J.T. (2008) Deep sequencing-based expression analysis shows major advances in robustness, resolution and inter-lab portability over five microarray platforms. *Nucleic Acids Res* 36; e141. doi:10.1093/nar/gkn705.
- Hofmann, C., Goldfine, I.D., Whittaker, J. (1989) The metabolic and mitogenic effects of both insulin and insulin-like growth factor are enhanced by the transfection of insulin receptors into NIH3T3 fibroblasts. *J Biol Chem* 264; 8606-8611.
- Holmes, G.B., Mann, R.A. (1992) Possible epidemiological factors associated with rupture of the posterior tibial tendon. *Foot and Ankle* 13; 70-79.
- Hopkins, C., Fu, S-C., Chua, E., Hu, X., Rolf, C., Mattila, V.M., Qin, L., Yung, P.S-H., Chan, K-M. (2016). Critical review on the socio-economic impact of tendinopathy. *Asia-Pacific J Sports Med, Arthroscopy, Rehab Tech* 4; 9-20.
- Hornbeck, P.V., Zhang, B., Murray, B., Kornhauser, J.M., Latham, V., Skrzypek, E. (2015) PhosphoSitePlus, 2014: mutations, PTMs and recalibrations. *Nucleic Acids Res* 43; D512-520.
- Hu, H.H., Chen, D.Q., Wang, Y.N., Feng, Y.L., Cao, G., Vaziri, N.D., Zhao, Y.Y. (2018) New insights into TGF- $\beta$ /Smad signaling in tissue fibrosis. *Chem Biol Interact* 292; 76-83. doi:10.1016/j.cbi.2018.07.008.
- Huang, T-F., Perry, S.M., Soslowsky, L.J. (2004) The effect of overuse activity on Achilles tendon in an animal model: a biomechanical study. *Ann Biomed Eng* 32; 336-341.

- Huang, H., Zhang, J., Sun, K., Zhang, X., Tian, S. (2011) Effects of repetitive multiple freeze-thaw cycles on the biomechanical properties of human flexor digitorum superficialis and flexor pollicis longus tendons. *Clin Biomech* 26; 419-423.
- Huang, R.S., Gamazon, E.R., Ziliak, D., Wen, Y., Im, H.K., Zhang, W., Wing, C., Duan, S., Bleibel, W.K., Cox, N.J., Dolan, M.E. (2011) Population differences in microRNA expression and biological implications. *RNA Biol* 8; 692-701.
- Huang, X., Yuan, T., Tschannen, M., Sun, Z., Jacob, H., Du, M., Liang, M., Dittmar, R.L., Liu, Y., Liang, M., Kohli, M., Thibodeau, S.N., Boardman, L., Wang, L. (2013) Characterisation of human plasma-derived exosomal RNAs by deep sequencing. *BMC Genomics* 14; 319.
- Huang, A.H. (2017) Coordinated development of the limb musculoskeletal system: tendon and muscle patterning and integration with the skeleton. *Dev Biol* 429; 420-428. doi:10.1016/j.ydbio.2017.03.028.
- Huang, H-Y., Lin, Y-C-D., Li, J., Huang, K-Y., Shrestha, S., Hong, H-C., Tang, Y., Chen, Y-G., Jin, C-N., Yu, Y., Xu, J-T., Li, Y-M., Cai, X-X., Zhou, Z-Y., Chen, X-H., Pei, Y-Y., Hu, L., Su, J-J., Cui, S-D., Wang, F., Xie, Y-Y., Ding, S-Y., Luo, M-F., Chou, C-H., Chang, N-W., Chen, K-W., Cheng, Y-H., Wan, X-H., Hsu, W-L., Lee, T-Y., Wei, F-X., Huang, H-D. (2020) miRTarBase 2020: updates to the experimentally validated microRNA–target interaction database. *Nucleic Acids Res* 48; D148–D154. doi.org/10.1093/nar/gkz896.
- Hüttemann, M., Kadenbach, B., Grossman, L.I. (2001) Mammalian subunit IV isoforms of cytochrome c oxidase. *Gene* 267; 111-123.
- Ide, J., Kikukawa, K., Hirose, J., Iyama, K., Sakamoto, H., Mizuta, H. (2009) The effects of fibroblast growth factor-2 on rotator cuff reconstruction with a cellular dermal matrix grafts. *Arthroscopy* 25; 608-616.
- Indrieri, A., Carrella, S., Romano, A., Spaziano, A., Marrocco, E., Fernandez-Vizarra, E., Barbato, S., Pizzo, M., Ezhova, Y., Golia, F.M., Ciampi, L., Tammara, R., Henao-Mejia, J., Williams, A., Flavell, R.A., de Leonibus, E., Zeviani, M., Surace, E.M., Banfi, S., Franco, B. (2019) miR-181a/b downregulation exerts a protective action on mitochondrial disease models. *EMBO Mol Med* 11: e8734.
- Innes, J.F., Clegg, P. (2010) Comparative rheumatology: what can be learnt from naturally occurring musculoskeletal disorders in domestic animals? *Rheumatol* 49; 1030-1039.
- Ireland, D., Harrall, R., Curry, V., Holloway, G., Hackney, R., Hazleman, B., Riley, G. (2001) Multiple changes in gene expression in chronic human tendinopathy. *Matrix Biology* 20; 159-169.
- Ivan, M., Harris, A.L., Martelli, F., Kulshreshtha, R. (2008) Hypoxia response and microRNAs: no longer two separate worlds. *J Cell Mol Med* 12; 1426-1431.
- Jelinsky, S.A., Rodeo, S.A., Li, J., Gulotta, L.V., Archambault, J.M., Seeherman, H.J. (2011) Regulation of gene expression in human tendinopathy. *BMC Musculoskelet Disord* 12; 86. doi:10.1186/1471-2474-12-86.
- Johnson, M.A., Polgar, J., Weightman, D., Appleton, D. (1973) Data on the distribution of fibre types in thirty-six human muscles: an autopsy study. *J Neuro Sci* 18; 111-129.

- Jones, G.C., Corps, A.N., Pennington, C.J., Clark, I.M., Edwards, D.R., Bradley, M.M., Hazleman, B.L., Riley, G.P. (2006) Expression profiling of metalloproteinases and tissue inhibitors of metalloproteinases in normal and degenerate human Achilles tendon. *Arthritis Rheum* 54; 832-842.
- Jones, J.A., Stroud, R.E., O'Quinn, E.C., Black, L.E., Barth, J.L., Elefteriades, J.A., Bavaria, J.E., Gorman, J.H., Gorman, R.C., Spinale, F.G., Ikonomidis, J.S. (2011) Selective microRNA suppression in human thoracic aneurysms: relationship of miR-29a to aortic size and proteolytic induction. *Circ Cardiovasc Genet* 4; 605-613. doi:10.1161/CIRCGENETICS.111.960419.
- Jordan, K., Clarke, A.M., Symmons, D.P., Fleming, D., Porcheret, M., Kadam, U.T., Croft, P. (2007). Measuring disease prevalence: a comparison of musculoskeletal disease using four general practice consultation databases. *Br J Gen Pract* 57; 7-14.
- Jung, H.J., Suh, Y. (2014) Circulating miRNAs in ageing and ageing-related diseases. *J Genet Genom* 41; 465-472.
- Kagan, V.E., Jiang, J., Tyurina, Y.Y., Desbourdes, C., Cottet-Rouselle, C., Dar, H.H., Verma, M., Tyurin, V.A., Kapralov, A.A., Cheikhi, A., Mao, G., Stolz, D., St.Croix, C.M., Watkins, S., Shen, Z., Li, Y., Greenberg, M.L., Tokarska-Schlattner, M., Boissan, M., Lacombe, M-L., Eband, R.M., Chu, C.T., Mallapalli, R.K., Bayir, H., Schlattner, U. (2016) NDPK-D (NM23-H4)-mediated externalization of cardiolipin enables elimination of depolarized mitochondria by mitophagy. *Cell Death Differ* 23; 1140-1151.
- Kaller, M., Liffers, S-T., Oeljeklaus, S., Kuhlmann, K., Röh, S., Hoffmann, R., Warscheid, B., Hermeking, H. (2011) Genome-wide characterisation of miR-34a induced changes in protein and mRNA expression by a combined pulsed SILAC and microarray analysis. *Mol Cell Proteomics* 10; M111.010462. doi:10.1074/mcp.M111.010462.
- Kalson, N.S., Malone, P.S., Bradley, R.S., Withers, .PJ., Lees, V.C. (2012) Fibre bundles in the human extensor carpi ulnaris tendon are arranged in a spiral. *J Hand Surg Eur* 37; 550-554.
- Kalvari, I., Nawrocki, E.P., Argasinska, J., Quinones-Olvera, N., Finn, R.D., Bateman, A., Petrov, A.I. (2018) Non-coding RNA analysis using the Rfam database. *Curr Protoc Bioinformatics* 62; e51. doi:10.1002/cpbi.51.
- Kapacee, Z., Richardson, S.H., Lu, Y., Starborg, T., Holmes, D.F., Baar, K., Kadler, K.E. (2008) Tension is required for fibroblast formation. *Matrix Biology* 27; 371-375.
- Kapacee, Z., Yeung, C-Y.C., Lu, Y., Crabtree, D., Holmes, D.F., Kadler, K.E. (2010) Synthesis of embryonic tendon-like tissue by human marrow stromal/mesenchymal stem cells requires a three-dimensional environment and transforming growth factor  $\beta$ 3. *Matrix Biology* 29; 668-677.
- Karagkouni, D., Paraskevopoulou, M.D., Chatzopoulos, S., Vlachos, I.S., Tastsoglou, S., Kanellos, I., Papadimitriou, D., Kavakiotis, I., Maniou, S., Skoufos, G., Vergoulis, T., Dalamagas, T., Hatzigeorgiou, A.G. (2018) DIANA-TarBase v8: a decade-long collection of experimentally supported miRNA-gene interactions. *Nucleic Acids Res* 46; D239-D245. doi:10.1093/nar/gkx1141.
- Karbowski, M., Youle, R.J. (2003) Dynamics of mitochondrial morphology in healthy cells and during apoptosis. *Cell Death Differ* 10; 870-880.

- Kastelic, J., Galeski, A., Baer, E. (1978) The multicomposite structure of tendon. *Connect Tissue Res* 6; 11-23.
- Katayama, H., Kogure, T., Mizushima, N., Yoshimori, T., Miyawaki, A. (2011) A sensitive and quantitative technique for detecting autophagic events based on lysosomal delivery. *Chem Biol* 18; 1042-1052.
- Kawanishi, Y., Nakasa, T., Shoji, T., Hamanishi, M., Shimizu, R., Kamei, N., Usman, M.A., Ochi, M. (2014) Intra-articular injection of synthetic microRNA-210 accelerates avascular meniscal healing in rat medial meniscal injured model. *Arthritis Res Therap* 16; 488. doi:10.1186/s13075-014-0488-y.
- Kharaz, Y.A., Tew, S.R., Peffers, M.J., Canty-Laird, E.G., Comerford, E. (2016) Proteomic differences between native and tissue-engineered tendon and ligament. *Proteomics* 16; 1547-1556.
- Kim, S.Y., Chun, E., Lee, K-Y. (2011) Phospholipase A<sub>2</sub> of peroxiredoxin 6 has a critical role in tumor necrosis factor-induced apoptosis. *Cell Death Differ* 18; 1573-1583.
- Kim, D., Sung, Y.M., Park, J., Kim, S., Kim, J., Park, J., Ha, H., Bae, J.Y., Kim, S., Baek, D. (2016) General rules for functional microRNA targeting. *Nat Genet* 48; 1517-1526. doi:10.1038/ng.3694.
- Kimura, S., Fujita, N., Noda, T., Yoshimori, T. (2009) Monitoring autophagy in mammalian cultured cells through the dynamics of LC3. Chapter 1 In: *Methods in Enzymology*, Volume 452. Elsevier. doi:10.1016/S0076-6879(08)03601-X.
- Kjær, M. (2004) Role of extracellular matrix in adaptation of tendon and skeletal muscle to mechanical loading. *Physiol Rev* 84; 649-698.
- Kohler, J., Popov, C., Klotz, B., Alberton, P., Prall, W.C., Haasters, F., Müller-Deubert, S., Ebert, R., Klein-Hitpass, L., Jakob, F., Schieker, M., Docheva, D. (2013) Uncovering the cellular and molecular changes in tendon stem/progenitor cells attributed to tendon aging and degeneration. *Aging Cell* 12; 988-999. doi:10.1111/accel.12124.
- Komatsu, M., Waguri, S., Koike, M., Sou, Y-S., Ueno, T., Hara, T., Mizushima, N., Iwata, J-I., Ezaki, J., Murata, S., Hamazaki, J., Nishito, Y., Iemura, S-I., Natsume, T., Yanagawa, T., Uwayama, J., Warabi, E., Yoshida, H., Ishii, T., Kobayashi, A., Yamamoto, M., Yue, Z., Uchiyama, Y., Kominami, E., Tanaka, K. (2007) Homeostatic levels of p62 control cytoplasmic inclusion body formation in autophagy-deficient mice. *Cell* 131; 1149-1163.
- Komatsu, M., Kurokawa, H., Waguri, S., Taguchi, K., Kobayashi, A., Ichimura, Y., Sou, Y-S., Ueno, I., Sakamoto, A., Tong, K.I., Kim, M., Nishito, Y., Iemura, S-I., Natsume, T., Ueno, T., Kominami, E., Motohashi, H., Tanaka, K., Yamamoto, M. (2010) The selective autophagy substrate p62 activates the stress responsive transcription factor Nrf2 through inactivation of Keap1. *Nat Cell Biol* 12; 213-223. doi:10.1038/ncb2021.
- Kowalski, M.P., Krude, T. (2015) Functional roles of non-coding Y RNAs. *Int J Biochem Cell Biol* 66; 20-29. doi:10.1016/j.biocel.2015.07.003.
- Kozomara, A., Birgaoanu, M., Griffiths-Jones, S. (2019) miRBase: from microRNA sequences to function. *Nucleic Acids Res* 47; D155-D162. doi:10.1093/nar/gky1141.

- Krämer, A., Green, J., Pollard, J., Tugendreich, S. (2014) Causal analysis approaches in Ingenuity Pathway Analysis. *Bioinformatics* 30; 523-530. doi:10.1093/bioinformatics/btt703.
- Kraus-Hansen, A.E., Fackelman, G.E., Becker, C., Williams, R.M., Pipers, F.S. (1992) Preliminary studies on the vascular anatomy of the equine superficial digital flexor tendon. *Equine Vet J* 24; 46-51.
- Krol, J., Loedige, I., Filipowicz, W. (2010) The widespread regulation of microRNA biogenesis, function and decay. *Nat Rev Genet* 11; 597-610.
- Kubo, K., Ikebukuro, T., Tsunoda, N., Kanehisa, H. (2008) Changes in oxygen consumption of human muscle and tendon following repeat muscle contractions. *Eur J Appl Physiol* 104; 859-866.
- Kulshreshtha, R., Ferracin, M., Wojcik, S.E., Garzon, R., Alder, H., Agosto-Perez, F.J., Davuluri, R., Liu, C-G., Croce, C.M., Negrini, M., Calin, G.A., Ivan, M. (2007) A microRNA signature of hypoxia. *Mol Cell Biol* 27; 1859-1867.
- Laguette, M-J., Abrahams, Y., Prince, S., Collins, M. (2011) Sequence variants within the 3'-UTR of the COL5A1 gene alters mRNA stability: implications for musculoskeletal soft tissue injuries. *Matrix Biology* 30; 338-345.
- Lam, K.H., Parkin, T.D.H., Riggs, C.M., Morgan, K.L. (2007) Descriptive analysis of retirement of Thoroughbred racehorses due to tendon injuries at the Hong Kong Jockey Club (1992-2004). *Equine Vet J* 39; 143-148.
- Langberg, H., Skovgaard, D., Petersen, L.J., Bülow, J., Kjær, M. (1999) Type I collagen synthesis and degradation in peritendinous tissue after exercise determined by microdialysis in humans. *J Physiol* 521; 299-306.
- Lau, A., Wang, X-J., Zhao, F., Villeneuve, N.F., Wu, T., Jiang, T., Sun, Z., White, E., Zhang, D.D. (2010) A noncanonical mechanism of Nrf2 activation by autophagy deficiency: direct interaction between Keap1 and p62. *Mol Cell Biol* 30; 3275-3285.
- Lee, K-P., Shin, Y.J., Cho, S.C., Lee, S-M., Bahn, Y.J., Kim, J.Y., Kwon, E-S., Jeong, D.Y., Park, S.C., Rhee, S.G., Woo, H.A., Kwon, K-S. (2014) Peroxiredoxin 3 has a crucial role in the contractile function of skeletal muscle by regulating mitochondrial homeostasis. *Free Radic Biol Med* 77; 298-306.
- Lee, K.J., Clegg, P.D., Comerford, E.J., Canty-Laird, E.G. (2018) A comparison of the stem cell characteristics of murine tenocytes and tendon-derived stem cells. *BMC Musculoskel Dis* 19; 116. doi:10.1186/s12891018-2038-2.
- Lemasters, J.J. (2014) Variants of mitochondrial autophagy; Types 1 and 2 mitophagy and micromitophagy (Type 3). *Redox Biology* 2; 749-754.
- Lian, O.B., Engebretsen, L., Bahr, R. (2005). Prevalence of jumper's knee among elite athletes from different sports – a cross sectional study. *Am J Sports Med* 33; 561-567.
- Lichtwark, G.A., Wilson, A.M. (2005) In vivo mechanical properties of the human Achilles tendon during one-legged hopping. *J Exp Biol* 208; 4715-4725.

- Lino Cardenas, C.L., Henaoui, I.S., Courcot, E., Roderburg, C., Cauffiez, C., Aubert, S., Copin, M-C., Wallaert, B., Glowacki, F., Dewaeles, E., Milosevic, J., Maurizio, J., Tedrow, J., Marcet, B., Lo-Guidice, J-M., Kaminski, N., Barbry, P., Luedde, T., Perrais, M., Mari, B., Pottier, N. (2013) miR-199a-5p is upregulated during fibrogenic response to tissue injury and mediates TGFbeta-induced lung fibroblast activation by targetting caveolin-1. *PLoS Genet* 9; e1003291. doi:10.1371/journal.pgen.1003291.
- Linsen, S.E.V., de Wit, E., Janssens, G., Heater, S., Chapman, L., Parkin, R.K., Fritz, B., Wyman, S.K., de Bruijn, E., Voest, E.E., Kuersten, S., Tewari, M., Cuppen, E. (2009) Limitations and possibilities of small RNA digital gene expression profiling. *Nat Methods* 6; 474-476.
- Lippai, M., Löw, P. (2014) The role of the selective adaptor p62 and ubiquitin-like proteins in autophagy. *Biomed Res Int* 2014; 832704.
- Littlewood, C., May, S., Walters, S. (2013). Epidemiology of rotator cuff tendinopathy: a systematic review. *Shoulder and Elbow* 5; 256-265.
- Liu, J., Shi, W., Wu, C., Ju, J., Jiang, J. (2014) miR-181b as a key regulator of the oncogenic process and its clinical implications in cancer. *Biomed Reports* 2; 7-11. doi:10.3892/br.2013.199.
- Liu, K.E., Frazier, W.A. (2015) Phosphorylation of the BNIP3 C-terminus inhibits mitochondrial damage and cell death without blocking autophagy. *PLoS ONE* 10; e0129667. doi:10.1371/journal.pone.0129667.
- Liu, J., Han, W., Chen, L., Tang, K. (2016) Mechanism of osteogenic and adipogenic differentiation of tendon stem cells induced by sirtuin 1. *Mol Med Rep* 14; 1643-1648.
- Liu, Y., Song, Y., Zhu, X. (2017) MicroRNA-181a regulates apoptosis and autophagy process in Parkinson's Disease by inhibiting p38 mitogen-activated protein kinase (MAPK)/c-Jun N-terminal kinases (JNK) signalling pathways. *Med Sci Monit* 23; 1597-1606. doi:10.12659/MSM.900218.
- Livak, K.J., Schmittgen, T.D. (2001) Analysis of relative gene expression data using real-time quantitative PCR and the  $2^{-\Delta\Delta C_T}$  method. *Methods* 25; 402-408.
- Loiacono, C., Palermi, S., Massa, B., Belviso, I., Romano, V., di Gregorio, A., Sirico, F., Sacco, A.M. (2019) Tendinopathy: pathophysiology, therapeutic options and role of nutraceuticals. A narrative literature review. *Medicina* 55; 447. doi:10.3390/medicina55080447.
- Lopes, A.D., Hespanhol, L.C., Yeung, S.S., Costa, L.O.P. (2012). What are the main running-related musculoskeletal injuries? A systematic review. *Sports Med* 42; 891-905.
- López-Otín, C., Blasco, M.A., Partridge, L., Serrano, M., Kroemer, G. (2013) The hallmarks of aging. *Cell* 153; 1194-1217.
- Loppini, M., Longo, U.G., Niccoli, G., Khan, W.S., Maffulli, N., Denaro, V. (2015). Histopathological scores for tissue-engineered, repaired and degenerated tendon: a systematic review of the literature. *Current Stem Cell Res Therap* 10; 43-55.
- Lu, D., Liu, L., Ji, X., Gao, Y., Chen, X., Liu, Y., Zhao, X., Li, Y., Li, Y., Jin, Y., Zhang, Y., McNutt, M.A., Yin, Y. (2015) The phosphatase DUSP2 controls the activity of the transcription activator STAT3 and regulates TH17 differentiation. *Nat Immunol* 16, 1263–1273. doi:10.1038/ni.3278.

- Lu, Y-F., Liu, Y., Fu, W-M., Xu, J., Wang, B., Sun, Y-X., Wu, T-Y., Xu, L-L., Chan, K-M., Zhang, J-F., Li, G. (2017) Long noncoding RNA H19 accelerates tenogenic differentiation and promotes tendon healing through targeting miR-29b-3p and activating TGF- $\beta$ 1 signalling. *FASEB J* 31; 954-964.
- Lui, P.P.Y., Cheuk, Y.C., Hung, L.K., Fu, S.C., Chan, K.M. (2007) Increased apoptosis at the late stage of tendon healing. *Wound Rep Reg* 15; 702-707.
- Lui, P.P., Fu, S-C., Chan, L-S., Hung, L-K., Chan, K-M. (2009) Chondrocyte phenotype and ectopic ossification in collagenase-induced tendon regeneration. *J Histochem Cytochem* 57; 91-100.
- Lui, P.P.Y., Maffulli, N., Rolf, C., Smith, R.K.W. (2011) What are the validated animal models for tendinopathy? *Scan J Med Sci Sports* 21; 3-17.
- Lundin, A., Delsing, L., Clausen, M., Ricchiuto, P., Sanchez, J., Sabirsh, A., Ding, M., Synnergren, J., Zetterberg, H., Brolén, G., Hicks, R., Herland, A., Falk, A. (2018) Human iPS-derived astroglia from a stable neural precursor state show improved functionality compared with conventional astrocytic models. *Stem Cell Rep* 10; 1030-1045.
- Ly, S., Navaroli, D.M., Didiot, M-C., Cardia, J., Pandarinathan, L., Alterman, J.F., Fogarty, K., Standley, C., Lifshitz, L.M., Bellve, K.D., Prot, M., Echeverria, D., Corvera, S., Khvorova, A. (2017) Visualisation of self-delivered hydrophobically modified siRNA cellular internalization. *Nucleic Acids Res* 45; 15-25.
- Maeda, E., Shelton, J.C., Bader, D.L., Lee, D.A. (2009) Differential regulation of gene expression in isolated tendon fascicles exposed to cyclic tensile strain in vitro. *J Appl Physiol* 106; 506-512.
- Maffulli, N., Reaper, J., Ewen, S.W.B., Waterston, S.W., Barrass, V. (2006) Chondral metaplasia in calcific insertional tendinopathy of the Achilles tendon. *Clin J Sports Med* 16; 329-334.
- Maffulli, N., Longo, U.G., Franceschi, F., Rabitti, C., Denaro, V. (2008) Movin and Bonar scores assess the same characteristics of tendon histology. *Clin Orthop Relat Res* 466; 1605-1611.
- Maganaris, C.N., Paul, J.P. (2000) In vivo human tendinous tissue stretch upon maximum muscle force generation. *J Biomech* 33; 1453-1459.
- Magnusson, S.P., Qvortrup, K., Larsen, J.O., Rosager, S., Hanson, P., Aagaard, P., Krogsgaard, M., Kjær, M. (2002) Collagen fibril size and crimp morphology in ruptured and intact Achilles tendons. *Matrix Biol* 21; 369-377.
- Magnusson, S.P., Hansen, M., Langberg, H., Miller, B., Haraldsson, B., Westh, E.K., Koskinen, S., Aagaard, P., Kjær, M. (2007) The adaptability of tendon to loading differs in men and women. *Int J Exp Path* 88; 237-240.
- Massagué, J. (2012) TGF $\beta$  signalling in context. *Nat Rev Mol Cell Biol* 13; 616-630. doi:10.1038/nrm3434.
- Mattick, J.S., Makunin, I.V. (2006) Non-coding RNA. *Hum Mol Genet* 15; R17-R29. doi:10.1093/hmg/ddl1047.
- Matuszewski, P.E., Chen, Y-L., Szczesny, S.E., Lake, S., Elliott, D.M., Soslowsky, L.J., Dodge, G.R. (2012) Regional variation in human supraspinatus tendon proteoglycans: decorin, biglycan and aggrecan. *Connect Tissue Res* 53; 343-348.

- Maurer, B., Stanczyk, J., Jüngel, A., Akhmetshina, A., Trenkmann, M., Brock, M., Kowal-Bielecka, O., Gay, R.E., Michel, B.A., Distler, J.H.W., Gay, S., Distler, O. (2010) microRNA-29a, a key regulator of collagen expression in systemic sclerosis. *Arthritis Rheum* 62; 1733-1743. doi:10.1002/art.27443.
- McCarron, J.G., Wilson, C., Sandison, M.E., Olson, M.L., Girkin, J.M., Saunter, C., Chalmers, S. (2013) From structure to function: mitochondrial morphology, motion and shaping in vascular smooth muscle. *J Vasc Res* 50; 357-371.
- McCoy, M.K., Cookson, M.R. (2011) DJ-1 regulation of mitochondrial function and autophagy through oxidative stress. *Autophagy* 7; 531-532.
- McHugh, M.L. (2012) Interrater reliability: the kappa statistic. *Biochemia Medica* 22; 276-282.
- McWilliams, T.G., Prescott, A.R., Allen, G.F.G., Tamjar, J., Munson, M.J., Thomson, C., Muqit, M.M.K., Ganley, I.G. (2016) *mito*-QC illuminates mitophagy and mitochondrial architecture in vivo. *J Cell Biol* 214; 333-345.
- McWilliams, T.G., Prescott, A.R., Montava-Garriga, L., Ball, G., Singh, F., Barini, E., Muqit, M.M.K., Brooks, S.P., Ganley, I.G. (2018) Basal mitophagy occurs independently of PINK1 in mouse tissues of high metabolic demand. *Cell Metab* 27; 439-449. doi:10.1016/j.cmet.2017.12.008.
- Mendias, C.L., Gumucio, J.P., Lynch, E.B. (2012) Mechanical loading and TGF- $\beta$  change the expression of multiple miRNAs in tendon fibroblasts. *J Appl Physiol* 113; 56-62.
- Millar, N.L., Wei, A.Q., Molloy, T.J., Bonar, F., Murrell, G.A.C. (2009) Cytokines and apoptosis in supraspinatus tendinopathy. *J Bone Joint Surg (Br)* 91-B; 417-424.
- Millar, N.L., Hueber, A.J., Reilly, J.H., Xu, Y., Fazzi, U.G., Murrell, G.A.C., McInnes, I.B. (2010). Inflammation is present in early human tendinopathy. *Am J Sports Med* 38; 2085-2091. doi:10.1177/0363546510372613.
- Millar, N.L., A.J., Reilly, J.H., Kerr, S.C., Campbell, A.L., Little, K.J., Leach, W.J., Rooney, B.P., Murrell, G.A.C., McInnes, I.B. (2012). Hypoxia: a critical regulator of early human tendinopathy. *Ann Rheum Dis* 71; 302-310.
- Millar, N.L., Gilchrist, D.S., Akbar, M., Reilly, J.H., Kerr, S.C., Campbell, A.L., Murrell, G.A.C., Liew, F.Y., Kurowska-Stolarska, M., McInnes, I.B. (2015) MicroRNA29a regulates IL-33-mediated tissue remodelling in tendon disease. *Nat Commun* 6; 6774. doi:10.1038/ncomms7774.
- Miller, B.F., Olesen, J.L., Hansen, M., Døssing, S., Cramer, R.M., Welling, R.J., Langberg, H., Flyvbjerg, A., Kjær, M., Babraj, J.A., Smith, K., Rennie M.J. (2005) Coordinated collagen and muscle protein synthesis in human patella tendon and quadriceps muscle after exercise. *J Physiol* 567; 1021-1033.
- Miñones-Moyano, E., Porta, S., Escaramís, G., Rabionet, R., Iraola, S., Kagerbauer, B., Espinosa-Parrilla, Y., Ferrer, I., Estivill, X., Martí, E. (2011) microRNA profiling of Parkinson's disease brains identifies early down regulation of miR-34b/c which modulate mitochondrial function. *Hum Mol Genet* 20; 3067-3078. doi:10.1093/hmg/ddr210.
- Miyazono, Y., Hirashima, S., Ishihara, N., Kusukawa, J., Nakamura, K., Ohta, K. (2018) Uncoupled mitochondria quickly shorten along their long axis to form indented spheroids, instead of rings, in a fission-independent manner. *Sci Rep* 8; 350. doi:10.1038/s41598-017-18582-6.

- Mizushima, N., Yoshimori, T. (2007) How to interpret LC3 immunoblotting. *Autophagy* 3; 542-545.
- Mokone, G.G., Gajjar, M., September, A.V., Schwellnus, M.P., Greenberg, J., Noakes, T.D., Collins, M. (2005) The guanine-thymine dinucleotide repeat polymorphism within the tenascin-c gene is associated with Achilles tendon injuries. *Am J Sports Med* 33; 1016-1021.
- Molloy, T.J., Kemp, M.W., Wang, Y., Murrell, G.A.C. (2006) Microarray analysis of the tendinopathic rat supraspinatus tendon: glutamate signalling and its potential role in tendon degeneration. *J Appl Physiol* 101; 1702-1709.
- Monboisse, J.C., Braquet, P., Randoux, A., Borel, J.P. (1983) Non-enzymatic degradation of acid-soluble calf skin collagen by superoxide anion: protective effect of flavonoids. *Biochem Pharmacol* 32; 53-58.
- Montava-Garriga, L., Ganley, I.G. (2020) Outstanding questions in mitophagy: what we do and do not know. *J Mol Biol* 432; 206-230. doi:10.1016/j.jmb.2019.06.032.
- Morell, C., Bort, A., Vara-Ciruelos, D., Ramos-Torres, Á., Altamirano-Dimas, M., Díaz-Laviada, I., Rodríguez-Henche, N. (2016) Up-regulated expression of LAMP2 and autophagy activity during neuroendocrine differentiation of prostate cancer LNCaP cells. *PLoS ONE* 11; e0162977. doi:10.1371/journal.pone.0162977.
- Morikawa, M., Derynck, R., Miyazono, K. (2016) TGF- $\beta$  and the TGF- $\beta$  family: context-dependent roles in cell and tissue physiology. *Cold Spring Harb Perspect Biol* 8; a021873. doi:10.1101/cshperspect.a021873.
- Morita, W., Dakin, S.G., Snelling, S.J.B., Carr, A.J. (2017) Cytokines in tendon disease. *Bone Joint Res* 6; 656-664.
- Morrison, D.K. (2012) MAP kinase pathways. *Cold Spring Harb Perspect Biol* 4; a011254. doi:10.1101/cshperspect.a011254.
- Mosca, M.J., Rashid, M.S., Snelling, S.J., Kirtley, S., Carr, A.J., Dakin, S.G. (2018) Trends in the theory that inflammation plays a causal role in tendinopathy: a systematic review and quantitative analysis of published reviews. *BMJ Open Sport Exerc Med* 4; e000332. doi:10.1136/bmjsem-2017-000332.
- Moser, B., Hochreiter, B., Herbst, R., Schmid, J.A. (2017) Fluorescence colocalisation microscopy analysis can be improved by combining object recognition with pixel-intensity-correlation. *Biotechnol J* 12; 1600332.
- Mouw, J.K., Ou, G., Weaver, V.M. (2014) Extracellular matrix assembly: a multiscale deconstruction. *Nat Rev Mol Cell Biol* 15; 771-785.
- Movin, T., Gad, A., Reinholt, F.P., Rolf, C. (1997) Tendon pathology in long-standing achillodynia. Biopsy findings in 40 patients. *Acta Orthop Scand* 68; 170-175.
- Murray, R.C., Dyson, S.J., Tranquille, C., Adams, V. (2006). Association of type of sport and performance level with anatomical site of orthopaedic injury diagnosis. *Equine Vet J Suppl* 36; 411-416.
- Myerson, M.S. (1996) Adult acquired flatfoot deformity. *J Bone Joint Surg* 78-A; 780-792.

- Naguibneva, I., Ameyar-Zazoua, M., Poleskaya, A., Ait-Si-Ali, S., Groisman, R., Souidi, M., Cuvellier, S., Harel-Bellan, A. (2006) The microRNA miR-181 targets the homeobox protein Hox-A11 during mammalian myoblast differentiation. *Nat Cell Biol* 8; 278-284. doi:10.1038/ncb1373.
- Nakanishi, Y., Okada, T., Takeuchi, N., Kozono, N., Senju, T., Nakayama, K., Nakashima, Y. (2019) Histological evaluation of tendon formation using a scaffold-free three-dimensional-bioprinted construct of human dermal fibroblasts under in vitro static tensile culture. *Regen Therap* 11; 47-55.
- Nallamshetty, S., Chan, S.Y., Loscalzo, J. (2013) Hypoxia: a master regulator of microRNA biogenesis and activity. *Free Radic Biol Med* 64; 20-30. doi:10.1016/j.freeradbiomed.2013.05.022.
- Narendra, D.P., Kane, L.A., Hauser, D.N., Fearnley, I.M., Youle, R.J. (2010) p62/SQSTM1 is required for Parkin-induced mitochondrial clustering but not mitophagy; VDAC1 is dispensable for both. *Autophagy* 6; 1090-1106.
- Nassar, F.J., Talhouk, R., Zgheib, N.K., Tfayli, A., El Sabban, M., El Saghir, N.S., Boulos, F., Jabbour, M.N., Chalala, C., Boustany, R-M., Kadara, H., Zhang, Z., Zheng, Y., Joyce, B., Hou, L., Bazarbachi, A., Calin, G., Nasr, R. (2017) microRNA expression in ethnic specific early stage breast cancer: an integration and comparative analysis. *Sci Rep* 7; 16829. doi:10.1038/s41598-017-16978-y.
- Nell, E.M., van der Merwe, L., Cook, J., Handley, C.J., Collins, M., September, A.V. (2012) The apoptosis pathway and the genetic predisposition to Achilles tendinopathy. *J Orthop Res* 30; 1719-1724.
- Nichols, A.E.C., Muscat, S.N., Miller, S.E., Green, L.J., Richards, M.S., Loiselle, A.E. (2021) Impact of isolation method on cellular activation and presence of specific tendon cell subpopulations during in vitro culture. *FASEB J* 35; e21733. doi:10.1096/fj.202100405R.
- Nielsen, R.H., Holm, L., Malmgaard-Clausen, N.M., Reitelseder, S., Heinemeier, K.M., Kjær, M. (2014) Increase in tendon protein synthesis in response to insulin-like growth factor-I is preserved in elderly men. *J Appl Physiol* 116; 42-46.
- Nirmalanandhan, V.S., Dressler, M.R., Shearn, J.T., Juncosa-Melvin, N., Rao, M., Gooch, C., Bradica, G., Butler, D.L. (2007) Mechanical stimulation of tissue engineered tendon constructs: effect of scaffold materials. *J Biomech Eng* 129; 919-923.
- Noren Hooten, N., Fitzparick, M., Wood, W.H., De, S., Ejiogu, N., Zhang, Y., Mattison, J.A., Becker, K.G., Zonderman, A.B., Evans, M.K. (2013). Age-related changes in microRNA levels in serum. *Aging* 5; 725-740.
- O'Reilly, S. (2016) MicroRNAs in fibrosis: opportunities and challenges. *Arthritis Res Therap* 18; 11. doi:10.1186/s13075-016-0929-x.
- Okatsu, K., Saisho, K., Shimanuki, M., Nakada, K., Shitara, H., Sou, Y-S., Kimura, M., Sato, S., Hattori, N., Komatsu, M., Tanaka, K., Matsuda, N. (2010) P62/SQSTM1 cooperates with Parkin for perinuclear clustering of depolarized mitochondria. *Genes Cells* 15; 887-900.
- Oliva, F., Piccirilli, E., Berardi, A.C., Frizziero, A., Tarantino, U., Maggulli, N. (2016) Hormones and tendinopathies: the current evidence. *Br Med Bull* 117; 39-58.

- Olivieri, F., Spazzafumo, L., Santini, G., Lazzarini, R., Albertini, M.C., Rippo, M.R., Galeazzi, R., Abbatecola, A.M., Marcheselli, F., Monti, D., Ostan, R., Cevenini, E., Antonicelli, R., Franceschi, C., Procopio, A.D. (2012). Age-related differences in the expression of circulating microRNAs: miR-21 as a new circulating marker of inflammaging. *Mech Ageing Dev* 133; 675-685.
- Olivieri, F., Rippo, M.R., Procopio, A.D., Fazioli, F. (2013) Circulating inflamma-miRs in aging and age-related diseases. *Front Genet* 4; 121. doi:10.3389/fgene.2013.00121.
- Oryan, A., Goodship, A.E., Silver, I.A. (2008) Response of a collagenase-induced tendon injury to treatment with a polysulphated glycosaminoglycan (Adequan). *Connect Tissue Res* 49; 351-360.
- Oshlack, A., Robinson, M.D., Young, M.D. (2010) From RNA-seq reads to differential expression results. *Genome Biol* 11; 220. doi:10.1186/gb-2010-11-12-220.
- Ouyang, Y-B., Lu, Y., Yue, S., Giffard, R.G. (2012) miR-181 targets multiple Bcl-2 family members and influences apoptosis and mitochondrial function in astrocytes. *Mitochondrion* 12; 213-219.
- Ouyang, D., Xu, L., Zhang, L., Guo, D., Tan, X., Yu, X., Qi, J., Ye, Y., Liu, Q., Ma, Y., Li, Y. (2016) miR-181a-5p regulates 3T3-L1 cell adipogenesis by targeting Smad7 and Tcf7l2. *Acta Biochim Biophys Sin* 48; 1034-1041. doi.org/10.1093/abbs/gmw100.
- Ozata, D.M., Gainetdinov, I., Zoch, A., O'Carroll, D., Zamore, P.D. (2019) PIWI-interacting RNAs: small RNAs with big functions. *Nat Rev Genet* 20; 89-108. doi:10.1038/s41576-018-0073-3.
- Paavola, M., Kannus, P., Järvinen, T.A.H., Khan, K., Józsa, L., Järvinen, M. (2002) Current concepts review: Achilles tendinopathy. *J Bone Joint Surg* 84-A; 2062-2076.
- Palikaras, K., Lionaki, E., Tavernarakis, N. (2018) Mechanisms of mitophagy in cellular homeostasis, physiology and pathology. *Nat Cell Biol* 20; 1013-1022.
- Panina, Y., Germond, A., Masui, S., Watanabe, T.M. (2018) Validation of common housekeeping genes as reference for qPCR gene expression analysis during iPS reprogramming process. *Sci Rep* 8; 8716. doi:10.1038/s41598-018-26707-8.
- Park, J.S., Kang, D.H., Bae, S.H. (2015) p62 prevents carbonyl cyanide *m*-chlorophenyl hydrazine (CCCP)-induced apoptotic cell death by activating Nrf2. *Biochem Biophys Res Comm* 464; 1139-1144.
- Park, S-H., Lee, A-R., Choi, K., Joung, S., Yoon, J-B., Kim, S. (2019) TOMM20 as a potential therapeutic target of colorectal cancer. *BMB Rep* 52; 712-717.
- Parry, D.A.D., Craig, A.S., Barnes, G.R.G. (1978a) Tendon and ligament from the horse: an ultrastructural study of collagen fibrils and elastic fibres as a function of age. *Proc R Soc Lond B* 203; 293-303.
- Parry, D.A.D., Barnes, G.R.G., Craig, A.S. (1978b) A comparison of the size distribution of collagen fibrils in connective tissues as a function of age and a possible relation between fibril size distribution and mechanical properties. *Proc R Soc Lond B* 203; 305-321.
- Parsons, S. (2014) Tibialis posterior tendon rupture. In: Bentley, G. (ed) *European Surgical Orthopaedics and Traumatology*. Springer, Berlin, Heidelberg. doi:10.1007/978-3-642-34746-7\_151.

- Parzych, K.R., Klionsky, D.J. (2014) An overview of autophagy: morphology, mechanism and regulation. *Antiox Redox Signal* 20; 460-473.
- Passos, J.F., Nelson, G., Wang, C., Richter, T., Simillion, C., Proctor, C.J., Miwa, S., Olijslagers, S., Hallinan, J., Wipat, A., Saretzki, G., Rudolph, K.L., Kirkwood, T.B.L., von Zglinicki, T. (2010) Feedback between p21 and reactive oxygen production is necessary for cell senescence. *Mol Syst Biol* 6; 347.
- Patterson-Kane, J.C., Wilson, A.M., Firth, E.C., Parry, D.A.D., Goodship, A.E. (1997a) Comparison of collagen fibril populations in the superficial digital flexor tendons of exercised and nonexercised Thoroughbreds. *Equine Vet J* 29; 121-125.
- Patterson-Kane, J.C., Firth, E.C., Goodship, A.E., Parry, D.A.D. (1997b) Age-related differences in collagen crimp patterns in the superficial digital flexor tendon core region of untrained horses. *Aust Vet J* 75; 39-44.
- Patterson-Kane, J.C., Rich, T. (2014) Achilles tendon injuries in elite athletes: lessons in pathophysiology from their equine counterparts. *ILAR J* 55; 86-99.
- Pease, L.I., Clegg, P.D., Proctor, C.J., Shanley, D.J., Cockell, S.J., Peffers, M.J. (2017) Cross platform analysis of transcriptomic data identifies ageing has distinct and opposite effects on tendon in males and females. *Sci Rep* 7; 14443. doi:10.1038/s41598-017-14650-z.
- Peffers, M.J., Thorpe, C.T., Collins, J.A., Eong, R., Wei, T.K.J., Screen, H.R.C., Clegg, P.D. (2014) Proteomic analysis reveals age-related changes in tendon matrix composition, with age- and injury-specific matrix fragmentation. *J Biol Chem* 289; 25867-25878. doi:10.1074/jbc.M114.566554.
- Peffers, M.J., Fang, Y., Cheung, K., Wei, T.K.J., Clegg, P.D., Birch, H.L. (2015) Transcriptome analysis of ageing in uninjured human Achilles tendon. *Arthritis Res Therap* 17; 33. doi:10.1186/s13075-015-0544-2.
- Peffers, M., Collins, J., Loughlin, J., Proctor, C., Clegg, P.D. (2016) A proteomic analysis of chondrogenic, osteogenic and tenogenic constructs from ageing mesenchymal stem cells. *Stem Cell Res Therap* 7; 133-148.
- Perkins, N.R., Reid, S.W., Morris, R.S. (2005). Risk factors for injury to the superficial digital flexor tendon and suspensory apparatus in Thoroughbred racehorses in New Zealand. *NZ Vet J* 53; 184-192.
- Piantadosi, C.A., Carraway, M.S., Babiker, A., Suliman, H.B. (2008) Heme oxygenase-1 regulates cardiac mitochondrial biogenesis via Nrf2-mediated transcriptional control of nuclear respiratory factor-1. *Circ Res* 103; 1232-1240.
- Platt, D., Wilson, A.M., Timbs, A., Wright, I.M., Goodship, A.E. (1994) Novel force transducer for the measurement of tendon force in vivo. *J Biomech* 27; 1489-1493.
- Pomeroy, G.C., Pike, R.H., Beals, T.C., Manoli, A. (1999) Acquired flatfoot in adults due to dysfunction of the posterior tibial tendon. *J Bone Joint Surg* 81-A; 1173-1182.
- Pop-Bica, C., Pintea, S., Cojocneanu-Petric, R., del-Sal, G., Piazza, S., Wu, Z-H., Alencar, A.J., Lossos, I.S., Berindan-Neagoe, I., Calin, G.A. (2018) miR-181 family-specific behaviour in different cancers: a meta-analysis view. *Cancer Metastasis Rev* 37; 17-32.

Poulsen, R.C., Knowles, H.J., Carr, A.J., Hulley, P.A. (2014) Cell differentiation versus cell death: extracellular glucose is a key determinant of cell fate following oxidative stress exposure. *Cell Death Dis* 5; e1074. doi:10.1038/cddis.2014.52.

Pradervand, S., Weber, J., Lemoine, F., Consales, F., Paillusson, A., Dupasquier, M., Thomas, J., Richter, H., Kaessmann, H., Beaudoin, E., Hagenbüchle, O., Harshman, K. (2010) Concordance among digital gene expression, microarrays, and qPCR when measuring differential expression of microRNAs. *BioTechniques* 48; 219-222.

Pryce, B.A., Watson, S.S., Murchison, N.D., Staverosky, J.A., Dünker, N., Schweitzer, R. (2009) Recruitment and maintenance of tendon progenitors by TGF $\beta$  signalling are essential for tendon formation. *Development* 136; 1351-1361.

R Core Team (2020) R: a language for environment and statistical computing. R Foundation for Statistical Computing, Vienna, Austria. URL <http://www.R-project.org/>.

Rahman, S., Islam, R. (2011) Mammalian Sirt1: insights on its biological functions. *Cell Commun Signal* 9; 11. doi:10.1186/1478-811X-9-11.

Rains, J.L., Jain, S.K. (2011) Oxidative stress, insulin signalling and diabetes. *Free Radical Biol Med* 50; 567-575.

Rane, S., He, M., Sayed, D., Vashistha, H., Malhotra, A., Sadoshima, J., Vatner, D.E., Vatner, S.F., Abdellatif, M. (2009) Downregulation of miR-199a derepresses hypoxia-inducible factor-1 $\alpha$  and sirtuin 1 and recapitulates hypoxia preconditioning in cardiac myocytes. *Circ Res* 104; 879-886. doi:10.1161/CIRCRESAHA.108.193102.

Reardon, R.J.M, Boden, L.A., Mellor, D.J., Love, S., Newton, J.R., Stirk, A.J., Parkin, T.D.H. (2012) Risk factors for superficial digital flexor tendinopathy in Thoroughbred racehorses in hurdle starts in the UK (2001-2009). *Equine Vet J* 44; 564-569.

Reardon, R.J.M, Boden, L.A., Mellor, D.J., Love, S., Newton, J.R., Stirk, A.J., Parkin, T.D.H. (2013) Risk factors for superficial digital flexor tendinopathy in Thoroughbred racehorses in steeplechase starts in the United Kingdom (2001-2009). *Vet J* 195; 325-330.

Reed, K.N., Wilson, G., Pearsall, A., Grishko, V.I. (2014) The role of mitochondrial reactive oxygen species in cartilage matrix destruction. *Mol Cell Biochem* 397; 195-201.

Rezaei, T., Amini, M., Hashemi, Z.S., Mansoori, B., Rezaei, S., Karami, H., Mosafer, J., Mokhtarzadeh, A., Baradaran, B. (2019) microRNA-181 serves as a dual-role regulator in the development of human cancers. *Free Radic Biol Med* 152; 432-454. doi:10.1016/j.freeradbiomed.2019.12.043.

Riasat, K., Bardell, D., Goljanek-Whysall, K., Clegg, P.D., Peffers, M.J. (2020) Epigenetic mechanisms in tendon ageing. *Br Med Bull* 135; 90-107. doi:10.1093/bmb/ldaa023.

Ribitsch, I., Gueltekin, S., Keith, M.F., Minichmair, K., Peham, C., Jenner, F., Egerbacher, M. (2019) Age-related changes of tendon fibril micro-morphology and gene expression. *J Anat* doi:10.1111/joa.13125.

Rifkin, D.B. (2005) Latent Transforming Growth Factor- $\beta$  (TGF- $\beta$ ) binding proteins: orchestrators of TGF- $\beta$  availability. *J Biol Chem* 280; 7409-7412. doi:10.1074/jbc.R400029200.

- Riley, G. (2008). Tendinopathy – from basic science to treatment. *Nat Clin Prac* 4; 82-89.
- Riss, T.L., Moravec, R.A., Niles, A.L., Duellman, S., Benink, H.A., Worzella, T.J., Minor, L. (2013 (updated 2016)) Cell viability assays. In: Markossian, S., Sittampalam, G.S., Grossman, A. et al. editors. *Assay guidance manual* (internet). Bethesda (MD): Eli Lilly & Company and the National Center for Advancing Translational Sciences; 2004. Available from: <https://www.ncbi.nlm.nih.gov/books/NBK144065/>
- Rojas-Ríos, P., Simonelig, M. (2018) piRNAs and PIWI proteins: regulators of gene expression in development and stem cells. *Development* 145; dev161786. doi:10.1242/dev.161786.
- Rooney, S.I., Torino, D.J., Baskin, R., Vafa, R.P., Kuntz, A.F., Soslowsky, L.J. (2017) Rat supraspinatus tendon responds acutely and chronically to exercise. *J Appl Physiol* 123; 757-763.
- Roush, S., Slack, F.J. (2008) The let-7 family of microRNAs. *Trends Cell Biol* 18; 505-516. doi:10.1016/j.tcb.2008.07.007.
- Runwal, G., Stamatakou, E., Siddiqi, F.H., Puri, C., Zhu, Y., Rubinsztein, D.C. (2019) LC3-positive structures are prominent in autophagy-deficient cells. *Sci Rep* 9; 10147. doi:10.1038/s41598-019-46657-z.
- Rupaimoole, R., Slack, F.J. (2017) microRNA therapeutics: towards a new era for the management of cancer and other diseases. *Nat Rev Drug Discov* 16; 203-222. doi:10.1038/nrd.2016.246.
- Russo, V., Mauro, A., Martelli, A., di Giacinto, O., di Marcantonio, L., Nardinocchi, D., Berardinelli, P., Barboni, B. (2015) Cellular and molecular maturation in fetal and adult ovine calcaneal tendons. *J Anat* 226; 126-142.
- Saltiel, A.R., Pessin, J.E. (2002) Insulin signalling pathways in time and space. *Trends Cell Biol* 12; 65-71.
- Sánchez-Martín, P., Komatsu, M. (2018) p62/SQSTM1 - steering the cell through health and disease. *J Cell Sci* 131; jcs222836. doi:10.1242/jcs.222836.
- Scott, A., Bahr, R. (2009) Neuropeptides in tendinopathy. *Front Biosci* 14; 2203-2211.
- Scott, A., Khan, K.M., Heer, J., Cook, J.L., Lian, O., Duronio, V. (2005) High strain mechanical loading rapidly induces tendon apoptosis - an ex vivo rat tibialis anterior model. *Br J Sports Med* 39; e25. doi:10.1136/bjism.2004.015164.
- Scott, M.S., Ono, M. (2011) From snoRNA to miRNA: dual function regulatory non-coding RNAs. *Biochimie* 93; 1987-1992.
- Screen, H.R.C., Shelton, J.C., Bader, D.L., Lee, D.A. (2005) Cyclic tensile strain upregulates collagen synthesis in isolated tendon fascicles. *Biochem Biophys Res Comm* 336; 424-429.
- Screen, H.R., Berk, D.E., Kadler, K.E., Ramirez, F., Young, M.F. (2015) Tendon functional extracellular matrix. *J Orthop Res* 33; 793-799.
- Seirafi, M., Kozlov, G., Gehring, K. (2015) Parkin structure and function. *FEBS J* 282; 2076-2088.
- Selbach, M., Schwanhäusser, B., Thierfelder, N., Fang, Z., Khanin, R., Rajewsky, N. (2008) Widespread changes in protein synthesis induced by microRNAs. *Nature* 455; 58-63. doi:10.1038/nature07228.

Schmidt, O., Pfanner, N., Meisinger, C. (2010) Mitochondrial protein import: from proteomics to functional mechanisms. *Nat Rev Mol Cell Biol* 11; 655-667.

Schroeder, A., Mueller, O., Stocker, S., Salowsky, R., Leiber, M., Gassmann, M., Lightfoot, S., Menzel, W., Granzow, M., Ragg, T. (2006) The RIN: an RNA integrity number for assigning integrity values to RNA measurements. *BMC Molecular Biol* 7; 3. doi:10.1186/1471-2199-7-3.

Sharma, P., Maffulli, N. (2005) Tendon injury and tendinopathy: healing and repair. *J Bone Joint Surg* 87-A; 187-202.

Shukunami, C., Takimoto, A., Nishizaki, Y., Yoshimoto, Y., Tanaka, S., Miura, S., Watanabe, H., Sakuma, T., Yamamoto, T., Kondoh, G., Hiraki, Y. (2018) Scleraxis is a transcriptional activator that regulates the expression of Tenomodulin, a marker of mature tenocytes and ligamentocytes. *Sci Rep* 8, 3155. doi.org/10.1038/s41598-018-21194-3.

Singer, E.R., Barnes, J., Saxby, F., Murray, J.K. (2008). Injuries in the event horse: training versus competition. *Vet J* 175; 76-81.

Smith, R.K.W., Jones, R., Webbon, P.M. (1994) The cross-sectional areas of normal equine digital flexor tendons determined ultrasonographically. *Equine Vet J* 26; 460-465.

Smith, R.K.W., Zunino, L., Webbon, P.M., Heinegard, D. (1997) The distribution of cartilage oligomeric matrix protein (COMP) in tendon and its variation with tendon site, age and load. *Matrix Biol* 16; 255-271.

Smith, R.K., Birch, H., Patterson-Kane, J., Firth, E.C., Williams, L., Cherdchutham, W., van Weeren, W.R., Goodship, A.E. (1999) Should equine athletes commence training during skeletal development? Changes in tendon matrix associated with development, ageing, function and exercise. *Equine Vet J Suppl* 30; 201-209.

Smith, R.K.W., Gerard, M., Dowling, B., Dart, A.J., Birch, H.L., Goodship, A.E. (2002a) Correlation of cartilage oligomeric matrix protein (COMP) levels in equine tendon with mechanical properties: a proposed role for COMP in determining function-specific mechanical characteristics of locomotor tendons. *Equine Vet J Suppl* 34; 241-244.

Smith, R.K.W., Birch, H.L., Goodman, S., Heinegard, D., Goodship, A.E. (2002b) The influence of ageing and exercise on tendon growth and degeneration – hypotheses for the initiation and prevention of strain-induced tendinopathies. *Comp Biochem Physiol Part A* 133; 1039-1050.

Song, Y., Du, Y., Zou, W., Luo, Y., Zhang, X., Fu, J. (2018) Involvement of impaired autophagy and mitophagy in Neuro-2a cell damage under hypoxic and/or high-glucose conditions. *Sci Rep* 8; 3301. doi:10.1038/s41598-018-20162-1.

Soriano-Arroquia, A., House, L., Tregilgas, L., Canty-Laird, E., Goljanek-Whysall, K. (2016) The functional consequences of age-related changes in microRNA expression in skeletal muscle. *Biogeront* 17; 641-654.

- Soslow, L.J., Thomopoulos, S., Tun, S., Flanagan, C.L., Keefer, C.C., Mastaw, J., Carpenter, J.E. (2000) Overuse activity injures the supraspinatus tendon in an animal model: a histologic and biomechanical study. *J Shoulder Elbow Surg* 9; 79-84.
- Sperveslage, J., Hoffmeister, M., Henopp, T., Klöppel, G., Sipos, B. (2014) Establishment of robust controls for the normalisation of miRNA expression in neuroendocrine tumours of the ileum and pancreas. *Endocrine* 46; 226-230.
- Spiesz, E.W., Thorpe, C.T., Chaudhry, S., Riley, G.P., Birch, H.L., Clegg, P.D., Screen, H.R.C. (2015) Tendon extracellular matrix damage, degradation and inflammation in response to in vitro overload exercise. *J Orthop Res* 33; 889-897.
- Springer, W., Kahle, P.J. (2011) Regulation of PINK1-Parkin-mediated mitophagy. *Autophagy* 7; 266-278.
- Stavast, C.J., Erkeland, S.J. (2019) The non-canonical aspects of microRNAs: many roads to gene regulation. *Cells* 8; 1465. doi:10.3390/cells8111465.
- Stenvang, J., Petri, A., Lindow, M., Obad, S., Kauppinen, S. (2012) Inhibition of microRNA function by anti-miR oligonucleotides. *Silence* 3; 1. doi:10.1186/1758-907X-3-1.
- Stephens, P.R., Nunamaker, D.M., Butterweck, D.M. (1989) Application of a Hall-effect transducer for measurement of tendon strains in horses. *Am J Vet Res* 50; 1089-1095.
- Su, Z., Yang, Z., Xu, Y., Chen, Y., Yu, Q. (2015) microRNAs in apoptosis, autophagy and necroptosis. *Oncotarget* 6; 8474-8490.
- Sugg, K.B., Lubardic, J., Gumucio, J.P., Mendias, C.L. (2014) Changes in macrophage phenotype and induction of epithelial-to-mesenchymal transition genes following acute Achilles tenotomy and repair. *J Orthop Res* 32; 944-951.
- Szabadkai, G., Simoni, A.M., Chami, M., Wieckowski, M.R., Youle, R.J., Rizzuto, R. (2004) Drp-1-dependent division of the mitochondrial network blocks intraorganellar Ca<sup>2+</sup> waves and protects against Ca<sup>2+</sup>-mediated apoptosis. *Mol Cell* 16; 59-68.
- Szekerczés, T., Gógl, A., Illyés, I., Mandl, J., Borka, K., Kiss, A., Schaff, Z., Lendvai, G., Werling, K. (2020) Autophagy, mitophagy and microRNA expression in chronic Hepatitis C and autoimmune hepatitis. *Pathol Oncol Res* 26; 2143-2151.
- Taira, T., Saito, Y., Niki, T., Iguchi-Arigo, S.M.M., Takahashi, K., Ariga, H. (2004) DJ-1 has a role in antioxidative stress to prevent cell death. *EMBO Reports* 5; 213-218.
- Tan, S., Yu, C.Y., Sim, Z.W., Low, Z.S., Lee, B., See, F., Min, N., Gautam, A., Chu, J.J.H., Ng, K.W., Wong, E. (2019) Pomegranate activates TFEB to promote autophagy-lysosomal fitness and mitophagy. *Sci Rep* 9; 727. doi:10.1038/s41598-018-37400-1.
- Tan, G.-K., Pryce, B.A., Stabio, A., Brigande, J.V., Wang, C.J., Xia, Z., Tufa, S.F., Keene, D.R., Schweitzer, R. (2020) Tgfβ signalling is critical for maintenance of the tendon cell fate. *eLIFE* 9; e52695.
- Tekirdag, K.A., Korkmaz, G., Ozturk, D.G., Agami, R., Gozuacik, D. (2013) *MIR181A* regulates starvation- and rapamycin-induced autophagy through targeting of *ATG5*. *Autophagy* 9; 374-385. doi:10.4161/auto.23117.

- Thankam, F.G., Boosani, C.S., Dilisio, M.F., Dietz, N.E., Agrawal, D.K. (2016) microRNAs associated with shoulder tendon matrix disorganisation in glenohumeral arthritis. *PLoS ONE* 11; e0168077. doi:10.1371/journal.pone.0168077.
- Thankam, F.G., Chandra, I.S., Kovilam, A.N., Diaz, C.G., Volberding, B.T., Dilisio, M.F., Radwan, M.M., Gross, R.M., Agrawal, D.K. (2018) Amplification of mitochondrial activity in the healing response following rotator cuff tendon injury. *Sci Rep* 8; 17027.
- Thankam, F.G., Boosani, C.S., Dilisio, M.F., Agrawal, D.K. (2018) microRNAs associated with inflammation in shoulder tendinopathy and glenohumeral arthritis. *Mol Cell Biochem* 437; 81-97.
- Thankam, F.G., Boosani, C.S., Dilisio, M.F., Gross, R.M., Agrawal, D.K. (2019) Genes interconnecting AMPK and TREM-1 and associated microRNAs in rotator cuff tendon injury. *Mol Cell Biochem* 454; 97-109.
- Thomopoulos, S., Williams, G.R., Gimbel, J.A., Favata, M., Soslowky, L.J. (2003) Variation of biomechanical, structural and compositional properties along tendon to bone insertion site. *J Orthop Res* 21; 413-419.
- Thorpe, C.T., Streeter, I., Pinchbeck, G.L., Goodship, A.E., Clegg, P.D., Birch, H.L. (2010) Aspartic acid racemization and collagen degradation markers reveal an accumulation of damage in tendon collagen that is enhanced with aging. *J Biol Chem* 285; 15674-15681.
- Thorpe, C.T., Udeze, C.P., Birch, H.L., Clegg, P.D., Screen, H.R.C. (2012) Specialization of tendon mechanical properties results from interfascicular differences. *J R Soc Interface* 9; 3108-3117.
- Thorpe, C.T., Klemm, C., Riley, G.P., Birch, H.L., Clegg, P.D., Screen, H.R.C. (2013a) Helical sub-structures in energy-storing tendons provide a possible mechanism for efficient energy storage and return. *Acta Biomaterialia* 9; 7948-7956.
- Thorpe, C.T., Udeze, C.P., Birch, H.L., Clegg, P.D., Screen, H.R.C. (2013b) Capacity for sliding between tendon fascicles decreases with ageing in injury prone equine tendons: a possible mechanism for age-related tendinopathy? *Europ Cells Mat* 25; 48-60.
- Thorpe, C.T., Riley, G.P., Birch, H.L., Clegg, P.D., Screen, H.R.C. (2014) Fascicles from energy-storing tendons show an age-specific response to cyclic fatigue loading. *J R Soc Interface* 11; 20131058.
- Thorpe, C.T., Spiesz, E.M., Chaudhry, Screen, H.R.C., Clegg, P.D. (2015a) Science in brief: Recent advances into understanding tendon function and injury risk. *Equine Vet J* 47; 137-140.
- Thorpe, C.T., Chaudhry, S., Lei, I.I., Varone, A., Riley, G.P., Birch, H.L., Clegg, P.D., Screen, H.R.C. (2015b) Tendon overload results in alterations in cell shape and increased markers of inflammation and matrix degradation. *Scand J Med Sci Sports* 25; e381-e389. doi:10.1111/sms.12333.
- Thorpe, C.T., Godinho, M.S.C., Riley, G.P., Birch, H.L., Clegg, P.D., Screen, H.R.C. (2015c) The interfascicular matrix enables fascicle sliding and recovery in tendon, and behaves more elastically in energy storing tendons. *J Mech Behav Biomed Mater* 52; 85-94.
- Thorpe, C.T., Riley, G.P., Birch, H.L., Clegg, P.D., Screen, H.R.C. (2016a) Fascicles and interfascicular matrix show adaptation for fatigue resistance in energy storing tendons. *Acta Biomaterialia* 42; 308-315.

- Thorpe, C.T., Karunaseelan, K.J., Hin, J.N.C., Riley, G.P., Birch, H.L., Clegg, P.D., Screen, H.R.C. (2016b) Distribution of proteins within different compartments of tendon varies according to tendon type. *J Anat* 229; 450-458.
- Thorpe, C.T., Peffers, M.J., Simpson, D., Halliwell, E., Screen, H.R.C., Clegg, P.D. (2016c) Anatomical heterogeneity of tendon: Fascicular and interfascicular tendon compartments have distinct proteomic composition. *Sci Rep* 6; 20455. doi:10.1038/srep20455.
- Thorpe, C.T., Riley, G.P., Birch, H.L., Clegg, P.D., Screen, H.R.C. (2017) Fascicles and interfascicular matrix show decreased fatigue life with ageing in energy storing tendons. *Acta Biomater* 56; 58-64.
- Tong, X., Wang, S., Lei, Z., Li, C., Zhang, C., Su, Z., Liu, X., Zhao, J., Zhang, H-T. (2020) MYOCD and SMAD3/SMAD4 form a positive feedback loop and drive TGF- $\beta$ -induced epithelial–mesenchymal transition in non-small cell lung cancer. *Oncogene* 39; 2890–2904. doi:10.1038/s41388-020-1189-4.
- Toy-Miou-Leong, M., Cortes, C.L., Beaudet, A., Rostène, W., Forgez, P. (2004) Receptor trafficking via the perinuclear recycling compartment accompanied by cell division is necessary for permanent neurotensin cell sensitisation and leads to chronic Mitogen Activated Protein Kinase activation. *J Biol Chem* 279; 1636-12646. doi:10.1074/jbc.M303384200.
- Tsai, W-C., Chang, H-N., Yu, T-Y., Chien, C-H., Fu, L-F., Liang, F-C., Pang, J-H.S. (2011) Decreased proliferation of aging tenocytes is associated with down-regulation of cellular senescence-inhibited gene and up-regulation of p27. *J Orthop Res* 29; 1598-1603.
- Tsang, J., Zhu, J., van Oudenaarden, A. (2007) microRNA-mediated feedback and feedforward loops are recurrent network motifs in mammals. *Mol Cell* 26; 753-767.
- Tully, L.J., Murphy, A.M., Smith, R.K.W., Hulin-Curtis, S.L., Verheyen, K.L.P., Price, J.S. (2014) Polymorphisms in TNC and COL5A1 genes are associated with risk of superficial digital flexor tendinopathy in National Hunt Thoroughbred racehorses. *Equine Vet J* 46; 289-293.
- Usman, M.A., Nakasa, T., Shiji, T., Kato, T., Kawanishi, Y., Hamanishi, M., Kamei, N., Ochi, M. (2015) The effect of administration of double stranded microRNA-210 on acceleration of Achilles tendon healing in a rat model. *J Orthop Sci* 20; 538-546.
- Valadkhan, S., Gunawardane, L.S. (2013) Role of small nuclear RNAs in eukaryotic gene expression *Essays Biochem* 54; 79-90. doi:10.1042/bse0540079.
- Victoria, B., Nunez Lopez, Y.O., Masternak, M.M. (2017) microRNAs and the metabolic hallmarks of aging. *Mol Cell Endocrin* 455; 131-147.
- Villa, E., Marchetti, S., Ricci, J-E. (2018) No parkin zone: mitophagy without parkin. *Trends Cell Biol* 28; 882-895. doi:10.1016/j.tcb.2018.07.004.
- Waddington, C.H. (1968) Towards a theoretical biology. *Nature* 218; 525-527. doi:10.1038/218525a0.
- Wang, M-X., Wei, A., Yuan, J., Clippe, A., Bernard, A., Knoop, B., Murrell, G.A.C. (2001) Antioxidant enzyme peroxiredoxin 5 is upregulated in degenerative human tendon. *Biochem Biophys Res Comm* 284; 667-673.

- Wang, Z., Gerstein, M., Snyder, M. (2009) RNA-seq: a revolutionary tool for transcriptomics. *Nat Rev Genet* 10; 57-63. doi:10.1038/nrg2484.
- Wang, X., Chen, X., Meng, Q., Jing, H., Lu, H., Yang, Y., Cai, L., Zhao, Y. (2015) miR-181b regulates cisplatin chemosensitivity and metastasis by targeting TGF $\beta$ R1/Smad signaling pathway in NSCLC. *Sci Rep* 5; 17618. doi:10.1038/srep17618.
- Wang, B., Guo, J., Feng, L., Suen, C-W., Fu, W-M., Zhang, J-F., Li, G. (2016) Mir124 suppresses collagen formation of human tendon derived stem cells through targeting egr1. *Exp Cell Res* 347; 360-366.
- Ward, C.W., Lawrence, M.C. (2009) Ligand-induced activation of the insulin receptor: a multi-step process involving structural changes in both the ligand and the receptor. *BioEssays* 31; 422-434.
- Watkins, J.P., Auer, J.A., Gay, S., Morgan, S.J., (1985) Healing of surgically created defects in the equine superficial digital flexor tendon – collagen-type transformation and tissue morphologic reorganization. *Am J Vet Res* 46; 2091-2096.
- Watts, A.E., Nixon, A.J., Yeager, A.E., Mohammed, H.O. (2012) A collagenase gel/physical defect model for controlled induction of superficial digital flexor tendonitis. *Equine Vet J* 44; 576-586.
- Watts, A.E., Millar, N.L., Platt, J., Kitson, S.M., Akbar, M., Rech, R., Griffin, J., Pool, R., Hughes, T., McInnes, I.B., Gilchrist, D.S. (2017) MicroRNA29a treatment improves early tendon injury. *Mol Therap* 25; 2415-2426. doi:10.1016/j.ymthe.2017.07.015.
- Webb, M., Malhotra, J., Tham, C-S., Goddeeris, M., McMillin, D.W., Tozzo, E. (2017) A novel mitophagy assay for skeletal myotubes. *Open Access J Neurol Neurosurg* 4; 555649. doi:10.19080/OAJNN.2017.04.555649.
- Webbon, P.M. (1978) A histological study of macroscopically normal equine digital flexor tendons. *Equine Vet J* 10; 253-259.
- Wertz, J., Galli, M., Borchers, J.R. (2013) Achilles tendon rupture – risk assessment for aerial and ground athletes. *Sports Health* 5; 407-409.
- Wightman, B., Ha, I., Ruvkun, G. (1993) Post transcriptional regulation of the heterochronic gene lin-14 by lin-4 mediates temporal pattern formation in *C. elegans*. *Cell* 75; 855-862.
- Williams, R.B., Harkins, L.S., Hammond, C.J., Wood, J.L. (2001). Racehorse injuries, clinical problems and fatalities recorded on British racecourses from flat racing and National Hunt racing during 1996, 1997 and 1998. *Equine Vet J* 33; 478-486.
- Wilmink, J., Wilson, A.M., Goodship, A.E. (1992) Functional significance of the morphology and micromechanics of collagen fibres in relation to partial rupture of the superficial digital flexor tendon in racehorses. *Res Vet Sci* 53; 354-359.
- Wilson, A.M., McGuigan, M.P., Su, A., van den Bogert, A.J. (2001) Horses damp the spring in their step. *Nature* 414; 895-899.
- Wilson, A.M., Goodship, A.E. (1994) Exercise-induced hyperthermia as a possible mechanism for tendon degeneration. *J Biomechanics* 27; 899-905.

- Wren, T.A., Yerby, S.A., Beaupre, G.S., Carter, D.R. (2001) Mechanical properties of the human Achilles tendon. *Clin Biomech* 16; 245-251.
- Wu, Y.F., Mao, W.F., Zhou, Y.L., Wang, X.T., Liu, P.Y., Tang, J.B. (2016) Adeno-associated virus-2-mediated TGF $\beta$ 1 microRNA transfection inhibits adhesion formation after digital flexor tendon injury. *Gene Therap* 23; 167-175.
- Xiao, F., Zuo, Z., Cai, G., Kang, S., Gao, X., Li, T. (2009) miRecords: an integrated resource for microRNA-target interactions. *Nucleic Acids Res* 37; D105-D110. doi:10.1093/nar/gkn851.
- Xie, W., Li, M., Xu, Q., Huang, N., He, J., Zhang, Y. (2013) miR-181a regulates inflammation responses in monocytes and macrophages. *PLoS ONE* 8; e58639. doi:10.1371/journal.pone.0058639.
- Xu, J., Wang, Y., Tan, X., Jing, H. (2012) MicroRNAs in autophagy and their emerging roles in crosstalk with apoptosis. *Autophagy* 8; 873-882.
- Xu, D., Tahara, H. (2013) The role of exosomes and microRNAs in senescence and aging. *Adv Drug Deliv Rev* 65; 368-375.
- Yamakuchi, M., Ferlito, M., Lowenstein, C.J. (2008) miR-34a repression of SIRT1 regulates apoptosis. *Proc Natl Acad Sci* 105; 13421-13426.
- Yang, Y., Topol, L., Lee, H., Wu, J. (2003) *Wnt5a* and *Wnt5b* exhibit distinct activities in coordinating chondrocyte proliferation and differentiation. *Development* 130; 1003-1015. doi:10.1242/dev.00324.
- Yang, C., Tabatabaei, S.N., Ruan, X., Hardy, P. (2017) The dual regulatory role of miR-181a in breast cancer. *Cell Physiol Biochem* 44; 843-856.
- Yates, A.D., Achuthan, O., Akanni, W., Allen, J., Allen, J., Alvarez-Jarreta, J., Amode, M.R., Armean, I.M., Azov, A.G., Bennett, R., Bhai, J., Billis, K., Boddu, S., Marugán, J.C., Cummins, C., Davidson, C., Dodiya, K., Fatima, R., Gall, A., Giron, C.G., Gil, L., Grego, T., Haggerty, L., Haskell, E., Hourlier, T., Izuogo, O.G., Janacek, S.H., Juettemann, T., Kay, M., Lavidas, I., Le, T., Lemos, D., Gonzalez Martinez, J., Maurel, T., McDowall, M., McMahon, A., Mohanan, S., Moore, B., Nuhn, M., Oheh, D.N., Parker, A., Parton, A., Patricio, M., Sakthivel, M.P., Salam, A.I.A., Schmitt, B.M., Schuilenburg, H., Sheppard, D., Sycheva, M., Szuba, M., Taylor, K., Thormann, A., Threadgold, G., Vullo, A., Walts, B., Winterbottom, A., Zadissa, A., Chakiachvili, M., Flint, B., Frankish, A., Hunt, S.E., Ilesley, G., Kostadima, M., Langridge, N., Loveland, J.E., Martin, F.J., Morales, J., Mudge, J.M., Muffato, M., Perry, E., Ruffier, M., Trevanion, S.J., Cunningham, F., Howe, K.L., Zerbino, D.R., Flicek P. (2020) Ensemble 2020. *Nucleic Acids Res* 48; D682-D688. doi:10.1093/nar/gkz966.
- Yatsenko, A.S., Shcherbata, H.R. (2014) *Drosophila* miR-9a targets the ECM receptor dystroglycan to canalize myotendinous junction formation. *Dev Cell* 28; 335-348.
- Ye, Y., He, X., Lu, F., Mao, H., Zhu, Z., Yao, L., Luo, W., Sun, X., Wang, B., Qian, C., Zhang, Y., Lu, G., Zhang, S. (2018) A lincRNA-p21/miR-181 family feedback loop regulates microglial activation during systemic LPS- and MPTP-induced neuroinflammation. *Cell Death Dis* 9; 803. doi:10.1038/s41419-018-0821-5.
- Yeung, C-Y.C., Gossan, N., Lu, Y., Hughes, A., Hensman, J.J., Bayer, M.L, Kjær, K.E., Kadler, K.E., Meng, Q-J. (2014) Gremlin-2 is a BMP antagonist that is regulated by the circadian clock. *Sci Rep* 4; 5183. doi:10.1038/srep05183.

- Yin, Z., Hu, J.-J., Yang, L., Zheng, Z.-F., An, C.-R., Wu, B.-B., Zhang, C., Shen, W.-L., Liu, H.-H., Chen, J.-L., Heng, B.-C., Guo, G.-J., Chen, X., Ouyang, H.-W. (2016) Single-cell analysis reveals a nestin+ tendon stem/progenitor cell population with strong tenogenic potentiality. *Sci Adv* 2; e1600874.
- Yoboue, E.D., Devin, A. (2012) Reactive oxygen species-mediated control of mitochondrial biogenesis. *Int J Cell Biol* 2012; 403870. doi:10.1155/2012/403870.
- Yokota, A., Gimbel, J.A., Williams, G.R., Soslowsky, L.J. (2005) Supraspinatus tendon composition remains altered long after tendon detachment. *J Shoulder Elbow Surg* 14 (Suppl S); S72-S78.
- Youle, R., Narendra, D. (2011) Mechanisms of mitophagy. *Nat Rev Mol Cell Biol* 12; 9-14.
- Yu, J.M., Wu, X., Gimble, J.M., Guan, X., Freitas, M.A., Bunnell, B.A. (2011) Age-related changes in mesenchymal stem cells derived from rhesus macaque bone marrow. *Aging Cell* 10; 66-79. doi:10.1111/j.1474-9726.2010.00646.x.
- Yu, T.-Y., Pang, J.-H.S., Wu, K.P.-H., Chen, M.J.-L., Chen, C.-H., Tsai, W.-C. (2013) Aging is associated with increased activities of matrix metalloproteinase-2 and -9 in tenocytes. *BMC Musculoskel Dis* 14; 2. doi.org/10.1186/1471-2474-14-2.
- Yuan, J., Murrell, G.A.C., Wei, A.-Q., Wang, M.-X. (2002) Apoptosis in rotator cuff tendinopathy. *J Orthop Res* 20; 1372–1389.
- Zarucco, L., Taylor, K.T., Stover, S.M. (2004) Determination of muscle architecture and fiber characteristics of the superficial and deep digital flexor muscles in the forelimbs of adult horses. *Am J Vet Res* 65; 819-827.
- Zhang, W., Liu, H.T. (2002) MAPK signal pathways in the regulation of cell proliferation in mammalian cells. *Cell Res* 12; 9-18.
- Zhang, H., Bosch-Marce, M., Shimoda, L.A., Yee, S.T., Jin, H.B., Wesley, J.B., Gonzalez, F.J., Semenza, G.L. (2008) Mitochondrial autophagy is an HIF-1-dependent adaptive metabolic response to hypoxia. *J Biol Chem* 283; 10892-10903. doi:10.1074/jbc.M800102200.
- Zhang, J., Ney, P.A. (2009) Role of BNIP3 and NIX in cell death, autophagy and mitophagy. *Cell Death Differ* 16; 939-946.
- Zhang, J., Li, F., Williamson, K.M., Tan, S., Scott, D., Onishi, K., Hogan, M.V., Wang, J.H.-C. (2021) Characterization of the structure, vascularity and stem/progenitor cell populations in porcine Achilles tendon (PAT). *Cell Tissue Res* 384; 367-387. doi:10.1007/s00441-020-03379-3.
- Zhao, D., Li, Y., Li, Y., Jiang, Z., Shen, D., Zhao, Z., Wang, F. (2018) miR-181a regulates the chondrogenic differentiation in pig peripheral blood mesenchymal stem cells. *Int J Clin Exp Pathol* 11; 947-955.
- Zheng, H., Liu, J., Tycksen, E., Nunley, R., McAlinden, A. (2019) MicroRNA-181a/b-1 over-expression enhances osteogenesis by modulating PTEN/PI3K/AKT signalling and mitochondrial metabolism. *Bone* 123; 92-102.
- Zhi, F., Wang, Q., Deng, D., Shao, N., Wang, R., Xue, L., Wang, S., Xia, X., Yang, Y. (2014) miR-181b-5p downregulates NOVA1 to suppress proliferation, migration and invasion and promote apoptosis in astrocytoma. *PLoSOne* 9; e109124. doi:10.1371/journal.pone.0109124.

Zhou, Y., Zheng, X., Chen, L.-J., Xu, B., Jiang, J.-T. (2019) microRNA-181b suppresses the metastasis of lung cancer cells by targeting sex determining region Y-related high mobility group-box 6 (Sox6). *Pathol Res Pract* 215; 335-342.

Zhu, L., Chen, S., Chen, Y. (2011) Unravelling the biological functions of Smad7 with mouse models. *Cell Biosci* 1; 44. doi:10.1186/2045-3701-1-44.

Zhu, L.-M., Yang, M. (2019) The suppression of miR-181 inhibits inflammatory responses of osteoarthritis through NK- $\kappa$ B signalling pathway. *Eur Rev Med Pharmacol Sci* 23; 5567-5574.

Zuskov, A., Freedman, B.R., Gordon, J.A., Sarver, J.J., Buckley, M.R., Soslowky, L.J. (2020) Tendon biomechanics and crimp properties following fatigue loading are influenced by tendon type and age in mice. *J Orthop Res* 38; 36-42.